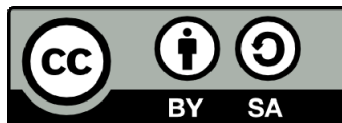




UNIVERSITAT_{DE}
BARCELONA

Nutrient supply impacts osteocytic specification by regulating a nuclear transcription program

Cristina Sánchez de Diego



Aquesta tesi doctoral està subjecta a la llicència **Reconeixement- Compartitqual 4.0. Espanya de Creative Commons.**

Esta tesis doctoral está sujeta a la licencia **Reconocimiento - Compartitqual 4.0. España de Creative Commons.**

This doctoral thesis is licensed under the **Creative Commons Attribution-ShareAlike 4.0. Spain License.**



UNIVERSITAT DE
BARCELONA

DOCTORAL PROGRAM in BIOMEDICINE

“Nutrient supply impacts osteocytic specification by regulating a nuclear transcription program”

Doctoral thesis
submitted by:

Thesis conducted under the
direction of:

Cristina Sanchez De Diego **Dr. Francesc Ventura Pujol**

This PhD Thesis was carried out in the department of **Ciencias Fisiológicas-Bellvitge. Universidad de Barcelona**

ABBREVIATIONS

AdipoR	Adiponectin Receptor
AGEs	Advance Glycation End Products
AhR	Aryl Hydrocarbon Receptor
AlpI	Alcaline Phosphatase
AP- 1	Activated Protein 1
ASARM	Acidic Serine-Aspartate Rich Mepe Associated
ATF4	Activating Transcription Factor 4.
ATP	Adenosine Triphosphate
B.Ar	Bone Area
B.Pm	Bone Perimeter
Bglap	Bone Gamma-Carboxyglutamic Acid-Containing Protein
BMD	Bone Mineral Density
BM-MSC	Bone Marrow Mesenchymal Stem Cell
BMP	Bone Morphogenetic Protein
BMP-R	Bmp Receptor
BMU	Basic Multicellular Unit
BTB	Tramtrack And Bric-À-Brac Domain
BV	Bone Volume
bZIP	Basic-Region Leucine Zipper
ChIP	Chromatin Immunoprecipitation
CNC	Cap “N” Collar
CS	Citrate synthase
Ct	Cycle Threshold
Ct.Th.	Cortical Thickness
CTR	C-Terminal Region

CUL3	Cullin3 E3 Ligase
Cx43	Connexin 43
Dlx	Distal Less Homeobox
DM	Diabetes Mellitus
DMF	Dimethyl Fumarate
DMP1	Dentin Matrix Protein 1
DMSO	Dimethyl Sulfoxide
DNA	Deoxyribonucleic Acid
DSPP	Dentin Sialophosphoprotein
ECM	Extracellular Matrix
eNOS	Endothelial Nitrogen Oxygen Species
ER	Endoplasmatic Reticulum
ERK	Extracellular Signal-Regulated Kinase
ERα/β	Estrogen Receptor-A/B
ETS	Electron Transfer Capacity
FBS	Fetal Bovine Serum
FF or F/F	Floxed
FGF23	Fibroblast Growth Factor 23
FoxOs	Forkhead Transcription Factor
GFP	Green Fluorescence Protein
GLUT	Glucose Transporters
GSH	Reduced Glutathione
GSK-3	Glycogen Synthase Kinase-3
GSSG	Oxidized Glutathione
HA	Hydroxyapatite
HAT	Histone Acetyltransferases
HbSS	Homozygous Sickle Cell Disease
hESCs	Human Embrionic Stem Cells
HIF- α	Hypoxia Inducible Factor 1 α

HIFs	Hypoxia Inducible Transcription Factors
HSCs	Hematopoietic Stem Cells
IBSP	Integrin- Binding Sialoprotein; Also Called Bone Sialoprotein
Id1	Inhibitor of DNA Binding 1
IGF-I	Insulin Like Grow Factor 1
IVR	Intervening Region
JNK	Stress-Activated Protein Kinase/Jun N-Terminal Kinase
KEAP1	Kelch-Like ECH-Associated Protein
KO	Knock-Out
LCS	Lacunocanalicular System
LEP-R	Leptin Receptors
lncRNA	Long Non-Coding RNA
LRP	Low-Density Lipoprotein-Related Receptor
MAPK	Mitogen-Activated Protein Kinases
M-CSF	Macrophage Colony-Stimulating Factor
miR	Microna
mPTP	Mitochondrial Permeability Transition Pore
MS	Multiple Sclerosis
MSC	Mesenchymal Stem Cell
Msx2	Homeobox-Containing Protein Muscle Segment Homeobox (<i>Msh</i>) Homolog
mtDNA	Mitochondrial DNA
N.Oc	Steocyte Number
NCPs	Non Collagenous Proteins
nDNA	Nuclear DNA
NEH	Nrf2-Ech Homology Domains
NF-κB	Nuclear Factor Kappa-Light-Chain-Enhancer Of Activated B Cells
NOS	Nitrogen Oxygen Species

NRF2	Nuclear Factor Erythroid 2-Related Factor
NTR	N-Terminal Region
OB	Osteoblast
OC	Osteocalcin
ON	Osteonectin. Also Named Sparc Or Bm40.
OPG	Osteoprotegerin. Also Named Ocif, Osteoclast Inhibitory Factor.
OPGL	Osteoprotegerin Ligand
OPN	Osteopontin. Also Named Spp1.
ORF	Open Reading Frame
Osx	Osterix. Also Named As Sp7
OVX	Ovariectomized
PCR	Polymerase Chain Reaction
PGC1	Peroxisome Proliferator-Activated Receptor Gamma Coactivator 1-Alpha
PGE₂	Prostaglandin E2
PHEX	Phosphate-Regulating Neutral Endopeptidase On Chromosome X
pHi	Intracellular Ph
PI3K	Phosphoinositide 3-Kinase
PKA	Cyclic Amp (Camp)-Dependent Protein Kinase, Protein Kinase A
PKC	Protein Kinase C
PRC	Pgc-Related Coactivator
PTH	Parathyroid Hormone
PTHrp	Parathyroid Hormone-Related Protein
qPCR	Quantitative PCR
RANK	Receptor Activator Of Nf-Kb
RANKL	Rank Ligand. Also Named As Opgl, Trance Or Odf

RGD	Arg-Gly-Asp Peptide
ROS	Reactive Oxygen Species
RT-PCR	Real Time Pcr
Runx2	Runt Related Transcription Factor 2. Also Named Cbfa1 And Aml3
SCs	Satellite Cells
SDS	Sodium Dodecyl Sulfate
SDS-PAGE	Sodium Dodecyl Sulfate Polyacrylamide Gel Electrophoresis
SERMs	Selective Estrogen Receptor Modulators
SIBLING	Small Integrin-Binding Ligand N-Linked Glycoproteins
SIRT1	Sirtuin 1
Smad	Contraction Of Sma And Mad (Mothers Against Decapentaplegic)
Smurf	Smad Ubiquitin Regulatory Factor 1
SOST	Sclerostin
Sp7	Specificity Protein Transcription Factor 7. Also Named Osterix.
SPP1	Secreted Phosphoprotein-1. Also Named Osteopontin.
T1D	Type 1 Diabetes Mellitus
T2D	Type 2 Diabetes Mellitus
TAK	Tgf β -Activated Kinase
Tb.N	Trabecular Number
Tb.Sp.	Trabecular Space
Tb.Th	Trabecular Thickness
TBP	Tata Binding Protein
TGFβ	Transforming Growth Factor B
TNF	Tumor Necrosis Factor
TNFR	Tumor Necrosis Factor Receptor
TV	Tissue Volume
ucOCN	Undercarboxylated Osteocalcin

VDR	Vitamin D Receptor
VEGF	Vascular Endothelial Growth Factor
Wnt	Wingless-Related Integration Site, Or Wingless-Type Mmtv Integration Site Family.
WT	Wild Type

CONTENTS

INTRODUCTION

CHAPTER I: THE BONE.....	15
1. THE SKELETON	15
2. BONE STRUCTURE	15
3. COMPONENTS OF BONE	19
3.1. <i>Bone Cells</i>	19
3.2. <i>Extracellular matrix</i>	21
4. BONE MINERALIZATION.....	26
CHAPTER II: THE AMAZING OSTEOCYTE.....	28
1. THE IMPORTANCE OF OSTEOCYTES.....	28
1.1. <i>Regulation of bone mineralization</i>	28
1.2. <i>Regulation of bone remodeling by osteocytes</i>	29
1.3. <i>Bone damage repair in aged bones</i>	31
1.4. <i>Mechanosensing</i>	32
1.5. <i>Regulation of calcium levels in plasma</i>	33
1.6. <i>Endocrine regulation</i>	34
2. OSTEOCYTOGENESIS	36
CHAPTER III: BONE METABOLISM.....	39
1. NUTRIENT SUPPLY IN BONE	39
2. BIOENERGETICS IN OSTEOBLAST AND OSTEOCYTE DIFFERENTIATION	40
3. CONTROL OF BONE CELL METABOLISM	43
CHAPTER IV: GENETIC REGULATION OF OSTEOCYTOGENESIS	48
1. MECHANISMS FOR GENE EXPRESSION CONTROL	48
2. PGC-1 PROTEIN FAMILY	50
3. NRF2 TRANSCRIPTION FACTOR.....	54
CHAPTER V: BONE PATHOLOGY.....	61
1. OSTEOPOROSIS.....	61
2. DIABETES MELLITUS, GLUCOSE AND BONE HEALTH	64
3. ROS AND BONE HEALTH.....	66
<u>HYPOTESIS AND OBJECTIVES</u>	
OBJECTIVES	71

RESULTS

CHAPTER I: GLUCOSE RESTRICTION ACTIVATES PGC-1A TO PROMOTE OSTEOCYTE DIFFERENTIATION..... 73

1. GLUCOSE RESTRICTION PROMOTES OSTEOCYTE DIFFERENTIATION. 73
2. GLUCOSE SUPPLY MODIFIES OSTEOBLAST AND OSTEOCYTE METABOLISM. 77
3. GLUCOSE RESTRICTION MODIFIES MITOCHONDRIAL CONTENT AND MORPHOLOGY. 81
4. GLUCOSE RESTRICTION EFFECTS ON OSTEOCYTOGENESIS DEPEND ON AMPK..... 86
5. PGC-1 ENHANCES OSTEOCYTIC DIFFERENTIATION IN RESPONSE TO REDUCED GLUCOSE SUPPLY. 89
6. PGC-1A/B CONTRIBUTE TO MAINTAIN BONE HOMEOSTASIS *IN VIVO*. 96

CHAPTER II: NRF2 FUNCTION IN BONE HOMEOSTASIS AND OSTEOCYTE DIFFERENTIATION.....101

1. INCREASED OXPHOS ACTIVITY AND ROS GENERATION ARE ASSOCIATED TO OSTEOCYTOGENESIS 101
2. INCREASED NRF2 ACTIVITY DURING OSTEOCYTOGENESIS 107
3. NFE2L2 DELETION IN OSTEOCYTES CAUSES OSTEOPENIA AND IMPAIRS OSTEOCYTE-SPECIFIC GENE EXPRESSION 109
4. NRF2 ACTIVITY REGULATES OSTEOCYTE-SPECIFIC GENE EXPRESSION 117
5. DMF TREATMENT PRESERVES BONE MASS AND OSTEOCYTIC GENE EXPRESSION IN OVARECTOMY-INDUCED OSTEOPOROSIS 131

DISCUSSION

CHAPTER I: THE OSTEOCYTES.....136

1. THE IMPORTANCE OF OSTEOCYTES AND CHALLENGES IN THEIR STUDY 136

CHAPTER II: METABOLISM AND DIFFERENTIATION.....141

1. OSTEOBLAST-TO-OSTEOCYTE TRANSITION IS ASSOCIATED TO AN INCREASE IN OXPHOS ACTIVITY AND ROS GENERATION. 141
2. GLUCOSE RESTRICTION PROMOTES METABOLIC REPROGRAMMING AND DIFFERENTIATION IN OSTEOCYTES 142
3. PGC-1 ENHANCES OSTEOCYTIC DIFFERENTIATION IN RESPONSE TO REDUCED GLUCOSE SUPPLY. 143
4. NRF2 ENHANCES OSTEOCYTIC DIFFERENTIATION IN RESPONSE TO AN INCREASE IN ROS LEVELS DURING METABOLIC REPROGRAMMING. 145

CHAPTER III: NEW THERAPEUTIC TARGETS FOR OSTEOPOROSIS.149

1. ANTI-DIABETIC DRUGS AND BONE HEALTH. 149
2. ANTI-OXIDANTS AND BONE HEALTH..... 150
3. NRF2 AS A THERAPEUTIC TARGET FOR OSTEOPOROSIS 151

MATERIAL AND METHODS:

CHAPTER I: CELL CULTURE	156
1. CELL CULTURE AND MAINTENANCE	156
2. CULTURE DISHES AND COLLAGEN COATING	159
3. CELL LINES	160
3.1. <i>IDG-SW3</i>	160
3.2. <i>Platinum-E</i>	162
4. PRIMARY CELL CULTURES	163
4.1. <i>Isolation of osteoblasts and osteocytes</i>	163
4.2. <i>Osteoblast isolation. Short protocol</i>	168
5. CRISPR/Cas9 TECHNOLOGY.....	170
6. CELL TREATMENTS.....	172
CHAPTER II: BACTERIA	174
1. GROWTH CONDITIONS	174
2. PREPARATION OF COMPETENT CELLS.....	175
3. BACTERIAL TRANSFORMATION: HEAT-SHOCK METHOD	176
4. PLASMID ISOLATION: MINI-PREP AND MAXI-PREP	177
5. DIGESTION	178
7. GLYCEROL STOCK	178
CHAPTER III: RETROVIRUS	180
1. PRODUCTION OF RETROVIRUS	180
2. TRANSDUCING CELLS WITH RETROVIRUS.	182
CHAPTER IV: MOLECULAR BIOLOGY	185
1. RNA ISOLATION.....	185
2. MRNA RETRO TRANSCRIPTION (RT-PCR).....	187
3. ISOLATION OF MITOCHONDRIAL AND NUCLEAR DNA.....	187
4. QUANTITATIVE PCR (qPCR).....	189
5. DNA SEQUENCING BY SANGER METHOD.	192
6. CELL LYSIS AND PROTEIN QUANTIFICATION: BCA ASSAY	193
7. SDS-POLYACRYLAMIDE GEL ELECTROPHORESIS (PAGE) AND WESTERN BLOT.....	194
7.1. <i>SDS-Polyacrylamide gel electrophoresis (PAGE)</i>	195
7.2. <i>Protein transfer and membrane blocking</i>	196
7.3. <i>Immunoblotting</i>	197
8. CHROMATIN IMMUNOPRECIPITATION (CHIP)	199
8.1. <i>Cross-linking</i>	199
8.2. <i>DNA Sonication</i>	200
8.3. <i>Inmunoprecipitation</i>	202
8.4. <i>DNA clean up</i>	206
9. F-ACTIN CYTOSKELETON STAINING WITH PHALLOIDINS	207
10. ALKALINE PHOSPHATASE STAINING:	209

11. ALIZARIN RED STAINING	210
CHAPTER V: CELL VIABILITY AND PROLIFERATION.....	211
1. TUNEL ASSAY <i>IN VITRO</i>	211
2. BRDU.....	212
CHAPTER VI: METABOLISM	216
1. ATP BIOLUMINESCENCE ASSAY.....	216
2. GLUCOSE UPTAKE	217
3. LACTATE ASSAY	218
4. GSSG AND GSH DETERMINATION.....	219
4.1. GLUTATHIONE DETERMINATION BY OPA METHOD	219
4.2. GLUTATHIONE DETERMINATION BY DTNB ASSAY	224
5. INTACT CELL RESPIROMETRY	227
6. MITOCHONDRIAL ISOLATION	229
7. CITRATE SYNTHASE ACTIVITY	231
8. FLUOROPHORES FOR METABOLIC DETERMINATION.	234
8.1. <i>Mitotracker staining.</i>	234
8.2. <i>CellROX staining</i>	235
8.3. <i>MitoSOX</i>	235
9. HYDROGEN PEROXIDASE ASSAY WITH AMPLEX RED	237
10. LIVE CELL IMAGING BY CONFOCAL MICROSCOPY	238
11. FLOW CYTOMETRY.....	239
CHAPTER VII: IN VIVO APPROACHES.....	242
1. MOUSE COLONY GENERATION AND MAINTENANCE.	242
2. ACTIVATION OF CRE RECOMBINASE WITH TAMOXIFEN.	243
3. MOUSE GENOTYPING.....	245
4. OVARECTOMY	246
5. ORAL GAVAGE.....	250
6. TISSUE DISSECTION AND BLOOD COLLECTION	252
7. MICRO-CT: MICRO-COMPUTED TOMOGRAPHY	254
7.1. <i>Sample obtention and Imaging</i>	255
7.2. <i>Image Reconstruction</i>	258
7.3. <i>Micro-CT calibration for BMD</i>	263
7.4. <i>Micro-CT analysis</i>	265
CHAPTER VIII: HISTOMORPHOMETRIC ANALYSIS.	268
1. PARAFFIN PROCESSING OF TISSUE	268
1.1. <i>Decalcification</i>	268
1.2. <i>Dehydratation</i>	269
1.3. <i>Preparation of paraffin blocks</i>	270
1.4. <i>Microme sectioning</i>	270
1.5. <i>Histological stains</i>	271

CHAPTER IX: BIOINFORMATICS	276
CHAPTER 10: STATISTICAL ANALYSIS.....	277
BIBLIOGRAPHY	278



INTRODUCTION

CHAPTER I: THE BONE

1. The skeleton

In vertebrates, the skeleton is a body system composed by bones and cartilages, and it is in close relationship with bands of fibrous connective tissue: the ligaments and the tendons. In the case of bone made skeletons, bones provide a hard-dense connective tissue to supports the structure of the body and give protection to internal organs while cartilage, a semi-rigid form of connective tissue, provides flexibility and smooth surfaces for movement. Ligaments and tendons attach muscles to bones and transmit the forces produced in muscle contraction, permitting locomotion. Bone skeletons also provide a reservoir of phosphate and calcium ions and regulate its circulating levels (Shaker & Deftos, 2013). Moreover, recent advances have highlighted the importance of the skeleton as an endocrine organ that modulates glucose tolerance and testosterone production by secretion of bone-specific proteins (Karsenty, 2014). In fact, bone is in continuous crosstalk with other organs such as adipose tissue, pancreas or kidney (Guntur & Rosen, 2012; Karsenty, 2014; Edgardo Rodríguez-Carballo et al., 2015). Bone also houses the process of hematopoiesis and influences immune system maturation (Manilay & Zouali, 2014). All these evidences emphasize the importance of bone for the well-function of the whole organism and point out the necessity for a deeper understanding of bone biology.

2. Bone structure

Bone tissue is a mineralized connective tissue made up of cells (osteoblasts, osteocytes and osteoclasts), vessels and inorganic crystals. Bone structure and function are dependent on complex interactions between those cells, matrix, cell-derived factors, and others systemic factors that govern the equilibrium between bone formation and destruction.

To achieve its mechanical, biological and chemical functions, bone is organized in a hierarchical, fractal-like manner, from nanostructures to millimeter-sized structures (Figure 1).

At the **nanosstructural level**, cross-linked type I collagen mineralized with nanocrystalline carbonated hydroxyapatite to form a composite material in which mineral provides stiffness while collagen provides ductility and resilience, protecting hydroxyapatite from breaking (Burr & Alle, 2019). This combination maximized load carrying capacity by distributing the forces around discontinuities in bone and reducing stress in the bone matrix. Collagen fibers in bone forms fiber bundles arranged parallel to each other forming sheets (lamellae structure). Recent studies suggest that lamellae are arranged in a helicoidal way in which collagen orientation changes slightly from lamella to lamella through 180 degrees cycles (Varga et al., 2013). These layers are also oriented with respect to the dominant stress in bone. For instance, in bone under tension, collagen fibers are predominantly longitudinal oriented whereas in regions that are usually under compression, collagen fibers are transversely orientated (McMahon et al., 1995)a. Despite its importance, the mechanisms that govern collagen orientation remain unknown. One hypothesis suggests that it is the osteoblast who determine collagen orientation and that the mineral is just deposited in spaces between collagen fibrils (Blair et al., 2017). Another alternative theory suggest that the collagen is deposited without any preferred orientation and that the deposition of charged mineral triggers the orientation of both, collagen and mineral (Burr & Alle, 2019).

At the **microscopic levels**, collagen fibers are organized in different ways, depending on the rate and location on which the bone, and the functional needs of the tissue:

- **Woven Bone:** this is primarily a repairing tissue that we can found in, forming the callus during fracture healing, in response to inflammation, such as in osteomyelitis or in the region of the growth plate during endochondral ossification. Woven bone is a tissue rapidly formed and hence the collagen fibers within it are rapidly mineralized and lack any preferred organization. It presents a lattice structure, with large pores present within the mineralized structure (Baron, 2000).

- **Primary bone:** primary bone is new bone made in a space where bone has not previously existed, although it may be formed from an existing surface of other tissue. This tissue appears in the embryonic development and in fracture repair (Burr & Alle, 2019). There are three different types of primary bone that differ in their microscopic organization, and hence in their mechanical properties:

– **Primary lamellar bone:** This structure is found in the periosteum and on the surface of bone marrow cavity and trabeculae within the marrow. It is characterized by a series of parallel laminar sheets, with a few vascular channels. Therefore, it is a very strong structure that provides mechanical function. It has also a rapid turnover, then it serves to support calcium metabolism.

– **Plexiform or fibrolamellar bone:** This structure is rarely found in humans, and it is typically found in animals that grow rapidly. It is a combination of non-lamellar bone, which forms a core subtracts, and primary lamellar bone, which is deposited on the surface. It provides a way to rapidly increase bone strength.

– **Primary osteons:** primary osteons are formed by progressive in-filling of enlarged vascular channels present in the lamellar bone. Cells are arranged in several concentric layers around the vascular canal until only a small vascular canal remains.

• **Secondary bone:** Secondary bone is the newly deposited bone in a place where previously existed bone has been resorbed. Secondary bone is arranged in secondary osteons or harvesian system, which consists on a lamellae structure surrounding a central harvesian canal that carries the neurovascular bundle. Harvesian vessels are connected in a vascular plexus by Volkmann's canals that run between them in a transverse direction. These secondary osteons are characterized by being larger than primary osteons, having more concentric lamellae, and having a cement line at its outer boundary. Cement lines serves as fiber reinforcement to the bone tissue and constitute the point at which osteoclastic bone resorption stops and bone formation begin (Skedros et al., 2005).

• **Interstitial bone:** Interstitial bone are traces of old bone in a region of bone remodeling. This bone appears to be lamellar but disorganized because its lamellae are incomplete. As it is older than the osteonal bone, it is more highly mineralized and more susceptible to accumulation of microcracks (Burr et al., 2015).

At the **macroscopic level**, bone can be classified into cortical or compact bone and trabecular or cancellous bone:

• **Cortical or compact bone:** Represents 80% of the skeleton. Cortical bone is the main component of the diaphysis or outer part of the long and short bones. It is a dense compact tissue (<5% of porosity) with low turnover rate and high resistance. Cortical bone is organized in osteons around the Harvesian canal where

blood vessels and nerves pass through. Cortical bone provides support and protection(Burr & Alle, 2019).

- **Trabecular, cancellous or spongy bone:** it is primary found in the metaphyses of long bones, as well as in the vertebrae, ribs and iliac crest. It is composed of plates and rods of bone that comprise only 25-30% of the total tissue volume, with the remainder being marrow space. It is characterized by having a higher turnover rate than compact bone. In trabecular bone, the lamellae are arranged in half osteons which are dispose in parallel to the trabecular surface. These trabeculae are highly interconnected, and this characteristic provides higher strength to the bone. The architecture of cancellous bone is characterized by parameters such as the number of trabeculae (Tb.N), its thickness (Tb.Th) and the distance between them (Tb.Sp.). Each of these factors contributes to the overall of cancellous bone volume. Modifications in each of these parameters affect in a different way to the bone strength (Cohen et al., 2010). For instance, the loss of complete trabeculae reduces the strength and stiffness of bone by two or three times more than does losing the same amount of bone via trabecular thinning, since the loss of trabecular connectivity reduces the capacity of bone to direct stresses, and hence its capacity of bearing weight. Spaces between trabecular structures are a niche of bone marrow cells and support the formation of blood cells.

Bone surfaces, except at joints, are surrounded by the periosteum, an external layer of dense irregular connective tissue that contains the bone progenitor cells, osteoblast, osteoclasts, blood vessels, nerve fibers.

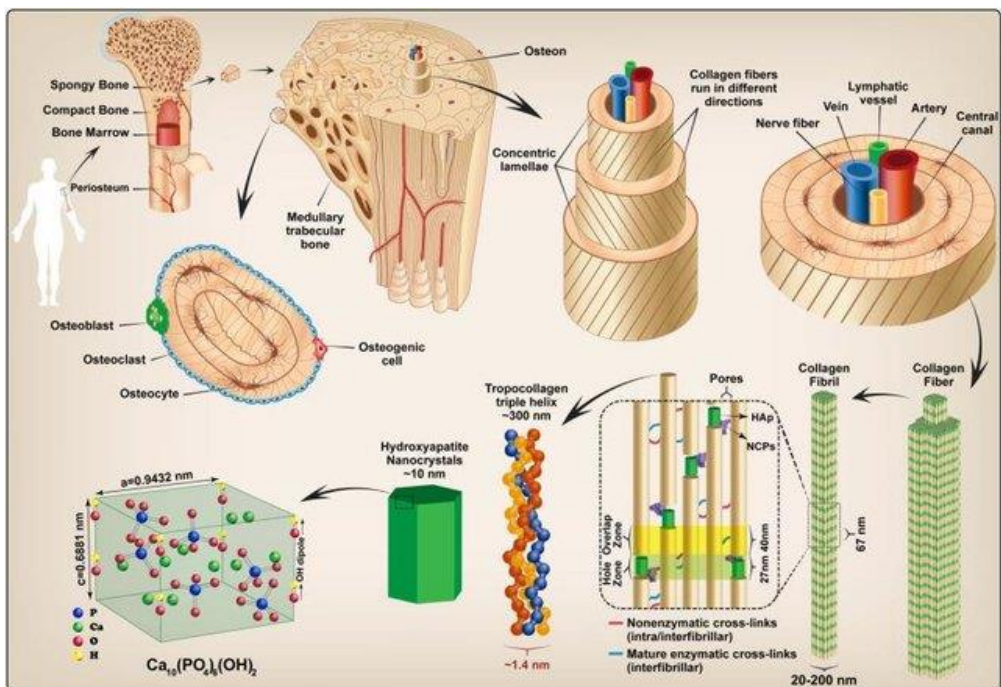


Figure 1. The highly specialized ultrastructure of bone tissue-organization and composition (obtained from (Teixeira et al., 2019))

3. Components of bone

3.1. Bone Cells

Bone consists of four major types of cells: osteoblasts, osteoclasts, osteocytes, and bone lining cells. Each cell type has a unique function and is found in different locations in bones; however, the four cell types work coordinated in the process of bone remodeling to adapt to changing situations and regulate calcium homeostasis. Bone is a highly dynamic organ that is continuously resorbed by osteoclasts and formed by osteoblasts. By its part, osteocytes act as mechanosensors and orchestrators of the process. The function of bone lining cells is not well clear, but these cells seem to play an important role in coupling bone resorption to bone formation. Remodeling enable the bone..... repair cracks etc...

- **Osteoblast:** Osteoblast are cuboidal cells located along the bone surface. Osteoblast are post-mitotic cells that arise from bone-marrow derived mesenchymal stem cells (BM-MSCs) in a process marked by the expression of different transcription factors. However, only a few osteoblasts will eventually differentiate into osteocytes (Rutkovskiy et al., 2016). Others may remain in a low

differentiated stage and retain their capacity to divide and generate new osteogenic cells. Those form a layer of inactive osteoblasts called bone lining cells. Others remain as mature osteoblasts, which are characterized by the presence of large amounts of rough endoplasmic reticulum that enables them to synthesize the components that constitute important for the extracellular matrix, including type I collagen and other non-collagenous proteins. They also secrete matrix vesicles that promote the mineralization of the organic matrix and BMPs to induce bone differentiation (Mohamed, 2008).

- **Bone lining cells.** Bone lining cells are quiescent flat-shaped osteoblasts that cover the bone surfaces, where neither bone resorption nor bone formation occur. Bone lining cells functions are not completely understood, but it has been shown that these cells prevent the direct interaction between osteoclasts and bone matrix, when bone resorption should not occur. They also participate in osteoclast differentiation, producing osteoprotegerin (OPG) and the receptor activator of nuclear factor kappa-B ligand (RANKL) (Miller et al., 1989).

- **Osteoclasts:** Osteoclasts are large multinucleated phagocytic cells derived from the macrophage-monocyte cell lineage. Osteoclasts are involved in bone resorption, contributing to bone remodelling and long-term maintenance of blood calcium homeostasis (Bar-Shavit, 2007).

- **Osteocytes:** Osteocytes are the major cell type of bone, constituting up to 95% of the total cell content. Osteocytes derive from osteoblasts that became buried in the mineralized matrix. At the end of the process, each osteocyte is located in a lacunae, surrounded by matrix, and communicated with other osteocytes via prolongations which cross the matrix through channels called canaliculi. Osteocytes act as orchestrators of bone remodeling through regulation of both osteoclast and osteoblast activities. Osteocytes have an important endocrine role. They secrete soluble factors that not only target cells on the bone surface but also regulate distant organs, such as kidney, muscle, and other tissues (Mohamed, 2008).

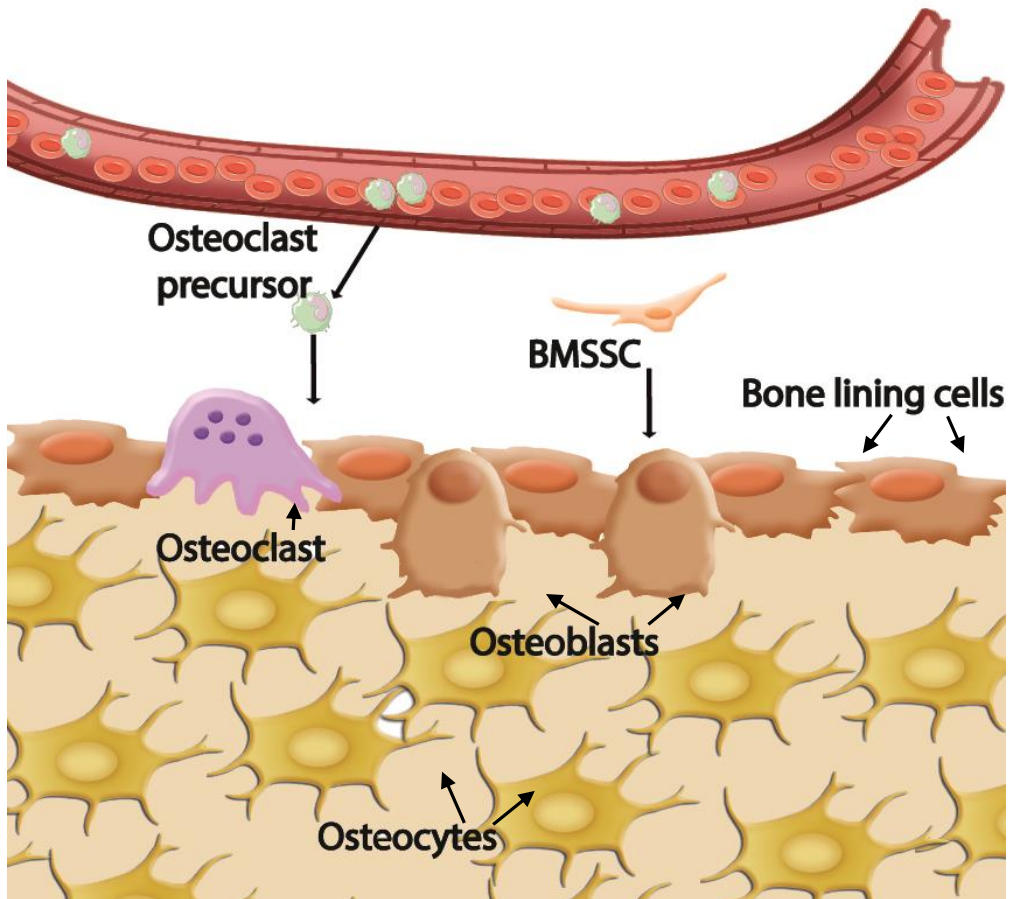


Figure 2. Cell types in bone. Schematic representation of the different cell types found in bone.

3.2. Extracellular matrix

Bone extracellular matrix is mainly produced by the osteoblasts. Generally, calcified bone is composed by around 50-70% mineral content, 20-40% secreted organic matrix and <3% of lipids. The remainder (about 10%) is composed of water, that can be bound to the collagen-mineral interface or can flow freely through canalicular and vascular channels in bone. Unbound water is redistributed during bone loading, and probably contributes to cell signaling. As bone mineralizes, water content declines, and this makes bone stiffer. The equilibrium between water and mineral content is important since drier bones tend to be more brittle and therefore break more easily (Burr & Akkus, 2013).

Bone mineral provides mechanical rigidity and load-bearing strength to bone. The mineral content of bone is mostly hydroxyapatite (HA) $[\text{Ca}_{10}(\text{PO}_4)_6(\text{OH})_2]$, with small amounts of carbonate, magnesium, sodium and potassium in addition to calcium and phosphate. Bone hydroxyapatite crystals are very small (≈ 200 Å) compared with geologic hydroxyapatite crystals. This property, together with the presence of carbonate substitutions, increases the solubility of hydroxyapatite. Thanks to this property, bone can react quickly to the mineral demands of the body (Clarke, 2008).

The organic component provides elasticity and flexibility to bone and serves as a scaffold in bone mineralization. The organic fraction of the bone is mainly composed by type I collagen (which is a tripe-helical molecule containing two α (I) chains (encoded by *Col1a1* gene) and one β (I) chain (encoded by *Col1a2* gene). The expression of genes encoding for type I collagen is widely used as a marker for osteoblast differentiation and mutations in these genes lead to osteogenesis imperfecta, a disorder characterized mainly by bone fragility derived from abnormal assembly of bone collagen (Fedarko, 2013; Makareeva & Leikin, 2013). Type I collagen is synthesized as a precursor, which consists of an N-terminal propeptide, central collagen domain and C-terminal propeptide. After translation, procollagen chains translocate into the lumen of rough endoplasmic reticulum (ER) where they undergo several posttranscriptional modifications including, hydroxylation and glycosylation. Vitamin C have proved to be necessary for the proper type I collagen hydroxylation (Ather & Harding, 2009; Murad et al., 1981). Still in the ER, transient association between molecular chaperones and pro-collagen chain domains promotes winding of the triple helix from the carboxy terminal toward the amino terminal. After post-translational modification and folding, procollagen molecules are transported through Golgi and secreted to the extracellular matrix where procollagen amino and carboxy proteinases cleavage N- and C-propeptides, producing 300 nm-long collagen triple helix bounded by short terminal peptides (telopeptides). These mature collagen molecules assemble into fibers, with a banding pattern that can be observed by electron microscopy. Polymerization of type I collagen is dependent on fibronectin, a minor constituent of the bone matrix produced by osteoblasts (Velling et al., 2002).

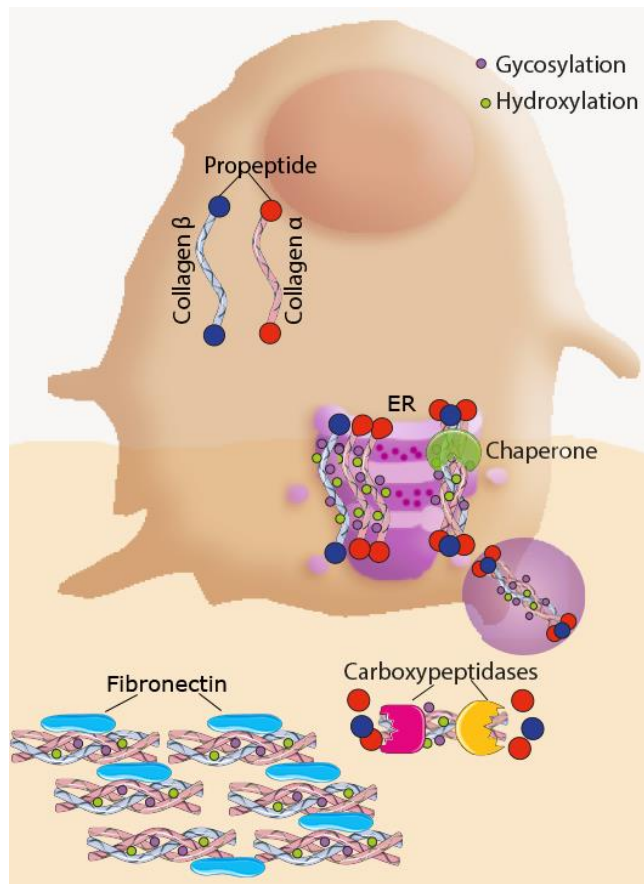


Figure 3. Collagen synthesis. procollagen chains are synthesized as precursors composed by N-terminal propeptide, central collagen domain and C-terminal propeptide. In the Endoplasmic Reticulum (ER) collagen precursors are hydroxylated, glycosylated and wined with the help of chaperones. Triple helix of procollagen is secreted to the extracellular matrix where carboxypeptidases cleavage N- and C-propeptides. After binding to fibronectin, mature collagen polymerize and assemble into fibers with a band pattern.

Other non-collagenous proteins (NCPs) are also synthesized by bone cells, representing 5-10% of the organic phase. NCPs interact with collagen fibrils and may function as “glue” enhancing the resistance of bone to fracture. NCPs also facilitate crystal nucleation, crystal growth, shape, and orientation. Among these, the most important are the SIBLING family proteins together with Osteonectin (ON) and Osteocalcin (OC).

Osteonectin (ON), also referred to as secreted protein acidic and rich in cysteine, or SPARC, is the most abundant non-collagenous polypeptide expressed in mineralized tissues. ON is a phosphoprotein which contains a collagen-binding domain and an HA binding region, so the mature forms link the mineral and collagen

phases, contributing to the proper organization of the bone matrix. Osteonectin also inhibits cellular proliferation through arrest of cells in the G1 phase of the cell cycle, and contribute to osteoblast maturation and survival(Burr et al., 2015).

Osteocalcin (OC) or bone Gla protein accounts for up to 20% of non-collagenous proteins in the bone. It is synthesized by mature osteoblasts and then undergo γ -carboxylation of glutamic acids. This process occurs intracellularly and is dependent of vitamin-K. Finally, osteocalcin is secreted and incorporated in the mineral matrix. Some uncarboxylated osteocalcin escapes incorporation into matrix and reaches the bloodstream(Seibel et al., 2006) where it act on pancreatic β cells to enhance insulin secretion and thus influence glucose metabolism(Norris & Carr, 2013). Only around 25% of circulating osteocalcin consists of intact osteocalcin, the remaining immunoreactivity comprised N-terminal, mid-region, mid-region-C-terminal and C-terminal fragments, that are released as a consequence of bone resorption. Plasma concentrations of these fragments are used as a marker for bone resorption(Cundy et al., 2014).

Fibronectin, a minor constituent of bone matrix, is one of the first proteins produced by osteoblasts, and directs the initial deposition of collagen fibrils Continued presence of fibronectin is also required to maintain the integrity of the collagenous matrix.

The small integrin-binding ligand N-linked glycoprotein (SIBLING) family is a group extracellular proteins present in mineralized tissues. This family is characterized by the presence of a RGD (Arg-Gly-Asp) domain important for integrin interaction and a "Acidic Serine-Aspartate Rich MEPE associated (ASARM) motif which is involved in the inhibition of the mineralization. The most important members are: of osteopontin (OPN), bone sialoprotein (BSP or IBSP)), dentin matrix protein 1 (DMP1), dentin sialophosphoprotein (DSPP) and matrix extracellular phosphoglycoprotein (MEPE).

- **Osteopontin (OPN)**, also known as secreted phosphoprotein 1 (SPP1) is a ubiquitous protein expressed by osteocytes, osteoblasts and osteoclasts. OPN has been identified as the bridge between the cells and HA crystals, mediating the bone attachment to the extracellular matrix (Sodek et al., 2000). Its phosphorylated forms binds HA and inhibit bone mineralization (W. Addison et al., 2009).

- **Bone sialoprotein (BSP)**, also called Integrin-binding sialoprotein (IBSP) is expressed by osteoblasts, osteoclasts, osteocytes and chondrocytes. BSP is involved in the nucleation process of HA crystal (Harris et al., 2000).

BSP also mediates osteoblast and osteoclast attachment to the extracellular matrix via integrin receptors (Bernards et al., 2008).

- **Dentix Matrix Protein 1 (DMP1)** is mainly expressed by osteocytes and mature osteoblasts, and hence it can be used as a marker for osteocyte differentiation. When phosphorylated, full-length DMP1 has been shown to inhibit the formation and growth of HA; however, its dephosphorylated form and its two fragments act as nucleators of HA formation (He et al., 2003; Staines et al., 2012)

- **Dentin sialophosphoprotein (DSPP)** is a ubiquitous protein. DSPP is proteolytically processed to two fragments: dentin phosphoprotein and dentin sialoprotein (DSP), both of which have important functions for mineralization (Boskey, Maresca, Doty, Sabsay, & Veis, 1990).

- **MEPE**, is primarily expressed by osteocytes and hence used as a marker for osteocyte differentiation (Nampei et al., 2004). The activity of MEPE is dependent on its state of cleavage and its phosphorylation. The phosphorylated form of MEPE inhibits bone mineralization in three different ways: (1) decreasing the expression of the type II sodium-dependent Pi cotransporter NPT2a, and hence decrease Pi uptake in the kidney (Marks et al., 2008); (2) enhancing Pi secretion by promoting FGF23 expression (Martin et al., 2011); and (3) binding to HA crystals (W. N. Addison et al., 2008). However, truncated forms of MEPE enhance osteogenesis by promoting osteoprogenitor adhesion (Sprowson et al., 2008).

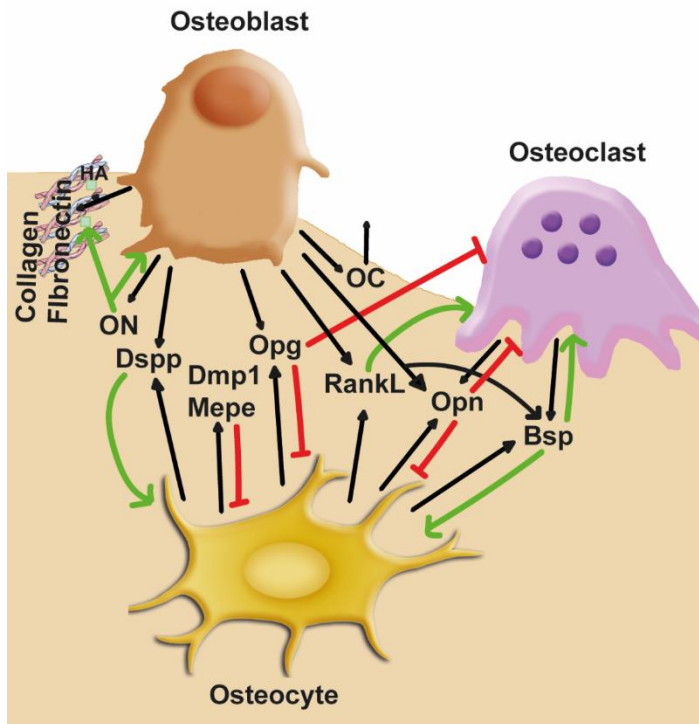


Figure 4. A schematic figure detailing the expression and function of the principal non-collagenous proteins present in bone matrix (BM). Osteonectin (ON) expressed by osteoblast link the mineral and collagen phases of BM. Osteocalcin (OC) is secreted by osteoblast and incorporated to the BM. Fibronectin released by osteoblast is associated to collagen and directs the direction of collagen fibrils. Figure X also represents the family of SIBLING proteins. OPN expressed by osteocytes, osteoblast and osteoclasts mediates the bone attachment to the extracellular matrix but when phosphorylated inhibit bone mineralization. BSP, expressed by osteoblasts, osteocytes and osteoclasts, has a pivotal role. On one side acts as a HA nucleator in bone mineralization and on the other increases osteoclastogenesis. DMP1 and MEPE are both produced by osteocytes and inhibit bone mineralization. DSSP is produced by osteoblast and osteocytes and promotes biomineralization.

4. Bone mineralization

During development, bone usually replaces solid and avascular mesenchymal tissue, mainly mineralized cartilage or fibrocartilage. This process takes place thanks to the coordinated work of the different cell types in bone. The extracellular matrix of bone is separated from general extracellular fluid by a tight epithelial layer of osteoblasts, which are also responsible for the secretion of bone organic matrix. As bone continues growing, some osteoblasts are incorporated into the matrix as living cells, and continue the differentiation process, becoming osteocytes. In parallel, mesenchymal stem cells are committed to precursor osteoblasts and recruited to

the bone surface in order to maintain an actively forming layer. At the apical surface, osteoblasts secrete proteins involved in the synthesis of the extracellular matrix including type I collagen and other matrix organizing proteins such as fibronectin, osteocalcin and osteopontin. The organic matrix secreted is called osteoid and serves as a template for inorganic matrix formation. Moreover, alkaline phosphatase is also bound to the apical surface of osteoblast and works to supply the phosphate needed for bone mineralization (Blair et al., 2017)

Bone mineralization occurs in two phases. In the primary mineralization, the calcium and phosphate ions are firstly incorporated into the collagen matrix. This process occurs rapidly, over 2–3 weeks, and accounts for roughly 70% of the final mineral content. In the secondary mineralization, mineral crystals mature. This process takes much longer, up to a year or more.

In the process of mineralization, calcium phosphate, along with large amounts of calcium carbonate, are deposited in empty zones between the ends of collagen fibrils. As bone matures, hydroxyapatite crystals reduce their level of impurities and enlarge by crystal growth and aggregation. As the extracellular fluid does not contain enough concentration of ions to allow its spontaneous precipitation, osteoblasts synthesize extracellular matrix vesicles that serve as protected microenvironments in which calcium and phosphate concentrations can increase sufficiently. Matrix extracellular vesicles also contain a nucleational core composed of proteins and a complex of acidic phospholipids, calcium, and inorganic phosphate in a sufficient concentration to precipitate. Macromolecules also bind to growing crystal surfaces to determine the size, shape, and number of crystals formed. As bone matures, the carbonate content is reduced and mineral crystals grow laterally, becoming more plate-like, and orient themselves given place to a mature bone with its characteristic structure.

CHAPTER II: THE AMAZING OSTEOCYTE

1. The importance of osteocytes

Of the major cell types in bone, osteocytes make up over 90% to 95% of total bone cells in the adult skeleton. No longer considered passive placeholders in bone, osteocytes have recently emerged as major orchestrators of bone remodeling, physical mechanosensors, hematopoietic niche cells, and endocrine regulators of whole-body metabolism.

Despite its importance for whole body homeostasis, little is known about osteocyte biology. For this reason, in this thesis we will try to understand the main mechanisms governing osteocyte differentiation and physiology. The contribution of osteocyte to each of these functions will be detailed in the next sections.

1.1. Regulation of bone mineralization.

Osteocytes contribute to the development and maintenance of the extracellular matrix by regulating bone mineralization at local and systemic levels. Osteocytes express DMP1, MEPE and PHEX, proteins that are involved in the mineralization process (Schaffler & Kennedy, 2012). DMP1 is a highly phosphorylated protein expressed in the canaliculi of osteocytes during the initial steps of mineralization. More exactly, Dmp1 is found in the gap region between collagen type 1 fibrils, where it might regulate hydroxyapatite formation through its phosphate groups (He et al., 2003). MEPE, as DMP1, belongs to SIBLING family and contains a highly phosphorylated region, which in this case acts as a potent inhibitor of mineralization. MEPE acts directly on osteoblasts and inhibit their bone formation activity (Gowen et al., 2003). By its part, PHEX is a type 1 cell-surface zinc metalloprotease present in the plasma membrane of osteoblasts and osteocytes. PHEX interact with DMP1 and contributes to enhance bone mineralization. In parallel, PHEX binds to MEPE and prevent the release of the protease-resistant MEPE-ASARM peptide, an inhibitor of mineralization (Rowe et al., 2005). PHEX also regulates the expression of FGF23, a phosphaturic factor predominantly expressed by osteocytes (S. Liu et al., 2003). Once synthesized, FGF23 is released and travels through the blood stream to the kidney, where it inhibits 1α -hydroxylase activity and

NPT2, a sodium-phosphate cotransporter present in the proximal tubule. Suppression of 1-alpha-hydroxylase activity reduces its ability to activate vitamin D and subsequently impairs calcium absorption while inhibition of NPT2 decreases the reabsorption and increases excretion of phosphate. Both activities reduce the amount of phosphate available for bone mineralization.

Osteocytes might also have a key role in the organization of bone mineral deposition. As late osteoblasts differentiate into osteocytes, they lay down small mineralized spherical structures within the type I collagen fibers surrounding them. These mineralized structures are initially associated with the dendritic processes of the developing osteocytes. Eventually increase in size, coalesce and surround the mineralizing cells (Barragan-Adjemian et al., 2006). This hypothesis evidences that the process of osteocyte differentiation and bone mineralization are linked.

1.2. Regulation of bone remodeling by osteocytes

Bone remodeling is a process where mature bone is degraded, and new bone is formed to repair microdamage and respond to the body demands of calcium and phosphate. Osteocytes detect and respond to mechanical and hormonal stimuli to coordinate the function of osteoblasts and osteoclasts through the release of several proteins. It is of special interest the molecular triad of osteoprotegerin (OPG), the receptor activator of nuclear factor-kappaB (RANK) and the receptor activator of nuclear factor-kappaB ligand (RANKL) which functions as a pivotal molecular link. RANKL, a member of the tumour necrosis factor (TNF) cytokine family, binds RANK receptor at the surface of precursors of osteoclasts and activate them, mediating osteoclastogenesis. By its part, osteoprotegerin (OPG), acts as a decoy receptor for RANKL, preventing it from binding to and activating RANK on the osteoclast surface. Thus, the biological effects of OPG on bone cells include the inhibition of terminal stages of osteoclast differentiation, suppression of the activation of mature osteoclasts and induction of apoptosis (Theoleyre et al., 2004). In consequence, the ratio between RANKL/OPG is used as a marker for bone resorption and is mainly controlled by osteocytes. Osteocytes can communicate with osteoclasts through other secreted factors such as macrophage colony stimulating factor (M-CSF) (Boyce & Xing, 2007), and vascular endothelial growth factor (VEGF) (Sipola et al., 2006). In addition alternative biochemical signals, such as NO, PGE₂, and ATP travel through the lacunocanalicular system and stimulate osteoblast differentiation (Heino et al., 2004; Nagata et al., 1994; Vezeridis et al., 2006).

Not only healthy osteocytes, but also apoptotic osteocytes play a key role in bone remodeling associated to microdamage. Microdamage causes a spatial

gradient of apoptotic osteocytes around the site that diminishes with distance (Verborgt et al., 2002). Those apoptotic osteocytes enhance osteoclastogenesis in a direct and indirect way. On one hand, apoptotic osteocytes increase the secretion of RANKL, and, on the other, they communicate with healthy osteocytes and induce them to secrete M-CSF and VEGF (Al-Dujaili et al., 2011). At the same time, osteocytes induce new bone formation at sites of fracture damage by recruiting mesenchymal stem cells via the secretion of osteopontin (Raheja et al., 2008).

Osteocytes also impact on osteoblast function by regulating the levels of sclerostin (SOST), an antagonist of Wnts that acts as an inhibitor of bone formation. Mechanical stimulation and elevation of parathyroid hormone (PTH) are anabolic signals that downregulate sclerostin expression in osteocytes to induce bone formation. In fact, cortical bone areas exposed to high mechanical strain exhibit a reduction in sclerostin associated with higher bone formation while sclerostin expression is high in unloaded bones.

Taken together, these findings suggest that osteocytes secrete several proteins and small molecules that coordinate osteoclast bone resorption and osteoblast bone formation to face up to the necessities of calcium and phosphate and maintain bone mass and structure (Teresita Bellido, 2014; Robling et al., 2008).

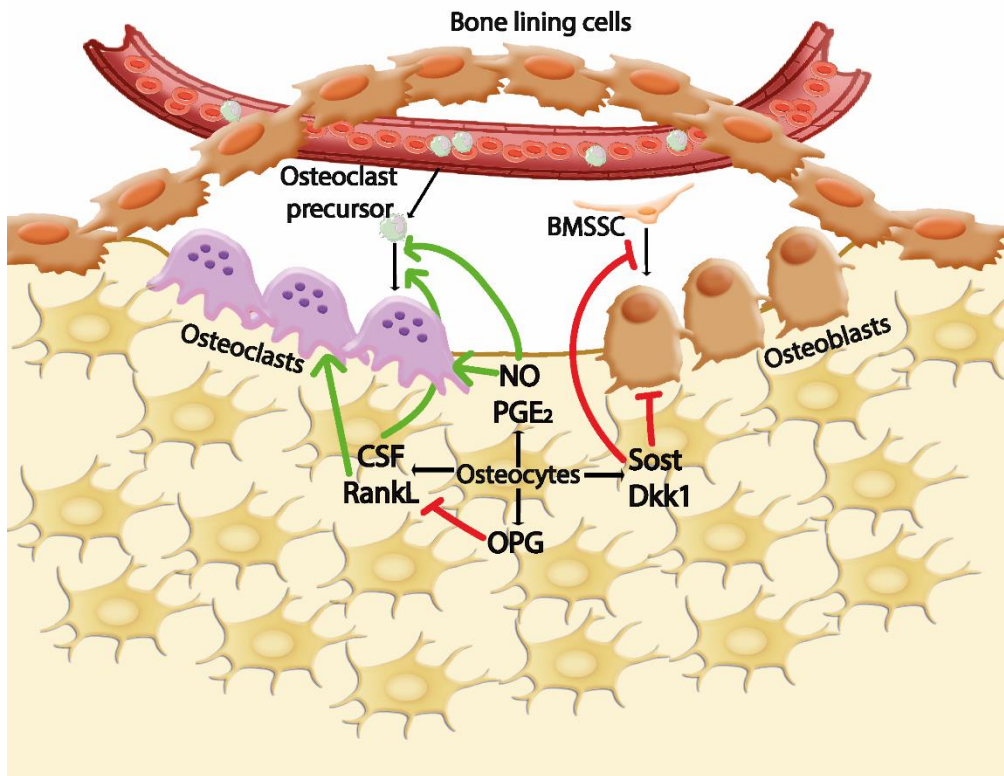


Figure 5. Schematic Basic Multicellular Unit (BMU) activated to execute the bone remodeling cycle. Green arrows represent activation, while red lines represent inhibition.

1.3. Bone damage repair in aged bones

In aged bone, the mineralized phase is increased in detriment of the organic phase. Cortical of long bones becomes thinner and more porous, and trabeculas are reduced in size and number. Thus, aged bones become more fragile and are more likely to break (Almeida & O'Brien, 2013). These changes are linked to a decrease in the number of osteoblasts and osteoclasts and hence in a reduction of bone remodeling. At this point osteocytes are interesting cells since they participate in the repair of the micro-damage or micro-cracks in aged bones, leading to the renovation of the aged bone, and maintaining bone integrity. Moreover, osteocytes regulate osteoblast and osteoclast differentiation and activity. In fact, suppression of autophagy in osteocytes results in a low rate of bone remodeling and mimic the impact of aging on the (Jilka & O'Brien, 2016; Onal et al., 2013).

With age, osteocyte autophagy is decreased while osteocyte apoptosis increases therefore, this is thought to be a key mechanism to initiate aging in bone.

When a micro-crack is produced, bone fluid is altered, reducing oxygen levels. Osteocytes detect them, and suffer apoptosis. Then, the neighboring viable osteocytes release signals to recruit osteoclasts to remove the damaged bone, including TNF- α , IL-6, IL-11 (Dallas et al., 2013; Murshid, 2017). Healthy osteocytes release also VEGF, a vascular growth factor crucial in the neo-angiogenesis, which is the first step in the arrival of osteoclasts to the damaged zone, and so the remodeling process is initiated (Jilka et al., 2013).

1.4. Mechanosensing

Thanks to its location in bone and their complex dendritic network the osteocytes are constantly exposed to the canalicular fluid that flows through the lacunocanalicular systems. When a bone is mechanically loaded, there are several stimuli that could be detected by bone cells. These include the physical deformation of the bone matrix itself, the load-induced flow of canalicular fluid through the lacunocanalicular network, or electrical streaming potentials that are generated when the ions of the canalicular fluid pass the charged surfaces of the lacunocanalicular walls and/or cell membrane. Although little is known, it has been proposed that there is a baseline flow of canalicular fluid driven by the extravascular pressure, which is altered as a result of intermittent mechanical loading (Weinbaum et al., 1994). Bone cells, and specially osteocytes, are exposed to fluid flow shear stress that is sensed through their cell body, the glycocalyxes on the surfaces of their dendrites, or the bending of cilia.

One of the earliest events that occurs in response to mechanical stimulation is the increase in intracellular calcium. During the differentiation from osteoblasts to osteocytes there is a switch in the expression of voltage-operated calcium channels from low voltage activated calcium channels (L-type channel) to high voltage activated calcium channels. This changes make osteocytes more responsible to fluid stress than osteoblast. (X. L. Lu et al., 2012). Soon after this rapid change in calcium signaling NO, ATP, and prostaglandin are released to induce an anabolic response. Shear stress stimulates the activity of endothelial form of NOS (eNOS) present in osteocytes, and hence the release of NO. In bone, NO inhibits resorption and promotes bone formation (Zaman et al., 1999). Shear stress in osteocyte also increases the secretion of ATP in response to extracellular calcium or mechanical stimulation (Bonewald, 2011; Genetos et al., 2005). Increase in ATP levels is needed for the activation of P2X7 nucleotide receptor, an ATP-gated ion channel involved in the release of prostaglandin in response to mechanical load. Prostaglandins are one of the key effectors of load-related osteogenic responses. In osteocytes, fluid flow-

induced shear stress stimulates the rapid release of PGE₂ through hemichannels associated with integrins. Glycocalyxes of the osteocyte dendrites are necessary for integrin attachment to hemichannels in this process (Cherian et al., 2005). The release of PGE₂ signals in an autocrine/paracrine manner to the osteocytes to enhance gap junction function and increase the expression of connexin 43 (Cx43).

As in bone remodeling, osteocytes stimulated by mechanical loading regulate the function of other cell types in a paracrine manner. Osteocytes under mechanical loading reduces the release of negative regulators of the Wnt/ β -catenin pathway such as SOST and DKK1 (Robling et al., 2008) to enhance osteoblast differentiation, proliferation, and matrix production (Dallas et al., 2013). On the other hand, unloading increases RANKL expression in osteocytes, which may be responsible for the bone loss associated with unloading (Xiong et al., 2011). Other genes known to be regulated by loading and by unloading include E11, a marker for the early osteocyte, PHEX, MEPE, and DMP1 (Gluhak-Heinrich et al., 2003; W. Yang et al., 2005; K. Zhang et al., 2006).

1.5. Regulation of calcium levels in plasma

Osteocytes are able to remove their perilacunar matrix in a process called “osteocyte osteolysis”, releasing calcium to the bloodstream. This process is induced by Parathyroid hormone (PTH) and PTH related peptide (PTHrP) (T. Bellido et al., 2005) through the activation of PTH receptor 1 (PTHR1) (Tsourdi et al., 2018). When PTH binds PTHR1 in osteocytes, activates G α protein initiating a signaling pathway that end up with the upregulation of *RankL* and *Sost* expression. RANKL and SOST acts in a paracrine manner enhancing osteoclastogenesis and reducing osteoblast differentiation and synthesis of bone matrix, respectively (Wein, 2018). The consequence is a local demineralization and proteolysis of the lacunar and pericanalicular matrix (Tsourdi et al., 2018).

The osteolytic activity is enhanced under calcium-demanding conditions, for example during lactation. (Kovacs, 2016). In these exceptional circumstance, osteocytes express markers of osteoclasts, such as tartrate-resistant acid phosphatase (TRAP), cathepsin K, carbonic anhydrase 2 and ATP6V0D2, a vacuolar ATPase associated with osteoclastic bone resorption (Kogawa et al., 2013; Wein, 2018) (Kogawa et al., 2013). Indeed, in lactating calcium-deficient conditions, osteocytes stimulated by PTH/PTHrP reduce perilacunar pH to liberate rapidly readily accessible pools of calcium. The relative contribution of this pathway versus osteoclastic bone resorption is still unclear and more studies are required to define osteocytic perilacunar remodeling.

1.6. Endocrine regulation

At first glance, osteocytes may appear to be isolated inside the mineralized matrix, however, thanks to lacunocanalicular system osteocytes are connected with other osteocytes, osteoblasts and the vasculature. The lacunocanalicular system is filled with proteoglycans located in the glycocalyx of the osteocytes that act as sieves allowing the rapid passage of smaller molecular mass molecules (<70 kDa) and slowing down passage of larger molecules. Inside the lacunocanalicular system circulates the canalicular fluid, that carries solutes to and from the osteocyte. The connectivity between the canalicular fluid and vasculature allows osteocytes to be exposed to circulating hormones from distant tissues, but it would also provide a conduit for hormones and other molecular mediators secreted by osteocytes into the circulation to exert effects on distant target organs (Fritton & Weinbaum, 2009). Therefore, the osteocytic network represents an endocrine tissue that plays a vital role in the regulation of phosphate and glucose homeostasis.

FGF23 has emerged as one of the most important osteocyte-secreted endocrine factors. FGF23 is a 32-kDa protein member of the FGF family. FGF-23 is produced by the osteocyte when serum phosphate levels are increased to protect the organism against the deleterious effects of an excess of circulating phosphate (alterations in the skeletal mineralization, chronic kidney disease, formation of extra-skeletal calcifications, including vascular calcifications, ventricular hypertrophy among others) (Faul et al., 2011; Tresguerres et al., 2020). In the presence of Klotho, FGF23 binds to FGF receptors (FGFRs) (Dallas et al., 2013). One of the major targets of FGF23 is the kidney, where it decreases expression of the sodium/phosphate cotransporters NaPi-IIa and NaPi-IIc. This leads to increased urinary excretion of phosphate (Gattineni et al., 2009). Additionally, high FGF23 levels are known to down-regulate the expression of 1- α hydroxylase, which is required for the conversion of 25-hydroxyvitamin D to the active vitamin D metabolite, 1,25-dihydroxyvitamin D [1,25(OH)₂D] (Shimada et al., 2004). This reduction in 1,25(OH)₂D levels results in decreased expression of NaPi-IIb in the intestine, therefore reducing phosphate absorption (Miyamoto et al., 2005).

The signaling between the osteocyte and the kidney is bidirectional because 1,25(OH)₂D induces expression of FGF23 by the osteocyte suggesting a negative feedback loop (S. Liu et al., 2006). In addition to 1,25(OH)₂D, several other factors have been shown to modulate serum FGF23 levels such as intake of dietary phosphorous (Perwad et al., 2005), PTH levels (Lavi-Moshayoff et al., 2010), as well as DMP-1, MEPE and PHEX expression. PTH secreted by the parathyroid gland

increases FGF23 expression *in vivo*. Interestingly, FGF23 is also able to act reciprocally on the parathyroid gland to decrease PTH secretion. Furthermore, sclerostin regulates the synthesis of FGF23 (Ryan et al., 2013) in a paracrine way since it modulate DMP-1, PHEX, MEPE and FGF23 expression.

Osteocytes, together with osteoblasts, participate in whole-body energy metabolism and body composition. It is known that undercarboxylated osteocalcin (ucOCN) is a potent regulator of insulin secretion and insulin sensitivity. However, decreased ucOCN does not explain reduced body fat in mice with induced-osteoblast deficiency, indicating the presence of additional mechanisms in which osteocytes play a key role (Yoshikawa et al., 2011). Recent research indicates that osteocytes influence body adiposity without altering serum insulin or glucose levels and through a ucOCN-independent mechanism that involves regulation of serum Sclerostin levels. Sclerostin interacts with the negatively charged β -propeller domains of the low-density lipoprotein-related receptor 5 (Lrp5) and Lrp6 Wnt coreceptors (Veverka et al., 2009), and thereby prevents the propagation of Wnt signals leading to the stabilization of the downstream transcription factor β -catenin. Outside of the skeleton, sclerostin is present in serum (Arasu et al., 2012; Ardawi et al., 2012), and circulating levels, are influenced by sex hormones and PTH levels (Drake et al., 2010; U. Il Mödder et al., 2011; U. I. Mödder et al., 2011). Increased levels of Sclerostin has been also associated to type 2 diabetics (García-Martín et al., 2012) and with increased body mass index and fat mass (Urano et al., 2012). Recent cross-sectional analysis reported that serum sclerostin levels exhibit a positive correlation with fasting glucose production and indices of hepatic and adipose insulin resistance as well as a negative correlation with whole-body glucose disposal and insulin clearance rate (Daniele et al., 2015). Sclerostin favors adipogenesis and adipose hypertrophy via the suppression of Wnt signaling in adipocytes, which are particularly sensitive to Wnt signaling. Wnt ligands are produced by preadipocytes, and their expression levels or downstream signaling must be suppressed to initiate adipogenesis (Bennett et al., 2002). Suppression of Wnt signaling by sclerostin in adipose tissue leads to an overall increase in fat mass and adipocyte size (S. P. Kim et al., 2017). Moreover, sclerostin represses long-chain fatty acid oxidation and enhances fatty acid synthesis, altering adipocyte metabolism (S. P. Kim et al., 2017). Controversially, in white adipose tissue, sclerostin increase the expression of UCP1 and hence induce beige adipogenesis, which contribute negatively to obesity (Fulzele et al., 2017). Further studies are needed to understand the contribution of the Wnt signaling inhibitor sclerostin on white, brown, or beige fat development and its relevance for lipid metabolism.

2. Osteocytogenesis

At the end of the bone formation phase, osteoblasts can either become quiescent and remain as inactive osteoblasts or bone lining cells, undergo apoptosis or become embedded in bone as osteocytes. The proportion of osteoblasts that follow each of these fates may be dependent on the animal species, the age and type of bone and hormonal or disease status, but it has been described that only, about 5–20% will continue the differentiation process. During osteocytogenesis, mature osteoblasts are gradually embedded within the surrounding extracellular matrix, and then transformed to preosteocytes or osteoid osteocytes. Later, when the osteoid becomes mineralized, the preosteocytes mature into osteocytes. This osteoblast-to-osteocyte transition is often referred to as osteocytogenesis (X. Chen et al., 2018; Dallas & Bonewald, 2010). A few years ago this was considered a passive process but at present is regarded as an active process, driven by substantial changes in gene expression, morphology and metabolism (Dallas et al., 2013).

In this process, osteoblasts undergo striking morphological changes from a cuboidal to stellate shape with multiple neuron-like cytoplasmic dendrites that interconnect with the dendrites from neighboring osteocytes and cells on the bone surface (Palumbo et al., 1990). As the cell body of mature osteocytes resides in small lacunar spaces within mineralized osteoid, the cytoplasm diminishes considerably during differentiation, (Holtrop, 1975). Osteocytes are well interconnected with neighbors through an extensive network of the long, slender cytoplasmic processes in the channels (canaliculi) connected by gap junctions (Noble, 2008). Typically, the osteocyte-to-osteocyte distance is maintained within 20–30 μm for effective diffusion of molecules (Sugawara et al., 2005). Formation of dendrites requiring cleavage of collagen and other matrix molecules by specific metalloproteinases (Holmbeck et al., 2005; Robin et al., 2016) as well as regulation of cytoskeletal proteins and molecules involved in cell motility. For instance, localization of actin binding proteins, such as fimbrin, filamin and α -actinin (Kamioka et al., 2004), is modified during osteoblast to osteocyte transition. Osteocytes are also enriched in a number of proteins important in cytoskeletal function, including CapG, destrin, cdc42 and E11/gp38 (Billiard et al., 2003; Guo et al., 2010a; Paic et al., 2009). CapG and Capzb are members of the gelsolin family that are important in regulating actin filament length by capping their barbed positive ends (Cooper & Sept, 2008). Destrin is a member of the actin depolymerizing factor/cofilin family that regulates assembly and disassembly of actin filaments (Sarmiere & Bamburg, 2004). These proteins regulate actin polymerization and depolymerization dynamics, which are critical for cell motility, membrane ruffling and extension of cell processes. E11, also called

podoplanin, highly expressed in osteocytes that are embedding or have recently embedded and regulates actin cytoskeleton dynamics (Keqin Zhang et al., 2006).

Concurrently with the changes in morphology, cells downregulate key molecular markers specific to osteoblasts, such as Col1a1, alkaline phosphatase (ALP), and osteocalcin (OCN). Meanwhile, they start to express some osteocyte-specific markers, including connexin43 (CX43), podoplanin (also called as E11/gp38), dentin matrix protein 1 (DMP1), phosphate-regulating neutral endopeptidase on chromosome X (PHEX), matrix extracellular phosphoglycoprotein (MEPE), fibroblast growth factor 23 (FGF23), and sclerostin (SOST). (X. Chen et al., 2018) CX43 is associated with gap junction for maintenance of the intercellular communication and response (Civitelli, 2008); DMP1, PHEX, and MEPE are considered as the major regulators of mineralization (Rowe, 2012); FGF23 is responsible for phosphate absorption (Yoshiko et al., 2007). SOST is thought to be uniquely expressed in mature osteocytes as a negative regulator of osteoblast differentiation (Poole et al., 2005). Previous studies demonstrated that genetic ablation of these markers in the knockout animal models would result in defective osteocyte differentiation and abnormalities in bone morphogenesis.

Due to their location embedded within bone, oxygen supply osteocytes is limited, therefore, osteocytes increase the expression of proteins associated with resistance to hypoxia (Guo et al., 2010b). It is believed that oxygen tension may regulate the osteocytogenesis process (Hirao et al., 2007) and hypoxia may also play a role in disuse-mediated bone resorption. As oxygen, nutrient supply might be also compromised and act as a signal governing osteocyte differentiation. In this thesis we will analyze the role of glucose in osteocytogenesis and the associated molecular mechanisms that drive osteocyte differentiation upon glucose restriction.

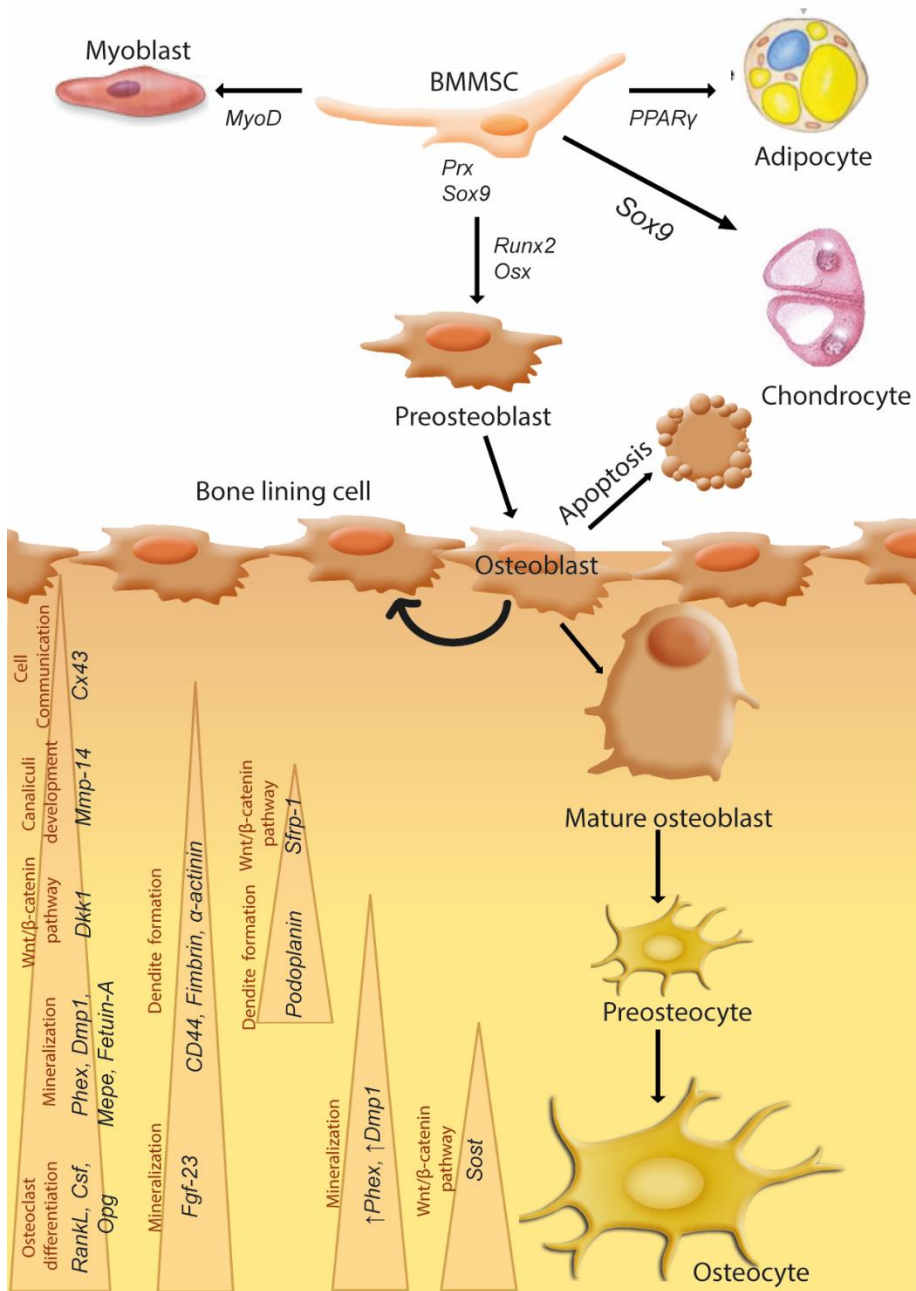


Figure 6. Osteocytogenesis. Representation of the osteocyte differentiation process and the main differentiation markers of each step.

CHAPTER III:

BONE METABOLISM

1. Nutrient supply in bone

Healthy bone requires a substantial blood flow to supply oxygen and nutrients, and to eliminate carbon dioxide and other metabolic waste products. It is estimated that about 5.5% to 11% of the cardiac output is received by the skeleton to fulfill the requirements of the bone cells (osteoblasts, osteocytes and osteoclasts), the marrow (hematopoietic lineage cells, stromal cells and adipocytes), and endothelial cells (Marenzana & Arnett, 2013). Blood does not diffuse directly through the mineralized matrix of the bone, so nourish the cells within calcified tissues represent a special problem. Therefore, bone cells must be within 250 μm of their blood supply. This is one reason that explains why the average diameter of a trabecula is about 200 μm and for what human bone is structured in osteons disposed around a blood vessel. This arrangement of cells provides a geometrically efficient system for supplying the maximum amount of bone tissue with the minimum number of vessels (Mishra & Knothe Tate, 2003). Those vessels are formed by an angiogenesis that occurs in association with osteogenesis. The coordination between both processes is driven by common signal molecules, and factors secreted by osteoblast such as VEGF, Notch and Noggin (Grosso et al., 2017).

In long bones, the nutrient artery, together with one or two veins, enters the bone through the nutrient foramen. Once inside the marrow cavity, the artery ramifies into ascending and descending branches that run longitudinally within the medullary cavity. Each one of these branches divides into cortical branches that pass through endosteal canals and feed the Haversian system with arterial blood. Finally, the vessels drain to venules on the periosteal surface of the bone. This organization allows a relative high intramedullary pressure which contributes to the movement of interstitial fluid in bone. Measurement of blood flow to the skeleton is technically difficult, however, it has been established that the blood flow for cortical bone and periosteum is 5 ml/min·100g and for trabecular bone is 20 ml/min·100g (McCarthy, 2006). Once in the Haversian canal, solutes have to diffuse through a lacunocanalicular system (LCS) to support bone cells, specially osteocytes. These LCS channels are filled with a thin pericellular matrix secreted by the osteocytes that acts as a chromatographic column, regulating fluid/solid transport to and from

osteocytes. In consequence, transport to bone cells will be influenced by the size, shape of the molecule. On the other hand, mechanical loading and vascular pressure also drive interstitial fluid flow within the LCS and augment solute diffusion in bone (L. Wang, 2018).

All this data highlights the complexity of nutrient supply in bone. The diffusion of nutrients to osteocytes will not only depend on bone structure but also on characteristics of the molecule (size, charges) and a complex interplay of different forces that includes mechanical loading. So, it is plausible that as osteocytes differentiate, receiving nutrient supply become challenging, therefore, osteocytes have to adapt their metabolism to this new environment in order to survive.

2. Bioenergetics in osteoblast and osteocyte differentiation

Most studies on the control of cell fate decisions address the contributions of changes in transcriptional programming, epigenetic modifications, and biochemical differentiation cues. However, recent studies have found that other aspects of cell biology also make important contributions to regulating cell fate decisions. These cues include four main aspects of cell biology: metabolism, reactive oxygen species (ROS), intracellular pH (pHi), and cell morphology (Tatapudy et al., 2017)

The metabolic state of a cell is the result of a complex array of inputs, including cell signaling, availability of nutrients and oxygen, energy needs, and biomass demands. These inputs and demands influence the rate of ATP production from glycolysis versus oxidative phosphorylation, as well as the rate of side reactions that produce anabolic intermediates. As cells differentiate, the change in these inputs shifts the metabolic state. In most cases, metabolic changes are propagated by signaling molecules, including AMPK, HIF1 α , AKT, and Myc. AMPK is activated by high [AMP]/[ATP] ratios under low nutrient availability and metabolic stress. Activation of this pathway increases glycolytic energy production, activates FOXO proteins to promote the expression of antioxidants and autophagy genes, and restricts growth by inhibiting mTOR (Ito & Suda, 2014; Mihaylova & Shaw, 2011; Tatapudy et al., 2017). This stress response program is important for maintaining cellular homeostasis in general and in some cases, they can have instructive roles in promoting differentiation.

Moreover, the signaling pathways are influenced by their proximity to nutrients and oxygen. This spatial relationship appears to be particularly important in the skeleton given its complex architecture and heterogeneity of bone cell types. In consequence, to understand the metabolic activity of bone cells we need to

consider anatomy of bone with relation to its vascular supply. Although the human skeleton is highly vascularized, blood flow varies substantially between different skeletal microenvironments. Estimates from studies using microspheres reported the highest flow in the metaphysis and lowest flow in the growth plate (Anetzberges et al., 2004). During the formation of the long bones, chondrocytes of the growth plate differentiate in the absence of blood vessels in a hypoxic environment. In this setting, upregulation of the hypoxia inducible factor 1 α (HIF-1 α) shifts the metabolic program toward glycolysis over oxidative phosphorylation and appears to activate gene programs that promote matrix synthesis in chondrocytes (H. K. W. Kim et al., 2009; Pfander et al., 2003; Tatapudy et al., 2017). In contrast, the appearance of osteoblasts in developing mouse limbs and cranial bone coincides with the invasion of blood vessels near sites of nascent primary ossification (Kronenberg, 2003). Similarly, in the setting of long bone fracture, the formation of the avascular soft callus by chondrocytes requires HIF-1 α and remains devoid of osteoblasts until the invasion of blood vessels (Shen et al., 2009). Microenvironments described in mineralized bone not only contribute to cell fate and differentiation but also influence bone remodeling by compartmentalizing osteoblasts, osteoclasts, and blood vessels. Presumably, this type of arrangement would provide a controlled environment in which the metabolic activity of osteoclasts and osteoblasts would take place in a regulated manner (Hauge et al., 2001)

Glucose is a major nutrient for osteoblasts. Primary calvarial osteoblasts preferentially take up glucose via Glut1, although they also express other glucose transporters, such as Glut3 and Glut4 (J. Wei et al., 2015). In osteoblasts, most of the glucose carbons are secreted as lactate regardless of oxygen conditions (Esen & Long, 2014). The phenomenon of lactate production from glucose under aerobic conditions is similar to the Warburg effect, observed in many cancer cells. In preosteoblast, aerobic glycolysis is stimulated by the stabilization of HIF1 α and increases osteoblast production and bone formation (Regan et al., 2014). However, during mineralization, oxidative phosphorylation increases (Komarova et al., 2000). Thus, aerobic glycolysis is not only a prominent metabolic feature of osteoblasts, but it also is likely to be integral to the osteoblast phenotype.

At first sight, the prominence of aerobic glycolysis could seem counterintuitive to the energy requirement of osteoblasts. However, although mature osteoblasts generally exhibit little proliferation *in vivo*, they are biosynthetically active since they are responsible for the production of large amounts of extracellular matrix proteins. Aerobic glycolysis therefore may be necessary for providing metabolic intermediates to support the synthesis of matrix proteins. For instance, glucose carbons were shown to contribute significantly to amino acids in collagen (FLANAGAN & NICHOLS,

1964). Additionally, aerobic glycolysis in osteoblasts may be coupled with the active secretion of citrate that is structurally important for the formation of apatite nanocrystals in bone (Costello et al., 2012; DIXON & PERKINS, 1952). The high citrate output by osteoblasts could mean an elevated mitochondrial citrate level that suppresses pyruvate entering the TCA cycle. Moreover, active removal of citrate from the mitochondria (cataplerosis) may increase the reliance of osteoblasts on glycolysis for energy production. On the other hand, it is also plausible that aerobic glycolysis in osteoblasts may serve to reduce redox stressors until a mature phenotype is attained (Riddle & Clemens, 2017).

Wnt signaling is a major mechanism for stimulating bone accrual in both mice and humans. Recent work has linked the bone anabolic function of Wnt with increased aerobic glycolysis in osteoblast-lineage cells (Esen et al., 2013). Specifically, Wnt3a, Wnt7b, and Wnt10b, which are known to promote osteoblast differentiation, also stimulate glucose consumption and lactate production. In contrast, Wnt5a does not induce neither osteoblastogenesis nor glycolysis in those cells. Mechanistically, Wnt3a signals mainly through Lrp5 to activate mTORC2 and Akt that, in turn, acutely increase the protein abundance of a number of key glycolytic enzymes such as hexokinase 2, phosphofructokinase 1, 6-phosphofructo-2-kinase/fructose-2,6-bisphosphatase 3, and lactate dehydrogenase (W. C. Lee et al., 2017). Furthermore, the reprogramming of glucose metabolism by Wnt3a lowers nuclear acetyl-coA levels and suppresses histone acetylation, affecting the epigenetics of osteoblast precursors and hence favoring osteoblast over adipocyte differentiation (Karner et al., 2016).

Glucose metabolism in osteoprogenitors is also essential for runt-related transcription factor 2 (*Runx2*) to exert transcriptional control of collagen type I synthesis and osteoblast differentiation. Glut1-dependent glucose uptake promotes RUNX2 nuclear import by inhibiting its phosphorylation by adenosine monophosphate-activated protein kinase (AMPK) and subsequent proteasomal degradation. In fact, when glucose uptake is compromised in osteoblast progenitors, RUNX2 is degraded and collagen synthesis and osteoblast development stalled (J. Wei et al., 2015).

As osteoblasts began to mineralize, ATP levels peaked in association with the accumulation of abundant mitochondria with high-transmembrane potentials and an increase in oxygen consumption rate. In consequence, fully differentiated osteoblasts appear to diversify fuel sources to burn both glucose and fatty acids and to engage oxidative phosphorylation over glycolytic pathways to maintain ATP production (Guntur et al., 2014). However, whether changes in energy production by osteoblasts occur along mitochondrial biogenesis has not been studied directly.

Early histological studies noted that mature osteoblasts maintain a greater number of mitochondria than progenitors or bone lining cells (PRITCHARD, 1952) which raises the possibility that osteoblast maturation is accompanied by mitochondrial biogenesis. But, alternatively, it is possible that the expected increase in ATP demand during osteoblast differentiation could be achieved by altering mitochondrial localization, increasing mitochondrial fusion and membrane potentials to enhance energy production (Komarova et al., 2000).

Despite glucose, fatty acids constitute another source of energy for differentiated osteoblast. However, in this case the relative concentrations and degree of saturation may make fatty acids differ in their functions. Several *in vitro* studies have demonstrated that long-chain saturated fatty acids can inhibit calvarial osteoblast differentiation (Gunaratnam et al., 2013; Yeh et al., 2014) whereas long-chain polyunsaturated fatty acids (n-3) has shown a potential benefit for skeletal health (Lau et al., 2013). Recently, it has been demonstrated that Wnt-LRP5 signaling enhances β -oxidation of fatty acids and is necessary for optimal osteoblast differentiation. Nevertheless, we should consider that the amount of fatty acids in bone cells that is used for ATP production is currently unknown and the direct effect of fatty acids on mitochondrial oxygen consumption and ATP production has also not been addressed to date (W. C. Lee et al., 2017).

Whereas a lot of questions remains unsolved about the role of nutrients in osteoblast differentiation, even more needs to be addressed regarding osteocyte differentiation. It can be envisioned that additional reprogramming of the metabolic machinery occurs during terminal differentiation of osteoblasts into osteocytes, however the molecular mechanisms and its implications remains completely unknown.

3. Control of bone cell metabolism

Metabolic flexibility of bone cells is achieved by signaling molecules and transcription factors, which work in synergy to couple extracellular signals to downstream bioenergetics. The optimization of global fuel metabolism and energy expenditure in mammals depends on both paracrine and endocrine/neuroendocrine networks, including:

- **Leptin:** Leptin, peptide hormone produced by adipocytes, serves as a monitor of overall energy availability. Leptin acts on specific neurons in the hypothalamus to regulate food intake: high serum leptin levels inhibit food intake while lower serum leptin and stimulate feeding. Leptin is also a primary regulator of reproductive function. In the bone, leptin receptors (LEP-R) have been found in osteoblasts progenitors that populate postnatal bone (T. Thomas et al., 1999) but

they are not expressed in the calvaria, long bone, or primary mouse osteoblast cultures (Ghilardi et al., 1996). In osteoblast lineages, leptin increases osteoblast proliferation and induce the expression of markers associated to differentiated osteoblast, including alkaline phosphatase activity, collagen synthesis, and matrix mineralization (Cornish et al., 2002; T. Thomas et al., 1999; H.-T. Wang et al., 2012). However, the role of Leptin *in vivo* is controversial. In contrast to the mitogenic effects observed *in vitro*, *in vivo* studies suggest Leptin suppresses osteoblast proliferation and bone acquisition in young mice (Ducy et al., 2000). In fact, ablation of LEP-R in osteoprogenitors increases bone volume secondary to an increased mineral apposition rate and increased numbers of marrow progenitors. Within the brain, leptin inhibits serotonin production, which in turn increases the sympathetic tone and leads to the activation of β 2-adrenergic receptors expressed by osteoblasts (Ducy et al., 2000).

- **Adiponectin:** Like leptin, adiponectin is produced by adipocytes and appears to influence skeletal metabolism. Adiponectin is a the 28-kDa protein that undergoes oligomerization to form low (trimers), middle (hexamers), and high (12-18mer) molecular weight forms (Pajvani et al., 2003). The distribution of adiponectin among these complexes contributes to the hormone's pleiotropic effects (Pajvani et al., 2004). Although adiponectin acts on several tissues, its primary functions appear to be increasing tissue insulin sensitivity and reducing hepatic glucose production. Adiponectin receptors (AdipoR1 and AdipoR2) are expressed in osteoblasts but not in osteoblast progenitors (Berner et al., 2004). *In vitro* studies suggest that adiponectin acts as a mitogen and stimulates osteoblast proliferation via activation of the AMPK and MAP kinase signaling pathways (Kanazawa et al., 2007; Luo et al., 2005). Adipose-derived adiponectin exhibits age-related effects on osteoblast function. *In vivo* studies suggest that the hormone has age-related effects on skeletal homeostasis. In growing mice (from 6–14 wk of age), adiponectin appears to suppress bone acquisition. As mice age (36 week of age), adiponectin acts within the brain to suppress the actions of leptin and reduce the sympathetic tone, inducing osteoblast proliferation and bone formation (Kajimura et al., 2013).

- **Insulin:** Pancreatic β -cells secrete insulin in response to elevations in blood glucose levels and regulates the metabolism of glucose, lipids, and amino acids. Patients with type 1 diabetes can develop early-onset osteopenia or osteoporosis, have increased risk of fragility fracture, and display defects in bone healing and regeneration after fracture (Janghorbani et al., 2007; Kemink et al., 2000; K. M. Thrailkill, 2000). Patients with type 2 diabetes also exhibit increased fracture risk, but they may have normal or even elevated bone mineral density (BMD) (Bonds et al., 2006; Janghorbani et al., 2007; Nicodemus & Folsom, 2001). The mechanisms by

which alterations in glucose homeostasis affect bone mass and strength are quite complex and can include alterations in matrix deposition, glucotoxicity in bone cells, and the modification of collagen by advanced glycation end products (AGEs) (Kalaitzoglou et al., 2016; Keenan & Maddaloni, 2016; Napoli et al., 2017). Osteoblasts express insulin receptors (IR) and insulin stimulation is mitogenic and enhances osteoblast differentiation *in vitro* (Craig et al., 1989; Levy et al., 1986; Ohya & Amagasa, 1994; D. M. Thomas et al., 2009). Insulin treatment of osteoblast cultures also suggested insulin is necessary to carry out the synthesis of collagen and matrix mineralization through recycling of vitamin C and the transport of phosphate (Kunkler et al., 1991; Qutob et al., 1998). More in details, IR together with IGF1R lead to the activation of phosphatidylinositol 3-kinase and mitogen-activated protein kinase signaling by phosphorylating insulin receptor substrate (IRS) proteins (331), which are important for skeletal homeostasis (Gómez et al., 2016; Ogata et al., 2000)

- **Enterohepatic hormones:** Loss of certain gut-derived hormones that participate in the control of whole-body energy homeostasis are associated with low bone mass. Ghrelin, a growth hormone secreted to increase appetite, stimulates osteoblast proliferation and augments osteoclastogenesis (Delhanty et al., 2014; Van Der Velde et al., 2012). Incretins binds to GIP receptors expressed in osteoblasts and activates cAMP and intracellular calcium signaling, enhancing osteoblastic function (Yamada et al., 2008; Zhong et al., 2003). Fibroblast growth factor 21 (FGF21), a liver-derived modulator of glucose and lipid metabolism regulates bone mass, longitudinal bone growth and bone turnover associated with lactation (X. Wang et al., 2015; S. Wu et al., 2012).

These extrinsic stimuli, as well as other disturbances in nutrient availability, modify key metabolic signaling pathways in bone cell lines contributing to reprogramming the bioenergetics of bone. Osteoblast bioenergetic and differentiation programs are coupled through common signaling molecules. This would provide a flexible mechanism for optimizing energy production and expenditure as osteoblasts transit from the proliferative to mineralization phase of their life cycles:

- **AMPK.** AMPK is a heterotrimeric protein that functions as a molecular sensor to adjust ATP production in response to changes in cellular stress and energy status. Increases in the cellular AMP-to-ATP ratio induce allosteric activation of the kinase domain, which then activates catabolic pathways to generate ATP while inhibits anabolic pathways and other ATP-consuming processes. AMPK is expressed in osteoblasts, and its activity is higher in undifferentiated cultures and decreases as osteoblasts differentiate *in vitro* (Joungmok Kim et al., 2016; Shah et al., 2010).

Studies also performed *in vitro* shows that transient activation of AMPK pathway with AICAR and metformin increases cell proliferation, type I collagen production, alkaline phosphatase activity, and mineral deposition (Cortizo et al., 2006; W. G. Jang, Kim, Lee, et al., 2011; Kanazawa et al., 2007; Shah et al., 2010). However, the constitutively active form of AMPK α inhibits matrix mineralization (Kasai et al., 2009). Such discrepancies seem to indicate that osteoblast differentiation only precise a transient activation of AMPK during specific stages. In fact, the ability of primary mouse osteoblasts to differentiate normally *in vitro* depended on an early rise in AMPK activity and a decline at later times (Riddle & Clemens, 2017). The early induction of AMPK is mechanistically linked to autophagy, suggesting that early catabolic changes are important for determining the energy source for osteoblast respiration, and downregulation of these components may be required for induction of glycolysis, which is essential for the final anabolic stages of differentiation (Xi et al., 2016).

- **mTOR/TSC2:** mTOR represents an intracellular hub that integrates intracellular and extracellular signals that affect cell growth, energy metabolism, and autophagy (Laplanche & Sabatini, 2012). mTOR associates with distinct regulatory adaptors to form two related complexes. Raptor associates with the TORC1 complex to control protein synthesis, ribosome biogenesis, and nutrient transport (Hara et al., 2002), whereas Rictor is a component of the TORC2 complex that regulates cell survival, metabolism, and cytoskeletal organization (Dos et al., 2004). In *Osx*-expressing cells, mTORC1-generated signals are required for osteoblast differentiation (J. Chen & Long, 2015) while mTORC2 seems to be important for mesenchymal cells (J. Chen et al., 2015). Moreover, recent work by Riddle et al. suggests that the osteoblast differentiation program is linked to whole body metabolism through mTOR signaling (Riddle et al., 2014).

- **Wnt/ β -catenin:** Wnt/ β -catenin is an anabolic pathway that is activated at different stages of the osteoblast life cycle to promote differentiation (Maupin et al., 2013). The anabolic effects of Wnt signaling are dependent on signaling via mTORC1 and include the activation of known regulators of cellular metabolism. Additionally, Wnt signaling regulates osteoblast differentiation by affecting epigenetic mechanisms that are linked to glucose metabolism and the levels of nuclear acyl-CoA (Karner et al., 2016).

- **GSK-3:** Osteoblasts express two different isoforms of glycogen synthase kinase-3 (GSK-3) GSK-3 α and GSK-3 β . GSK-3 inhibits IR and Wnt- β catenin activity, therefore is associated with reduced osteoblast differentiation and function (Kugimiya et al., 2007).

- **HIFs:** The hypoxia-inducible transcription factors (HIFs) mediate the cellular response to hypoxia by activating genes controlling bioenergetics, oxygen supply, and consumption (Prabhakar & Semenza, 2012). Under hypoxia, HIFs promote angiogenesis and serves as a molecular switch diverting energy production from oxidative to glycolytic metabolism (Papandreou et al., 2006). In bone, HIFs coordinate the angiogenesis and osteogenic processes and regulate glucose metabolism (Riddle et al., 2009). In human MSCs, HIF-1 α is stabilized even under normoxic conditions, and activates aerobic glycolysis and the expression of glycolytic genes (Regan et al., 2014). In these cells, osteogenic differentiation reversed the normoxic HIF-1 α stabilization and glycolytic metabolism and activated mitochondrial biogenesis (M. et al., 2012) .

- **FoxOs:** The FoxOs are a subclass of the a conserved forkhead transcription factor family, which regulate the activity of genes controlling cellular proliferation, stress tolerance, and life span (Accili & Arden, 2004) in response to insulin, IGFs, nutrients, and many other external stimuli. In osteoblasts, the four transcription factors are highly expressed and modulate redox balance, protein synthesis, and osteoblast differentiation through the activation of specific gene programs, including β -catenin, ATF4, and RUNX2 (Ambrogini et al., 2010; Iyer et al., 2013; Rached et al., 2010).

The link between metabolism and differentiation of osteoblasts have been widely studied and a number of molecular pathways involved have been identified. However, little is known about the contribution of these signaling pathways to the osteoblast-osteocyte transition and deeper understanding is needed.

CHAPTER IV: GENETIC REGULATION OF OSTEOCYTOGENESIS

1. Mechanisms for gene expression control

Genetic regulation is a multistep process that involves chromatin and several chromatin-interacting protein complexes including transcription factors, co-activators and co-repressors.

Chromatin is a complex, plastic, and multifaceted cluster of proteins, DNA, and RNA that regulate gene expression. It is built in a hierarchical manner starting with DNA forming single base-pairs up to whole genomes. Genomes are organized into distinct domains, called Topologically Associating Domains. TADs are regions of the chromatin that exhibit higher preference for internal interactions compared to interactions with adjacent domains (Jerković et al., 2020). TADs have been shown to be important for gene regulation by restricting the interaction of cell-type specific enhancers with their target genes (Krefting et al., 2018). Therefore, TADs act as genomic units of gene regulation.

histones act as "bouncers" and histone modifications determine whether transcription factors gain access to a particular site of the DNA. These modifications include methylation of arginine (R) residues; methylation, acetylation, ubiquitination, ADP-ribosylation, and sumolation of lysines (K); and phosphorylation of serines and threonines. In general, acetylation of histones loosens bindings and promotes transcription. Most modifications are distributed in localized patterns within the upstream region, the core promoter, the 5' end of the open reading frame (ORF) and the 3' end of the ORF (Li et al., 2007). Indeed, the location is crucial for its effect on transcription and modifications in this pattern of location can alter its function. The principal histone modifications and its location are summarized in figure X (Landry et al., 2003)

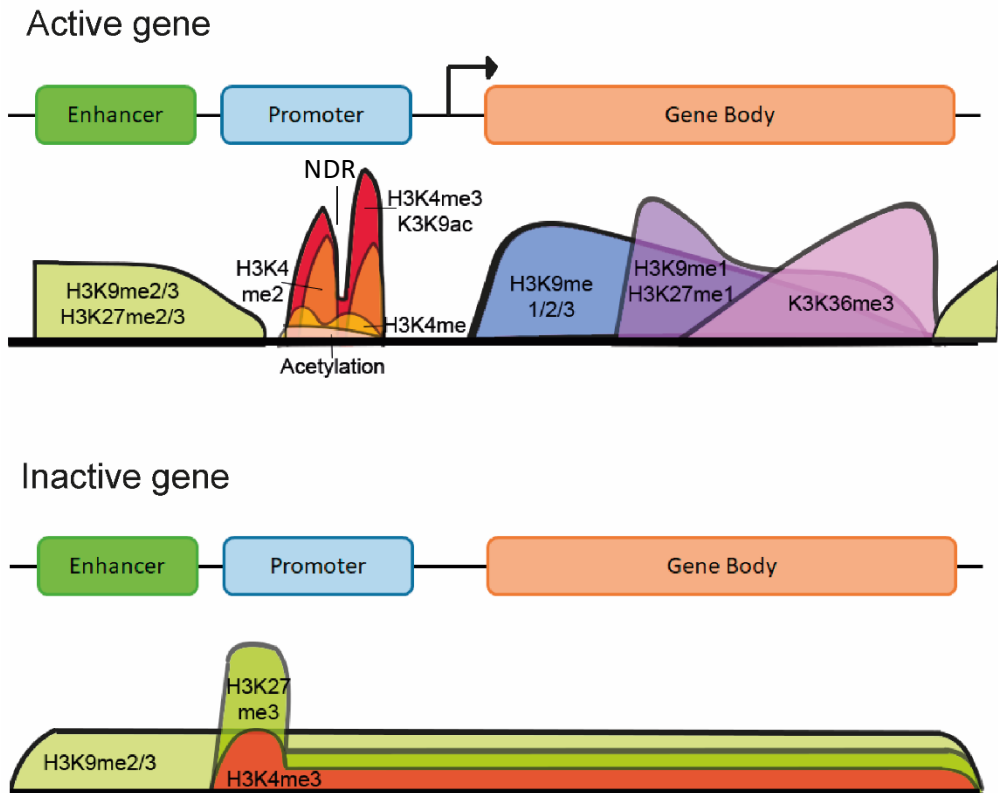


Figure 7. Distribution of histone modifications on active and silenced genes. Modification patterns differ on actively transcribed and silenced genes. Nucleosomes within the promoters of actively transcribed genes carry high levels of active modifications such as acetylation and methylation of H3K4. At the transcriptional start site there is a nucleosome-depleted region (NDR) within the promoter where the transcription factors bind. Other active modifications such as methylation of H3K79 are present in the body of these genes. Inactive genes, are mark with silencing modifications, such as H3K9 methylation and H4K20 methylation, along the whole gene. Indeed, H3K27 methylation is enriched in the promoter. These modifications can be bound by heterochromatic proteins and, thus, this chromatin area can condense, as seen in heterochromatin. Data obtained from (Barth & Imhof, 2010)

Transcription factors bind to DNA in a sequence-specific manner and mark a gene for activation or repression. As transcription factors generally lack the enzymatic activities necessary to modify chromatin, unwind DNA, and recruit RNA polymerase II, they generally dock other coregulators to achieve this task. Corepressors and coactivators usually exist as multiprotein complexes in the nucleus and are recruited by transcription factors in response to cellular signals. Coactivators often contain the enzymatic activities necessary for an alteration in chromatin structure from a quiescent state to one allowing active gene transcription.

Transcriptional coactivator proteins can be highly regulated by hormones and signal transduction pathways (Spiegelman & Heinrich, 2004). Although coactivators function in a variety of ways, three main mechanisms have been described:

- **Histone modification:** some coactivators modify histones to allow greater access of other proteins to the DNA. Examples: p300 and CBP, histone acetyltransferases (HATs)(Hermanson et al., 2002).
- **Recruitment of RNA polymerase II:** Coactivators that bind to transcription factors, recruit RNA polymerase II and interact with the general transcription apparatus. Examples: members of the Mediator complex. (Malik & Roeder, 2000)
- **ATP-dependent DNA unwinding activity:** these coactivators alter the positioning of nucleosomes along DNA promoting further binding of transcription factors. Examples: protein complexes of the yeast SWI/SNF family (or their mammalian homologs BRG1 or BRM (Lemon et al., 2001).

2. PGC-1 Protein family

PGC-1 (PPAR γ coactivator-1) is a family of coactivators that integrates signaling pathways in the control of cellular metabolism. It is expressed in several tissues, especially those with very high oxidative metabolism, such as heart, skeletal muscle, kidney, brown fat, brain, and liver(Martínez-Redondo et al., 2015).

PGC-1 family is constituted by three coactivators (PGC-1 α , PGC-1 β and PGC-related coactivator (PRC)) that share a common structure and several motifs. The first member of the PGC-1 family was identified in brown fat and named as PPAR γ -interacting protein or PGC-1 α (Puigserver et al., 1998). PGC-1 α shares extensive sequence identity with the second member of the family, PGC-1 β . Homology between PGC-1 α and PGC-1 β is clustered in several distinct domains, including an N-terminal activation domain (40%), a central regulatory domain (35%), and a C-terminal RNA binding domain (48%) (J. Lin et al., 2002). PGC-related coactivator (PRC) has more limited homology (Andersson & Scarpulla, 2001) including the activation domain and RNA binding domain. Sequence analysis reveals that the PGC-1 family of coactivators is conserved in many chordate species, including primates, rodents, ruminants, birds, amphibians, and fishes (Figure 8).

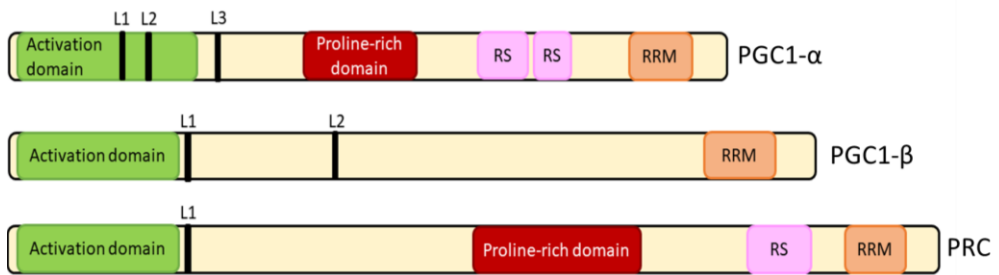


Figure 8. Domain structure of PGC-1 coactivators. The most relevant structural and functional domains of the three most important members of the PGC-1 family of transcriptional coactivators.

PGC-1 coactivators are highly versatile and interact with many different transcription factors through a central region. Therefore, they activate distinct biological programs in different tissues. In addition, PGC-1 α has three functional LXXLL motifs involved in the binding of many nuclear receptors. At the N-terminal regions, PGC-1 coactivators bind several HAT-containing proteins, including CBP, p300, and SRC-1 (Puigserver et al., 1999). These proteins acetylate histones and remodel chromatin to allow access of additional transcription factors for gene activation. The PGC-1 α transcriptional activator complex is able to displace repressor proteins, such as histone deacetylase, on its target promoters, leading to augmented gene transcription (Borgius et al., 2002, Guan et al., 2005). PGC-1 α also harbors a Ser/Arg-rich domain and an RNA binding domain and has been shown to couple pre-mRNA splicing with transcription (Monsalve et al., 2000).

PGC-1 α and β coactivate a subset of transcription factors (NRF-1 and NRF-2, PPAR α PPAR δ ERR α and TR) that directly regulate the expression of certain nuclear-encoded mitochondrial genes (Vega et al., 2000), (Wang et al., 2003), (Huss et al., 2002, Huss et al., 2004, Kamei et al., 2003, Mootha et al., 2004, Schreiber et al., 2004), (Zhang et al., 2004b). The simultaneous stimulation by PGC-1 α and β of mitochondrial genes leads to increased enzymatic capacity for fatty-acid β -oxidation, Krebs cycle, and oxidative phosphorylation (OXPHOS). Importantly, PGC-1 α and β also induce the expression of genes involved in heme biosynthesis, ion transport, mitochondrial translation, and protein import and can stimulate mitochondrial biogenesis and increased respiratory function (St-Pierre et al., 2003, Wu et al., 1999). As PGC-1 stimulate mitochondrial-based respiration, it also increases the expression of SOD and glutathione peroxidase, as well as enzymes responsible for glutathione biosynthesis (St-Pierre et al., 2003) to prevent a deleterious increase in ROS.

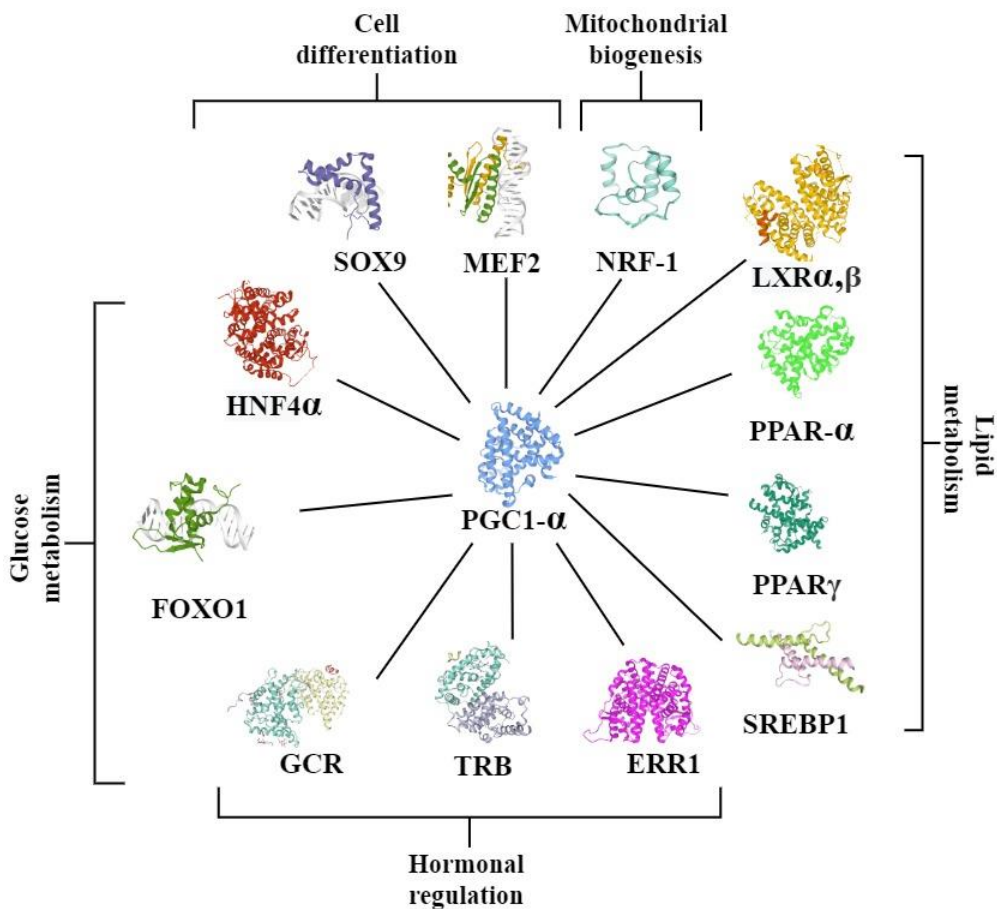


Figure 9. Principal functions of PGC-1 α . PGC-1 α binds and activates several transcription factors with different biological roles including mitochondrial biogenesis, glucose and lipid metabolism, hormonal regulation, cell differentiation. Abbreviations: SRY-Box Transcription Factor 9 (SOX-9), Myocyte-specific enhancer factor 2 (MEF2), Nuclear respiratory factor 1 (NRF1), liver X receptor alpha and beta (LXR α,β), Peroxisome proliferator-activated receptor alpha (PPAR- α), Plasminogen activator inhibitor 1 RNA-binding protein (SERBP1), Steroid hormone receptor ERR1 (ERR1), Thyroid hormone receptor beta (TRb), Glucocorticoid receptor (GCR), Forkhead box protein O1 (FOXO1), Hepatocyte Nuclear Factor 4 (HNF4 α).

The diverse effects of PGC-1 α and β on cellular energy metabolism require their activities be tightly controlled (Figure 9). PGC-1 α protein has a very short half-life (~2.3 hr) and is greatly stabilized following phosphorylation at three sites (T262, S265, and T298) by p38 MAP kinase (Knutti et al., 2001, Puigserver et al., 2001). These modifications also enhance the transcriptional activity of PGC-1 α by displacing p160 myb binding protein (p160MBP), a strong transcriptional suppressor (Fan et al., 2004). Phosphorylation of PGC-1 α at residues T177 and S538 by AMPK also contribute to enhance PGC-1 α activity and to induce mitochondrial oxidative

metabolism in response several physiological stresses. PGC-1 α is also phosphorylated by glycogen synthase kinase 3b (GSK3b). In this case, phosphorylation by GSK3b favors PGC-1 α ubiquitination and proteolytic degradation. PGC-1 α activity is also regulated by acetylation/deacetylation. Acetylation of PGC-1 α , which is carried out by GCN5, γ inhibits PGC-1 α intrinsic transcriptional activity and induces its translocation to inactive chromatin domains, preventing its binding to target gene promoters. On the other hand, deacetylation by sirtuin 1 (SIRT1) activates PGC-1 α transcriptional activity in a NAD⁺-dependent way. Deacetylation of PGC-1 α by SIRT1 depends on its prior phosphorylation by AMPK. Indicating that different posttranslational modifications converge to regulate PGC-1 α transcriptional activity in a coordinated manner in response to a physiological stimulus.

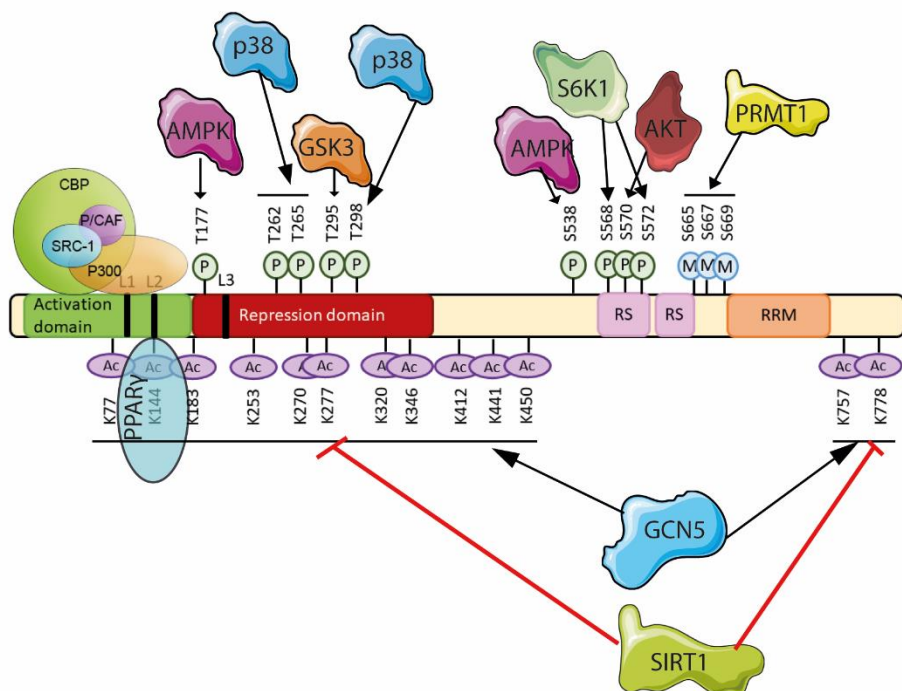


Figure 10. Regulation of PGC1- α activity. Schematic representation of the main posttranslational modifications known to regulate PGC-1 α transcriptional activity.

In addition to posttranslational mechanisms, many studies have clearly demonstrated that the PGC-1 coactivators are regulated at the transcriptional level in response to a variety of nutritional and environmental stimuli. The promoter of PGC-1 α contains two conservative binding sites for myocyte enhancer factor 2 (MEF2) and one CRE-binding site for the cAMP response element-binding protein

(CREB)(Esterbauer et al., 1999). Activation of the cAMP signaling pathway is a major mechanism underlying the induction of PGC-1 α in several different cell types. In fact, the proximal promoter of PGC-1 α contains a functional CREB binding site that is required for cAMP response (Herzig et al., 2001).

One main function of PGC-1 coactivators is enhancing energy production. However, additional functions have emerged in several tissues. One of the most important is promoting cell differentiation. For instance Both PGC-1 α and PGC-1 β facilitate the terminal differentiation of erythroid cells during embryonic development (Cui et al., 2014). In skeletal muscle, PGC-1 α -mediated switch from type II fibers to type I slow, oxidative fibers, increasing muscular resistance (Rasbach et al., 2010). In the liver, PGC-1 α regulate gluconeogenesis in response to fasting (Puigserver et al., 2003) whereas PGC-1 β induce hepatic lipogenesis metabolism in response to specific nutritional stimuli (J. Lin et al., 2005; Nagai et al., 2009). PGC-1 α promotes brown fat differentiation of MSCs (P. L. Huang et al., 2011)

These studies suggest that each member of the family may modulate mitochondrial activity in a specific and subtle manner that depends on the tissue and physiological context and evidence the relevance of PGC-1 coactivators in multiple biological processes beyond the strict control of the mitochondrial oxidative metabolism. Given this pleiotropic function, and the metabolism reprogramming observed during osteocytogenesis, it could be expected to find that PGC-1 family members play also a role in the osteoblast to osteocyte transition.

3. NRF2 Transcription factor

Nuclear factor, erythroid 2-like 2 (*NFE2L2*), also known as NF-E2-Related Factor 2 (NRF2), is a transcription factor that regulates the expression of a wide array of genes encoding for antioxidant enzymes and other proteins responsible for the detoxification of xenobiotics. Among them, these are of special interest NAD(P)H quinone oxidoreductase 1 (*NQO1*), Heme oxygenase-1 (*HO-1*), glutathione S-transferase (*GST*) and Glutamate-Cysteine Ligase Catalytic Subunit (*GCLC*) (Jaramillo & Zhang, 2013).

NRF2 (59, 108) belongs to the cap “n” collar (CNC) subfamily of basic-region leucine zipper (bZIP) transcription factors that includes NRF1 (18), NRF3 (79), NF-E2 p45 subunit (K Itoh et al., 1995; Tonelli et al., 2018). NRF2 is a modular protein with seven Nrf2-ECH homology domains (Neh1–7), each of which fulfills different functions, which are summarized in Figure 11.

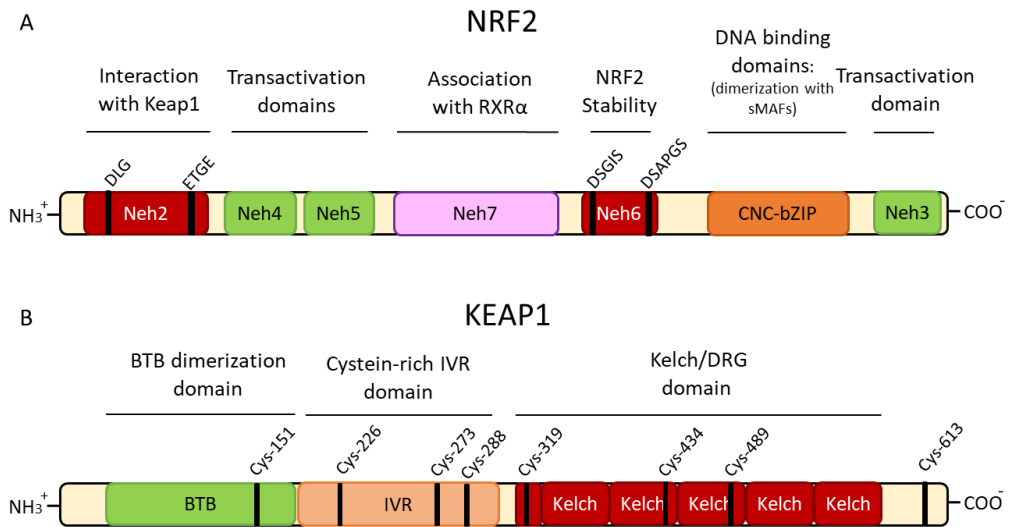


Figure 11. Functional domains of NRF2 and its ubiquitin ligase KEAP1. (A) Schematic structure of NRF2. NRF2 comprises seven Nrf2-ECH homology (Neh) domains, Neh1-Neh7. Among these domains, Neh2 and Neh6 are important for binding with the negative regulators KEAP1 and β -TrCP, respectively, and consequently causing Nrf2 ubiquitination and degradation. Neh1 contains a basic-region leucine zipper (bZIP) domain that is important for interacting with small MAF (sMAF) proteins and DNA. Neh3, Neh4, and Neh5 domains are necessary for transactivation. Neh7 is important for binding with RXR α , a Nrf2 repressor. (B) Schematic structure of KEAP1. KEAP1 comprises an N-terminal region (NTR), a broad complex, Tramtrack and Bric-à-Brac (BTB) domain, an intervening region (IVR), six Kelch repeats, and a C-terminal region (CTR). Among these domains, BTB domain is responsible for the homodimerization of Keap1 and the binding with Cullin3 E3 ligase (CUL3). BTB also harbors cysteine residues, which are reactive to electrophiles and reactive oxygen species (ROS). IVR consists of reactive cysteine residues, including C226, C273 and C288. DRG domain is responsible for Nrf2 binding to DLG and ETGE motifs. NRF2 indicates nuclear factor erythroid 2-related factor 2; KEAP 1, Kelch-like ECH-associated protein 1; RXR α , retinoid X receptor α ; BTB, Broad-Complex, Tramtrack, and Bric-a-Brac; IVR, intervening region; DRG, double glycine repeats.

Besides mediating stress-stimulated induction of antioxidant and detoxification genes, NRF2 contributes to adaptation by upregulating the repair and degradation of damaged macromolecules, and by modulating intermediary metabolism. In the latter case, NRF2 inhibits lipogenesis, supports β -oxidation of fatty acids, facilitates flux through the pentose phosphate pathway, and increases NADPH regeneration and purine biosynthesis (Hayes & Dinkova-Kostova, 2014). Furthermore, NRF2 has been shown to regulate mitochondrial bioenergetics. In particular, NRF2 increases mitochondrial membrane potential, oxygen consumption and ATP production (Holmström et al., 2013). On the contrary, cells deficient in *Nrf2* prefers aerobic glycolysis to produce ATP, which is then used by the F1/Fo-ATPase for maintenance of the mitochondrial membrane potential (Holmström et al., 2013). These observations suggest NRF2 plays a key role in metabolic reprogramming.

NRF2 activity and abundance are tightly regulated at the transcriptional, post-transcriptional, and post-translational level to ensure that its activity increases during redox perturbation, inflammation, growth factor stimulation and nutrient/energy fluxes.

At transcriptional level, *Nfe2l2* is regulated by several transcription factors. *Nfe2l2* is induced by aryl hydrocarbon receptor (AhR) in response to polycyclic aromatic hydrocarbon exposure and other xenobiotics (Miao et al., 2005). Indeed, the *Nfe2l2* promoter contains a binding site for nuclear factor NF- κ B, which allows it to be induced by inflammatory stimuli (Rushworth et al., 2012). Within this promoter, we also found ARE-like sequences which provide a positive feedback mechanism to amplify NRF2 effects (Kwak et al., 2002). Oncogenic Kras and B-Raf, Myc (Denicola et al., 2011), the phosphoinositide 3-kinase (PI3K)-Akt pathway (Mitsuishi et al., 2012), and the Notch signaling pathway (Wakabayashi et al., 2014) have also been reported to augment *Nfe2l2* transcription.

At post-transcriptional level, several miRNAs have been identified to control NRF2 levels in the cell. Increased miR-144 is associated with reduced NRF2 levels in patients with homozygous sickle cell disease (HbSS)(Sangokoya et al., 2010). Moreover miR-28 in human MCF7 breast cancer cells (M. Yang et al., 2011); miR-27a, miR142-5p, miR-144, and miR-153 in human SH-SY5Y neuroblastoma cells (Narasimhan et al., 2012); and miR-93 in human MCF10A mammary epithelial cells and T47D breast cancer cells(B. Singh et al., 2013) decreased *NRF2* mRNA and protein levels.

At post-translational level, NRF2 abundance within the cell is tightly regulated by ubiquitination and proteasomal degradation. Under homeostatic conditions, NRF2 has a short half-life of approximately 10–30 min (Nguyen et al., 2003). In this case, two molecules of KEAP1 are bound to the Neh2 domain of NRF2 at the ETGE and DLG motifs (via their Kelch-repeat domain)(Tong et al., 2006). KEAP1 functions as an adaptor protein for the Cul3 E3 ubiquitin ligase, which is responsible for the continuous ubiquitylation and degradation of NRF2 (Cullinan et al., 2004) maintaining NRF2 basal levels extremely low. In response to oxidative stress, Keap1 is oxidized at reactive cysteine residues, resulting in KEAP1 inactivation, NRF2 stabilization and translocation into the nucleus (Ken Itoh et al., 2003) (Figure 12). Beside oxidative stress, several cytoplasmic proteins interfere with KEAP1-NRF2 interaction. These include the ubiquitin-binding protein p62 (Copple et al., 2010), BRCA2 (PALB2) (J. Ma et al., 2012), phosphoglycerate mutase 5 (PGAM5) (Lo & Hannink, 2008), dipeptidyl-peptidase 3 (DPP3) (Hast et al., 2013), and Wilms tumor gene on X chromosome (WTX) (Camp et al., 2012), p21 (W. Chen et al., 2009) and BRCA1 (Gorrini et al., 2013) among others. Additionally, KEAP1-mediated regulation

of NRF2 activity can be modulated by post-translational modifications of NRF2. Protein kinase C (PKC) phosphorylates Ser40 in the Neh2 domain of NRF2, disrupting KEAP1-NRF2 association and thus promoting NRF2 activation (H.-C. Huang et al., 2002).

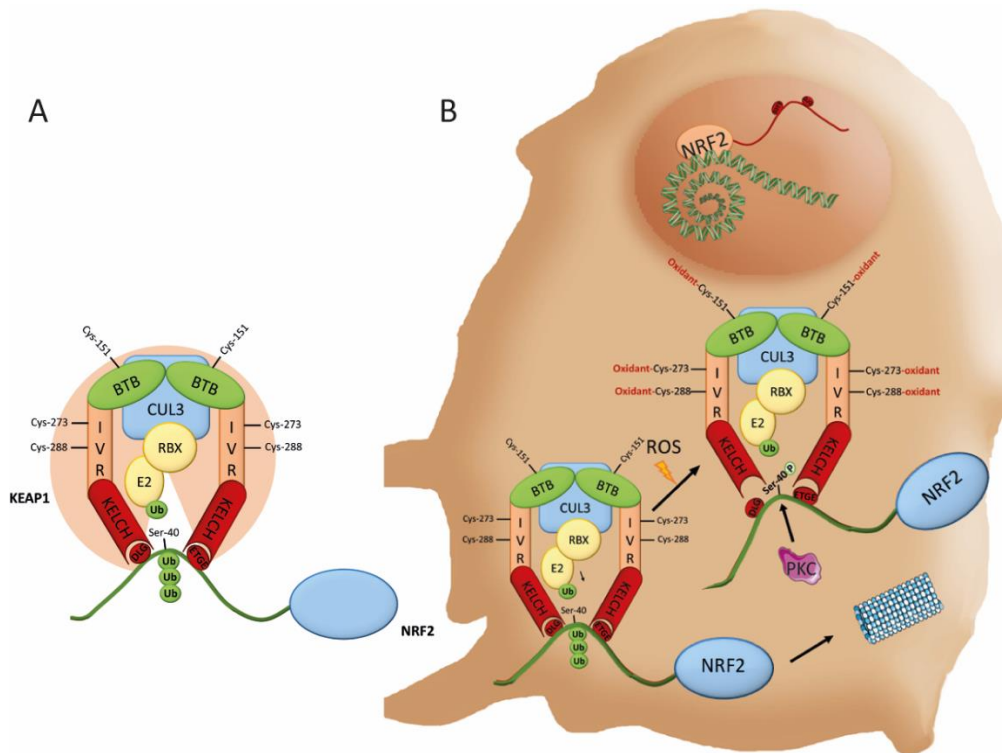


Figure 12. Interaction between KEAP1 and NRF2. (A) The Keap1 homodimer binds one molecule of Nrf2 through the ETGE and DLG motifs of Nrf2. The lysine residues (K) are clustered between the two motifs and represent ubiquitination targets. (B) Under normal conditions, Nrf2 is constantly ubiquitinated through Keap1 and degraded in the proteasome. ROS and other electrophiles target cysteine residues present in IVR and BTB domains of KEAP1 inducing its inactivation. Then, NRF2 is released and accumulates in the nucleus where it activates many cytoprotective genes. Phosphorylation of NRF2 by PKC or other kinases also contribute to the stabilization and activation of the protein. NRF2 indicates nuclear factor erythroid 2-related factor 2; KEAP 1, Kelch-like ECH-associated protein 1; BTB, Broad-Complex, Tramtrack, and Bric-a-Brac; IVR, intervening region; DRG, double glycine repeats; RBX, Ring Box Protein; PKC, Protein Kinase C.

Besides KEAP1, other negative regulators control the degradation of NRF2. β -TrCP binds to DSGIS and the DSAPGS motifs of Neh6 domain. Then, β -TrCP Gsk-3 β -mediated phosphorylation of the Neh6 domain of NRF2 and SCF E3 ubiquitin ligase induce proteasomal degradation of NRF2. Thus, NRF2 activity could potentially be enhanced by some kinases, such as extracellular signal-regulated kinase (ERK), p38 MAP kinase (MAPK), PI3K and PKC, through the inhibition of Gsk-3 β (Rada et al.,

2011). E3 ubiquitin ligase synoviolin (Hrd1) is another ubiquitin ligase that interacts with the Neh4 and Neh5 domains of NRF2 through its C-terminal domain and causes NRF2 ubiquitylation and subsequent degradation (T. Wu et al., 2014)

Once in the nucleus, NRF2 cannot bind DNA on their own and has to heterodimerize with members of the sMAF protein family (MafF, MafG, and MafK) to act as transcriptional regulator (Katsuoka et al., 2005; Motohashi et al., 2002). Then, NRF2-sMAF complex binds, in a sequence-specific manner, to the antioxidant response element in the promoter region of NRF2 target genes. The regulation of NRF2 activity is also controlled by the availability of these binding partners. The sMAFs (MafF, MafG and MafK) are members of the bZIP family of transcription factors. They are characterized by a basic domain that binds DNA, and a leucine zipper that mediates homo- or hetero-dimerization with CNC proteins and Bach proteins (Kannan et al., 2012). But the sMAF proteins lack the transactivation domain, thus sMAF homodimers have been shown to act as transcriptional repressors in overexpression experiments (Kimura et al., 2007). Therefore, changes in the abundance or activity of the participant molecules of the network can lead to major changes in the regulation of gene expression (Motohashi et al., 2000).

Once the complex NRF2-sMAF is formed, it binds to the ARE sequences in the DNA. However there is a small fraction of NRF2 binding sites that did not contain an ARE, indicating that NRF2 probably interacts with other DNA-binding proteins (Malhotra et al., 2010). Motif analysis of NRF2 binding sites identified the consensus motifs for other transcription factors, such as FOS, MAFb, LHX3 and MEF2A (Malhotra et al., 2010).

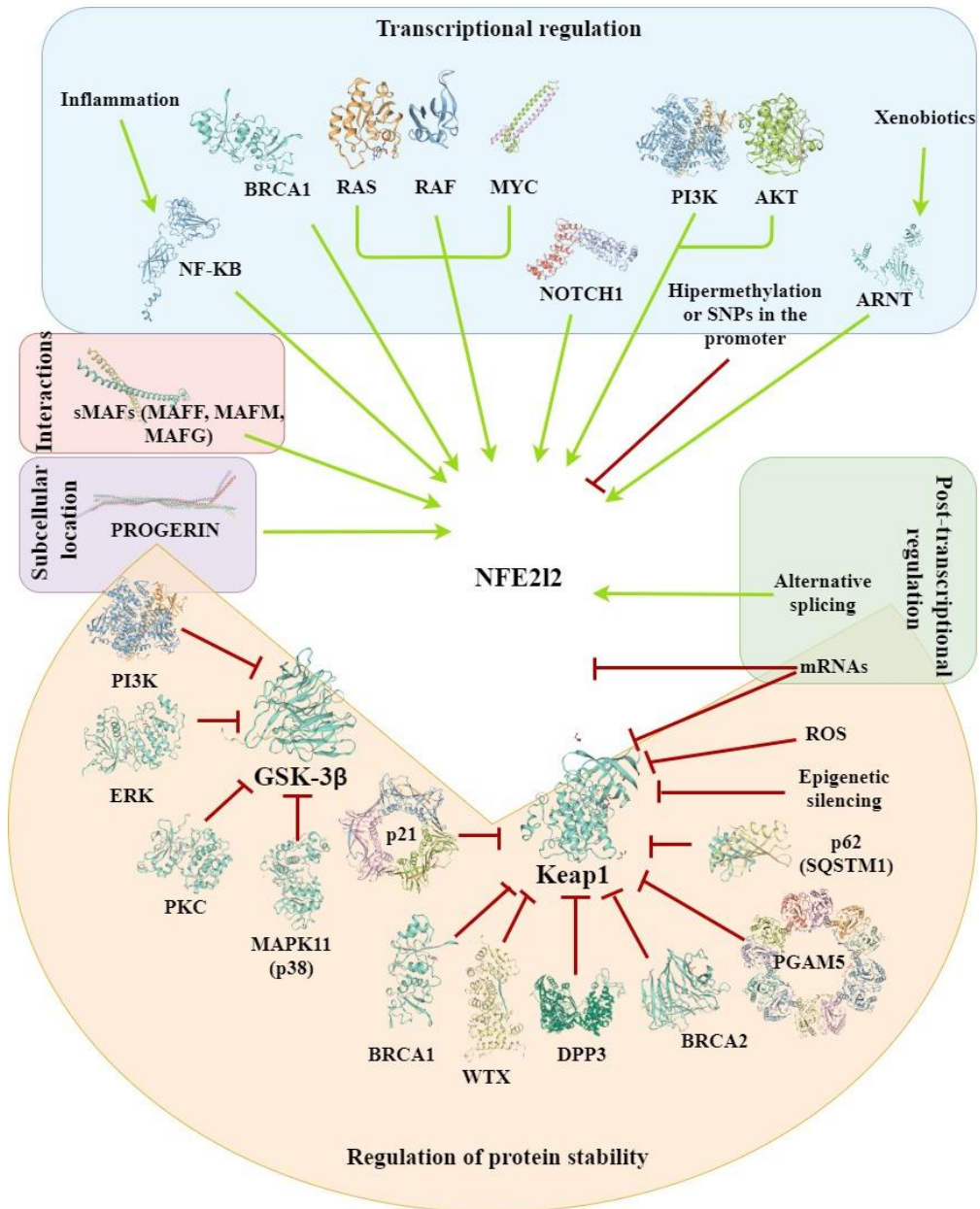


Figure 13. Mechanisms of regulation of Nrf2 activity. The mechanisms of modulation of Nrf2 activity include the regulation of transcription, mRNA processing, translation, subcellular localization, protein stability, and availability of binding partners. Arrows indicate activating regulation, and bars indicate inhibitory regulation. NOTCH1, Neurogenic locus notch homolog protein 1; PI3K, Phosphatidylinositol 3-kinase; AKT, Proline-rich AKT1 substrate 1; ARNT, Aryl hydrocarbon receptor nuclear translocator; ROS, Reactive oxygen species; BRCA1, breast cancer susceptibility 1; DPP3 Dipeptidyl peptidase 3; WTX, APC membrane recruitment protein 1; PKC, Protein kinase C; ERK, Mitogen-activated protein kinase 3; NF-κB, nuclear factor-κB; PI3K, phosphoinositide 3-kinase.

The whole-genome mapping of NRF2 binding sites indicated that the majority of NRF2 binding sites lie outside the promoter-proximal region (Hirotsu et al., 2012). Some of these binding sites could be located in the promoter region of long non-coding RNAs (lncRNAs) (Guttman et al., 2009) or enhancers. The generation of chromatin state maps by profiling combinations of epigenetic marks, in addition to NRF2 binding in a given cell type will allow the identification of regulatory elements provide unique insights into NRF2-mediated transcriptional regulation (Tonelli et al., 2018).

Analyses of the genome-wide distribution of NRF2 have identified new sets of target genes whose products are not involved in response to oxidative stress, evidencing new functions for NRF2. Among them, we find genes controlling in cell proliferation and differentiation. In this model, the Keap1-Nrf2 system will translates environmental stresses into regulatory network signals that will determine cell fate decision. Several examples are found in different cell lineages. For instance, NRF2 deficiency blocks adipogenesis (Pi et al., 2010) while activation of NRF2 stimulates neural differentiation (Zhao et al., 2009), drives myeloid differentiation of hematopoietic stem cells (HSCs) (Murakami et al., 2014), contribute to differentiation of erythrocytes (Kawatani et al., 2011) and megakaryocytes (Motohashi et al., 2010). On the other hand, NRF2 is necessary for the maintenance and proliferation of stem cells and progenitors. It has been found that NRF2 controls self-renewal and pluripotency of human embryonic stem cells (hESCs) (J. Jang et al., 2014), supports proliferation of satellite cells (SCs) in muscle (Al-Sawaf et al., 2014) and enhance proliferation and differentiation of Neuronal progenitor cells (NPCs) (Kärkkäinen et al., 2014). In bone NRF2 activation inhibits osteoclast differentiation (Hyeon et al., 2013) and chondrocyte maturation (Hinoi et al., 2007). The role of NRF2 in osteoblasts and osteocytes is unclear. Some studies suggest that NRF2 inhibit osteoblast differentiation by direct binding to RUNX2 (Hinoi et al., 2006) and that *Nfe2l2*-deficiency increased bone acquisition and mass (Park et al., 2014b; Pellegrini et al., 2017). Other studies revealed that deletion of *Nfe2l2* in female mice results in a deficit in postnatal bone acquisition and increased bone loss (Ibáñez et al., 2014; J.-H. H. Kim et al., n.d.; Pellegrini et al., 2017). Similarly, moderate NRF2 activation by heterozygous deletion of Keap1 led to sexual dimorphic results with higher bone mass in males but not in female mice (Yin et al., 2020). All these previous studies have the limitation that genetic modifications affected all the murine cells and tissues, then we cannot exclude the influence of paracrine and endocrine factors. Therefore, studies with cell-type specific knockout mice of NRF2 would provide more insight in their specific role in bone biology and pathophysiology.

CHAPTER V:

BONE PATHOLOGY

1. OSTEOPOROSIS

Osteoporosis is a chronic disease characterized by decreased bone mass and microarchitectural deterioration of bone tissue, resulting in a loss of bone strength and consequent increased risk of fracture. Osteoporotic fractures usually affect hip, vertebrae, distal forearm and other body positions with a large proportion of trabecular bone (Pouresmaeili et al., 2018). Diagnosis of osteoporosis is challenging, and in consequence, prevalence and incidence of this disease are difficult to estimate. Even though approximately 1.66 million hip fractures occur each year worldwide. As the number of vertebral and hip fractures increases exponentially with advancing age, WHO expect that the incidence would increase four-fold by 2050 because of the population ageing. The age-adjusted incidence rates are higher in affluent developed countries than in sub-Saharan Africa and Asia. Within those countries with a high fracture incidence, rates are three- to four-fold greater among women (*WHO | 5. Population nutrient intake goals for preventing diet-related chronic diseases*, n.d.). These reasons make osteoporosis the major cause of morbidity and disability in older people and impose a considerable economic burden on health services worldwide. Thereby great efforts should be done in order to understand this disease.

Osteoporosis is initiated by an imbalance between bone resorption and formation that can be influenced by non-modifiable and modifiable risk factors. Non-modifiable risk factors include gender (osteoporosis has higher prevalence in women), age (fracture risk increases with age), race (osteoporosis is more common among Caucasians), and genetics (polymorphisms in the vitamin D receptor (VDR) gene (Pouresmaeili et al., 2013; Remes et al., 2005), the type I collagen (COL1A1) gene (Grant et al., 1996; Tural et al., 2013), the estrogen receptor- α (ER α) (Ioannidis et al., 2004; Y. Yamada et al., 2002)) increased the risk of osteoporosis (Pouresmaeili et al., 2018). Other conditions, such as Diabetes Mellitus (DM), Rheumatoid Arthritis, Hyperthyroidism or multiple sclerosis, have been also linked to osteoporosis and bone loss. Among modifiable research factors, research studies give special importance to diet and lifestyle (Pouresmaeili et al., 2018). Historically, calcium and vitamin D are the primary limiting nutrients considered for osteoporosis prevention in older adults (Sunyecz, 2008). More recent studies have related additional

nutrients with bone health, such as vitamins A, B, C, E, K; minerals (potassium, magnesium, silicon); and macronutrients (protein and fats) (Sahni et al., 2015). Other recommended prevention approaches include engaging in regular exercise, avoiding smoking and limiting alcohol intake.

Management of osteoporosis involves treating and preventing fractures and using medicines to strengthen bones. In a first attempt, non-pharmacological can be assayed. This includes adequate calcium and vitamin D intake, weight-bearing exercise, smoking cessation, limitation of alcohol/caffeine consumption, and fall-prevention techniques (Delaney, 2006). Pharmacological therapy aims to reduce the risk of fractures (Figure 14). Medications to treat osteoporosis can be divided in two categories:

- **Antiresorptive agents** to decrease the rate of bone resorption. This category includes bisphosphonates, RANKL inhibitors, hormonal therapy with estrogens, estrogen agonists/antagonists also called selective estrogen receptor modulators (SERMs), parathyroid hormone analogues, and calciton (Pavone et al., 2017).

- **Anabolic agents** to increase the rate of bone formation. This category includes Sclerostin inhibitors and analogs of Parathyroid Hormone (PTH) and parathyroid Hormone-Related Protein (PTHrp)(Pavone et al., 2017).

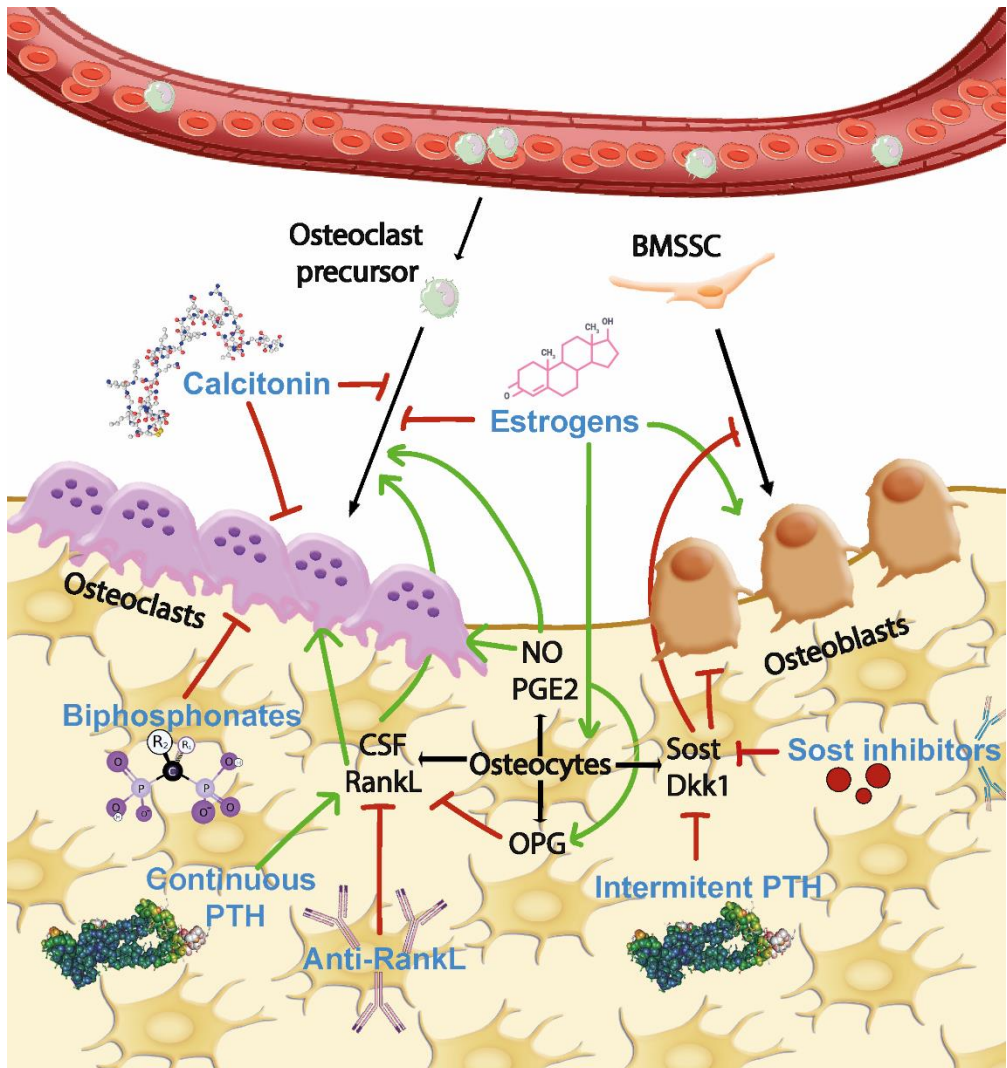


Figure 14. Principal treatments for osteoporosis. Pharmacological treatment for osteoporosis includes antiresorptive agents to inhibit osteoclast function (bisphosphonates, RANKL inhibitors, parathyroid hormone analogues (PTH), calcitonin and estrogens) and anabolic agents to increase the rate of bone formation (Sclerostin (Sost) inhibitors and analogs of Parathyroid Hormone (PTH)).

Therapeutic strategy will depend on several factors such as age, sex, previous injury story and risk of fracture. Although the broad number of therapeutic options, there still remain multiple unmet needs in the field of osteoporosis and fracture care, for example, the primary prevention of osteoporosis in young individuals (to reach a high peak bone mass), the optimization of the use of imaging techniques, the use of nonmedical treatment options and surgical techniques of fracture healing and the development of new osteoporosis treatment with lower side effects.

In most of the cases, bisphosphonates constitute the first therapeutic option. Bisphosphonates are highly effective at limiting the bone loss that occurs in many disorders characterized by increased osteoclast-mediated bone resorption, including senile osteoporosis in both men and women, glucocorticoid-associated osteoporosis, and malignancies metastatic to bone. Although they are generally well tolerated, potential adverse effects may limit bisphosphonate use in some patients. Some adverse effects that may occur with bisphosphonate therapy, such as gastroesophageal irritation, were recognized. Other more serious potential complications, including osteonecrosis of the jaw (ONJ) and severe suppression of bone turnover (Kennel & Drake, 2009). The increase in BMD and bone volume triggered by bisphosphonates is usually linked to an increase in bone stiffness and strength, which increase the risk of fracture (Sroga & Vashishth, 2012). Moreover, the use of bisphosphonates also causes a decrease in bone heterogeneity and reduction of bone turnover (Fleisch, 2003). Both effects combined can lead to bone failure.

2. Diabetes Mellitus, glucose and bone health

Diabetes Mellitus (DM) is a chronic metabolic disorder characterized by the presence of hyperglycemia due to a damage in the insulin-producing cells of the pancreas (type 1) or to the inability of the cells to respond properly to insulin (type 2). Uncontrolled high blood sugar can lead to complications such as retinopathy, nephropathy, neuropathy, cardiovascular events and osteoporosis. In the context of bone health, children and adolescent with Type 1 Diabetes Mellitus (T1D) have lower BMD levels and higher risk of suffer osteoporosis in later life (Lettgen et al., 1995). Several defects in bone cell differentiation have been found in T1D models. Experiments in animal models of insulin deficiency found downregulation of *Runx2* in the early course of diabetes (H. Lu et al., 2003). Downregulation of *Runx2* was linked to a decreased expression of its target genes including *Mmp-9*, *Mmp-13*, *Ibsp*, *Col1*, *Phex*, *DMP-1*, *Opn* and *Oc*, *Osterix* and *Alpl* (Fowlkes et al., 2008) which also reflects a decreased osteoblast activity. Furthermore, T1D is associated to low systemic levels of insulin and insulin like growth factor-1 (IGF-1), as well as, reduced protein levels of IGF-1 receptor (IGF-1R) and insulin receptor (IR) in bone marrow stromal cells (BMSCs). IGF-1 stimulates growth and differentiation of mesenchymal stem cells into osteoblast both *in vivo* and *in vitro* (Crane et al., 2013; Xian et al., 2012) and is essential for bone mineralization (Bouillon, 1992). Insulin binds to IR present in osteoblasts and induce collagen production. In fact, mice lacking the IR in osteoblasts have lower number of osteoblasts and present decreased trabecular bone formation, as well as lower osteocalcin levels (Fulzele et al., 2010). By its part,

mice lacking the IR in osteoprogenitor cells have post-natal growth restriction (Fulzele et al., 2010) and decreased bone strength (K. Thrailkill et al., 2014). Besides differentiation, viability and activity of osteoblasts are also compromised in T1D. Low numbers of osteoblasts and low osteoid formation was found in mice with STZ-mediated diabetes (J. et al., 2016). The reduced numbers of osteoblasts observed could be a consequence of an increased apoptosis of osteoprogenitor cells induced by high levels of oxidative stress, another consequence of diabetes in bone (Hamada et al., 2007; E. Weinberg et al., 2014). Advanced Glycation Ends Products (AGES), which have been found increased in diabetic bones, trigger bone marrow stromal cells apoptosis through inflammatory and oxidative stress-inducing mechanisms (Evgeny Weinberg et al., 2013).

Due to its location within the osteoid, osteocytes are more inaccessible to high glucose environment, however they are also affected in T1D. T1D enhances the inhibition of WNT pathway by increasing *Sost* gene expression and protein levels by osteocytes (Hie et al., 2011). Upregulation of *Sost* can be triggered either by high levels of glucose or AGEs (J. Y. Kim et al., 2013; Tanaka et al., 2015). T1D animal models also showed a reduction in lacunar and osteocyte density, probably caused by the decrease in osteoblast differentiation as well as a reduction in osteocyte viability (Lai et al., 2015; Portal-Núñez et al., 2010; Villarino et al., 2006).

Osteogenesis and bone remodeling in T1D are also affected by osteoclast activity. Peripheral blood derived osteoclasts isolated from humans with T1D are less sensitive to OPG than controls (Mabilleau et al., 2008), and shows increased activity of soluble RANKL (Tsentidis et al., 2016). In addition, bone *Rankl* mRNA levels are increased in studies of STZ-induced diabetes (Bortolin et al., 2015) whereas changes in the expression of OPG remains unclear. Some studies show downregulation of OPG expression in T1D animal models (Motyl et al., 2009) while others found increased OPG gene expression in T1D (Loureiro et al., 2014) and in chronic hyperglycemic conditions (Bortolin et al., 2015; Cunha et al., 2014), which suggests a possible mechanism of adaptive protection. But, even if those compensatory mechanisms exists, studies in long term insulinopenic rodent models demonstrate upregulation of genes associated with osteoclast activity such as cathepsin K, and tartrate-resistant acid phosphatase (TRAP) (Hie et al., 2007), as well as increased markers of bone turnover such as C-terminal telopeptide (Kathryn M. Thrailkill et al., 2016).

The contribution of Diabetes Mellitus Type 2 (T2D) to osteoporosis is more controversial. Several mechanisms are involved and some of them may have contradictory effects. On one hand, obesity linked to T2D is associated with higher BMD, probably through mechanical loading and hormonal factors, including insulin,

estrogen, and leptin production (Felson et al., 1993; Wakasugi et al., 1993). Hyperinsulinemia also promotes bone formation (Reid et al., 1993). On the other hand, glucose, when present in high levels in the blood, interacts with several proteins to generate a high concentration of advanced glycation end-products (AGEs) in collagen that may reduce bone strength (Paul & Bailey, 1996) and stimulate apoptosis of osteoblasts (Alikhani et al., 2007). Moreover, in T2D, glycosylated hemoglobin levels correlate positively with sclerostin levels and with measures of insulin resistance (García-Martín et al., 2012; Zhou et al., 2013), but negatively with alkaline phosphatase (ALPL) (Zhou et al., 2013). In consequence, increased levels of AGEs results in deficient bone formation and increased bone fragility. Furthermore, glycosuria, produced as consequence of hyperglycemia, increases the amount of calcium excreted in the urine (hypercalciuria), accelerating bone loss. In addition, microvascular complications of diabetes might reduce blood flow to bone and contribute to bone loss and fragility (Vogt et al., 1997; Wientroub et al., 1980).

In summary, T1D is associated with poor differentiation of BMMSC towards osteoblasts, and osteoblast toward osteocytes, as well as a reduction in cell viability of these three cell lines. On the other hand, T1D is associated with enhanced activity of osteoclasts. Both factors contribute to reduce bone mineral density and increase bone fragility and fracture risk. These effects can be triggered either by glucose itself and its derivative products or to the reduction in insulin signaling. However, the contribution of each factor is not clear yet, and further investigations are needed. This lack of information is especially critical in the case of osteocytes. Due to their relative inaccessibility, data regarding the effects of DM and glucose on osteocyte activity or cell survival is more limited than with other cell types. Due to the importance of glucose in bone homeostasis we think that further studies are needed to unveil the role of glucose in osteocyte differentiation and function.

3. ROS and Bone Health

ROS are radical and non-radical oxygen species that result from the partial reduction of oxygen (Ray et al., 2012a). Cellular ROS include the superoxide anion (O_2^-), hydrogen peroxide (H_2O_2), and hydroxyl radical ($OH\cdot$) that arise either as byproducts of aerobic metabolism or as defense mechanisms against xenobiotics or bacterial invasion (Schieber & Chandel, 2014). Under physiological conditions, ROS act as signaling molecules that are important for adaptation to changes in nutrient supply and the oxidative environment (J. Zhang et al., 2016). In fact, ROS have the capacity to target several transducer proteins, ion channels and transporters (Ca^{2+} and mitochondrial permeability transition pore [mPTP]), and thus, impact on

cell growth, differentiation, migration and death. In particular, ROS are also known to be involved in modulating tyrosine kinase phosphorylation pathways either directly by stimulating tyrosine kinase receptors or indirectly by inhibiting tyrosine phosphatases (Wauquier et al., 2009; D. Xu et al., 2002). Among the molecular pathways that can be regulated by ROS, we have to highlight NF- κ B, MAPKs, KEAP1-NRF2 and PI3K-AKT (J. Zhang et al., 2016) which have been shown to play a key role in bone differentiation. However, increased ROS levels or changes in their compartmentalization can dysregulate oxidation of proteins, lipids and nucleic acids (J. Zhang et al., 2016). Therefore, the ROS concentration is in a dynamic equilibrium and is modulated by cellular processes that produce and eliminate ROS.

Deregulation of the redox balance in cells and tissues is known as oxidative stress. Oxidative stress has been broadly described to play roles in aging and associated complications (Krause, 2007) such as degenerative diseases, cancer, cardiovascular diseases, ischemia–reperfusion injury, arthritis, diabetes and neurological disorders (Valko et al., 2007). Besides these pathologies, accumulating evidence suggests that bone biology is particularly affected by the redox balance. It seems that ROS production specially promotes bone resorption and oxidative stress has been linked to several bone pathogenesis including osteoporosis, bone tumour development, diabetes-induced bone complications and joint inflammatory diseases.

Because osteoclasts and immune cells such as macrophages and dendritic cells share some common features, it seems feasible that ROS can contribute to osteoclast activation, and therefore its role in osteoclast has also been investigated. In primary mouse bone marrow stromal cells (BMSCs) and calvaria osteoblasts increased intracellular ROS levels mediates ERK phosphorylation and nuclear translocation. Once active, ERK induce *RANKL* mRNA and protein expression (Bai et al., 2005). Likewise, ROS activates transcription factor 3 (ATF-3) which contributes to increased gene expression of *RANKL* (J. R. Chen et al., 2008). Further analysis also demonstrated that ROS promote phosphorylation of cAMP response element-binding protein (CREB)/ATF-2 and its binding to the CRE domain in the *RANKL* promoter region (Bai et al., 2005). Secreted *RANKL* binds to its cognate receptor *RANK* to induce NF- κ B activation, leading to osteoclast differentiation, activation and maturation. In osteoclast ROS production is needed for the activation of *RANKL*-induced osteoclastogenesis (N. K. Lee et al., 2005) while enhancing antioxidant systems of osteoclasts inhibits osteoclastogenesis (Lean et al., 2005). In ovariectomised mice, oxidative stress and T-cell activation induce the production of TNF α , a cytokine that promotes osteoclast differentiation. This effect might

contribute to the mechanisms underlying bone loss during menopause (Grassi et al., 2007).

On the other hand, oxidative stress suppresses bone formation by inhibiting osteoblast differentiation. Hydrogen peroxide-induced oxidative stress suppresses the osteoblastic differentiation process in primary mouse BMSCs and reduces alkaline phosphatase (ALPL) activity, and type I collagen production (LIU et al., 2004). In these studies, nuclear phosphorylation of the transcription factor RUNX2 and colony-forming unit-osteoprogenitor (CFU-O) formation also were reduced (Arai et al., 2007). It seems that ROS also influence osteoblast lifespan, since overexpression of ROS scavenging enzymes protects osteoblastic cells from ROS-induced apoptosis (Linares et al., 2009). The complete molecular mechanisms by which ROS hamper osteoblast differentiation are still unclear, however, it is known that H_2O_2 stimulates ERK1/2 phosphorylation as well as phospholipase C- γ 1 and ERK-dependent NF- κ B activation, resulting in impaired osteoblastic differentiation (Bai et al., 2004). Moreover, in conditions of oxidative stress, as occurs with aging or estrogen deficiency, ROS phosphorylates p66shc. Active p66shc acts as a scaffold and promotes the association between FOXO transcription factors and β -catenin, diverting the pool of β -catenin. By decreasing β -catenin levels, ROS inhibits Wnt-induced osteoblastic gene expression and can play a role in causing increased osteoblast and osteocyte apoptosis (Manolagas & Almeida, 2007). Conversely, ROS induce chondrocyte terminal differentiation and hypertrophy, a crucial step for endochondral ossification (Morita et al., 2007).

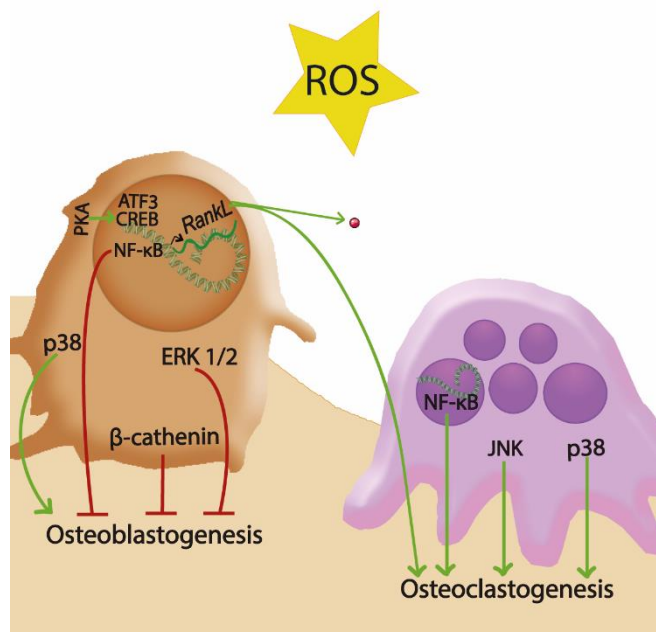


Figure 15. Effects of ROS on bone. ROS induce osteoclast activity through the activation of NF- κ B (NF- κ B, nuclear factor- κ B), JNK (Jun N-Terminal Kinase) and p38 signalling pathways. Moreover, ROS inhibit bone formation through NF- κ B (NF- κ B, nuclear factor- κ B), ERK1/2 and β -catenin molecular pathways.

Because of the crucial roles of ROS and oxidative stress in bone turnover, the potential use of antioxidants as treatments for osteoporosis and bone inflammatory diseases would be of major interest. However, as the role of ROS in osteogenesis is not fully understood, further studies will be needed to investigate whether antioxidant treatment strategies might be beneficial or detrimental to bone health. Such strategies could strongly impact morbidity and mortality, as well as the social and economic burden associated with osteoporosis



HYPOTHESIS AND OBJECTIVES

Glucose supply and cell metabolism regulates osteocyte differentiation by activating transcriptional programs.

OBJECTIVES

The main objective of this thesis is to determine the key factors that regulate the osteocytic differentiation, as well as understanding the role of glucose metabolism in bone cell differentiation.

• Objective 1: Study the role of glucosa in osteocytic differentiation. To achieve this, we define the following objectives:

- Determine the influence of glucose concentration in osteocyte differentiation.

- Identify the molecular pathways that connect the metabolism with osteocyte differentiation.

- Evaluate the role of PGC1 α in osteocyte differentiation.

• Objective 2: Analyze the role of ROS and NRF2 in osteocyte differentiation.

- Analyze the effect of ROS in osteocyte differentiation.

- Analyze the activity of NRF2 pathway during osteocyte differentiation.

- Evaluate the effect of NRF2 in osteocyte differentiation.



RESULTS

CHAPTER I:

GLUCOSE RESTRICTION ACTIVATES PGC-1 α TO PROMOTE OSTEOCYTE DIFFERENTIATION

1. Glucose restriction promotes osteocyte differentiation.

Glucose is a major source of energy for osteoblasts, but as they differentiate, maintaining an adequate nutrient supply results challenging. We hypothesize that it could constitute a signal to induce osteoblast-to-osteocyte transition. In consequence, we investigated the effects of different glucose concentrations on bone cell specification. We differentiated the pre-osteocytic IDG-SW3 cell line with differentiation culture medium containing 1, 5 or 25 mM glucose. We observed that selected glucose concentrations did not affect cell viability (Figure 1 A-B) or proliferation of IDG-SW3 cells (Figure 1 C)

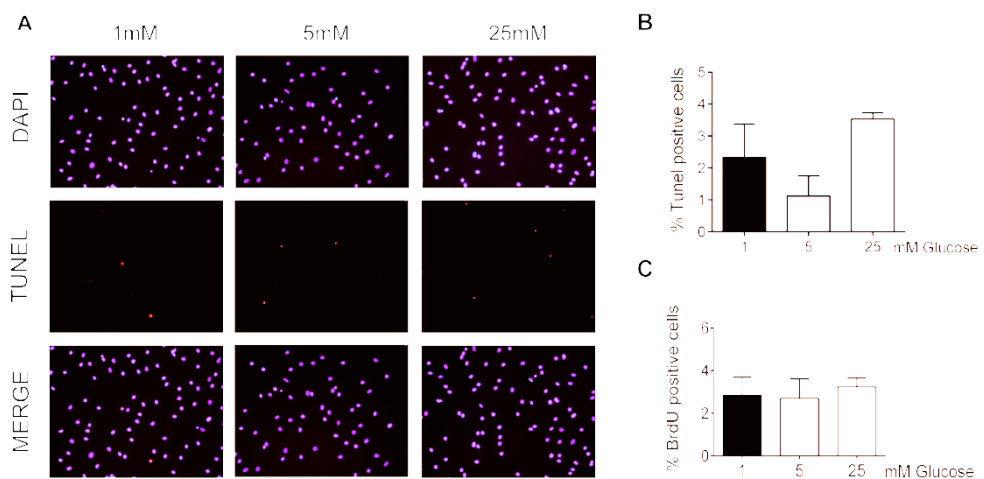


Figure 1. Glucose supply does not affect cell proliferation neither viability. (A and B) TUNEL staining of IDG-SW3 differentiated for 14 days in the presence of 1, 5 or 25 mM glucose. Representative images (A) and quantitative analysis (B) of TUNEL staining. Results are plotted as mean \pm SEM of three independent experiments. (C) Proliferation rate of IDG-SW3 differentiated for 14 days in presence of 1, 5 or 25 mM glucose. Results are expressed as percentage of BrdU+ cells. Data are plotted as mean \pm SEM of three independent experiments.

Confluent IDG-SW3 cells differentiated into osteocytes after 21 days in culture at 37°C. At day 14 of differentiation, IDG-SW3 cells start to express osteocyte markers, so they can be considered as early osteocytes (Woo et al., 2011). Therefore, we followed IDG-SW3 cells differentiation from day 0 to day 14 to analyze the first steps of osteocyte differentiation. Alkaline phosphatase and Alizarin Red staining showed the ability of IDG-SW3 cells to differentiate into mature osteoblasts and revealed a decrease in the formation of calcium deposits (Alizarin Red) when cultured in 25 mM glucose (Figure 2 A).

To facilitate the follow-up of the osteoblast-to-osteocyte transition, IDG-SW3 cells carry a *Dmp1*-GFP reporter, so at the stage of early osteocyte, they start to express GFP. Our data showed a negative correlation between osteocytic *Dmp1*-GFP expression and glucose supply. Low glucose supply enhanced expression of *Dmp1*-GFP. On the contrary, high glucose concentrations hampered *Dmp1*-GFP expression (Figures 2 A-B).

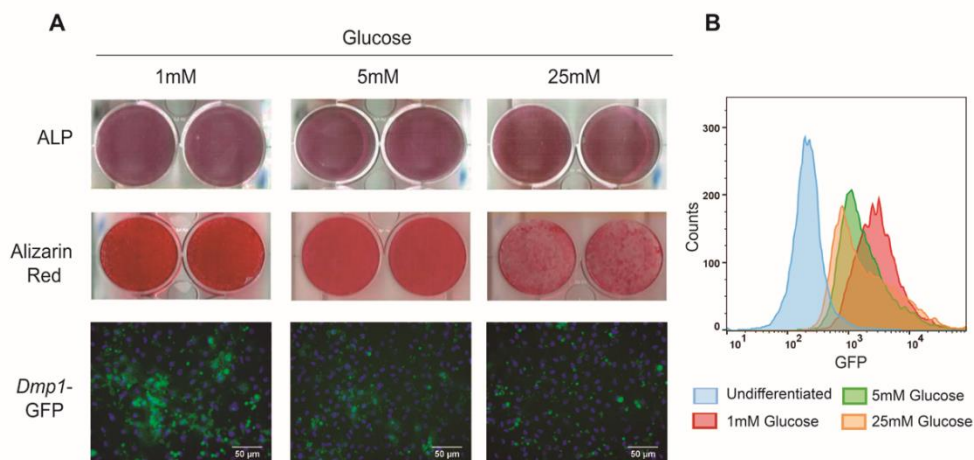


Figure 2. Effect of glucose supply in osteocyte differentiation. (A) Representative images of alkaline phosphatase staining (ALP), Alizarin Red staining and visualization of *Dmp1*-GFP expression in IDG-SW3 differentiated for 14 days in the presence of 1, 5 or 25 mM glucose. Cell nuclei were stained with DAPI (blue). (B) Flow cytometry analysis of *Dmp1*-GFP expression in IDG-SW3 undifferentiated and differentiated for 14 days in the presence of 1, 5 or 25 mM glucose.

To characterize further the induced phenotype, we analyzed the expression of gene markers for osteoblasts and osteocytes. As it has been previously described, mRNA levels of osteoblastic genes (*Alpl*, *Col1a1*, *Bglap* or *Atf4*) peaked at the 7th day and decreased thereafter, whereas expression osteocytic markers increased at day 14 (Figure 3). In our study, we found that a high glucose regime reduced the levels of osteoblastic genes, such as *Bglap*, *Osterix* or *Dkk1*. More importantly, glucose restriction significantly increased the expression of the osteocyte markers *Dmp1* and *Fgf23* (Figure 3).

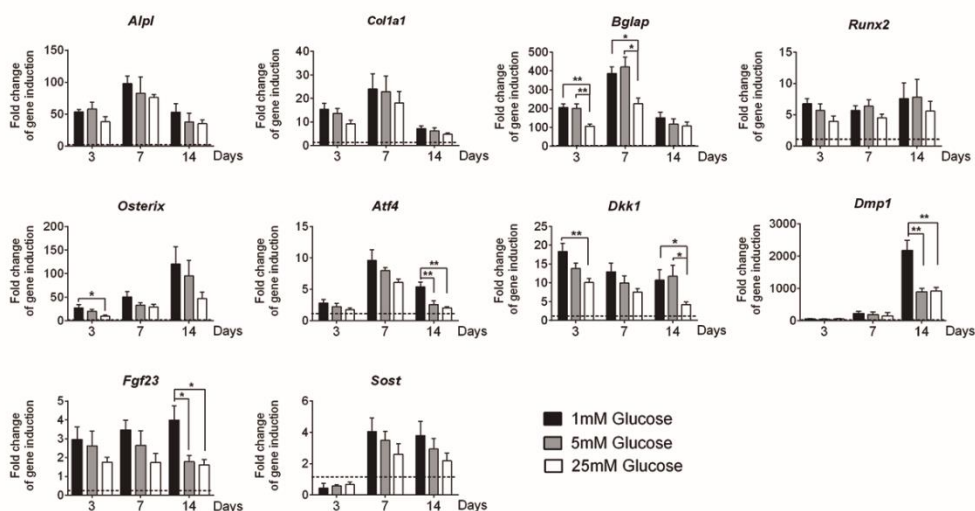


Figure 3. Gene expression profiling during IDG-SW3 differentiation under different glucose regimes. Quantification of mRNA expression of osteoblast and osteocyte gene markers during IDG-SW3 differentiation (at 3, 7 and 14 days) in the presence of 1, 5 and 25 mM glucose. mRNA levels were measured by RT-qPCR and normalized to *Tbp* expression. Results are plotted as expression relative to undifferentiated IDG-SW3 or osteocytes cultured in 5 mM glucose (mean \pm SEM of five to seven independent experiments). * p <0.05, ** p <0.01 and *** p <0.001 using one-way ANOVA.

Although IDG-SW3 cells maintain their capacity to differentiate, they are an immortalized cell line, therefore account with several drawbacks linked to these models. Therefore, we wonder whether the effects shown in IDG-SW3 cells would be replicated by a more physiological model. So, we investigated the effect of glucose concentration in gene expression profile of osteocytes (Figure 4 A) and bone organotypic cultures (Figure 4 B) maintained for 4 and 5 days respectively, under different glucose regimes. As with IDG-SW3 cells, low-glucose media increased expression of some osteocytic genes (*Dkk1*, *Dmp1*, *Fgf23* or *Sost*) in both models.

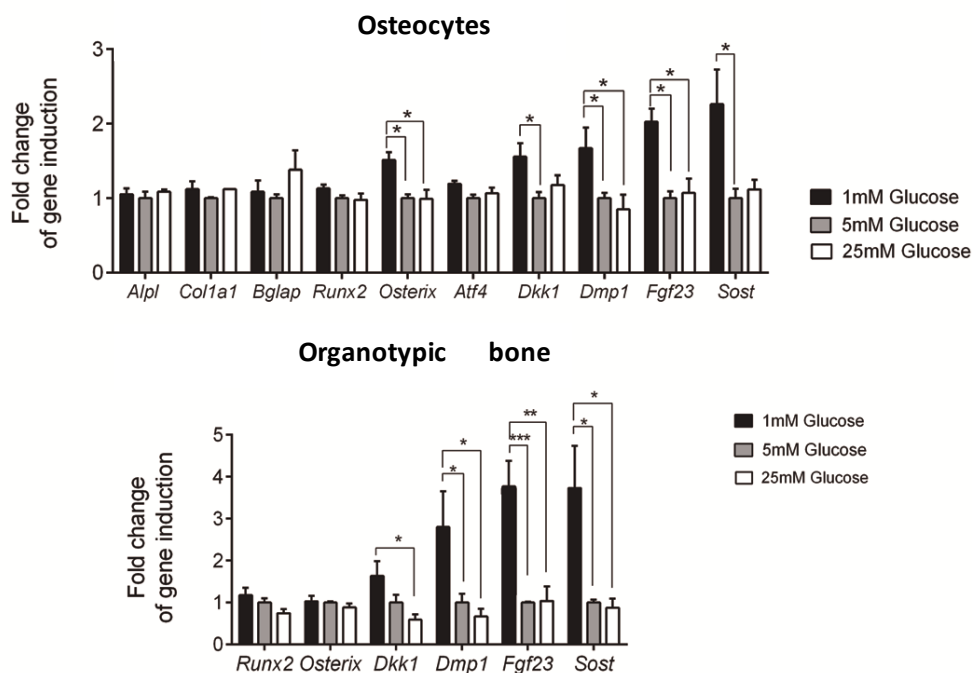


Figure 4. Impact of glucose supply in primary cultures. Quantification of mRNA expression levels in (A) primary osteocytes and (B) organotypic cultures from mouse femur maintained in the presence of 1, 5 or 25 mM glucose for 4 and 5 days respectively. Results are plotted as expression relative to in 5 mM glucose media. mRNA levels were measured by RT-qPCR and normalized to *Tbp* expression. Results plot as mean \pm SEM of five to seven independent experiments. * $p < 0.05$, ** $p < 0.01$ and *** $p < 0.001$ using Student's t-test.

The effects of glucose supply observed could be attributed to differences in osmotic pressure of the different culture mediums. Therefore, we compared the effects of changes in osmotic pressure induced by mannitol in the transcriptional program of IDG-SW3 cells. We conclude that the effects of distinct glucose concentrations in the osteocytic transcriptional program were independent of changes in the osmotic pressure (Figure 5). Altogether, these data demonstrated that glucose restriction favors osteocytic gene expression.

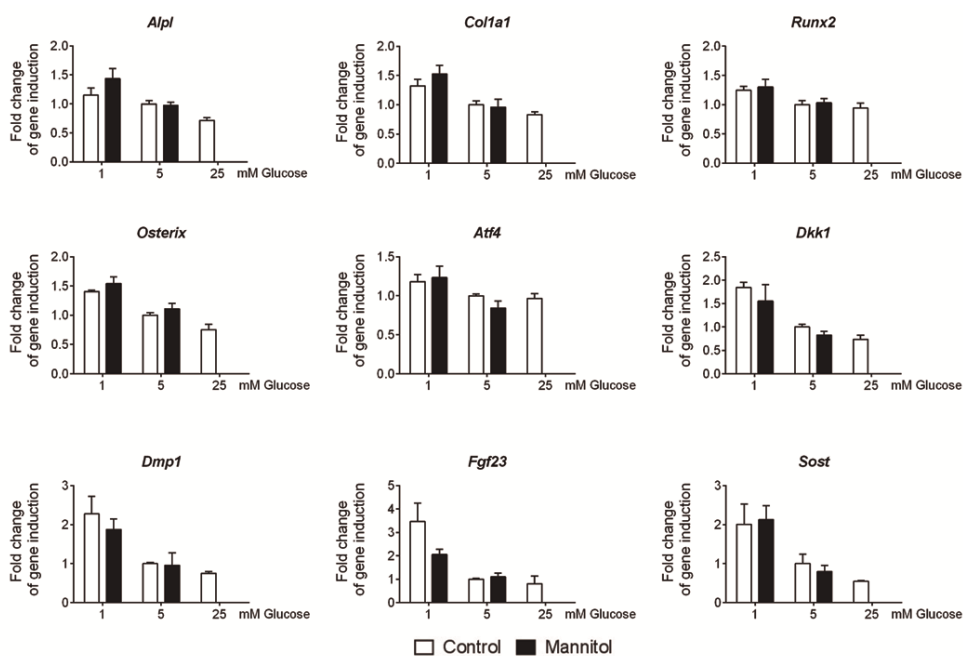


Figure 5. Effect of osmotic pressure in osteocyte differentiation. Quantification of mRNA expression levels in IDG-SW3 cells differentiated in the presence of 1, 5 or 25 mM glucose or in the presence of 1mM glucose plus 24 mM mannitol and 5 mM glucose plus 20 mM mannitol. Results are plotted as expression relative to IDG-SW3 cultured in 5 mM glucose. mRNA levels were measured by RT-qPCR and normalized to *Tbp* expression. Results plot as mean \pm SEM of six independent experiments. * $p < 0.05$, ** $p < 0.01$ and *** $p < 0.001$ using Student's t-test.

2. Glucose supply modifies osteoblast and osteocyte metabolism.

During differentiation, osteoblasts suffer a metabolic reprogramming. Therefore, we aimed to understand the effect of different glucose concentrations on the metabolism of osteocyte-like cells. We observed that IDG-SW3 cells differentiated in low glucose conditions had decreased intracellular ATP levels compared to normoglycemia or hyperglycemia, which suggests a compromised energy supply (Figure 6 A). Osteoblast are highly glycolytic cells that undergoes aerobic glycolysis even in the presence of oxygen. One of the consequences of this process is the production of lactate. In consequence, we assayed lactate released by IDG-SW3 cells during the initial steps of differentiation (24 hours) and after complete differentiation (14 days). As expected, either at 24 h or after differentiation, low glucose medium reduced the amount of lactated released by IDG-SW3, while high glucose regime enhanced lactate production (Figure 6 B). For a further

characterization of metabolic reprogramming, we also analyzed glucose uptake capacity after differentiation for 14 days in 1, 5 and 25 mM glucose. Glucose uptake was tested at 10 μ M glucose for all conditions. Low glucose exposure significantly increased the uptake capacity for glucose whereas glucose enriched media decreased it (Figure 6 C).

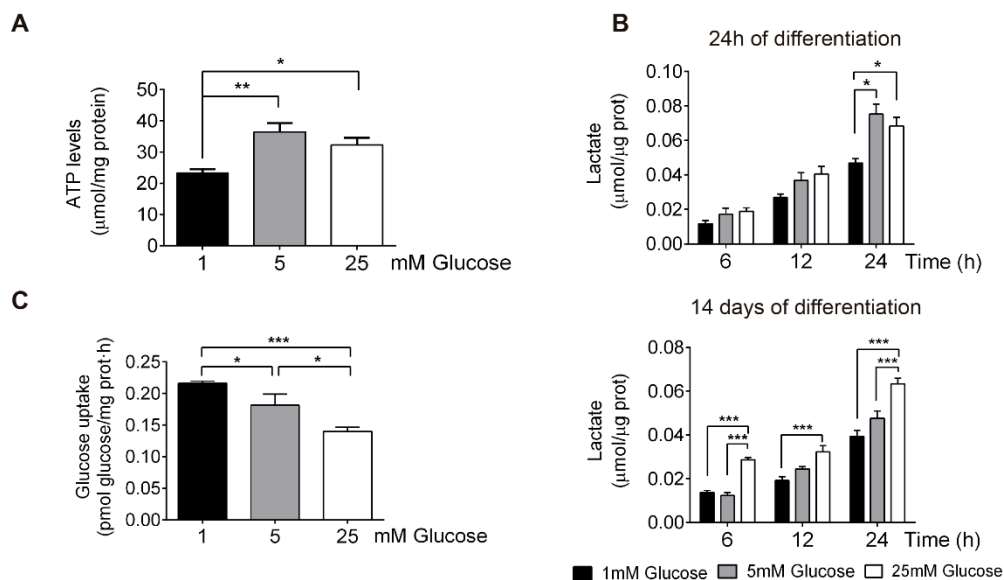


Figure 6. Metabolic profile induced by glucose supply. (A) ATP levels in IDG-SW3 after 14 days of differentiation in the presence of 1, 5 or 25 mM glucose. (B) Quantification of lactate release in predifferentiated IDG-SW3 cultured in 1, 5 or 25 mM glucose media for 24 hours, and in IDG-SW3 differentiated for 14 days in the presence of 1, 5 or 25 mM glucose. (C) Determination of the maximal uptake capacity for glucose in IDG-SW3 cells differentiated for 14 days in the presence of 1, 5 or 25 mM glucose.

We also investigated the bone cell metabolism in primary osteoblasts cultured for 10 days with different glucose concentrations. In this case, mature primary osteoblasts cultured in 1mM glucose were still able to maintain ATP levels (Figure 7 A). However, as IDG-SW3 cells, osteoblast cultured under 25mM glucose released higher levels of lactate (Figure 7 B). Again, glucose uptake capacity in osteoblasts behave in a similar way than in IDG-SW3, as it was found increased under low glucose conditions (Figure 7 C). These data suggested a sparing effect in glucose-restricted conditions, maximizing uptake and reducing lactate release and vice versa under hyperglycemic conditions. These adaptations allow mature osteoblasts in culture to maintain energetic balance and anaerobic glycolysis even at 1mM glucose.

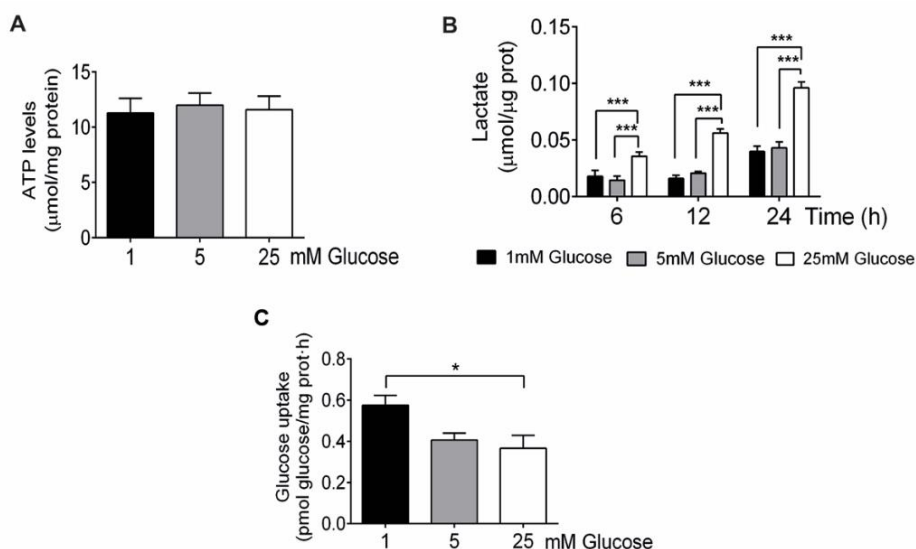


Figure 7. Metabolic profile in primary mature osteoblasts under different glucose supplies.

(A) ATP levels in osteoblasts after 10 days of differentiation in the presence of 1, 5 or 25 mM glucose. (B) Quantification of lactate release in osteoblasts differentiated for 10 days in the presence of 1, 5 or 25 mM glucose. (C) Determination of the maximal uptake capacity for glucose in osteoblast differentiated for 10 days in the presence of 1, 5 or 25 mM glucose. Glucose uptake was tested at 10 μ M glucose for all conditions.

In order to understand better the differences observed in ATP and lactate production, we evaluated mitochondrial respiration in intact, differentiated IDG-SW3 cells under different glucose supplies. We determined routine O_2 consumption, leak state (uncoupled respiration after addition of oligomycin into the assay), electron transfer capacity (after FCCP addition, (ETS)) and coupled respiration. Surprisingly, we did not find significant differences in respiratory parameters among the three groups; however we observed a slightly increase in routine respiration when cells were cultured with 25 mM glucose (Figure 8 A). These data indicate that IDG-SW3 cells were able to maintain O_2 consumption under glucose-restriction conditions. We also measured mitochondrial membrane potential by flow cytometry. As expected, it was also unmodified by the different glucose regimes. Therefore, these data suggested that cells adapt to meet energy demands by increasing glucose uptake and through the diversion of glucose to mitochondrial respiration.

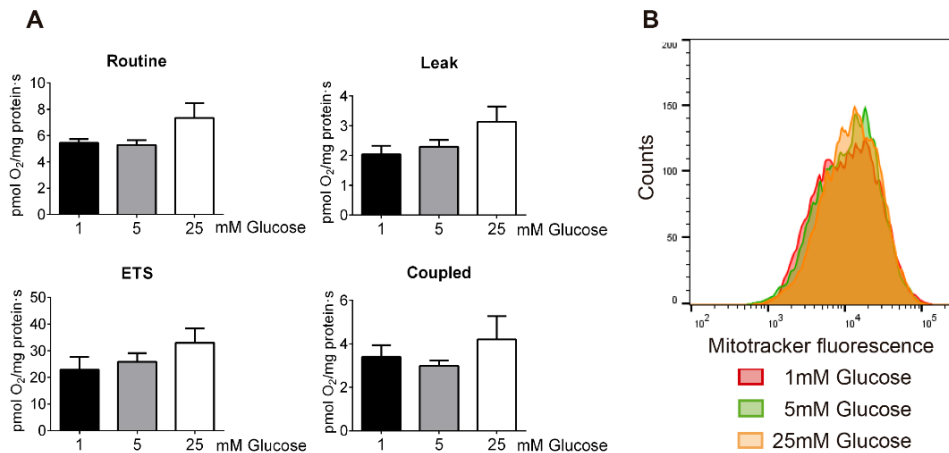


Figure 8. Mitochondrial respiration in IDG-SW3 cells under different glucose supply. (A) Determination of routine oxygen consumption, leak respiration (uncoupled), electron transfer capacity (ETS) and coupled respiration of IDG-SW3 differentiated for 14 days in the presence of 1, 5 or 25 mM glucose. 700,000 IDG-SW3 cells were incubated in the respirometry chamber with 1, 5, or 25 mM glucose in α -MEM without FBS during the analysis. All results were expressed relative to protein content. Results are plotted as mean \pm SEM of four to eight independent experiments. (B) Flow cytometry analysis of IDG-SW3 cells differentiated for 14 days in the presence of 1, 5 or 25 mM glucose and labeled with Mitotracker-Deep-Red. * $p < 0.05$, ** $p < 0.01$ and *** $p < 0.001$ using one-way ANOVA.

We performed the same experiments of oxygen consumption in osteoblast cultured for 7 days with different glucose concentration. As for IDG-SW3, differences in respiratory parameters between osteoblast cultured in 1 mM and 5 mM glucose were not significant. Similarly, we observed increased routine respiration in cells cultured with 25 mM glucose. Moreover, in this case we observed a significant increase of leak respiration in osteoblast cultured with 25 mM glucose (Figure 9). These results evidence that osteoblasts, as IDG-SW3 cells, were able to maintain O₂ consumption under low glucose conditions.

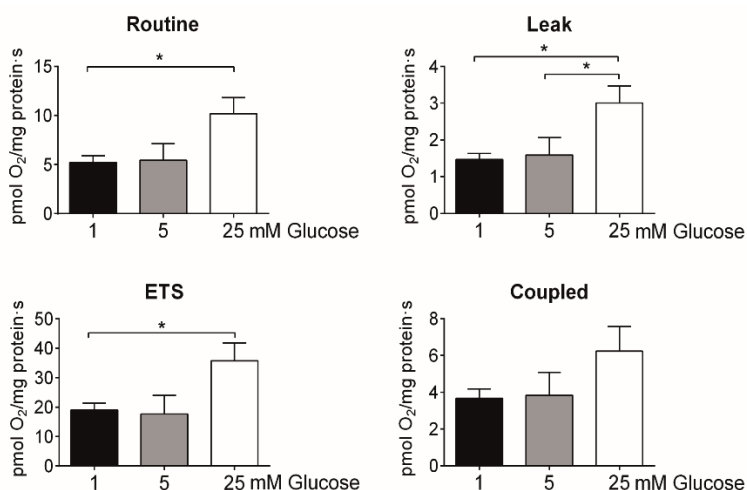


Figure 9. Oxygen consumption in osteoblasts under different glucose supply. (A) Determination of routine oxygen consumption, leak respiration (uncoupled), electron transfer capacity (ETS) and coupled respiration of osteoblast differentiated for 7 days in the presence of 1, 5 or 25 mM glucose. 700,000 osteoblasts were incubated in the respirometry chamber with 1, 5, or 25 mM glucose in α -MEM without FBS during the analysis. All results were expressed relative to protein content. Results are plotted as mean \pm SEM of four to eight independent experiments.

3. Glucose restriction modifies mitochondrial content and morphology.

In order to further identify the changes in energy metabolism induced by glucose supply, we quantified the expression of genes involved in glycolysis and mitochondrial function. Glucose is transported into bone cells via facilitative glucose transporters (GLUT). Of all the existing isoforms, GLUT1 (*Slc2a1*) is by far the glucose transporter most expressed in IDG-SW3 and bone cells during the whole process of osteocyte specification (Figure 10 A) (referencia). In addition, different glucose concentrations did not induce a significant switch between GLUT family members (Figure 10 B). Different glucose conditions did not also alter the expression of solute transporters; however, it enhance the expression of glycolytic genes such as *Pfkfb3* and *Hk2* in IDG-SW3 cells (Figure 10 C). The expression of *Cox4i1* and the genes involved in mitochondrial fusion/fission *Mtf2* and *Opa1* did not show significant differences between distinct glucose regimes (Figure 10 C)

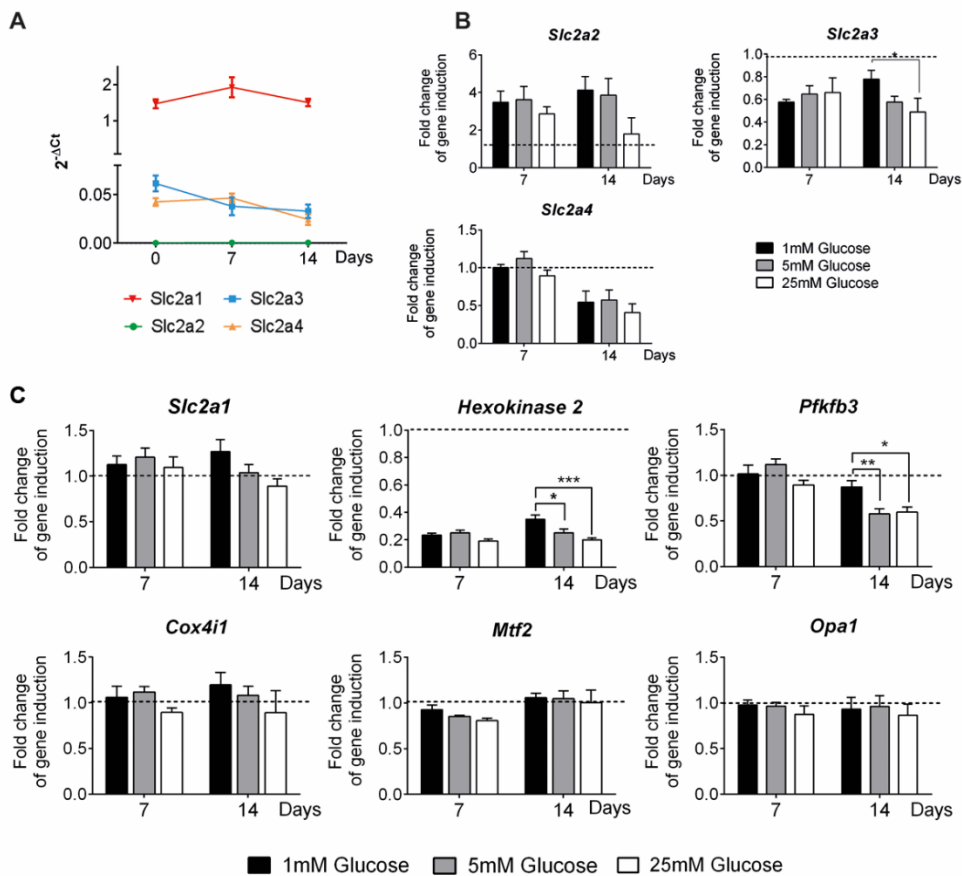


Figure 10. Figure 11. Changes in glycolytic gene expression and mitochondrial function induced by different glucose concentrations along osteocytic differentiation. (A) mRNA expression levels of the different GLUT Family Members (SLC2a) in IDG-SW3 differentiated for 14 days in 5 mM glucose media. mRNA expression was quantified by RT-qPCR and normalized to *Tbp* expression. Results are plotted as $2^{-\Delta Ct}$ (mean \pm SEM of six independent experiments). (B) mRNA expression levels of *Slc2a2*, *Slc2a3* and *Slc2a4* during IDG-SW3 differentiation in 1, 5 and 25 mM glucose media. mRNA levels were quantified by qRT-PCR, normalized by *Tbp* and plotted as expression relative to undifferentiated IDG-SW3 (mean \pm SEM of six independent experiments). (C) mRNA expression levels of glycolytic and mitochondrial genes in IDG-SW3 differentiated for 14 days in the presence of 1, 5 or 25 mM glucose. mRNA expression levels were measured by RT-qPCR and normalized to *Tbp* expression. Results were plotted as expression relative to undifferentiated IDG-SW3 (mean \pm SEM of six independent experiments).

Similar results were obtained in osteoblast, where low glucose concentrations upregulated the expression of glycolytic genes (*Pfkfb3* and *Hk2*) but did not alter the expression of the glucose transporter *Slc2a1* neither mitochondrial genes (*Cox4i1*, *Mtf2* and *Opa1*) (Figure 11).

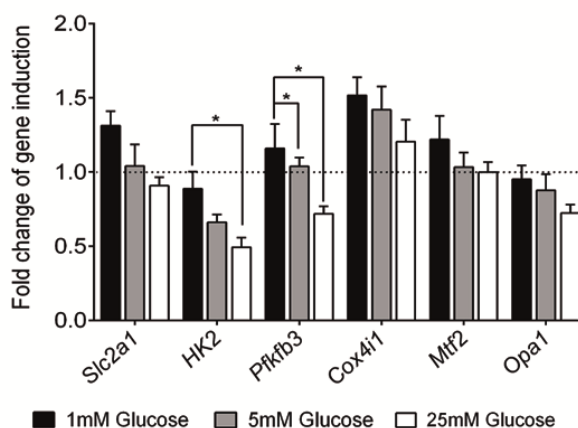


Figure 11. Changes in glycolytic gene expression and mitochondrial function induced by different glucose concentrations in osteoblasts. mRNA expression levels of glycolytic and mitochondrial genes in primary osteoblasts differentiated for 10 days in the presence of 1, 5 or 25 mM glucose. Results are plotted as expression relative to undifferentiated primary osteoblasts (mean \pm SEM of six independent experiments).

Since mitochondria are remarkable dynamic organelles that respond to changes in energy demands, we wondered whether glucose concentration could modify mitochondrial content and function. In differentiated IDG-SW3, reduced glucose supply increased the ratio of mitochondrial DNA (mtDNA) respective to nuclear DNA (Figure 12 A). This increase in mtDNA was consistent with an increase in the protein levels of members of the different OXPHOS complexes (Figure 12 B). Respiratory function not only depends on mitochondrial content but also on mitochondrial organization. Emerging evidence showed that mitochondria continuously adjust their shape, size and network organization through fusion/fission events, to regulate their function (Galloway et al., 2012). Confocal images showed dramatic differences in mitochondrial structure and network among the three conditions. IDG-SW3 cells differentiated in 1 mM glucose media arranged their mitochondria in elongated tubules, with higher branching, forming reticular networks (Figure 12 C). In contrast, hyperglycemic conditions increased mitochondrial the formation of ring-like structures a characteristic of mitochondrial fragmentation processes (Figure 12C).

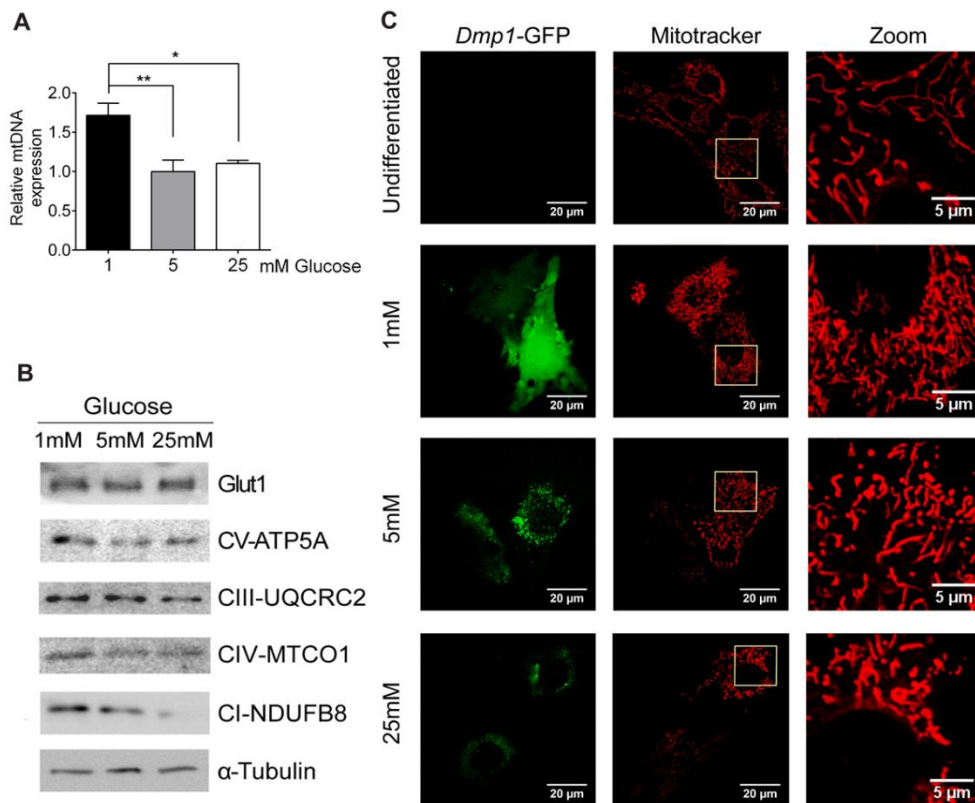


Figure 12. Mitochondrial function in osteocyte differentiation under different glucose concentrations. (A) Quantification of mtDNA (tRNA-Glu) in IDG-SW3 differentiated for 14 days in the presence of 1, 5 or 25 mM glucose. mtDNA copy number was measured by qPCR and normalized relative to nuclear DNA (Dmp1 and Fgf23). Results are plotted as mean \pm SEM of six independent experiments. (C) Immunoblot analysis of the expression of Glut1 and mitochondrial complexes in IDG-SW3 differentiated for 14 days in the presence of 1, 5 or 25 mM glucose. (D) Visualization of mitochondrial in IDG-SW3 differentiated for 14 days in the presence of 1, 5 or 25 mM glucose. Dmp1-GFP was visualized and mitochondria were stained with Mitotracker-Deep-Red. * $p < 0.05$, ** $p < 0.01$ and *** $p < 0.001$ using one-way ANOVA.

In a similar way, low glucose concentrations increased the ratio of mitochondrial DNA (mtDNA) respective to nuclear DNA (Figure 13 A) and the protein levels of members of the different OXPHOS complexes (Figure 13 B) in osteoblast cell cultures. In these cells, glucose also modify mitochondrial morphology. Confocal images demonstrated that osteoblast differentiated in 1 mM glucose media formed bigger reticular networks of elongated mitochondria. On the other hand, hyperglycemic conditions increased ring-like structures (Figure 13 C).

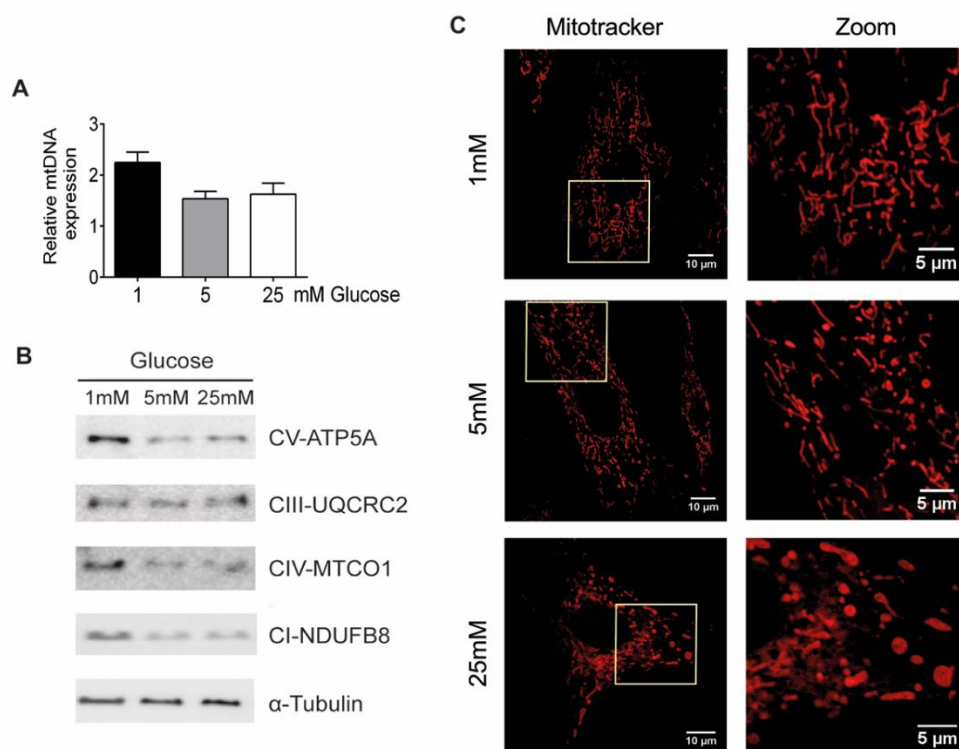


Figure 13. Mitochondrial function in osteoblast primary cell cultures. (A) Quantification of mtDNA in primary osteoblasts differentiated for 10 days in the presence of 1, 5 or 25 mM glucose. Results are plotted as expression relative to undifferentiated primary osteoblasts (mean \pm SEM of four independent experiments). (B) Analysis of the levels of mitochondrial complexes in primary osteoblasts differentiated for 10 days in the presence of 1, 5 or 25 mM glucose. (C) Visualization of mitochondria in primary osteoblasts differentiated for 10 days in the presence of 1, 5 or 25 mM glucose. * $p < 0.05$, ** $p < 0.01$ and *** $p < 0.001$ using one-way ANOVA.

It has been demonstrated that elongated mitochondria are more resistant to mitophagy and more efficient at producing ATP through enhanced cristae density and ATP synthase dimerization (Gomes et al., 2011). In addition, it is known that ring-like and fragmented mitochondria structures arise from cellular stresses (Yu et al., 2006). Therefore, these data suggest that during osteocyte differentiation, glucose-restriction stimulates glycolytic pathways, increases mitochondrial DNA and efficiency in an effort to maintain ATP levels.

4. Glucose restriction effects on osteocytogenesis depend on AMPK

Nutrient starvation acts as a signal that activates AMPK and mTORC1 energy sensors (Carroll & Dunlop, 2017). Thus, we determined the activation state of signaling pathways likely to be involved in the metabolic and genetic reprogramming of osteocytes. We analyzed early activation of these pathways during the first hours of differentiation and after complete differentiation. In response to glucose-restriction, AMPK and its substrate ACC became phosphorylated in IDG-SW3 (Figures 14 A-B). Similarly, the stress kinase p38-MAPK was also activated either at 24 hours or after 14 days.

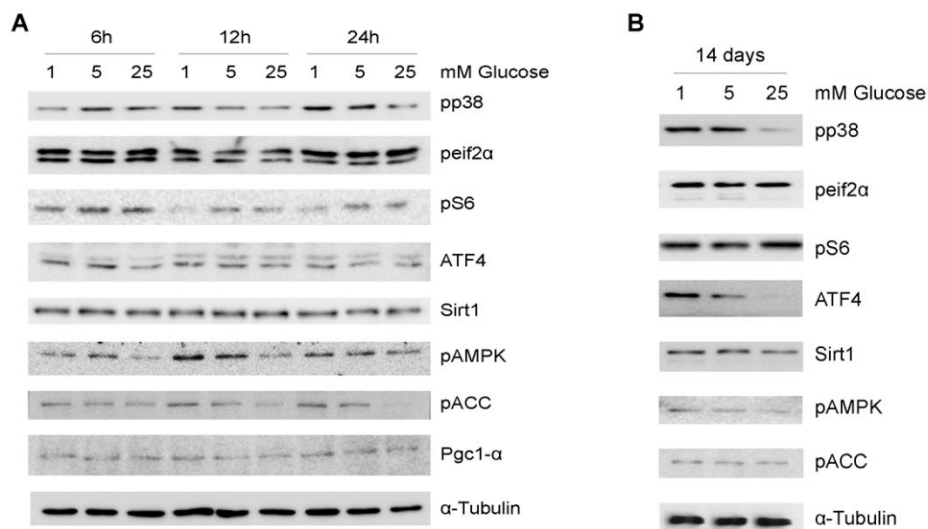


Figure 14. Signaling pathways involved in metabolic and genetic reprogramming of osteocytes. Immunoblots from IDG-SW3 cells (A) cultured in 1, 5 and 25 mM glucose media for 6, 12 and 24 hours or (B) after 14 days of differentiation in 1, 5 and 25 mM glucose media.

We also analyzed AMPK and mTORC1 pathways in osteoblast primary cultures, obtaining similar results than in IDG-SW3. Similarly, in osteoblasts, AMPK and its substrate ACC became phosphorylated in response to glucose-restriction (Figures 15 A-B). The stress kinase p38-MAPK was also activated either at 24 hours or after 14 days (Figures 15 A-B).

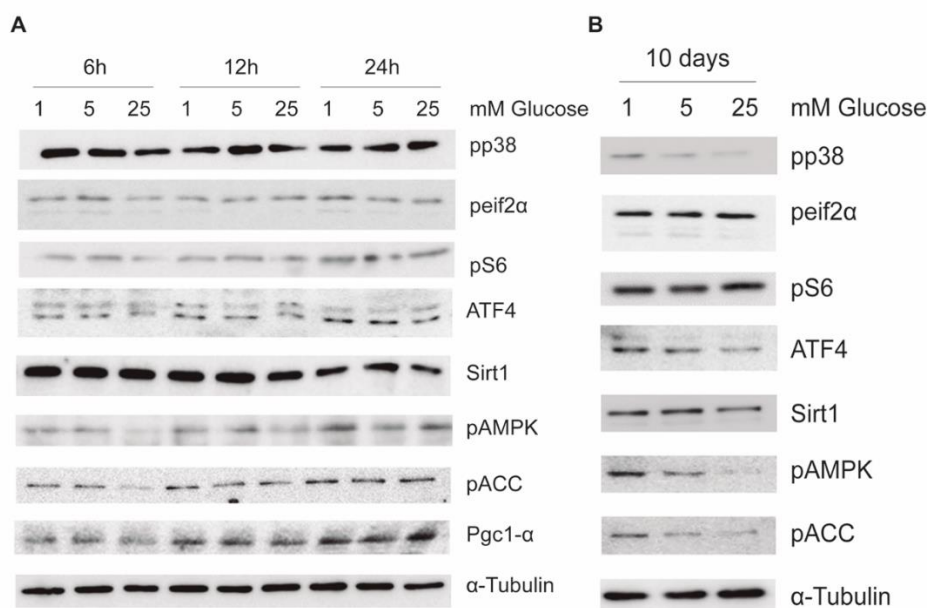


Figure 15. Signaling pathways involved in glucose restriction in osteoblasts. Immunoblots from primary osteoblasts (A) during the first 24 hours of differentiation in 1, 5 or 25 mM glucose media or (B) after 10 days of differentiation in 1, 5 and 25 mM glucose media.

Effects of AMPK exert its activity on mitochondrial biogenesis through the activation of PGC-1 (PGC-1 α and β) (Hardie, 2018). The PGC-1 family of transcriptional coactivators translate physiological signals into the expression of nuclear-encoded mitochondrial genes (Villena, 2015). The activity of PGC-1 family members is mainly regulated by post-translational, including phosphorylation by AMPK and p38 and deacetylation by SIRT1 (Fan et al., 2004; Gerhart-Hines et al., 2007; Jager et al., 2007). Therefore, to further characterize the role of AMPK/SIRT/PGC1 α/β pathways in osteocyte reprogramming and differentiation, we treated IDG-SW3 cells with different chemical modulators of these pathways. The activation of AMPK by Aicar during differentiation increased the expression of gene markers for osteoblasts (*Runx2* and *Osterix*) and osteocytes (*Dmp1*, *Fgf23* and *Sost*) (Figure 16). Similarly, the activation of SIRT1 by SRT2104 treatment induced the expression of late osteocyte markers (Figure 16) while its inhibition with sirtinol reduced the levels of *Osterix* and *Fgf23*. These results suggested that the activation of AMPK/SIRT1 enhances osteocytic differentiation. We also evaluated whether induction of mitochondrial fusion and elongation was sufficient for the activation of osteocyte transcription program. The chemical modulator Mdivi-1 inhibits mitochondrial fission and, in consequence, it increases the number of elongated mitochondria and their reticular network (Cassidy-Stone et al., 2008). Inhibition of

mitochondrial fission by Mdivi-1 during osteocytic differentiation only induced expression of *Sost* whereas reduced the expression of *Osterix* and *Dmp1* (Figure 16). These results suggest that mitochondrial reorganization is not a sufficient inducer of osteocytogenesis.

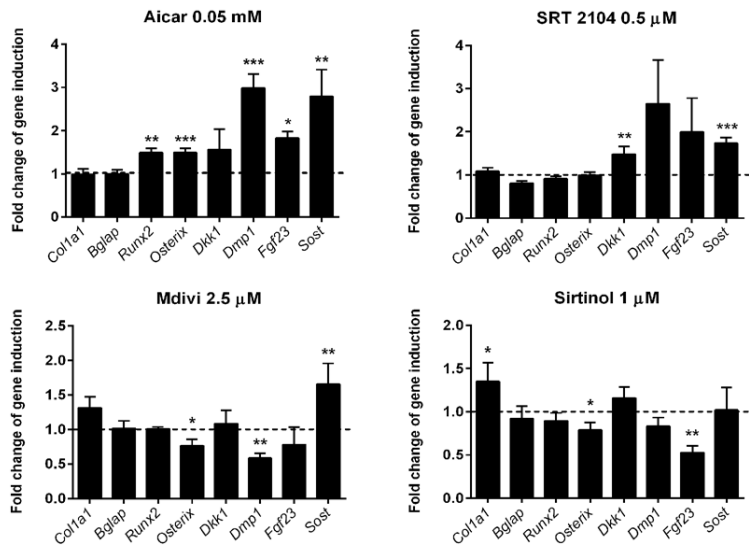


Figure 16. Activation of AMPK/SIRT/PGC1 α / β pathways induce osteocyte differentiation in IDG-SW3 cells. mRNA expression of osteoblastic and osteocytic genes in IDG-SW3 differentiated for 14 days in 5mM glucose and treated with 0.05mM Aicar (activator of AMPK), 0.5 μ M SRT2104 (activator of SIRT1), 1 μ M Sirtinol (inhibitor of SIRT1) and 2.5 μ M Mdivi (inhibitor of mitochondrial fission). mRNA levels were measured by RT-qPCR and normalized to *Tbp* expression. Results were plotted as expression relative to untreated IDG-SW3 (mean \pm SEM of five independent experiments).

We validate these results in bone organotypic cultures treated with the same chemical modulators of AMPK/SIRT/PGC-1 α / β pathways. The activation of AMPK by Aicar in bone organotypic cultures increased the expression of osteocyte genes (*Dmp1*, *Fgf23* and *Sost*) but did not modify the levels of osteoblast genes (*Runx2* and *Osterix*) (Figure 17). Likewise, the activation of SIRT1 by SRT2104 treatment induced the expression of late osteocyte markers but its inhibition with sirtinol did not cause significant changes in the expression of osteoblast neither osteocyte gene markers (Figure 17). These results confirmed that the activation of AMPK/SIRT1 is sufficient to induce osteocytic differentiation.

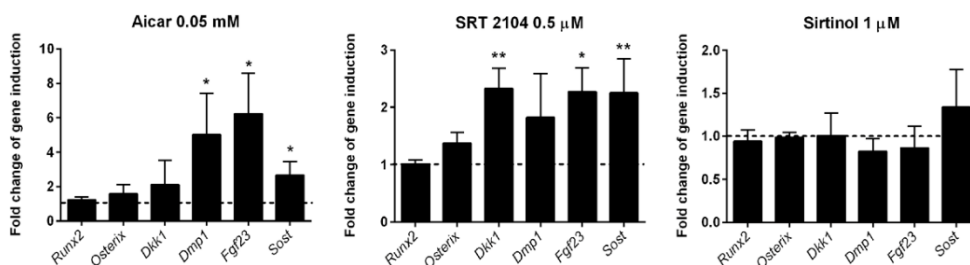


Figure 17. Activation of AMPK/SIRT/PGC1 α / β pathways induce osteocyte differentiation in bone organotypic cultures mRNA expression of osteoblastic and osteocytic genes in from mouse femur. Organotypic cultures were maintained in 5mM glucose media and treated with 0.05mM Aicar, 0.5 μ M SRT2104 and 1 μ M sirtinol for 5 days. mRNA levels were measured by RT-qPCR and normalized to *Tbp* expression. Results were expressed as gene expression relative to untreated organotypic cultures (mean \pm SEM of five independent experiments). *p<0.05, **p<0.01 and ***p<0.001 using Student's t-test.

5. PGC-1 enhances osteocytic differentiation in response to reduced glucose supply.

At this point, our results indicate that PGC-1 family of transcription factors have a relevant role in osteocyte differentiation. Therefore, we determined the expression of *Ppargc1a* and *b* genes during the osteoblast to osteocyte transition in IDG-SW3 cells. Proliferative IDG-SW3 cells expressed higher levels of *Ppargc1a* compared to *Ppargc1b*. Moreover, differentiated cells shifted further towards a major expression of *Ppargc1a* over *Ppargc1b* (Figure 18A). However, mRNA levels of *Ppargc1a* or *Sirt1* did not change among the three culture conditions in IDG-SW3 (Figure 18B)

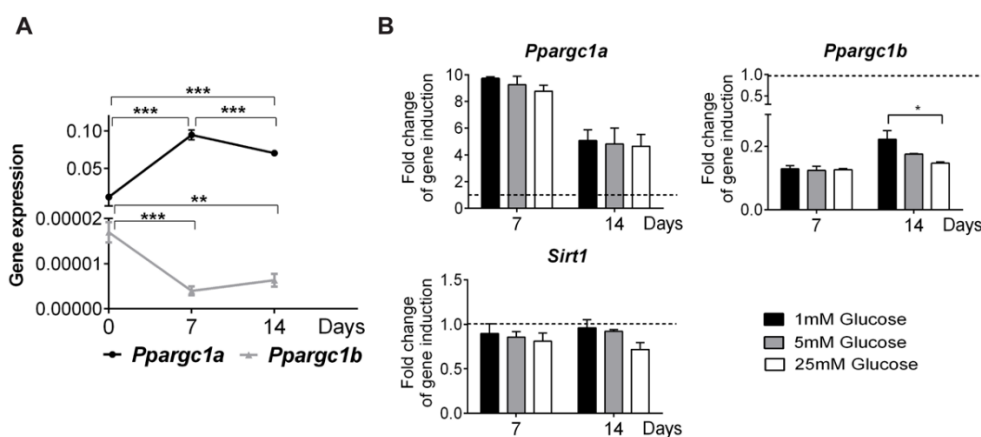


Figure 18. Expression of PGC-1 family of transcription factors during osteocytic differentiation. (A) mRNA expression levels of the different isoforms of PGC-1 in IDG-SW3

differentiated for 14 days in 5mM glucose media. mRNA expression was quantified by RT-qPCR and normalized to *Tbp* expression. Results are plotted as $2^{-\Delta\Delta Ct}$ (mean \pm SEM of six independent experiments). (B) mRNA expression levels of *Ppargc1a*, *Ppargc1b* and *Sirt1* during IDG-SW3 differentiation in 1, 5 and 25mM glucose media. mRNA levels were quantified by RT-qPCR, normalized by *Tbp* and plotted as expression relative to undifferentiated IDG-SW3 (mean \pm SEM of six independent experiments). * $p < 0.05$, ** $p < 0.01$ and *** $p < 0.001$ using Student's t-test.

Likewise, osteoblast presented 10-fold higher basal expression of *Ppargc1a* than *Ppargc1b*. But, in this case, glucose restriction induced *Ppargc1a* and *Ppargc1b* mRNA expression (Figure 19).

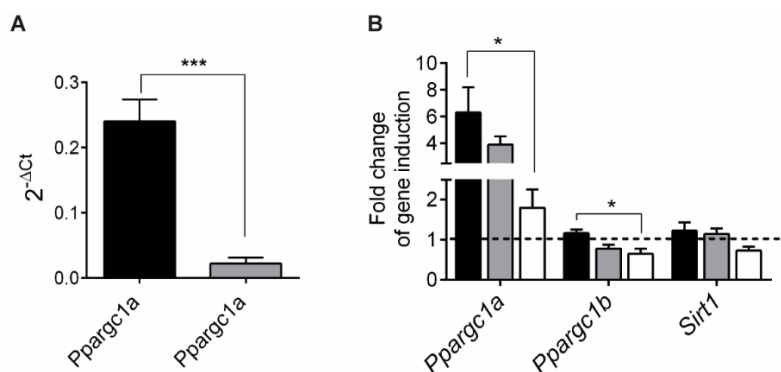


Figure 19. Expression of PGC-1 family in osteoblast. (A) mRNA expression levels of the different isoforms of PGC-1 in osteoblasts cultured with 5mM glucose media. mRNA expression was quantified by RT-qPCR and normalized to *Tbp* expression. Results are plotted as $2^{-\Delta\Delta Ct}$ (mean \pm SEM of five independent experiments). (B) mRNA expression levels of *Ppargc1a*, *Ppargc1b* and *Sirt1* in osteoblast differentiated with 1, 5 and 25mM glucose media for 10 days. mRNA levels were quantified by RT-qPCR, normalized by *Tbp* and plotted as expression relative to osteoblast cultured for 24h (mean \pm SEM of six independent experiments). * $p < 0.05$, ** $p < 0.01$ and *** $p < 0.001$ using Student's t-test.

Ppargc1a and *b* play redundant roles by regulating gene expression programs through their interaction with a variety of transcription factors such as NRF2, ERRA, PPARs, or MEF2. *In silico* analysis of the promoters of the osteocyte genes *Dmp1*, *Fgf23* and *Sost* revealed conserved potential binding sites for PGC-1 co-activated factors. We confirmed the recruitment of PGC-1 to these regulatory regions by chromatin immunoprecipitation (ChIP). Overexpression of PGC-1 α and its activation with Aicar increased PGC-1 α occupancy of *Fgf23* and *Sost* promoters in IDG-SW3 cells (Figure 20).

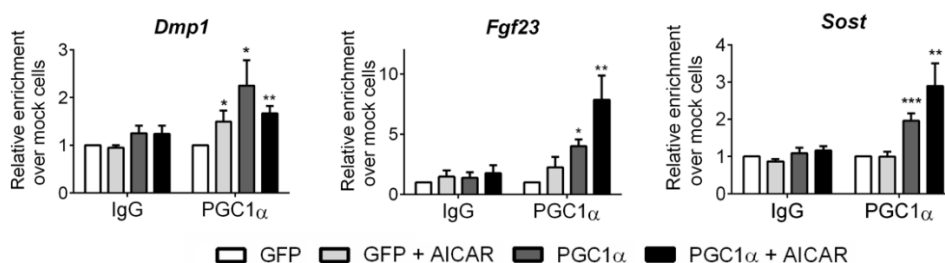


Figure 20. PGC1- α binds to osteocytic promoters. Chromatin immunoprecipitation of IDG-SW3 cells infected with control GFP or PGC-1 α expression vectors and differentiated in 5mM glucose media for 5 days in the presence or absence of 0.5mM Aicar. Results were normalized to input chromatin and plotted relative to untreated IDG-SW3 cells infected with control GFP vector (mean \pm SEM of four independent experiments). *P<0.05, **P<0.01 and ***P<0.001 using Student's t-test.

We then wonder whether the binding of PGC-1 α was able to induce the expression of osteocyte genes. Lentiviral overexpression of PGC-1 α in IDG-SW3 (Figure 21 A) and primary osteoblasts (Figure 21 B) increased mRNA levels of osteoblastic (*Col1a1*, *Bglap*, *Osx*) and osteocytic (*Dkk1*, *Fgf23* and *Sost*) genes.

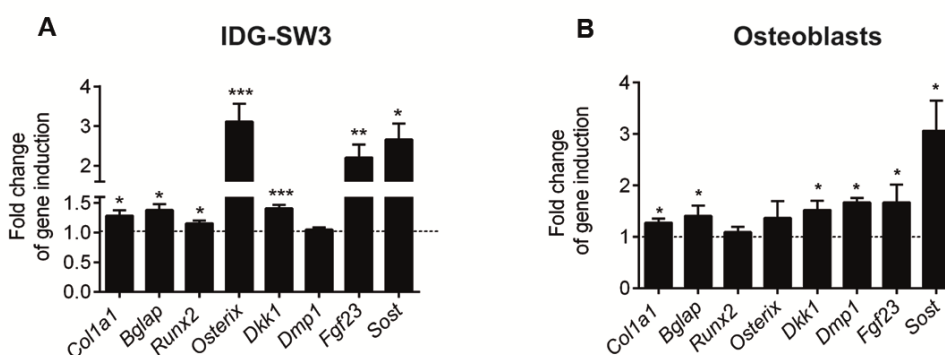


Figure 21. PGC-1 overexpression induce in osteocyte differentiation. mRNA expression levels of (A) IDG-SW3 cells and (B) primary osteoblasts infected with PGC-1 α expression vectors and differentiated in 5mM glucose media for 5 days. mRNA expression levels were measured by RT-qPCR and normalized to *Tbp* expression. Results were plotted as expression relative to cells infected with GFP vector (mean \pm SEM of six to eight independent experiments)

To further characterize the role of PGC-1 α/β in bone cells, we generated primary osteoblasts and osteocytes deficient in both isoforms. For the generation of those cell cultures, we obtained osteoblast and osteocytes from transgenic mice that harbor the alleles of *Ppargc1a* and *Ppargc1b* floxed. Then, cells were infected with CRE-recombinase or mocked vectors to generate knock-out and wild-types cells respectively. As expected, *Ppargc1a* and *Ppargc1b* mRNA levels were significantly reduced in both osteoblasts (Figure 22 A) and osteocytes (Figure 22 B). *Ppargc1a/b*

deletion did not affect either cell viability (Figure 22 C-D) or proliferation (Figure 22 E).

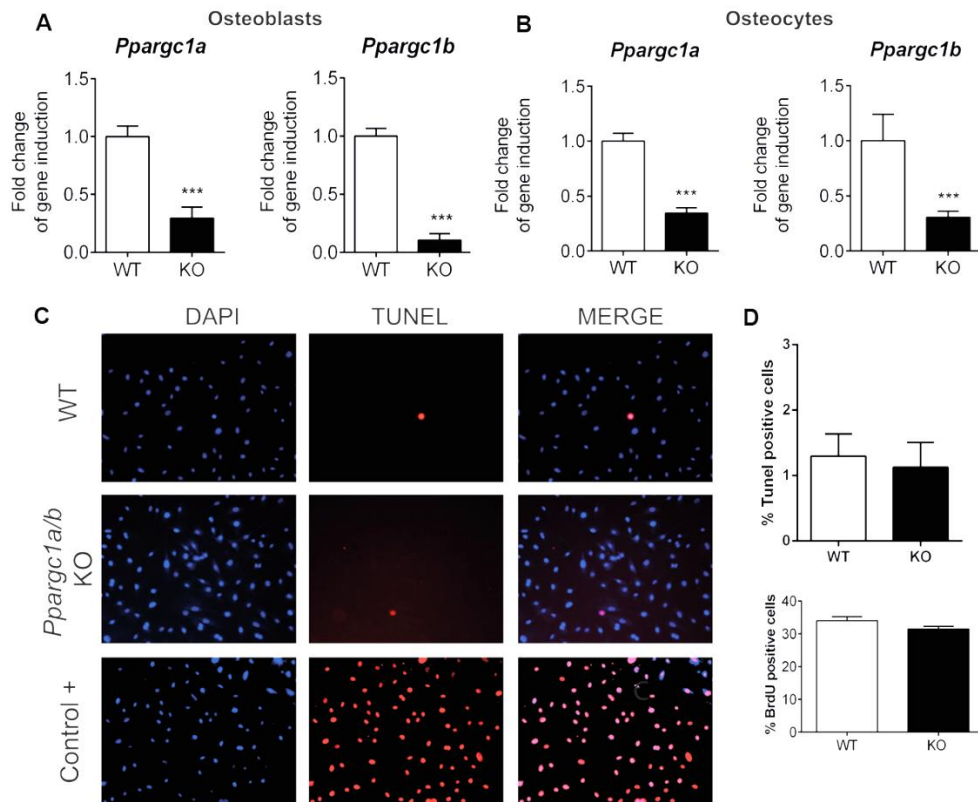


Figure 22. Loss of PGC-1 α/β does not affect cell viability. mRNA expression levels of *Ppargc1a* and *Ppargc1b* in primary osteoblast wild-type and KO for *Ppargc1a/b*. Results were plotted as mean \pm SEM of six independent experiments. (B) mRNA expression levels of *Ppargc1a* and *Ppargc1b* in primary osteocytes wild-type and KO for *Ppargc1a/b*. Results were plotted as mean \pm SEM of six independent experiments. (C-D) TUNEL staining of primary osteoblasts wild-type and KO for *Ppargc1a/b*. Representative images (C) and quantitative analysis (D) of TUNEL staining. Results are plotted as mean \pm SEM of three independent experiments. (E) Proliferation rate of primary osteoblasts wild-type and KO for *Ppargc1a/b*. Results are expressed as percentage of BrdU⁺ cells. Data are plotted as mean \pm SEM of three independent experiments.

PGC-1 family controls mitochondrial dynamics, therefore we examined the effects of *Ppargc1a/b* deletion on mitochondria content and organization. We found that *Ppargc1a* and *Ppargc1b* ablation hampered the increase in mitochondrial DNA (mtDNA) induced by glucose restriction (Figure 23 A) and reduced morphological reorganization (Figure 23 B). Taken together, these results evidence that deletion *Ppargc1a/b* impact mitochondrial function without affecting cell viability or proliferation.

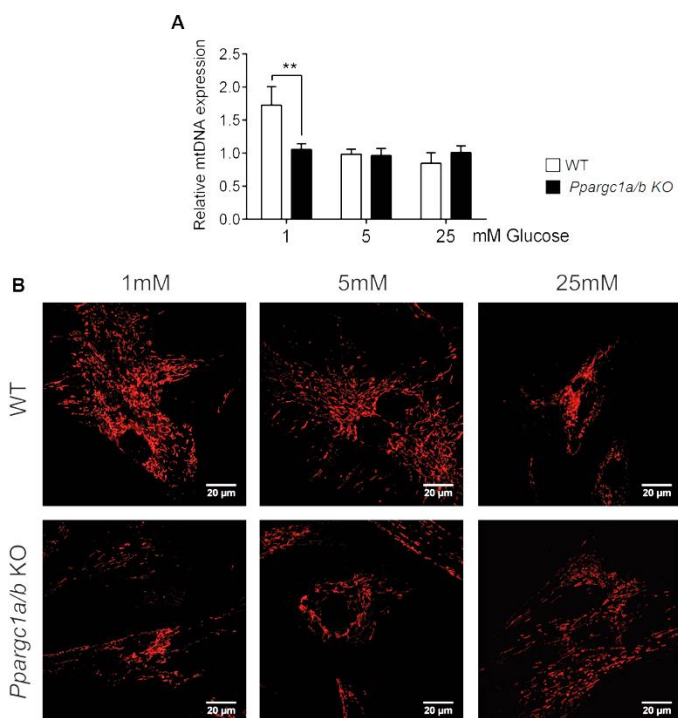


Figure 23. Loss of PGC-1 α/β reduce mitochondrial content and organization. (A) Quantification of mtDNA in primary osteoblasts, wild-type and KO for *Ppargc1a/b*, differentiated for 10 days in the presence of 1, 5 or 25 mM glucose. Results are plotted relative to the content of wild type osteoblasts cultures at 5 mM glucose as mean \pm SEM of four independent experiments. * $p < 0.05$, ** $p < 0.01$ and *** $p < 0.001$ using one-way ANOVA. (B) Visualization of mitochondria in primary osteoblasts wild-type and KO for *Ppargc1a/b* differentiated for 10 days in the presence of 1, 5 or 25 mM glucose.

Once we have determined that osteoblast and osteocytes deficient for *Ppargc1a/b* are viable, we analyzed the effect of this deletion on osteocyte specification program. Deficiency of *Ppargc1a/b* in primary osteoblasts or osteocytes decreased the levels of *Runx2* and *Osterix* irrespective of the glucose regime (Figure 24 A-B). Furthermore, deletion of *Ppargc1a/b* genes abolished the induction of the *Dmp1*, *Fgf23* and *Sost* mRNAs caused by glucose restriction (Figure 24 A-B). Osteocytes are also a source of molecules that regulate generation and activity of osteoclasts, such as OPG and RANKL. As deletion of *Ppargc1a/b* affects to osteocyte differentiation, it might also alter bone resorption induced by osteocytes. Therefore, we determined the expression of *Opg*, *RankL* and the ratio *Opg/RankL* in osteocytes control and deficient for *Ppargc1a/b* under different glucose supplies. We found that deletion of *Ppargc1a/b* decreased *Opg/RankL* ratio (Figure 24 C). Altogether, these results proved that PGC-1 co-activators act as regulators of osteocyte gene expression.

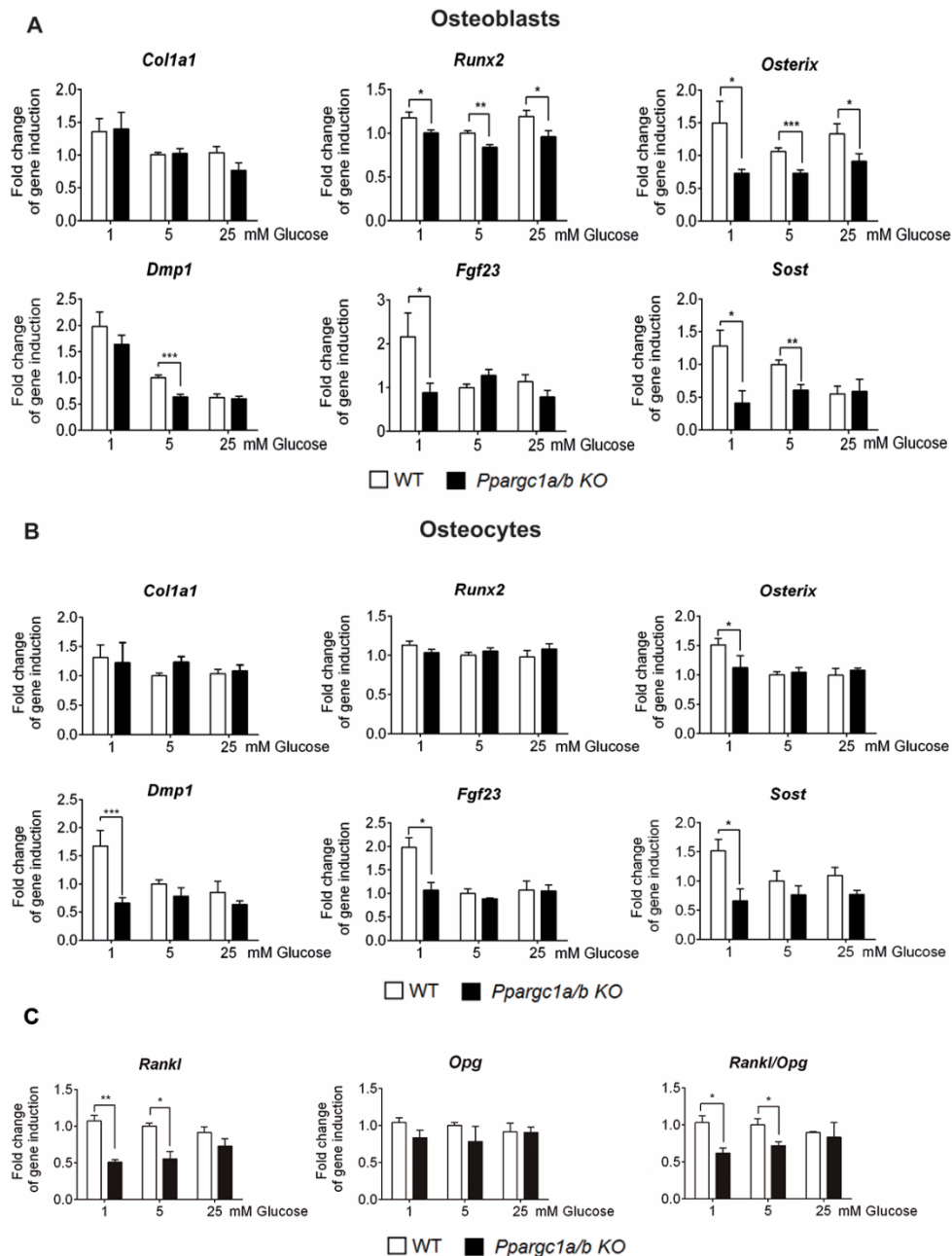


Figure 24. Role of PGC-1 in osteocyte differentiation. mRNA expression levels of osteocytic and osteoblastic genes in (A) primary osteoblasts and (B) primary osteocytes wildtype and knockout for PGC-1 α/β . Osteoblasts and osteocytes were isolated from calvarias obtained from *Ppargc1a/b*^{fl/fl} mice and infected with pMSCV-Puro or pMSCV-puro-Cre-ERT2 vectors. Infected cells were cultured for five days in 1, 5 or 25 mM glucose media. (C) mRNA expression levels of *Rankl*, *Opg* and *Rankl/Opg* expression ratio in primary osteocytes wild-type and KO for *Ppargc1a/b* cultured in 1, 5, and 25 mM

glucose media. Results were plotted as mean \pm SEM of three independent experiments. mRNA expression levels were measured by RT-qPCR and normalized to *Tbp*. Results are plotted as expression relative to control infection (mean \pm SEM of six independent experiments). * $p < 0.05$, ** $p < 0.01$ and *** $p < 0.001$ using Student's t-test.

Rearrangement of the cytoskeletal organization is a hallmark of osteocytes. In consequence, we examined the arrangement of actin cytoskeleton in IDG-SW3 cells cultured in different glucose concentrations but we could not observe any particular difference among the three conditions (Figure 25).

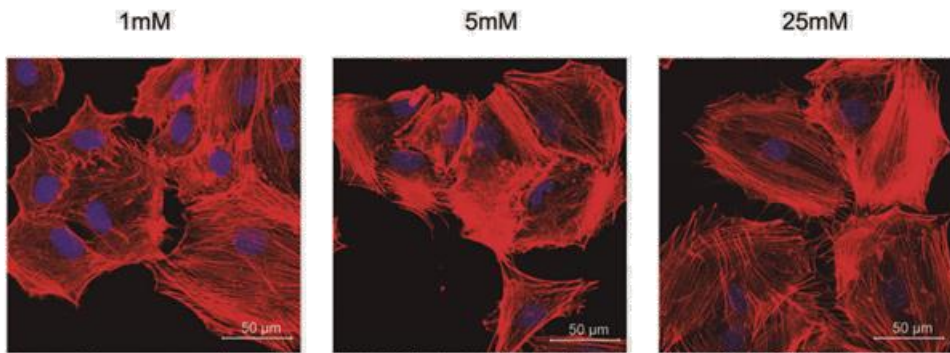


Figure 25. Glucose supply does not alter actin cytoskeleton organization. Maximum Intensity Projection of IDG-SW3 differentiated in 1, 5, or 25 mM glucose media for 14 days and stained with Alexa 488-phalloidin (red) and DAPI (blue).

We also analyzed whether PGC-1 α/β could somehow influence cytoskeletal organization of osteoblast (Figure 26 A) and osteocytes (Figure 26 B). We compared PGC-1 actin cytoskeleton of cells wild type or deficient in *Ppargc1a/b*. As glucose supply, *Ppargc1a/b* deletion did not produce any significant alteration of actin fibers in bone cells.

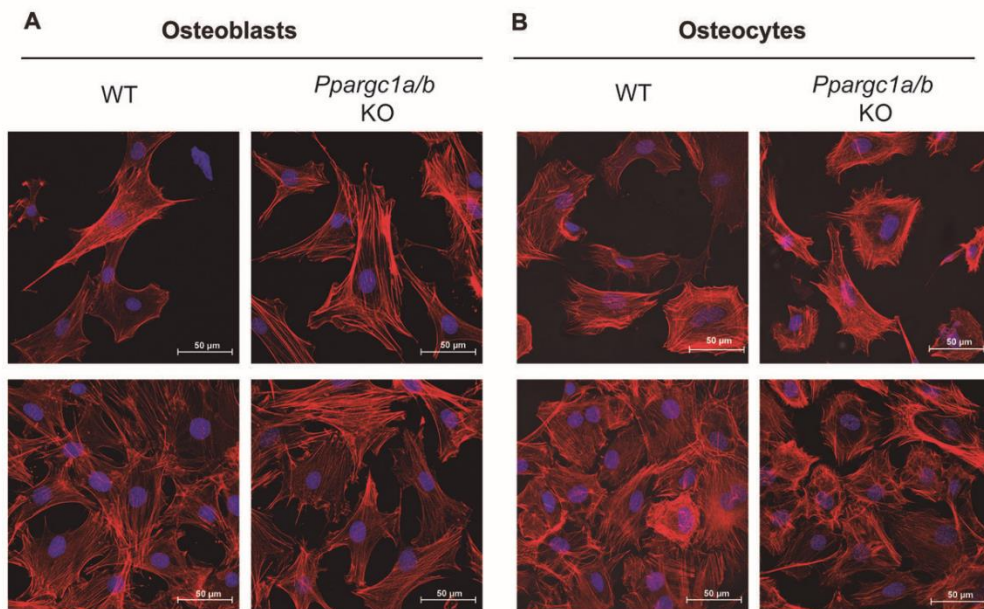


Figure 26. Deletion of *Ppargc1a* and *Ppargc1b* does not alter actin cytoskeleton organization. Maximum Intensity Projection of (A) osteoblasts and (B) osteocytes wild-type and KO for *Ppargc1a/b* stained with Alexa 488-phalloidin (red) and DAPI (blue).

6. PGC-1 α/β contribute to maintain bone homeostasis *in vivo*.

We explored further the role of *Ppargc1a/b* in bone formation and homeostasis in mice. Transgenic mice for Cre under the control of the *2.3-Col1a1* promoter (Dacquin et al., 2002a) allowed deletion of *Ppargc1a* and *Ppargc1b* in osteoblasts and osteocytes (hereafter *Ppargc1a* f/f; *Ppargc1b* f/f; *Col1a1*-Cre (KO)). *Ppargc1a/b* deletion did not affect either body weight or femur length. As expected, *Ppargc1a* and *Ppargc1b* mRNA levels in calvaria from KO mice were significantly reduced in both male and female mice (Figure 27).

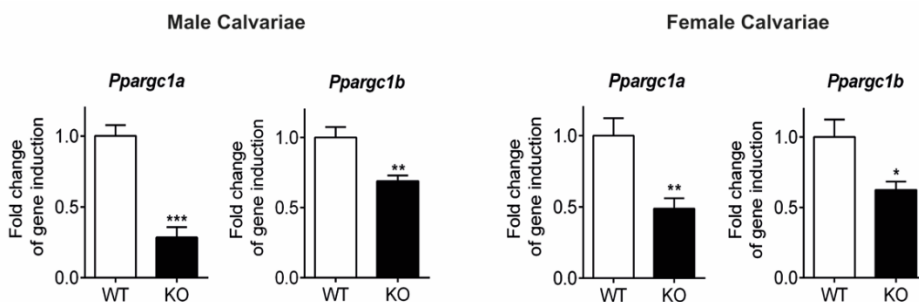


Figure 27. *Ppargc1a* and *Ppargc1b* expression levels in *Ppargc1a/b* deficient (KO) mice. mRNA expression levels of *Ppargc1a* and *Ppargc1b* in calvaria obtained from *Ppargc1a/b* conditional knockout (*Ppargc1a/b* f/f; *Col1a1*-Cre) and control male and female mice. Results were plotted as mean \pm SEM of eight independent animals. mRNA expression levels were measured by RT-qPCR and normalized to *Tbp* expression. * $p < 0.05$, ** $p < 0.01$ and *** $p < 0.001$ using Student's t-test.

We used micro-computed tomography scanning (μ CT) to analyze bone structure of distant femurs in male and female mice. In eight week-old mice, deletion of *Ppargc1a* and *Ppargc1b* led to a decrease in both trabecular and cortical bone architecture. KO male mice presented lower cortical bone volume (BV) associated with reduced cortical thickness (Ct.Th) while bone perimeter (B.Pm) around the midshaft was not affected (Figure 28 A). Additionally, distal femurs in males also presented less trabecular bone volume (BV/TV) resulting from a significantly lower trabecular number (Tb.N) and thickness (Tb.Th) (Figure 28 A). Trabecular analysis of distal femurs in KO females also showed a significant reduction in trabecular bone volume (BV/TV), trabecular number (Tb.N) and thickness (Tb.Th). However, reduction in cortical bone parameters were lower in magnitude and did not reach significant differences (Figure 28 B).

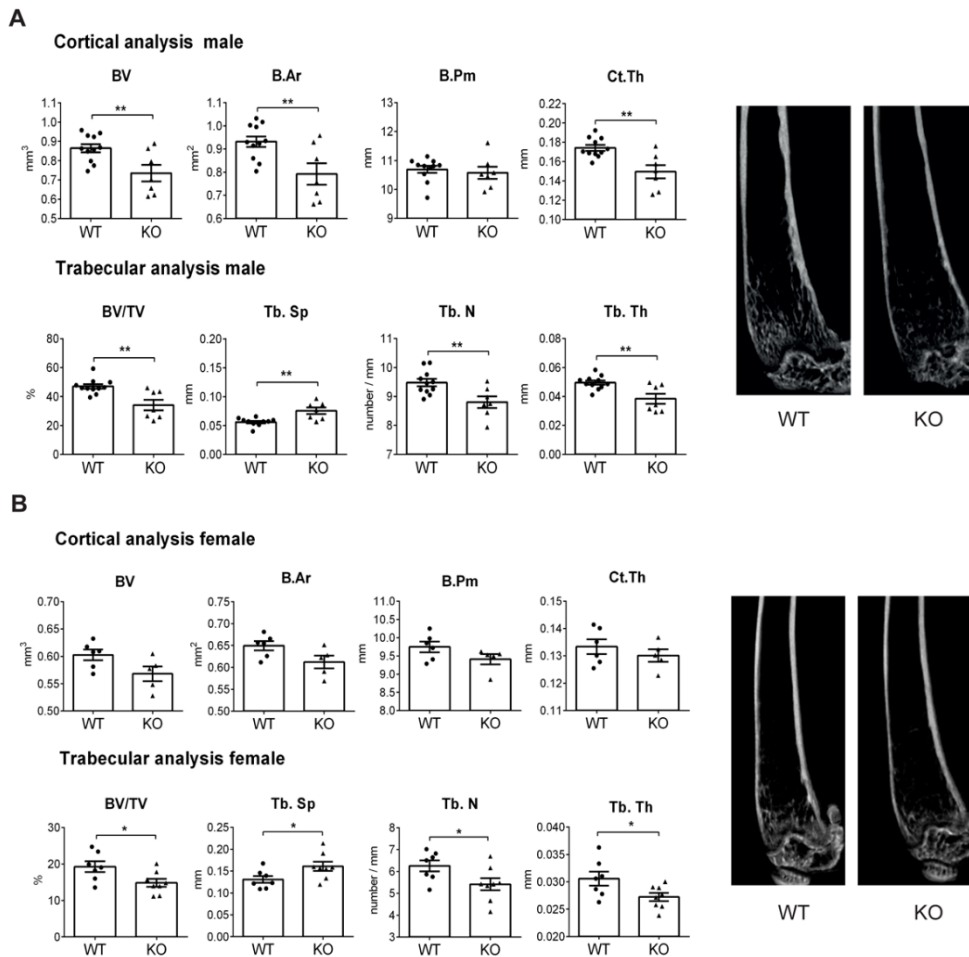


Figure 28. Bone phenotype of *Pparg1α/β* conditional knockout mice. μ CT analysis and representative images of femurs obtained from male (A) or female (B) *Pparg1α/b^{f/f};Col1a1-Cre* and control (*Pparg1α/b^{f/f}*) mice. Results were plotted as mean \pm SEM of eight to eleven independent animals. * $p < 0.05$, ** $p < 0.01$ and *** $p < 0.001$ using Student's t-test.

Then, we performed histological techniques to discover any alteration on bone structure arising as a consequence of PGC-1 α/β deletion. We stained both WT and KO femurs with Hematoxylin-Eosin and Masson's trichrome. Neither of them revealed any alteration of bone structure or collagen deposition (Figure 29 A-B). Furthermore, we did not find differences in the number of osteocytes per bone area (N.Oc/B.Ar) or the number of empty lacunae in cortical bone, indicating that the osteopenic phenotype occurs without significant changes in either osteocytes density or viability (Figure 29 C).

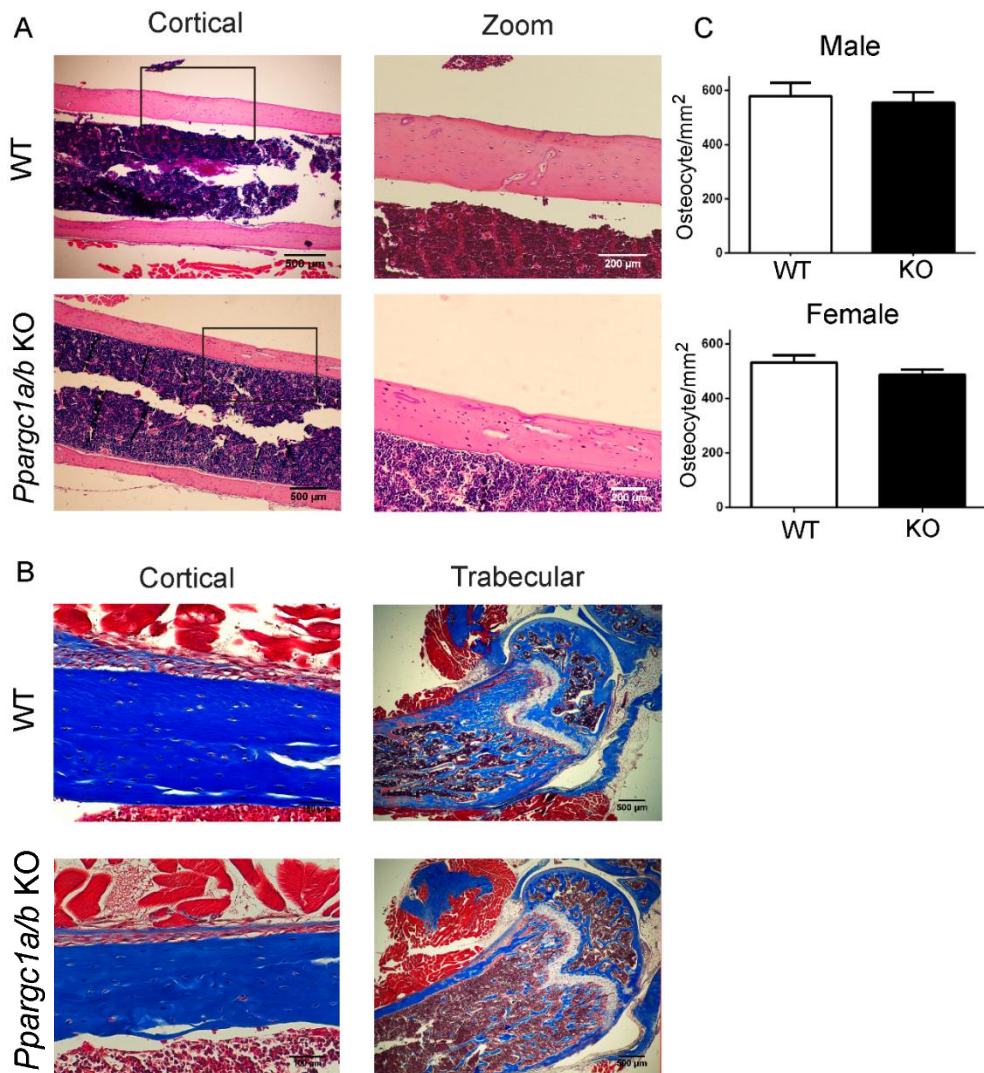


Figure 29. Histological analysis of femurs of *Ppargc1a* and *Ppargc1b*-deficient mice. (A) Representative images of longitudinal sections of femur from wild type (WT) and *Ppargc1a/b* knock-out (KO) mice stained with haematoxylin and eosin. Images were taken at 4x and 10x magnification. (B) Representative images of longitudinal sections from middle and distal femur from wild type (WT) and *Ppargc1a/b* knock-out (KO) mice stained with Masson's trichrome stain. Images were taken at 2x and 20x magnification. (C) Osteocyte number normalized by bone area. Results are shown as mean \pm SEM of 12 different fields from 8 different animals.

In order to clarify the underlying reason for the osteopenic phenotype of the KO mice, we analyzed the expression of osteoblast and osteocyte genes from

calvaria. KO male and female mice displayed a reduced expression of osteocyte genes, including *Dmp1*, *Fgf23* and *Sost*, and increased levels of osteoblastic gene such as *Bglap*, *Runx2* or *Osx* (Figure 30 A, C). We also wondered whether osteocytes deficient for *Ppargc1 α/β* could activate bone resorption. Therefore, we analyzed the expression of *Rankl* and *Opg*. We found a reduced ratio of *Rankl/Opg* expression in calvaria (Figure 30 B,D). These data suggest that although *Ppargc1 α/β* affects the expression of *Rankl* and *Opg* in osteocytes, osteopenia in young *Ppargc1 α/β* -deficient mice does not depend on the induction of *Rankl/Opg* ratio in osteocytes. In conclusion, our data demonstrate the relevant role of PGC-1 in co-activation of the osteoblast and osteocyte transcriptional programs.

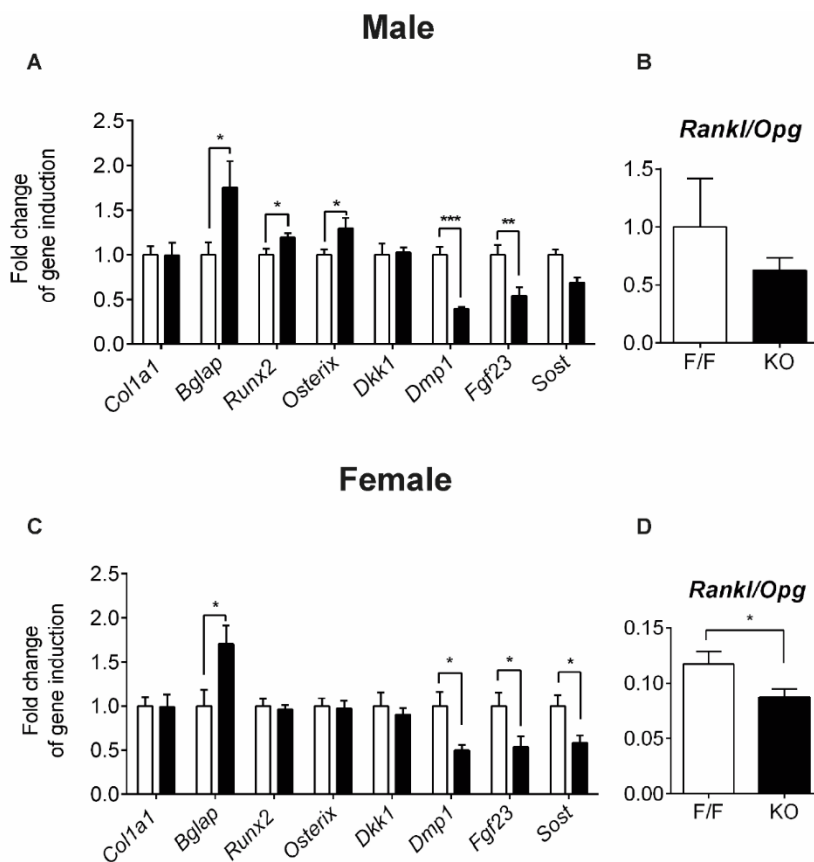


Figure 30. Osteoblastic and osteocytic gene expression levels in *Ppargc1 α/β* deficient (KO) mice (A,C) mRNA expression levels of osteocytic and osteoblastic genes in calvaria obtained from PGC-1 α/β conditional knock-out (*Ppargc1 α/β f/f; Col1a1-Cre*) and control (A) male and female (B) mice. Results are plotted as mean \pm SEM of eight independent animals. (B,D) *Rankl/Opg* expression ratio in calvaria obtained from *Ppargc1 α/β* conditional knockout (*Ppargc1 α/β f/f; Col1a1-Cre*) and control male (C) and female (D) mice. mRNA expression levels were measured by RT-qPCR and normalized to *Tbp* expression. * $p < 0.05$, ** $p < 0.01$ and *** $p < 0.001$ using Student's t-test.

CHAPTER II: NRF2 FUNCTION IN BONE HOMEOSTASIS AND OSTEOCYTE DIFFERENTIATION

1. Increased OXPHOS activity and ROS generation are associated to osteocytogenesis

Confluent IDG-SW3 cells constitute a well-established model of osteocytogenesis (Woo et al., 2011). As we have demonstrated in the previous chapter, IDG-SW3 cells differentiate into osteocytes after 14-21 days in culture. At fourteen days, they express gene markers characteristic of early osteocytes. Previous reports from our group suggested that during osteocyte differentiation a metabolic reprogramming towards oxidative phosphorylation occurs (Sánchez-de-Diego et al, 2019). Therefore, we used IDG-SW3 to investigate mitochondrial dynamics during osteocyte specification. As differentiation progresses, cells increased their content in mitochondrial DNA (mtDNA), which indicates an increase in the number of mitochondria per cell (Figure 31 A). In parallel, differentiation enhanced the mitochondrial membrane potential and increased protein levels of different OXPHOS complexes, suggesting that the newly formed mitochondria were metabolically active (Figures 31 B-C).

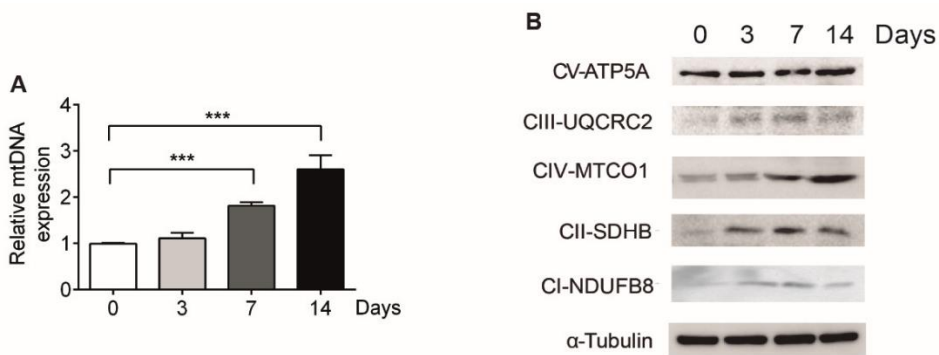


Figure 31. Osteocytic differentiation increases mitochondrial function. (A) Quantification of mtDNA in undifferentiated IDG-SW3 and after 3, 7 and 14 days of differentiation. Results are plotted as expression relative to undifferentiated IDG-SW3 (mean \pm SEM; n=7). (B) Analysis of the levels of mitochondrial complexes in undifferentiated IDG-SW3 and after 3, 7 and 14 days of differentiation. * $p < 0.05$, ** $p < 0.01$ and *** $p < 0.001$ using Student's t-test.

In order to understand better the differences observed in mitochondria content, we evaluated mitochondrial respiration in intact, IDG-SW3 cells during the differentiation process. We determined routine O_2 consumption, leak state (uncoupled respiration after addition of oligomycin into the assay), electron transfer capacity (after FCCP addition, (ETS). we did not find significant differences in routine and ETS parameters; however, we observed a slightly increase in routine respiration during differentiation (Figure 32). These results seems to indicate that there is a reprogramming if mitochondrial function during differentiation.

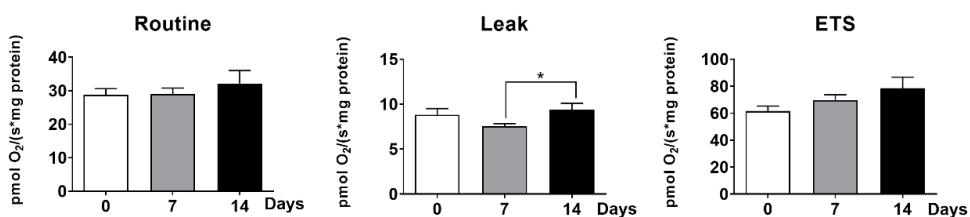


Figure 32. Mitochondrial respiration in IDG-SW3 during differentiation. Determination of routine oxygen consumption, leak respiration (uncoupled) and electron transfer capacity (ETS) of IDG-SW3 differentiated for 0, 7 and 14 days. 700,000 IDG-SW3 cells were incubated in the respirometry chamber with α -MEM. All results were expressed relative to protein content. Results are plotted as mean \pm SEM of four independent experiments. * $p < 0.05$, ** $p < 0.01$ and *** $p < 0.001$ using one-way ANOVA.

To determine whether changes in mitochondrial respiratory transport chain were linked to alteration of ROS levels, we assessed oxidative stress in these cells. During osteocytogenesis we observed a progressive induction of total and mitochondrial ROS (Figure 33). These results indicates that a metabolic reprogramming towards oxidative phosphorylation occurs during differentiation and produce an increase in mitochondrial function that raise ROS levels.

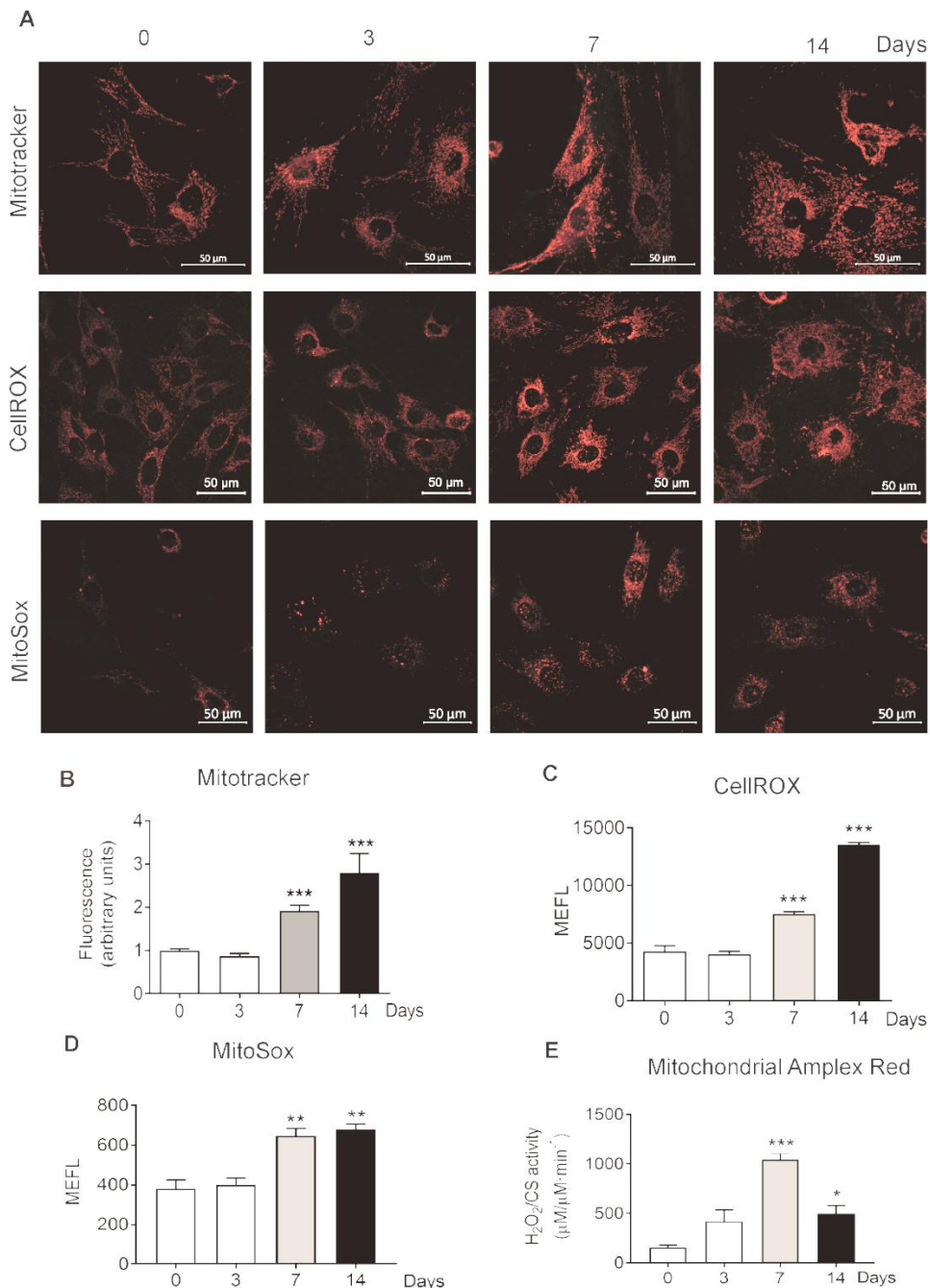


Figure 33. The increase of mitochondria function during osteocytogenesis trigger an increase in ROS levels. (A) Visualization of mitochondria and Reactive Oxygen Species with Mitotracker Deep Red, CellRox Deep Red and MitoSox in undifferentiated IDG-SW3 and after 3, 7 and 14 days of differentiation. (B) Flow cytometry analysis of mitochondrial membrane potential of undifferentiated IDG-SW3 and after 3, 7 and 14 days of differentiation. Results are plotted as expression relative to

undifferentiated IDG-SW3 (mean \pm SEM; n= 8). (C) Flow cytometry analysis of Reactive Oxygen Species in undifferentiated IDG-SW3 and after 3, 7 and 14 days of differentiation. Results are plotted as Molecules of Equivalent Fluorescein (mean \pm SEM; n=4). (D) Flow cytometry analysis of mitochondrial Reactive Oxygen Species in undifferentiated IDG-SW3 and after 3, 7 and 14 days of differentiation. € Determination of Mitochondrial Reactive Oxygen species by Amplex Red staining) Flow cytometry analysis of Reactive Oxygen Species in undifferentiated IDG-SW3 and after 3, 7 and 14 days of differentiation. Results are plotted as Molecules of Equivalent Fluorescein (mean \pm SEM; n=4). Results are plotted as Molecules of Equivalent Fluorescein (mean \pm SEM; n=4). *p<0.05, **p<0.01 and ***p<0.001 using Student's t-test.

Then, we aimed to validate these results in primary cultures of osteoblasts and osteocytes. Therefore, we compared the mitochondrial content of murine primary osteoblasts and osteocytes. Osteocytes displayed a 30-40% increased mitochondrial number per cell compared to osteoblasts (Figure 34 A). However, confocal images showed that differentiation do not significantly affect to mitochondrial configuration. Both primary osteoblast and osteocytes arranged their mitochondria in elongated tubules, forming networks that has been shown to be more efficient at producing ATP (Gomes et al., 2011). As in IDG-SW3, these networks follow a similar pattern than ROS staining, suggesting that mitochondrial activity is the major source of ROS in these cells (Figure 34 B).

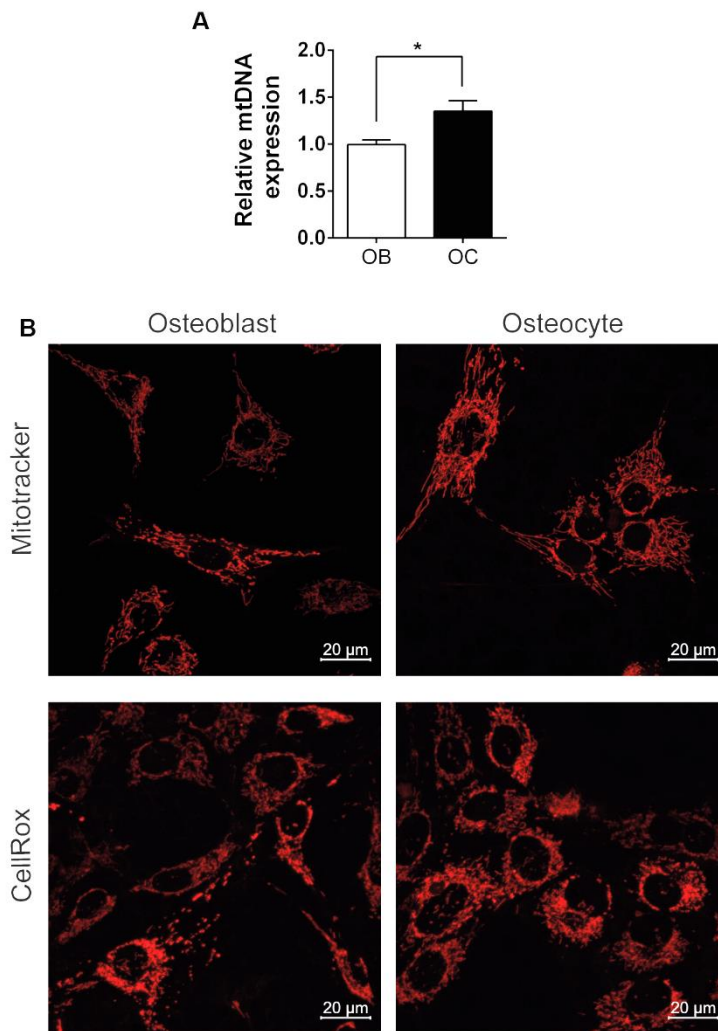


Figure 35. Mitochondria and ROS in osteoblasts and osteocytes. (A) Quantification of mtDNA in osteoblast and osteocyte primary cultures. Results are plotted as expression relative to osteoblasts (mean \pm SEM; n=6). (B) Visualization of mitochondria with Mitotracker Deep Red in murine osteoblasts and osteocytes.

One of the most important intracellular scavengers of ROS is reduced glutathione (GSH), and its ratio with oxidized glutathione (GSSG) is used as a marker of increased ROS levels. Therefore, we measured GSSG/GSH ratio and confirmed the alteration in redox status by measuring. GSSG/GSH ratio increases during osteocytogenesis and peaked at day 7 of differentiation (Figure 35 A and B). Within mitochondria, GSH do not only act as ROS scavenger but also regulates mitochondrial ATP production by modifying critical protein sulfhydryl redox states that influence nicotinamide adenine dinucleotide (NADH) and flavin adenine

dinucleotide (FADH₂) generation and electron flow in the electron transport chain (ETC). Therefore, we decided to analyze the levels of mGSH and mGSSG. We observed a decrease of mGSH from day 7 of differentiation whereas mGSSG increased during the whole differentiation process (Figure 35 C and D)

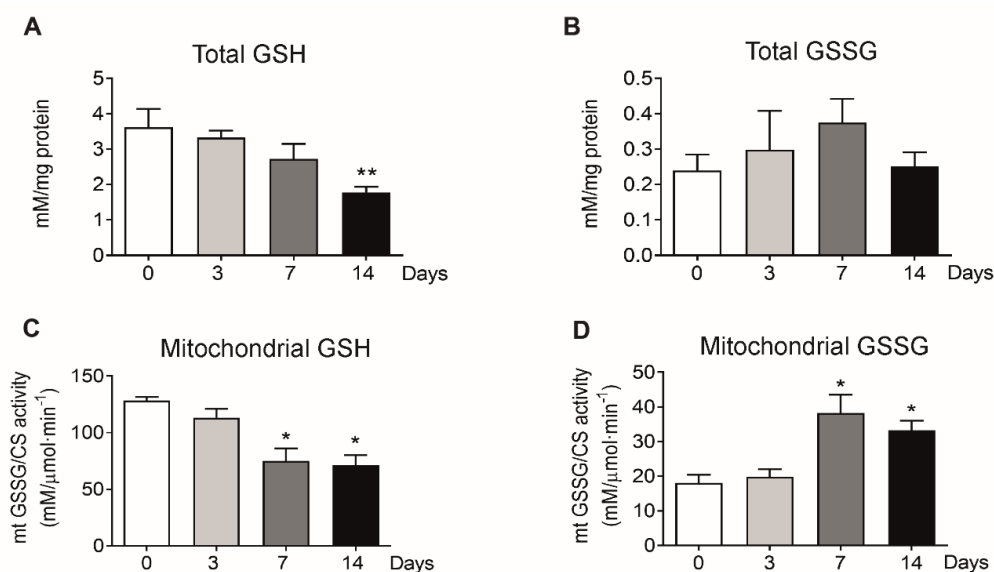


Figure 35. Osteocytogenesis induce oxidation of total and mitochondrial GSH. (A and B) total levels of GSH and GSSG in undifferentiated IDG-SW3 and after 3, 7 and 14 days of differentiation. (C and D) Mitochondrial GSH (mGSH) and GSSG (mGSSG) levels in undifferentiated IDG-SW3 and after 3, 7 and 14 days of differentiation Results are plotted as mean \pm SEM (n=4). *p<0.05, **p<0.01 and ***p<0.001 using Student's t-test.

2. Increased NRF2 activity during osteocytogenesis

Within the cells, NRF2 is a major oxidative stress sensor responsible for the induction of an antioxidant response. Then we hypothesized that the increase in ROS levels and the GSSG/GSH ratio might induce NRF2 levels and activity. We found a significant increase in total NRF2 protein levels in IDG-SW3 cells after 7 and 14 days of differentiation. On the contrary, the protein levels of the NRF2-repressor, KEAP1, slightly lowered upon time (Figure 34 A-B). NRF2 target genes NAD(P)H dehydrogenase quinone 1 (*Nqo1*) and glutamate-cysteine ligase catalytic subunit (*Gclc*) were transcriptionally activated during IDG-SW3 differentiation (Figure 34C) confirming the activation of NRF2 during osteocyte differentiation. Similarly, transcription of *Nfe2l2* increased throughout osteocytogenesis, whereas *Keap1*

mRNA levels remained unaltered until the 14th day when they also rised (Figure 36C).

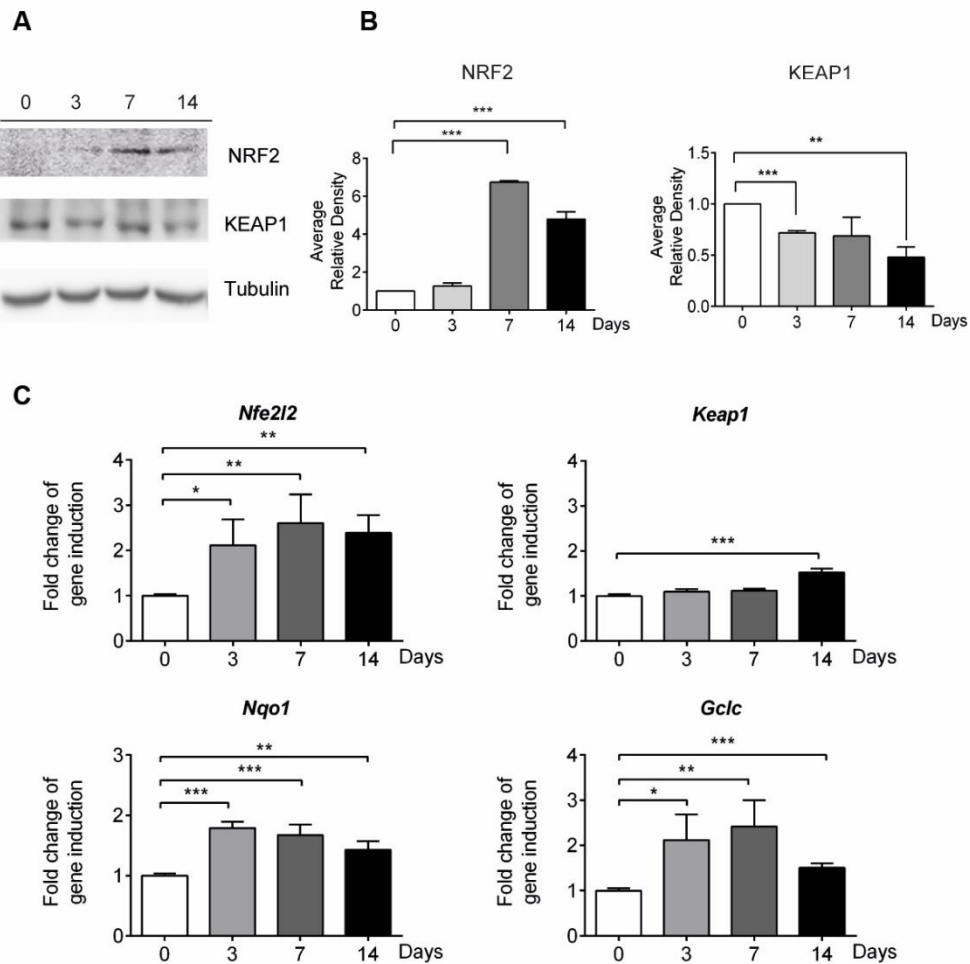


Figure 36. NRF2 activity during osteocytogenesis. (A) Undifferentiated IDG-SW3 cells and after 3, 7 and 14 days of differentiation were analysed for NRF2 and KEAP1 protein expression. Tubulin levels were used as a protein load control. (B) NRF2 and KEAP1 levels were quantified and normalized by tubulin levels. Results are plotted as mean \pm SEM (n=3). (C) mRNA expression of *Keap1*, *Nfe2l2* and its target genes in undifferentiated IDG-SW3 and after 3, 7 and 14 days of differentiation. mRNA levels were quantified by qRT-PCR, normalized by *Tbp* and plotted as expression relative to undifferentiated IDG-SW3 (mean \pm SEM; n=8) Results are plotted as $2^{-\Delta\Delta Ct}$ (mean \pm SEM; n=6). * $p < 0.05$, ** $p < 0.01$ and *** $p < 0.001$ using Student's t-test.

We confirmed the obtained results in primary cultures isolated from mice. Osteocytes displayed higher expression of *Nfe2l2* mRNA than primary osteoblasts. Likewise, the basal levels of NRF2 target genes were also higher in primary osteocyte than osteoblast. On the contrary, *Keap1* mRNA levels were similar in both cells (Figure 37). Altogether, these findings suggest that osteoblast-to-osteocyte transition requires an increase in NRF2 activity.

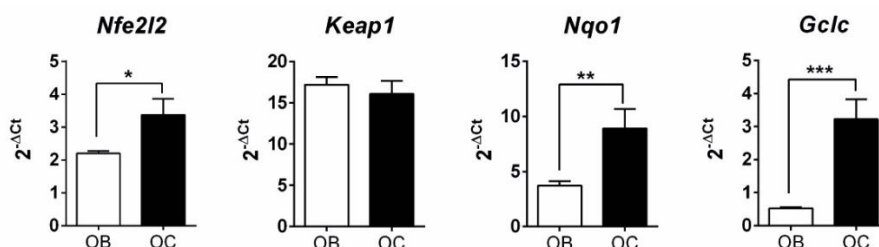


Figure 37. NRF2 activity in osteoblast and osteocyte cultures. mRNA expression of *Keap1*, *Nfe2l2* and its target genes in primary cultures of osteoblasts and osteocytes. mRNA expression was quantified by RT-qPCR and normalized to *Tbp* expression. Results are plotted as $2^{-\Delta\Delta Ct}$ (mean \pm SEM; n=6). * $p < 0.05$, ** $p < 0.01$ and *** $p < 0.001$ using Student's t-test.

3. *Nfe2l2* deletion in osteocytes causes osteopenia and impairs osteocyte-specific gene expression

Previous studies reported conflicting results on the effects of whole-body deletion of *Nfe2l2* in the bone mass of male mice. Moreover, information about the role of NRF2 in each bone cell type has not been studied and needs to be addressed. To determine the function of NRF2 in osteocytes, we bred *Dmp1-CreERT2* mice with *Nfe2l2^{fl/fl}* mice (Powell et al., 2011) to eliminate *Nfe2l2* expression in mature osteoblasts and osteocytes. In these mice, Cre recombinase is fused to a triple mutant form of the human estrogen receptor which does not bind its natural ligand (17 β -estradiol) at physiological concentrations. To activate CRE recombinase, we administered low doses of tamoxifen to three-week-old mice. Using this strategy we minimized the effects of tamoxifen on bone turnover in mice while we still achieved a robust and restricted activation of the transgene in osteocytes and mature osteoblasts (Powell et al., 2011; Zhong, et al. 2015; McKenzie et al., 2019; Kang et al., 2016; Kim et al., 2012). Four weeks after deletion, we visualized bone in male and female mice in distal femurs by micro-computed tomography scanning (μ CT) and histological analysis. Deletion of *Nfe2l2* led to a decrease in both trabecular and cortical bone architecture. *Dmp1-CreERT2:Nfe2l2^{fl/fl}* (hereafter *Dmp1/Nfe2l2-KO*) male mice presented lower cortical bone volume (BV) associated with reduced

cortical thickness (Ct.Th) while bone perimeter (B.Pm) around the midshaft was not affected (Figure 38 A-B). Moreover, distal femurs in males also presented less trabecular bone volume (BV/TV) resulting from a significantly lower trabecular number (Tb.N) and thickness (Tb.Th) (Figure 38A-B). Trabecular analysis of distal femurs in *Dmp1/Nfe2l2*-KO females also showed a significant reduction in trabecular bone volume (BV/TV), trabecular number (Tb.N) and thickness (Tb.Th), although this reduction of trabecular parameters was lower in magnitude than in males (Figure 38 C-D). Female bone parameters revealed a significant reduction of cortical thickness in *Dmp1/Nfe2l2*-KO females (Figure 38 C-D) while other cortical parameters remained unaltered.

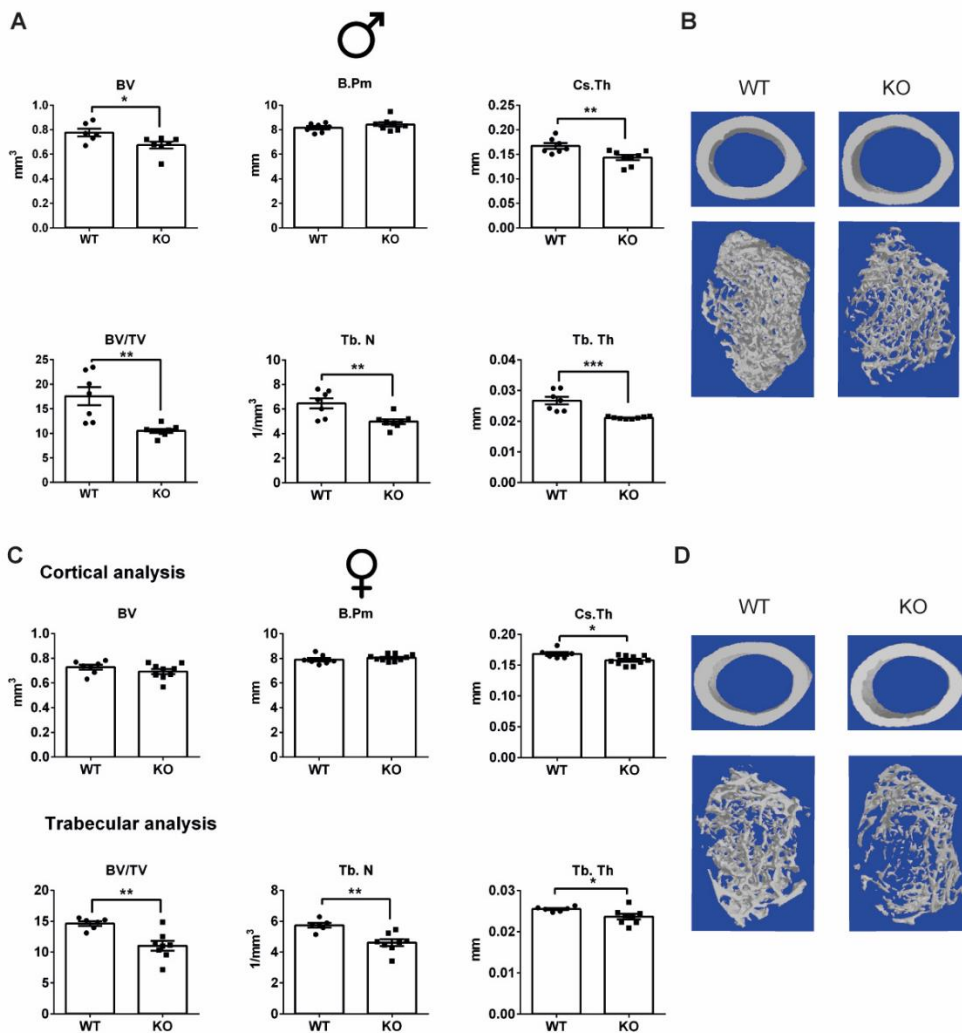


Figure 38. Bone phenotype of mice with *Nfe2l2* conditional deletion in osteocytes. μ CT analysis and representative images of femurs obtained from male (A and B) or female (C and D) *Nfe2l2^{f/f};Dmp1-Cre-Ert2* and control (*Nfe2l2^{f/f}*) mice. Results are plotted as mean \pm SEM of seven to eleven independent animals. * p <0.05, ** p <0.01 and *** p <0.001 using Student's t-test.

In order to clarify the mechanism by which deletion of *Nfe2l2* in mature osteoblasts and osteocytes provokes osteopenia, we analyzed the expression of osteoblastic and osteocytic genes. As expected, expression of the NRF2 targets genes *Nqo1* and *Gclc* were reduced in both male and female bones. *Dmp1/Nfe2l2*-KO male and female mice also displayed a reduced expression of osteocyte genes, including *Dmp1*, *Mepe* and *Sost*. Additionally, the expression of other osteoblast genes (*Runx2* or *Osx*) was reduced in *Dmp1/Nfe2l2*-KO mice (Figure 39).

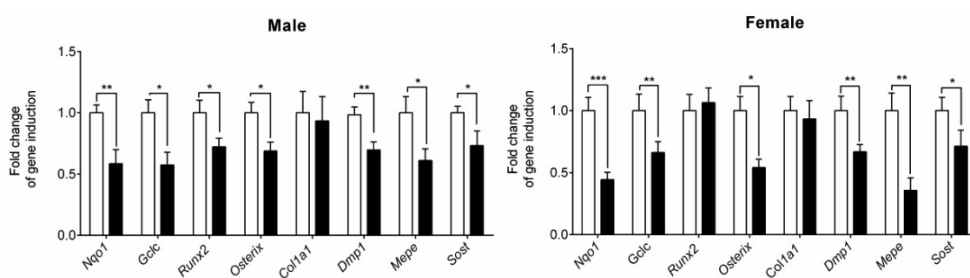


Figure 39. Osteoblastic and osteocytic gene expression levels in *Dmp1/Nfe2l2*-KO mice. mRNA levels in calvaria obtained from NRF2 conditional knock-out (*Nfe2l2^{f/f};Dmp1-Cre-Ert2*) and control (*Nfe2l2^{f/f}*) mice. mRNA expression levels were measured by RT-qPCR and normalized to *Tbp* expression. Results are plotted as mean \pm SEM of seven to eleven independent animals. * p <0.05, ** p <0.01 and *** p <0.001 using Student's t-test.

Reduced osteocyte gene expression occurred without significant changes the density of osteocytes per bone area (N.Oc/B.Ar) in either males (Figure 38 A-B) and females (Figure 38 E-F). Moreover, the number of osteoclasts and its activity was significantly higher in male *Dmp1/Nfe2l2*-KO mice (Figure 40 A, C) whereas this increase was not significant in female mice (Figure 38 E, G). We confirmed the increase in osteoclastic activity by qRT-PCR. We observed an increase of *Trap* expression in male *Dmp1/Nfe2l2*-KO but not in females (Figure 38 D-H). These effects in osteoclasts took place without any alteration of *Rankl/Opg* expression (Figure 40 D-H).

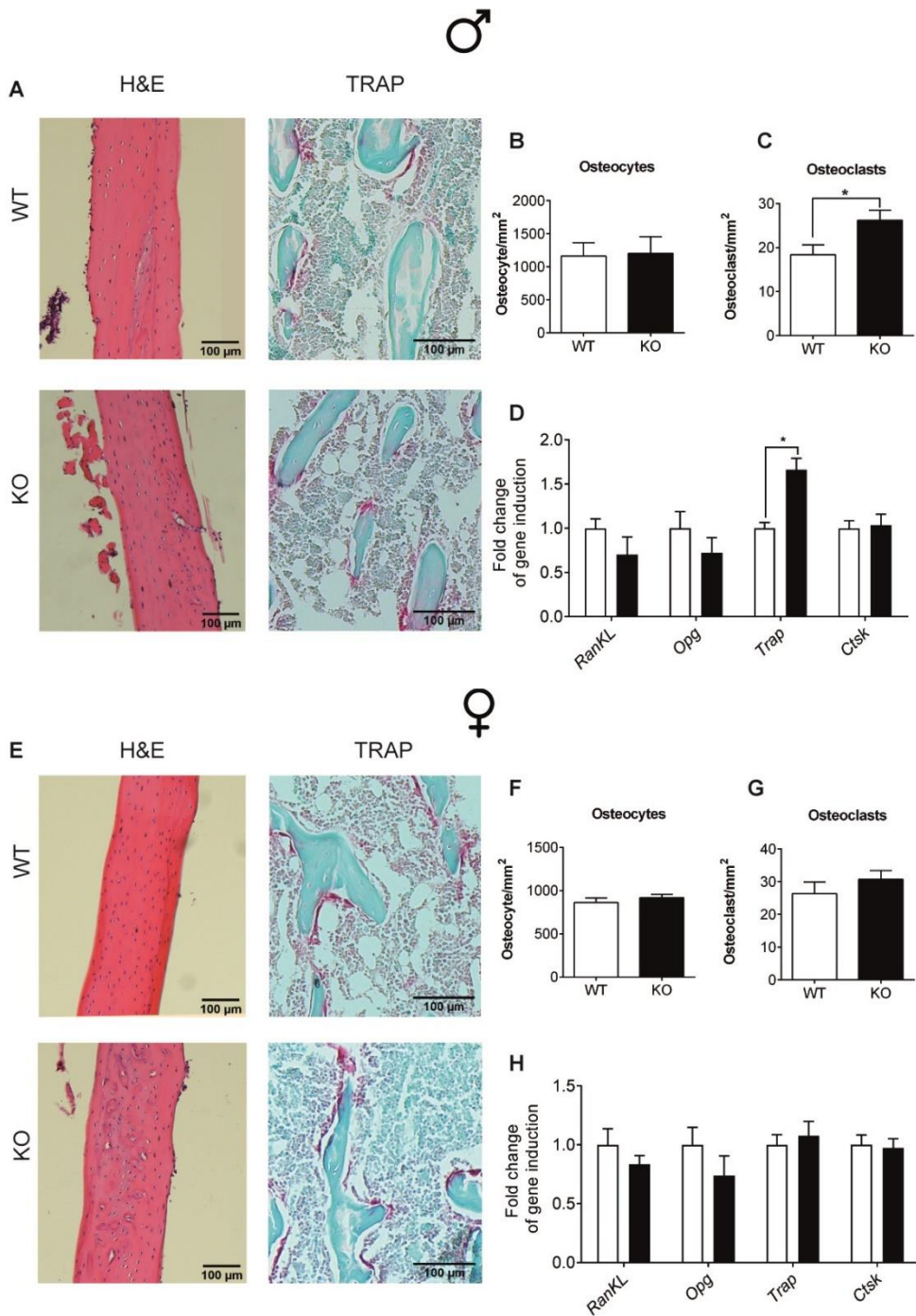


Figure 40. Histological analysis of femurs obtained from mice deficient of NRF2 in osteocytes. (A and E) Representative images of longitudinal sections of femur from male (A) and female (E) wild type (WT) and NRF2 knock-out (KO) mice stained with hematoxylin and eosin and TRAP. Images were

taken at 4x magnification. (B and F) Osteocyte number per area of cortical bone in male (B) and female (F) wild type (WT) and *Nfe2l2^{fl/fl};Dmp1-Cre-Ert2* knock-out (KO) mice. (C and G) Osteoclast number per area of trabecula determined by TRAP staining from male (C) and female (G) wild type (WT) and *Nfe2l2^{fl/fl};Dmp1-Cre-Ert2* knock-out (KO) mice. (D and H) mRNA expression levels of relevant genes of osteoclast function from calvaria obtained from NRF2 conditional knock-out (*Nfe2l2^{fl/fl};Dmp1-Cre-Ert2*) and control (*Nfe2l2^{fl/fl}*) mice. mRNA expression levels were measured by RT-qPCR and normalized to *Tbp* expression. Results are plotted as mean \pm SEM of seven to eleven independent animals. * $p < 0.05$, ** $p < 0.01$ and *** $p < 0.001$ using Student's t-test.

Given the results obtained, we aimed to establish also the impact of *Nfe2l2* deletion in the previous steps of osteoblast differentiation. Osteoblast-specific *Nfe2l2* mutant mice were generated by means of a Cre recombinase adjacent to the 2.3-*Col1a1* promoter *Nfe2l2;Col1a1-Cre* (hereafter *Col1a1/Nfe2l2-KO*), which drives constitutive expression of Cre exclusively in osteoblasts from E14 (Dacquin et al., 2002b) As *Dmp1/Nfe2l2-KO* mice, *Col1a1/Nfe2l2-KO* males presented lower trabecular bone volume (BV/TV) and less trabecular number (Tb.N) and thickness (Tb.Th) in distal femur (Figure 39 A-B). However, *Col1a1/Nfe2l2-KO* male mice did not present major defects in cortical bone volume (Figure 39 A-B). For its part, female *Col1a1/Nfe2l2-KO* mice did not show changes in cortical bone parameters (Figure 39C and D). Moreover, trabecular bone of *Col1a1/Nfe2l2-KO* female mice was also unaffected by *Nfe2l2* deletion (Figure 39 C and D).

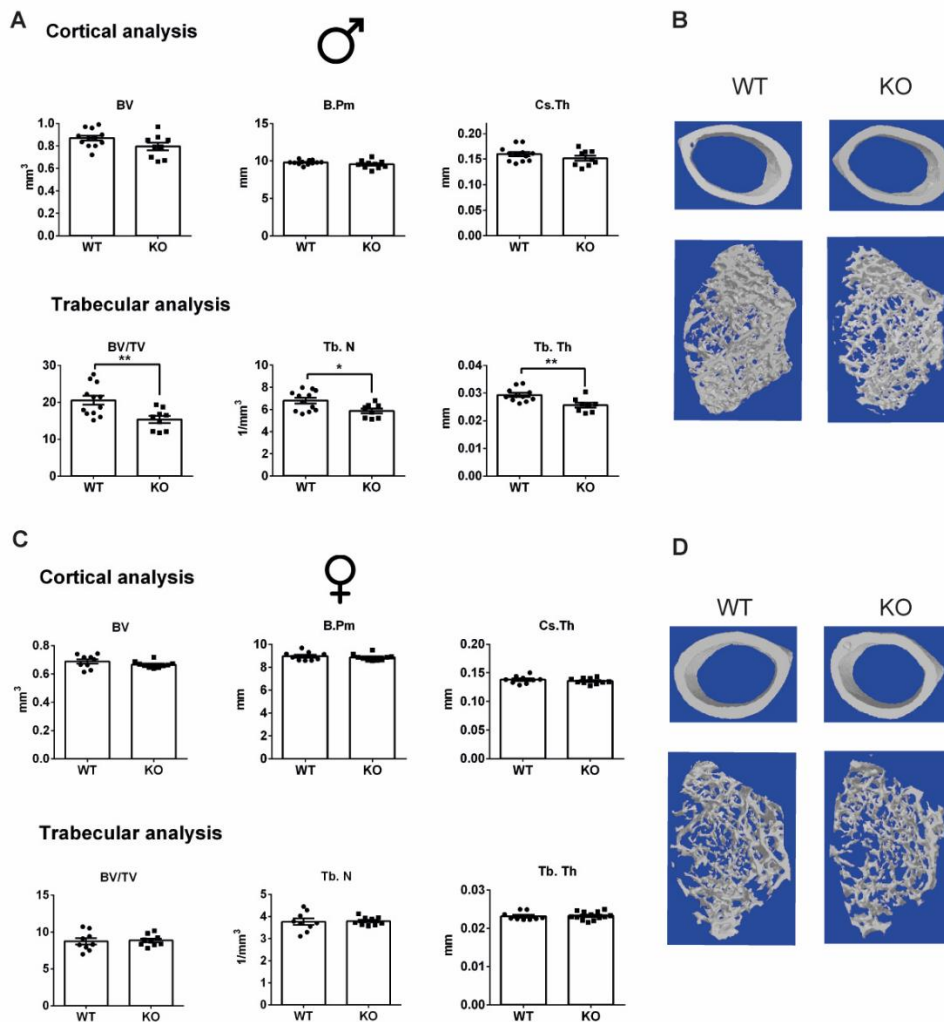


Figure 41. Bone phenotype of mice with *Nfe2l2* conditional deletion in osteoblasts. (A-D) μ CT analysis and representative images of femurs obtained from male (A and B) or female (C and D) *Nfe2l2^{fl/fl};Col1a1-Cre* and control (*Nfe2l2^{fl/fl}*) mice. Results are plotted as mean \pm SEM of nine to eleven independent animals. * $p < 0.05$, ** $p < 0.01$ and *** $p < 0.001$ using Student's t-test.

In order to understand the phenotypical differences observed between *Dmp1/Nfe2l2-KO* and *Col1a1/Nfe2l2-KO* mice, we analyzed the gene expression of calvaria obtained from *Dmp1/Nfe2l2-KO* and WT animals. Expression of the NRF2 targets genes *Nqo1* and *Gclc* were reduced in both male and female bones to a similar extent than in *Dmp1/Nfe2l2-KO* mice, indicating an effective deletion of *Nfe2l2*. (Figure 40). *Col1a1/Nfe2l2-KO* male and female mice also displayed reduced levels of *Dmp1*, *Mepe* and *Sost* mRNA, but no major changes in the expression of other osteoblastic genes, such as *Runx2* or *Osx*, were observed (Figure 40).

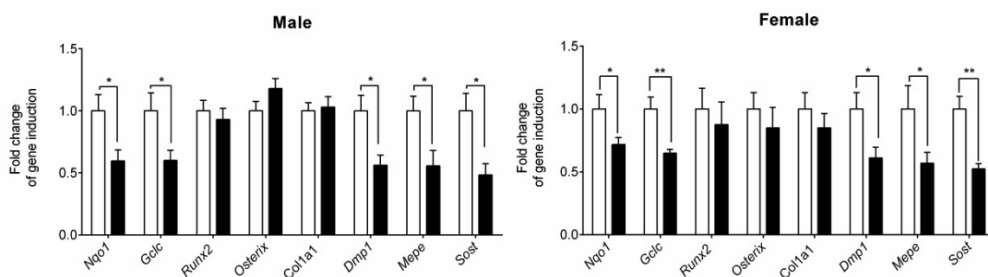


Figure 42. Osteoblastic and osteocytic gene expression levels in *Col1a1/Nfe2l2*-KO mice mRNA levels in calvaria obtained from NRF2 conditional knock-out (*Nfe2l2^{fl/fl}; Col1a1-Cre*) and control (*Nfe2l2^{fl/fl}*) mice. mRNA expression levels were measured by RT-qPCR and normalized to *Tbp* expression. Results are plotted as mean \pm SEM of nine to eleven independent animals. * $p < 0.05$, ** $p < 0.01$ and *** $p < 0.001$ using Student's t-test.

Similarly to *Dmp1/Nfe2l2*-KO mice, the number of osteocytes were unaltered and the number of osteoclasts was significantly higher in male but not in female *Col1a1/Nfe2l2*-KO mice (Figure 43). In conclusion, our data demonstrate a sexually dimorphic, relevant role of NRF2 in osteocyte gene expression and function *in vivo* that results in lower bone mass and increased number of osteoclasts.

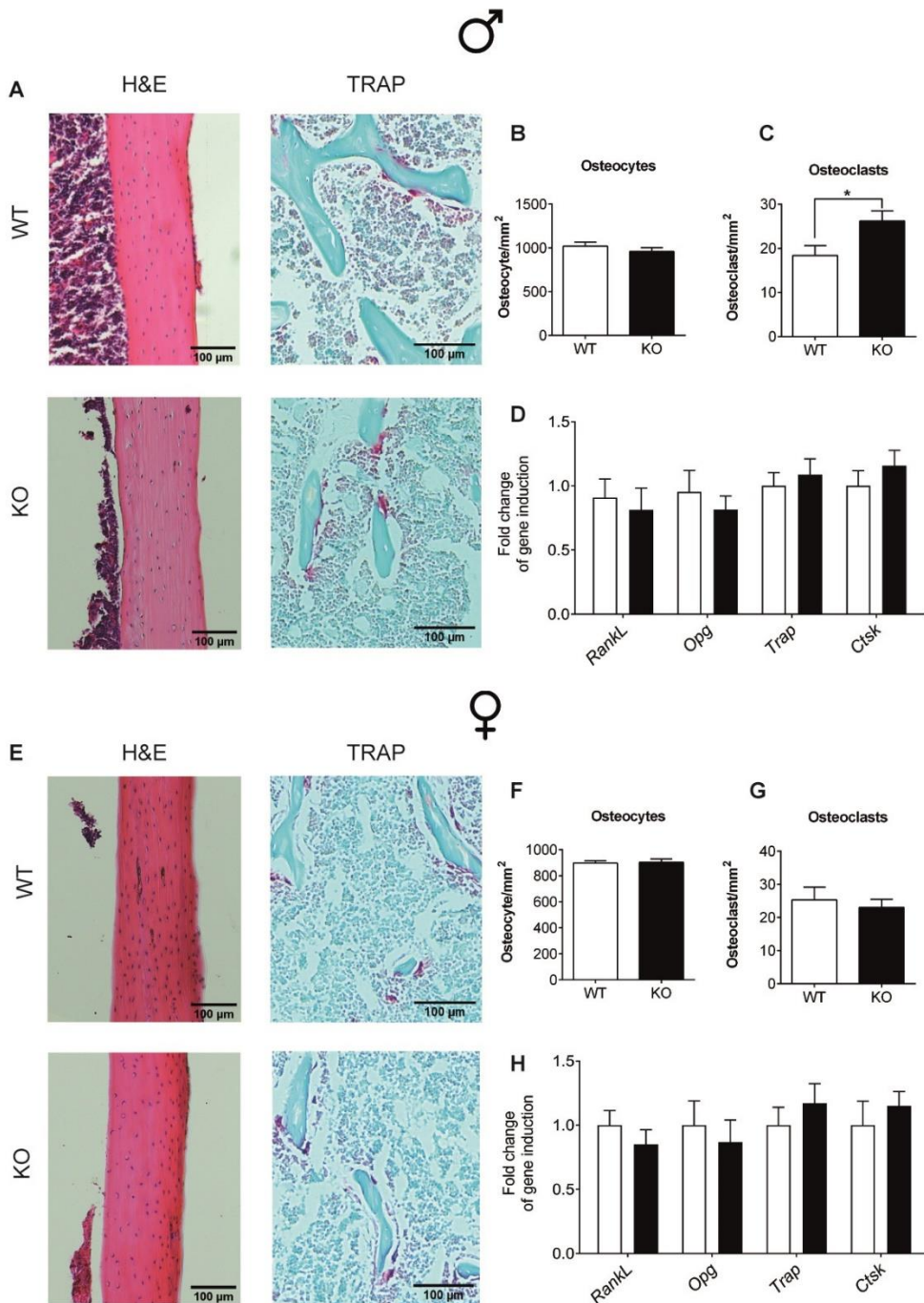


Figure 43. Histological analysis of femurs obtained from mice deficient of NRF2 in osteoblast. (A and E) Representative images of longitudinal sections of femur from male (A) and female (E) wild type (WT) and NRF2 knock-out (KO) mice stained with hematoxylin and eosin and TRAP. Images were

taken at 4x magnification. (B and F) Osteocyte number per area of cortical bone in male (B) and female (F) wild type (WT) and *Nfe2l2^{fl/fl};Col1a1-Cre* knock-out (KO) mice. (C and G) Osteoclast number per area of trabecula determined by TRAP staining from male (C) and female (G) wild type (WT) and *Nfe2l2^{fl/fl};Col1a1-Cre-Ert2* knock-out (KO) mice. (D and H) mRNA expression levels of relevant genes of osteoclast function from calvaria obtained from NRF2 conditional knock-out (*Nfe2l2^{fl/fl};Col1a1*) and control (*Nfe2l2^{fl/fl}*) mice. mRNA expression levels were measured by RT-qPCR and normalized to *Tbp* expression. Results are plotted as mean \pm SEM of seven to eleven independent animals. * $p < 0.05$, ** $p < 0.01$ and *** $p < 0.001$ using Student's t-test.

4. NRF2 activity regulates osteocyte-specific gene expression

Our data suggest that some of the effects observed *in vivo* arise from alteration of the paracrine communication between distinct bone cell types. Therefore, we sought to uncover the role of NRF2 deficiency and overexpression at different steps of osteocyte differentiation *in vitro*. To this end, we used CRISPR/Cas9 technology to generate IDG-SW3 clones deficient for *Nfe2l2* or *Keap1*. We infected IDG-SW3 cells with pLKO (a lentiviral plasmid with puromycin resistance) alone or coinfecting with pX458 containing the sequence for sgNrf2 or sgKeap1 (Romero et al., 2017) (Figure 44). We selected the infected cells with 5 μ g/ml for 48h. Then, we analyzed the expression of NRF2 target genes in the obtained pools of IDG-SW3 cells (Figure 42). We observed a slight reduction of the expression of NRF2 target genes in cells infected with sg*Nfe2l2*. On the contrary, cells infected with sg*keap1* tended to have increased levels of NRF2 target genes. However, neither of these changes in gene expression were significant. These results suggest the presence of non-genetically-engineered cells within the pool. Therefore, to avoid the effects of contaminants, we decided to generate single-cell clones.

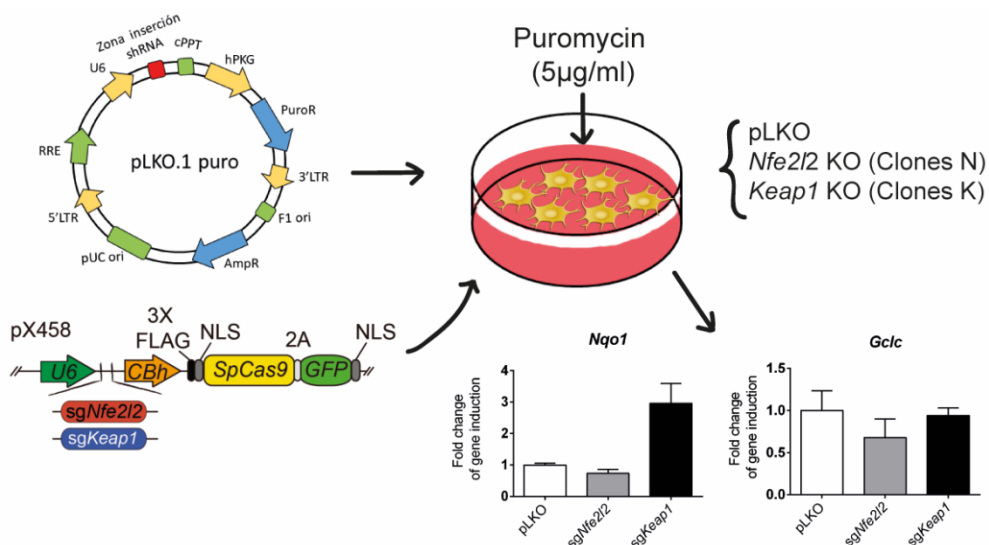


Figure 44. Schematic representation of the generation of IDG-SW3 cell knock-out for *Nfe2l2* or *Keap1*. IDG-SW3 were infected with the lentiviral vectors pLKO (puromycin resistance) alone (pLKO pool) or coinfecting with pX458 containing the sequence to target the genes *Nfe2l2* (*sgNfe2l2*) or *Keap1* (*sgKeap1*). We generated two different pools of each vector. Infected cells were selected with 5µg/ml for 48h. 24h post selection the expression of NRF2 target genes in each pool were analyzed. mRNA expression levels were measured by RT-qPCR and normalized to *Tbp* expression. Results are plotted as expression relative to IDG-SW3 cells infected with pLKO (mean ± SEM of two independent experiments). *p<0.05, **p<0.01 and ***p<0.001 using Student's t-test.

We generated 3 clones for pLKO, 18 clones for *sgNfe2l2* and 18 clones for *sgKeap1*. We sequenced the targeted region of the genomes in all the obtained clones (Figure 45 A). We found that pLKO clones showed no mutations in *Nfe2l2* nor *Keap1*. Only 4 of the 18 clones obtained from the infection with *sgNfe2l2* displayed mutation in the sequence of *Nfe2l2*. When mutated, *sgNfe2l2* clones presented alterations in both alleles of the gene. Finally, we were not able to generate IDG-SW3 deficient in KEAP1 since none of the 18 clones for *sgKeap1* displayed mutation in the sequence. To confirm that the genomic editing by CRISPR/Cas9 has effectively abolish NRF2 activity we analyzed the levels of NRF2 target genes in the selected clones (Figure 45 B). In all the cases, genome editing of *Nfe2l2* resulted in a dramatic reduction in the expression of *Nfe2l2* and its target genes. No significant differences were found in *Nfe2l2* and *Gclc* mRNA levels between the two selected pLKO clones, however, we found that pLKO.1 had higher expression of *Nqo1*. Significant differences were also found in the expression of *Nfe2l2* and *Nqo1* among the different clones *sgNfe2l2* clones.

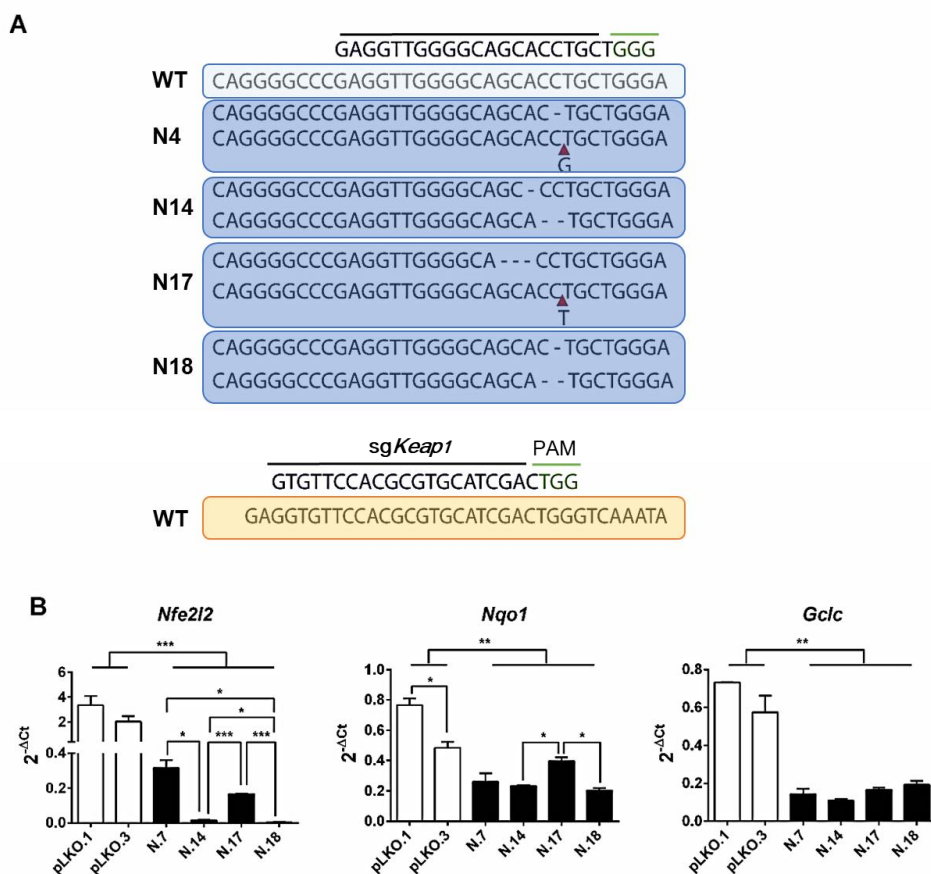


Figure 45. Validation of single-cell clones knocked-out for *Nfe2l2*. (A) Genome sequencing of the *Nfe2l2* target locus for the different sg *Nfe2l2* single-cell clones obtained. The sequences content the sg*Nfe2l2* binding site (black) and PAM sequence (green) Red arrows indicate insertion event. All clones were screened by Sanger Sequencing. (B) Expression levels of NRF2 target genes in the indicated single-cell clones obtained from infection with sg*Nfe2l2*. mRNA expression levels were measured by RT-qPCR and normalized to *Tbp* expression. Results are plotted as $2^{-\Delta Ct}$ (mean \pm SEM of three independent experiments). * $p < 0.05$, ** $p < 0.01$ and *** $p < 0.001$ using Student's t-test.

In recent years, several chemical activators of NRF2 have been developed. Among them, dimethyl fumarate (DMF) was shown to activate NRF2 and the antioxidant response and has been approved for treatment of multiple sclerosis or psoriasis (Linker et al., 2011). To corroborate that the changes in gene expression observed were triggered by disruption of *Nfe2l2*, we treated two selected clones (pLKO.3 and N.7) with 5 μ M DMF. As expected, pLKO.3 cells had increased levels of Nrf2 transcriptional targets, however, N.7 was refractory to the effect of DMF (Figure 46 A). Original IDG-SW3 constitute a model for osteocyte differentiation but we cannot guarantee that they conserve the capacity of differentiation after the

genetically-engineering process. Therefore, we examine the capacity of pLKO.3 and N.7 to differentiate *in vitro* and whether the expression of the human NRF2 could restore the phenotype. With this purpose, we infected pLKO.3 and N.7 with lentiviral vectors for *GFP* or the human *NFE2L2* gene and cultured the cells in differentiation medium for 5 days. We then analyzed the expression of NRF2 target genes, as well as gene markers for osteoblast and osteocyte differentiation (Figure 46 B). As expected, N.7 showed reduced levels of *Nqo1* and *Gclc*. Infection with human *NFE2L2* increased the levels of NRF2 target genes in pLKO.3 and rescue the levels of *Nqo1* and *Gclc* mRNAs in N7. Likewise, overexpression of *NFE2L2* in pLKO.3 significantly increased the expression of osteoblastic genes (*Runx2* and *Osterix*) while it only triggered a slight induction of the osteocyte gene *Dmp1*. Abrogation of *Nfe2l2* did not affect the expression of osteoblastic genes in N7, but it reduced the levels of *Dmp1*. However, expression levels of *Dmp1* could not be restored by overexpression of *NFE2L2* in N7. Rescue with NRF2 neither modified gene expression of osteoblastic genes in N7. Finally, we compare the expression of two osteocyte genes, *Dmp1* and *Fgf23* among two different control clones (pLKO.1, pLKO.3) and the knockout clone N7. Each clone presented different expression levels of osteocyte genes, independently of *Nfe2l2* status (Figure 46 C). Taking together these results demonstrated that we were able to generate *Nfe2l2* Knocked-out clones of IDG-SW3 cells. However, this process altered the capacity of IDG-SW3 to differentiation towards osteocytes. Consequently, we considered that Crispr/Cas9 genetically-engineered cells do not constitute a suitable model to study osteocyte differentiation and therefore we decided to investigate other approaches.

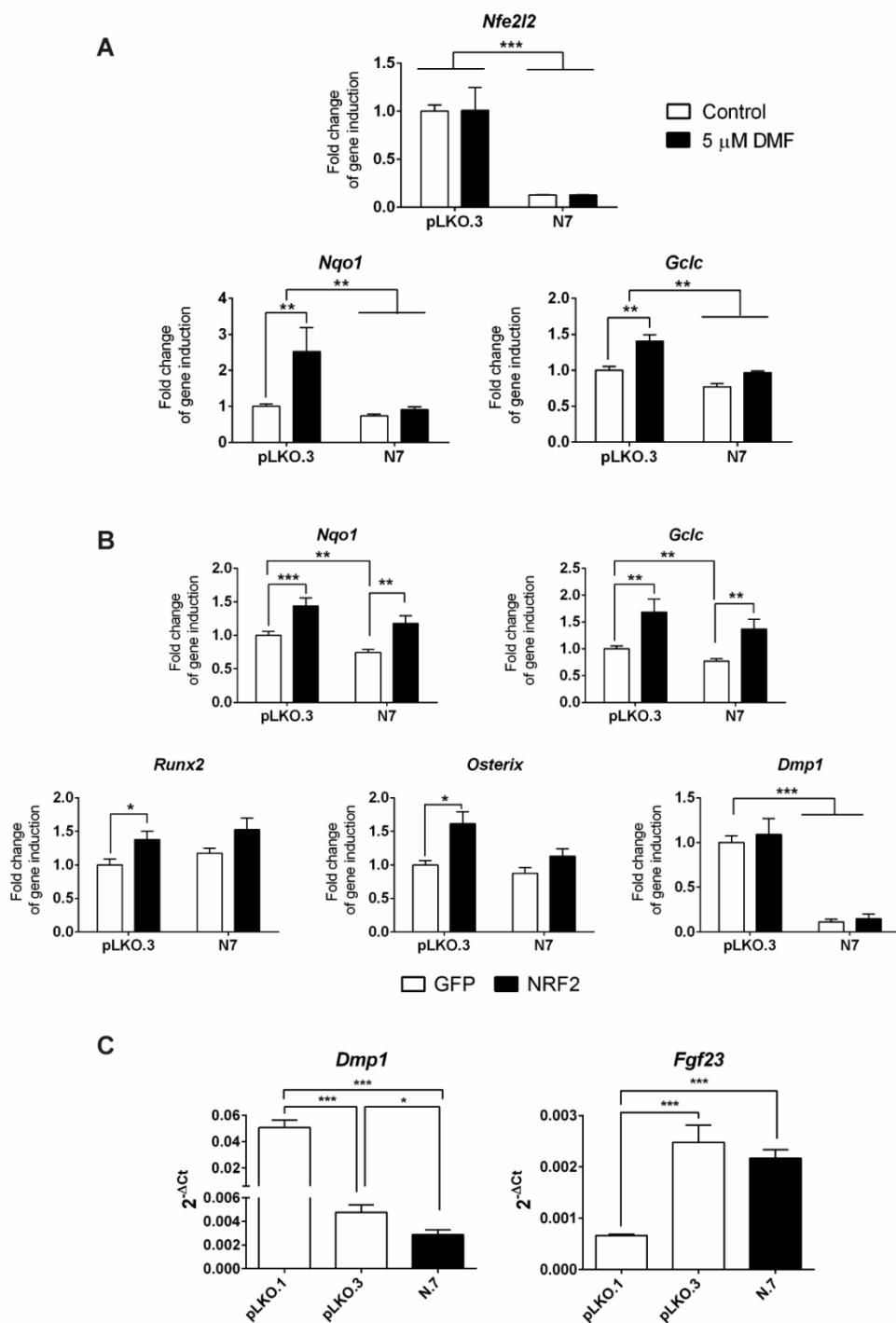


Figure 46. CRISPR/Cas9 genetically engendered clones present alteration in osteocyte differentiation. (A) Expression levels of NRF2 target genes in the control clone pLKO.3 and the clone N7 which harbor a mutation in *Nfe2l2* gene. All clones treated with 5 μ M DMF for 48 hours. mRNA levels were quantified by qRT-PCR, normalized by *Tbp* and plotted as expression relative to untreated pLKO.1 clone (mean \pm SEM; n=6) (B) Expression levels of NRF2 target genes and gene markers for osteoblast and osteocyte differentiation in pLKO.3 and N7 clones infected with *GFP* or *NFE2L2* overexpression vectors. mRNA levels were quantified by qRT-PCR, normalized by *Tbp* and plotted as expression relative to pLKO.1 clone infected with GFP (mean \pm SEM; n=6) (C) Expression levels of the osteocytic genes *Dmp1* and *Fgf23* in two control clones (pLKO.1 and pLKO.3) and the clone N7 with a mutation in *Nfe2l2*. mRNA expression levels were measured by RT-qPCR and normalized to *Tbp* expression. Results are plotted as $2^{-\Delta\Delta Ct}$ (mean \pm SEM of three independent experiments). *p<0.05, **p<0.01 and ***p<0.001 using Student's t-test.

To identify further cell-autonomous effects of *Nfe2l2* deletion, we look for other more physiological models. With this aim, we generated primary osteoblasts and osteocytes deficient for NRF2. We obtained osteoblast and osteocytes from transgenic mice that harbor the alleles of *Nfe2l2* floxed. Those cells were infected with CRE-recombinase or mocked vectors to generate knock-out and wild-types cells respectively. Then, we analyzed cell viability of osteoblast and osteocytes, wild-type and deficient for NRF2. We found that deletion of NRF2 in osteoblast slightly increased the number of death cells (Figure 47 A). This reduction of cell viability was even more significant in the case of osteocyte deficient for NRF2 (Figure 47 B).

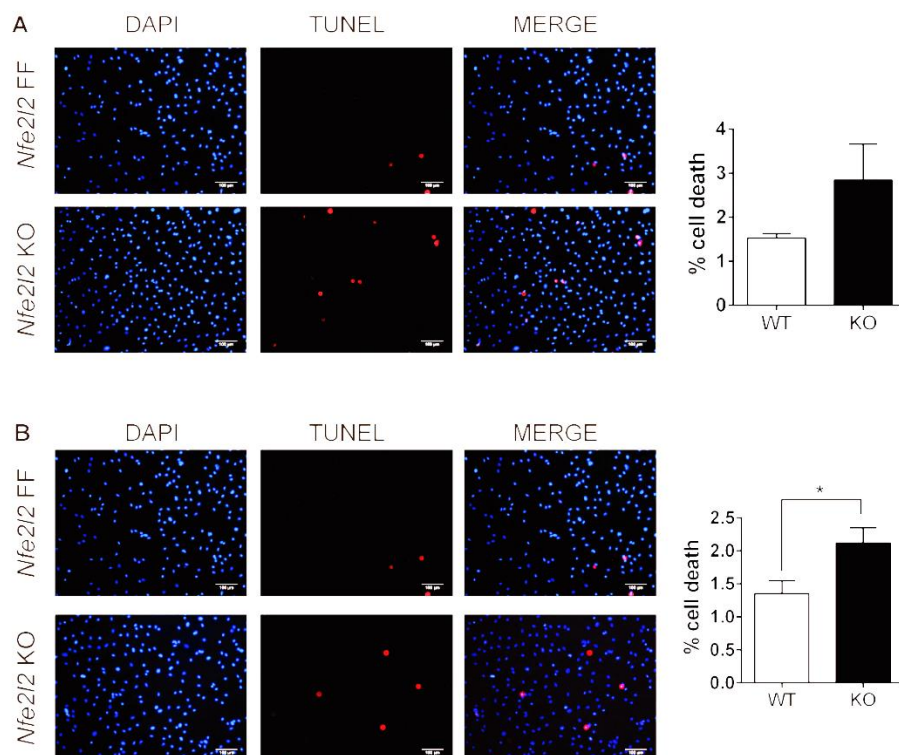


Figure 47. Loss of NRF2 affects cell viability. analysis of TUNEL staining in primary osteoblasts (n=6) (A) and osteocytes (n=10) (B) wild-type and KO for NRF2. Results are plotted as mean \pm SEM of three independent experiments. (E) Proliferation rate of primary osteoblasts wild-type and KO for *Ppargc1a/b*. Results are expressed as percentage of BrdU⁺ cells. Data are plotted as mean \pm SEM of three independent experiments.

As expected, expression of the NRF2 targets genes *Nqo1* and *Gclc* were strongly reduced. Osteoblasts and osteocytes displayed a reduced expression of osteocytic genes, including *Dmp1*, *Mepe*, *Fgf23* and *Sost* whereas major osteoblastic genes such as *Runx2*, *Osterix* or *Col1a1* were unaffected (Figure 48 A-B). Moreover, analysis of osteocytes overexpressing NRF2 showed the inverse effects, increased *Nqo1* and *Gclc* mRNA levels and the higher expression of the osteocytic genes *Dmp1*, *Mepe*, *Fgf23* and *Sost* (Figure 48 C).

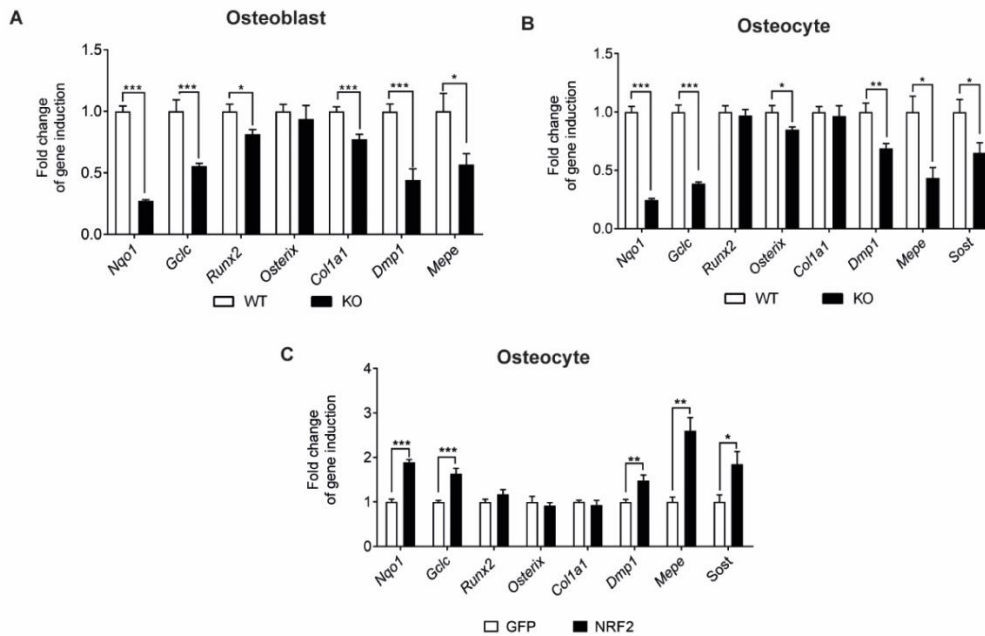


Figure 48. *Nrf2* controls osteocyte-specific gene expression. (A and B) mRNA expression levels of osteoblastic and osteocytic genes in (A) primary osteoblasts and (B) primary osteocytes wild type and knockout for NRF2. mRNA expression levels were measured by RT-qPCR and normalized to *Tbp* expression. Results were plotted as expression relative to wild-type cells (mean \pm SEM of nine independent experiments). (C) mRNA expression in primary osteocytes infected with NRF2 expression vectors. mRNA expression levels were measured by RT-qPCR and normalized to *Tbp* expression. Results were plotted as expression relative to cells infected with GFP vector (mean \pm SEM of six independent experiments). * $p < 0.05$, ** $p < 0.01$ and *** $p < 0.001$ using Student's t-test.

Mechanistically, increased expression of osteocytic genes upon activation of NRF2 could be directly triggered by the transcriptional effects of NRF2 or could be indirectly caused, emerging as a consequence of the decreased ROS levels upon activation of the anti-oxidative machinery. We tested this hypothesis by treatment of osteocytes deficient for *Nfe2l2* with 1mM N-acetyl-cysteine (NAC). Antioxidant treatment slightly reduced expression levels of NRF2 target genes in control osteocytes whereas in osteocytes deficient for *Nfe2l2* these responses were blunted (Figure 49). Either treatment of NAC or deficiency of *Nfe2l2* has no major effects on *Runx2* or *Col1a1* expression, and only slightly decreased *Osterix* mRNA levels in *Nfe2l2* deficient osteocytes (Figure 49). We confirmed that *Nfe2l2* deficiency reduced the levels of *Dmp1*, *Mepe* and *Sost*. More importantly, antioxidant effects of NAC not only did not alter expression of *Dmp1* in control or after *Nfe2l2* deletion but reduced *Mepe* and *Sost* mRNA expression independently of the *Nfe2l2* status (Figure 49).

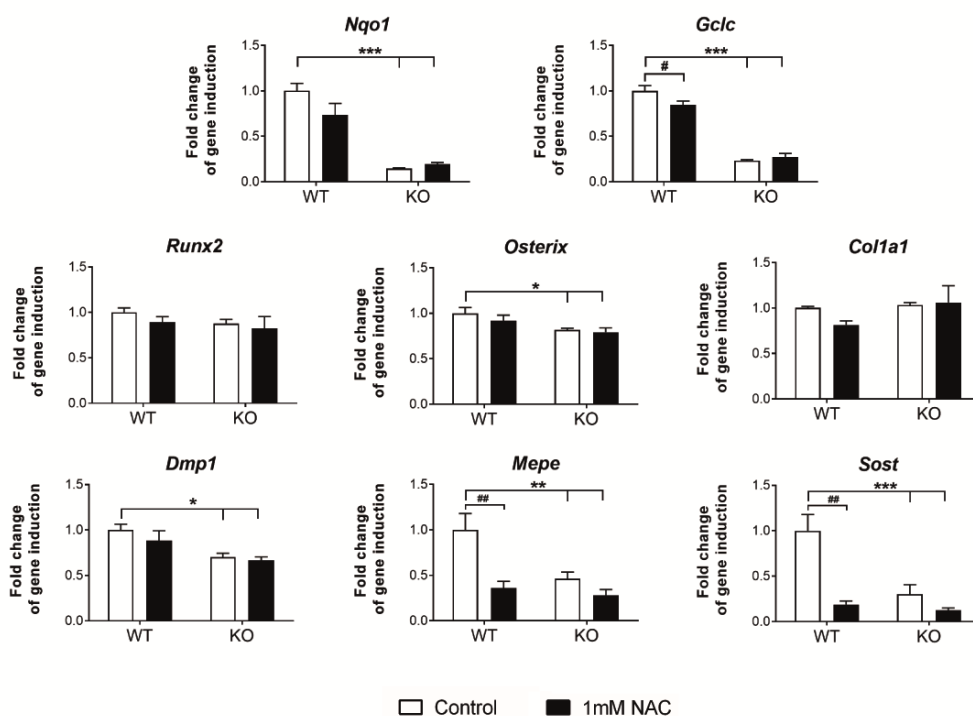


Figure 49. Modification of ROS and glutathione levels with NAC is not the main responsible mechanism for osteocyte differentiation. Primary osteocytes from *Nfe2l2^{fl/fl}* mice were infected with pMSCV-puro-Cre-ERT2 and treated with 1 μ g/ml tamoxifen to induce Cre recombination. Osteocytes were cultured for 48h in presence or absence of 1mM N-acetylcysteine (NAC, a ROS scavenger). Results were plotted as expression relative to cells infected with puromycin vector (mean \pm SEM of six independent experiments). * $p < 0.05$, ** $p < 0.01$ and *** $p < 0.001$ using Student's t-test.

NAC is a source of cysteins and can change redox thiol signaling independently of ROS status. Therefore, at this point we were unable to distinguish if the changes observed were produced by the effect of NAC in glutathione levels, or in ROS scavenging directly. Therefore, we treated osteocytes with Trolox, water-soluble analogue of vitamin E that acts as an antioxidant without affecting to glutathione. Supplementation with the analogue of vitamin E increased expression levels of NRF2 target genes in control osteocytes whereas in osteocytes deficient for *Nfe2l2* these responses were blunted (Figure 50). As for NAC, either treatment of Trolox or deficiency of *Nfe2l2* has no major effects on *Runx2* or *Col1a1* expression, and only slightly decreased *Osterix* mRNA levels in *Nfe2l2* deficient osteocytes (Figure 49). In the same way, antioxidant effects of Trolox not only did not alter expression of *Dmp1* in control or after *Nfe2l2* deletion but reduced *Mepe* and *Sost* mRNA expression independently of the *Nfe2l2* status (Figure 50).

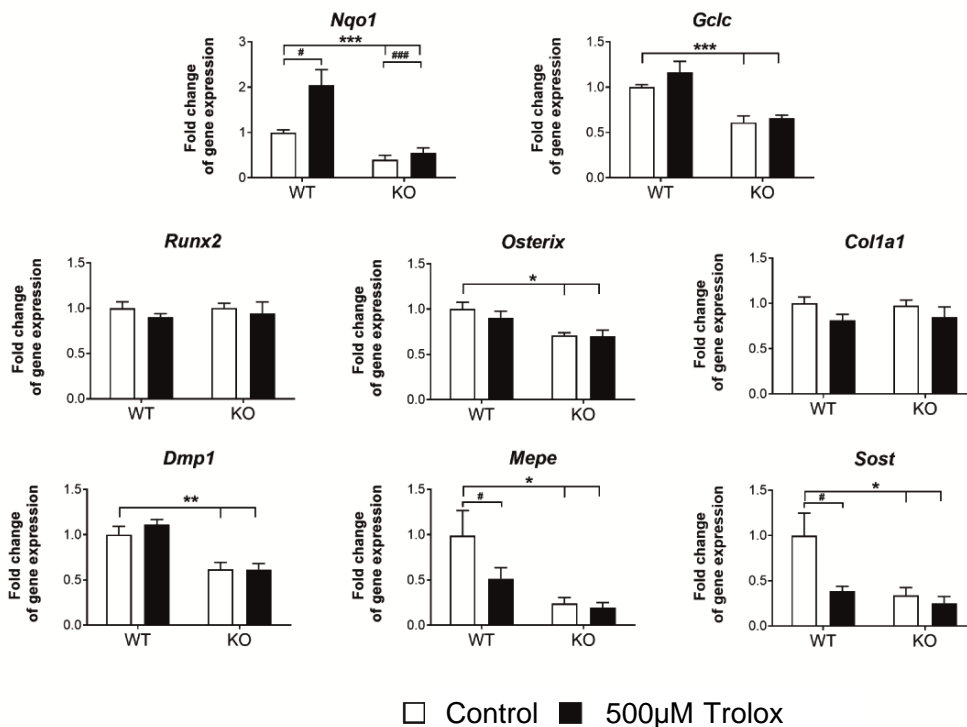


Figure 50. Reduction of total ROS levels hampers osteocyte differentiation. Primary osteocytes from *Nfe2l2^{fl/fl}* mice were infected with pMSCV-puro-Cre-ERT2 and treated with 1µg/ml tamoxifen to induce Cre recombination. Osteocytes were cultured for 48h in presence or absence of 500µM Trolox (a vitamin E analogue). Results were plotted as expression relative to cells infected with puromycin vector (mean ± SEM of six independent experiments). *p<0.05, **p<0.01 and ***p<0.001 using Student's t-test.

Previous experiments suggested that the main source of ROS during osteocyte differentiation were the mitochondria. To test this hypothesis, we analyzed the effect of MitoQ, a mitochondrial ROS scavenger, in osteocyte differentiation. Antioxidant treatment slightly increased levels of *Nqo1*, but did not affect *Gclc*, another NRF2 target gene in control osteocytes and osteocytes deficient for *Nfe2l2* (Figure 51). This result suggest that the antioxidant response induced by MitoQ is not mediated by NRF2. As for NAC or Trolox, either treatment of MitoQ or deficiency of *Nfe2l2* has no major effects on *Runx2* or *Col1a1* expression (Figure 51). Once again, *Nfe2l2* deficiency reduced the levels of *Dmp1*, *Mepe* and *Sost*. More importantly, as NAC and Trolox did not alter expression of *Dmp1* in control osteocytes but reduced *Mepe* and *Sost* mRNA expression independently of the *Nfe2l2* status (Figure 51). Altogether, the data suggests that ROS are important for osteocyte differentiation.

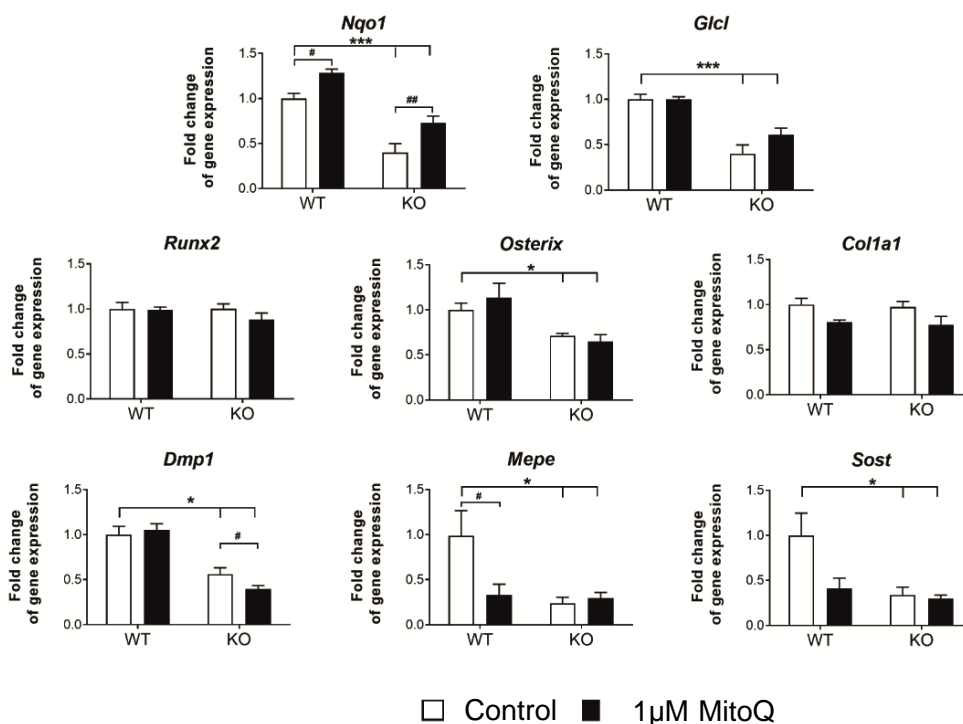


Figure 51. Reduction of mitochondrial ROS levels hampers osteocyte differentiation. Primary osteocytes from *Nfe2l2^{fl/fl}* mice were infected with pMSCV-puro-Cre-ERT2 and treated with 1µg/ml tamoxifen to induce Cre recombination. Osteocytes were cultured for 48h in presence or absence of 500µM Trolox (a vitamin E analogue). Results were plotted as expression relative to cells infected with puromycin vector (mean ± SEM of six independent experiments). * $p < 0.05$, ** $p < 0.01$ and *** $p < 0.001$ using Student's t-test.

To confirm further whether the expression of the osteocytic genes was modulated by NRF2, we treated osteocytes deficient for *Nfe2l2* with 5µM DMF. This dose is far below the maximum serum concentration of DMF when clinically administrated (www.accessdata.fda.gov/drugsatfda_docs/label/2013/204063lbl). As expected, DMF treatment increased *Nqo1* and *Gclc* expression levels in control osteocytes whereas osteocytes *Nfe2l2*-deficient osteocytes were refractory to changes upon DMF addition (Figure 48). DMF has no major effects on *Runx2*, *Osx* or *Col1a1* expression but strongly induced expression of *Dmp1*, *Mepe* and *Sost* mRNA expression in control cells. These responses were severely hampered in osteocytes deficient for *Nfe2l2* (Figure 52). Altogether, the data suggests that NRF2 activity leads to transcriptional activation of these genes.

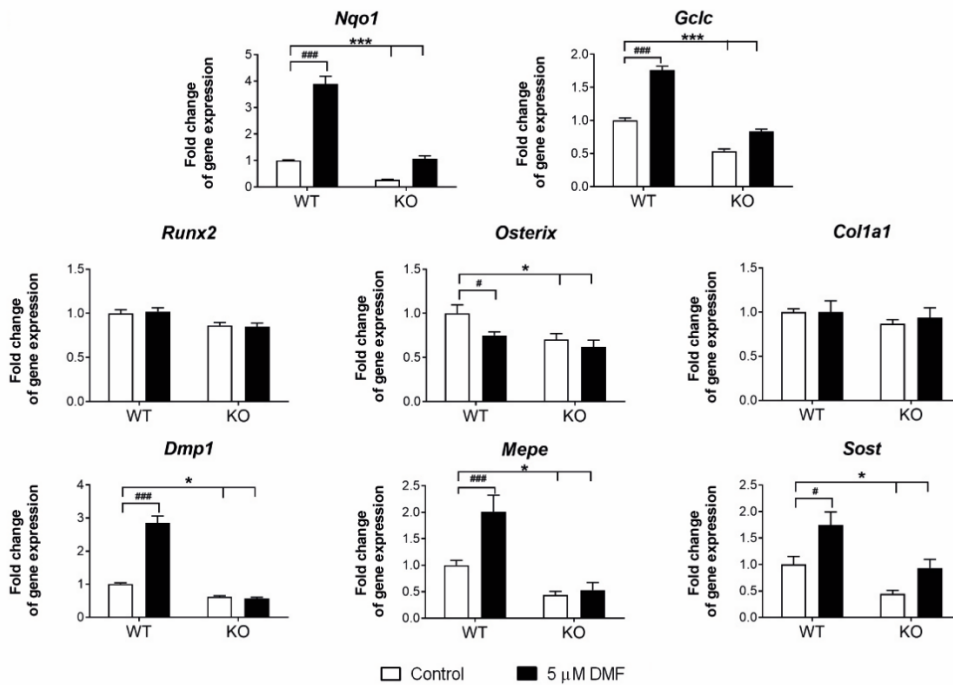


Figure 52. Activation of NRF2 induce osteocyte transcription program. Primary osteocytes transduced as above were cultured for 48h in presence or absence of 5μM dimethyl fumarate (DMF). Results were plotted as expression relative to cells infected with GFP vector (mean ± SEM of ten independent experiments). * $p < 0.05$, ** $p < 0.01$ and *** $p < 0.001$ using Student's t-test.

NRF2 is a transcription factor that preferential binding to ARE regions within the genome which usually lie outside the promoter-proximal region. Most of those NRF2 binding sites are placed in enhancers that act as binding platforms for transcription factors and are characterized by specific chromatin signatures of histone methylation and acetylation. In order to understand better the mechanism by which NRF2 promotes osteocyte differentiation, we analyzed the possible gene regulatory elements of three of the principal osteocyte genes (*Dmp1*, *Mepe* and *Sost*). Genomic analysis indicated that *Dmp1*, *Mepe* and additional SIBLING (Small Integrin-Binding Ligand, N-linked glycoproteins) family members such as *Dspp*, *Ibsp* or *Spp1* share the same topologically associated domain (TAD) in human chromosome 4 (Figure 53 A). Within the same TAD, we found the known NRF2 target *Abcg2* located in close vicinity to the osteocytic genes. Bioinformatic analysis of whole-genome NRF2-ChIPSeq data (GSE113497G) showed that this TAD is highly enriched in NRF2 binding sites (Figure 53 B) We confirmed the binding of NRF2 to the regulatory region of *Dmp1* by ChIP assays in primary osteocytes after DMF activation (Figure 53 C).

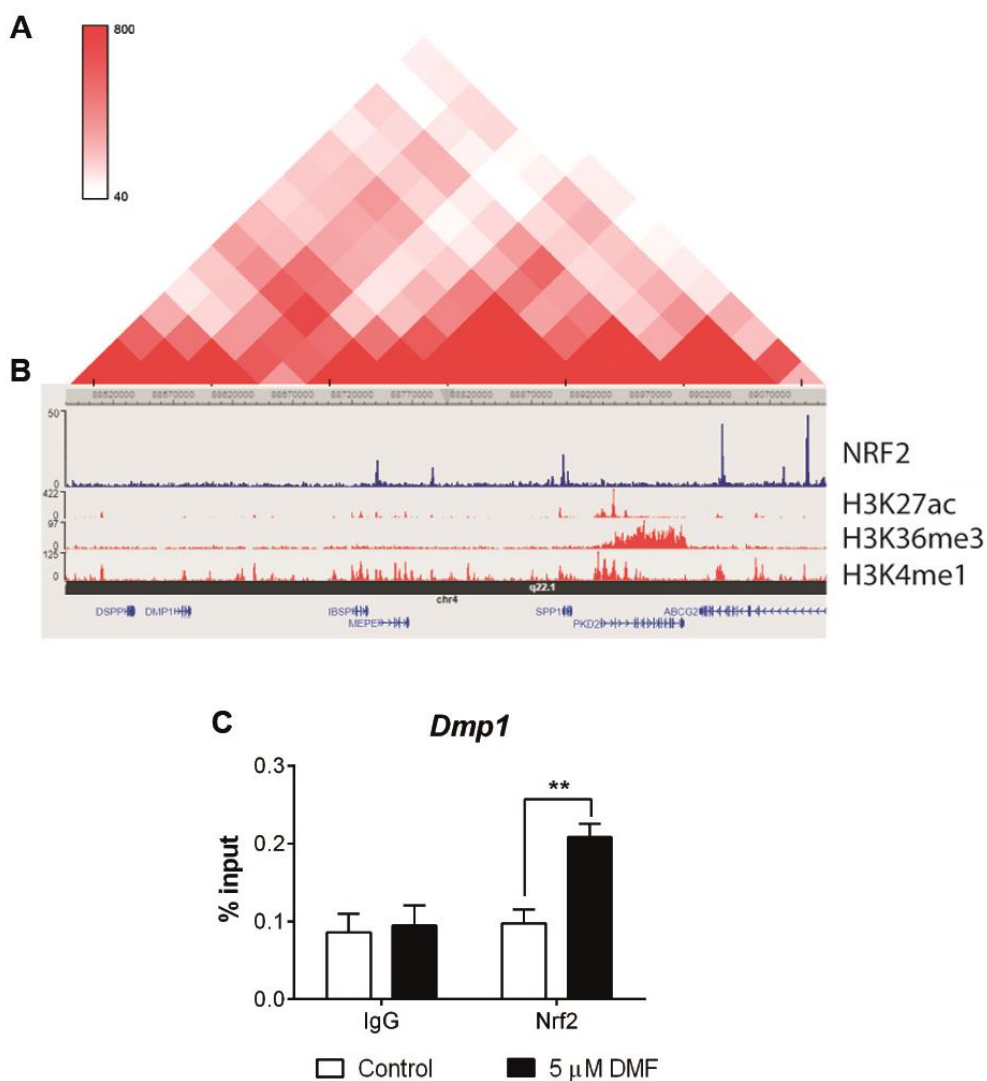


Figure 53. Sibling proteins are organized in a TAD regulated by NRF2 (A) Topological domain and looping structure indicated by Hi-C data from (Dixon et al., 2015) in MSC. The schematic shows TAD (red-shaded triangle) containing the SIBLING family of proteins. (B) ChIP-seq data showing NRF2 binding sites in A549 cells (data obtained from GSE113497), as well as active promoter/enhancer associated histone mark H3K27ac, gene body associated histone mark H3K36me3 and promoter associated histone mark H3K4me3 obtained from human osteoblast epigenome. (C). Chromatin immunoprecipitation from osteocytes cultured in the presence or absence of 5 μ M DMF for 48 hours. Results were normalized to input chromatin and plotted relative to untreated osteocytes (mean \pm SEM; n=5). *P<0.05, **P<0.01 and ***P<0.001 using Student's t-test.

Similarly, whole-genome NRF2-ChipSeq data (GSE113497G) showed a strong NRF2 binding site in a distal enhancer located 3' of the *Sost* gene (Figure 54 A-B). This

distal enhancer has been shown to be sufficient for inducing the expression of *Sost* (Sebastian and Loots, 2018; Collette et al., 2012). We also confirmed the binding of NRF2 to the regulatory region of *Sost* by ChIP assays in primary osteocytes after DMF activation (Figure 54 C). In conclusion, the data suggests that NRF2 activates expression of *Dmp1*, *Mepe* and *Sost* through direct binding to their regulatory regions.

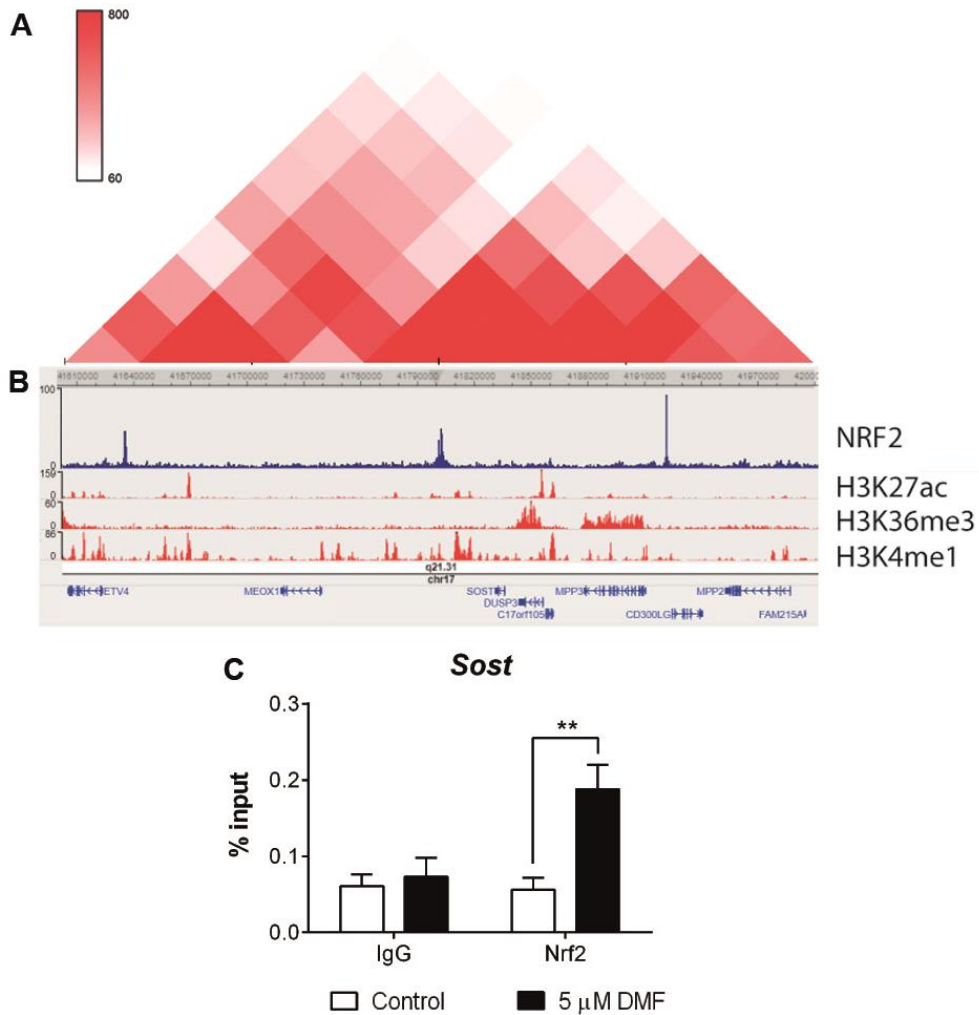


Figure 54. The osteocytic gene *Sost* belongs to a TAD regulated by NRF2 (A) Topological domain and looping structure indicated by Hi-C data from (Dixon et al., 2015) in MSC. The schematic shows TAD (red-shaded triangle) containing the gene *Sost* (B) ChIP-seq data showing NRF2 binding sites in A549 cells (data obtained from GSE113497), as well as active promoter/enhancer associated histone mark H3K27ac, gene body associated histone mark H3K36me3 and promoter associated histone mark H3K4me3 obtained from human osteoblast epigenome. (C) Chromatin immunoprecipitation from osteocytes cultured in the presence or absence of 5μM DMF for 48 hours. Results were normalized to

input chromatin and plotted relative to untreated osteocytes (mean \pm SEM; n=5). *P<0.05, **P<0.01 and ***P<0.001 using Student's t-test.

5. DMF treatment preserves bone mass and osteocytic gene expression in ovariectomy-induced osteoporosis

Oxidative stress has been implicated in numerous disorders. In the past decade, Nrf2-ARE pathway activation has been studied for the treatment of many disorders including chronic kidney disease, multiple sclerosis, hepatotoxicity or rheumatoid arthritis (Yamamoto et al., 2018). However, information about potential beneficial effects of pharmacological activation of NRF2 in bone pathologies is scarce (Yamaguchi et al., 2018; Bollag et al., 2019). We analyzed the effects of DMF in osteopenia induced by ovariectomy (OVX), an established model to induce osteoporotic bone loss. Ovariectomized mice were treated with 100mg/kg of DMF for 8 weeks. Then, we used MicroCT analysis to assess bone health. We found that cortical bone parameters were not significantly modified by either ovariectomy or DMF treatment (Figure 55A and B). However, ovariectomized mice displayed decreased trabecular bone mass, mostly due to a reduced number of trabeculae. More importantly, treatment with DMF restored the trabecular bone mass and increased the number of trabeculae and their thickness in ovariectomized mice (Figure 55 A and B).

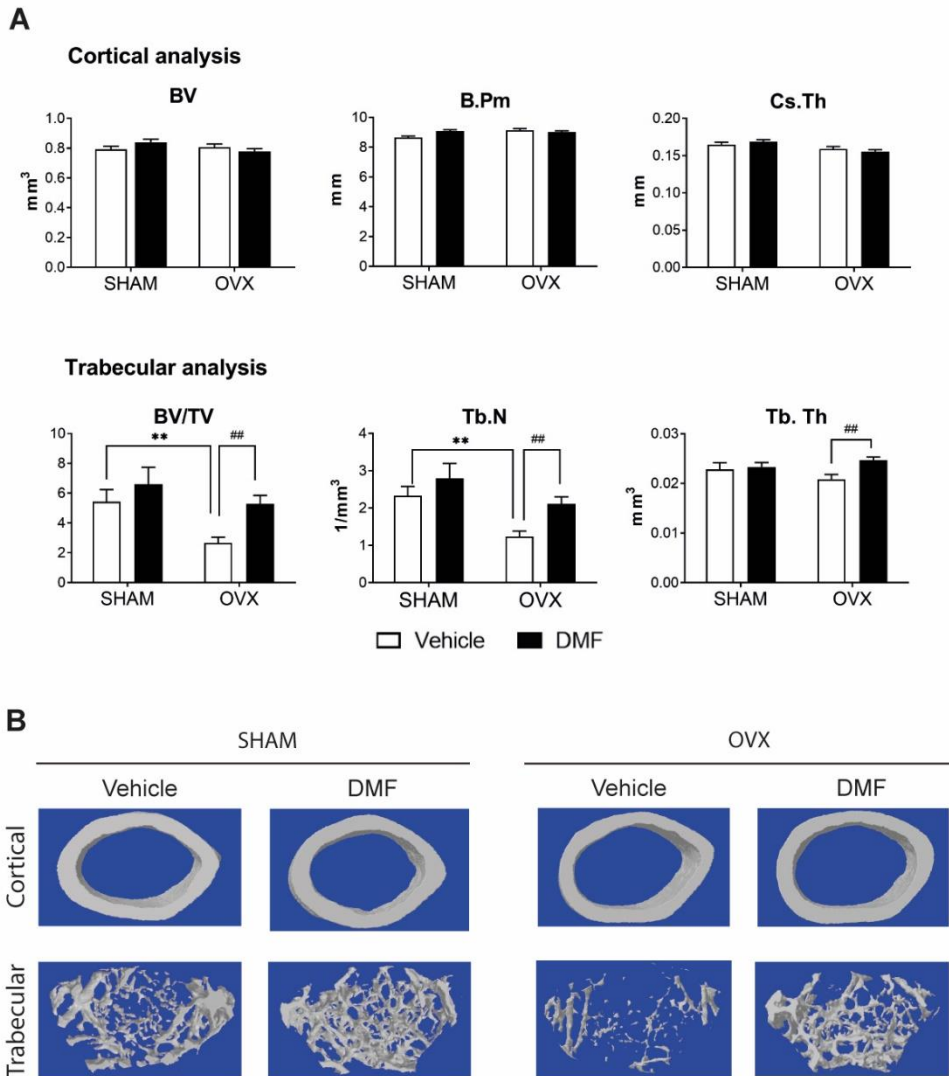


Figure 55. Dimethylfumarate (DMF) reduces bone loss induced by ovariectomy. (A) MicroCT analysis of femurs obtained from ovariectomized (OVX) and sham operated (SHAM) mice treated with 100 mg/kg of dimethylfumarate (DMF) or vehicle. (B) Representative images of cortical and trabecular section of femurs obtained from OVX and SHAM mice treated with 100 mg/kg of DMF or vehicle. Results are plotted as mean \pm SEM of seven to eleven independent animals. * $P < 0.05$, ** or ## $P < 0.01$, *** or ### $P < 0.001$ using Student's t-test. * refer to statistics performed against SHAM mice treated with vehicle. Similarly, # refers to significance between OVX mice treated with vehicle or DMF.

To analyze the effects of DMF treatment in osteocyte differentiation, we isolated RNA from mice calvaria. Gene expression analysis indicated that ovariectomy led to decreased levels of *Nfe2l2*, whereas DMF treatment restored the levels of *Nfe2l2* and increased the levels of its target *Nqo1* (Figure 56). Ovariectomized mice also had reduced expression of *Dmp1*, *Osx*, and *Sost*, whereas DMF treatment was able to rescue their gene expression in bone (Figure 52).

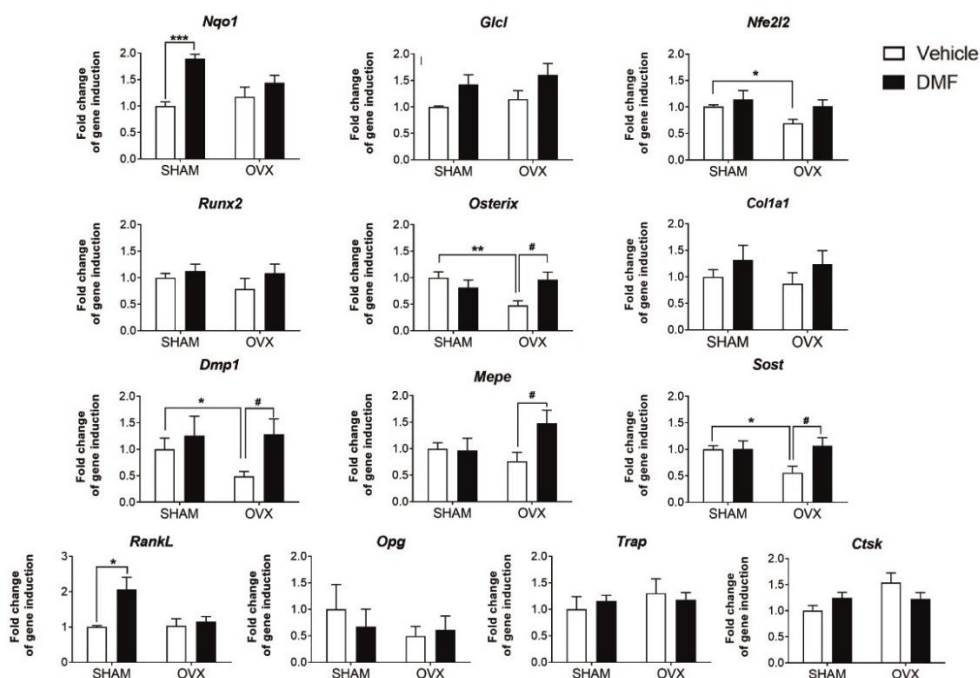


Figure 56. Dimethylfumarate (DMF) effect on bone gene expression after ovariectomy. mRNA levels in calvaria obtained from ovariectomized (OVX) and sham operated (SHAM) mice treated with 100 mg/kg of dimethylfumarate (DMF) or vehicle. mRNA expression levels were measured by RTqPCR and normalized to *Tbp* expression. Results are plotted as mean \pm SEM of seven to eleven independent animals. * $P < 0.05$, ** or ## $P < 0.01$, *** or ### $P < 0.001$ using Student's *t*-test. * refer to statistics performed against SHAM mice treated with vehicle. Similarly, # refers to significance between OVX mice treated with vehicle or DMF. * refer to statistics performed against SHAM mice treated with vehicle. Similarly, # refers to significance between OVX mice treated with vehicle or DMF.

Ovariectomy (OVX), like menopause, stimulates bone resorption by increasing osteoclast (OC) number and activity. In our model, histomorphometric measurements showed that the number of osteoclasts was significantly higher in OVX mice (Figure 53), even though the ratio *RankL*/*Opg* was not modified (Figure 56). Treatment with DMF reduced this increase in osteoclast number (Figure 57A and

B). On the other hand, neither ovariectomy nor DMF treatment induced significant changes in osteocyte number (Figure 57C and D).

These results demonstrate that DMF treatment restored the expression of the osteocytic genes *Dmp1*, *Osx*, and *Sost* and was effective in rescuing the osteopenic phenotype after ovariectomy.

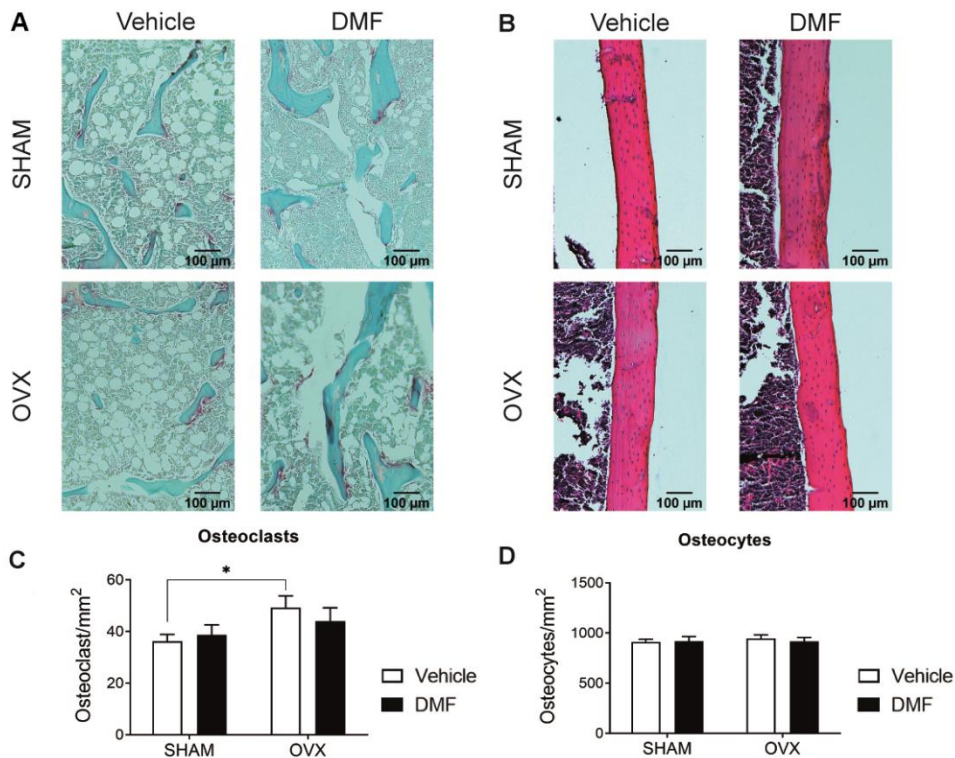


Figure 57. Dimethylfumarate (DMF) effect on bone histology after ovariectomy. (A) mRNA levels in calvaria obtained from ovariectomized (OVX) and sham operated (SHAM) mice treated with 100 mg/kg of dimethylfumarate (DMF) or vehicle. mRNA expression levels were measured by RTqPCR and normalized to *Tbp* expression. Results are plotted as mean \pm SEM of seven to eleven independent animals. (A and B) Representative images of longitudinal sections of femur from OVX and SHAM mice treated with 100 mg/kg of DMF or vehicle stained with (A) TRAP or (B) hematoxylin. Images were taken at 4x and 10x magnification, respectively. (C) Osteoclast number per area of trabeculae determined by TRAP staining from OVX and SHAM mice treated with 100 mg/kg of DMF or vehicle. Results are plotted as mean \pm SEM of seven to eleven independent animals. (D) Osteocyte number per area of cortical bone in femur from OVX and SHAM mice treated with 100 mg/kg of DMF or vehicle. Results are plotted as mean \pm SEM of seven to eleven independent animals. * $P < 0.05$, ** or ## $P < 0.01$, *** or ### $P < 0.001$ using Student's *t*-test. * refer to statistics performed against SHAM mice treated with vehicle. Similarly, # refers to significance between OVX mice treated with vehicle or DMF.



DISCUSSION

CHAPTER I: THE OSTEOCYTES.

1. The importance of osteocytes and challenges in their study

Before osteocytes were recognized as active essential bone cells, it was assumed that bone biology mainly took place on the bone surface and not within the bone. Osteoblasts forming bone and osteoclasts resorbing bone were considered the major players to maintain bone homeostasis. It was thought that osteoblasts and osteoclasts were regulated mainly by external factors such as parathyroid hormone, PTH or 1,25 dihydroxyvitamin D₃, and autocrine factors secreted by these two cell types. According to this model, osteoblasts secreted factors that regulate osteoclast activity and vice versa, osteoclasts released molecules to regulate osteoblast activity. At that time, osteocytes were left out of the picture and all the research in therapies for bone pathologies were focused to modify either osteoclast's or osteoblast's activities.

However, the development of new technologies make possible the study of osteocytes. Since then, osteocytes have not longer been considered as passive placeholders in bone. On the contrary, osteocytes have demonstrated to fulfill a wide amount of functions inside and outside the bone. Osteocytes have recently emerged as major orchestrators of bone remodeling, physical mechanosensors, hematopoietic niche cells and regulators of both phosphate and calcium homeostasis. (Dallas et al., 2013; Karsenty and Olson, 2016; Sato et al., 2013). In fact, the effect of osteocytes goes far beyond the bone, acting as endocrine controllers of whole-body metabolism. Osteocytes regulate primary lymphoid organs, control fat metabolism and increase muscle biogenesis and function (Brotto & Bonewald, 2015; Sato et al., 2013). Moreover, proteins released by osteocytes, such as FGF23 impact on kidney, heart and liver functions (Bonewald & Wacker, 2013; S. Singh et al., 2016). As osteocytes play a key role in whole body homeostasis, the abnormal or missing osteocyte function has been linked to several pathologic or disease conditions including sclerosteosis, hypophosphatemic rickets, osteoporosis, necrotic bone, aging and others. Therefore, novel therapeutics are being envisaged to target osteocyte factors, however, nowadays little is still know about the biology of this cell

type (Bonewald, 2017). Despite new techniques have arisen in the last years to study the bone, the localization of osteocytic cells within the matrix still difficult accessibility and study of these highly specialized cells. Calcified matrix supposes an additional challenge to perform common and basic approaches such as histology, and even after decalcification treatment, the remaining calcium content hampers the cutting and adhesion of the tissue to the glass. The development of the micro-computed tomography technology has revolutioned the bone field, as it makes possible the study of bone structure, obtaining a complete 3D picture nondestructively.

Working with osteocytes primary cultures *in vitro* is also challenging. The encasement of osteocytes within the mineralized matrix hampers their isolation and limit the yield of extraction. Therefore, despite osteocytes are the most abundant cells in the bone, the total number of cells obtained per animal is much lower than that for other bone cells such as osteoblasts or bone marrow mesenchymal stem cells. This problem has motivated scientists to improve the current protocols available, which are based on a series of demineralization and digestion steps of the bone particles (Bernhardt et al., 2020; Nijweide et al., 2003; Stern et al., 2012). But, even with all these efforts, the actual isolation methods are still tedious, had poor yield and contain a small fraction of other cells types such as cells from the hematopoietic lineage, osteoblasts and fibroblasts. Furthermore, primary osteocyte isolations are highly heterogeneous and may include cells of different stages of differentiation (Klein-Nulend et al., 2008). Moreover, as fully differentiated cells, osteocytes do not divide *in vitro*, which also reduce the potential cells available for experiments, while the small fraction of contaminants (fibroblasts and osteoblasts) can quickly overgrowth the culture. Furthermore, when osteocytes are detached their surrounding matrix, they dedifferentiate, and even when cultured in collagen coated plates, they lose their osteocyte-like phenotype. All these reasons limit the life span of osteocyte-rich cultures to one week and can affect the results obtained.

Due to all the limitations of *in vitro* cultures of isolated osteocytes, *ex vivo* bone organ cultures have raised as a convenient alternative. Cultured bone explants maintain the natural position of osteocytes within the extracellular mineralized matrix, thus preserving the *in vivo* 3D distribution. In addition, in bone organ cultures, the innate proportion of osteocytes compared with other cells (osteoblasts, osteoclasts, bone marrow cells, and endothelial cells) is maintained. Alternatively, *ex-vivo* bone organ cultured can be enriched in osteocytes by a series of EDTA-collagenase digestions. Moreover, *ex vivo* bone organ cultures allow the study of the effects of both genetic and pharmacologic manipulations on bone cells. More importantly, *ex vivo* bone organ cultures can be established with bones from

multiple species, including humans. For instance, fragments of anterior iliac crest, hip or knee can be obtained as surgical waste material. It is thought that *ex vivo* bone organ cultures will facilitate the translation of research findings into the clinic (Teresita Bellido & Delgado-Calle, 2020). However, this approach does not lack of several disadvantages, such as deficiency of blood supply, culture media perfusion, cell death and cell migration out of the bones after longer periods of culture, as well as the need to use highly rich culture media for applications requiring long-term culture. Moreover, due to the high ratio of extracellular matrix and bone cells, the total amount of biological material obtained is very low. On the other hand, cells cannot be isolated or visualized. Both facts limit the number of techniques that can be used for the study of the sample. Current research efforts are focused on reducing these limitations, such as the incorporating bioreactors that increase tissue perfusion and the development of chorioallantoic membrane culture systems (Abubakar et al., 2016).

Due to the difficulties associated with working with osteocytes, some experiments were carried out in osteoblasts as they are easier to isolate and maintain. Several approaches have been published to successfully isolate mesenchymal precursors and osteoblasts from bone. The method for primary osteoblast isolation from calvaria was firstly designed in 1964 by Peck (Peck et al., 1964), but high degree of contamination in the culture by fibroblasts was noticed. Previous researchers in our laboratory had developed a modification of Peck's protocol to isolate osteoblast with high efficiency and purity. This protocol consists on two serial digestions with collagenase. But, the necessity of isolating osteocytes makes us to modify the original protocol to obtain both cell lines from the same biological material. For this purpose, we add several steps of EDTA decalcification and collagenase digestion. We realized that this modification reduced even more the contamination with fibroblast and increased the yield of osteoblasts obtained. We use calvaria from new-born mice in order to avoid dealing with highly calcified tissue. Another advantage of working with osteoblast cultures is their capacity to survive longer than osteocytes. Osteoblast can be maintained *in vitro* up to three weeks without losing their phenotype. Moreover, they can be frozen and thaw maintaining a high viability and differentiation capacity. These properties allow us to study *in vitro* the molecular signalling governing the osteoblast biology and the pathways that controls differentiation, motility, adhesion, division or survival of osteoblasts. However, primary cultures of osteoblasts rarely differentiate to osteocytes *in vitro*. This fact makes us to wonder about the inputs regulating the final stage of osteogenic differentiation. For instance, the hypoxic environment, high confluence and the presence of a stiff extracellular matrix seems to be a necessary (Hirao et al.,

2007; Jeonghyun Kim & Adachi, 2019; Mullen et al., 2013), together with restrictions in the nutrient intake (Sánchez-de-Diego et al., 2019).

In the last years, the importance of osteocyte study increases while the problems regarding the generation of primary osteocyte cultures remains unsolved. Therefore, several cell lines have been developed to overcome this limitation. Existing cell lines such as MLO-Y4 (Yoichi Kato et al., 1997) and MLO-A5 (Y Kato et al., 2001) have several important drawbacks including transformation, constitutive expression of the large T antigen, absence of SOST/sclerostin or FGF-23 expression, and/or absence of a mineralized matrix. Therefore, better cell model systems are needed that demonstrate the gene expression profiles and function seen in primary osteocytes. In 2011, an Immortomouse/*Dmp1*-GFP-derived bone cell line (IDG-SW3) was established. This cell line was capable of overcoming many of the limitations of existing osteocytic cell lines, since cells were able to proliferate at 33°C in the presence of γ -IFN and to differentiate when cultured at 37°C in the absence of IFN- γ under differentiation conditions (Woo et al., 2011). In our lab, we confirmed that IDG-SW3 are able to express a full osteogenic differentiation profile from late osteoblast to late osteocyte including detectable levels of *Sost*, *Fgf-23* and *Dmp1* mRNA using real-time PCR (Figure 3) (Woo et al., 2011). Moreover, GFP reporter paralleling osteogenic differentiation (*Dmp1*-GFP) was very useful, enabling us to live monitoring osteocyte transition in our experiments (Figure 2). For all these reasons, the acquisition of this cell line in the laboratory has been an extremely valuable experimental tool. However, IDG-SW3 are not exempt of drawbacks. IDG-SW3 cannot be transfected with common transfection methods (PEI, calcium phosphate, Lipofectamine, DOTAP) and lentiviral particles are the only effective delivery method for genetic manipulations. Moreover, as IDG-SW3 differentiate, they increase in size, complexity and autofluorescence complicating the interpretation of data obtained from fluorescence experiments and limiting the application of flow cytometry and confocal microscopy. Finally, we evidenced that the IDG-SW3 is not a suitable model for the application of CRISPR/Cas9 technology since the process of single-cell clone generation produce several cells population with different basal potential of differentiation (figure 44). Heterogeneity in differentiation potential of the different control clones can mask the effect of the genetic manipulation.

During this thesis, *in vitro* culture of primary osteoblasts and osteocytes, as well as cell lines have been the main approach for studying signalling and molecular interactions in bone. However, when performing experiments *in vitro* many physiological interactions are lost, and the relative contribution of the process to bone health can be misinterpreted. Therefore, we always confirmed our hypothesis in mice models in order to evaluate the impact of the described mechanisms over

the whole organism. For instance, the importance of the PGC-1 α/β and NRF2 was tested in mice with ablation of those proteins in bone cells. Tissue specific knock-out allows us to evaluate the function of the studied proteins exclusively in osteoblasts and osteocytes, reducing the impact that these modifications can have in other organs that also could affect at bone homeostasis. Nowadays, in our laboratory we have two different mice strains that harbor Cre recombinase under the control of the promoter for *Col1a1* or *Dmp1*, to perform deletions specifically in osteoblasts or osteocytes, respectively. We have observed that, for some proteins, such as NRF2, the results obtained varied depending on the cell line where the deletion is made (Figures 36 and 39). These effects might help us to have a deeper knowledge about the contribution of each molecular mechanism in the different steps of bone cell differentiation.

CHAPTER II: METABOLISM AND DIFFERENTIATION.

1. Osteoblast-to-osteocyte transition is associated to an increase in OXPHOS activity and ROS generation.

Like other metabolically active cells, bone cells regulate their rate of fuel consumption and catabolism to accommodate changing energy demands at different stages in their life spans. Such metabolic flexibility is achieved by signaling molecules and transcription factors which work in concert to connect extracellular inputs with downstream bioenergetic pathways (Riddle & Clemens, 2017). BMMSCs and osteoblasts in early stages of specification rely on glycolysis to generate ATP, initiate collagen synthesis and stabilize RUNX2 expression (Guntur et al., 2018; J. Wei et al., 2015). Accordingly, molecular signals that determine osteoblast specification, such as Wnt, PTH or HIF-1, also promote aerobic glycolysis in osteoblast progenitors (Esen et al., 2013, 2015; Regan et al., 2014). However, osteocytes contribute little to glucose consumption in murine bones compared to osteoprogenitors and osteoblasts (Galloway et al., 2012). In fact, it has been recently shown that bone accumulates a significant fraction of postprandial fatty acids that seems to be crucial for mature osteoblasts and osteocytes (Quinn et al., 2010). Osteocyte transition and network formation processes are likely to demand high levels of energy, however, in the adult human skeleton, osteocytes are entrapped in their own mineralized matrix that only leaves space for 24 ml of extracellular fluid in the whole skeleton (Buenzli & Sims, 2015), restricting the access to nutrients. Therefore, osteocytes must adapt their metabolism to satisfy their high energy demands in a nutrient-restricted environment. In recent years, we and others have demonstrated that, a shift of the metabolic machinery towards a higher mitochondrial function occurs during the transition of osteoblasts into osteocytes in order to optimize energy production and fulfill the functional demands (Hirao et al., 2007; Sánchez-de-Diego et al., 2019; Stegen et al., 2016). Accordingly, our data corroborate the increase in mitochondrial mass and function during osteocytogenesis (Figures 31-33). This link between metabolic reprogramming and cellular specification was already well established for

other models of cell specification. For example, higher mitochondrial biogenesis and function is related to the final stage of neurogenesis, astrocytogenesis, hepatic differentiation and erythropoiesis (Regan et al., 2014; Riddle & Clemens, 2017).

Mitochondria is the mayor source for ROS, which mainly arise as byproducts of oxidative phosphorylation. As expected, we observed that the levels of ROS levels increased in parallel with the increase in mitochondrial respiration (Figures 32-33). Unregulated accumulation of ROS has been shown to be a major contributor to aging and several diseases that include osteoporosis and bone diseases (Callaway & Jiang, 2015). On the other hand, physiological levels of ROS mediate mitochondria-nucleus crosstalk and function as a rheostat to coordinate cellular metabolism with chromatin remodeling, gene expression, cell cycling, DNA repair and cell differentiation (Bigarella et al., 2014). We found that slight variations in ROS content, at non-toxic levels can actually contribute to osteocyte specification as shown for other mesenchymal stem cell differentiation processes (Atashi et al., 2015; K. S. Kim et al., 2010; G.-S. Liu et al., 2012).

These data indicate for the first time that metabolic reprogramming occurs in parallel with osteocyte differentiation and that probably both processes will be interdependent. Now, the next question to address is which molecular signals and pathways involved in the initiation and coordination of both events.

2. Glucose restriction promotes metabolic reprogramming and differentiation in osteocytes

In this study, we identified that a reduced supply of glucose facilitates the expression of osteocytic genes in osteoblast/osteocyte precursors. These effects take place in parallel with an increase in mtDNA and mitochondrial function. On the other hand, culture medium with high glucose concentration impaired osteoblast and osteocyte gene expression and altered mitochondrial organization (Figures 6-9, 12-13). Not surprisingly, hyperglycemic microenvironments have been previously associated with a reduction in osteocyte number and function (Rinker et al., 2014) while bone turnover and remodeling have been found to be compromised in diabetic conditions (Kalaitzoglou et al., 2016). These results evidence that glucose is a key regulator for both metabolic reprogramming and osteocyte differentiation.

Consistent with its role as regulator of energy homeostasis, we found an inverse correlation between AMPK activity and glucose supply, even when ATP levels were maintained (Figures 6-7, 14-15). These results agree with new evidence showing that AMPK became activated by phosphorylation at Thr172, not only by

sensing low cellular energy but also low glucose supply (S. C. Lin & Hardie, 2018; C. S. Zhang et al., 2017). We also demonstrated that activation of AMPK with AMP analogs in normoglycemia is sufficient to induce osteocyte gene expression in IDG-SW3 cells and organotypic bone cultures (Figures 16,17). AMPK activation in osteocytes also decreases *Rankl* and increases *Sost* expression to delicately coordinate bone turnover (Kanazawa et al., 2018). Indeed, studies using whole-body and osteoblast-specific genetic abrogation of AMPK activity showed lower cortical and trabecular bone density and enhanced bone turnover (Jeyabalan et al., 2012; Kanazawa et al., 2018). Our data also demonstrate that activation of SIRT1 by SRT2104 led to increased osteocyte gene expression program in IDG-SW3 cells and organotypic bone cultures (Figures 16,17). In a similar way, mice fed on a diet supplemented with SRT2104 showed an increase in bone mineral density which was dependent on *Sirt1* activity (Mercken et al., 2014). Moreover, SIRT1 activation with resveratrol gives protection against osteoporosis in both mice and humans (Ornstrup et al., 2014). The beneficial role of SIRT1 in bone formation and remodeling were further confirmed in whole-body and osteoblast-specific *Sirt1*-deficient mice, which displayed low bone mass phenotype (Cohen-Kfir et al., 2011).

These results evidence that glucose restriction itself is sufficient to activate molecular signaling pathways involved in metabolic reprogramming and to promote osteocyte specification program.

3. PGC-1 enhances osteocytic differentiation in response to reduced glucose supply.

We identified a key role of PGC-1, downstream of AMPK, in the coordination of mitochondrial biogenesis and osteocyte specification in cultured cells and in murine models. PGC-1 α and β seems to play a redundant transcriptional role in many tissues since noticeable phenotypes were only observed when the expression of both coactivators was abolished (Villena, 2015). Interestingly, we observed that osteoblasts and osteocytes express *Ppargc1a* in preference to *Ppargc1b*. Moreover, osteoblast-to-osteocyte transition further increased this tendency (Figure 18 A). On the contrary, PGC-1 β is the main member of the PGC-1 family expressed in osteoclasts and is specifically required for osteoclast function (W. Wei et al., 2010; Y. Zhang et al., 2018).

To study the importance of PGC-1 family members in bone homeostasis, we abrogate the expression of both proteins in osteoblasts and osteocytes in order to avoid possible compensatory effects. Our data show, for the first time, that PGC-1 α/β also have a fundamental role in osteoblast/osteocyte function and bone

homeostasis (Figure 28). Furthermore, we discovered that the effects of glucose in osteocyte differentiation were dependent to the activation of the AMPK/PGC-1 pathway, since osteoblasts deficient in *Ppargc1a* and *b* were refractory for glucose restriction (Figure 24).

PGC-1 co-activates specific transcription factors, including NRF1, NRF2, PPARs, ER α , ERR α and MEF2C (Villena, 2015). Co-activation of diverse transcription factors by PGC-1 has been shown to deeply affect developmental transcriptional programs such as erythropoiesis, chondrogenesis and differentiation of hepatocytes, cardiomyocytes and brown adipocytes (Cui et al., 2014; Wanet et al., 2017). Our data show that this would be also the case for osteocytogenesis, since several of this transcription factors, such as ER α , NRF2, PPARs, ERR α and MEF2C, positively regulate osteocyte gene expression (Kramer et al., 2012; Stechschulte et al., 2016). In fact, it has been already demonstrated that ER α transcription factor affect bone mineral density only in male mice (K. Lee et al., 2003; Windahl et al., 2013) and therefore it could account for the milder osteopenic phenotypes that we obtained in female. Moreover, PGC-1 α binds to the *Fgf23* or *Sost* gene promoters (Figure 30) whereas overexpression and loss-of-function experiments produce effects on the expression of *Dmp1*, *Dkk1*, *Fgf23*, *Sost* or *Osx* genes (Figure 24, 30). We found numerous conserved binding sites for known transcription factors in the promoter and enhancer regions of *Fgf23*, *Sost*, *Dmp1* and *Osx* genes, including MEF2C, ER α , NRF2, PPARs and ERR α that could mediate their regulation by PGC1- α . However, at present, the transcription factors directly involved in this co-activation in specific gene promoters are still unknown and would require further investigation.

Although we have studied the effects of *Ppargc1a/b* deletion in osteoblast and osteocyte cell cultures, in our experiments *in vivo*, *Ppargc1a/b* were deleted in both osteoblasts and osteocytes. Therefore, we are unable to distinguish the relative contribution of PGC-1 of each cell type in bone homeostasis.

Altogether, we identified that a reduced supply of glucose facilitates metabolic reprogramming during osteoblast to osteocyte transition and increased the expression of osteocytic genes in osteoblast/osteocyte precursors. These effects were dependent to the activation of the AMPK/PGC-1 pathway, and its deficiency leads to osteopenia. Altogether, we have uncovered a central role of PGC-1-mediated transcriptional program leading to osteocyte specification. However, further studies should be done to understand the contribution of PGC-1 in each stage of osteocyte differentiation.

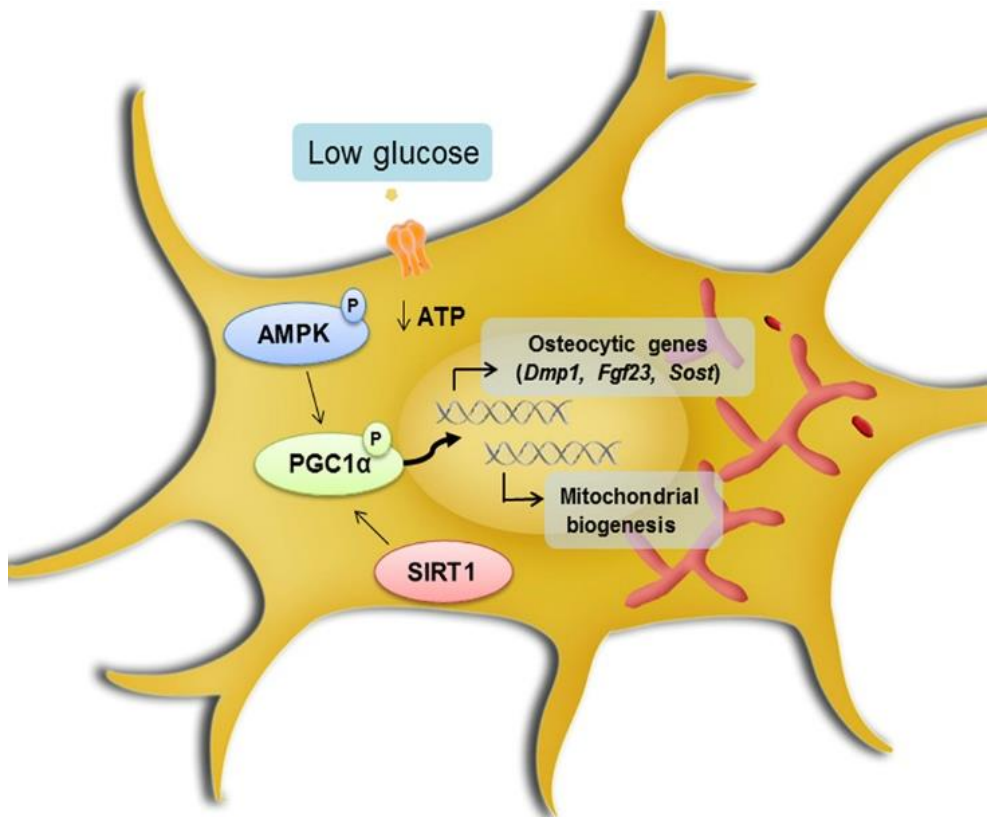


Figure 1. Glucose Restriction Promotes Osteocyte Specification by Activating a PGC-1 α -Dependent Transcriptional Program. Reduced supply of glucose induce metabolic reprogramming in osteocytes to fulfill the energetic demands. During differentiation osteocyte increase glucose uptake and mitochondrial number and function. These effects took place in parallel with an increased expression of osteocytic genes. Glucose reduction triggers the activation of the AMPK/PGC-1 pathway. Once active, PGC-1 migrates to the nucleus where it binds to different transcription factors and induce the expression of genes involved in mitochondrial biogenesis and osteocyte differentiation.

4. NRF2 enhances osteocytic differentiation in response to an increase in ROS levels during metabolic reprogramming.

In this study, we also identified that as a consequence to their increase in mitochondrial function, ROS levels increases during osteocyte differentiation (Figure 31-33). Physiological levels of ROS act as an important signal mediator, activating different molecular pathways including NF- κ B, MAPKs, Keap1-Nrf2-ARE and PI3K-Akt, ion channels such as Ca²⁺ and mPTP (J. Zhang et al., 2016). Activation of some of this signaling pathways, such as MAPK or PI3K-AKT, had been already associated with osteoblast differentiation (W. Huang et al., 2007; Eddie Rodríguez-Carballo et

al., 2016; Sánchez-De-Diego et al., 2019). In this study we focus on the role of Keap1-Nrf2-ARE in osteocyte differentiation. Consistent with its function as regulator of oxidative stress, we found a correlation between NRF2 activity, mitochondrial activity and ROS levels during osteocytogenesis (figure 31-34). Moreover, NRF2 activity increases mitochondrial function as a feed-forward loop (Holmström et al., 2013).

The role of NRF2-KEAP1 in bone homeostasis had been previously studied in several animal models, however its effects remained unclear. It seemed that it may depend on factors, such as age, sex or high vs. low activation levels (Park et al., 2014a; Pellegrini et al., 2017; Yin et al., 2020). For instance, some studies revealed that deletion of *Nfe2l2* in female mice results in a deficit in postnatal bone acquisition and increased bone loss (Ibáñez et al., 2014; J.-H. H. Kim et al., n.d.; Pellegrini et al., 2017). However, similar *Nfe2l2*-deletion approaches in male mice led to controversial results. Some studies reported increased bone acquisition and mass (Park et al., 2014a; Pellegrini et al., 2017) whereas others showed reduced bone density, load-driven bone formation, and increased radiation-induced bone loss (Rana et al., 2012; Role of Nrf2 in bone metabolism, 2015). Similarly, moderate NRF2 activation by heterozygous deletion of *Keap1* led to sexual dimorphic results with higher bone mass in males but not in female mice (Yin et al., 2020). All these previous studies have the limitation that genetic modifications affected to all the murine cells and tissues, then alterations in paracrine and endocrine factors could influence bone homeostasis. Therefore, to address the unresolved issues of the role of NRF2 in bone cells, we analyze cortical and trabecular bone parameters in cell-type specific knockout mice of NRF2. We developed two different models, *Dmp1/Nfe2l2*-KO and *Col1a1/Nfe2l2*-KO to delete *Nfe2l2* in osteocytes and osteoblast and osteocytes respectively. In both models, the effect of NRF2 deletion on bone mass is more pronounced in male mice confirming the sexual dimorphism observed by other studies (Figures 36, 39) and provide additional information to understand this effect. Although in our study deletion was performed only in the osteoblast/osteocyte lineages, dimorphic effects in bone parameters correlate with differential changes in osteoclast numbers. Supporting this hypothesis, it has been shown that dissimilar expression of cytoprotective genes, *Rankl/Opg* ratio or osteoclast numbers correlate with different effects of *Nfe2l2* deletion in bone maintenance depending on the sex (Figures 38,41) (Pellegrini et al., 2017; Yin et al., 2020). Furthermore, NRF2 has been shown to negatively regulate the expression of cytokines that induce osteoclastogenesis, such as IL-1 α , IL1 β , IL6, TNF α or RANKL (Amarasekara et al., 2018; Kobayashi et al., 2016; Narimiya et al., 2019) Therefore, is plausible to suggest that deletion of *Nfe2l2* in osteocytes and mature osteoblasts would increase paracrine osteoclastogenic signaling. In the other hand, interaction between NRF2

activation and signaling downstream of the sex steroid receptors could contribute to this sex-specific differential regulation. For instance, NRF2 displays transcriptional cooperation with ERs, which differentially affects bone parameters in female and male mice (Khalid & Krum, 2016). Similarly, NRF2 modifies androgen receptor (AR) transactivation whose function in osteocytes is required for proper bone homeostasis (Sinnesael et al., 2012). NRF2 has been shown to negatively regulate the expression of cytokines that induce osteoclastogenesis, such as IL-1 α , IL1 β , IL6, TNF α or RANKL (Amarasekara et al., 2018; Kobayashi et al., 2016; Narimiya et al., 2019). Therefore, we suggest that deletion of *Nfe2l2* in osteocytes and mature osteoblasts would increase paracrine osteoclastogenic signaling.

Interestingly, *Dmp1/Nfe2l2*-KO mice of both sexes display severe osteopenia, while *Col1a1/Nfe2l2*-KO mice only exhibit subtle osteopenia in males and non-significant changes in bones of females (Figures 36, 39). We observed that levels of CRE expression, deletion of *Nfe2l2*, and expression of its target genes *Nqo1* and *Gclc* were modified similarly in both models, arguing against different deleting efficiency. It is possible that deletion in the late embryonic and neonatal period (in *Col1a1/Nfe2l2*-KO) compared to deletion at postnatal P21-28 (in *Dmp1/Nfe2l2*-KO) could reprogram compensatory mechanisms in the former to keep bone formation and turnover. For instance, whereas *Runx2* and *Osterix* expression was significantly diminished in *Dmp1/Nfe2l2*-KO mice, it remains unaltered in *Col1a1/Nfe2l2*-KO of both sexes. Alternatively, it is possible that *Nfe2l2* deletion in osteoblasts (*Col1a1/Nfe2l2*) or in osteocytes (*Dmp1/Nfe2l2*) could somehow differentially modify their function and/or paracrine crosstalk to osteoclasts. For instance, NRF2 deletion *in vitro* increases osteoblast proliferation although no differences had been found in the total number of osteocytes. More detailed studies are required to explore further these possibilities.

Independent of sex and the *in vivo* deletion model NRF2 activity induces transcriptional activation of a topologically associated domain (TAD) containing the SIBLING family of extracellular proteins (Figure 37, 40). These results were confirmed *in vitro*, using both genetically and pharmacological models (Figure 46, 48). The SIBLING protein family is a structurally and phylogenetically homogeneous group located in the human chromosome 4 which comprises *Dspp*, *Dmp1*, *Mepe*, *Osteopontin*, *Spp1*, and *Ibsp*. The expression of SIBLING gene group is specific for bone cell types where they are required for proper bone mineralization (Bouleftour et al., 2015) and its defects led to osteoporosis. SIBLING proteins share significant levels of functional redundancy and they seem to appear along with the generation of the bony skeleton in the vertebrate lineage, highlighting their importance for the bone tissue. Whole-genome Chip-Seq assays and our Chip assays in osteocytes show

that this TAD, which also contains the canonical NRF2-activated gene *Abcg2*, bound NRF2, strongly suggesting that NRF2 activity has a key role in the regulation of SIBLING proteins in osteoblasts and osteocytes (Figure 49). Similarly, NRF2 bound in whole-genome Chip-Seq assays and our Chip assays to the 3' region of the *Sost* gene (Figure 50). This region has been shown to be essential for its osteocyte-specific expression and shown to be responsible of Van Buchem disease, a rare autosomal recessive disorders that results from osteoblast hyperactivity (Sebastian & Loots, 2018). Altogether, our results demonstrate an important role of NRF2 activity in the regulation of a number of relevant osteocyte-specific genes in vitro and in vivo.

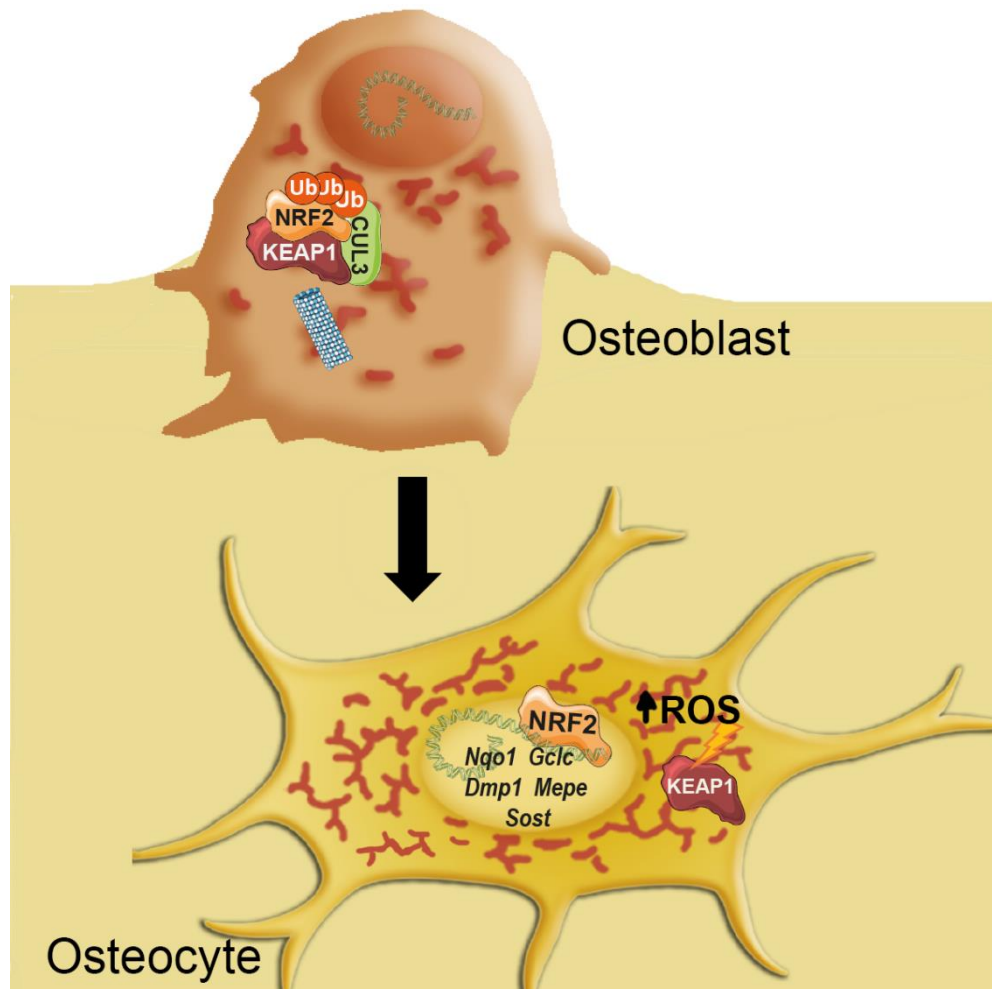


Figure 2. NRF2 function in osteocytes is required for bone homeostasis and drives osteocytic gene expression. We previously showed that nutrient restriction promotes the osteocyte transcriptional program and is associated to increased mitochondrial biogenesis. Increased mitochondrial biogenesis and function increases ROS levels and consequently, NRF2 activity during osteocytogenesis. Once active, NRF2 migrate to the nucleus where it binds to ARE sequences. Despite

antioxidant genes, we found active binding sites for NRF2 in TADs containing SIBLING proteins and *Sost* genes.

CHAPTER III: NEW THERAPEUTIC TARGETS FOR OSTEOPOROSIS.

1. Anti-diabetic drugs and bone health.

Our results show that a high glucose regimen impairs osteocyte differentiation *in vitro*. In this line, high blood sugar levels have been associated with lower mineral density and Diabetes Mellitus is considered as a risk factor for osteoporosis. Diabetes affects bones through hyperinsulinemia, glucose metabolism impairment, disruption of bone microvascular function and muscle endocrine function and presentation of advanced glycosylation of end-products in collagen. These factors, attenuate bone remodeling by decreasing both bone formation and resorption. It is speculated that low turnover of bone in diabetes may lead to defective microfracture repairs and, their accumulation contributes to decreased bone quality (Krakauer et al., 1995; Rubin, 2015). Several studies have demonstrated that the exact glycemic control can result in enhanced bone turnover while poorly glycemic control in diabetic patients can lead to imbalance of osteoblast/osteoclast activity and impaired bone formation (Okazaki et al., 1997; Rosato et al., 1998; Viégas et al., 2011). Therefore, drugs to control glucose blood levels might have a positive impact on bone health.

Glucose-lowering therapies target different aspects of glucose metabolism, including insulin sensitivity (metformin and thiazolidinediones [TZDs]), insulin secretion and bioactivity (sulfonylureas, glucagon-like peptide 1 [GLP-1] analogues, dipeptidyl peptidase 4 [DPP-4] inhibitors and insulin analogues), and modulation of blood glucose levels by either increased excretion (sodium–glucose cotransporter 2 [SGLT2] inhibitors) or delaying its appearance following nutrient digestion (α -glucosidase inhibitors) (Lecka-Czernik, 2017). Some of these drugs have already demonstrated to improve bone quality. Metformin, together with sulfonylureas account for more than 70% of prescriptions for diabetes (Krakauer et al., 1995).

Although there is no correlation between their use and incidence of fractures, strong experimental evidence suggests that metformin may be beneficial for bone since it activates a pro-osteoblastic regulatory cascade via RUNX2 and AMPK (S. C. Chen et al., 2017; W. G. Jang, Kim, Bae, et al., 2011). In this study we have demonstrate that activation of AMPK is sufficient to induce osteocyte differentiation (Figures 16,17), therefore, the use of metformin might also improve osteocyte function. Similarly, some research suggests that glimepiride, a second-generation sulfonylurea, may enhance osteoblastic differentiation in high glucose conditions via the phosphoinositide 3-kinase (PI3K)/Akt/eNOS pathway and bone formation in ovariectomized rats (Fronczek-Sokół & Pytlik, 2014; P. Ma et al., 2014).

However, other drugs used for diabetes control such as Thiazolidinediones (TZDs) are detrimental for bone health. TZD are PPAR γ selective agonists, therefore, they stimulate adipocyte differentiation while they inhibit osteoblast differentiation (Ali et al., 2005). On the other hand, PPAR γ expression results in osteoclast proliferation and bone resorption (W. Wei & Wan, 2011).

In this study we unveiled the importance of PGC-1 for bone homeostasis. In parallel, accumulating evidences have indicated that PGC-1 α is involved in the regulation of T2DM. In consequence, PGC-1 α could be considered as a novel therapeutic strategy for diabetes and the associated pathologies such as osteoporosis. In fact, activation of PGC-1 α with 6-C- β -d-glucopyranosyl-(2S,3S)-(+)-5,7,3',4'-tetrahydroxydihydroflavonol (GTDF), an adiponectin receptor 1 (AdipoR1) agonist in osteoblasts restored osteopenia without improving diabetes (Khan et al., 2015).

Together with our results, these evidences highlight the importance of glucose control for bone health. Moreover, although further studies are needed, current evidence demonstrate the impact of different anti-diabetic drugs in osteoporosis and could contribute to improve the selection of anti-diabetic treatment in a context of bone fragility.

2. Anti-oxidants and bone health.

Oxidative stress occurs as a result of a disbalance between the production of ROS and the levels of antioxidants. This can arise as a consequence of both physiological events, such as aging and hormonal changes (Almeida et al., 2007; Finkel & Holbrook, 2000; Sendur et al., 2009) and pathological conditions related to the production of inflammatory cytokines, exogenous and endogenous toxins, radiation exposure and drug therapies (Ray et al., 2012b; Tilg et al., 2008). Oxidative

stress alters bone remodeling process causing an unbalance between osteoclast and osteoblast activities, that can lead to metabolic bone diseases and skeletal system disorders including osteoporosis. In particular, oxidative stress activates the differentiation of pre-osteoclasts in osteoclasts and strengthens the bone resorption. Moreover high levels of ROS induce the apoptosis of osteoblasts and osteocytes and block the osteoblast activity and differentiation (Kikuyama et al., 2002; Romagnoli et al., 2013).

Clinical studies show a positive correlation between low levels of antioxidants and bone loss, and this is also linked to an increase of markers of bone resorption. Antioxidants have complementary effects in bone health. *In vivo* and *in vitro* data indicates that antioxidants contribute to the differentiation of osteoblasts and bone formation (Banfi et al., 2008; Ji et al., 2008), while reduce osteoclast differentiation and activity (Domazetovic et al., 2017). Previous studies reported that administration of NAC or ascorbate in ovariectomized mice and rats abolishes ovariectomy-induced bone loss, while l-buthionine-(S,R)-sulphoximine (BSO), a specific inhibitor of glutathione synthesis, causes substantial bone loss (Lean et al., 2003). Moreover, administration of antioxidants such as vitamin C, E, N-acetyl-cysteine (NAC), has beneficial effects in individuals with osteoporosis (Hall & Greendale, 1998; Mainini et al., 2012; Morton et al., 2001; Sanders et al., 2007). However, little is known about the mechanism of action of antioxidants in bone cells and their effects in osteoblast and osteocyte activity. We analyzed the effect of NAC in osteocyte differentiation, and we found that NAC did not modified the expression of osteoblastic genes whereas it decreased the expression of osteocyte genes (Figure 47). The implication of these changes should be further studied. Moreover, most of studies are made in conditions under high oxidative stress, whereas the effects of antioxidants on normal bone health have not been analyzed yet. Here we have found that ROS are important signaling molecules that regulate osteocyte differentiation. Therefore, it seems important to asses that administration of antioxidants do not hamper osteocyte differentiation under non-oxidative stress conditions.

3. NRF2 as a therapeutic target for osteoporosis

The transcription factor NRF2 and its principal negative regulator, KEAP 1, are critical in the maintenance of redox, metabolic and protein homeostasis, as well as the regulation of inflammation. Thus, NRF2 activation provides cytoprotection against numerous pathologies including chronic diseases autoimmune, neurodegenerative and metabolic disorders and cancer initiation (Cuadrado et al., 2019). This expanded recognition of NRF2 as a potential drug target has sparked the

interest of the pharmaceutical industry and led to the development of several NRF2 modulators. The most successful NRF2 activator to date is the fumaric acid ester dimethyl fumarate (DMF) (BG-12 or Tecfidera, from Biogen) that was approved in 1994 for the treatment of psoriasis (Höxtermann et al., 1998) and repurposed in 2014 by FDA and EMA for relapsing-remitting multiple sclerosis (MS)(Fox et al., 2012; Gold et al., 2012; Schimrigk et al., 2006; Z. Xu et al., 2015) after showing clinical effectiveness

(www.accessdata.fda.gov/drugsatfda_docs/label/2014/204063s003s008s010lbl.pdf). DMF has a good tolerability and safety profile in humans and most common adverse events were flushing and gastrointestinal events, which were of mild or moderate severity and appear to be largely manageable (Narapureddy & Dubey, 2019)

In this study we demonstrated that activation of NRF2 induce osteocyte differentiation, and that its deficiency results in osteopenia (Figures 36-37, 39-40, 46, 48). Although alteration of NRF2 expression or their target genes has never been linked to osteoporosis before (Feng et al., 2018), we observed that ovariectomy in mice reduce the expression and function of NRF2 (Figure X). Given these results we hypothesized that activation of NRF2 could become effective for bone pathologies. Nowadays, bisphosphonates remain the first-line and most cost-effective treatment option for osteoporosis, but there is increasing concern about their long-term safety. For instance, bisphosphonates have been associated with increased risk of atypical fractures as they change bone's nanoscale material properties affecting the toughness of the bone (Lloyd et al., 2017). Therefore, new medications with novel mechanisms to treat osteoporosis are needed. Our data demonstrate that treatment with DMF prevented the deleterious effects of ovariectomy in the skeleton. Bone mass and architecture was mostly protected in both the cortical and trabecular compartments. In addition, we found a decreased number of osteoclasts in DMF treated mice. Treatment with DMF also restored the expression of *Dmp1*, *Mepe* and *Sost* in ovariectomized mice therefore improving osteocyte function and their inhibitory effects on osteoclasts. However, we cannot exclude a direct effect of DMF on reduction of recruitment and activation of osteoclasts through attenuation of ROS signaling as previously reported (Yamaguchi et al., 2018) or effects mediated by additional signaling pathways inhibited by DMF such as NF- κ B (Meili-Butz et al., 2008). Finally we did not see differences in collagen synthesis, therefore we believe that DMF won't modify the composition of the extracellular matrix, avoiding the increased risk of atypical fractures linked to bisphosphonates(Lloyd et al., 2017). These experiments evidence a promising future for DMF in bone disorders, however, further studies should be performed to optimize dosing and to fully understand the bone protecting mechanisms of DMF.



CONCLUSIONS

- Osteocytes are cells difficult to study. Nowadays, the most relevant tools to unveil their biology are primary cultures and the cell line IDG-SW3.

- Osteocyte differentiation relies on the expression of some osteocytic genes that are clustered in TADs.

- Osteocyte differentiation is linked to a metabolic reprogramming characterized by an increase in mitochondrial function, and ROS production.

- Glucose restriction enhance both osteocyte differentiation and metabolic reprogramming.

- High glucose levels hamper osteocyte differentiation and decrease mitochondrial function.

- Osteocyte differentiation mediated by glucose restriction depends on the activation of AMPK-PGC1 α pathway.

- PGC1 α induce osteocyte differentiation by acting as a co-transcription factor for osteocytic genes. PGC1 α binds to the promoter of *Dmp1*, *Fgf23* and *Sost*, and activate its transcription.

- Loss of PGC1 α/β produce osteopenia and reduce the capacity of osteocytes to differentiate.

- The increase in ROS levels that occurs in osteocyte differentiation activates NRF2.

- NRF2 binds to enhancer and promoters of osteocyte genes, inducing osteocyte differentiation.

- Loss of NRF2 in osteoblasts and osteocytes produce mild osteopenia through two mechanisms: hampering the capacity of osteocytes to differentiate and increasing the activity and number of osteoclast. These effects are sex-dependent.

- Osteoporosis is associated with alteration in NRF2 signaling pathway and ROS. Therefore, activation of NRF2 with DMF is a potential treatment for osteoporosis.

-



MATERIALS AND METHODS

CHAPTER I: CELL CULTURE

During this doctoral thesis, different cell lines and primary cultures had been used with different purposes. Each cell model has their own advantages and drawbacks, and it is important to choose the best model to answer our questions.

Primary cultures are those directly generated from animal tissues. They do not survive long time since, in the best scenario, they stop dividing after a few numbers of passages and get senescent. Moreover, primary cultures obtained from fully differentiated cells, have lost their capacity to divide so they just last a few days. On the other side, primary cultures maintain their fundamental cellular functions including the expression of cellular markers and signaling and genetic integrity. So primary cell models are the closest experimental tools available to mimic *in vivo* processes.

Cell lines arose from primary cultures that have been immortalized or transformed in some manner. These altered cell lines typically exhibit abnormal or uncontrolled metabolic function and proliferative capacities in culture as a result of intracellular changes. Further, the unnatural state can result in altered growth characteristics, single or multiple genetic abnormalities and aberrant signaling pathways. On the other hand, the immortalization allows us to culture cell lines for longer periods of time. However, we must consider that, as we increase the number of passages, selective pressures increase, and it can drive the cell population further from their original state. Cell lines can be also specifically designed to achieve a particular experimental process.

1. Cell culture and maintenance

Each primary culture or cell line have their own nutritional requirements; therefore, specific culture medium must be used for their maintenance. During this thesis, three different commercial recipes have been used (Table 1):

- **DMEM:** Dulbecco Modified Eagle Medium. (01-055-1A, Biological Industries)

- **Alpha-MEM:** Minimum Essential Medium Eagle Alpha Modification (M8042, Sigma).

- **Alpha-MEM without glucose** (06-1043-01-1A Biological Industries)

The main differences between them are the amino acid and vitamin composition and the Glucose concentration (25 mM in DMEM, 5 mM in alpha-MEM, and 0mM in alpha-MEM without glucose).

If not otherwise specified, the mediums were supplemented with:

- **10% Fetal Bovine Serum (FBS)**
- **2 mM glutamine (Gln),**
- **1 mM sodium pyruvate (Pyr),**
- **100 U/ml Penicillin and 0.1 mg/ml Streptomycin** (1% P/S commercial solution).

For **osteogenic differentiation medium**, alpha-MEM medium was supplemented with **50 µg/ml ascorbic acid** and **4 mM β-glycerophosphate**.

For **ostecyte culture medium**, FBS of osteogenic differentiation medium was replaced by **5% heat-inactivated FBS** and **5% heat-inactivated CFS** (calf serum).

For culture medium with controlled glucose supply, the corresponding amount of 1mM D-Glucose was added to obtain 1mM, 5mM, 25mM glucose medium. The stock was previously filtered and kept at -20°C.

DMEM	IDG-SW3 proliferation medium	Osteogenic differentiation medium	Glucose controlled differentiation medium	ostocyte culture medium
		Alpha-MEM 10% FBS	Alpha-MEM non glucose 10% FBS	Alpha-MEM
DMEM	Alpha-MEM 10% FBS	10% FBS	2 mM Glun 1mM Pyr	5% heat-inactivated FBS
10% FBS	10% FBS	2 mM Gln	1% P/S	5% heat-inactivated FBS
2 mM Gln	2 mM Gln	1mM Pyr	Glucose up to 1mM, 5mM or 25mM	5% heat-inactivated CFS
1mM Pyr	1mM Pyr	1% P/S	50 µg/ml ascorbic acid	2 mM Gln
1% P/S	1% P/S	50 µg/ml ascorbic acid	4 mM β-glycerophosphate	1mM Pyr
		4 mM β-glycerophosphate	4 mM β-glycerophosphate	1% P/S

Table 1. Basic components of the principal cell culture medium used.

In our lab, the cells are maintained in a cell incubator at 37°C in a 5% CO₂ humidified atmosphere.

For passaging, cells are washed with PBS and detached using 0.25% Trypsin-0.02% EDTA solution (03-050-1A, Biological Industries).

For long term storage, cells are cryopreserved in liquid nitrogen. Briefly, cell cultured at 70-90% of confluence are collected and resuspended in 1.5 mL of freezing medium (DMEM or alpha-MEM medium containing 10-20% FBS and 10% DMSO (Dimethyl Sulfoxide; Sigma). Cell suspensions are placed in 2 ml cryogenic vial and frozen immediately at -80°C. A few days later, move the vial to nitrogen liquid container



Helpful
TIPS

Tips to improve cell viability after freeze-thaw process.

- Increase the concentration of FBS up to 20% to improve cell preservation and thaw.
- DMSO is toxic for the cells, so avoid long exposures in liquid state. Froze and thaw the cells as fast as you can.

2. Culture dishes and collagen coating

All the used cells are adherent and were grown over a plastic surface treated to improve cell attachment (Corning dishes). IDG-SW3 and osteocytes must be grown in cultured dishes coated with 5 $\mu\text{g}/\text{cm}^2$ collagen type I to avoid losing their original phenotype. For the coating of culture dishes, we proceed as follows (Table 2.):

- Prepare a stock solution of **0.2M of acetic acid**. Dissolve 515 μL of Glacial acetic acid in 44.5mL of milliQ water. Use 0.22 μM filter to sterilize the solution and keep it at 4°C.
- Prepare a solution of **50 $\mu\text{g}/\text{ml}$ Type I Collagen in 20mM acetic acid**.

Reagent	Stock	Final concentration	Volume for 50mL
Collagen Type I, rat tail (08-115, Sigma)	2920 $\mu\text{g}/\text{ml}$	50 $\mu\text{g}/\text{ml}$	0.856 ml
Acetic Acid solution	0.2M	20mM	5 ml
Sterile milliQ water	-	-	44.14mL

Table 2. Preparation of collagen coating mix.

- Distribute the collagen mix to the culture dishes as follows (Table 3):

Culture plate	Volume of collagen mix
100 mm	7.8 mL
60 mm	2.8 mL
6-well	1mL/well
12-well	400 $\mu\text{l}/\text{well}$
24-well	200 $\mu\text{l}/\text{well}$

Table 3. Volumes for the coating of culture plates.

- Incubate the cell dishes at least for **1h at room temperature** or at 37°C.

- **Remove the excess of collagen and keep it at 4°C.** Collagen excess can be reused up to 5 times.

Coated plates can be stored at 4°C. If needed, collagen plates can be sterilized by overnight exposure to UV light in a sterile tissue culture hood.

3. Cell lines

Two different cell lines have been used in this thesis with two very different objectives: IDG-SW3 to mimic the process of osteocytogenesis and Platinum-E for the generation of lentiviral particles

3.1. IDG-SW3

IDG-SW3 (for Immortomouse/Dmp1-GFP-SW3) is a cell line obtained from long bone chips of mice that carried a **Dmp1 promoter driving GFP** expression and that expressed a **thermolabile SV40 large T-antigen regulated by IFN- γ** (Woo et al., 2011). SV40 large T-antigen induces cell division and is a common technique for cell immortalization and generation of cell lines. Unlike other cell lines, T-antigen is only expressed under proliferative conditions (33°C and in presence of IFN- γ) and their levels drop dramatically after 24h in normal culture conditions (37°C and in absence of IFN- γ). In the absence of the large T-antigen, IDG-SW3 cells do not proliferate and recover their original phenotype, resembling primary bone cells in the osteogenic environment.

Dmp1-GFP is a marker for osteocytic differentiation. Under immortalized conditions, IDG-SW3 are GFP-negative. After 3 days of culture with osteogenic medium, IDG-SW3 cells start to express low levels of *Dmp1*-GFP and begin osteocytic differentiation. By the day 14, GFP should have increased and be uniformly distributed across the culture surface (Woo et al., 2011).

As they differentiate, IDG-SW3 express osteoblastic and osteocytic markers. In an early stage, as mature osteoblast, they express alkaline phosphatase and produce and mineralize a type I collagen matrix. Like early osteocytes, they express *E11/gp38*, *Dmp1*, *MEPE*, and *Phex*. In a final stage of differentiation, they develop a dendritic morphology and express *Sost* and *Fgg23*. We demonstrated the expression of most of these cell markers in the section of Results, Figure 3.

For proliferation, IDG-SW3 should be maintained in **alpha-MEM medium supplemented with 50 U/mL of INF- γ at 33°C** with 5% CO₂. For differentiation, IDG-SW3 are cultured with **osteogenic differentiation medium at 37°C** with 5% CO₂. IDG-SW3 should be grown on **dishes coated with 0.15 mg/ml rat tail type I collagen** (Figure 1).

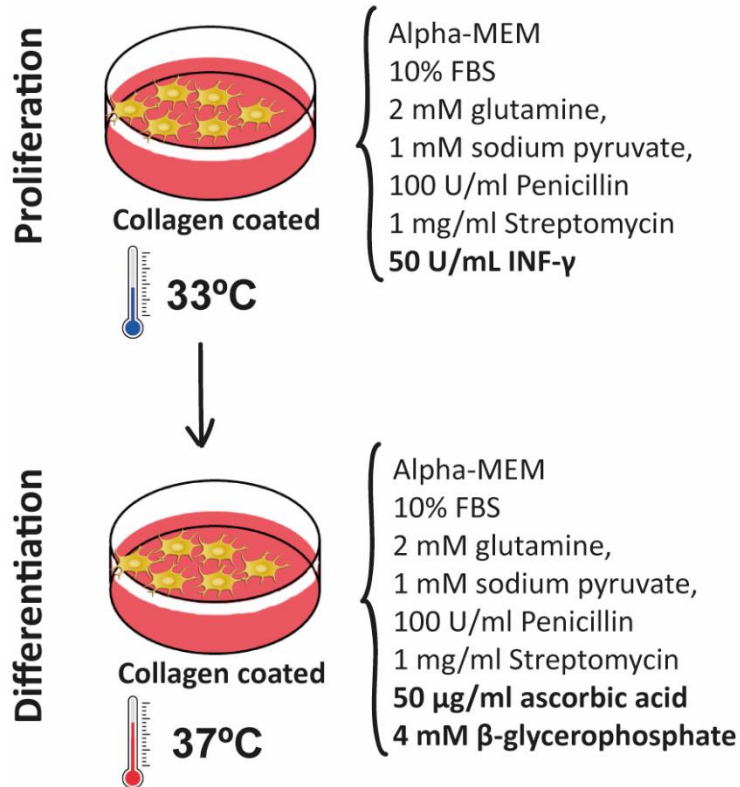


Figure 1. Schematic representation of IDG-SW3 cells culture conditions.



Helpful TIPS

Tips when working with IDG-SW3.

- IDG-SW3 establish strong cell-to-cell interactions, so they are **hard to detached**. Some tricks are the following:
 - Keep your stock dish **subconfluent ~80-85%**
 - Take it easy. Be patient and **let trypsin act for up to 5-10 min.**
- The **differentiation capacity of IDG-SW3 becomes reduced with passages**. So:
 - **Work with low passes**
 - If your differentiation experiments start to **fail**, cells do not express differentiation markers or do not respond to treatments, do not get worried. Take it easy and **try thawing a new cell vial.**
 - **Be careful** if you plan a **CRISPR/Cas9** experiment. Ensure that the effects are not clonal artefacts.
- Remember, **differentiated IDG-SW3 express GFP**. If fluorescence assays are performed, be careful when selecting the fluorophores.
 - **Collagen** (synthesized by IDG-SW3 and added in the process of plate coating), is a highly **autofluorescent molecule** and can produce high background when working with fluoresce. Be careful, **choose the channel that minimize** your background fluorescence and **add the adequate controls**.

3.2. Platinum-E

The Platinum-E (Plat-E) Cell Line is a potent retrovirus packaging cell line derived from the 293T cell line. Plat-E has been genetically engineered to express the retroviral proteins (gag, pol, ecotropic env) under the control of EF1 α promoter. This system ensures longer stability and higher yield of the retroviral proteins than other conventional NIH-3T3 based retroviral packaging cell line. In presence of drug selection, Plat-E cells can be kept in good condition in for at least 4 months in the presence of drug selection, and can produce retroviruses with an average titer of 1×10^7 infectious units/ml.

Moreover, during the incorporation of packaging genes, Plat-E cells acquire Blasticidine and Puromycin resistance. Thus, Plat-E are maintained in complete DMEM (DMEM with 10% Fetal Bovine Serum (FBS), 2 mM glutamine, 100 U/ml Penicillin and 0.1 mg/ml Streptomycin) supplemented with 5 µg/ml Blasticidine and 1 µg/ml Puromycin.

Retroviral generation will be explained Chapter 3.

4. Primary cell cultures

In his thesis, two different types of primary cell cultures had been generated: osteoblast and osteocyte. For osteoblast obtention, two different protocols are set up in the lab: a long one that allows the obtention of osteoblast and osteocytes from the same bone pieces, and an alternative shorter one. In this thesis, osteoblasts were mainly obtained following the first protocol. However, I will also detail the shorter version, which had been used only in specific situations. Osteoblasts isolated with both protocols shared similar morphology and had similar expression levels of osteoblast gene markers.

4.1. Isolation of osteoblasts and osteocytes

The primary osteoblast and osteocytes were obtained from mice calvaria and limbs maintained in differentiation α -MEM. Osteocyte culture dish must be previously coated with collagen.

The yield of osteocyte isolation is quite low, therefore, a minimum of 5-7 individuals is required. Moreover, yield is dramatically reduced in older pups.



Helpful
TIPS

- This protocol takes about **5-7 hours** since you take the pups until you have the cell culture. So:
 - Take it easy and plan well your time.
 - If you have less than 4-5 animals consider aborting the mission. The poor number of cells obtained might not worth your efforts.
- **The age of the pups is critical for obtaining a good yield.** When possible, pups that were born the same day. If this is not possible, use P0 to P3 pups. Do not try to isolate osteocytes from **pups older than P4-P5 since the yield will be too poor.**

Materials and Methods

Start the protocol with **coating the tissue culture plastic** with type I collagen as described in “1.2.Culture dishes and collagen coating” section. Sterilize all dissection equipment in 70% ethanol prior to use. Prepare the **solutions that you will need for this protocol** (table 4):

Solution	Recipe
Collagenase Solution	<p><u>For 5 calvaria, and for one digestion</u> (you will need a total of 6 digestions):</p> <p>3 mg collagenase II 1 ml trypsin (0.25% Trypsin-EDTA) Up to 5 ml with alpha-MEM + 100 U/ml Penicillin and 0.1 mg/ml Streptomycin.</p> <p>Filter with 0.22 μm filter and keep it at 4°C</p>
EDTA Solution	<p><u>For 5 calvaria (8mL), and for one digestion</u> (you will need a total of 3 digestions):</p> <p>5mM EDTA dissolved in PBS. 0.1% bovine serum albumin (BSA) Adjust the pH of the solution to 7.4.</p> <p>Filter with 0.22 μm filter and keep it at 4°C.</p>

Table 4. Solution needed for osteocyte and osteoblast isolation.

- **Prewarmed Alpha-MEM** with 100 U/ml Penicillin and 0.1 mg/ml Streptomycin.

Remember to prewarm the amount of digestion solution that you are going to need prior to its use. Proceed as follows:

- Take 5-7 pups and place them inside sterile culture hood. Euthanize one pup by decapitation. Proceed with the **dissection of the calvaria and the limbs**
 - **Dissection of the calvaria** (Figure 2):
 - Clean pup head with 70% ethanol.
 - With a scissor, make two incisions in the lateral of the head, from the neck to the ears (Figure 2, step 1).
 - Use a clamp to hold the head by the eyes. Pull the skin away (Figure 2, step 1).

- Clean the calvaria by immersion in PBS with 100 U/ml Penicillin and 0.1 mg/ml and scratch softly the surface in order to remove the periosteum.
- Remove muscles and fibrotic tissue from sutures and edges with scissors. Remove the internal sutures of the calvaria and cut it in small pieces (Figure 2, step 2).
- Pool calvaria into 50 ml tube containing Alpha-MEM containing antibiotics (Figure 2, step 3).

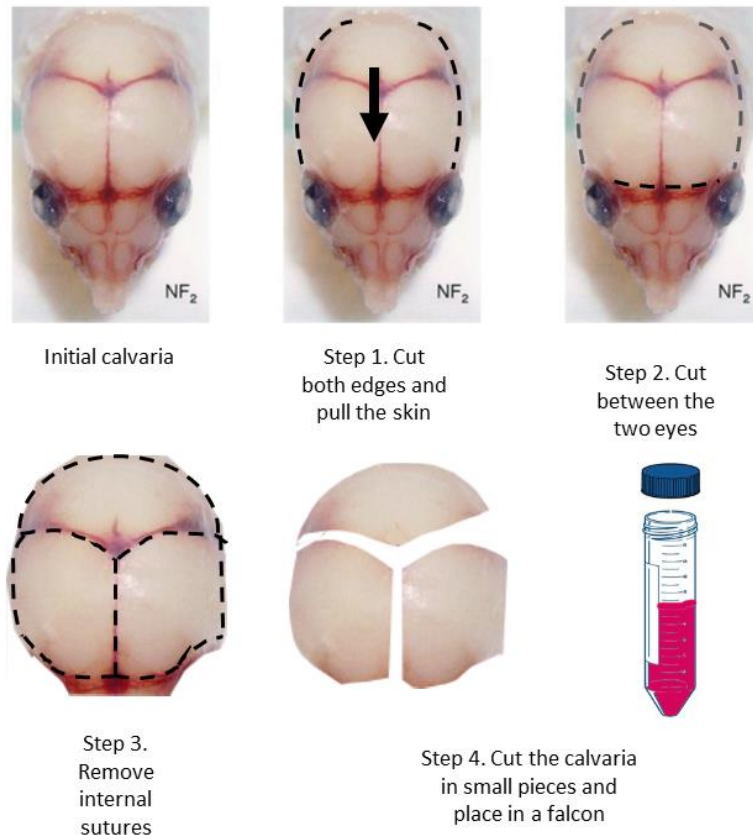


Figure 2. Dissection of mice calvaria.

➤ Dissection of the limbs

- Clean pup head with 70% ethanol
- Pull the skin of the limb away.
- Obtain the tibiae, femora, humeri, radius and ulna. With Dressing Forceps localize the bone within the limb and carefully pull it out.

Materials and Methods

- Clean the bones by immersion in PBS with 100 U/ml Penicillin and 0.1 mg/ml and scratch softly the surface in order to remove the periosteum.
- Pool the bones of the limb with the calvaria into 50 ml tube containing Alpha-MEM containing antibiotics.
- **Repeat** the dissection of calvaria and limb for each pup and pool all the bones.
- **Rinse the bones** three times with α -MEM containing antibiotics.
- Start with the digestions:
 - **Digestion 1:** Add 5 mL of collagenase mix and incubate for 25 min on a shaking/rotating platform at 37 °C. Remove and discard the collagenase, rinse the bone pieces with 5 ml PBS and discard the rinse. Cells released from this digest are primarily fibroblastic.
 - **Digestion 2:** Add 5 mL of collagenase mix and incubate for 25 min on a shaking/rotating platform at 37 °C. Remove and discard the collagenase, rinse the bone pieces with 5 ml PBS and discard the rinse. Cells released from this digest are a mixture of fibroblasts and osteoblasts.
 - **Digestion 3:** Add 5 mL of collagenase mix and incubate for 25 min on a shaking/rotating platform at 37 °C. Remove and discard the collagenase, rinse the bone pieces with 5 ml PBS and discard the rinse. Cells released from this digest are of fibroblasts and osteoblasts.
 - **Digestion 4:** Incubate the bone pieces in 5 ml EDTA for 25 min on a shaking/rotating platform at 37 °C. Remove and discard the EDTA, rinse the bone pieces with 5 ml PBS and discard the rinse.
 - **Digestion 5:** Add 5 mL of collagenase mix and incubate for 25 min on a shaking/rotating platform at 37 °C. Transfer the collagenase mix to a 50 ml centrifuge tube containing 20 mL of differentiation medium. Rinse the bone pieces with PBS and transfer the rinse to the same tube. This digestion contains mainly osteoblasts.
 - **Digestion 6:** Incubate the bone pieces in 5 ml EDTA for 25 min on a shaking/rotating platform at 37 °C. Transfer the EDTA solution to the previous 50 ml centrifuge tube. Rinse the bone pieces with PBS and transfer the rinse to the same tube. This digestion contains mainly osteoblasts.
 - **Digestion 7:** Add 5 mL of collagenase mix and incubate for 25 min on a shaking/rotating platform at 37 °C. Transfer the collagenase mix to the previous 50 ml centrifuge tube. Rinse the bone pieces with PBS and transfer the rinse to the same tube. This digestion contains mainly osteoblasts.

Centrifuge the falcon containing digestions 5 to 7 at 1000 g, resuspend in culture media and seed on one or two normal culture plate with differentiation medium.

- **Digestion 8:** Incubate the bone pieces in 5 ml EDTA for 25 min on a shaking/rotating platform at 37 °C. Transfer the EDTA solution to a new 50 ml centrifuge tube containing osteocyte culture medium. Rinse the bone pieces with PBS and transfer the rinse to the same tube. This digestion contains mainly osteocytes.

- **Digestion 9:** Add 5 mL of collagenase mix and incubate for 25 min on a shaking/rotating platform at 37 °C. Transfer the collagenase mix to the previous 50 ml centrifuge tube. Rinse the bone pieces with PBS and transfer the rinse to the same tube. This digestion contains mainly osteocytes.

Centrifuge the falcon containing digestions 8 and 9 at 1000 g, resuspend in osteocyte culture medium and seed on one collagen coated plate. The cells will attach within 24 h and should be used within 7 days of plating to prevent loss of phenotype or overgrowth by osteoblasts.

Seed the bone pieces in a collagen coated 6-well plate. Some osteocyte will migrate from the bone to the coated plate in the next 72 h, increasing the yield.



Helpful
TIPS

Osteoblast and osteocyte are highly dependent of cell-to-cell interactions. Therefore, maintaining a good confluency is critical in bone primary cultures. **Low confluence decreases cell proliferation and viability and can end up in the death of the cellular culture.** Confluence is especially critical when the culture is established.

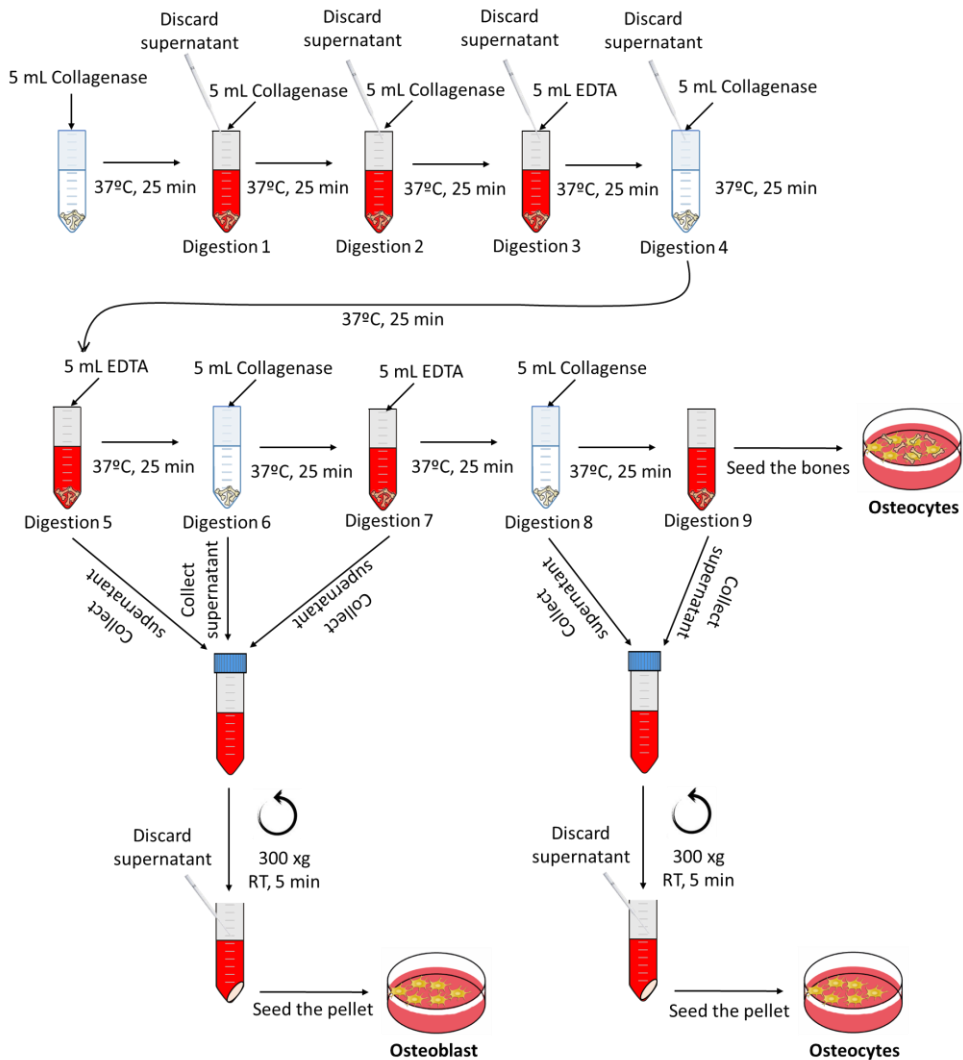


Figure 3. Schematic workflow of osteoblast and osteocyte isolation protocol.

4.2. Osteoblast isolation. Short protocol

In this case, we will only use the calvaria. As for osteocyte and osteoblast isolation, a minimum of pups is needed. Age of the pups is also critical for obtaining a good yield. Pups from P0 to P3 are recommended.

Before starting the protocol, prepare the **collagenase digestion mix** as described in table 4.

- Take 5 pups and place them inside sterile culture hood. Euthanize one pup by decapitation. Proceed with the **dissection of the calvaria** as explained in the previous section (Figure 2).

- **Digestion 1:** Add 5 ml digestion mix. Incubate at 37°C 5 minutes, in a shaking bath.

- Discard the supernatant as it mainly contains fibroblasts.

- **Digestion 2:** Add fresh 5 ml digestion mix. Incubate for 20 minutes at 37°C in a shaking bath. Shake by hand for a few seconds and incubate other 20 minutes at 37°C in a shaking bath. Transfer the digestion to a new 50 ml centrifuge tube containing 10mL α -MEM and incubate at 37°C until the whole procedure is completed.

- **Digestion 3:** Add 5 ml digestion mix to calvaria. Again, incubate for 20 minutes at 37°C in a shaking bath. Shake by hand for a few seconds and incubate other 20 minutes at 37°C in a shaking bath. Pool the digestion with the supernatant obtained in digestion 2.

Centrifuge the falcon containing digestions 2 and 3 at 1000 g, resuspend in differentiation medium and seed in one or two culture plates. Remember that confluence will influence your results.

Seed the bone pieces in a collagen coated 6-well plate. Some osteocytes will migrate from the bone to the coated plate in the next 72 h.

Experiments should be performed between passages 3 to 6, normally the cells begin to go under senescence after 3 weeks in culture.

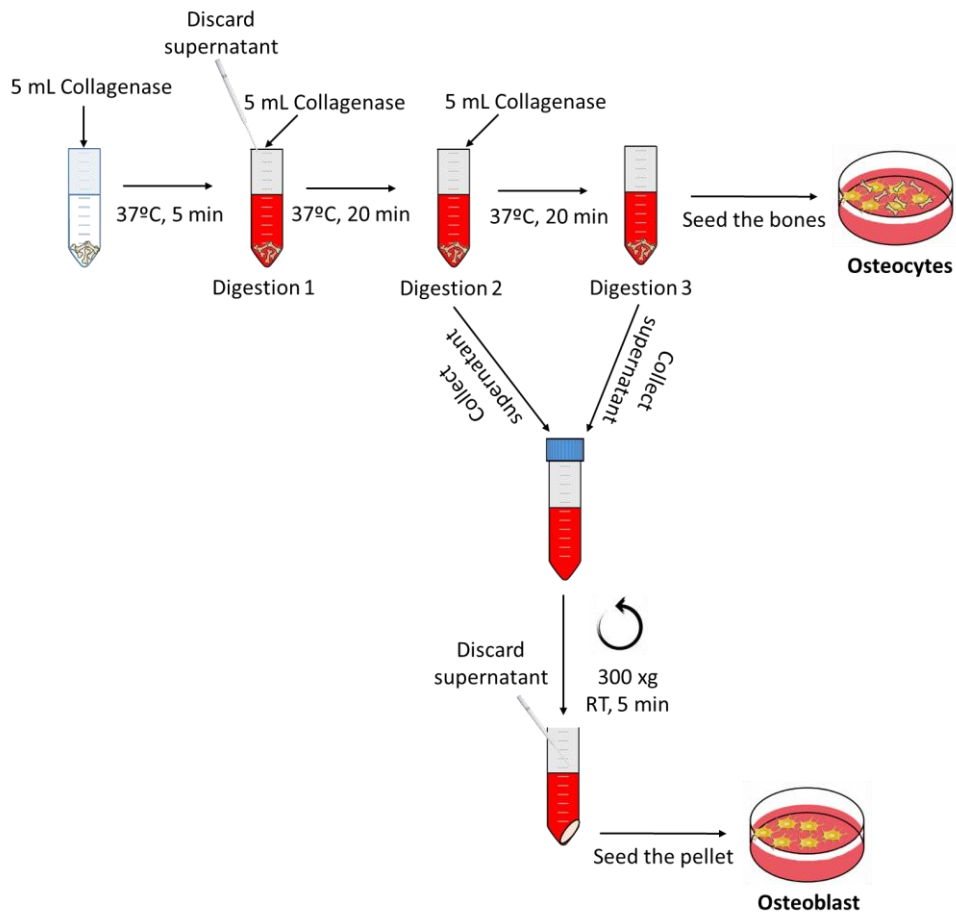


Figure 4. Schematic workflow of osteoblast isolation protocol.

5. CRISPR/Cas9 technology

The CRISPR/Cas9 technology is a technology used to edit genomes within cells or organism. It consists on an enzyme, Cas9 (or "CRISPR-associated protein 9") that uses CRISPR (clustered regularly interspaced short palindromic repeats) sequences as a guide to recognize and cleave specific strands of DNA that are complementary. In this thesis, aimed to knocked down the genes *Keap1* and *Nfe2l2* using CRISPR/CAS9 in IDG-SW3.

As IDG-SW3 are hard to transfect, we used lentiviral vector to deliver the sequences encoding for *Nfe2l2* and *Keap1* sgRNA as well as Cas9. Both vectors were generated and kindly donated by Dr. Papagiannakopoulos (Romero et al., 2017). Sequence for sgRNA are detailed in table 5.

sgRNA	Sequence
sgNRF2.3	5' GAGGTTGGGGCAGCACCTGCT 3'
sgKEAP1.4	5' GTGTTCCACGCGTGCATCGAC 3'

Table 5. Sequence of sgRNA used for CRISPR/Cas9

As the lentiviral plasmids used were bigger than usual, we needed to modify the protocol of retrovirus generation which is detailed in Chapter 3. Therefore, for generation of CRISPR/Cas9 genetically engineered cell with lentivirus, proceed as follows:

- Seed Plat-E cells and **transfect them with the envelop and lentiviral plasmid** as described in section “3.1. Production of retrovirus”.
- 72 h post-infection, **harvest and filtrate the virus with a 0.45 µm** cellulose acetate filter.
- **Concentrate viral particles to increase the infection yield.** Centrifuge the virus at 36,000g for 90 min at 4°C. Resuspend the virus in 100-200 µL
- **Transduce IDG-SW3** with the concentrate lentiviral preparations. If lentiviral vector does not encode for any protein for selection (as in this case), **co-infect the concentrated CRISPR/Cas9 lentiviral plasmid with a plasmid for antibiotic resistance** in a ratio from 1:10 to 1:50. For the cell transduction, proceed as explained in section “2.3. Transducing cells with retrovirus”. Use an empty lentiviral vector or a puromycin resistance vector as control.
 - **Select transduced cells with 5 µg/ml of puromycin.**
 - **Seed the survival cells in a 100 mm culture plate at very low density** (from 25.000 to 100.000 cells in total) and wait for colony formation.
 - **Transfer each colony into an individual well.** To do this, put a drop of trypsin over the colony and wait until they become rounded and starts to detach. Aspirate the colony with a pipette. Then transfer the colony to an individual well of a 6-well plate. All the cells should come from the same clone.
 - **Expand the cells and obtain DNA for sequencing** as described in Chapter IV, section “5. DNA sequencing by Sanger Method”. Briefly, copy a fragment of DNA containing the edition site for CRISPR. Mix the purified product of DNA with the sequencing primer and send it for Sanger sequencing. All primers used for DNA sequencing are detailed in Table 6.



Helpful TIPS

Most of cell lines have two copies of the same gene. When editing genomes with CRISP/Cas9 different events can occur in each copy of the gene, resulting in a cell population with two different sequences. This difficult the screening by sequencing. To discover the sequence of each copy you might sequence the forward and reverse sequences.

The positive pools were checked for NRF2 knock-down. As NRF2 is difficult to detect by western blot we used the expression of NRF2 target genes, quantified by qRT-PCR, as an indirect measure of the activity of NRF2.

Primer	Sequence	Product length
<i>Keap1</i>	Fw: 5' GGTCTGGAAGCTGGCTTATGGGGA 3' Rv: 5' AAGTAACCGCCCGCTGTGTAGAT 3'	1126 bp
<i>Keap1_seq1</i>	5' CTCATCAGCCGGGATGATCTGAAC 3'	N/A
<i>Keap1_seq2</i>	5' TTATAGGAGTGTGCCACTACACC 3'	N/A
<i>Nfe2l2</i>	Fw: 5' TCCCGTCCCTAGGTCCTTGTTC 3' Rv: 5' CCAAGTCGTAGAACGGGGTTGG 3'	844 bp
<i>Nfe2l2_seq1</i>	5' CGAGCAGGCTATCTCCTAGTCTC 3'	N/A
<i>Nfe2l2_seq2</i>	5' TCAGAGCTTCTCCACACCCCA 3'	N/A

Table 6: Primers used for gene sequencing of *Nfe2l2* and *Keap1*

6. Cell treatments

In this thesis several cell treatments had been used in order to induce or inhibit specific signalling pathways. Table 7 summarized some of the drugs used for this aim:

Reagent	Description	Stock	Diluted in	Dose
Aicar	Activator of AMPK	100mM	DMSO	50 μ M
Dimethylfumarate (DMF)	Inhibitor of Keap1	5mM	DMSO	5 μ M
Mdivi	Inhibitor of mitochondrial fission	5 mM	DMSO	5 μ M
N-acetylcysteine (NAC)	ROS scavenger	100mM	Water	1mM
Puromycin	Selection of infected cells	1 mg/mL	Water	5 μ g/mL
Tamoxifen	Activation of ERT2 inducible proteins	1 mM	Ethanol	1 μ M
Sirtinol	Inhibitor of SIRT1	0.5 mM	DMSO	1 μ M
SRT2104	Activator of SIRT1	0.3 mM	DMSO	0.5 μ M

Table 7. Drugs used for cell treatments.



Helpful TIPS

- Most of the drugs are hydrophobic and must be dissolved in DMSO. However, **DMSO is toxic for the cells at > 0.1% final concentration (v/v)**. So, try to make the stocks as concentrated as possible.
- **Dilutions of NAC are extremely acidic** and need to be neutralized (pH 7.4) before added to the medium.
- **Most of the drugs lose their activity with freeze-thaw cycles.**

Prepare small aliquots and avoid freezing and thawing them multiple times.

CHAPTER II: BACTERIA

In this thesis, bacteria were mainly used as a tool for the cloning of DNA plasmids. Therefore, of all the different bacteria used in the labs, we worked with the stain **DH5 α of *E.Coli***. This stain can be transformed with high efficiency and produce big amounts of DNA. These features have made DH5 α the most used model for DNA cloning.

1. Growth Conditions

Escherichia coli bacteria were growth in Luria-Bertani (LB) media, at 37°C and 250 rpm agitation or in agar plaques with LB-Agar (solid LB). Both mediums are prepared as follows:

For 1 L of liquid LB:

- Weight the LB components:
 - 10 g Bacto-tryptone
 - 5 g Yeast extract
 - 10 g NaCl
- Add milliQ water up to 1 L
- Adjust the pH at 7.5
- Sterilize by autoclaving.

For LB-agar plaques (around 40 plaques)

- Prepare 1 L of LB agar:
 - 10 g Bacto-tryptone
 - 5 g Yeast extract
 - 10 g NaCl
 - 7.5 g Bacto-Agar
- Adjust the **pH at 7.55**
- **Sterilize by autoclaving.**

- **Let it cold slowly** until it gets below 55°C. **Add the selection antibiotics.** Before adding them, be sure that the mix is cold enough as antibiotics degrade with heat. We mainly use Ampicillin at 50 µg/mL final concentration. Mix gently to avoid forming excess bubbles.

- **Distribute the liquid in the plaques** in sterile conditions (pour around 20 mL per plaque) and maintain them uncovered and horizontal until they solidify (around 15-20 min).

- When the plaques are solid, **storage them face down at 4°C.**



Antibiotics degrades with time. Plaques older than 6 months should be thrown away and plaques older than 3 months should be used with caution.

2. Preparation of Competent Cells

As DNA is a highly hydrophilic molecule, normally it cannot pass through the cell membrane of bacteria. Competent cells are bacteria with small holes in their membrane that allows the internalization of exogenous DNA to enter in. For induce competence in laboratory conditions, we follow the CaCl₂ method, which is recommended for DH5α *E.coli* strain. This method suspends the bacteria in a solution containing a high concentration of calcium to destabilizes their cell membrane. For this method, prepare:

- A solution of 0.1M CaCl₂ and sterilize by autoclaving.
- 100mL of LB media. Of those, save 2 mL of LB for blank.
- 5 ml DH5α bacterial culture, growth overnight at 37°C, 250 rpm in LB free of antibiotics.

Proceed as follows:

- Transfer **3 ml of overnight culture** into the 100 mL of LB media.
- Allow cell to growth at 37°C and 250 rpm, until **OD₆₀₀= 0.4**.
- Transfer cells to centrifuge bottles, and place **cells on ice for 20 mins**.
- Centrifuge cells at **4°C for 10 mins, at 3000 g**.
- Pour off media and resuspend cells in **15 mL of cold 0.1M CaCl₂** by progressive addition of volume. First resuspend in 1 mL, then add volume until 5 mL and finally 15 mL

- Transfer the suspended cells into 50 mL polypropylene falcon tubes and **incubate on ice for 30 minutes**.
- Centrifuge cells at **4°C for 10 min, at 3000 g**.
- Pour supernatant and resuspend the cells in **8 mL of cold 0.1M CaCl₂ containing 15% glycerol**.
- Transfer **250 µL into Eppendorf tubes placed on liquid nitrogen**, for shock-freezing. Cells stored at -80°C can be used for transformation for up to 6 months.
- Test the efficiency by transform 1 ng of DNA in 100 ml competent bacteria. In our terms, an acceptable efficiency should result in 10⁶ transformed bacteria.



Helpful
TIPS

Since CaCl₂ is added, **cells must remain cold** for the rest of the procedure. transport tubes on ice and resuspend on ice. This is critical to maintain cell viability.

Avoid vortexing or excess pipetting, especially when the cells have been resuspended in CaCl₂, to avoid cell lysis.

3. Bacterial transformation: Heat-shock method

Bacterial transformation is a process of horizontal gene transfer by which bacteria take up foreign genetic material (naked DNA) from the environment. In the laboratory we take advantage of this capacity to introduce the plasmid of our interest into bacteria for their replication and storage. There are several methods to insert introduce DNA into a bacterial host. We used the **heat-shock method** in competent DH5α. The procedure is the following:

- **Thaw competent bacteria** on ice. If less than one vial is needed, through the leftovers, do not refreeze it.
 - Prepare **50 µl of competent bacteria and add 0,1-1 µg of plasmid** of interest. If working with a ligation product, transform 1/3 or 2/3 (ligation/bacterial volumes) to ensure a correct efficiency of transformation. Gently mix by flicking the bottom of the tube with your finger a few times.
 - Prepare a **black tube** and keep it in parallel. Prepare 50 µl of competent bacteria and add a similar volume of water. Gently mix by flicking the bottom of the tube with your finger a few times.
 - **Incubate on ice for 30'**, to allow the DNA to bind to bacterial membrane.
 - Immerse the Eppendorf **1'30'' at 42°C or 2' at 37°C**. Do it rapidly, generating a heat-shock.

- **Place rapidly the tubes on ice**, generating a shock of temperatures. Incubate for **2'**.
- **Add 300 μL of LB** and incubate for **30' at 37°**, and 250 rpm.
- **Streak out 50-100 μL** (or the whole volume if working with ligation products) of bacteria in **LB-Agarose Petri dishes containing the selection antibiotic**. Use sterile glass beads to spread the volume. As antibiotics have been incorporated to the agar, only transformed bacteria will grow. Moreover, with this method, cells grow forming individual clones derived from a single cell.
 - Incubate the plates upside down overnight, at 37°C.
 - The next day, **pick one individual colony and seed it in 5 ml liquid LB** with the selection antibiotic. Growth at 37°C, 250 rpm overnight for generate a pre-culture from a single cell clone.



Helpful TIPS

- **DNA is very sticky and contaminate your pipettes** very easily. If a plasmid has contaminated your pipettes, some bacteria can incorporate and undesired DNA and grow in medium with antibiotics. To avoid problems:
 - **Clean your pipettes** regularly
 - **Use filtered tips** when needed
 - **Always check your bacteria clone**. Isolate plasmid DNA with a mini-prep, digest it and run it on an electrophoresis gel.
- **Plasmids are fragile. Avoid pipetting** or vortex as you can break them. Mix then gently with your fingers when needed.
- **The efficiency of bacterial transformation depends on the size of the plasmid** (among other factors). If possible, design plasmid as small as you can.

4. Plasmid isolation: Mini-PREP and Maxi-PREP

We use transformed bacteria cells to obtain high amount of copies of our plasmid of interest in a short period of time. Many methods have been developed to clone plasmid DNA with bacteria. These methods invariably involve three steps: growth of the bacterial culture, harvesting, lysis, and DNA purification. In the lab we have two different commercial kits to isolate plasmids from a bacterial culture. **Mini-Prep DNA preparation and Maxi-Prep** are collected in Table 8. We will decide to use one or another depending on the final objective. We generally perform Mini-Preps to test our plasmid, in order to know if the cloning strategy has worked and the new

plasmid has been correctly generated. Once the clone has been tested, we perform MAXI-preps of the tested clones to generate plasmids for cell transfection. Commercial kits were used following manufacturer instructions

	Mini-PREP	MAXI-Prep
Starting culture	1-5 ml	200-300 ml
Purification Kits used	GenElute™ Plasmid Miniprep Kit (PLN70-1KT; Sigma)	QIAGEN Plasmid Maxi Kit (12165; Qiagen) GenElute™ HP Plasmid Maxiprep Kit (NA0310-1KT; Sigma)
Yield	Final volume: 50 µl. Concentration: 20-100 ng/ml	Final volume: 300 µl. Concentration: 1-2 µg/ml

Table 8. Commercial kits for plasmid isolation.

5. Digestion

Plasmids contain specific target sites for restriction enzymes. In first term, they are used to manipulate and modify the plasmids. However, they can also be employed as a tool to analyze and cloned vector. If the patter of digestions of a plasmid coincide with the expected one, it is likely that we have obtained the desired vector. To make a DNA digestion we proceed as follows:

- **Prepare the digestion mix:**
 - **1 µg of DNA plasmid**
 - **1 µL of each restriction enzyme.** For double or triple enzymatic digestion more than one enzyme can be add at the same time.
 - **1µL of digestion buffer (10x).** Each enzyme has their own digestion buffer. If multiple enzymes are used, chose the digestion buffer that gives the maximum activity of the combination.
 - **Up to 10 µL of milliQmilliQ water**
- **Incubate 1h or overnight** in a humid incubator at the adequate temperature.

The result of the digestion could be checked in electrophoresis using a 1-2% agarose gel.

7. Glycerol stock

The bacteria colonies can be stored at -80°C for several years. Generating a glycerol stock allows to rapidly generate a culture of bacteria, skipping transformation and pre-culture steps. Glycerol stocks are generated from a pre-culture containing the colony of interest. To generate 1 mL of stock **mix 800 μL of the bacteria culture with 200 μL of 80% Glycerol sterile preparation**. The final glycerol concentration is 20%. As the glycerol is toxic for the cells, freeze rapidly once the glycerol has been added. When you need to grow the bacteria again, scratch with a sterile tip in the frozen surface and inoculate in 5 ml LB containing the antibiotic. Grow bacteria as usual. Avoid thaw of the stock.

CHAPTER III:

RETROVIRUS

Primary cell cultures and the cell line IDG-SW3 are hard to transfect with common transfection methods, therefore, retroviral infection played a key role in gene silencing and ectopic expression of proteins. In this thesis, retrovirus we generated in virus facilities. Then target cells were infected. The protocols of both steps are detailed in the following sections.

1. Production of retrovirus

Retrovirus used for gene infection were generated in Platinum-E cells. These cells have been genetically modified to express all the retroviral genes required for packaging of RNA and assembly of viral particles (gag, pol, env). Nevertheless, previous experience in the lab recommends to transfect our viral vector together with a plasmid that encodes for the envelope (VSG-V gene) in order to improve the efficiency of viral production in presence of polybrene. Plasmids used for production of retroviral particles are shown in **Error! Reference source not found.9**.

Plasmid	Protein	Resistance	Origen
pMD2.G	VSV-G	Ampicillin	Dr. M. Parra's lab
pMSCV-GFP	GFP	Ampicillin	Dr. M. Parra's lab
pMSCV-NRF2	Human NRF2	Ampicillin	Generated in our lab
pMSCV-PGC1 α	Human PGC1 α	Ampicillin	Generated in our lab
pMSCV-Puro	puromycin resistance	Ampicillin	Dr. M. Parra's lab
pMSCV-Puro-Cre-ERT2	Cre puromycin resistance Tamoxiden inducible	Ampicillin	22776, Adgene
pSECC-Keap1.4	CRISPR/Cas9 against mouse Keap1	Ampicillin	Dr. Papagiannakopoulos' lab
pSECC-Nrf2.4	CRISPR/Cas9 against mouse <i>Nfe212</i>	Ampicillin	Dr. Papagiannakopoulos' lab

Table 9. Plasmid used for retrovirus production

To generate the retroviral particles, proceed as follows:

- 24 h prior transfection, **seed Plat-E cells in DMEM without selective antibiotics** (Blasticidine and Puromyci). The cells should achieve 60-75% confluence at the time of transfection.

- **Start the protocol to transfect Plat-E** with the selected plasmid using Lipofectamine LTX. In first place, prepare following solutions (tables 10 and 11):

- **Dilution 1:**

Reagent	For one 100mm plate	For one well of a 6-wells
Opti-MEM	875 μ L	175 μ L
Lipofectamine LTX	35 μ L	7 μ L

Table 10. Reagents for Dilution 1 of LTX transfection protocol

- **Dilution 2:**

Reagent	For one 100mm plate	For one well of a 6-wells
Opti-MEM	875 μ L	175 μ L
Retroviral plasmid	8 μ g	1,6 μ g
Envelop plasmid (pMD2.G)	2 μ g	0,4 μ g
Plus reagent	10 μ L	2 μ L

Table 11. Reagents for Dilution 2 of LTX transfection protocol

- **Add dilution 2 to dilution 1.** Mix gently and **incubate for 15 min.**
- **Distribute the volume drop by drop** in a 100 mm plate or a well of a 6-well plate containing 8 mL or 2 mL or medium without antibiotics, respectively.
- Place the dishes in the virus culture room and **leave the cells 48-72 h with the transfection medium.**
- 24-28 h post-transfection **evaluate the expression of GFP** (if any of the transfected retroviral plasmid codifies for it). This can be used as a control of the transfection efficiency.
- 48-72 h after transfection, **harvest the retroviral supernatants and filter them with a cellulose acetate filter of 0.45 μ m** to remove cellular debris.



Helpful TIPS

- **When you filter the retrovirus:**
 - **Do not use nitrocellulose filters**, they bind proteins present on the membranes of the retrovirus and destroy them.
 - **Do not use filters of 0.22 μm** , they will retain virus particles and the supernatant won't be infectious.
- **Retroviral supernatants can be stored at 4°C up to 10 days** before losing their efficiency.
- **For longer storage periods, freeze the retrovirus at -80°C.** Avoid thaw and freezing cycles as they decrease the efficiency.

2. Transducing cells with retrovirus.

We used the following protocol to transduce adherent cells that are hard to transfect, as osteoblasts, osteocytes or IDG-SW3. In all the cases, the effectivity for retroviral infection was very high. The general protocol used in the lab proceeds as follows:

- 24 h prior transfection, **seed the cells in a 6-well plate to achieve 20-40% confluence** the next day. For osteoblasts, osteocytes and IDG-SW3, seeds **7-8 \cdot 10⁵ cells per well**. If antibiotic selection is going to be performed, do not forget to seed extra-wells.
- Next day, for each well of a 6-well plate prepare the infection mix (Table 12):

Reagent	For one well of a 6-wells
Virus supernatant	200-500 μL
Polybrene (1 mg/mL)	5 μL
Complete medium	Up to 1 mL

Table 12. Mix for cell transduction with lentiviral particles

- **Centrifuge plates at 400 g for 30 minutes at 32°C.** This will increase the efficient of transduction.
- **After 24 hours, remove and discard the virus-containing medium** and replace it with fresh medium.
- **Incubate for additional 24-48 hours** to allow higher expression levels of ectopic proteins.
- If needed, **select the cells with antibiotics.** For osteoblast, osteocytes and IDG-SW3 we used 5 µg/mL of puromycin for 48 h.
- When using an **inducible system, add** the appropriate treatment. We used 1 µM Tamoxifen to activate Cre-ERT2 protein.
- **Remove selection** media and add fresh media for additional 24 hours for recovery.
- **Harvest** the cells for analysis as usual.



- **Co-transfections can be performed.** In this case pour up to 250 µL of each supernatant.
- **Each cell line has a different optimal concentration of antibiotic for selection.** Use non-transfected cells as controls to know when puromycin has already killed all the non-infected cells.
- **Selection** of cells and **induction** of certain proteins (such as Cre-ERT2) **can be performed at the same time** if needed.
- **The expression levels of GFP varies among cell lines.** In some cases, expression is very low, and it is not visible until 72h post-transduction. If GFP expression is used as a control of transduction, take it with care since sometimes expression of GFP is not detected, even when cells have been effectively infected

CHAPTER IV:

MOLECULAR BIOLOGY

1. RNA isolation

RNA was isolated from cells and tissues using TRIsure reagent (Bioline, ref. BIO-38033) and following the manufacturer instructions. The protocol used proceeds as follows:

- **Step1: Lysis.**

- **For cells:** Lyse cells directly in the culture dish by adding **500 µL of TRIsure** per 1 well of a 6-well plate and freeze the samples or continue with the protocol. With a blue tip, **scrape** the cells. Then, pipette the cell lysate several times to ensure enough cell disruption.



Freezing point: Samples can be storage at -80°C for at least one month.

- **For bone tissues:** **Cut the bone** in small pieces and place them in a 2 mL Eppendorf. **Add 500 µL of TRIsure per each half calvaria or 1 mL of TRIsure for long bones** (one femur and one tibia).



Freezing point: Freeze immediately in liquid nitrogen or dry ice to avoid RNA degradation. At this stage samples can be stored for at least one month at -80°C However, try to process samples as soon as possible as RNA decays with time.

Thaw the samples on ice. **Homogenize the tissue with the polytron for 30''**. Homogenization should be done on ice to avoid sample overheating.

- **Step 2: Phase separation.** Incubate the samples for 5 min at room temperature. Add **100 µL of chloroform per 500 µL of TRIsure** used. Vortex the tubes or **shake them vigorously** by hand for 15 seconds. Incubate the samples for 3' at room temperature. **Centrifuge samples at 12,000 xg for 20' at 4°C**. The sample will split in two phases: a pale green organic phase, a solid interphase made of proteins and a colorless aqueous phase (upper phase) that contains the RNA.

- **Step 3: RNA precipitation:** Use a 200 µL pipete to **transfer the aqueous phase into a new Eppendorf**. **Add 1 µl of glycogen** in the aqueous phase to facilitate


Materials and Methods

RNA precipitation. Precipitate RNA with **250 μL of isopropyl alcohol per 500 μL of TRIreure** used. Vortex the tubes or **shake them vigorously** by hand for 15 seconds. Incubate the sample 10 min at room temperature. Then, centrifuge at **12,000 xg for 20'** at **4°C**.




Use double tips to remove the supernatants. Place a white tip over a blue tip to make a narrower tip and avoid pellet disturbance.

- **Step 4: RNA wash:** Remove the supernatant. **Add 500 μL of 75% ethanol** to wash the pellet. Vortex and **centrifuge at 7,500 xg for 5'**.

 **Freezing point:** Samples can be storage for one week at 4°C or one month at -20°C.

- **Step 5: Hydration the RNA:** **Air-dry the pellet** and dissolve in **15 μL of DEPC-treated water** by pipetting the solution up and down. Incubate **10' at 55°C** for complete re-hydration.

 **Freezing point:** Samples can be storage at -80°C or proceed to RNA retrotranscription.



Pellets can be air-dry at room temperature. Alternatively, they can be placed in the thermoblock at 45°C or under a lighten bulb to speed the drying step.

- **Step 6: Quantification:** Use a Nanodrop to assess the purity and concentration of the RNA.

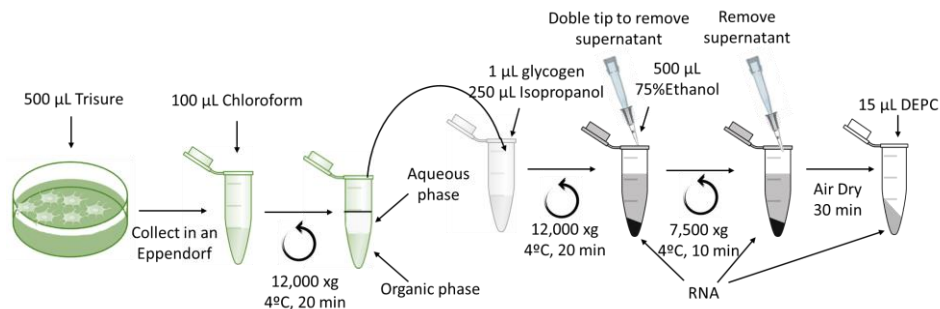


Figure 5. Schematic workflow of RNA isolation protocol.

2. mRNA retrotranscription (RT-PCR)

Retrotranscription (RT) is the process of copying RNA into cDNA. 1-3 µg RNA were retrotranscribed to cDNA using High Capacity cDNA Reverse Transcription Kit (Applied Biosystems). A general recipe was performed as follows (Table 13):

Reagent	Volume for 30 µL reaction	Volume for 50 µL reaction
RNA	1-2 µg contained in 15 µL	2-3 µg contained in 15 µL
Buffer	3 µL	5 µL
dNTP Mix	1'2 µL	1'2 µL
Random primers	3 µL	5 µL
Retrotranscriptase	1,5 µL	2,5 µL
DEPC-treated water	Up to 15 µL	Up to 50 µL

Table 13. Reaction mix for retrotranscription.

3. Isolation of mitochondrial and nuclear DNA

Mouse mitochondrial DNA (mtDNA) is a double-stranded circular DNA of 16.6-kb, which encodes genes for transfer RNAs (tRNA), ribosomal RNAs and 13 subunits of the oxidative phosphorylation (OXPHOS) complexes I, III, IV, and V. MtDNA replication is independent of nuclear and the ratio mtDNA/nDNA is a marker of overall mitochondrial number. Quantitative PCR (qPCR) is the method generally used for the quantification of mtDNA/nDNA. But, before qPCR is performed, isolation of mtDNA and nDNA is needed.

To start the protocol, cells are seeded in a 6-well plate (we seeded 200,000 cells/well). After treatments, cells are collected in an Eppendorf either by trypsinization or scrapping. None of the methods interfere in the final outcome. Then, to isolate both DNAs from the same sample proceed as follows:

- **Wash the cells** with 200 µL of cold PBS. Centrifuge at maximum speed for 10' at room temperature.
- Add **600 µL of Nuclei Lysis Solution** (50 mM TRIS-HCL pH 8.0, 10mM EDTA pH 8.0 and 2% SDS) and lysate the cells by pipetting.
- Add **3 µL of RNase A** and mix by inversion 2-5 times. **Incubate at 37°C for 15-30'**. To improve cell lysis mix by inversion time to time.

- Add **20 μL of Proteinase K** and incubate at **45°C 1-3h or overnight**.



Eventually open when they are left at 45°C overnight. If this happens, the sample will dry. To avoid this, place some weight on the Eppendorf tubes.

- Add **200 μL of 6M NaCl** and vortex vigorously for 20". Place the samples **on ice for 5'**.
- Centrifuge the samples at **maximum speed for 4-8'** for protein precipitation. Check that pellet is consistent. If not, centrifuge again.
- Transfer the supernatant to a **new Eppendorf containing 600 μL of isopropanol at room temperature**. Mix by inversion until DNA becomes visible.
- Centrifuge at **maximum speed for 1' at room temperature**. A small white pellet must be seen at this step. Remove the supernatant using double tip.
- Add **600 μL of 75% ethanol** at room temperature and vortex to clean up the DNA.
- Centrifuge at **maximum speed for 1' at room temperature**. Remove the supernatant using double tip. Air-dry the pellet.



Pellets can be air-dry at room temperature. Alternatively, they can be placed in the thermoblock at 45°C or under a light bulb to speed the drying step.

- Suspend the pellet in **30 μL of millQ water**. Rehydrate the pellet by incubating it 1h at 65°C or overnight at 4°C.
- Quantify DNA obtained. If needed, dilute it to obtain a solution of 6 $\mu\text{g}/\text{ml}$.

Finally, for quantification of mtDNA/nDNA ratio we performed a qPCR with Syber Green as explained in section "4.4. quantitative PCR (qPCR)". The primers used for mtDNA determination were *Nd4*, *RNA16S* and *tRNA_Glu*, while the primers used for nDNA determination were *Dmp1*, *Fgf23* and *Sost*. Sequences and PCR conditions are detailed in section "4.4. quantitative PCR (qPCR)".

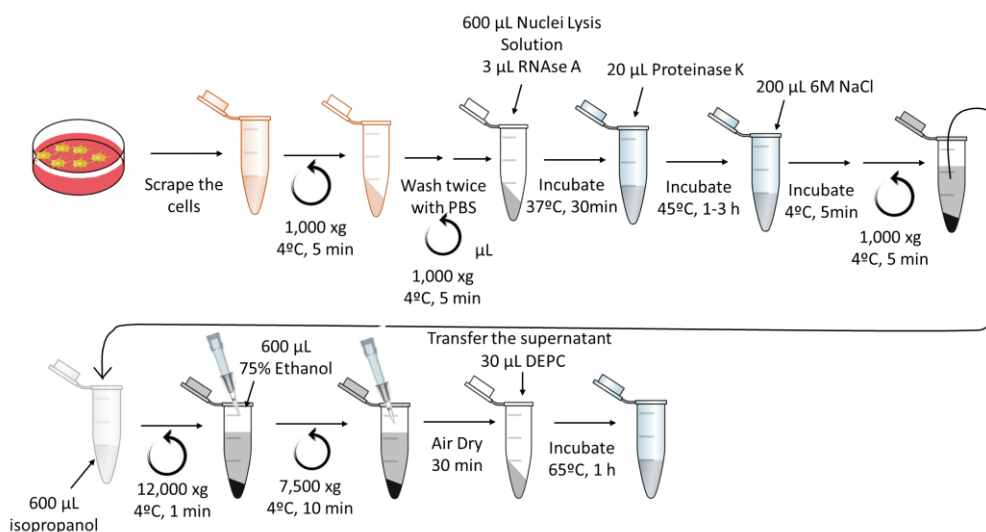


Figure 6. Schematic workflow of nuclear and mitochondrial DNA isolation protocol.

4. Quantitative PCR (qPCR)

Quantitative PCR (qPCR) is used to detect, characterize and quantify nucleic acids (not only RNA) for numerous applications. qPCR was performed in the ABI Prism 7900 HT Fast Real-Time PCR System using 384-well plates. Two different protocols were used:

- mRNA quantification with Taqman probes:** Taqman probes were used to determine the levels of mRNA and therefore, gene expression. TaqMan® probes consist of an 18-22 bp oligonucleotide probe which is labeled with a reporter fluorophore at the 5' end and a quencher fluorophore at the 3' end. In this stage, the quencher and the fluorophore remain in proximity to each other, and thus, the fluorescence of the reporter dye remains quenched. During PCR, the probe anneals specifically in an internal region of the PCR product, between the forward and reverse primer. The polymerase then carries out the extension of the primer. Then, the 5' exonuclease activity of the polymerase cleaves the probe, releasing the reporter molecule away from the quencher. As result, the fluorescence intensity of the reporter dye increases. This process is repeated in every cycle and does not interfere with the accumulation of PCR product. Designed Taqman assays (Applied Biosystems) were used to quantify mRNA levels. The recipe for one reaction is detailed in Table 14. Reaction were carried out always in duplicates. Taqman probes used in this thesis are listed in Table 15:

Reagent	Volume
cDNA	1 μ L (50-100 ng)
Taqman	0,5 μ L
SensiFast	5,5 μ L
MilliQwater	4,5 μ L

Table 14. Reaction mix for Taqman qPCR. Volumes are calculated for 1 well of a 384-well plate

Gene name	Taqman Probe ID
<i>Acp5 (Trap)</i>	Mm00475698_m1
<i>Alpl</i>	Mm 00475834_m1
<i>Atf4</i>	Mm 00515325_g1
<i>Bglap 3</i>	Mm00649782_gH
<i>Col1a1</i>	Mm 00801666_g1
<i>Cox4i1</i>	Mm 01250094_m1
<i>Ctsk (Cathepsin K)</i>	Mm00484039_m1
<i>Dkk1</i>	Mm 00438422_m1
<i>Dmp1</i>	Mm 01208363_m1
<i>Fgf23</i>	Mm 00445621_m1
<i>Gapdh</i>	Mm99999915_g1
<i>Gclc</i>	Mm00802655_m1
<i>Mepe</i>	Mm02525159_s1
<i>Mfn2</i>	Mm 00500120_m1
<i>Nfe2l2</i>	Mm00477784_m1
<i>Nqo1</i>	Mm01253561_m1
<i>Pfkfb3</i>	Mm 00504650_m1
<i>Pparg1b</i>	Mm 00504730_m1
<i>PPARGC1A</i>	Hs 01016730_g1
<i>Ppargc1a</i>	Mm 04331182_m1
<i>Runx2</i>	Mm 03003491_m1
<i>Scl2a1</i>	Mm 00441480_m1
<i>Sost</i>	Mm 00470479_m1
<i>Sp7</i>	Mm00504574_m1
<i>Tbp</i>	Mm 01277042_m1
<i>Tnfrsf11b (Opg)</i>	Mm00435454_m1
<i>TNFSF11 (RankL)</i>	Mm00441906_m1

Table 15. Taqman probes for qPCR.

• **qPCR with Sybr green:** SYBR® Green is a fluorescent dye that intercalates between the DNA bases. When bound to DNA, the dye becomes less mobile, causing its energy to be released as fluorescence. In consequence, the fluorescence measured at the end of each amplification cycle determine relatively or absolutely the amount of DNA amplified. Beside Syber green, two primers have to be designed for the amplification of the desired fragment. We used Sybr green to quantify mtDNA, nDNA, chromatin, expression levels of a fragment of a gene. The recipe for one reaction is detailed in Table 16. Reaction were carried out always in triplicates. Sequence of primers and reaction conditions are detailed in table 17.

Reagent	Volume
Sample	2 µL
SYBR Selected Master Mix	5 µL
Primers 5 µM	0,8 µL/each
MilliQ water	1,4 µL

Table 16. Reaction mix for Sybr Green qPCR. Volumes are calculated for 1 well of a 384-well plate

Gene	Primer sequences	qPCR Conditions (T annealing/ amplification time)
<i>Dmp1</i>	Fw: 5' AGCACCAGCAGGAAGGTCTCTACCC 3' Rv: 5' GTCTCCCGCCCACTAACAGATCCCA 3'	67°C, 30''
<i>Fgf23</i>	Fw: 5' GGAAGCCCAACATCCTGCGTTCTG 3' Rv: 5' GGCTATTTCTAGCTCAGGGGCCGGT 3'	67°C, 30''
<i>Nd4</i>	Fw: 5' CGCACATGGCCTCACATCACT 3' Rv: 5' ACGGCTGTGGATCCGTTCTAGT 3'	67°C, 30''
<i>Ppargc1a</i>	Fw: 5' ACTTGAGAAGCTCTGAGCAGGGACG 3' Rv: 5' TGCAGCAAACACACCCACAGG 3'	70°C, 60''
<i>Ppargc1b</i>	Fw: 3' GACGCTCTGAAGGACGGGGC 3' Rv: 5' CTCGGGAGGCTGGGCACTGT 3'	70°C, 60''
<i>RNA16S</i>	Fw: 5' TCGGCAAACAAGAACCCCGCCT 3' Rv: 5' TCTCCGAGGTCACCCAACCGAA 3'	67°C, 30''
<i>Sost</i>	Fw: 5' CGCCCGGTTTCATGGTCTGTTGTTTC 3' Rv: 5' CCGTGCCTCATCTGCCTACTTGTGC 3'	67°C, 30''
<i>tRNA_Glu</i>	Fw: 5' CCCAGTACTACCATCATCAAGT 3' Rv: 5' GATGTTTGGGAGATTGGTTGATGT 3'	67°C, 30''

Table 17. Primer sequence and reaction conditions used for qPCR with Sybr Green.

5. DNA sequencing by Sanger Method.

Sanger sequencing is a method of DNA sequencing based on the selective incorporation of chain-terminating dideoxynucleotides by DNA polymerase during *in vitro* DNA replication. Sanger sequencing reaction was performed in the Genomic Facility in Parc Cientific of Barcelona. Before sequencing sample samples must be prepared. This step depends on the nature of the DNA to sequence:

- For plasmid sequencing: we can use the whole plasmid for sequencing. Proceed as follows:

- Purify the plasmid with MaxiPrep or MiniPrep kits.
- Place 100ng of plasmid per each kb of DNA to be sequenced in PCR Eppendorf.
- Mix it with 5 pmol of the primer for sequencing.
- Incubate at 80°C in the thermocycle for lyophilization.

- For genomic DNA sequencing: Genomic DNA cannot be sequenced directly, and several steps are needed:

- Isolate genomic DNA as described in section 4.3. Isolation of mitochondrial and nuclear DNA.
- Make multiple copies of the fragment of interest by PCR.
- Run the PCR in an 1.5-2% agarose gel and in the transilluminator, cut the band corresponding to your PCR product.
- Purify the PCR product using the kit Qiagen PCR purification kit following manufacturer instructions. For further information, DNA purification step is detailed in section “4.7.4. DNA Clean up”.
- Place 100ng of purified DNA per each Kb of DNA to be sequenced in PCR Eppendorf.
- Mix it with 5 pmol of the primer for sequencing.
- Incubate at 80 °C in the thermocycler for lyophilization.

Lyophilized DNA can be storage at 4°C or room temperature until its sequencing.



Helpful TIPS

- **When designing the primers for DNA sequencing:**
 - Avoid annealing temperatures lower than **50°C**
 - Use primers purified by **HPLC**
 - Primers must be longer than **18 bp**.
 - Try to maintain a **G-C** content around **50-55%**
 - **Keep a safety margin from the site for your primers binding to the beginning of the sequence of your interest.** The first nucleotides are not sequenced sometimes.
 - **Design primers close to the sequence of your interest**, as the sequencing advances, the quality is reduced.
- **Purification of PCR products have a very low yield, therefore:**
 - **DNA sequencing might be poor and could sequence small part of the DNA.** Therefore, try to focus in the most important part.
 - **Sequencing is quite powerful.** Send your samples even if the quantity is lower than minimum required.

6. Cell lysis and Protein quantification: BCA assay

Total protein is used as a normalization measure for data obtained in several techniques, and it is also used to equalize the amount of protein load in Western Blot. To quantify proteins, we used Pierce™ BCA Protein Assay Kit (Thermo Scientific), which is compatible with the detergents used for cell lysis.

Unless other method is specified, cells are lysed with SB lysis buffer (500 mM Tris-HCl, pH 6.8; 2% SDS; 10% glycerol) on ice. For one well of a 6-well plate, cells are lysate with 200 µl of SB. Then, cells are scraped with a scraper or a yellow tip. Cell lysate can be aliquoted and stored at -20°C.



Helpful
TIPS

- Cell lysates from osteoblast and IDG-SW3 with SB get very viscous and sticky, and it is difficult to handle. You can work with a **1:3 dilution of SB buffer** or **heat** the cell lysate.
- **SB buffer doesn't need to be supplemented with proteases and phosphatases inhibitors**, as it instantly denaturalizes all the proteins

To determine protein concentration with BCA Protein Assay Kit, proceed as follows:

- **Dilute the samples** if they are too concentrated to avoid saturation.
- **Make a standard** of BSA albumin fraction V. Make 8 serial dilution (1:2) from 10mg/ml to 0 mg/ml (10, 5, 2.5, 1.25, 0.625, 0.313, 0.156 mg/ml)
- Take a 96-well plate. In each well place **15 µL of sample and 200 µL of BCA mix**, which contains **Reactive A and reactive B** in a proportion **24:1**. Incubate for **30'** at **37°C**



Helpful
TIPS

- The BCA reaction start when reactive A and B are mixed, **so add the reaction mix very quickly to all the wells**. Use a **multichannel pipette**.
 - **Measure all the samples in duplicate**.
- Read the plate at **562 nm** using Xfluo4 program.
 - Use the standard curve to obtain a regression equation. Then calculate protein concentration of the samples by inferring in the regression equation obtained.

7. SDS-Polyacrylamide gel electrophoresis (PAGE) and Western Blot.

Western Blot is a tool for the evaluation and quantification of protein levels within a cell culture or tissue. In the first step, proteins are separated in an electrophoresis according to their electrophoretic mobility. Then proteins are transferred to a PVDF membrane and incubated with antibodies against them. Finally, a secondary antibody conjugated with a peroxidase is used to visualize the results. All these steps are further detailed in the next sections:

7.1. SDS-Polyacrylamide gel electrophoresis (PAGE).

Samples are denaturalized with LSB buffer (final concentration of 1% SDS, 5% glycerol, 0.001% bromophenol blue, 0.313 M Tris-Cl, pH 6.8, 1% 2-mercaptoethanol (or DTT)). LSB contains high SDS concentration that inserts interact with amino acids and give a net negative charge to the protein/detergent complex. Therefore, proteins will be attracted by the positive pole in an electrophoretic field and will migrate proportionally to their size. Once LSB is added, samples can be boiled at 95°C for 5 min to increase the denaturalization of the proteins. Moreover, boiled cell lysates get less sticky and are easier to handle.



Helpful
TIPS

In some cases, **boiling of samples leads to a decrease in signal** due to aggregation of proteins therefore heating samples at or close to boiling is not always recommended.

To separate the proteins, two different gels are made:

- **Stacking gel:** concentrate the proteins and prepare them for its correct separation (table 18).
- **Running gel:** forms a network to separate the proteins. The percentage of of acrylamide determines the pore size and the resolution of the separation. We used gels with 8-12% of acrylamide (table 18).

Materials and Methods

	Stacking buffer	Running Buffer		
		8%	10%	12%
Stacking Buffer 4x (0.4% SDS 0.5 M Tris-HCl pH 6.8)	1.25 mL	-	-	-
Running Buffer 4x (0.4% SDS 1.5 M Tris-HCl pH 8.8)	-	2.5 mL	2.5 mL	2.5 mL
40% Acrylamide/Bis Solution, 37.5:1 (Bio-Rad)	0.525 mL	2 mL	2.5 mL	3 mL
MilliQ	3.225 mL	5.5 mL	5.25 mL	5 mL
10% APS (Ammonium Persulfate; Sigma)	100 µL	100 µL	100 µL	100 µL
TEMED (Merck)	10 µL	10 µL	10 µL	10 µL

Table 18. Composition of SDS-PAGE gel for electrophoresis. Recipe for one gel, 10x10 cm.

Once gels had polymerized, load 20–30 µg of total protein into the wells of the SDS-PAGE gel, along with molecular weight marker (PageRuler, ThermoFisher). Then fill the bucket with electrophoresis buffer (2.5 mM Tris-HCl, pH = 8.3; 19.2 mM Glycine, 1% SDS). Run the gel at 90 V until the front pass through the stacking gel and gets into the running gel. Turn up the voltage until 120 V and run the gel until the front reach the lower zone.

7.2. Protein transfer and membrane blocking

Proteins of the gel are transfer to a PVDR membrane using semi-dry system in Fast Semi-Dry Machine (from Bio-Rad). For this protocol, two buffers are used:

- **Cathode Buffer:**
 - 40 mM 6-aminocaproic acid
 - 20 % methanol
- **Anode Buffer:**
 - 0.3 M Tris-Base
 - 20% methanol



As the methanol evaporates rapidly, **prepare stock without methanol**. Add methanol when one bottle starts to be used. This will elongate the use of the buffer.

The protocol follows as indicated:



From now until the end of the protocol:

- **Avoid the membrane to get dry.**
- **Do not touch the membrane with your hands.** Use the forceps.

- **Cut 8 x 5 cm PVDF membrane.**
- **Activate PVDF membrane** by immersion in methanol for 1-3'. Leave it in cathode buffer while preparing the stack.
- **Cut 6 pieces of 8'5 x 6 cm of Whatman Paper** for each gel. **Soak** 3 Whatman paper in Cathode buffer, and 3 in Anode buffer.
- **Prepare the stack as follows** (Figure 3).

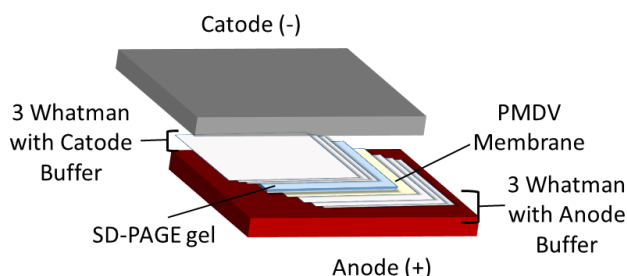


Figure 7: Scheme for protein transference in semi-dry transfer system.

- **Block the membrane:** Incubate the membrane for 1 hour at room temperature using 5-10 % non-fatty milk in TBS-T to avoid unspecific binding of the antibody.

7.3. Immunoblotting

In this step, the target protein is identified via antigen-antibody specific reactions. The protocol proceeds as follows:

- **Wash** the blocked membrane with TBS-T for **10 minutes**. Repeat the wash **three times**.
- **Incubate** the membrane with appropriate dilutions of **primary antibody** in 5% BSA in TBS-T. For this, make individual bags containing the membrane and the antibody solution and place them at **4°C in gentle agitation overnight**. If weekend is coming, you can incubate the antibody for 48-72 h. Antibodies used are listed in table 19.

Materials and Methods

- After incubation, **transfer the antibody to a falcon and keep it at 4°C** for further uses.
- **Wash** the membrane with TBS-T for **10 minutes**. Repeat the wash **three times**.
- **Incubate** the membrane with the recommended dilution of **conjugated secondary antibody** in 1% milk in TBS-T at **room temperature for 1 h**.
- **Wash** the membrane with TBS-T for **10 minutes**. Repeat the wash **three times**.
- **Imaging of the membrane**: For signal generation, **incubate** the membranes with a Chemiluminescence Detection Kit for HRP (**EZ-ECL Kit**) (20-500-500, Biological Industries) following the kit manufacturer's recommendations. Remove excess reagent and cover the membrane in transparent plastic wrap. **Acquire image using LAS3000** (Nikon).

Antibody	Dilution	Secondary	Expected molecular weight	Supplier
α-tubulin	1:2000	Mouse	55 kDa	Sigma
ATF4				
KEAP1 (F-10)	1:100	Mouse	60-64 KD	sc-514914 Santa Cruz Technologies
NRF2 (A-10)	1:100	Mouse	95-110 KD	sc-365949 (Santa Cruz Technologies)
Oxphos cocktail	1:100	Mouse	CV-ATP5A 55 KD CIII_UQCRC2 48 KD CIV-MTCO1 40 KD CII_SDHB 30 KD CI_NDUFB8 20 KD	Ns607300 (Mitoscience)
pAMPK	1:100			
PEIF2α	1:100			
p-p38 MAPK(Thr180/Tyr182)	1:100	Rabbit	43 KDa	92115 (Cell Signalling)
pS6	1:100			
SIRT1	1:100	Rabbit	110 KDa	07-131 (Millipore)
PGC1α	1:100	Mouse	130 KDa	ab54481 (Abcam)

Table 19: Antibodies used for immunoblotting in Western Blot assay.

8. Chromatin Immunoprecipitation (ChIP)

The Chromatin Immunoprecipitation aims to determine whether specific proteins are associated with specific genomic regions, for instance transcription factors with promoter regions of their target genes.

The ChIP protocol is composed by several steps that include fixation of the proteins, immunoprecipitation, DNA purification and measure of co-immunoprecipitated DNA by qPCR. It is important to start with a great number of cells. This protocol is adapted for working with a confluent entire 6-well plate.

8.1. Cross-linking

- **Fixate cells with 1% PFA.** To fixate the cells, follow these steps:
 - **Prepare fresh 18.5% in milliQ water.** For 5 mL add 0.925g of PFA and 4.8 mL of milliQ water. Stir and heat until almost complete dissolution.




PFA solution should become clear. If this do not happen, add up to 35 μL of 1N KOH to adjust the pH and allow complete dissolution.

- In each well, **add 54 μL of 18.5% formaldehyde in 1 ml of growth media without FBS.** Incubate **10 min at room temperature** with gentle agitation.
- **Add 100 μL of 2.5M Glycine** to each well to stop the reaction. **Incubate 5 min at room temperature** with gentle agitation.
- Place the plaques **on ice** for the rest of the procedure. **Wash twice with cold PBS.**
- **Add 1 ml PBS supplemented with proteases and phosphatases inhibitors** (table 20). Collect cells by **scrapping**. **Pool al the cells** of one 6-well plate in the same tube to homogenize the experimental conditions and increase the initial number of cells.
- **Centrifuge at 1000 g, 5 minutes at 4°C.** Check if the pellet is consistent. If not, centrifuge again.
- **Remove supernatant.**



Freezing point: Pellet can be storage at -80°C

- Resuspend pellet in 1ml SDS Lysis Buffer (table 19) supplemented with proteases and phosphatases inhibitors. Make aliquots of 320 μ l.

 **Freezing point:** Aliquots can be storage at -80°C


Proteinase Inhibitors		
Inhibitor	Stock and dissolvent	Working concentration
Leupeptin	5 mg/ml Water	5 μ g/ml
Aprotinin	2 mg/ml Hepes 10mM pH8	2 μ g/ml
Pepstatin	1 mg/ml 10% Acetic acid, 90% Ethanol	1 μ g/ml
Benzamidine	10 mg/ml Water	100 μ g/ml
PMSF (phenylmethylsulfonyl fluoride)	100 mM Isopropanol	1 mM
Phosphatase Inhibitors		
Inhibitor	Stock and dissolvent	Working concentration
NaF	1 M Water	10 mM
β -Glycerol phosphate	1 M Water	10 mM
Na_2VO_4 (Sodium orthovanadate)	100 mM Water, pH = 10	200 mM

Table 20. Protease and phosphatase inhibitors.

8.2. DNA Sonication

Sonication is a method to break the chromatin in random fragments. For CHIP we aim to generate small chromatin fragments between 200-1000bp. Each IDG-SW3 cells and osteoblast aliquot of 320 μ l, was sonicated 8 cycles for 10" each cycle (8x10"), in **duty-cycle set at 5-6**. The number of cycles will depend on the cell model, confluence and fixative conditions you are working with.

Then, **centrifuge the extracts at 15.000 g x 10 minutes at 4°C** to remove the chromatin that has not been sonicated. Collect supernatants.

 **Freezing point:** Supernatants can be storage at -80°C



- During sonication, **sample get warm**. To avoid this, place the tube **in ice while you sonicate** it.
- **Avoid formation of foam** by maintaining the tip near to the bottom. If you form foam, let the tube rest until the air gets out and continue. Otherwise sample will no sonicate properly.
- **Sonicate all the tubes by cycles**. That's allow the samples to rest between sonication turns. Sonicate the first tube 10'', next continue with the next tube until all the tubes get the first pulse. Then, star with the first tube the second cycle in the same way.
- You need **to test the better conditions for sonication** in your model. The first time make a sonication probe. Take 5 aliquots of your model and sonicate them for 4, 6, 7, 8 and 10 cycles of 10''. Then run 10 μl of the sonicated samples in an agarose gel. You have to see a degradation patter with fragments ranging from 100 to 1000 bp (Figure 4).
 - Be careful with the volume of the aliquots since it might interfere in the sonication results. Bigger or smaller volumes might modify the sonication efficiency.
 - An alternative to sonication is enzyme-based chromatin digestion. However, DNA binding proteins, or chromatin modification can influence chromatin digestion, creating a bias in the fragmentation. This might be critical for some studies.
 - Chromatin is very sticky and **can contaminate your pipette**. Be careful, **clean** your pipettes regularly. Use **filter tips** if necessary.

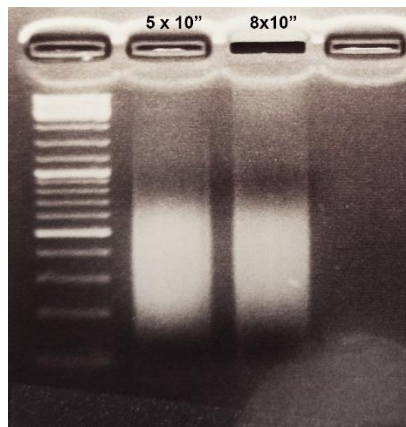


Figure 8. Probes of Chromatin sonication in IDG-SW3 cells. Chromatin fragments after sonication of IDG-SW3 cells for 5 and 8 cycles of 10'' (5x10'' and 8x10'' respectively).

8.3. Immunoprecipitation.

In this step antibodies are used to bind transcription factor-DNA complexes. Before starting the protocol, prepare all the buffers needed (table 21). The protocol is the following:

- **Make 100 μ l aliquots of sonicated chromatin** per each immunoprecipitation. Make one plus aliquot for the negative (IgG) and another if you want to add a positive control (anti-RNA pol II). Separate also **20 μ l for INPUT**. Keep them at 4°C during the immunoprecipitation step.



- If more than more than 3 IP are going to be done, thaw more than one aliquot and **mix before slit them** to homogenize the conditions.
- It is highly recommendable to use an IgG made in the same species that the antibody against the protein of interest.

- To each aliquot, **add 900 μ l Dilution Buffer** supplemented with protease and phosphatase inhibitors.

- **Add 1 μ g of their correspondent antibody** to each tube. Incubate the samples with the antibody **overnight rotating at 4°C**.



As long as you can, **use polyclonal antibodies**. That would enhance the chances of target the protein, if eventually some epitopes results blocked.

- Add **20 μ L Magna ChIP Protein A+G Magnetic Beads** (16-663; Millipore). **Incubate 1 hour at 4°C** on rotating platform
- **Collect the beads using a magnetic rack.** Aspirate supernatant carefully.
- **Wash the beads.** Add **1 mL** of the following wash buffers and incubate **5-10' in rotation at 4°C.** Use the sequence that follows:
 - **2x Low Salt Buffer**
 - **2x High Salt Buffer**
 - **1x LiCl Buffer**
 - **2x Wash with TE buffer**



- **Washings can be performed for 5' or 10'.** Start trying washing for 5' and if you find high interspecific binding, increase the washing time up to 10'.
- **LiCl interferes with the charges and the Magnetic Beads** are softly attracted by the rack. Remove the LiCl washing buffer carefully by pipetting.
- Chromatin is very sticky, and some contaminations might remain in the Eppendorf. **Transfer the sample to a new Eppendorf** before the last TE washing to remove any rest of chromatin.

- Prepare **200 μ L of fresh elution buffer per IP and 100 μ L per input.**
- **Resuspend the beads in 100 μ L of fresh elution buffer.** Take the **inputs** and add **50 μ L of fresh elution buffer** to each tube. Mix gently by hand and **incubate 15' at room temperature.**
 - Use a Magnetic rack to separate the beads. **Collect the supernatant** in a new tube.
 - **Add new 100 μ L of fresh elution buffer to each IP and 50 μ L to each input sample.** Mix gently by hand and again incubate **15' at room temperature.**
 - Use a Magnetic rack to separate the beads. **Collect the supernatant** in the previous tubes.

Materials and Methods

- **Reverse crosslinking of the DNA and the proteins.** Add **8 μL 5M NaCl** in each **bead-elution** (final volume 200 μL) and add **4 μL 5M NaCl** for the **inputs**. **Incubate overnight at 65°C.**



Eppendorfs eventually open when they are left at 65°C overnight. If this happen, the sample will dry. To avoid this, place some weigh on the Eppendorf tubes.

- Let the Eppendorfs cool down. Add **0.5-1 μL of RNase A** and incubate **30' at 37°C.**
- Degrade the proteins present in the sample. Add **13 μL of fresh proteinase K mix** (Table 19) to each bead-elution and input. Incubate 1-2h at 45°C.
- Continue to DNA clean up.

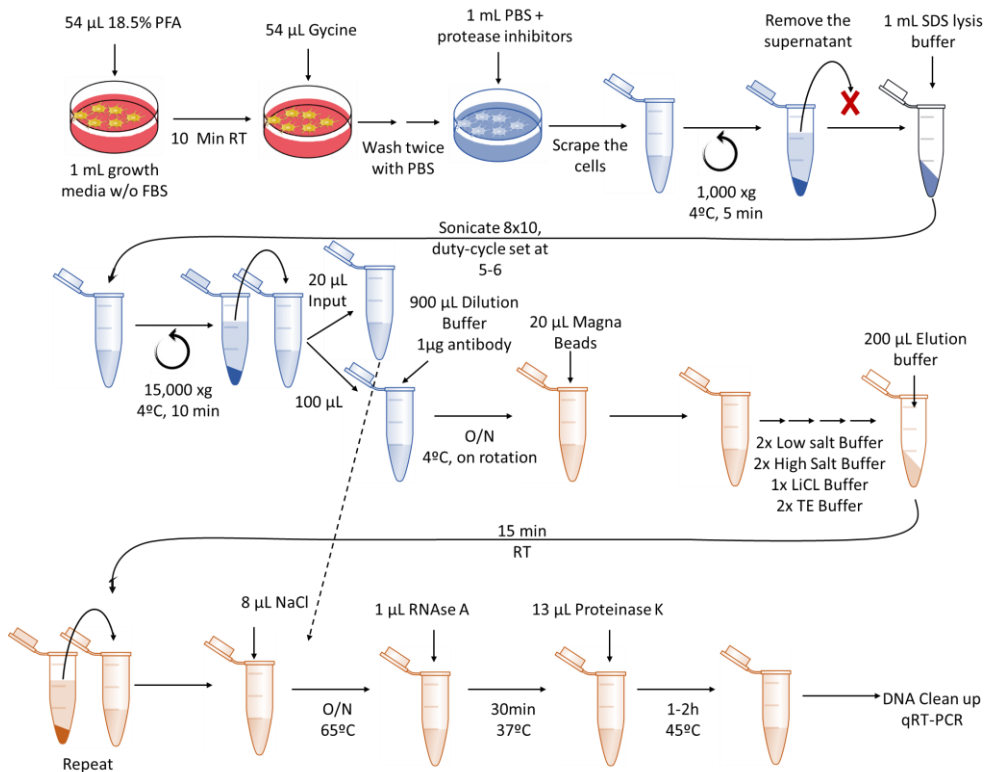


Figure 9. Schematic workflow of ChIP protocol.

Material and Methods

Buffer	Composition	Recipe
SDS-Lysis Buffer	1% SDS	<u>For 50 mL:</u> 0.5 g SDS
	10 mM EDTA	0.186 g EDTA
	50 mM Tris	0.302 g TRIS
Dilution Buffer	0.01% SDS	<u>For 50 mL:</u> 50 µL 10% SDS
	1.1% Triton x100	2.76 mL 20% Triton
	1.2 mM EDTA	2.2 mg EDTA
	16.7 mM Tris-HCl	101 mg Tris-HCl
	167 mM NaCl	488 mg NaCl
High Salt Buffer	0.1% SDS	<u>For 500 mL:</u> 0.5 g SDS
	1% Triton x100	5 mL Triton x100
	2 mM EDTA	0.375 g EDTA
	20 mM Tris-HCl	1.211 g Tris-HCl
	500 mM NaCl	15.6 g NaCl
Low Salt Buffer	150 mM NaCl	<u>For 500 mL:</u> 4.383 g NaCl
LiCl Buffer	0.25M LiCl	<u>For 500 mL:</u> 5.298 g NaLi
	1% NP-40	5 mL NP-40
	1% sodium deoxycholate (NaDOC)	5 g NaDOC
	1 mM EDTA	0.186 g EDTA
	10 mM Tris	0.605 g Tris
Elution Buffer (make it fresh!)	1%SDS	<u>For 200 µL (one IP)</u> 10 µL 20% SDS
	0.1 M NaHCO ₃	20 µL 1M NaHCO ₃
		170 µL MilliQ water
Proteinase K mix (make it fresh!)	0.154 M EDTA	<u>For 13 µL (one sample):</u> 4 µL 0.5M EDTA
	0.615 M Tris-HCl pH=6.5	8 µL 1M Tris-HCl pH= 6.5
	Proteinase K	1 µL Proteinase K

Table 21: Composition of CHIP buffer and the recipe for the volumes usually prepared.

8.4. DNA clean up.

Use the kit **Qiagen PCR purification kit** to remove any contaminants your samples prior analyzing the ChIP by qRT-PCR. You should start with a total volume of 222 μ L. Proceed as follows:

- Add **666 μ L of QG buffer**. Mix it several times by inversion.
- Add **222 μ L of Isopropanol**. Mix several times by inversion.
- Place **half of the mix in a column**. Centrifuge **1' at 13,000 rpm at room temperature**.
 - Throw the flow through. **Add the other half** of the volume. **Centrifuge 1' at 13,000 rpm at room temperature**.
 - Throw the flow through. Add **500 μ L of QG buffer** again. **Centrifuge 1' at 13,000 rpm at room temperature**.
 - Throw the flow through. Clean with **750 μ L of buffer PE**. Centrifuge **1' at 13,000 rpm at room temperature**.
 - Throw the flow through. **Centrifuge again 1' at 13,000 rpm at room temperature**.
 - Throw the flow through. **Let the column dry**.
 - **Add 50 μ L of buffer EB**. Wait some minutes. Centrifuge **1' at 13,000 rpm at room temperature in a new Eppendorf** to collect the final sample.

Analyze the samples by qRT-PCR with using SYBR Green as explain in Section “4.3. Quantitative PCR (qPCR)”. Use 1 μ L of the sample for each well and the primers designs against the putative promoter. Primer used for ChIP analysis in this thesis are listed in table 22.

Gene	Primer sequences	PCR Conditions (T annealing/ amplification time)
<i>Dmp1</i>	Fw: 5' AGCACCAGCAGGAAGGTCTCTACCC 3' Rv: 5' GTCTCCCGCCCACTAACAGATCCCA 3'	70°C, 30''
<i>Fgf23</i>	Fw: 5' GGAAGCCCCAACATCCTGCGTTCTG 3' Rv: 5' GGCTATTCTAGCTCAGGGGCCGGT 3'	70°C, 30''
<i>Sost</i>	Fw: 5' CGCCCGTTTCATGGTCTGGTTGTTTC 3' Rv: 5' CCGTGCCTCATCTGCCTACTTGTGC 3'	70°C, 30''

Table 22: Primers used and PCR conditions for ChIP analysis

9. F-Actin Cytoskeleton Staining with Phalloidins

Phalloidin is a bicycling peptide belonging to a family of toxins isolated from *Amanita phalloides*. Phalloidins conjugated with different labels are commonly used to stain cytoskeleton. Labeled phalloidins have similar affinity for large and small filaments, binding in a stoichiometric ratio of one phalloidin molecule per actin subunit in cells. Unlike antibodies, the binding affinity does not change with the different species or tissue sources used. Therefore, phalloidins can be used to visualize and quantify F-actin in cryopreserved tissue section, cell cultures or cell-free preparation. In this thesis, we only applied phalloidin staining to cell cultures.

As for other immunocytofluorescence stains, cells have to be seed over glass coverslips at 40-60% confluence. For this, a coverslip is place in the bottom of a well of 24-well plates. For osteoblast and osteocytes, the glass was coated with collagen as described in Section “1.2.Culture dishes and collagen coating”).

The protocol for phalloidin stain proceeds as follows:

- **Fix the cells with 4% PFA.** Incubate for **15’ at room temperature** with gentle agitation.
 - **Rinse three times** with cold PBS.
 - ❄️ **Stop point:** You can keep the cells at 4°C until you perform the staining.
 - Permeabilize the cells with 0.1% triton x-100 in PBS. Incubate for **15’ at room temperature** with gentle agitation.
 - **Rinse three times** with cold PBS.
 - **Block** non-specific staining with 1% BSA in PBS. Incubate for **30’ at room temperature** with gentle agitation. This step is not necessary



If you need to perform additionally histological staining, proceed to incubation with primary and secondary antibodies between these two steps.

- Prepare **staining solution**. Dissolve **5 μ L of 40X methanolic stock** solution into **100 μ L of PBS with 1% BSA** for each coverslip to be staining. Incubate for **30’ at room temperature in the dark**. To avoid evaporation, add water in between the wells of the plate to create a wet chamber.
 - **Rinse three times** with cold PBS.
 - Stain nuclei with DAPI. Add **1 μ g/mL of DAPI diluted in PBS**. Incubate for **15 min at room temperature in the dark**.

- **Rinse three times** with cold PBS.
- **Mount the Coverslip** slides with Prolong[®] Gold Antifade Reagent (Life Technologies). To do so, **drop a 15 μ l drop of mounting media** over a slide and **put over it side-down the glass cover** with your immune-stained cells. Allow to dry the mounting media in perfectly horizontal for a few hours. For long-term storage, store slides flat at 4°C protected from light.



- **Do not let the cells dry** during the protocol. Ensure they are always wet and in a humidified atmosphere
- When mounting the cells:
 - Be careful to **not to lose the surface where the cells are**.
 - **Remove the excess of water**, to avoid bubbles.
 - **Do not be stingy with Prolong[®]**. Add it in excess to avoid bubbles and clean it once it is dry.

We also tried to apply the protocol in tissue section to study the dendrites and cytoskeleton of osteocytes. However, resolution obtained was poor, and we were not able to observe the dendrites or the connections between osteocytes. Perhaps, histological sections of 7 μ m are too small and connections between cells might be lost. Maybe, femurs should be cryoprotected in 30% sucrose (w/v) and cut in thicker sections of 20-50 μ m (Figure 5).

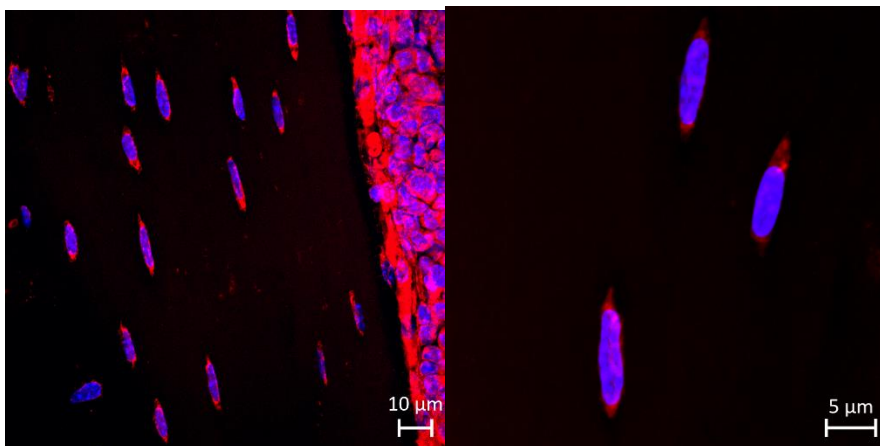


Figure 10. Representative images of Phalloidin stain of bone sections of 7 μ m.

10. Alkaline phosphatase staining:

Alkaline phosphatase activity is important for the mineralization of bone and represents a useful biochemical marker of bone formation. Activity of Alkaline phosphatase was semi-quantitative determined *in vitro* using Sigma-Aldrich Alkaline Phosphatase kits.

The protocol was performed in **6-well plates**. If working with bone cells, **seed them at confluence to induce differentiation**. For IDG-SW or osteoblasts, plate 200,000 cells per well.

Before starting the protocol, prepare the alkaline-dye as follows:

- **Warm 48 ml distilled water at 18-26 °C.**
- **Dissolve contents of one Fast Blue RR Salt capsule or one Fast Violet B capsule in distilled water.**
- **Add 2 ml Naphthol AS-MX Phosphate Alkaline Solution** to diluted diazonium salt solution

Once the reagents are prepared, proceed as follows:

- Rinse the cells three times with warm PBS.
- **Fix the cells with 4% PFA.** Incubate for **15'** at **room temperature** with gentle agitation.
- **Rinse the cells** with milliQ running water for 45". Be careful cells do not detach.
- **Add alkaline-dye mixture** to the cells and incubate for **30'** at **18–26°C**. Protect immersed slides from direct light.
- **Discard alkaline-dye mixture and rinse the cells with milliQ running water for 2'.**
- Add **Mayer's Hematoxylin Solution for 10'** to stain the nuclei.
- **Rinse the cells.**
- **Evaluate under the microscope.**

11. Alizarin Red staining

Alizarin Red S (ARS) is an anthraquinone dye that has been widely used to evaluate calcium deposits in cell culture in a semi-quantitative way. Therefore, alizarin Red has been widely used to assess the capacity of mesenchymal stem cells to differentiate. Alizarin Red S-calcium forms a complex with calcium in a chelation process, given rise to a bright red stain.

The protocol proceed as follows:

- **Seed the cells in a 6-well plate.** If working with bone cells, seed enough cells to achieve confluence and thus facilitate cell differentiation. If working with IDG-SW3 or osteoblasts, seed 200,000 cells per well. Differentiate and treat the cells as usual.

- Remove culture medium and **rinse 3 times with PBS.**
- **Fix the cells in 4% PFA for 15' at room temperature** and gently shaking.
- Remove fixative and **rinse the cells 3 times with milliQ.**
- Add **1 mL of 40mM ARS per well.** Incubate at room temperature for **20-30'** with gentle shaking.

- Remove the dye and **rinse the cells 5 times** with milliQ
- **Analyze the results.** Inspect the cells using a phase microscope and take images.

Alternatively, ARS can be extracted with 10% acetic acid for quantification. Concentration of ARS can be calculated by measuring absorbance at 405 nm.



The reaction is not strictly specific for calcium, since magnesium, manganese, barium, strontium, and iron may interfere, but these elements usually do not occur in sufficient concentration to interfere with the staining.

CHAPTER V: CELL VIABILITY AND PROLIFERATION

1. TUNEL assay *in vitro*

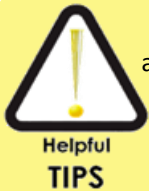
Cell viability was determined *in vitro* using In Situ Cell Death Detection Kit TMR Red (12 156 792 910, Roche). TUNEL assay detects single- and double-stranded DNA breaks that occur at the early stages of apoptosis. To achieve this, TUNEL reaction mixture contains the enzyme deoxynucleotidyl transferase TdT and tetramethyl-rhodamine-dUTP. During incubation, TdT catalyzes the incorporation of tetramethyl-rhodamine-dUTP to DNA strand break, which can be detected by fluorescence microscopy.

As for other immunocytofluorescence stains, cells have to be seeded over glass coverslips at 40-60% confluence. For this, coverslips are placed in the bottom of a well of a 24-well plates coated with collagen as described in section "1.2.Culture dishes and collagen coating". 30,000-40,000 cells were seeded and treated as indicated in the different experiments. Then, TUNEL assay can be performed as follows:

- **Fix the cells with 4% PFA.** Incubate for **1h at room temperature** with gentle agitation.
- **Rinse three times** with PBS.
- Permeabilize the cells with freshly prepared permeabilization buffer (0.1% Triton x-100 in 0.1% sodium citrate). Incubate for **2' on ice.**
- **Rinse three times** with cold PBS.
- For a positive control, treat one of the coverslip with DNase (3U/ml in 50 mM Tris-HCl, pH 7.5, 1mg/ml BSA) for 10' at room temperature. Leave the other coverslips in PBS at room temperature during that time.
- **Rinse three times** with cold PBS.
- Prepare 50 µl of TUNEL reaction mix per sample:
 - 25 µL of TUNEL Dilution Buffer
 - 22,5 µL of Labeling solution
 - 2,5 µL of enzyme solution.

Materials and Methods

- Add 50 μL of TUNEL reaction mix to each sample and incubate 60' at 37°C in a humidified atmosphere in the dark.
- **Rinse** with cold PBS for 5'. Repeat for three times.
- Add 1 $\mu\text{g}/\text{mL}$ of DAPI dilute in PBS. Incubate for 20' at room temperature.
- **Rinse** with PBS for 5'. Repeat for three times.
- **Mount the Coverslip** slides with Prolong[®] Gold Antifade Reagent (Life Technologies). To do so, **drop a 15 μL drop of mounting media** over a slide and **put over it side-down the glass cover** with your stained cells. Allow to dry the mounting media in perfectly horizontal for a few hours. For long-term storage, store slides flat at 4°C protected from light.



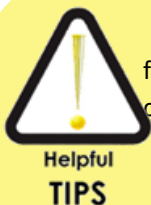
- Do not let the cells dry during the protocol. Ensure they are always wet and in a humidified atmosphere
- When mounting the cells:
 - Be careful to not to lose the surface where the cells are.
 - Remove the excess of water, to avoid bubbles.
 - Do not be stingy with Prolong[®]. Add it in excess to avoid bubbles and clean it once it is dry.

Samples were visualized in a fluorescence microscopy (microscope Nikon E800, Scientific and Technological center, CciT-Bellvitge). For each coverslip, we took 4 pictures from different fields. We used ImageJ for quantification of total nuclei and for the number of TUNEL positive cells.

2. BrdU

For quantification of cell proliferation, we used a fluorescence immunoassay based on the incorporation of the pyrimidine analogue BrdU instead of thymine during DNA synthesis and posterior detection of BrdU with antibodies conjugated to APC. We used BD Pharmagim BrdU Kit (552598; Biological Industries) and followed manufacture instructions. The protocol was as follows:

- Cells were seed at low confluency ($\approx 30\%$) and cultured and treated as indicated in each experiment. Then cells were trypsinized and collected in Eppendorfs.



- The protocol for BrdU staining has many fixation/permeabilization steps followed by centrifugation where a lot of cells might be lost. Therefore:

- Seed enough cells but do not let them to achieve the confluency. If needed used a 10 mm culture dish. We seed 300,000 cells in a 10 mm culture dish or 20,000 cells per well per 6-well plate and then we combine 6 wells per experimental condition.
- Remember to seed extra well for negative controls.
- Avoid changing the Eppendorf. Some cells can attach to the polypropylene tubes and we can lose them. Collect the cells in the same Eppendorf where the staining is going to be done.
- Increase centrifugation speed. In the original protocol, cells are centrifuged at 200 – 300 xg. However, many cells are lost. Increase the centrifugation speed up to 1,000 xg

- **Incubate the cells with 10 μ M BrdU in cell culture medium.** To do this, **dilute the BrdU stock (10 mg/ml) to a 1 mM solution** by adding 31 μ L to 1 mL of culture medium. Then add **10 μ L of 1 mM solution to each mL of cell culture.** Incubation time might range from 2 to 24h, depending on the proliferation rate of each cell line. If working with IDG-SW3, osteoblasts, and osteocytes, incubate the cells **for 6 h.**

- **Prepare the following buffers.**

- **Staining buffer:** 3% heat-inactivated FBS and 0.09% sodium azide in PBS

- **BD Perm/Whas Buffer:** Dilute the concentrated stock buffer 1:10 with deionized water. Store at 4°C.

- **DNase solution:** Thaw the vial of DNase solution. For each sample, take 30 μ L of stock DNase solution (1 mg/ml) and add 70 μ L of PBS to make a working solution of 300 μ g/mL. Refreeze the remaining DNase solution at -80°C

- **Rinse the cells, trypsinize and collect them in Eppendorfs.**


- If needed, **stain specific cell- surface markers** with antibodies.

- Rinse the cells with **1 mL of staining buffer.**


- **Fix and permeabilize the cells.** Resuspend the cells in **100 μ L of BD Cytfix/Cytoperm Buffer.** Incubate for **15-30' at room temperature.**

Materials and Methods

- Rinse the cells with **1 mL of 1x DB Perm/Wash buffer**. Centrifuge for **5' at 1,000 xg** and discard the supernatant.

 **Stop point:** At this step you can store your samples at 4°C overnight or indefinitely at -80°C. In both cases, wash the cells in staining buffer. Centrifuge for 5' at 1,000 xg and discard the supernatant. Then:

- **For overnight storage:** Resuspend the cells in **staining buffer** and store them at **4°C**. On the next day continue with the protocol.
- **For indefinite storage:** Resuspend the cells in **freezing medium** (10% DMSO, 90% heat-inactivated fetal bovine serum) and **store at -80°C**. When you thaw the sample, wash freshly thawed cells with staining buffer and **skip the next step of the protocol** (it is not necessary to permeabilize cells with BD Cystoperm Permeabilization Buffer Plus, directly repeat incubation with DB Cytofix/Cytoperm Buffer).
- Resuspend the cells in **100 µL of BD Cytoperm Permeabilization Buffer Plus**. Incubate for **10' on ice**.
 - Rinse the cells with **1 mL of 1x DB Perm/Wash buffer**. Centrifuge for **5' at 1,000 xg** and discard the supernatant.
 - Fix again the cells. Resuspend the cells in **100 µL of BD Cytofix/Cytoperm Buffer**. Incubate for **5' at room temperature**.
 - Rinse the cells with **1 mL of 1x DB Perm/Wash buffer**. Centrifuge for **5' at 1,000 xg** and discard the supernatant.
 - Treat the cells with DNase to expose incorporated BrdU. Resuspend the cells in **100 µL of diluted DNase (300 µg/mL)**. Incubate the cells for **1 h at 37°C**.
 - Rinse the cells with **1 mL of 1x DB Perm/Wash buffer**. Centrifuge for **5' at 1,000 xg** and discard the supernatant.
 - **Stain BrdU** and intracellular antigens with fluorescent antibodies. Dilute **1 µL of antibody stock solution in 50 µL of BD Perm/Was Buffer**. Resuspend the cells in **50 µL of BD Perm/Was Buffer containing diluted fluorescence anti-BrdU**. If you want to perform **additional intracellular staining**, add the specific antibodies against your target antigens at this step. Remember to leave some samples without staining to use them as **negative controls**. Incubate the cells for **20' at room temperature**.
 - Wash the cells with **1 mL of 1x DB Perm/Wash buffer**. Centrifuge for **5' at 1,000 xg** and discard the supernatant.
 - If you want to **analyze cell cycle**, stain total DNA. Resuspend the cells in **20 µL of 7-ADD solution**. If you do not want to perform cell cycle analysis, skip this step.
 - Resuspend the cells (with or without 7-ADD) in **1 mL of staining buffer**.

 **Stop point:** At this step you can **storage your samples at 4°C overnight**, protected from light prior to analysis by flow cytometry.

- **Acquire stained cells on a flow cytometer.** For optimal resolution, acquire using a **low flow rate** (no greater than 400 events per second).

CHAPTER VI:

METABOLISM

1. ATP bioluminescence assay

Amount of ATP in samples was detected by luciferin-luciferase-ATP reaction. In the luciferase reaction, light is emitted when luciferase oxidize luciferin in a reaction dependent on ATP. The emitted photons are proportional to ATP levels and can be detected by a luminometer. To determine ATP levels, the highly stable luciferin-luciferase reagent rLucHS (#K790-1000 Biovision,) was used following manufacturing instructions.



- rLucHS is light sensitive. Once added, it is recommended to perform all steps of assay in **subdued lighting**.
- rLucHS is very sensitive and is important to **avoid contamination with exogenous sources of ATP**, such as bacteria, fingerprints etc.

For ATP quantification, cells were seeded in 12-well plate. For IDG-SW3 and osteoblast, we seeded 50,000 cells per well and differentiated them as indicated in each experiment. After that, the protocol for ATP determination proceeds as follows:

- Aspirate the cell medium and **rinse cell twice with PBS**.
- **Lyse the cells** with the method of **Boiling water extraction** which allow to quench and lyse the cells at the same time with boiling water. Add **500 µl/well of boiling water** and lysate the cells repeated pipetting.



Pipettes with plastic tips lose accuracy when hot water is used. Therefore, use 1mL glass pipettes or Pasteur pipettes with mark in 500 µL.

- **Transfer the extracts to Eppendorfs and vortex** them vigorously.
- **Centrifuge the cells at 12 000 g and 4°C for 5 min**. Transfer **supernatants to new tubes and store at -80°C** until used. Keep the **pellet for protein**

normalization. Proteins can be extracted with RIPA buffer and quantified with BCA protein assay kit (#23223, Thermo Scientific) as explained in section “4.5. Cell lysis and Protein quantification: BCA assay”

- **Reconstitute rLucHS Reagent Mix with 1.1 ml StayBrite™ Reconstitution Buffer.** The reconstituted reagents can be stored at 4°C for 2 months.

- Make an **standard curve of ATP** ranging from 0-10 μM (0 μM , 0,062 μM , 0,35 μM , 0,5 μM , 1 μM , 5 μM , 10 μM)

- For each sample, mix **80 μM of milliQ H₂O with 10 μl of reconstituted rLucHS** in an Eppendorf tube. Make a common mix for all the samples.

- For each sample, take **90 μL of the reaction mix** and read the background in the luminometer. Then, add **10 μL of the sample** or standard curve, mix and read total luminescence.

- **Subtract background luminescence from total** and calculate levels of ATP in samples by interpolation on the standard curve.

- Use protein concentration to **normalize the levels of ATP.**

2. Glucose uptake

Glucose consumption was measured using radiolabeled 2-[¹⁴C]deoxyglucose (2DG). Due to its sensibility this assay has been employed extensively for studying glucose utilization in a variety of tissues. In fact, this protocol is still in use, however, the drawbacks derivate from the use of radioactivity have motivated several companies to release commercial kits that substitute radioactivity with other detection techniques such as luminescence or colorimetric assays.

Glucose and 2DG are transported through the same mechanisms into cells and both are phosphorylated by hexokinase. However, unlike glucose, the DG6P formed from 2DG accumulates because it cannot be converted to an analog of fructose 6-phosphate or be otherwise metabolized. Consequently, the levels of radioactivity accumulated will be a measure of the total glucose uptake, which includes glucose transport and its phosphorylation by hexokinase.

In our assay we analyzed the maximum uptake capacity, so the total concentration of glucose and 2DG was equal in all the conditions. The steps to evaluate glucose uptake are the following:

- Seed and treat the cells as usual.
- **Rinse the cells four times** with pre-warmed PBS.

- **Add PBS containing 50 Ci/mmol of 2-[¹⁴C]deoxyglucose and 10 μM cold 2-deoxy-glucose.** Incubate for 5' at 37 °C
- **Rinse the cells 4 times with cold PBS.**
- **Lyse the cells in 0.4 M NaOH**
- **Quantify the radioactivity** associated with the cells using a liquid scintillation counter.
- **Determine protein concentration by BCA** protein assay kit (#23223, Thermo Scientific) as explained in section “4.5. Cell lysis and Protein quantification: BCA assay”
- **Normalize radioactivity by protein content.**

3. Lactate assay

The concentration of L-Lactate was determined using an enzymatic reaction based on the oxidation of L-lactate to pyruvate by lactate dehydrogenase (LDH; Roche) in presence of NAD⁺ (Sigma Aldrich). NADH can be detected by absorbance (340 nm) or fluorescence (ex: 340 nm, Em: 460 nm) and its levels are proportional to the amount of L-Lactate in the samples. To determine L-Lactate concentration proceed as follows:

- **Seed the cells in a 12-well** plate and treat it as usual. If working with IDG-SW3 or osteoblasts, seed 50,000 cells per well.
- Before beginning the experiment, **rinse the cells with** PBS and change the medium of the cell culture and take a sample. If working in 12-well plate, add 500 μL of medium and take a sample of 50 μL.
- **Take a sample of culture medium at 6h, 12h and 24h.** Take the samples on ice to avoid lactate degradation and **freeze them at -80°C.** At **24h lyse the cells with SB** and storage the cell lysate at -20°C for protein quantification.
- The day of the assay prepare reaction and enzyme mix (table 23). Prepare enough volume for all the conditions. Carry out the experiment in triplicate:

Lactate buffer	Reaction mix (per well)	Enzyme mix (per well)
0.3 M hydrazine sulphate	200 μL Lactate buffer	2,5 μL LDH
0.87 M Glycine pH 9.5	0,331 mg NAD	7,5 μL MilliQ
	0,075 μL EDTA 0.5M pH 8	10 μL Lactate buffer

Table 23. Buffer used for L-Lactate determination.

- **Prepare a standard curve of L-Lactate** (Sigma) ranging from 0-10 mM (0, 0.156, 0.313, 0.625, 1.25, 2.5, 5, 10 mM).
 - In a **black-walled 96-well** plate (compatible for fluorescence assays), mix **100 μ L of Reaction mix with 10 μ L of the sample or 10 μ L of the standard curve.**
 - **Measure fluorescence at t_0** (ex: 340 nm, Em: 460 nm).
 - **Add 20 μ L of enzyme mix** to each well. Incubate **20' at room temperature.**
 - **Measure fluorescence at t_{20}** (ex: 340 nm, Em: 460 nm).
 - Calculate the NADH produced by **subtraction of t_0 from t_{20}** . calculate levels of ATP in samples by interpolation on the standard curve.
 - **Determine protein concentration by BCA** protein assay kit (#23223, Thermo Scientific) as explained in section "4.5. Cell lysis and Protein quantification: BCA assay"
 - Use protein concentration to **normalize the levels of lactate.**

4. GSSG and GSH determination.

Glutathione is the major intracellular low-molecular-weight thiol that plays a critical role in cellular defence against oxidative stress in tissues and cells. Therefore, measurement of glutathione (GSH), glutathione disulfide (GSSG), and related intermediates are important in assessing the redox and metabolic status of biological systems *in vivo* and *in vitro*. Cellular content of GSH and GSSG can be determined through fluorometric or colorimetric assays using O-phtalaldehyde (O-PA), a derivatizing agent, or DTNB respectively.

4.1. Glutathione determination by OPA method

O-PA is non-fluorescent until it reacts as a heterobifunctional reagent with a primary amine forming a fluorescent isoindole. In the assay, O-PA, which has a very low fluorescence background, reacts only with GSH (not GSSG), to generate strong fluorescence, so that GSH can be specifically quantified. To measure GSSG specifically, first the GSH present in the samples is quenched with NEM, preventing it from reacting with O-PA. Then, $\text{Na}_2\text{S}_2\text{O}_3$ reduces GSSG turning it into GSH, which is now reactive with O-PA. The measure of this GSH in the tube will be proportional to the levels of GSSG present in the sample.

Before starting the protocol, several buffers must be prepared. They are listed in table 24. All the buffers must be conserved at 4°C. KPi, DT and O-PA must be prepared at the time of the experiment. Buffer	Composition
Redox Quenching Buffer (RQB)	20 mM HCl 5 mM diethylenetriaminepentaacetic acid (DTPA) 10 mM ascorbic acid
6% Perchloric Acid (PCA)-RQB	850 µL PCA in 10 mL RQB
N-Ethylmaleimide (NEM)	7,5 mM NEM in RQB
1 M KPi (pH=7)	50 mL HK ₂ PO ₄ 1M 50 mL H ₂ KPO ₄ 1M
0,1 M KPi (pH= 6,9)	1:10 1M KPi in water
NaOH 1 M	2 g NaOH in 50 mL water
O-PA	5 mg/mL O-PA in methanol
Na₂S₂O₃	100 mM Na ₂ S ₂ O ₃ in RQB

Table 24. Recipes of buffers used for GSH determination

The protocol for determination of GSH and GSSG levels has 3 different steps (obtaining cellular extracts, GSH determination and GSSG determination) which are detailed in the following sub sections.

4.1.1. Obtaining cellular extracts.

Before starting the protocol, seed and treat the cells as usual. If working with IDG-SW3 seed $1.6 \cdot 10^6$ cells in a 10 cm culture dish. Proceed as follows to obtain a cell extract



Tissue levels of both GSH and GSSG fall into a range easily measurable by most currently used methods (1–10 mM and 0.01–0.05 mM, respectively). To have enough sensibility, seed a high number of cells.

- **Rinse the cells twice** directly in the tissue culture plate by adding cold PBS and rock gently. **Keep cells on ice.**

- **Lyse the cells with 750 μL of TCA-RQB buffer.** Scrape the cells from the surface and transfer the cell lysate into an Eppendorf.
- **Centrifuge for 5' at 12,000 xg at 4°C** to precipitate the proteins. Transfer the supernatant to a new tube and stored on ice. This supernatant contains GSH, GASSG, as well as acid-soluble sugars and other substances.
- **Keep the pellet for protein determination.** Wash it twice with 1 mL of TCA-RQB and centrifuge for 5' at 12,000 xg at 4°C. Resuspend with 1mL 1M NaOH and use BCA protein assay kit (#23223, Thermo Scientific) to quantify protein content as shown in section "4.5. Cell lysis and Protein quantification: BCA assay"



Protein pellet can be hard to resuspend. Sonicate the sample if needed.

4.1.2. GSH determination.

The protocol will be carried out in black 96-well **Costar plate with flat clear bottom**. All measures will be performed in triplicate.

- **Prepare a standard of GSH** ranging from 0 -100 mM (0, 1.56, 3.13, 6.25, 12.5, 25, 50 and 100 mM).
- For **each sample and each concentration** of the standard, **take two eppendorfs**, one for the determination of the background (blank) and other for the determination of total GSH (total).
- To perform triplicates, in each Eppendorf add 80 μL of the sample and **100 μL of 1M phosphate buffer** to neutralize the pH. **Add 8 μL of NEM into the blank tube and 8 μL of RQB buffer into the total tube.** Mix and incubate for **5' at room temperature** (Table 25).



- Addition of 1M phosphate buffer trigger the **precipitation of a salt**. This is normal.
- **Precipitation of the salt reduce the volume that you can use**, therefore, the quantities of the different reagents have been multiplied x4
- **Avoid taking salt in following steps** as it might interfere with the lectures

- **Centrifuge at max rpm for 5'** to remove the salts. Transfer the supernatant into a new tube.
- To each well of the 96-well Costar plate add **100 µL of 0.1M phosphate buffer, 15 µL of O-PA** freshly prepared and **47 µL of the blank or total Eppendorf**. Make triplicates of each one. Incubate 30' at room temperature in the dark (table 26).
- Measure fluorescence (ex: 365.5 nm; em: 430.20 nm) in a FLUOstar plate reader (CCiT)

	Blank		Total	
	X1	X4	X1	X4
Sample	20 µL	80 µL	20 µL	80 µL
1M KPi (pH=7)	25 µL	100 µL	25 µL	100 µL
NEM	2 µL	8 µL	-	-
RQB	-	-	2 µL	8 µL
5' incubation at room temp.				

Table 25. Preparation of cell extracts for GSH determination.

	Blank (x 1 well)	Total (x1 well)
Sample	47 µL	47 µL
0.1M KPi	100 µL	100 µL
O-PA	15 µL	15 µL

30' incubation at room temperature in the dark.

Table 26. Protocol for GSH measurement.

4.1.3. GSSG determination.

The protocol will be carried out in black **96-well Costar plate with flat clear bottom**. All measures will be performed in triplicate.

- **Prepare a standard of GSH** ranging from 0 to 10 mM (0, 0.078, 0.156, 0.313, 0.625, 1.25, 2.5, 5 and 10 mM).

- For each sample and each concentration of the standard, take two eppendorfs, one for the determination of the background (blank) and other for the determination of total GSH (total).

- To perform triplicates, in each Eppendorf add **180 µL of the sample and 100 µL of 1M phosphate buffer** to neutralize the pH. Add **24 µL of NEM into both blank and sample tube** to quench GSH contained in the sample. Do not add NEM to the standard. **Instead of NEM add 8 µL of RQB buffer into the standard tubes.** Mix and incubate for **5' at room temperature** (Table 27).



Remember that Addition of 1M phosphate buffer will trigger salt precipitation so make extra volume and avoid taking salt to the following steps.

- **Centrifuge at max rpm for 5' to remove the salts.** Transfer the **supernatant** into a new tube.

- Reduce GSSG with $\text{Na}_2\text{S}_2\text{O}_3$. **Add 20 µL of $\text{Na}_2\text{S}_2\text{O}_3$ to total tube and 20 µL of RQB buffer** to blank and standard patron tubes. **Incubate for 1h at room temperature in the dark.**

- To each well of the 96-well Costar plate add **100 µL of 0.1M phosphate buffer, 15 µL of O-PA** freshly prepared and **76 µL of the blank or total Eppendorf.** Make triplicates of each one. Incubate 30' at room temperature in the dark. Incubate 30' at room temperature in the dark (table 28).

- Measure fluorescence (ex: 365 5 nm; em: 430 20 nm) in a FLUOstar plate reader (CCiT)

	Blank		Total	
	X1	X4	X1	X4
Sample	45 µL	180 µL	45 µL	180 µL
1M KPi (pH=7)	25 µL	100 µL	25 µL	100 µL
NEM	6 µL	24 µL	6 µL	24 µL
5' incubation at room temperature				
$\text{Na}_2\text{S}_2\text{O}_3$	-	-	5 µL	20 µL
RQB	5 µL	20 µL	-	-
1h incubation at room temperature in the dark				

Table 27. Preparation of cell extracts for GSSG determination.

	Blank (x 1 well)	Total (x1 well)
Sample	76 μL	76 μL
0.1M KPi	100 μL	100 μL
O-PA	15 μL	15 μL

30' incubation at room temperature in the dark.

Table 28. Protocol for GSSG measurement.

4.2. Glutathione determination by DTNB assay

Glutathione determination by OPA method has low sensitivity, therefore, to determine mitochondria glutathione we decided to use the GSSG/GSH Quantification Kit (Sigma) based on DTNB assay. DTNB in presence of GSH is reduced to TNB (5-mercapto-2-nitrobenzoic acid) which has a maximum absorption at 412nm. To quantify GSSG and GSH from the same sample, firstly GSH is removed by adding the Masking reagent. Therefore, GSSG in the sample solution can be selectively determined by measuring the absorption ($\lambda_{\text{max}} = 412 \text{ nm}$) derived from a colorimetric reaction of DTNB (5,5'-dithiobis (2-nitrobenzoic acid)) coupled with the enzymatic recycling system. The quantity of GSH can also be determined by subtracting the amount of GSSG from the total amount of glutathione. The detection ranges of total glutathione and GSSG using in this kit are from 0.5 $\mu\text{mol/l}$ to 50 $\mu\text{mol/l}$ and from 0.5 $\mu\text{mol/l}$ to 25 $\mu\text{mol/l}$, respectively.

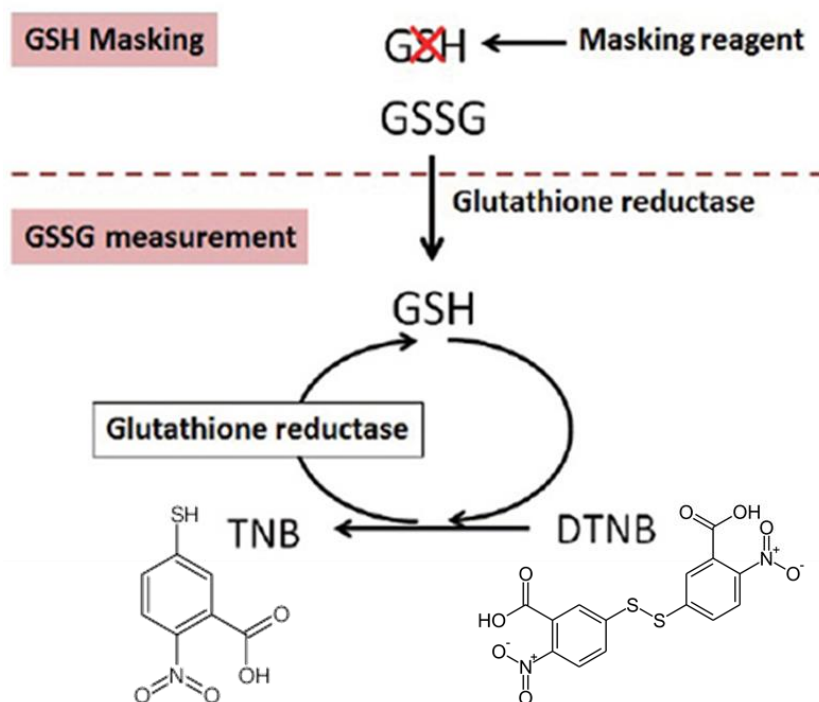


Figure 11. Principle of GSSG/GSH detection. Figure adapted from Sigma bulletin.

4.2.1. Sample preparation

- If working with mitochondria, isolate mitochondria as in section “6.6. Mitochondrial isolation”. If working with cells, collect the cells and wash them with PBS.
- Resuspend the mitochondria or cell pellet with **80 µl of 10 mmol/l HCl**.
- Lyse the sample by **freezing and thawing** twice.
- Add **20 µl of 5% SSA** and centrifuge at 8,000g for 10 minutes.
- Transfer the supernatant to a new tube, and add **900µl of distilled water** (ddH₂O) to reduce the SSA concentration to 0.5% for the assay.

Freezing point. At this point samples can be storage at -80°C. Do not storage samples at -20°C even for short time periods since GSH can get oxidized rapidly.

- **For GSSG measurement: Add 200 µl of the sample** to microtube, **4 µl of Masking solution**, and mix using vortex mixer. (Sample A)
- **For total glutathione measurement: Prepare 200 µl sample.** (Sample B)

4.2.2. Preparation of GSSG standard solution

- Mix 100 μl of **100 $\mu\text{mol/l}$ GSSG standard** solution and **300 μl of 0.5% SSA** solution in a microtube to prepare a 25 $\mu\text{mol/l}$ GSSG standard solutions. Prepare the following **GSSG standard solutions by serial dilution** using 0.5% SSA solution: **12.5, 6.25, 3.13, 1.57, 0.78, 0.39, 0.195 and 0 $\mu\text{mol/l}$.**

- Add **4 μl of Masking solution** to all prepared GSSG standard solutions, and mix using a vortex mixer.

4.2.3. Preparation of GSH standard solution

- Mix 100 μl of **200 $\mu\text{mol/l}$ GSH standard solution** and **300 μl of 0.5% SSA** solution in a microtube to prepare a 50 $\mu\text{mol/l}$ GSH standard solution. Prepare the following **GSH by serial dilutions** using 0.5% SSA solution: **12.5, 6.25, 3.13, 1.57, 0.78, 0.39, 0.195 and 0 $\mu\text{mol/l}$.**

4.2.4. Measurement

- **Add 40 μl of GSSG standard solution, GSH standard solution, Sample A, or Sample B to each well.** Make duplicates or triplicates of each condition.

- **Add 120 μl of Buffer solution** to each well.

- **Incubate the plate at 37 °C for 1 hour.** Close well the microplate to prevent evaporation of the solution.

- **Add 20 μl of Substrate working solution** to each well.

- **Add 20 μl of Coenzyme working solution** and then **20 μl of Enzyme working solution** to each well. Reaction starts immediately after the addition of Enzyme working solution, so use a multichannel pipette to avoid the reaction time lag of each well.

- **Incubate at 37°C for 10 minutes.** The O.D. increases linearly over 10 minutes after the start of reaction, so **read the absorbance at 405 or 415 nm at time zero** (after addition of enzyme working solution) **and after 10 minute.**

- **Determine the concentration of GSSG in the sample (Sample A) using a GSSG calibration curve.**

- **Determine the concentration of total glutathione (GSH + GSSG) in the sample (Sample B) using a GSH calibration curve.**

- **GSH concentration** is calculated using the following equation from the concentrations of total glutathione (GSH + GSSG) and GSSG.

$$\text{GSH} = \text{total glutathione (GSH + GSSG)} - \text{GSSG} \times 2$$

5. Intact cell respirometry

Small changes in cellular respiration may indicate significant mitochondrial differences. Therefore, analysis of mitochondrial function might be useful to understand mitochondrial health. Mitochondrial function of intact cells was measured by high-resolution respirometry (Oxygraph-2k, Oroboros Instruments) in collaboration with Pablo M. García-Roves and Pau Gama-Pérez.

The OROBOROS O2k is a MultiSensor all-in-one instrument for in-depth bioenergetic studies of mitochondria and chloroplasts. OROBOROS O2k has two chambers of 2 mL of maximum capacity that operate at 37.0 °C. To avoid cell precipitation, both chambers use PEEK stirrers that remove the medium with at 750 rpm. Data sampling is collected each 2" through a polarographic oxygen sensor.

To evaluate the different parameters, need to be determined:

- **Routine respiration** reflects the aerobic metabolic activity under routine culture conditions.
- **Leak respiration** is a dissipative component of respiration which is not available for performing biochemical work and thus is associated to heat production.
- **ETS respiration** is the maximum capacity of the electron transfer system.
- **Intrinsic uncoupling and decoupling** are evaluated as the flux control ratio between non-phosphorylating LEAK respiration (electron flow coupled to proton pumping to compensate for proton leaks) and ETS capacity.
- **Coupled respiration** is the result of subtracting leak respiration to routine respiration.

Before starting the protocol, calibration of the instrument is needed. First, both chambers are chemically sterilized (70% ethanol for 20 min in the stirred chambers) and temperature must be stabilized at 37 °C. The chambers are washed three times with distilled water and filled with medium. Then two calibrations are preformed:

7.1. Stabilization of the signal: the oxygen dissolved in the stirred medium and oxygen in gas phase needs to equilibrate. When signal is stable, a mark is set (Mark R1) delineating the period of a stable signal at air saturation.

7.2. Test contamination: Close the chamber. Oxygen should start to decrease. Leave O₂ slope stabilize and observe the signal. O₂ slope negative should be within the range of 2 to 4 pmol/(s*mL). Higher values indicate a biological contamination in the medium or O2k-chamber.

Once OROBOROS O2k is calibrated we can start the protocol. The cells are trypsinized and placed in the oxygraph chamber. For IDG-SW3, or osteoblast we placed between 1-1.5 million cells in 2.5 mL of culture medium. Lower cell quantity might reduce the resolution of the technique, while higher cell numbers might consume all the oxygen in the chamber before the end of the experiment. Save a sample of cells for protein quantification and normalization. Then, proceed as follows (Figure 9):

7.3. Place the cells inside the respiratory chamber. Leave the oxygen consumption rate to stabilize. This parameter is **routine respiration**.

7.4. Inject 1 µg/ml of oligomycin (2 µg/ml) into the oxygraph chamber and record cellular respiration until a stable oxygen flux signal is achieved. **This parameter is leak respiration.**

7.5. Titrate FCCP in 0.1 to 0.3 µM steps by injecting 1-3 µl of 0.2 to 1 mM FCCP (0.1 to 2 µM final concentration in the chamber) into the oxygraph chamber until the oxygen flux signal reaches its maximal levels. To be sure that it has reached the maximum signal, continue injecting FCCP until the oxygen signal start to decline. **This parameter is ETS.**

7.6. Inject 0.1 µM rotenone and 2.5 µM antimycin A. Record respiration until the oxygen flux signal decreases and stabilizes. This parameter is the background and will be subtracted to all the results.

7.7. Calculate Routine, leak, ETS and coupled. Remember to subtract the background.

7.8. Determine protein concentration by BCA protein assay kit (#23223, Thermo Scientific) as explained in section “4.5. Cell lysis and Protein quantification: BCA assay”

7.9. Use protein concentration to normalize the respiratory parameters.

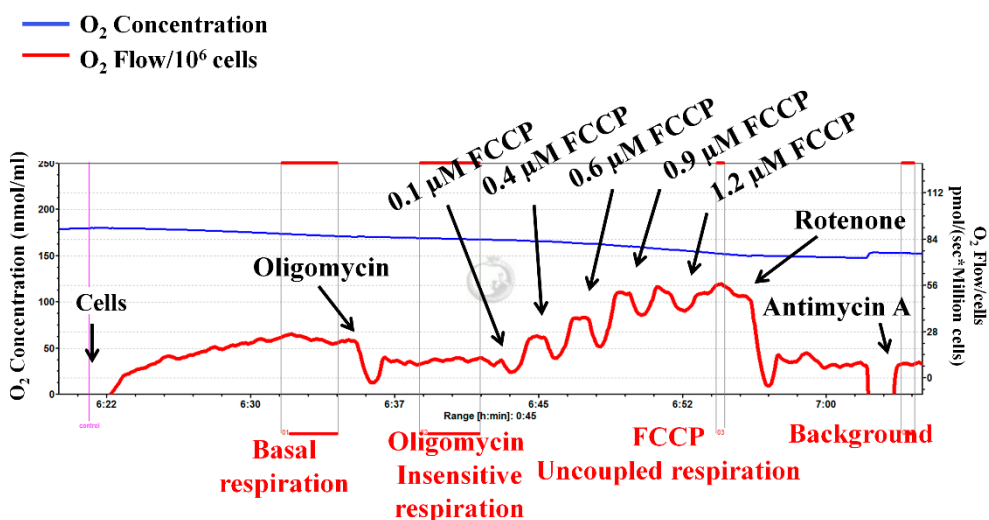


Figure 12. Schematic representation of Coupled and uncoupled respiration of intact cells. Representative respiratory traces of basal oxygen consumption, leak respiration measured in the presence of oligomycin (oligomycin-insensitive respiration) and sequential addition of FCCP using high-resolution respirometry. Thereafter, once a stable signal is reached, respiration is inhibited with the addition of rotenone and antimycin A and the remaining background respiration (non-mitochondrial respiration) is subtracted from all results. Oxygen consumption is expressed as pmol/(sec x number of cells).

6. Mitochondrial isolation

This protocol describes a sequential procedure to obtain functional mitochondria from culture plates. Mitochondrial isolation protocols involve two processes: cell disruption to break open the cells and release the cellular structures, and differential centrifugation to recover fractions that are enriched for mitochondria. The yield of the procedure is very low, so it is recommended to start with at least $1,2 \times 10^8$ cells (2-3 100 mm culture dishes at 90% confluence).

Before beginning the procedure, precool a glass potter for homogenization. Homogenization as well as the following steps must be performed at 4 °C to minimize the activation of damaging phospholipases and proteases. Then proceed as follows:

- **Trypsinize the cells** as usual and collect them on 15ml falcon tube. Mix the cells from 2-3 culture dishes of the same condition in the same falcon tube. Centrifuge the cells at 300g x 5 min.
- **Wash the cells** with 1x PBS.
- **Resuspend the pellet in 1 ml of MIB buffer.**



Alternatively, you can collect the cells by scrapping, but the yield might be slightly reduced. In this case, wash the cells once with 1x PBS. Add 600 μ L of ice-cold MIB and scrape the dish. Collect 2-3 culture dishes of the same condition in one 2mL Eppendorf.

- **Homogenize the cells using a glass potter.** Place the cell suspension in the potter and stroke it for 30. Ensure that the vessel is on ice during this step, not to remove the pestle above the liquid and to use a steady speed with continuous passes.
- To improve the cell lysis, **draw the solution into a 1 ml syringe using a 27 gauge needle** and expel it back into the Eppendorf on ice with a 27 gauge. Take care to expel the solution against the inside wall of the tube as to utilize that force for cell membrane disruption. Repeat the syringe steps for a total of five times.



For the first time, it is recommended to Check the degree of homogenization with a phase-contrast microscope: Naked nuclei (smooth spheres with obvious nucleoli inside), smaller organelles (dark, granular objects), and a small number of unbroken cells (large spheres with a granular appearance) should be present if cell lysis was successful.

Eight to nine naked nuclei for every whole cell is a very good result. Trying for anything better usually results in increasing the number of damaged nuclei, which increases the number of mitochondria trapped in the nuclear pellet during the first centrifugation.

8. **Centrifuge the homogenate at 500-600g at 4 °C for 10 min.** Mitochondria are in the supernatant after this first, low-speed spin, while cell membranes and unbroken cells are pelleted.
9. **Collect the supernatant** in a new 1.5 ml Eppendorf and **centrifuge** the tubes again in a fixed angle rotor at **7,000-10,000g, 4 °C for 10-15 min.**
10. Discard the supernatant and **resuspend the pellet** containing mitochondria in MIB buffer.
11. **Repeat the centrifugation step** (7,000-10,000g, 4 °C for 10-15 min).
12. Discard the supernatant and **resuspend the pellet containing mitochondria.** Resuspend the mitochondria in the small amount of buffer that remains after discarding the supernatant. Mitochondria retain their functionality for

a longer time, probably as a consequence of lower exposure to oxygen, when they are stored in a concentrated form.



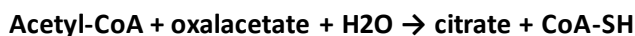
Mitochondria obtained might be contaminated with other organelles. If needed, perform a sucrose gradient to obtain highly pure mitochondria. However, increasing the purity of mitochondria with a sucrose gradient will reduce the yield of the protocol.

Buffer	Preparation
0.1 M Tris/MOPS	Dissolve 12.1 g of Tris in 500 ml of distilled water, adjust pH to 7.4 using MOPS powder, bring the solution to 1 liter and store at 4 °C. 20 mM HCl
0.1 M EGTA/Tris	Dissolve 38.1 g of EGTA in 500 ml of distilled water, adjust pH to 7.4 using Tris powder, bring the solution to 1 liter and store at 4 °C.
MIB buffer: 200mM sucrose 10mM TRIS/MOPS 1mM EGTA/Tris pH 7.4	Prepare 100 ml of MIB by adding 10 ml of 0.1 M Tris–MOPS 1 ml of EGTA/Tris 20 ml of 1 M sucrose. Bring the volume to 100 ml with distilled water. Adjust pH to 7.4. Filter to sterilize and store at 4°C

Table 29. Buffer used for mitochondria isolation.

7. Citrate Synthase activity

Citrate synthase, CS (EC 4.1.3.7), is an enzyme of the Krebs cycle. Although it is nuclear encoded, CS is localized on the mitochondrial matrix, therefore, is commonly used as a quantitative marker enzyme for the content of intact mitochondria. CS catalyzes the reaction of two-carbon acetyl CoA with four-carbon oxaloacetate to form six-carbon citrate, thus regenerating coenzyme



Materials and Methods

This reaction can be coupled to the reduction of DNTB, and production of TNB. The reaction product TNB has an intense absorption at 412 nm that increases linearly with time, up to 0.6-0.8 units of over 200 s.



Before starting the protocol, several buffers must be prepared. They are listed in table 30.

Buffer	Composition
Tris-HCl buffer (1.0 M, pH 8.1):	2.4228 g Tris 20 mL dH ₂ O Adjust pH to 8.1 with 37% HCl Store at 4°C
Tris-HCl buffer (0.1 M, pH 7.0): (PCA)-RQB	2 mL 1M Tris-HCl buffer, pH 8.1 15 mL dH ₂ O Adjust pH to 7 with concentrated HCl and fill up to 20 mL with dH ₂ O Store at 4°C
Triethanolamine-HCl buffer (0.5 M, pH 8.0) + EDTA (5 mM)	8.06 g triethanolamine 100 mL dH ₂ O adjust pH with 37 % HCl add 186.1 mg EDTA Store at 4°C
10% Triton X-100	add 90 mL dH ₂ O to 10 g (10 mL) Triton X-100. Store at 4°C
12.2 mM acetyl-CoA	25 mg acetyl CoA 2.5 mL dH ₂ O Store at -20°C
Triethanolamine-HCl-buffer (0.1 M, pH 8.0):	1 mL of 0.5 M triethanolamine-HCl-buffer of pH 8.0 4 mL dH ₂ O Prepare fresh every day
Oxalacetate (10 mM, pH 8.0)	0.6 mg oxalacetate 5 mL of 0.1 M triethanolamine-HCl-buffer of pH 8.0. Prepare fresh every day
DTNB (1.01 mM, pH 8.1).	2 mg DTNB 5 mL of 1 M Tris-HClbuffer of pH 8.1.

Material and Methods

Prepare fresh every day

Table 30: Buffers needed for CS activity

To measure CS activity, proceed as follows:

- In a well of a 96-well plate, add all reaction components (except for the 10 mM oxalacetate solution) in the given sequence. Like this the components are gently mixed and the reaction mixture turns yellow:

Component	Volumen	Final concentration
10% Triton X-100	5 µL	0.25%
Acetyl-CoA	5 µL	0.31mM
1.01 mM DTNB	20 µL	0.1 mM
Sample	20 µL	-
dH ₂ O	140 µL	-

Table 31. Reaction mix for CS activity determination

- Add 10 µL of oxaloacetate to start the reaction. Measure the absorbance at 412 nm at time zero and after 200ms.
- Calculate the citrate synthase activity using the following equation:

$$\text{units } (\mu\text{mole/ml/min}) = \frac{(\Delta A_{412})/\text{min} \times V(\text{ml}) \times \text{dil}}{\epsilon^{\text{mM}} \times L(\text{cm}) \times V_{\text{enz}}(\text{ml})}$$

Where:

dil - the dilution factor of the original sample

V(ml) – the reaction volume: · for assay in 96 well plate = 0.2 ml

Venz(ml) – the volume of the enzyme sample in ml

ϵ^{mM} (mM⁻¹ cm⁻¹) – the extinction coefficient of TNB at 412 nm is 13.6.

L(cm) – pathlength for absorbance measurement: · for 96 well plate, pathlength = 0.552 cm

8. Fluorophores for metabolic determination.



Helpful
TIPS

Remember:

- **Differentiated IDG-SW3 express GFP.** Be careful when selecting the fluorophores.
- **Collagen** (added in the process of plate coating and synthesized by IDG-SW3, osteoblast and osteocytes), is a highly **autofluorescent molecule** and can produce high background when working with fluoresce. Be careful, **choose the channel that minimize** your background fluorescence and **add the adequate controls.**

8.1. Mitotracker staining.

MitoTracker[®] dyes are cell permeable probes that contain a thiol-reactive chloromethyl moiety for mitochondrial labeling. To label mitochondria, cells are simply incubated with MitoTracker[®] probes, which passively diffuse across the plasma membrane and accumulate in active mitochondria. Its accumulation is dependent upon membrane potential. Once mitochondria are labelled, cells can directly be analyzed or can be fixed with an aldehyde-based reagent to allow further processing of the sample. The fluorescence resulting from MitoTracker[®] Oxidative Stress Reagents can be measured using traditional fluorescence microscopy, high-content imaging and analysis, microplate fluorometry, or flow cytometry (Ex: 581, Em:644). For cellular staining with MitoTracker deepRed[®] Reagent proceed as follows:

- Dilute the **1mM stock solution of MitoTracker deepRed[®] Reagent 1:10** in alpha Mem without FBS.
- **Aspirate the medium and rinse the cells** three times with warm PBS to remove the remaining FBS.
- Add **2.5 μ L of 100 μ M MitoTracker deepRed[®] solution to 1 mL of culture medium** to obtain a final concentration of 250 μ M.
- **Incubate the cells** for 20 min.
- **Rinse the cells three times with PBS**
- **Add complete medium and analyze**

8.2. CellROX staining

CellROX® Oxidative Stress Reagents are fluorogenic probes designed to reliably measure ROS in live cells. The cell-permeable reagents are non-fluorescent or very weakly fluorescent while in a reduced state and upon oxidation exhibit strong fluorogenic signal. Unlike CellROX® Green Reagent, that upon oxidation binds DNA accumulating in the nucleus and mitochondria; CellROX® Deep Red is localized in the cytoplasm. For cellular staining with CellROX® proceed as follows

- Add the CellROX® Reagent at a final concentration of **5 µM** to the cells. For 1 mL of culture medium, add 2 µL of CellROX® stock solution. Incubate for **30 minutes at 37°C**. You do not need to remove the medium as CellROX can work with medium containing FBS.
- Incubate the cells for **30 minutes at 37°C**.
- **Rinse the cells three times with PBS**
- **Add complete medium and analyze**

8.3. MitoSOX

Mitochondrial superoxide is generated as a byproduct of oxidative phosphorylation and can be determined by fluorescence probes such as MitoSOX. MitoSOX™ Red reagent is live-cell permeant selectively targeted to the mitochondria. Once in the mitochondria, MitoSOX™ Red reagent is selectively oxidized by superoxide and exhibits red fluorescence. MitoSOX™ Red reagent is not oxidized by other ROS- or reactive nitrogen species (RNS)-generating systems, and oxidation of the probe is prevented by superoxide dismutase. The oxidation product becomes highly fluorescent upon binding to nucleic acids. The fluorescence resulting from MitoSOX can be measured using traditional fluorescence microscopy, or flow cytometry (Ex: 581, Em: 644). For cellular staining with MitoTracker deepRed® Reagent proceed as follows:

For cellular staining with MitoTracker deepRed® Reagent proceed as follows:

- **Prepare 5 mM MitoSOX™** reagent stock solution by **dissolving the contents of one vial** (50 µg) of MitoSOX™ in **13 µL of dimethylsulfoxide (DMSO)** to make a 5 mM MitoSOX™ reagent stock solution
- **Dilute** the 5 mM stock solution of MitoSOX **1:5 in PBS** with glucose to generate 1mM stock solution.
- **Aspirate the medium and rinse the cells** with warm PBS

- Add **2 μL of 1mM MitoSOX™ solution to 1 mL of PBS with glucose** to obtain a final concentration of **2 μM** .
- **Incubate the cells** for 15 min.
- **Rinse the cells three times with warm PBS**
- **Add complete medium and analyze**



- **Low micromolar concentrations of MitoSOX 5–10 μM resulted in uncoupled mitochondria with reduced respiratory capacity (Figure 13).** In this case Redistribution of MitoSOX to the cytoplasm and nucleus occurred concomitant to mitochondrial uncoupling. Submicromolar MitoSOX had no adverse effects, therefore, reduce the concentration of MitoSOX as much as possible. For osteoblast and IDG-SW3, 1-2 μM MitoSOX are the optimal concentrations. Concentrations above 2 μM start damaging the mitochondria
- **GFP interferes with MitoSOX (Figure 14).** Excitation spectra of MitoSOX and GFP overlaps so try to avoid using GFP with working with MitSOX, if not possible:
 - **Analyze the images by confocal microscopy** rather than flow cytometry, so you can set the emission wavelength that you are going to collect.
 - Use a **spectral flow cytometer** to adjust the emission wavelength that you are going to collect.
 - Be careful with your flow cytometry data and **compensate** well.

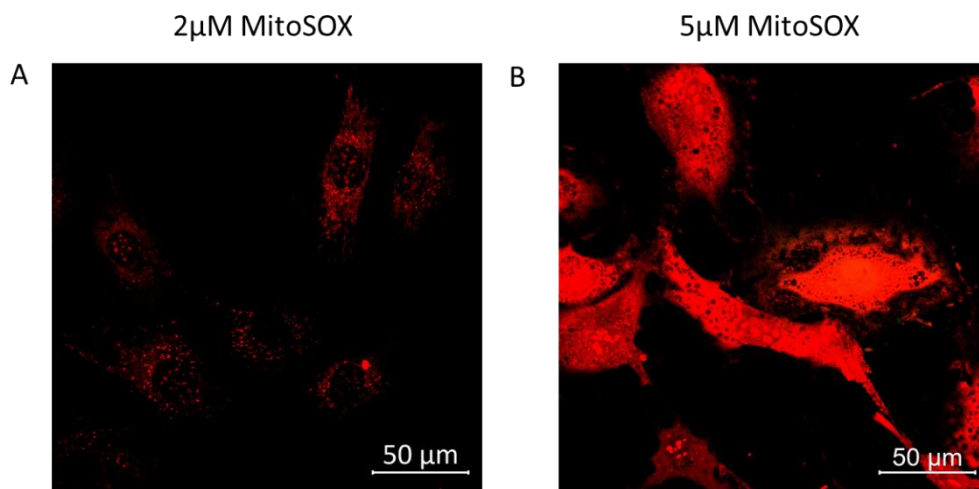


Figure 13. Effects of MitoSOX concentration. Low MitoSOX concentrations (A) stain mitochondria superoxide whereas higher MitoSOX concentrations (B) produce mitochondrial uncoupling and unspecific staining.

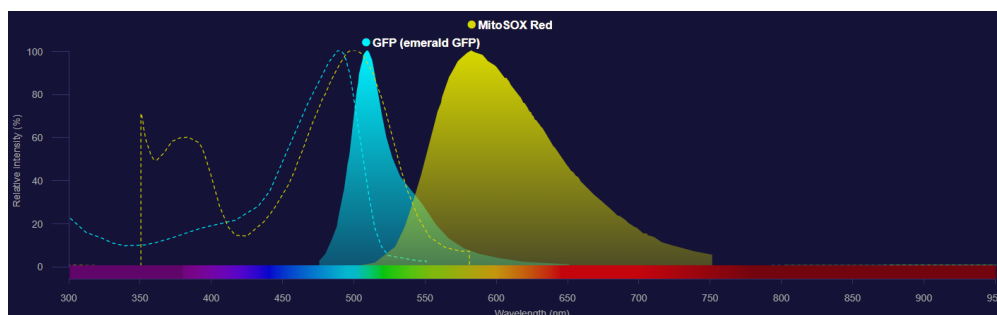


Figure 14. Excitation and emission spectrum of GFP (blue) and MitoSOX Red (yellow)

9. Hydrogen Peroxidase Assay with Amplex Red

The generation of Mitochondrial H_2O_2 was determined using Amplex™ Red Hydrogen Peroxide/Peroxidase Assay Kit (Thermofisher) following manufacturer's instructions.

Briefly, mitochondria were isolated as described previously. Mitochondrial pellets were diluted in 1x Reaction Buffer and incubated in presence of 100 μM Amplex® Red reagent and 0.2 U/mL HRP for 30 minutes at room temperature and protected from light. Fluorescence was measured in a fluorimeter (Ex: 550nm/ Em: 590 nm). H_2O_2 levels were quantified using a standard curve.

10. Live cell imaging by confocal microscopy

For confocal microscopy with living cells, cells have to be seed in a special cell culture dish. So prior starting the experiment, coat the cell culture dish with collagen as explained in “1.2. Culture dishes and collagen coating” section. Then proceed as follows:

- One or two days prior the experiment, seed the cells in the collagen coated plate. If working with IDG-SW3, osteoblast, or osteocytes, seed **40.000-60.000 cells/dish**.
- **Stain the cells with fluorophores** as indicated in section “6.5. Fluorophores for metabolic determination”
 - **Rinse the cells three times with PBS**
 - **Add complete medium and analyze the cells in a confocal microscopy with incubation chamber at 37°C and 5% FBS.**



Helpful TIPS

- **Avoid saturated images.** Use the condition with the highest expected intensity to set up the conditions of the microscope.
 - Fluorophores loose activity with thaw/ freezing cycles. **Make aliquots** and thaw only the amount needed.
 - **Different factors might affect the intensity** of the staining (the age of the reagents, thaw/freezing cycles, light, cell confluence...), and it may vary between days even in the same conditions. So:
 - Try to **compare conditions on the same day** and from the same experiment
 - **Seed extra wells to adjust the time and concentration of the staining** and set up the conditions of the microscope. If you have done a similar experiment before, start trying with those conditions and re-adjust them if needed. Remember in this case you will cannot compare between days.
 - Analyzing microscopy images with different cell types, or with cell types in different stages of differentiation might be tricky since some cells can have a higher staining intensity per area but, as they have different sizes, they can content a lower number of total molecules.

11. Flow cytometry

Flow cytometry is a technology that provides rapid multi-parametric analysis of single cells in solution. Flow cytometry can analyze long population of cells in a short period of time. The procedure is the following:

- **Plate the cells as usual to have a population of at least 10,000 cells** at the end of the protocol. As cells might be lost during the protocol, seed an excess of cells. If working with IDGs, osteoblast or osteocyte, **seed $1.2-1.6 \cdot 10^6$ cells in a 65mm cell culture dish** to achieve the confluence.

- **Stain the cells** as indicated in in section “6.5. Fluorophores for metabolic determination”

- **Rinse the cells three times with PBS**

- **Trypsinize the cells and collect them** in a 15 ml falcon.

- **Wash twice with PBS**

- **Resuspend the cell in PBS** containing P/S, Pyr and Glucose.

- **Filter the cells with a 70 μ m nylon mesh** to remove aggregates and avoid the obstruction of the flow cytometer channels. To filter the cells make a handmade filter as follows:

- Cut the tip of a blue pipette tip.

- Cut a 2 x 2 cm 70 μ m nylon mesh

- Place the nylon mesh at the end of the cut blue tip and introduce the whole complex inside another blue tip.

- Drop the cells inside the homemade filter with a pipette. Put small pressure on the mesh to help the liquid to flow. Be careful do not break the mesh.

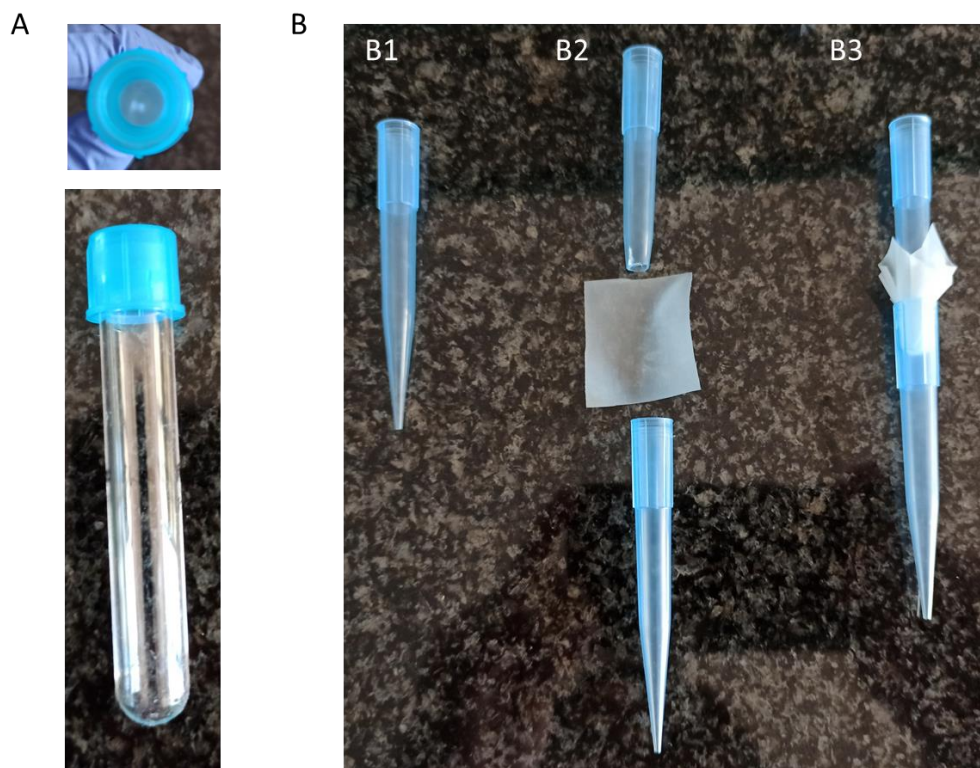


Figure 15. Commercial filter (A) vs handmade filter (B). To generate a handmade filter, take a blue tip (B1), cut the end and place a nylon mesh at the end of the cut blue tip (B2). Insert the mesh and the cut blue tip inside another blue tip (B3).

- **Add 7-ADD** if you want to assess cell viability.
- **Analyze the samples in the flow cytometer.** If needed, use 8-peak rainbow beads to calibrate the cytometer and compare between different days.



- Differentiated IDG-SW3 and osteoblast are difficult to detach by trypsinization. Sometimes they detach together from the well, forming a layer of cells difficult to break up. Therefore:
 - **Be patient** and let trypsin act for up to 5-10 min until cell connexion are lost.
 - **Break up cell aggregates by pipetting**
 - **Filter always the cells with a 70 μm nylon** mesh as they tend to form aggregates that could block the flow cytometer channels.
 - **Be careful when filter the cells as you might lose many cells in the process.** This is especially critical when you have low cell populations, or many cell aggregates.
- As IDG-SW3 differentiate, they **increase in size, complexity and autofluorescence** so:
 - **You might not differentiate if they have a higher concentration of the fluorophore** (or molecule to study) or if, as they are bigger, they have a **higher amount of fluorophore but lower concentration. Additional visualization with confocal microscopy might be useful in some situations.**
 - Autofluorescence can vary among conditions, so the base line might be different. Be careful and **add the adequate controls** (one sample without staining per each cells line or differentiation step, to analyse the background of each condition).

CHAPTER VII:

In Vivo Approaches

1. Mouse colony generation and maintenance.

Ppargc1a/b-deficient mice (*Ppargc1a/b;Col1a1-Cre*) were generated by crossing heterozygous *Col1a1-Cre* mice (Tg(*Col1a1-cre*)1Kry(21) with mice carrying loxP sites flanking exons 4 and 5 of the *Ppargc1a* (25) and exons 4 and 5 of *Ppargc1b* alleles (26). *Col1a1-Cre* mice were already available in our animal facilities while *Ppargc1a/b^{ff}* were kindly donated by Dr. Villena. *Ppargc1a/b^{ff}* and *Ppargc1a/b^{ff};Col1a1-Cre* (KO) mice were fertile and born in the Mendelian ratio. *Ppargc1a/b^{ff};Col1a1-Cre* (KO) were crossed with *Ppargc1a/b^{ff}* to obtain experimental KO animals (*Ppargc1a/b^{ff};Col1a1-Cre*) and controls (*Ppargc1a/b^{ff}*)

To delete *Nfe2l2* specifically in osteocytes, mice carrying loxP sequences flanking exon 5 of *Nfe2l2* gene (purchased from The Jackson Laboratory) were crossed with *Dmp1-cre/ERT2* transgenic line D77 (purchased from The Jackson Laboratory) that express tamoxifen-inducible Cre recombinase (*cre/ERT2*) under the control of the mouse dentin matrix protein 1 (*DMP1*) promoter to generate *Nfe2l2^{ff};Dmp1-cre/ERT2* mice. Heterozygous *Dmp1-cre/ERT2* mice with floxed *Nfe2l2* (*Nfe2l2^{fl}*) were crossed with *Nfe2l2^{ff}* to obtain experimental (*Nfe2l2^{ff};Dmp1-Cre/ERT2*) and control (*Nfe2l2^{fl/fl}*) mice. The resulting *Nfe2l2^{ff};Dmp1-cre/ERT2* mice were fertile and born at the anticipated Mendelian ratio. To induce recombination, Cre must be activated with 4-OH tamoxifen which can be administer to mice by intraperitoneal injections.

Osteoblast-specific *Nfe2l2*-deficient mice (*Nfe2l2^{ff};Col1a1-Cre*) were generated by crossing heterozygous *Col1a1-Cre* mice (Tg(*Col1a1-cre*)) with *Nfe2l2* floxed mice described previously. *Nfe2l2^{ff};Col1a1-Cre* (KO) mice were fertile and born at the Mendelian ratio.

Mice were housed under controlled conditions (12 h-light/12 h-dark cycle, 21 °C, 55% humidity) and fed *ad libitum* with water and a 14% protein diet (Teklad, 2014: Harlan-Tekland, Indianapolis, IN, USA). All animal experiments were performed in accordance with guidelines approved by the Ethical Committee for Animal Experimentation of the University of Barcelona and Generalitat de Catalunya (Spain)



Helpful TIPS

- To maintain the health of the colonies
 - **Avoid consanguinity.** Do not cross brother with brothers or parents with their offspring.
 - **Use young animals for breeding.** The fertility of mice (specially females) start to become reduced at 6-month age and most of them become infertile at 1-year.
 - **Sometimes mother start to eat their offspring.** This is relatively normal in their first birth. If this continue happening, try to identify the source of stress and try taking out the male. If this do not work, do not use that mother for breeding.

2. Activation of Cre recombinase with tamoxifen.

The advent of tamoxifen (Tm)-inducible Cre recombinases has greatly improved the ability to temporally control Cre-loxP recombination *in vivo*. In the case of *Dmp1-cre/ERT2* mice the addition of ERT2 domain reduce the unspecific expression of CRE recombinase in *Dmp1-cre* mice, in which Cre activity was detected in skeletal muscle fibers, certain cells in the cerebellum and the hindbrain and gastric and intestinal mesenchymal cells. Cre/ERT2 contains tamoxifen-inducible estrogen receptor (ERT2) fused to both ends of CRE recombinase. Under basal conditions, the activity of CRE is blocked by ERT2 domain. However, once 4 OH-tamoxifen binds ERT2 domain, CRE become active. Therefore, to activate *Dmp1-cre/ERT2*, 4 OH-tamoxifen or tamoxifen must be administered.



Helpful TIPS

- 4-OH tamoxifen is the active form of tamoxifen. When tamoxifen is administered, it is metabolized in the liver to its active form, so in principle there is no need to administer 4-OH tamoxifen (which is much expensive). However, if working with very small pups, liver might to be completely functional and the concentration of active 4-OH tamoxifen might be lower than for adults.

To induce recombination of the floxed *Nfe2l2* alleles, 3-weeks-old *Nfe2l2^{f/f}* (WT) and *Nfe2l2^{f/f}; Dmp1-Cre/Ert2* (KO) mice received a total of 5 intraperitoneal injections of 20 mg/kg tamoxifen free base (Sigma) with 48h in between. Tamoxifen powder was dissolved in ethanol at a concentration of 100mg/mL and then suspended in corn oil at a concentration of 20 mg/ml by shaking 1h at 37°C.



Helpful TIPS

- Some authors recommend injecting up to 50 $\mu\text{g/g}$ tamoxifen in corn oil (total volume of 50 μL) at P3, P5, P7, P14 and P21 with intraperitoneal injections. However, when we performed this protocol, **corn oil accumulated in the peritoneum of the pups, which died** after the second injection, between day 5 and 7. Therefore I recommend starting injections after weaning (P21).
- **Tamoxifen is highly hydrophobic and almost insoluble in water base solvents and it is even hard to dissolve in corn oil.** To facilitate the process, first suspend tamoxifen in ethanol at a concentration of 100 mg/ml and heat it at 37°C. Then, dilute the solution 1:50 in corn oil to obtain a solution of 20 mg/ml tamoxifen and heat it for 1h or overnight at 37°C.
 - **Tamoxifen is soluble in ethanol at 20 mg/ml** however at this concentration, ethanol will result toxic for mice when administer by IP injections. To reduce toxicity, mix it with corn oil. **So, increasing ethanol volume might be not a good idea to increase tamoxifen solubility.**
 - Mice at P21 are still very small and we have showed that corn oil might accumulate and become toxic, therefore, try to minimize the volume injected. **So, increasing total volume might be not a good idea to increase tamoxifen solubility.**
 - At room temperature, **the solubility of ethanol in corn oil is very low** (< 1mL of ethanol per 20 mL of corn oil). Therefore, if you reduce the concentration of tamoxifen in ethanol to facilitate its dissolution, you will have to increase the ethanol: corn oil rate to maintain the concentration of the final solution (20 mg/mL). At higher ethanol:corn oil ratios, both liquids become immiscible. **So, decreasing concentration of tamoxifen in corn oil is not a good idea.**
 - **Solubility of tamoxifen in ethanol, and ethanol in corn oil increase with temperature** (in fact 100% miscibility of ethanol and corn oil is achieved above 60°C). However, high temperatures might degrade tamoxifen; Therefore, **rising temperature more than 37°C is not a good idea.**
 - You can keep tamoxifen solution at 4°C for at least one week. However, as miscibility of ethanol in corn oil, and solubility of tamoxifen in ethanol are both reduced at low temperature, refrigeration of the solution might cause precipitation and two phase formation. If that occurs, heat the solution at 37°C from 30' to 1 h.
 - Try to administer the solution while it is warm. **Use your hands to keep it warm during transportation and administration.**

3. Mouse genotyping

For mouse genotyping, DNA was purified from a piece of ear or tail smaller than 3 mm. The DNA purification was performed using Nucleo Spin Kit (Macherey Nagel) following manufacturer instruction. Briefly, proceed as follows:

- **Digest the tissue** by incubation with **20 µL of Proteinase-K** diluted in **180 µL of buffer T1** for 3h or overnight at 55°C.
- For each sample, mix **200 µL of lysis buffer B3** (an SDS based solution) with **210 µL of 100% ethanol**. Add 410 µL to each sample to lysate the tissue and precipitate the DNA. **Mix by inversion** until the tissue is completely lysate. **Place** the solution **into a column** and **centrifuge for 1' at 11,000g**.
- Perform successive **washings** of the DNA as follows:
 - Wash the column with **500 of buffer BW**. Spin the column for **1' at 11,000g**.
 - Wash the column with **600 of buffer B5** with ethanol. Spin the column for **1' at 11,000g**.
 - **Dry the column**. Spin the column for **1' at 11,000g**.
- Elute the DNA with **100 µl of buffer BE or TE**.

The genes of interest were amplified by PCR using My Taq Mix 2x (Bio-25042, Biorline). The recipe used for PCR is detailed in table 32. Primers used for the genotyping of each mice and PCR conditions are listed in table 33. PCR products were run in an 1.5% agarose gel at 100 V for 20'.

Reagent	Volume per sample
DNA	2µl
Primers, 50 µM	0.25 µl
MyTaq Mix 2X	10 µl
MilliQ water	Up to 20 µL

Table 32. PCR mix for mice genotyping.

Gene	Primer sequences	PCR Conditions (T annealing, amplification time, cycles)	Fragment length
<i>Col1a1-Cre</i>	Fw: 5' CAGTCGTCGGAGCAGACGGGAGT 3' Rv: 5' AATCGCGAACATCTTCAGGTTCTGCG 3'	65°C, 30'', x40	200 bp
<i>Dmp1-Cre</i>	Fw: 5' ACTTTCATTACAGGTAGAGGAATCG 3' Rv: 5' TTGCTTTTCTGACCAGATGGA 3'	60°C, 30'', x28	244 bp
Internal control	Fw: 5' CTGTCCTGTATGCCTCTGG 3' Rv: 5' AGATGGAGAAAGGACTAGGCTACA 3'	60°C, 30'', x28	415 bp
<i>Nfe2l2^{f/f}</i>	Fw: 5' TCATGAGAGCTTCCAGACTC 3' Rv: 5' CAGCCAGCTGCTTGTTTTC 3'	60°C, 30'', x28	Wt: 272 bp Tg: 310 bp
<i>Ppargc1a^{f/f}</i>	Fw: 5' CACGCTTCATCCCATCTCTGT 3' Rv: 5' CAATTGTCAGTCCCAACTGTCT 3'	58°C, 45'', x35	Wt: 487 bp Tg: 555 bp
<i>Ppargc1b^{f/f}</i>	Fw: 3' GGCTACCGTGCTGCACTGTT 3' Rv: 5' ACAGATGCCCTTAAGGTGACATA 3'	58°C, 45'', x35	Wt: 166 bp Tg: 234 bp

Table 33: Primers and PCR conditions for genotyping of *Ppargc1a/b* and *Nfe2l2* mice colonies

4. Ovariectomy

Ovariectomy is the surgical excision of the ovaries and constitutes a well-established model for postmenopausal osteoporosis. In mice, soon after ovariectomy the loss of cancellous bone but not cortical bone occurs. These effects can be observed 8 weeks after ovariectomy.



The effect of ovariectomy depends on the age at which the procedure was performed and the mice strain. **The highest rate of bone loss was detected in C57BL/6J female mice ovariectomized at 8-week of age.**

Ovariectomy can be performed accessing ovaries by a single surgical incision in the back of the animal, double dorsolateral incisions, or a single ventral transverse incision on the middle part of the abdomen. We used a single incision in the back of the animal since it seemed less invasive than other methods. For the ovariectomization of mice, proceed as follows:

- **20' prior ovariectomy, inject 0.1mg/kg buprenorphine (Buprex).** Prepare a working solution of 0.1 mg/ml of Buprex in saline and inject about 200 μ L of the solution via subcutaneous. Buprex administered via intraperitoneal lasts up to 6h



Helpful
TIPS

Try to inject Buprex as far as possible of the surgical area and wait until its complete absorption. Otherwise, when you open the animal you will find a kind of capsule of jelling consistency that will difficult the surgery.

- **Anesthetize the animal with Isoflurane.** To induce anesthesia, soak a cotton with isoflurane and place it inside a container (anesthesia chamber). Place the animal in the anesthesia chamber and close it. Wait until the mice stops moving. Place the animal in the surgical area in a prone position, connected with isoflurane nose cone.



Helpful
TIPS

- **Be careful when inducing anesthesia**, if the **concentration in the anesthesia chamber is too high** (you soak too much the cotton or the container used is too small) or if **the animal spends too much time** inside it, **it might die.**

- **Acute exposure to isoflurane has been associated with central nervous system toxicity.** Symptoms include headache, nausea, dizziness, loss of consciousness, asphyxia. Severe occupational overexposures to isoflurane may result in death. So be careful and protect yourself. Use the activated carbon filter.

- Alternative anesthesia methods can be used, however, **isoflurane has the best recovery rates.**

- **Apply eye lubricant** frequently as needed to prevent corneal drying and damage.
- **Shave hair off** the flank area (between the hump and above the pelvis).
- **Desinfect skin** with iodine solution
- **Make an incision** in the skin of 2 cm **in the middle of the back, below the hump.**
- Carefully, **move the skin towards one side. Localize the ovarian fat pad.** With a scissors, **make an incision in the muscle** to access the ovary.

- With fine tying forceps, carefully **pull the ovarian fat pad out** of the incision, until you can see the ovary.
- Tightly clamp the region below the ovary. Using a sterile thread, **make one knot** in order to delimitate the area to be removed and finally **remove the ovary**.
- **Place the fat pad on its place again**. If needed, suture the muscle.
- **Move the skin towards the other side** and **repeat** the procedure.
- Close the incision with **horizontal mattress**. Put some staples if needed.



Helpful TIPS

Mice will do their best to remove the suture stitches. Even when the wound is in the back, they can scratch and break the stitches. If this happens, the wound might infect and become bigger. To avoid this:

- **Administer correctly the analgesia** for 4 days. If they feel fine, they will scratch less.
- **Avoid simple stitches** even interrupted stitches. Make small horizontal mattress as they are less accessible.
- Try to **dress the wound with a tough tape** to reduce their access to the wound. Do not use regular tape, as they are breakable and too sticky and might cause discomfort in the mice. Use tape for athletes (8c+ Sticky Tape).
- **Disinfect daily the wound with iodine**. Apply regeneration creams if needed (e.g. Blastostimulina, climbskin)
- If they remove the suture, evaluate the necessity to suture again. **If possible, do not suture again**. Disinfect twice a day and apply regeneration cream (Blastostimulona, climbskin).

- **Administer additional analgesia** (2 mg/kg of meloxicam). Make a stock solution of 5 mg/ml and inject 100 μ L via subcutanea. Meloxicam anesthesia will last up to 24h.

- **Place the animal in a warm place** until recovery.

Observe the animal daily for any inflammatory signs. Inspect and disinfect the surgical wound once or twice a day and look for any behavior that suggests pain. Administer anti-inflammatory (2 mg/kg of meloxicam) drugs for 3 days.

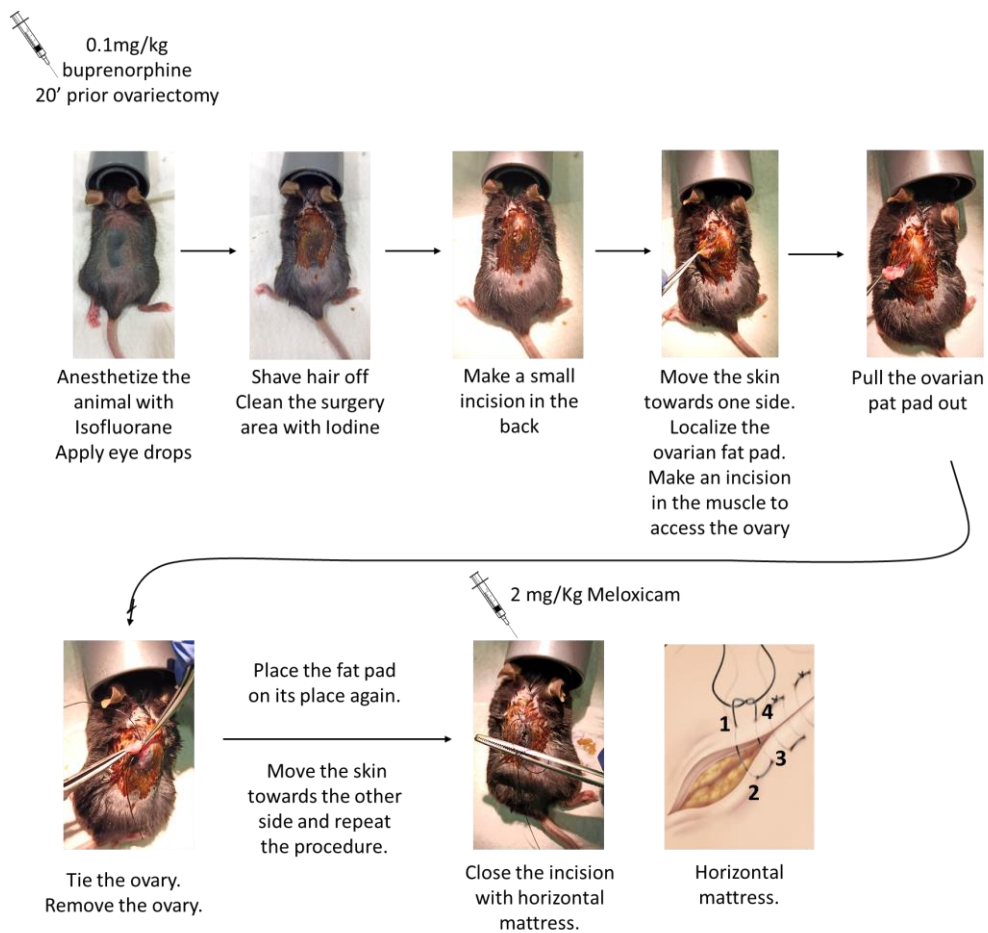


Figure 16. Schematic representation of ovariectomy process.



Helpful
TIPS

To reduce animal manipulation, after the analgesic in strawberry jelly (Royal). Dissolve the jelly in tap water and heat

- **Prepare the jelly following manufacturer instructions.** Dissolve the jelly in tap water. Use **less water** than the indicated by the manufacturer to obtain a more consist jelly. Heat it until boiling.
- Let the jelly cool down. You can use cold water. Add the metoxicam. **Add 100 μ L of 5 mg/ml metoxicam per portion.**
- **Place the jelly in small petri dish or in an ice bucket** and let it polymerize.
- **Give one portion per animal.** You can substitute subcutaneous injection by jelly portions **the second day after surgery.** **The first day after surgery, as mice do not eat much, I recommend to administer the analgesic by subcutaneous injection.**

5. Oral gavage

Liquid compounds may be administered directly into the stomach of mice via oral gavage. In this procedure we used a stainless-steel bulb tipped gavage needle attached to a syringe. Although a flexible cannula is preferred, a rigid one also worked well. The recommended maximum volume for administration is 1% of body weight (200-300 μ L). In our case, we used oral gavage to administer 100 mg/kg DMF daily for 8 weeks. For the administration of DMF proceed as follows:

- **Make a solution of 0.8% methylcellulose in hot PBS.** Agitate the mixture until the particles are thoroughly wetted and evenly dispersed. For complete solubilization, Solution should be cooled to 0-5 °C for 20-40'. Then continue agitation for at least 30 min, until complete dissolution of aggregates.



Methyl cellulose has a lower critical solution temperature (LCST) between 40 °C and 50 °C. At temperatures below the LCST, it is readily soluble in water; above the LCST, it is not soluble. However, preparing a solution of methyl cellulose with cold water is difficult because as the powder comes into contact with water, a gel layer forms around it, maintaining the powder as inside dry. This dramatically slows the diffusion of water into the powder. A better way to solubilize methyl cellulose is mixing the powder with hot water, so that the methyl cellulose particles are well dispersed and have a much higher effective surface area. Then and cool down this dispersion while stirring, leading to the much more rapid dissolution of those particles.

- **Prepare a solution of 20 mg/mL DMF (Sigma) in 0.8% methylcellulose (Sigma).** Per 1 mL of solution, add 20 mg of DMF in an Eppendorf containing 0,5 mL of methylcellulose. **Sonicate the mix on ice 3 times, 1' each time** or until complete dissolution.



DMF is a highly hydrophobic molecule and insoluble in almost everything. The solubility of DMF in aqueous buffers is very poor. It is slightly soluble in organic solvents such as ethanol (2 mg/ml), DMSO (5mg/mL) and Dimethyl formamide (DMF) (12 mg/mL). However, the amount of this solvents needed to administer 100 mg/kg of mice will exceed the maxim volume allowed for oral gavage and produce toxicity.

DMF can be dissolved in 0.8% methylcellulose. DMF form crystals that when place in methylcellulose or PBS, they precipitate. To enhance the solubility of DMF, sonicate the mix to break DMF crystals and to create an emulsion of methylcellulose that entrap DMF inside it. Do it on ice to avoid excessive warming of the mix.

- **Administer DMF by oral gavage** as follows:
 - **Immobilize the animal**, be sure that it cannot move the head.
 - Maintain the animal in an upright position and **pass the gavage needle along the side of the mouth**. Following the roof of the mouth, **advance the needle into the esophagus and toward the stomach**. If resistance is

encountered, you may be attempting to enter the trachea and you should redirect your needle.

- **After the needle is passed to the correct length, the compound may be injected.** If the animal coughs, chokes or begins to struggle after compound administration begins you may be injecting material into the lungs. If this occurs stop and withdraw the needle immediately. If it appears that material has been injected into the lungs the animal should be euthanized.

Complications of oral gavage include:

- **Passive reflux** if excessive material administered.
- **Aspiration pneumonia** if material injected into the trachea.
- **Pharyngeal, esophageal and gastric irritation** or injury due to incorrect technique or caustic substances.
- **Physical and/or psychological stress** to the animals.
- **Microaspiration of material into the lungs**



To reduce complications derived of oral gavage and facilitate handling, soak the gavage needle in honey. Honey will act as a lubricant, facilitating the pass of the needle through the throat and reducing the risk of irritation. Moreover, as mice love sweet things, they will be more collaborative.

6. Tissue dissection and blood collection

Animals were sacrificed at the end of the experiment and blood and tissue were collected for further analysis. To obtain the different sample, proceed as follows:

- Anesthetize the mice with a combination of **15 mg/kg xylazine and 80 mg/kg ketamine**. Assess anesthetic depth by testing the response to various stimuli (such as toe pinch or palpebral reflex). Wait until no response is detected.
- Proceed to **blood collection** as follows:
 - **Desinfect** the abdomen of the mice with 70% ethanol
 - **Open the abdominal cavity** making a V-cut through the skin and the abdominal wall.
 - Locate the heart. **Insert the needle through the diaphragm into the heart.**

- Gently **apply negative pressure** on the syringe plunger. Do it carefully as heart chamber may collapse if negative pressure is to great.
- **Withdraw the needle** after blood has been collected. Place the blood in an Eppendorf. You should be able to collect 300-900 μL depending on the animal size.
- **Perform a secondary method of euthanasia** to ensure that the animal is deceased.



Helpful
TIPS

- Use **23-25G needles** for blood collection.
 - Once inserted, **do not move the needle side-to-side** as this could lacerate the heart.
 - **If no blood appears**, slowly withdraw the needle so that it remains under the diaphragm and **redirect** in a slightly different direction.
 - Alternatively, you can **cut the diaphragm to have a better visualization of the heart**. However, once the diaphragm is broken, respiration starts to collapse and the animal die within a few minutes. Therefore, if possible keep the diaphragm intact, or act very quickly.
 - **If blood stops flowing, slowly rotate needle or move it slightly** in or out.
 - **Never pour the blood in the Eppendorf without removing the needle first**. This will produce hemolysis.
- **Let the blood to coagulate at room temperature** while you continue with the tissue dissection (from 30' to 3h).
 - **Centrifuge the Eppendorf 1,500 g for 15'** at room temperature.
 - **Transfer the serum** (clear upper phase) to a new Eppendorf and freeze it at -80°C
 - **Proceed to calvaria isolation**. Cut off the head of the animal. **Isolate the calvaria** and **remove the cartilage sutures** as explained in section "1.4.1. Isolation of osteoblast and osteocytes" Figure 2. **Cut the calvaria in small pieces**. If RNA is going to be isolated, place half calvaria in a 2 mL Eppendorf containing 500 μL TRISURE and freeze it immediately with liquid nitrogen
 - **Remove the lower limbs of the animal**. Pull the skin out. Break the foot by the ankle and pull up to the knee to remove the muscles of the tibia. Then remove the muscles of the femur. Prepare one leg for RNA isolation and one leg microCT analysis as follows:

- **For RNA isolation removing the bone marrow is needed.** With a needle, make a hole in the bottom of two 1 mL Eppendorfs. **Cut both edges** of tibia and femur and **place each bone in one of the the 1 mL Eppendorfs**. Place each Eppendorf inside a 1.5 mL Eppendorf. **Centrifuge for 15' at 7,000-10,000 g.** Clean the rest of tissue and bone marrow, cut both bones in small pieces and place them in a 2 mL Eppendorf containing 1mL TRISURE. Freeze it immediately with liquid nitrogen

- **For microCT.** Remove as much connective tissue as possible. Place the femur and the tibia inside a 2 mL Eppendorf containing **4% PFA**.

- If needed, remove additional tissues.

When tissue was obtained for further RNA or protein extraction, samples were immediately submerged in liquid nitrogen and subsequently stored at -80°C. For other purposes, samples were kept in 4% PFA.

7. Micro-CT: Micro-computed tomography

Micro computed tomography or "micro-CT" is X-ray imaging in 3D in a small scale with increased resolution. It really represents 3D microscopy, where very fine scale internal structure of objects is imaged non-destructively.

In micro-CT, X-rays are generated in an X-ray source, transmitted through the sample, and recorded by the X-ray detector as a 2D projection image. The gray levels of that image correspond to X-ray attenuation, which reflects the proportion of X-rays scattered or absorbed as they pass through each voxel. The sample is then rotated a fraction of a degree on the rotational stage, and another X-ray projection image is taken. This step is repeated through a 180-degree turn (or sometimes 360 degrees, depending on sample type). The series of X-ray projection images is then computed into cross-sectional images through the computational process called "reconstruction". These slices can be analyzed to quantify several parameters, and further processed into 3D models for visualization.

7.1. Sample obtention and Imaging

Long bones from mice were dissected, cleaned and fixed with PFA 4% for 24 hours. Then, an overnight wash with PBS was performed, and maintained at 4°C, in PBS supplemented with 50 µg/ml Sodium Azide, until scanning.

High resolution images from the femur were acquired using a micro tomographic imaging system (SkyScan; Bruker). For technical reasons, two different SkyScan machines were used in this thesis: SkyScan 1076 and Skyscan 1272. The specifications for each machine are detailed in table 34.

	SkyScan 1076	Skyscan 1272
X-ray generator	25W, 20-90kV	10W, 20-100 KV
X-ray detector	11 MP (4000x2672x12bits)	11MP (4032x2688 pixels)
Maximum resolution	9 µm	0.45 µm
Maximum object size	68mm x 200mm (20mm length per single scan)	75 mm in diameter using offset scan (27 mm in fast single scan)

Table 34. Technical Specification of SkyScan micro-CT machines.

All imagens were acquired in accordance with the recommendations of the American Society for Bone and Mineral Research (ASBMR). Some of the parameters to consider are the following:

- **Scanning medium:** Scanning in **air to enhance the contrast** between the specimen and the surrounding medium. However, **if tissue mineral density is going to be calculated, ASBMR recommends scanning the femurs in liquid medium**. The same scanning medium must be used for the calibration and the scanning of all samples that are to be compared.

- **X-Ray energy:** when X-rays pass through the sample, the interaction between photons and matter results in a transference of energy from the photons to the medium and the energy of the photon is attenuated. Depending on the X-ray energy, different processes with their own coefficient of attenuation will occur. In the case of micro-CT, when a photon hit an atom of the bone, it ejects one electron losing energy in this process (attenuation). As micro-CT systems produce

polychromatic beams (a spectrum of photon with different energies) in a range of 20-100KeV, two different effects are combined: Photoelectric and Compton effects. **At low energies (<50KeV) the photoelectric effect is dominant**, and the gamma photon energy is completely absorbed by the atom and transferred to the ejected electron. At this energy, the capacity to differentiate bone and marrow is enhanced but noise also become larger. **At high energies (>90 KeV), the Compton scattering is dominant** and the incident gamma photon transfers part of its energy to the struck electron, but, as the X-Ray is more energetic than the photoelectric effect, the remaining energy is scattered as a photon with a lower energy. In this case, the attenuation is proportional to the density of the material. The best results are obtained in the **medium range of X-Ray energy (50 to 90 KeV)** where both photoelectric effect and Compton scattering contribute to attenuation.

- **Beam hardening and filters:** Beam hardening is a consequence of using a polychromatic x-Ray energy. As the polychromatic X-ray beams passes through the sample, the lower-energy portion of the beam is preferentially stopped in the first layers of the sample. The result is a **beam that, has a higher average energy than the incident beam**. As the energy of X-Ray is increased through the sample, the capacity of the material to attenuate those X-ray is reduced. Therefore, **beam hardening causes that the edges of an object appear brighter than the center**, even if the material is the same throughout. Beam hardening can be reduced by placing a filter, such as an aluminum foil, in the X-ray path to narrow the energy spectrum or by applying mathematical correction during image reconstruction. Placing a filter will also reduce the noise of the image produce by the presence of other tissues in our sample that has less capacity to attenuate X-Rays (e.g. muscle, fat, etc).

- **Intensity: The information content of a voxel depends on the signal-to-noise ratio (SNR)** which is governed by **the sensibility of the detector and the number of incident photons**, which in turns depends on **the tube current (μA), the integration time for each projection (ms), and the number of times each projection is repeated (frame averaging)**. The SNR can be improved by increasing the integration time and the frame averaging; however, this will increase the total time of scanner and radiation exposure. Therefore, we must achieve an equilibrium between SNR and scanning time. Usually, for a determined resolution, exposure and current are predefined while averaging can be modified.

- **Voxel size and image resolution:** A voxel is the 3D unit of scan volume that results of the tomographic reconstruction. **Micro-CT images have isotropic voxels** (voxels that have all the three dimensions equal). **Voxel size depends on the resolution of the imagen** (as higher the resolution of the scan in, smaller the voxel

size is) and therefore, depends on **SNR**. This also implies that the resolution affect to the total scanning time (higher-resolution scans require longer acquisition times and generates longer data sets). Therefore, we should reach a **balance between resolution and scanning time**. The optimum balance will depend on the size of the structure that we are evaluating. **For mice femurs, differences in voxel size from 6 μm to 12 μm have little effects** on the evaluation of cortical bone and trabeculae. Voxel size higher than 12 μm produce blurred images that can cause underestimation of bone mineral density and overestimation of object thickness.

All the parameters used for femur scanning with both Skyscan micro-CTs are listed in table 35.

	SkyScan 1076	Skyscan 1272
Voltage	50 kV	60kV
Current	200 μA	166 μA
Exposure	800 ms	5600ms
Averaging	2	1
Resolution	9 μm	11 μm
Filter	1 mm Aluminum	1 mm Aluminum
Rotation step	1°	1°
Rotation degrees	180°	180°
Scanning medium	Air	Air
Time of scanning	8' per femur	13' per femur

Table 35. Parameters used for femur scanning with SkyScan micro-CT machines.

7.2. Image Reconstruction

Two-dimensional captures were subsequently reconstructed in order to later obtain 3D images using *NRecon* reconstruction software and in accordance with the recommendations of the American Society for Bone and Mineral Research (ASBMR). Different mathematical methods can be applied during reconstruction to reduce noise and improve the quality of the images.

Once the sample is loaded in *NRecon*, five different sections appears (start, setting, advanced, output and summary). Different parameters can be modified in the different sections:

- **Start section:** section where the projections can be view (Figure 10) . In this section we can modify:
 - **Region of interest (ROI):** When setting up the scan acquisition and reconstruction, it is critical to ensure that a sufficient amount of the sample is scanned and reconstructed to allow for reliable and reproducible morphology and density measurements. However, as bigger the region of interest is, longer the acquisition and reconstruction times are. So again, we should arrive to a tradeoff between time and ROI size. For femurs a squared **ROI of 759x759** pixels and **20 mm length is enough**. Be sure that the femur is placed in the center of the ROI.
 - **Preview: reconstructs one slice of choice.** Can be used to adjust several parameters.
 - **Fine Tuning:** Many parameters have to be adjusted manually in a try-and-error fashion using the preview function. The "fine-tuning" function **launches a series of previews**, helping you to compare and select the best one. You can use Fine Tuning to set Post-Alignment, Beam-Hardening correction, Ring-Artifacts reduction and Smoothing.

Materials and Methods

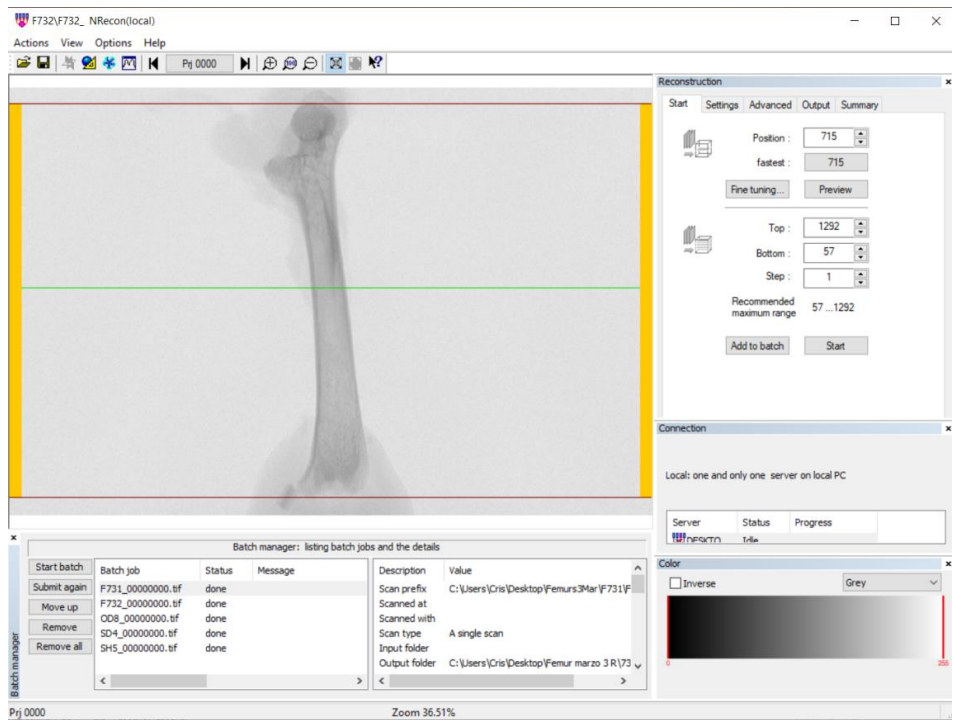


Figure 17. Start section of NRecon. Previsualization of bone shadow projection. Green line represents the stack that will be selected for reconstruction as a sample.

- **Settings:** This page includes (Figure 11):

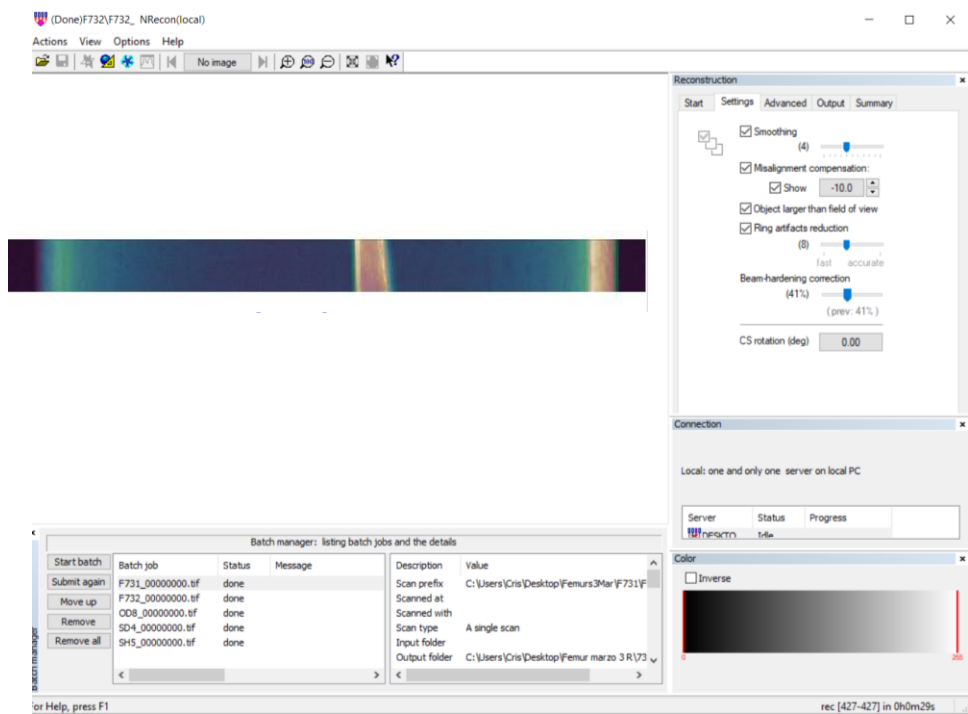


Figure 18. Settings page. The program shows an overlaid image of 2 shadow images at opposite positions (180 degrees apart), one of them flipped. As image is aligned, both images coincide.

- **Misalignment compensation:** This **compensates possible misalignment during acquisition**. Wrong alignment compensation would cause tails, doubling or blurring in the reconstructed image. To facilitate image alignment, the program displays an overlaid image of 2 shadow images at opposite positions (180 degrees apart), one of them flipped. When the image is aligned, both images coincide. However, it is always recommended to use the previewing to choose the post-alignment value (Figure 12). Misalignment compensation **must be set for each sample**



Figure 19. Preview of a misaligned bone.

- **Smoothing:** It smooths each pixel with a MxN neighborhood. It is used **reduce the noise**; however, high smoothing values introduce blurring for fine structures. Smoothing **must be conserved within the same experiment**. In general smoothing is set at **4%**

- **Ring artefact reduction:** Occasionally, minor problems such as a defective pixel on the detector, a defect in the scintillator that converts X-rays to visible light, or dust on the detector system will create an artifact that looks like rings or half rings around the rotation center of the reconstructed image. They can be reduced before the acquisition of the images (cleaning the detector, placing filters) or during the reconstruction step. This option reduces ring artifacts. It is applied on the projections before any other preprocessing steps. You can select the depth of the correction in a slider with 20 positions. It is generally not recommended to use an unnecessarily high value: blurring

may occur. Ring artefact reduction **must be conserved within the same experiment**. In general ring artefact reduction is set at **8**.

- **Beam hardening correction:** This option **compensates beam-hardening effect by linear transformation in the software**. Depth of correction (from 0 to 100) can be selected according to object density. To help us in the decision, we create a histogram of density. To do this, right-click on one side of the bone and drag the mouse to the other side. The program will show a histogram of density. If beam hardening correction is right, histogram should be flat. Beam hardening correction **must be conserved within the same experiment**. In general beam hardening correction is set between **31-41**.

- **Cs Rotation:** rotates the resulting cross-section image by a fixed angle.

- **Advanced (Figure 13):**

- **Smoothing:** μ CT data inherently include signal noise that should be reduced by filtering. **Removal of image noise** is best accomplished by a low-pass filter, but this essentially blurs the image. Enhancing the edge of the image, requires a high-pass filter, yet this may result in increased noise. Therefore, the filter applied should tradeoff both effects. Generally, a **Gaussian filter is used** as does well at balancing these competing objectives, is easy to implement, and is fast, even for large data sets. We should apply a minimum amount of filtering to avoid degrading the μ CT data and obtain a blurred image. The filter applied **must be conserved within the same experiment**.

- **Defect pixel masking** is another **type of ring artefact**. Sometimes, the presence of dust in the filter or in the detector block the X-rays, given rise to a shadow. The percentage of pixel masking can be correct from 3% to 50%. This percentage **must be conserved within the same experiment**. In general defect pixel masking is set between at **5%**.

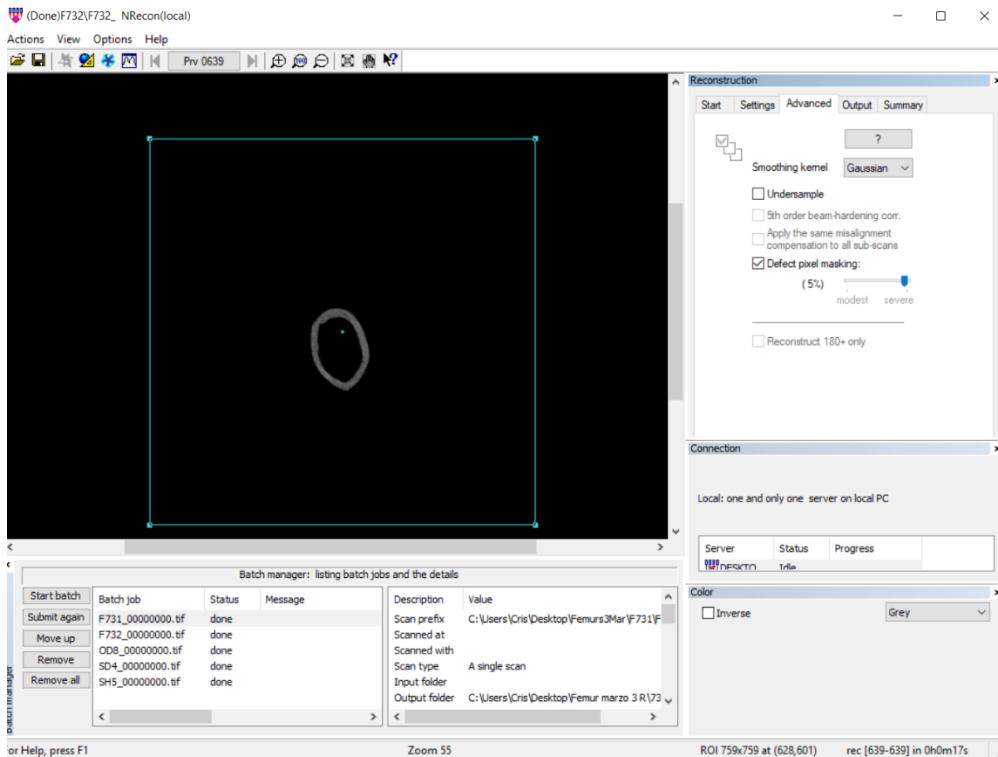


Figure 20: Advanced page. The square mark the area selected for reconstruction. In the middle of the square, we see the selected stack reconstructed as a sample.

- **Output:** This window/page offers possibilities to adjust parameters which influence the output images in format, size, color or dynamic range (Figure 14).

- **Histogram page:** This function **determines the pixels that will be used for the reconstruction based on their gray value**. The interval **must be conserved within the same experiment**. In general, the interval used is **0.01-0.08**.

- **File format:** Four output formats are provided: 8-bit BMP (0-255), 16-bit TIFF (0-65535), 8-bit JPEG (0-255) and 8-bit PNG (0-255). For further analysis in CtAN, **BMP** format is selected.

- **Destination:** Specify the output dataset. **Create a new folder for each reconstruction.**

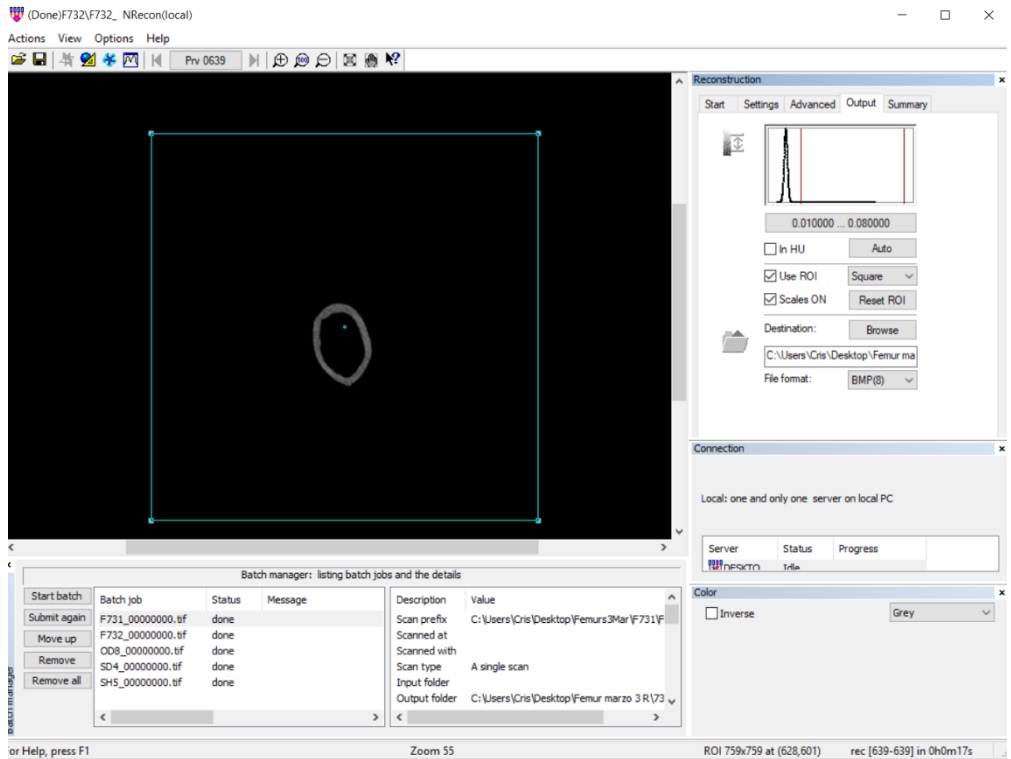


Figure 21. Output page. The square mark the area selected for reconstruction. In the middle of the square, we see the selected stack reconstructed as a sample. The histogram located in the upper right corner of the image determines the grey values that will be selected for reconstruction.

7.3. Micro-CT calibration for BMD

Different micro-CT systems often use different CT-value scales to assess tissue density. Therefore, ASBMR recommend to report bone density in milligrams per cubic centimeter of HA rather than CT values to minimize manufacturer dependency. In consequence, micro-CT must be calibrated using calibration phantoms. A calibration phantom is a cylinder of calcium hydroxyapatite (HA) with a known mineral density. These phantoms allow us to relate CT values to a mineral-equivalent value, normally in milligrams per cubic centimeter (mg/cm^3) of calcium

hydroxyapatite. Owing to the excellent linearity of modern μ CT systems, calibration is possible with only two phantoms of 0.25 mg/cm^3 and 0.75 mg/cm^3 .

To calibrate the machine, phantoms are scanned in the same conditions than in our samples. The images are reconstructed with the same parameters of the samples. Then calibrate BMD in CT-Analyser. Proceed as follows:

- **Open in CT-Analyser (“CTAn”)** the dataset of one BMD phantom scan (0.25 mg/cm^3 or 0.75 mg/cm^3).

- **Go to the region of interest (ROI) page of CTAn** and **choose a ROIs within the phantoms**. The cross-sectional ROIs should be set as a **circle, smaller than the phantom and excluding the exterior margin**. The vertical ranges of the ROIs for both phantoms should also exclude the part near the ends and need not run the whole length of the phantom (just one or two hundred cross-sections is sufficient).

- **Move to the binary page of CTAn**. A density histogram is shown, with two tabs above it, “from image” and “from dataset”. By default “from image” is selected, thus the histogram displayed is for the current cross-section level only. Change it to **“from dataset” to integrate the density histogram over the whole open dataset**. Then, click on the button on the far right under the heading “histogram”. This button will restrict the density histogram to the contents of the VOI.

- **Select the tab below the histogram entitled Hounsfield units**. Scroll to the bottom of the histogram table and you will see a statistical summary of the histogram data. The first value in the summary table is **“mean (total)”**. This is the mean density value of all the voxels within the VOI. At this stage in the calibration method the threshold values is not important as we need to measure the mean density of all the voxels within the phantom rod volumes of interest (VOIs).

- **Write down the number of mean (total) and repeat the process with the other phantom**.

- **Go to the file menu of CTAn and “preferences”**. Open the tab entitled **“histogram”**. Check that Hounsfield units are selected. Click on the **“calibrate”** button. A table will appear as. In this table, in the top row, enter the two BMD concentrations for the two phantoms of calcium hydroxyapatite (0.25 mg/cm^3 or 0.75 mg/cm^3). **In the second row, enter the two values measured and click OK**. Note that after entering these values, the formula displayed in the histogram window will change.

7.4. Micro-CT analysis

microCT analyses were carried out with the *CT-Analyser* (SkyScan) software. We assessed representing parameters of cortical and trabecular bone as well as bone mineral density.

- **Cortical measurements** were performed by delineating the femur medial cortex for 101 stacks around the femoral midshaft. Then we drew a polygonal ROI surrounding the cortical bone (Figure 15). Binary minimum threshold was established at 100 for images from SkyScan 1076 and at 50 for images from Skyscan 1272. Key parameters that must be assessed for cortical tissue are the following:

- **Bone volume (BV):** Volume of the region segmented as bone
- **Bone area (B.Ar):** Area of the region segmented as bone.
- **Bone perimeter (B.Pm.):** Perimeter of the region segmented as bone
- **Average cortical thickness (Ct.Th.)**

These parameters are not independent variables. BV can be modified by an expansion or contraction of the bone or by a modification of the cortical thickness. In the first case, the increase in BV will be joined to an increase in B.Ar and B.Pm without modifications in Ct.Th. This has been linked to alterations during the development or to compensatory mechanisms of bone in aging. In the second case, alteration of cortical thickness is seen in changes in adult bones.

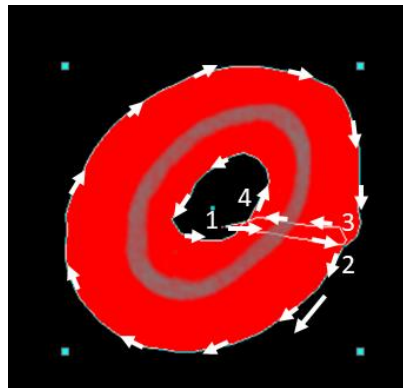


Figure 22. Schematic representation of the steps to create a cortical ROI

- **Trabecular measurements:** For trabecular measurements, manual VOI was employed, starting at 100 slices from the distal growth plate of the femur and extending to the diaphysis for 151 stacks. Thus, ROI was manually drawn a few voxels away the endocortical surface every 30 stacks (Figure 16). For reconstruction, binary minimum threshold was established at for images from SkyScan 1076 and at 50 for

images from Skyscan 1272. Key parameters that must be assessed for cortical tissue are the following:

- **Bone Volume fraction (BV/TV):** Ratio of the segmented bone volume to the total volume of the area of interest.
- **Trabecular Number (Tb.N):** Measure of the average number of trabecula per unit length
- **Trabecular Thickness (Tb.Th):** Mean thickness of trabecula.
- **Trabecular separation (Tb.Sp):** Mean distance between trabecula

All trabecula parameters can be measured using information from 2D or 3D images. Measurements made using 2D methods require assumptions about the underlying structure, therefore, ASBMR recommend using 3D model-independent measurements of Tb.N, Tb.Th and Tb.Sp. Although the magnitude of this parameters changes when analyzed in 2D and 3D models, the significant differences observed between the different groups of studies were maintained independently of the method used.

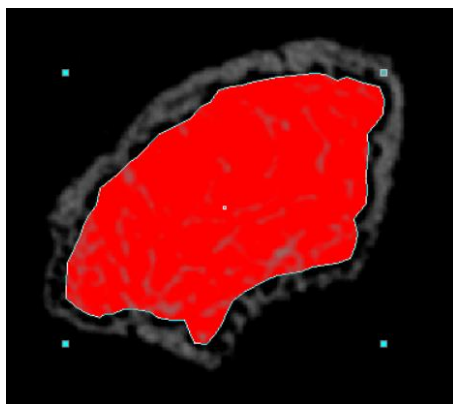


Figure 23. Representative representation of a trabecular ROI

- **Tissue mineral density:** TMD is calculated from the average attenuation value of the bone tissue only and does not include attenuation values from non-bone voxels. We assessed TMD using the same ROI and threshold than for the cortical analysis. However, the use of a polychromatic X-ray source, during image obtention produce several potential sources of artifacts that can alter attenuation values and therefore TMD measurements. These include beam hardening, partial-volume effects, photon starvation, photon scatter, and undersampling. Therefore, it is important to recognize that significant errors in TMD measurements can occur and data should be taken with care.

CHAPTER VIII: HISTOMORPHOMETRIC ANALYSIS.

For a better understanding of the changes observed in bone structure, we performed several histological techniques that are explained in the following sections. Most of the techniques explained were performed in the Histology Unit of the CMRB core facilities.

1. Paraffin processing of tissue

Paraffin processing of bone tissues have three different steps: decalcification of bone tissue, dehydration and preparation of paraffin blocks.

1.1. Decalcification

Before performing histological techniques, bones must be fixed and decalcified, otherwise they will not be cut by the microtome. Bones were fixed with 4% PFA for 24h. Then they were washed with PBS overnight and conserved in PBS with 50 µg/ml sodium azide until decalcification. Different techniques can be used to achieve decalcification:

- **Decalcifier 11 (00460, Surgipath):** commercial solution made of EDTA and HCl. After PBS washing, samples are placed in Decalcifier solution for 3 days.

- **EDTA solution:** Fixed bones are incubated with 16% EDTA in PBS pH 7.4 for at least 4 weeks. The solution is replaced every 3 days.



- Decalcification with **Decalcifier 11 is faster than with EDTA**, however, the **HCl can interfere with different techniques**, such as TRAP staining and some immunohistochemistry stains. Therefore, if possible, decalcify the bones with EDTA.

- To obtain good histological section it is very important to **decalcify the bones properly**. Check that the bone tissue is soft before proceeding to the next step. They should have a chewy consistency, like tendons. If you think they are not soft enough, leave them a few days more in EDTA.

- **Sometimes the midshaft of the bone is soft but the ends harder.** This is because the cartilage of the knee is harder than the decalcified bone. If this happen leave the bones one week more in EDTA just to be sure that the bone is completely decalcify. If none improvement is detected, proceed to the paraffin inclusion

1.2. Dehydration

Once bones have been decalcified, dehydrate samples in increasing concentrations of ethanol. The aim of this protocol is to displace the water from the tissue to further infiltrate it with the paraffin. For the identification of the samples, each femur is place inside a cassette. All cassettes are process at the same time. The protocol is automatized in a dehydration robot and can be performed overnight. The steps are the following.

- 70% ethanol, 1hour
- 90% ethanol, 1 hour
- 100% ethanol I, 1 hour
- 100% ethanol I, 1 hour
- 100% ethanol I, 1 hour
- Butyl alcohol, 1 hour
- Xylene I, 1 hour
- Xylene II, 1 hour
- Xylene III, 1 hour
- Paraffin I, 1 hours
- Paraffin II, overnight

1.3. Preparation of paraffin blocks.

After dehydration, cassettes are immersed in a paraffin bath (65 °C). The blocks are prepared individually as follows:

- Take a cassette from the paraffin bath and **remove the cover**.
- **Place the sample in a mold**.
- **Pour a little of liquid paraffin** in the mold and **orientate the femur**. This is a critical step. **All femurs must have the same orientation** if possible. Avoid that the sample touch the edges.
 - **Place the mold over the cold plate**. Do it carefully to avoid the femur lose the orientation. **Press softly** the sample to put it at the bottom of the mold.
 - **Place the cassette over the mold** to fix the sample and add some extra paraffin to fill up the cassette.
 - **Place the piece over the cold plate** and press for some seconds, until the cassette does not move.
 - **Leave the piece cool down for 30'**. Then **unmold** the cassette.
 - **Leave the paraffin cassette in the fridge (4°C)** until microtome sectioning.

1.4. Microme sectioning

A microtome is a tool used to cut extremely thin slices of material, known as sections. The microtome has a mechanism for advancing the block across the bladder. The distance (and therefore the thickness of the section) is usually set at 5-10 μm for paraffin embedded tissues. We made 7 μm sections of bone. To make microtome section proceed as follows:



To obtain good sections, the block must be very cold. Therefore:

- Place it in the freezer the night before.
 - Maintain the blocks in the cold plate.
 - Leave the tissue cool down in the freezer after removing the excess of paraffin.
-
- **Remove the excess of paraffin** surrounding the sample with a knife.
 - Place the paraffin block in the microtome and **make cuts of 10-20 μm until you reach the area of the bone desired**. Let the block to cool down again.

- **Make serial sections of 7 μm .** Leave the chain of sections floating on warm water bath to remove wrinkles.
- **Pick up sections from the water bath** using a glass microscopic slide.



- Leave the section on the water bath just the necessary time to remove the wrinkles. If paraffin stays for too long in the water, the tissue will start to break.
- Use Superfrost glass slides as they attract electrochemically the tissue and facilitate the picking up of the sections.

Dry the samples at 37°C. Leave them in the incubator at least overnight.

1.5. Histological stains



- Colorants used in histological stains can be used more than once. Do not throw away the excess, keep it for reutilization.
- Filter all the colorants before using them. Use bench paper to make homemade filters.
- Be very carefully when cleaning. If something is not well cleaned, and colorants mix, future stains can be ruined.
- Colorant stains not only your samples but also your clothes, the bench, etc. Be careful, use lab coat. Accidental staining of surfaces can be removed with bleach.

1.5.1. Dewax and Rehydration.

As most of colorants and reagents used for histological stains are water-based, samples must be dewaxed and rehydrated to allow them to penetrate inside the tissue.

Firstly, slides are placed in a bucket and heated in the oven at 60°C for 30' to ensure that all the water has been removed and to start the dewaxing process. The next steps of the protocol are automatized and performed in an auto-staining machine as follows:

- Xylene I, 5'
- Xylene II, 5'
- 100% ethanol, 5'

- 96% ethanol, 5'
- 80% ethanol, 5'
- 70% ethanol, 5'
- Distilled water, 5'

1.5.2. Hematoxilin-Eosin

Hematoxilin-Eosin (H&E) is one of the major tissue stainings used in histology. H&E is the combination of two histological stains: hematoxylin that stains cell nuclei blue, and eosin that stains the extracellular matrix and cytoplasm pink. The stain shows the general layout and distribution of cells and provides a general overview of a tissue sample's structure and helps us to quantify the number of cells within an area.

After dewaxing and rehydrating slides with water, start Hematoxilin-Eosin staining as follows:

- Place the slides in **Harris' hematoxylin for 8'**
- Wash with running **tap water for 5'**
- Place the slides in **Hydrochloric alcohol** (1% hydrochloric acid in 70% ethanol) to do nuclear differentiation.
 - Wash with **running tap water for 5'**
 - Place the slides in **alcoholic eosin bucket for 30''**
 - Proceed to **dehydration step**. Start with **ethanol 70%**

1.5.3. Goldner's Masson trichrome

Masson's trichrome is a three-colour staining protocol used in histology to distinguishing cells from surrounding connective tissue. Most recipes produce red keratin and muscle fibers, blue collagen and bone, light red or pink cytoplasm, and dark brown to black cell nuclei.

After dewaxing and rehydrating the slides with distilled water, proceed as follows:

- The day prior performing Goldner's Masson trichrome, **place the slides in Bouin's solution** (picric acid, acetic acid and formaldehyde in water) solution to improve tissue stain with acid dyes. Incubate overnight.
 - Wash in **running tap water for 10'** or until the yellow color of picric acid has disappear.
 - Place in **Weigert's Hematoxylin for 5'**.

- Wash in **running tap water for 5'**
- Wash in **ammoniacal water 3% for 3'**
- Wash in **running distilled water for 3'**
- Stain in **Xilidine Ponceau-Acid Fuchsine solution for 5'**
- Wash in running **distilled water for 5'**
- Differentiate in **phosphomolybdic-phosphotungstic acid solution for 5'**
- Stain in **Anilin Blue for 5'**
- Wash in **1% acetic acid for 2'**
- Wash in **running distilled water for 3'**
- Proceed to **dehydration step**. Start with ethanol **90%**

1.5.4. TRAP (Tartrate resistant acid phosphatase) staining

TRAP (Tartrate resistant acid phosphatase) staining is used for the staining of osteoclasts.

TRAP staining is not set up in CMRB facilities, therefore, all the material must be prepared in the lab before starting the staining. The components of all buffers needed are listed in Table 36:

Buffer	Recipe	Storage and stability
Basic incubation medium (Stock)	Per 1L 9.2 g sodium acetate, anhydrous 11.4 g sodium tartrate, dibasic dehydrate 2.8 mL glacial acetic acid Up to 1000 mL of dH ₂ O Adjust the pH to 4.7-5	Room temperature up to 6 months
Naphtol AS-BI phosphate buffer	Per 200 mL (one bucket): 50 mg Naphtol 2.5 mL 2-Ethoxiethanol	4°C up to 6 weeks
Sodium nitrite	Per 25 mL 1g of sodium nitrite (NaNO ₃) Up to 1000 mL of dH ₂ O	4°C for long storage
Pararosaniline dye	1 g Pararosaniline dye 20 mL 2M HCl (83 mL HCl in 417 mL dH ₂ O	Room temperature for long storage

Table 36. Solutions for TRAP stain

After dewaxing and rehydrating the slides with distilled water, proceed as follows:

- **Warm** 500 mL basic incubation solution (BI solution) to 37°C
- Fill 2 staining buckets with 200 mL/each of pre-warmed BI solution. Leave them at 37°.
- **Add 2 mL of naphthol-ether substrate** to one bucket of BI solution. Place slides into the bucket and incubate at **37°C for 1 hour**.
 - A few minutes before incubation time is up, mix **4 mL sodium nitrite solution and 4 mL pararosaniline dye**. Mix gently by hand for 30" and then **let sit for 2'**. Add this solution to the second pre-heated bucket of BI solution and mix well.
 - **Transfer the incubated slides from the first bucket to the second one** without rinsing. **Incubate at 37°C for 4-10 minutes**. During the incubation time check periodically under microscope for desired intensity of red in osteoclasts. Once the osteoclasts are pink, proceed rapidly to the next step to avoid unspecific staining.
 - **Rinse 3 times** with distilled water.
 - **Counterstain with a 0.02% fast green solution for 45"**.
 - Rinse with **running distilled** water for 5'.
 - Proceed to **dehydration step**. Start with **ethanol 90%**



BI solution with naphthol-ether can be reutilize for the staining of more than one bucket on the same time. However, the mix lose efficiency with the time. Therefore, if you reutilize BI solution with naphthol-ether, leave the second stain longer.

1.5.5. Dehydration

After most of the stains, a dehydration procedure is also needed before mounting. To dehydrate the slides proceed as follows:

- Dip the bucket 5 times in 70% ethanol
- Dip the bucket 5 times in 90% ethanol
- Dip the bucket 5 times in 96% ethanol
- Dip the bucket 5 times in 100% ethanol
- Change the slides to a clean and dry bucket and place it in Xylene I for 10'.

Materials and Methods

- Move the bucket to xylene II for 10'
- Move the bucket to xylene + eucalyptol for 10' or until all the water has disappeared.
- Mount immediately with DPX mounting media.



Helpful
TIPS

- Ethanol dehydrate the sample but also reduce the intensity of the stains. During dehydration protocol proceed fast. To obtain brighter stains, remove the first ethanol step (start with 90% ethanol). This is critical for Goldner's Masson trichrome.
- Do not be mean with DPX mounting media. Put an excess to avoid bubbles.
- Once the slides are dry, clean the slides with acetone. Clean the excess of DPX with acetone. Scrub gently with a paper and let it dry. Slides will seem foggy. Clean again with acetone to obtain perfect clear slides.

CHAPTER IX: BIOINFORMATICS

We used public databases to find putative regulatory regions and transcription factor binding sites that for our genes of interest.

In a first attempt we used ECR browser (<https://ecrbrowser.dcode.org/>) (Ovcharenko et al., 2004) to find conserved regions upstream and downstream our genes of interest that could be susceptible to act as regulatory regions.

We used Hi-C data from (Dixon et al., 2015) in MSC to assess Topological domain and looping structures involving the osteocytic genes. Data was visualized using 3D Genome Browser (<http://promoter.bx.psu.edu/hi-c/index.html>).

ChIP-seq data showing NRF2 binding sites in A549 cells was obtained from GSE113497 (Olagner et al., 2018) and visualized with IGV 2.0.8. program.

Finally histone marks H3K27ac, H3K36me3 and mark H3K4me3 of human osteoblast epigenome were obtained from Roadmaps Epigenomics project (https://egg2.wustl.edu/roadmap/web_portal/index.html) (Roadmap Epigenomics Consortium et al., 2015). This project joined and analyzed the information of 1,936 data to create 111 reference epigenomes, including primary osteoblast epigenome. All primary processed data are contained within Release 9 of the Human Epigenome Atlas (<http://www.pigenomeatlas.org>).

CHAPTER 10: STATISTICAL ANALYSIS

GraphPad Prism 6.0 software was used for graph representations and statistical analysis. The results are always expressed as mean \pm SEM. Unpaired two-tailed Student's t- test or two-way ANOVA were employed for statistical analysis. Differences were considered significant at p values lower than 0.05, and are represented in the figures as * p < 0.05; **, p < 0.01, and ***, p < 0.001.

BIBLIOGRAPHY

- Abubakar, A. A., Noordin, M. M., Azmi, T. I., Kaka, U., & Loqman, M. Y. (2016). The use of rats and mice as animal models in ex vivo bone growth and development studies. In *Bone and Joint Research* (Vol. 5, Issue 12, pp. 610–618). British Editorial Society of Bone and Joint Surgery. <https://doi.org/10.1302/2046-3758.512.BJR-2016-0102.R2>
- Accili, D., & Arden, K. C. (2004). FoxOs at the crossroads of cellular metabolism, differentiation, and transformation. In *Cell* (Vol. 117, Issue 4, pp. 421–426). [https://doi.org/10.1016/S0092-8674\(04\)00452-0](https://doi.org/10.1016/S0092-8674(04)00452-0)
- Addison, W., Masica, D., Gray, J., & McKee, M. D. (2009). Phosphorylation-Dependent Inhibition of Mineralization by Osteopontin ASARM Peptides is Regulated by PHEX Cleavage. *Journal of Bone and Mineral Research*, 090923081604075–44. <https://doi.org/10.1359/jbmr.090832>
- Addison, W. N., Nakano, Y., Loisel, T., Crine, P., & McKee, M. D. (2008). MEPE-ASARM Peptides Control Extracellular Matrix Mineralization by Binding to Hydroxyapatite: An Inhibition Regulated by PHEX Cleavage of ASARM. *Journal of Bone and Mineral Research*, 23(10), 1638–1649. <https://doi.org/10.1359/jbmr.080601>
- Al-Dujaili, S. A., Lau, E., Al-Dujaili, H., Tsang, K., Guenther, A., & You, L. (2011). Apoptotic osteocytes regulate osteoclast precursor recruitment and differentiation in vitro. *Journal of Cellular Biochemistry*, 112(9), 2412–2423. <https://doi.org/10.1002/jcb.23164>
- Al-Sawaf, O., Fragoulis, A., Rosen, C., Keimes, N., Liehn, E. A., Hölzle, F., Kan, Y. W., Pufe, T., Sönmez, T. T., & Wruck, C. J. (2014). Nrf2 augments skeletal muscle regeneration after ischaemia-reperfusion injury. *The Journal of Pathology*, 234(4), 538–547. <https://doi.org/10.1002/path.4418>
- Ali, A. A., Weinstein, R. S., Stewart, S. A., Parfitt, A. M., Manolagas, S. C., & Jilka, R. L. (2005). Rosiglitazone Causes Bone Loss in Mice by Suppressing Osteoblast Differentiation and Bone Formation. *Endocrinology*, 146(3), 1226–1235. <https://doi.org/10.1210/en.2004-0735>
- Alikhani, M., Alikhani, Z., Boyd, C., MacLellan, C. M., Raptis, M., Liu, R., Pischon, N., Trackman, P. C., Gerstenfeld, L., & Graves, D. T. (2007). Advanced glycation end products stimulate osteoblast apoptosis via the MAP kinase and cytosolic apoptotic pathways. *Bone*, 40(2), 345–353. <https://doi.org/10.1016/j.bone.2006.09.011>

- Almeida, M., Han, L., Martin-Millan, M., Plotkin, L. I., Stewart, S. A., Roberson, P. K., Kousteni, S., O'Brien, C. A., Bellido, T., Parfitt, A. M., Weinstein, R. S., Jilka, R. L., & Manolagas, S. C. (2007). Skeletal involution by age-associated oxidative stress and its acceleration by loss of sex steroids. *Journal of Biological Chemistry*, 282(37), 27285–27297. <https://doi.org/10.1074/jbc.M702810200>
- Almeida, M., & O'Brien, C. A. (2013). Basic biology of skeletal aging: Role of stress response pathways. *Journals of Gerontology - Series A Biological Sciences and Medical Sciences*, 68(10), 1197–1208. <https://doi.org/10.1093/gerona/glt079>
- Amarasekara, D. S., Yun, H., Kim, S., Lee, N., Kim, H., & Rho, J. (2018). Regulation of osteoclast differentiation by cytokine networks. In *Immune Network* (Vol. 18, Issue 1). Korean Association of Immunologists. <https://doi.org/10.4110/in.2018.18.e8>
- Ambrogini, E., Almeida, M., Martin-Millan, M., Paik, J. H., DePinho, R. A., Han, L., Goellner, J., Weinstein, R. S., Jilka, R. L., O'Brien, C. A., & Manolagas, S. C. (2010). FoxO-Mediated Defense against Oxidative Stress in Osteoblasts Is Indispensable for Skeletal Homeostasis in Mice. *Cell Metabolism*, 11(2), 136–146. <https://doi.org/10.1016/j.cmet.2009.12.009>
- Andersson, U., & Scarpulla, R. C. (2001). Pgc-1-related coactivator, a novel, serum-inducible coactivator of nuclear respiratory factor 1-dependent transcription in mammalian cells. *Molecular and Cellular Biology*, 21(11), 3738–3749. <https://doi.org/10.1128/MCB.21.11.3738-3749.2001>
- Anetzberges, H., Thein, E., Becker, M., Zwissles, B., & Messmer, K. (2004). Microspheres accurately predict regional bone blood flow. *Clinical Orthopaedics and Related Research*, 424, 253–265. <https://doi.org/10.1097/01.blo.0000128281.67589.b4>
- Arai, M., Shibata, Y., Pugdee, K., Abiko, Y., & Ogata, Y. (2007). Effects of reactive oxygen species (ROS) on antioxidant system and osteoblastic differentiation in MC3T3-E1 cells. *IUBMB Life*, 59(1), 27–33. <https://doi.org/10.1080/15216540601156188>
- Arasu, A., Cawthon, P. M., Lui, L. Y., Do, T. P., Arora, P. S., Cauley, J. A., Ensrud, K. E., & Cummings, S. R. (2012). Serum sclerostin and risk of hip fracture in older caucasian women. *Journal of Clinical Endocrinology and Metabolism*, 97(6), 2027–2032. <https://doi.org/10.1210/jc.2011-3419>
- Ardawi, M. S. M., Rouzi, A. A., Al-Sibiani, S. A., Al-Senani, N. S., Qari, M. H., & Mousa, S. A. (2012). High serum sclerostin predicts the occurrence of osteoporotic fractures in postmenopausal women: The center of excellence for osteoporosis research study. *Journal of Bone and Mineral Research*, 27(12), 2592–2602.

<https://doi.org/10.1002/jbmr.1718>

- Atashi, F., Modarressi, A., & Pepper, M. S. (2015). The role of reactive oxygen species in mesenchymal stem cell adipogenic and osteogenic differentiation: A review. In *Stem Cells and Development* (Vol. 24, Issue 10, pp. 1150–1163). Mary Ann Liebert Inc. <https://doi.org/10.1089/scd.2014.0484>
- Ather, S., & Harding, K. G. (2009). Wound management and dressings. In *Advanced Textiles for Wound Care* (pp. 3–19). Elsevier Inc. <https://doi.org/10.1533/9781845696306.1.3>
- Bai, X. C., Lu, D., Bai, J., Zheng, H., Ke, Z. Y., Li, X. M., & Luo, S. Q. (2004). Oxidative stress inhibits osteoblastic differentiation of bone cells by ERK and NF- κ B. *Biochemical and Biophysical Research Communications*, 314(1), 197–207. <https://doi.org/10.1016/j.bbrc.2003.12.073>
- Bai, X. C., Lu, D., Liu, A. L., Zhang, Z. M., Li, X. M., Zou, Z. P., Zeng, W. Sen, Cheng, B. L., & Luo, S. Q. (2005). Reactive oxygen species stimulates receptor activator of NF- κ B ligand expression in osteoblast. *Journal of Biological Chemistry*, 280(17), 17497–17506. <https://doi.org/10.1074/jbc.M409332200>
- Banfi, G., Iorio, E. L., & Corsi, M. M. (2008). Oxidative stress, free radicals and bone remodeling. In *Clinical Chemistry and Laboratory Medicine* (Vol. 46, Issue 11, pp. 1550–1555). <https://doi.org/10.1515/CCLM.2008.302>
- Bar-Shavit, Z. (2007). The osteoclast: A multinucleated, hematopoietic-origin, bone-resorbing osteoimmune cell. In *Journal of Cellular Biochemistry* (Vol. 102, Issue 5, pp. 1130–1139). <https://doi.org/10.1002/jcb.21553>
- Baron, R. (2000). Anatomy and Ultrastructure of Bone – Histogenesis, Growth and Remodeling. In *Endotext*. MDTText.com, Inc. <http://www.ncbi.nlm.nih.gov/pubmed/25905372>
- Barragan-Adjemian, C., Nicolella, D., Dusevich, V., Dallas, M. R., Eick, J. D., & Bonewald, L. F. (2006). Mechanism by which MLO-A5 late osteoblasts/early osteocytes mineralize in culture: Similarities with mineralization of lamellar bone. *Calcified Tissue International*, 79(5), 340–353. <https://doi.org/10.1007/s00223-006-0107-2>
- Barth, T. K., & Imhof, A. (2010). Fast signals and slow marks: the dynamics of histone modifications. In *Trends in Biochemical Sciences* (Vol. 35, Issue 11, pp. 618–626). Elsevier. <https://doi.org/10.1016/j.tibs.2010.05.006>
- Bellido, T., Ali, A. A., Gubrij, I., Plotkin, L. I., Fu, Q., O'Brien, C. A., Manolagas, S. C., & Jilka, R. L. (2005). Chronic elevation of parathyroid hormone in mice reduces expression of sclerostin by osteocytes: A novel mechanism for hormonal control of osteoblastogenesis. *Endocrinology*, 146(11), 4577–4583.

<https://doi.org/10.1210/en.2005-0239>

- Bellido, Teresita. (2014). Osteocyte-driven bone remodeling. In *Calcified Tissue International* (Vol. 94, Issue 1, pp. 25–34). NIH Public Access. <https://doi.org/10.1007/s00223-013-9774-y>
- Bellido, Teresita, & Delgado-Calle, J. (2020). Ex Vivo Organ Cultures as Models to Study Bone Biology. *JBMR Plus*, 4(3), jbm4.10345. <https://doi.org/10.1002/jbm4.10345>
- Bennett, C. N., Ross, S. E., Longo, K. A., Bajnok, L., Hemati, N., Johnson, K. W., Harrison, S. D., & MacDougald, O. A. (2002). Regulation of Wnt signaling during adipogenesis. *Journal of Biological Chemistry*, 277(34), 30998–31004. <https://doi.org/10.1074/jbc.M204527200>
- Bernards, M. T., Qin, C., Ratner, B. D., & Jiang, S. (2008). Adhesion of MC3T3-E1 cells to bone sialoprotein and bone osteopontin specifically bound to collagen I. *Journal of Biomedical Materials Research - Part A*, 86(3), 779–787. <https://doi.org/10.1002/jbm.a.31650>
- Berner, H. S., Lyngstadaas, S. P., Spahr, A., Monjo, M., Thommesen, L., Drevon, C. A., Syversen, U., & Reseland, J. E. (2004). Adiponectin and its receptors are expressed in bone-forming cells. *Bone*, 35(4), 842–849. <https://doi.org/10.1016/j.bone.2004.06.008>
- Bernhardt, A., Wolf, S., Weiser, E., Vater, C., & Gelinsky, M. (2020). An improved method to isolate primary human osteocytes from bone. *Biomedizinische Technik*, 65(1), 107–111. <https://doi.org/10.1515/bmt-2018-0185>
- Bigarella, C. L., Liang, R., & Ghaffari, S. (2014). Stem cells and the impact of ROS signaling. *Development (Cambridge)*, 141(22), 4206–4218. <https://doi.org/10.1242/dev.107086>
- Billiard, J., Moran, R. A., Whitley, M. Z., Chatterjee-Kishore, M., Gillis, K., Brown, E. L., Komm, B. S., & Bodine, P. V. N. (2003). Transcriptional profiling of human osteoblast differentiation. *Journal of Cellular Biochemistry*, 89(2), 389–400. <https://doi.org/10.1002/jcb.10514>
- Blair, H. C., Larrouture, Q. C., Li, Y., Lin, H., Beer-Stoltz, D., Liu, L., Tuan, R. S., Robinson, L. J., Schlesinger, P. H., & Nelson, D. J. (2017). Osteoblast differentiation and bone matrix formation in vivo and in vitro. In *Tissue Engineering - Part B: Reviews* (Vol. 23, Issue 3, pp. 268–280). Mary Ann Liebert Inc. <https://doi.org/10.1089/ten.teb.2016.0454>
- Bonds, D. E., Larson, J. C., Schwartz, A. V., Strotmeyer, E. S., Robbins, J., Rodriguez, B. L., Johnson, K. C., & Margolis, K. L. (2006). Risk of fracture in women with

- type 2 diabetes: The women's health initiative observational study. *Journal of Clinical Endocrinology and Metabolism*, 91(9), 3404–3410. <https://doi.org/10.1210/jc.2006-0614>
- Bonewald, L. F. (2011). The Amazing Osteocyte. *Journal of Bone and Mineral Research*, 26(2), 229–238. <https://doi.org/10.1002/jbmr.320>
- Bonewald, L. F. (2017). The Role of the Osteocyte in Bone and Nonbone Disease. In *Endocrinology and Metabolism Clinics of North America* (Vol. 46, Issue 1, pp. 1–18). W.B. Saunders. <https://doi.org/10.1016/j.ecl.2016.09.003>
- Bonewald, L. F., & Wacker, M. J. (2013). FGF23 production by osteocytes. In *Pediatric Nephrology* (Vol. 28, Issue 4, pp. 563–568). NIH Public Access. <https://doi.org/10.1007/s00467-012-2309-3>
- Bortolin, R. H., Abreu, B. J. D. G. A., Ururahy, M. A. G., De Souza, K. S. C., Bezerra, J. F., Loureiro, M. B., Da Silvada, F. S., Marques, D. E. D. S., De Batista, A. A. S., Oliveira, G., Luchessi, A. D., Lima, V. M. G. D. M., Miranda, C. E. S., Fook, M. V. L., Almeida, M. D. G., De Rezende, L. A., & De Rezende, A. A. (2015). Protection against T1DM-induced bone loss by zinc supplementation: Biomechanical, histomorphometric, and molecular analyses in STZ-induced diabetic rats. *PLoS ONE*, 10(5), e0125349. <https://doi.org/10.1371/journal.pone.0125349>
- Bouillon, R. (1992). Diabetic bone disease. Low turnover osteoporosis related to decreased IGF-I production. *Verhandelingen - Koninklijke Academie Voor Geneeskunde van België*, 54(4).
- Bouleftour, W., Bouet, G., Granito, R. N., Thomas, M., Linossier, M. T., Vandebossche, A., Aubin, J. E., Lafage-Proust, M. hélène, Vico, L., & Malaval, L. (2015). Blocking the expression of both bone sialoprotein (BSP) and osteopontin (OPN) impairs the anabolic action of PTH in mouse calvaria bone. *Journal of Cellular Physiology*, 230(3), 568–577. <https://doi.org/10.1002/jcp.24772>
- Boyce, B. F., & Xing, L. (2007). Biology of RANK, RANKL, and osteoprotegerin. In *Arthritis Research and Therapy* (Vol. 9, Issue SUPPL.1, p. S1). BioMed Central. <https://doi.org/10.1186/ar2165>
- Brotto, M., & Bonewald, L. (2015). Bone and muscle: Interactions beyond mechanical. In *Bone* (Vol. 80, pp. 109–114). Elsevier Inc. <https://doi.org/10.1016/j.bone.2015.02.010>
- Buenzli, P. R., & Sims, N. A. (2015). Quantifying the osteocyte network in the human skeleton. *Bone*, 75, 144–150. <https://doi.org/10.1016/j.bone.2015.02.016>
- Burr, D. B., & Akkus, O. (2013). Bone Morphology and Organization. In *Basic and Applied Bone Biology* (pp. 3–25). Elsevier Inc. <https://doi.org/10.1016/B978-0-12-416015-6.00001-0>

- Burr, D. B., & Alle, M. R. (2019). *Basic and Applied Bone Biology* (Vol. 1). Elsevier.
- Burr, D. B., Bellido, T., & White, K. E. (2015). Bone structure and function. In *Rheumatology: Sixth Edition* (Vols. 1–2, pp. 42–55). Elsevier Inc. <https://doi.org/10.1016/B978-0-323-09138-1.00006-1>
- Callaway, D. A., & Jiang, J. X. (2015). Reactive oxygen species and oxidative stress in osteoclastogenesis, skeletal aging and bone diseases. In *Journal of Bone and Mineral Metabolism* (Vol. 33, Issue 4, pp. 359–370). Springer Tokyo. <https://doi.org/10.1007/s00774-015-0656-4>
- Camp, N. D., James, R. G., Dawson, D. W., Yan, F., Davison, J. M., Houck, S. A., Tang, X., Zheng, N., Major, M. B., & Moon, R. T. (2012). Wilms tumor gene on X chromosome (WTX) inhibits degradation of NRF2 protein through competitive binding to KEAP1 protein. *Journal of Biological Chemistry*, 287(9), 6539–6550. <https://doi.org/10.1074/jbc.M111.316471>
- Carroll, B., & Dunlop, E. A. (2017). The lysosome: a crucial hub for AMPK and mTORC1 signalling. *Biochemical Journal*, 474(9), 1453–1466. <https://doi.org/10.1042/BCJ20160780>
- Cassidy-Stone, A., Chipuk, J. E., Ingerman, E., Song, C., Yoo, C., Kuwana, T., Kurth, M. J., Shaw, J. T., Hinshaw, J. E., Green, D. R., & Nunnari, J. (2008). Chemical Inhibition of the Mitochondrial Division Dynamin Reveals Its Role in Bax/Bak-Dependent Mitochondrial Outer Membrane Permeabilization. *Developmental Cell*, 14(2), 193–204. <https://doi.org/10.1016/j.devcel.2007.11.019>
- Chen, J., Holguin, N., Shi, Y., Silva, M. J., & Long, F. (2015). mTORC2 signaling promotes skeletal growth and bone formation in mice. *Journal of Bone and Mineral Research*, 30(2), 369–378. <https://doi.org/10.1002/jbmr.2348>
- Chen, J., & Long, F. (2015). mTORC1 signaling promotes osteoblast differentiation from preosteoblasts. *PLoS ONE*, 10(6). <https://doi.org/10.1371/journal.pone.0130627>
- Chen, J. R., Shankar, K., Nagarajan, S., Badger, T. M., & Ronis, M. J. J. (2008). Protective effects of estradiol on ethanol-induced bone loss involve inhibition of reactive oxygen species generation in osteoblasts and downstream activation of the extracellular signal-regulated kinase/signal transducer and activator of transcription 3/receptor activator of nuclear factor- κ B ligand signaling cascade. *Journal of Pharmacology and Experimental Therapeutics*, 324(1), 50–59. <https://doi.org/10.1124/jpet.107.130351>
- Chen, S. C., Brooks, R., Houskeeper, J., Bremner, S. K., Dunlop, J., Viollet, B., Logan, P. J., Salt, I. P., Ahmed, S. F., & Yarwood, S. J. (2017). Metformin suppresses adipogenesis through both AMP-activated protein kinase (AMPK)-dependent

- and AMPK-independent mechanisms. *Molecular and Cellular Endocrinology*, 440, 57–68. <https://doi.org/10.1016/j.mce.2016.11.011>
- Chen, W., Sun, Z., Wang, X. J., Jiang, T., Huang, Z., Fang, D., & Zhang, D. D. (2009). Direct Interaction between Nrf2 and p21Cip1/WAF1 Upregulates the Nrf2-Mediated Antioxidant Response. *Molecular Cell*, 34(6), 663–673. <https://doi.org/10.1016/j.molcel.2009.04.029>
- Chen, X., Wang, L., Zhao, K., & Wang, H. (2018). Osteocytogenesis: Roles of Physicochemical Factors, Collagen Cleavage, and Exogenous Molecules. In *Tissue Engineering - Part B: Reviews* (Vol. 24, Issue 3, pp. 215–225). Mary Ann Liebert Inc. <https://doi.org/10.1089/ten.teb.2017.0378>
- Cherian, P. P., Siller-Jackson, A. J., Gu, S., Wang, X., Bonewald, L. F., Sprague, E., & Jiang, J. X. (2005). Mechanical strain opens connexin 43 hemichannels in osteocytes: a novel mechanism for the release of prostaglandin. *Molecular Biology of the Cell*, 16(7), 3100–3106. <https://doi.org/10.1091/mbc.e04-10-0912>
- Civitelli, R. (2008). Cell-cell communication in the osteoblast/osteocyte lineage. In *Archives of Biochemistry and Biophysics* (Vol. 473, Issue 2, pp. 188–192). <https://doi.org/10.1016/j.abb.2008.04.005>
- Clarke, B. (2008). Normal bone anatomy and physiology. In *Clinical journal of the American Society of Nephrology: CJASN: Vol. 3 Suppl 3*. <https://doi.org/10.2215/CJN.04151206>
- Cohen-Kfir, E., Artsi, H., Levin, A., Abramowitz, E., Bajayo, A., Gurt, I., Zhong, L., D'Urso, A., Toiber, D., Mostoslavsky, R., & Dresner-Pollak, R. (2011). Sirt1 is a regulator of bone mass and a repressor of sost encoding for sclerostin, a bone formation inhibitor. *Endocrinology*, 152(12), 4514–4524. <https://doi.org/10.1210/en.2011-1128>
- Cohen, A., Dempster, D. W., Müller, R., Guo, X. E., Nickolas, T. L., Liu, X. S., Zhang, X. H., Wirth, A. J., Van Lenthe, G. H., Kohler, T., McMahon, D. J., Zhou, H., Rubin, M. R., Bilezikian, J. P., Lappe, J. M., Recker, R. R., & Shane, E. (2010). Assessment of trabecular and cortical architecture and mechanical competence of bone by high-resolution peripheral computed tomography: Comparison with transiliac bone biopsy. *Osteoporosis International*, 21(2), 263–273. <https://doi.org/10.1007/s00198-009-0945-7>
- Cooper, J. A., & Sept, D. (2008). New Insights into Mechanism and Regulation of Actin Capping Protein. In *International Review of Cell and Molecular Biology* (Vol. 267, pp. 183–206). [https://doi.org/10.1016/S1937-6448\(08\)00604-7](https://doi.org/10.1016/S1937-6448(08)00604-7)
- Copple, I. M., Lister, A., Obeng, A. D., Kitteringham, N. R., Jenkins, R. E., Layfield, R.,

- Foster, B. J., Goldring, C. E., & Park, B. K. (2010). Physical and functional interaction of sequestosome 1 with Keap1 regulates the Keap1-Nrf2 cell defense pathway. *Journal of Biological Chemistry*, 285(22), 16782–16788. <https://doi.org/10.1074/jbc.M109.096545>
- Cornish, J., Callon, K. E., Bava, U., Lin, C., Naot, D., Hill, B. L., Grey, A. B., Broom, N., Myers, D. E., Nicholson, G. C., & Reid, I. R. (2002). Leptin directly regulates bone cell function in vitro and reduces bone fragility in vivo. In *Journal of Endocrinology* (Vol. 175, Issue 2, pp. 405–415). <https://doi.org/10.1677/joe.0.1750405>
- Cortizo, A. M., Sedlinsky, C., McCarthy, A. D., Blanco, A., & Schurman, L. (2006). Osteogenic actions of the anti-diabetic drug metformin on osteoblasts in culture. *European Journal of Pharmacology*, 536(1–2), 38–46. <https://doi.org/10.1016/j.ejphar.2006.02.030>
- Costello, L. C., Franklin, R. B., Reynolds, M. A., & Chellaiah, M. (2012). The important role of osteoblasts and citrate production in bone formation: “Osteoblast Citration” as a new concept for an old relationship. In *Open Bone Journal* (Vol. 4, Issue 1, pp. 27–34). <https://doi.org/10.2174/1876525401204010027>
- Craigf, R. G., Rowe, D. W., Petersen, D. N., & Kream, B. E. (1989). Insulin increases the steady state level of α -1(I) procollagen mRNA in the osteoblast-rich segment of fetal rat calvaria. *Endocrinology*, 125(3), 1430–1436. <https://doi.org/10.1210/endo-125-3-1430>
- Crane, J. L., Zhao, L., Frye, J. S., Xian, L., Qiu, T., & Cao, X. (2013). IGF-1 Signaling is Essential for Differentiation of Mesenchymal Stem Cells for Peak Bone Mass. *Bone Research*, 1(2), 186–194. <https://doi.org/10.4248/BR201302007>
- Cuadrado, A., Rojo, A. I., Wells, G., Hayes, J. D., Cousin, S. P., Rumsey, W. L., Attucks, O. C., Franklin, S., Levonen, A. L., Kensler, T. W., & Dinkova-Kostova, A. T. (2019). Therapeutic targeting of the NRF2 and KEAP1 partnership in chronic diseases. In *Nature Reviews Drug Discovery* (Vol. 18, Issue 4, pp. 295–317). Nature Publishing Group. <https://doi.org/10.1038/s41573-018-0008-x>
- Cui, S., Tanabe, O., Lim, K.-C., Xu, H. E., Zhou, X. E., Lin, J. D., Shi, L., Schmidt, L., Campbell, A., Shimizu, R., Yamamoto, M., & Engel, J. D. (2014). PGC-1 coactivator activity is required for murine erythropoiesis. *Molecular and Cellular Biology*, 34(11), 1956–1965. <https://doi.org/10.1128/MCB.00247-14>
- Cullinan, S. B., Gordan, J. D., Jin, J., Harper, J. W., & Diehl, J. A. (2004). The Keap1-BTB Protein Is an Adaptor That Bridges Nrf2 to a Cul3-Based E3 Ligase: Oxidative Stress Sensing by a Cul3-Keap1 Ligase. *Molecular and Cellular Biology*, 24(19), 8477–8486. <https://doi.org/10.1128/mcb.24.19.8477-8486.2004>

- Cundy, T., Reid, I. R., & Grey, A. (2014). Metabolic bone disease. In *Clinical Biochemistry: Metabolic and Clinical Aspects: Third Edition* (pp. 604–635). Elsevier Inc. <https://doi.org/10.1016/B978-0-7020-5140-1.00031-6>
- Cunha, J. S., Ferreira, V. M., Maquigussa, E., Naves, M. A., & Boim, M. A. (2014). Effects of high glucose and high insulin concentrations on osteoblast function in vitro. *Cell and Tissue Research*, 358(1), 249–256. <https://doi.org/10.1007/s00441-014-1913-x>
- Dacquin, R., Starbuck, M., Schinke, T., & Karsenty, G. (2002a). Mouse $\alpha 1(I)$ -collagen promoter is the best known promoter to drive efficient Cre recombinase expression in osteoblast. *Developmental Dynamics*, 224(2), 245–251. <https://doi.org/10.1002/dvdy.10100>
- Dacquin, R., Starbuck, M., Schinke, T., & Karsenty, G. (2002b). Mouse $\alpha 1(I)$ -collagen promoter is the best known promoter to drive efficient Cre recombinase expression in osteoblast. *Developmental Dynamics*, 224(2), 245–251. <https://doi.org/10.1002/dvdy.10100>
- Dallas, S. L., & Bonewald, L. F. (2010). Dynamics of the Transition from Osteoblast to Osteocyte. *Annals of the New York Academy of Sciences*, 1192, 437–443. <https://doi.org/10.1111/j.1749-6632.2009.05246.x>
- Dallas, S. L., Prideaux, M., & Bonewald, L. F. (2013). The osteocyte: An endocrine cell . . . and more. In *Endocrine Reviews* (Vol. 34, Issue 5, pp. 658–690). <https://doi.org/10.1210/er.2012-1026>
- Daniele, G., Winnier, D., Mari, A., Bruder, J., Fourcaudot, M., Pengou, Z., Tripathy, D., Jenkinson, C., & Folli, F. (2015). Sclerostin and insulin resistance in prediabetes: Evidence of a cross talk between bone and glucose metabolism. *Diabetes Care*, 38(8), 1509–1517. <https://doi.org/10.2337/dc14-2989>
- Delaney, M. F. (2006). Strategies for the prevention and treatment of osteoporosis during early postmenopause. In *American Journal of Obstetrics and Gynecology* (Vol. 194, Issue 2 SUPPL., pp. S12-23). <https://doi.org/10.1016/j.ajog.2005.08.049>
- Delhanty, P. J. D., van der Eerden, B. C. J., & van Leeuwen, J. P. T. M. (2014). Ghrelin and bone. In *BioFactors* (Vol. 40, Issue 1, pp. 41–48). <https://doi.org/10.1002/biof.1120>
- Denicola, G. M., Karreth, F. A., Humpton, T. J., Gopinathan, A., Wei, C., Frese, K., Mangal, D., Yu, K. H., Yeo, C. J., Calhoun, E. S., Scrimieri, F., Winter, J. M., Hruban, R. H., Iacobuzio-Donahue, C., Kern, S. E., Blair, I. A., & Tuveson, D. A. (2011). Oncogene-induced Nrf2 transcription promotes ROS detoxification and tumorigenesis. *Nature*, 475(7354), 106–110.

<https://doi.org/10.1038/nature10189>

- DIXON, T. F., & PERKINS, H. R. (1952). Citric acid and bone metabolism. *The Biochemical Journal*, *52*(2), 260–265. <https://doi.org/10.1042/bj0520260>
- Domazetovic, V., Marcucci, G., Iantomasi, T., Brandi, M. L., & Vincenzini, M. T. (2017). Oxidative stress in bone remodeling: role of antioxidants. *Clinical Cases in Mineral and Bone Metabolism*, *14*(2), 209. <https://doi.org/10.11138/CCMBM/2017.14.1.209>
- Dos, D. S., Ali, S. M., Kim, D. H., Guertin, D. A., Latek, R. R., Erdjument-Bromage, H., Tempst, P., & Sabatini, D. M. (2004). Rictor, a novel binding partner of mTOR, defines a rapamycin-insensitive and raptor-independent pathway that regulates the cytoskeleton. *Current Biology*, *14*(14), 1296–1302. <https://doi.org/10.1016/j.cub.2004.06.054>
- Drake, M. T., Srinivasan, B., Mödder, U. I., Peterson, J. M., McCready, L. K., Riggs, B. L., Dwyer, D., Stolina, M., Kostenuik, P., & Khosla, S. (2010). Effects of parathyroid hormone treatment on circulating sclerostin levels in postmenopausal women. *Journal of Clinical Endocrinology and Metabolism*, *95*(11), 5056–5062. <https://doi.org/10.1210/jc.2010-0720>
- Ducy, P., Amling, M., Takeda, S., Priemel, M., Schilling, A. F., Beil, F. T., Shen, J., Vinson, C., Rueger, J. M., & Karsenty, G. (2000). Leptin inhibits bone formation through a hypothalamic relay: A central control of bone mass. *Cell*, *100*(2), 197–207. [https://doi.org/10.1016/S0092-8674\(00\)81558-5](https://doi.org/10.1016/S0092-8674(00)81558-5)
- Esen, E., Chen, J., Karner, C. M., Okunade, A. L., Patterson, B. W., & Long, F. (2013). WNT-LRP5 signaling induces warburg effect through mTORC2 activation during osteoblast differentiation. *Cell Metabolism*, *17*(5), 745–755. <https://doi.org/10.1016/j.cmet.2013.03.017>
- Esen, E., Lee, S. Y., Wice, B. M., & Long, F. (2015). PTH Promotes Bone Anabolism by Stimulating Aerobic Glycolysis via IGF Signaling. *Journal of Bone and Mineral Research*, *30*(11), 1959–1968. <https://doi.org/10.1002/jbmr.2556>
- Esen, E., & Long, F. (2014). Aerobic glycolysis in osteoblasts. *Current Osteoporosis Reports*, *12*(4), 433–438. <https://doi.org/10.1007/s11914-014-0235-y>
- Esterbauer, H., Oberkofler, H., Krempler, F., & Patsch, W. (1999). Human peroxisome proliferator activated receptor gamma coactivator 1 (PPARGC1) gene: cDNA sequence, genomic organization, chromosomal localization, and tissue expression. *Genomics*, *62*(1), 98–102. <https://doi.org/10.1006/geno.1999.5977>
- Fan, M., Rhee, J., St-Pierre, J., Handschin, C., Puigserver, P., Lin, J., Jäeger, S.,

- Erdjument-Bromage, H., Tempst, P., & Spiegelman, B. M. (2004). Suppression of mitochondrial respiration through recruitment of p160 myb binding protein to PGC-1 α : Modulation by p38 MAPK. *Genes and Development*, *18*(3), 278–289. <https://doi.org/10.1101/gad.1152204>
- Faul, C., Amaral, A. P., Oskouei, B., Hu, M. C., Sloan, A., Isakova, T., Gutiérrez, O. M., Aguilon-Prada, R., Lincoln, J., Hare, J. M., Mundel, P., Morales, A., Scialla, J., Fischer, M., Soliman, E. Z., Chen, J., Go, A. S., Rosas, S. E., Nessel, L., ... Wolf, M. (2011). FGF23 induces left ventricular hypertrophy. *Journal of Clinical Investigation*, *121*(11), 4393–4408. <https://doi.org/10.1172/JCI46122>
- Fedarko, N. S. (2013). Osteoblast/Osteoclast Development and Function in Osteogenesis Imperfecta. In *Osteogenesis Imperfecta: A Translational Approach to Brittle Bone Disease* (pp. 45–56). Elsevier Inc. <https://doi.org/10.1016/B978-0-12-397165-4.00005-8>
- Felson, D. T., Zhang, Y., Hannan, M. T., & Anderson, J. J. (1993). Effects of weight and body mass index on bone mineral density in men and women: The framingham study. *Journal of Bone and Mineral Research*, *8*(5), 567–573. <https://doi.org/10.1002/jbmr.5650080507>
- Feng, L., Wang, Y., Zhou, J., Tian, B., & Xia, B. (2018). Screening of differentially expressed genes in male idiopathic osteoporosis via RNA sequencing. *Molecular Medicine Reports*, *18*(1), 67–76. <https://doi.org/10.3892/mmr.2018.8985>
- Finkel, T., & Holbrook, N. J. (2000). Oxidants, oxidative stress and the biology of ageing. In *Nature* (Vol. 408, Issue 6809, pp. 239–247). <https://doi.org/10.1038/35041687>
- FLANAGAN, B., & NICHOLS, G. (1964). METABOLIC STUDIES OF BONE IN VITRO. V. GLUCOSE METABOLISM AND COLLAGEN BIOSYNTHESIS. *The Journal of Biological Chemistry*, *239*, 1261–1265. <http://www.ncbi.nlm.nih.gov/pubmed/14165936>
- Fleisch, H. (2003). Bisphosphonates in osteoporosis. In *European Spine Journal* (Vol. 12, Issue SUPPL. 2, p. S142). Springer. <https://doi.org/10.1007/s00586-003-0622-z>
- Fowlkes, J. L., Bunn, R. C., Liu, L., Wahl, E. C., Coleman, H. N., Cockrell, G. E., Perrien, D. S., Lumpkin, C. K., & Thrailkill, K. M. (2008). Runt-related transcription factor 2 (RUNX2) and RUNX2-related osteogenic genes are down-regulated throughout osteogenesis in type 1 diabetes mellitus. *Endocrinology*, *149*(4), 1697–1704. <https://doi.org/10.1210/en.2007-1408>
- Fox, R. J., Miller, D. H., Phillips, J. T., Hutchinson, M., Havrdova, E., Kita, M., Yang, M.,

- Raghupathi, K., Novas, M., Sweetser, M. T., Viglietta, V., & Dawson, K. T. (2012). Placebo-controlled phase 3 study of oral BG-12 or glatiramer in multiple sclerosis. *New England Journal of Medicine*, *367*(12), 1087–1097. <https://doi.org/10.1056/NEJMoa1206328>
- Fritton, S. P., & Weinbaum, S. (2009). Fluid and Solute Transport in Bone: Flow-Induced Mechanotransduction. *Annual Review of Fluid Mechanics*, *41*(1), 347–374. <https://doi.org/10.1146/annurev.fluid.010908.165136>
- Fronczek-Sokół, J., & Pytlik, M. (2014). Effect of glimepiride on the skeletal system of ovariectomized and non-ovariectomized rats. *Pharmacological Reports*, *66*(3), 412–417. <https://doi.org/10.1016/j.pharep.2013.12.013>
- Fulzele, K., Lai, F., Dedic, C., Saini, V., Uda, Y., Shi, C., Tuck, P., Aronson, J. L., Liu, X., Spatz, J. M., Wein, M. N., & Divieti Pajevic, P. (2017). Osteocyte-Secreted Wnt Signaling Inhibitor Sclerostin Contributes to Beige Adipogenesis in Peripheral Fat Depots. *Journal of Bone and Mineral Research*, *32*(2), 373–384. <https://doi.org/10.1002/jbmr.3001>
- Fulzele, K., Riddle, R. C., DiGirolamo, D. J., Cao, X., Wan, C., Chen, D., Faugere, M. C., Aja, S., Hussain, M. A., Brüning, J. C., & Clemens, T. L. (2010). Insulin Receptor Signaling in Osteoblasts Regulates Postnatal Bone Acquisition and Body Composition. *Cell*, *142*(2), 309–319. <https://doi.org/10.1016/j.cell.2010.06.002>
- Galloway, C. A., Lee, H., & Yoon, Y. (2012). Mitochondrial morphology-emerging role in bioenergetics. In *Free Radical Biology and Medicine* (Vol. 53, Issue 12, pp. 2218–2228). <https://doi.org/10.1016/j.freeradbiomed.2012.09.035>
- Gámez, B., Rodríguez-Carballo, E., Graupera, M., Rosa, J. L., Ventura, F., Rodríguez-Carballo, E., Graupera, M., Rosa, J. L., & Ventura, F. (2016). Class I PI-3-Kinase Signaling Is Critical for Bone Formation Through Regulation of SMAD1 Activity in Osteoblasts. *Journal of Bone and Mineral Research*, *31*(8), 1617–1630. <https://doi.org/10.1002/jbmr.2819>
- García-Martín, A., Rozas-Moreno, P., Reyes-García, R., Morales-Santana, S., García-Fontana, B., García-Salcedo, J. A., & Muñoz-Torres, M. (2012). Circulating levels of sclerostin are increased in patients with type 2 diabetes mellitus. *Journal of Clinical Endocrinology and Metabolism*, *97*(1), 234–241. <https://doi.org/10.1210/jc.2011-2186>
- Gattineni, J., Bates, C., Twombly, K., Dwarakanath, V., Robinson, M. L., Goetz, R., Mohammadi, M., & Baum, M. (2009). FGF23 decreases renal NaPi-2a and NaPi-2c expression and induces hypophosphatemia in vivo predominantly via FGF receptor 1. *American Journal of Physiology - Renal Physiology*, *297*(2). <https://doi.org/10.1152/ajprenal.90742.2008>

- Genetos, D. C., Geist, D. J., Liu, D., Donahue, H. J., & Duncan, R. L. (2005). Fluid shear-induced ATP secretion mediates prostaglandin release in MC3T3-E1 osteoblasts. *Journal of Bone and Mineral Research : The Official Journal of the American Society for Bone and Mineral Research*, 20(1), 41–49. <https://doi.org/10.1359/JBMR.041009>
- Gerhart-Hines, Z., Rodgers, J. T., Bare, O., Lerin, C., Kim, S.-H., Mostoslavsky, R., Alt, F. W., Wu, Z., & Puigserver, P. (2007). Metabolic control of muscle mitochondrial function and fatty acid oxidation through SIRT1/PGC-1alpha. *The EMBO Journal*, 26(7), 1913–1923. <https://doi.org/10.1038/sj.emboj.7601633>
- Ghilardi, N., Ziegler, S., Wiestner, A., Stoffel, R., Heim, M. H., & Skoda, R. C. (1996). Defective STAT signaling by the leptin receptor in diabetic mice. *Proceedings of the National Academy of Sciences of the United States of America*, 93(13), 6231–6235. <https://doi.org/10.1073/pnas.93.13.6231>
- Gluhak-Heinrich, J., Ye, L., Bonewald, L. F., Feng, J. Q., MacDougall, M., Harris, S. E., & Pavlin, D. (2003). Mechanical Loading Stimulates Dentin Matrix Protein 1 (DMP1) Expression in Osteocytes In Vivo. *Journal of Bone and Mineral Research*, 18(5), 807–817. <https://doi.org/10.1359/jbmr.2003.18.5.807>
- Gold, R., Kappos, L., Arnold, D. L., Bar-Or, A., Giovannoni, G., Selmaj, K., Tornatore, C., Sweetser, M. T., Yang, M., Sheikh, S. I., & Dawson, K. T. (2012). Placebo-controlled phase 3 study of oral BG-12 for relapsing multiple sclerosis. *New England Journal of Medicine*, 367(12), 1098–1107. <https://doi.org/10.1056/NEJMoa1114287>
- Gomes, L. C., Benedetto, G. Di, & Scorrano, L. (2011). During autophagy mitochondria elongate, are spared from degradation and sustain cell viability. *Nature Cell Biology*, 13(5), 589–598. <https://doi.org/10.1038/ncb2220>
- Gorrini, C., Baniasadi, P. S., Harris, I. S., Silvester, J., Inoue, S., Snow, B., Joshi, P. A., Wakeham, A., Molyneux, S. D., Martin, B., Bouwman, P., Cescon, D. W., Elia, A. J., Winterton-Perks, Z., Cruickshank, J., Brenner, D., Tseng, A., Musgrave, M., Berman, H. K., ... Gauthier, M. L. (2013). BRCA1 interacts with Nrf2 to regulate antioxidant signaling and cell survival. *Journal of Experimental Medicine*, 210(8), 1529–1544. <https://doi.org/10.1084/jem.20121337>
- Gowen, L. C., Petersen, D. N., Mansolf, A. L., Qi, H., Stock, J. L., Tkalcevic, G. T., Simmons, H. A., Crawford, D. T., Chidsey-Frink, K. L., Ke, H. Z., McNeish, J. D., & Brown, T. A. (2003). Targeted disruption of the osteoblast/osteocyte factor 45 gene (Of45) results in increased bone formation and bone mass. *Journal of Biological Chemistry*, 278(3), 1998–2007. <https://doi.org/10.1074/jbc.M203250200>
- Grassi, F., Tell, G., Robbie-Ryan, M., Gao, Y., Terauchi, M., Yang, X., Romanello, M.,

- Jones, D. P., Weitzmann, M. N., & Pacifici, R. (2007). Oxidative stress causes bone loss in estrogen-deficient mice through enhanced bone marrow dendritic cell activation. *Proceedings of the National Academy of Sciences of the United States of America*, *104*(38), 15087–15092. <https://doi.org/10.1073/pnas.0703610104>
- Grosso, A., Burger, M. G., Lunger, A., Schaefer, D. J., Banfi, A., & Di Maggio, N. (2017). It takes two to tango: Coupling of angiogenesis and osteogenesis for bone regeneration. In *Frontiers in Bioengineering and Biotechnology* (Vol. 5, Issue NOV, p. 68). Frontiers Media S.A. <https://doi.org/10.3389/fbioe.2017.00068>
- Gunaratnam, K., Vidal, C., Boadle, R., Thekkedam, C., & Duque, G. (2013). Mechanisms of palmitate-induced cell death in human osteoblasts. *Biology Open*, *2*(12), 1382–1389. <https://doi.org/10.1242/bio.20136700>
- Guntur, A. R., Gerencser, A. A., Le, P. T., DeMambro, V. E., Bornstein, S. A., Mookerjee, S. A., Maridas, D. E., Clemmons, D. E., Brand, M. D., & Rosen, C. J. (2018). Osteoblast-like MC3T3-E1 Cells Prefer Glycolysis for ATP Production but Adipocyte-like 3T3-L1 Cells Prefer Oxidative Phosphorylation. *Journal of Bone and Mineral Research*, *33*(6), 1052–1065. <https://doi.org/10.1002/jbmr.3390>
- Guntur, A. R., Le, P. T., Farber, C. R., & Rosen, C. J. (2014). Bioenergetics During Calvarial Osteoblast Differentiation Reflect Strain Differences in Bone Mass. *Endocrinology*, *155*(5), 1589–1595. <https://doi.org/10.1210/en.2013-1974>
- Guntur, A. R., & Rosen, C. J. (2012). Bone as an endocrine organ. In *Endocrine Practice* (Vol. 18, Issue 5, pp. 758–762). <https://doi.org/10.4158/EP12141.RA>
- Guo, D., Keightley, A., Guthrie, J., Veno, P. A., Harris, S. E., & Bonewald, L. F. (2010a). Identification of osteocyte-selective proteins. *Proteomics*, *10*(20), 3688–3698. <https://doi.org/10.1002/pmic.201000306>
- Guo, D., Keightley, A., Guthrie, J., Veno, P. A., Harris, S. E., & Bonewald, L. F. (2010b). Identification of osteocyte-selective proteins. *Proteomics*, *10*(20), 3688–3698. <https://doi.org/10.1002/pmic.201000306>
- Guttman, M., Amit, I., Garber, M., French, C., Lin, M. F., Feldser, D., Huarte, M., Zuk, O., Carey, B. W., Cassady, J. P., Cabili, M. N., Jaenisch, R., Mikkelsen, T. S., Jacks, T., Hacohen, N., Bernstein, B. E., Kellis, M., Regev, A., Rinn, J. L., & Lander, E. S. (2009). Chromatin signature reveals over a thousand highly conserved large non-coding RNAs in mammals. *Nature*, *458*(7235), 223–227. <https://doi.org/10.1038/nature07672>
- Hall, S. L., & Greendale, G. A. (1998). The relation of dietary vitamin C intake to bone mineral density: Results from the PEPI study. *Calcified Tissue International*, *63*(3), 183–189. <https://doi.org/10.1007/s002239900512>

- Hamada, Y., Kitazawa, S., Kitazawa, R., Fujii, H., Kasuga, M., & Fukagawa, M. (2007). Histomorphometric analysis of diabetic osteopenia in streptozotocin-induced diabetic mice: A possible role of oxidative stress. *Bone*, *40*(5), 1408–1414. <https://doi.org/10.1016/j.bone.2006.12.057>
- Hara, K., Maruki, Y., Long, X., Yoshino, K. ichi, Oshiro, N., Hidayat, S., Tokunaga, C., Avruch, J., & Yonezawa, K. (2002). Raptor, a binding partner of target of rapamycin (TOR), mediates TOR action. *Cell*, *110*(2), 177–189. [https://doi.org/10.1016/S0092-8674\(02\)00833-4](https://doi.org/10.1016/S0092-8674(02)00833-4)
- Hardie, D. G. (2018). Keeping the home fires burning: AMP-activated protein kinase. *Journal of the Royal Society, Interface*, *15*(138). <https://doi.org/10.1098/rsif.2017.0774>
- Harris, N. L., Rattray, K. R., Tye, C. E., Underhill, T. M., Somerman, M. J., D’Errico, J. A., Chambers, A. F., Hunter, G. K., & Goldberg, H. A. (2000). Functional analysis of bone sialoprotein: Identification of the hydroxyapatite-nucleating and cell-binding domains by recombinant peptide expression and site-directed mutagenesis. *Bone*, *27*(6), 795–802. [https://doi.org/10.1016/S8756-3282\(00\)00392-6](https://doi.org/10.1016/S8756-3282(00)00392-6)
- Hast, B. E., Goldfarb, D., Mulvaney, K. M., Hast, M. A., Siesser, P. F., Yan, F., Hayes, D. N., & Major, M. B. (2013). Proteomic analysis of ubiquitin ligase KEAP1 reveals associated proteins that inhibit NRF2 ubiquitination. *Cancer Research*, *73*(7), 2199–2210. <https://doi.org/10.1158/0008-5472.CAN-12-4400>
- Hauge, E. M., Qvesel, D., Eriksen, E. F., Mosekilde, L., & Melsen, F. (2001). Cancellous bone remodeling occurs in specialized compartments lined by cells expressing osteoblastic markers. *Journal of Bone and Mineral Research*, *16*(9), 1575–1582. <https://doi.org/10.1359/jbmr.2001.16.9.1575>
- Hayes, J. D., & Dinkova-Kostova, A. T. (2014). The Nrf2 regulatory network provides an interface between redox and intermediary metabolism. In *Trends in Biochemical Sciences* (Vol. 39, Issue 4, pp. 199–218). Elsevier Ltd. <https://doi.org/10.1016/j.tibs.2014.02.002>
- He, G., Dahl, T., Veis, A., & George, A. (2003). Dentin Matrix Protein 1 Initiates Hydroxyapatite Formation In Vitro. *Connective Tissue Research*, *44*(1), 240–245. <https://doi.org/10.1080/03008200390181726>
- Heino, T. J., Hentunen, T. A., & Väänänen, H. K. (2004). Conditioned medium from osteocytes stimulates the proliferation of bone marrow mesenchymal stem cells and their differentiation into osteoblasts. *Experimental Cell Research*, *294*(2), 458–468. <https://doi.org/10.1016/j.yexcr.2003.11.016>
- Hermanson, O., Glass, C. K., & Rosenfeld, M. G. (2002). Nuclear receptor

- coregulators: multiple modes of modification. *Trends in Endocrinology and Metabolism: TEM*, 13(2), 55–60. [https://doi.org/10.1016/s1043-2760\(01\)00527-6](https://doi.org/10.1016/s1043-2760(01)00527-6)
- Hie, M., Iitsuka, N., Otsuka, T., & Tsukamoto, I. (2011). Insulin-dependent diabetes mellitus decreases osteoblastogenesis associated with the inhibition of Wnt signaling through increased expression of Sost and Dkk1 and inhibition of Akt activation. *International Journal of Molecular Medicine*, 28(3), 455–462. <https://doi.org/10.3892/ijmm.2011.697>
- Hie, M., Shimono, M., Fujii, K., & Tsukamoto, I. (2007). Increased cathepsin K and tartrate-resistant acid phosphatase expression in bone of streptozotocin-induced diabetic rats. *Bone*, 41(6), 1045–1050. <https://doi.org/10.1016/j.bone.2007.08.030>
- Hinoi, E., Fujimori, S., Wang, L., Hojo, H., Uno, K., & Yoneda, Y. (2006). Nrf2 negatively regulates osteoblast differentiation via interfering with Runx2-dependent transcriptional activation. *The Journal of Biological Chemistry*, 281(26), 18015–18024. <https://doi.org/10.1074/jbc.M600603200>
- Hinoi, E., Takarada, T., Fujimori, S., Wang, L., Iemata, M., Uno, K., & Yoneda, Y. (2007). Nuclear factor E2 p45-related factor 2 negatively regulates chondrogenesis. *Bone*, 40(2), 337–344. <https://doi.org/10.1016/j.bone.2006.08.016>
- Hirao, M., Hashimoto, J., Yamasaki, N., Ando, W., Tsuboi, H., Myoui, A., & Yoshikawa, H. (2007). Oxygen tension is an important mediator of the transformation of osteoblasts to osteocytes. *Journal of Bone and Mineral Metabolism*, 25(5), 266–276. <https://doi.org/10.1007/s00774-007-0765-9>
- Hirotsu, Y., Katsuoka, F., Funayama, R., Nagashima, T., Nishida, Y., Nakayama, K., Engel, J. D., & Yamamoto, M. (2012). Nrf2-MafG heterodimers contribute globally to antioxidant and metabolic networks. *Nucleic Acids Research*, 40(20), 10228–10239. <https://doi.org/10.1093/nar/gks827>
- Holmbeck, K., Bianco, P., Pidoux, I., Inoue, S., Billingham, R. C., Wu, W., Chrysovergis, K., Yamada, S., Birkedal-Hansen, H., & Poole, A. R. (2005). The metalloproteinase MT1-MMP is required for normal development and maintenance of osteocyte processes in bone. *Journal of Cell Science*, 118(1), 147–156. <https://doi.org/10.1242/jcs.01581>
- Holmström, K. M., Baird, L., Zhang, Y., Hargreaves, I., Chalasani, A., Land, J. M., Stanyer, L., Yamamoto, M., Dinkova-Kostova, A. T., & Abramov, A. Y. (2013). Nrf2 impacts cellular bioenergetics by controlling substrate availability for mitochondrial respiration. *Biology Open*, 2(8), 761–770. <https://doi.org/10.1242/bio.20134853>

- Holtrop, M. E. (1975). The ultrastructure of bone. *Annals of Clinical and Laboratory Science*, 5(4), 264–271. <http://www.ncbi.nlm.nih.gov/pubmed/1163991>
- Höxtermann, S., Nüchel, C., & Altmeyer, P. (1998). Fumaric acid esters suppress peripheral CD4- and CD8-positive lymphocytes in psoriasis. *Dermatology*, 196(2), 223–230. <https://doi.org/10.1159/000017903>
- Huang, H.-C., Nguyen, T., & Pickett, C. B. (2002). Phosphorylation of Nrf2 at Ser-40 by protein kinase C regulates antioxidant response element-mediated transcription. *The Journal of Biological Chemistry*, 277(45), 42769–42774. <https://doi.org/10.1074/jbc.M206911200>
- Huang, P. L., Chen, Y. C., Chen, L. H., Juan, C. C., Ku, H. H., Wang, S. T., Chiou, S. H., Chiou, G. Y., Chi, C. W., Hsu, C. C., Lee, H. C., Chen, L. K., & Kao, C. L. (2011). PGC-1 α mediates differentiation of mesenchymal stem cells to brown adipose cells. *Journal of Atherosclerosis and Thrombosis*, 18(11), 966–980. <https://doi.org/10.5551/jat.7401>
- Huang, W., Yang, S., Shao, J., & Li, Y. P. (2007). Signaling and transcriptional regulation in osteoblast commitment and differentiation. In *Frontiers in Bioscience* (Vol. 12, Issue 8, pp. 3068–3092). NIH Public Access. <https://doi.org/10.2741/2296>
- Hyeon, S., Lee, H., Yang, Y., & Jeong, W. (2013). Nrf2 deficiency induces oxidative stress and promotes RANKL-induced osteoclast differentiation. *Free Radical Biology and Medicine*, 65, 789–799. <https://doi.org/10.1016/j.freeradbiomed.2013.08.005>
- Ibáñez, L., Ferrándiz, M. L., Brines, R., Guede, D., Cuadrado, A., & Alcaraz, M. J. (2014). Effects of Nrf2 Deficiency on Bone Microarchitecture in an Experimental Model of Osteoporosis. *Oxidative Medicine and Cellular Longevity*, 2014. <https://doi.org/10.1155/2014/726590>
- Ito, K., & Suda, T. (2014). Metabolic requirements for the maintenance of self-renewing stem cells. In *Nature Reviews Molecular Cell Biology* (Vol. 15, Issue 4, pp. 243–256). Nature Publishing Group. <https://doi.org/10.1038/nrm3772>
- Itoh, K., Igarashi, K., Hayashi, N., Nishizawa, M., & Yamamoto, M. (1995). Cloning and characterization of a novel erythroid cell-derived CNC family transcription factor heterodimerizing with the small Maf family proteins. *Molecular and Cellular Biology*, 15(8), 4184–4193. <https://doi.org/10.1128/mcb.15.8.4184>
- Itoh, Ken, Wakabayashi, N., Katoh, Y., Ishii, T., O'Connor, T., & Yamamoto, M. (2003). Keap1 regulates both cytoplasmic-nuclear shuttling and degradation of Nrf2 in response to electrophiles. *Genes to Cells*, 8(4), 379–391. <https://doi.org/10.1046/j.1365-2443.2003.00640.x>

- Iyer, S., Ambrogini, E., Bartell, S. M., Han, L., Roberson, P. K., De Cabo, R., Jilka, R. L., Weinstein, R. S., O'Brien, C. A., Manolagas, S. C., & Almeida, M. (2013). FOXOs attenuate bone formation by suppressing Wnt signaling. *Journal of Clinical Investigation*, *123*(8), 3409–3419. <https://doi.org/10.1172/JCI68049>
- J., P., K., H., C., H., Z., P., Q.X., G., Q., J., G., L., J., M., Z., Q., C., B., Q.N., D., Z.H., B., X.Y., J., D.L., F., Peng, J., Hui, K., Hao, C., Peng, Z., Gao, Q. X., ... Fu, D. L. (2016). Low bone turnover and reduced angiogenesis in streptozotocin-induced osteoporotic mice. *Connective Tissue Research*, *57*(4), 277–289. <https://doi.org/10.3109/03008207.2016.1171858> LK - http://WT3CF4ET2L.search.serialssolutions.com?sid=EMBASE&issn=16078438&id=doi:10.3109%2F03008207.2016.1171858&atitle=Low+bone+turnover+and+reduced+angiogenesis+in+streptozotocin-induced+osteoporotic+mice&stitle=Connect.+Tissue+Res.&title=Connective+Tissue+Research&volume=57&issue=4&page=277&epage=289&a_ualast=Peng&aufirst=Jia&aunit=J.&aufull=Peng+J.&coden=CVTRB&isbn=&pages=277-289&date=2016&aunit1=J&aunitm=
- Jager, S., Handschin, C., St.-Pierre, J., & Spiegelman, B. M. (2007). AMP-activated protein kinase (AMPK) action in skeletal muscle via direct phosphorylation of PGC-1. *Proceedings of the National Academy of Sciences*, *104*(29), 12017–12022. <https://doi.org/10.1073/pnas.0705070104>
- Jang, J., Wang, Y., Kim, H.-S., Lalli, M. A., & Kosik, K. S. (2014). Nrf2, a Regulator of the Proteasome, Controls Self-Renewal and Pluripotency in Human Embryonic Stem Cells. *STEM CELLS*, *32*(10), 2616–2625. <https://doi.org/10.1002/stem.1764>
- Jang, W. G., Kim, E. J., Bae, I. H., Lee, K. N., Kim, Y. D., Kim, D. K., Kim, S. H., Lee, C. H., Franceschi, R. T., Choi, H. S., & Koh, J. T. (2011). Metformin induces osteoblast differentiation via orphan nuclear receptor SHP-mediated transactivation of Runx2. *Bone*, *48*(4), 885–893. <https://doi.org/10.1016/j.bone.2010.12.003>
- Jang, W. G., Kim, E. J., Lee, K. N., Son, H. J., & Koh, J. T. (2011). AMP-activated protein kinase (AMPK) positively regulates osteoblast differentiation via induction of Dlx5-dependent Runx2 expression in MC3T3E1 cells. *Biochemical and Biophysical Research Communications*, *404*(4), 1004–1009. <https://doi.org/10.1016/j.bbrc.2010.12.099>
- Janghorbani, M., Van Dam, R. M., Willett, W. C., & Hu, F. B. (2007). Systematic review of type 1 and type 2 diabetes mellitus and risk of fracture. In *American Journal of Epidemiology* (Vol. 166, Issue 5, pp. 495–505). <https://doi.org/10.1093/aje/kwm106>
- Jaramillo, M. C., & Zhang, D. D. (2013). The emerging role of the Nrf2-Keap1 signaling

- pathway in cancer. In *Genes and Development* (Vol. 27, Issue 20, pp. 2179–2191). Cold Spring Harbor Laboratory Press. <https://doi.org/10.1101/gad.225680.113>
- Jerković, I., Szabo, Q., Bantignies, F., & Cavalli, G. (2020). Higher-Order Chromosomal Structures Mediate Genome Function. In *Journal of Molecular Biology* (Vol. 432, Issue 3, pp. 676–681). Academic Press. <https://doi.org/10.1016/j.jmb.2019.10.014>
- Jeyabalan, J., Shah, M., Violette, B., & Chenu, C. (2012). AMP-activated protein kinase pathway and bone metabolism. In *Journal of Endocrinology* (Vol. 212, Issue 3, pp. 277–290). <https://doi.org/10.1530/JOE-11-0306>
- Ji, H. J., Lee, S. H., Han, B. K., Zang, H. L., Seo, S. B., Kyung, M. W., Ryoo, H. M., Kim, G. S., & Baek, J. H. (2008). N-acetylcysteine stimulates osteoblastic differentiation of mouse calvarial cells. *Journal of Cellular Biochemistry*, 103(4), 1246–1255. <https://doi.org/10.1002/jcb.21508>
- Jilka, R. L., Noble, B., & Weinstein, R. S. (2013). Osteocyte apoptosis. In *Bone* (Vol. 54, Issue 2, pp. 264–271). <https://doi.org/10.1016/j.bone.2012.11.038>
- Jilka, R. L., & O'Brien, C. A. (2016). The Role of Osteocytes in Age-Related Bone Loss. In *Current Osteoporosis Reports* (Vol. 14, Issue 1, pp. 16–25). Current Medicine Group LLC 1. <https://doi.org/10.1007/s11914-016-0297-0>
- Kajimura, D., Lee, H. W., Riley, K. J., Arteaga-Solis, E., Ferron, M., Zhou, B., Clarke, C. J., Hannun, Y. A., Depinho, R. A., Guo, E. X., Mann, J. J., & Karsenty, G. (2013). Adiponectin regulates bone mass via opposite central and peripheral mechanisms through foxo1. *Cell Metabolism*, 17(6), 901–915. <https://doi.org/10.1016/j.cmet.2013.04.009>
- Kalaitzoglou, E., Popescu, I., Bunn, R. C., Fowlkes, J. L., & Thrailkill, K. M. (2016). Effects of Type 1 Diabetes on Osteoblasts, Osteocytes, and Osteoclasts. *Current Osteoporosis Reports*, 14(6), 310–319. <https://doi.org/10.1007/s11914-016-0329-9>
- Kamioka, H., Sugawara, Y., Honjo, T., Yamashiro, T., & Takano-Yamamoto, T. (2004). Terminal differentiation of osteoblasts to osteocytes is accompanied by dramatic changes in the distribution of actin-binding proteins. *Journal of Bone and Mineral Research*, 19(3), 471–478. <https://doi.org/10.1359/JBMR.040128>
- Kanazawa, I., Takeno, A., Tanaka, K. I., Notsu, M., & Sugimoto, T. (2018). Osteoblast AMP-activated protein kinase regulates postnatal skeletal development in male mice. *Endocrinology*, 159(2), 597–608. <https://doi.org/10.1210/en.2017-00357>
- Kanazawa, I., Yamaguchi, T., Yano, S., Yamauchi, M., Yamamoto, M., & Sugimoto, T. (2007). Adiponectin and AMP kinase activator stimulate proliferation,

- differentiation, and mineralization of osteoblastic MC3T3-E1 cells. *BMC Cell Biology*, 8. <https://doi.org/10.1186/1471-2121-8-51>
- Kannan, M. B., Solovieva, V., & Blank, V. (2012). The small MAF transcription factors MAFF, MAFG and MAFK: Current knowledge and perspectives. In *Biochimica et Biophysica Acta - Molecular Cell Research* (Vol. 1823, Issue 10, pp. 1841–1846). Elsevier. <https://doi.org/10.1016/j.bbamcr.2012.06.012>
- Kärkkäinen, V., Pomeschchik, Y., Savchenko, E., Dhungana, H., Kurronen, A., Lehtonen, S., Naumenko, N., Tavi, P., Levonen, A.-L., Yamamoto, M., Malm, T., Magga, J., Kanninen, K. M., & Koistinaho, J. (2014). Nrf2 Regulates Neurogenesis and Protects Neural Progenitor Cells Against A β Toxicity. *STEM CELLS*, 32(7), 1904–1916. <https://doi.org/10.1002/stem.1666>
- Karner, C. M., Esen, E., Chen, J., Hsu, F. F., Turk, J., & Long, F. (2016). Wnt protein signaling reduces nuclear Acetyl-CoA Levels to suppress gene expression during osteoblast differentiation. *Journal of Biological Chemistry*, 291(25), 13028–13039. <https://doi.org/10.1074/jbc.M115.708578>
- Karsenty, G. (2014). Bone as an Endocrine Organ. In *Cellular Endocrinology in Health and Disease* (pp. 193–205). Elsevier Inc. <https://doi.org/10.1016/B978-0-12-408134-5.00012-3>
- Kasai, T., Bandow, K., Suzuki, H., Chiba, N., Kakimoto, K., Ohnishi, T., Kawamoto, S. I., Nagaoka, E., & Matsuguchi, T. (2009). Osteoblast differentiation is functionally associated with decreased AMP kinase activity. *Journal of Cellular Physiology*, 221(3), 740–749. <https://doi.org/10.1002/jcp.21917>
- Kato, Y., Boskey, A., Spevak, L., Dallas, M., Hori, M., & Bonewald, L. F. (2001). Establishment of an osteoid preosteocyte-like cell MLO-A5 that spontaneously mineralizes in culture. *J Bone Miner Res*, 16(9), 1622–1633. http://www.ncbi.nlm.nih.gov/entrez/query.fcgi?cmd=Retrieve&db=PubMed&dopt=Citation&list_uids=11547831
- Kato, Yoichi, Windle, J. J., Koop, B. A., Mundy, G. R., & Bonewald, L. F. (1997). Establishment of an osteocyte-like cell line, MLO-Y4. *Journal of Bone and Mineral Research: The Official Journal of the American Society for Bone and Mineral Research*, 12(12), 2014–2023. <https://doi.org/10.1359/jbmr.1997.12.12.2014>
- Katsuoka, F., Motohashi, H., Ishii, T., Aburatani, H., Engel, J. D., & Yamamoto, M. (2005). Genetic Evidence that Small Maf Proteins Are Essential for the Activation of Antioxidant Response Element-Dependent Genes. *Molecular and Cellular Biology*, 25(18), 8044–8051. <https://doi.org/10.1128/mcb.25.18.8044-8051.2005>

- Kawatani, Y., Suzuki, T., Shimizu, R., Kelly, V. P., & Yamamoto, M. (2011). Nrf2 and selenoproteins are essential for maintaining oxidative homeostasis in erythrocytes and protecting against hemolytic anemia. *Blood*, *117*(3), 986–996. <https://doi.org/10.1182/blood-2010-05-285817>
- Keenan, H. A., & Maddaloni, E. (2016). Bone Microarchitecture in Type 1 Diabetes: It Is Complicated. In *Current Osteoporosis Reports* (Vol. 14, Issue 6, pp. 351–358). Current Medicine Group LLC 1. <https://doi.org/10.1007/s11914-016-0338-8>
- Kemink, S. A. G., Hermus, A. R. M. M., Swinkels, L. M. J. W., Lutterman, J. A., & Smals, A. G. H. (2000). Osteopenia in insulin-dependent diabetes mellitus: Prevalence and aspects of pathophysiology. *Journal of Endocrinological Investigation*, *23*(5), 295–303. <https://doi.org/10.1007/BF03343726>
- Kennel, K. A., & Drake, M. T. (2009). Adverse Effects of Bisphosphonates: Implications for Osteoporosis Management. *Mayo Clinic Proceedings*, *84*(7), 632–638. [https://doi.org/10.1016/s0025-6196\(11\)60752-0](https://doi.org/10.1016/s0025-6196(11)60752-0)
- Khalid, A. B., & Krum, S. A. (2016). Estrogen receptors alpha and beta in bone. In *Bone* (Vol. 87, pp. 130–135). Elsevier Inc. <https://doi.org/10.1016/j.bone.2016.03.016>
- Khan, M. P., Kumar Singh, A., Joharapurkar, A. A., Yadav, M., Shree, S., Kumar, H., Gurjar, A., Mishra, J. S., Tiwari, M. C., Kumar Nagar, G., Kumar, S., Ramachandran, R., Sharan, A., Jain, M. R., Kumar Trivedi, A., Maurya, R., Godbole, M. M., Gayen, J. R., Sanyal, S., & Chattopadhyay, N. (2015). Pathophysiological mechanism of bone loss in type 2 diabetes involves inverse regulation of osteoblast function by pgc-1 α and skeletal muscle atrogenes: Adipor1 as a potential target for reversing diabetes-induced osteopenia. *Diabetes*, *64*(7), 2609–2623. <https://doi.org/10.2337/db14-1611>
- Kikuyama, A., Fukuda, K., Mori, S., Okada, M., Yamaguchi, H., & Hamanishi, C. (2002). Hydrogen peroxide induces apoptosis of osteocytes: Involvement of calcium ion and caspase activity. *Calcified Tissue International*, *71*(3), 243–248. <https://doi.org/10.1007/s00223-001-1110-2>
- Kim, H. K. W., Bian, H., Aya-Ay B, J., Garces, A., Morgan, E. F., & Gilbert, S. R. (2009). Hypoxia and HIF-1 α expression in the epiphyseal cartilage following ischemic injury to the immature femoral head. *Bone*, *45*, 280–288. <https://doi.org/10.1016/j.bone.2009.03.665>
- Kim, J.-H. H., Singhal, V., Biswal, S., Thimmulappa, R. K., & DiGirolamo, D. J. (n.d.). Nrf2 is required for normal postnatal bone acquisition in mice. *Bone Research*, *2*(1). <https://doi.org/10.1038/boneres.2014.33>
- Kim, J. Y., Lee, S. K., Jo, K. J., Song, D. Y., Lim, D. M., Park, K. Y., Bonewald, L. F., & Kim,

- B. J. (2013). Exendin-4 increases bone mineral density in type 2 diabetic OLETF rats potentially through the down-regulation of SOST/sclerostin in osteocytes. *Life Sciences*, 92(10), 533–540. <https://doi.org/10.1016/j.lfs.2013.01.001>
- Kim, Jeonghyun, & Adachi, T. (2019). Cell Condensation Triggers the Differentiation of Osteoblast Precursor Cells to Osteocyte-Like Cells. *Frontiers in Bioengineering and Biotechnology*, 7, 288. <https://doi.org/10.3389/fbioe.2019.00288>
- Kim, Joungmok, Yang, G., Kim, Y., Kim, J., & Ha, J. (2016). AMPK activators: mechanisms of action and physiological activities. *Experimental & Molecular Medicine*, 48(4), e224. <https://doi.org/10.1038/emm.2016.16>
- Kim, K. S., Choi, H. W., Yoon, H. E., & Kim, I. Y. (2010). Reactive oxygen species generated by NADPH oxidase 2 and 4 are required for chondrogenic differentiation. *The Journal of Biological Chemistry*, 285(51), 40294–40302. <https://doi.org/10.1074/jbc.M110.126821>
- Kim, S. P., Frey, J. L., Li, Z., Kushwaha, P., Zoch, M. L., Tomlinson, R. E., Da, H., Aja, S., Noh, H. L., Kim, J. K., Hussain, M. A., Thorek, D. L. J., Wolfgang, M. J., & Riddle, R. C. (2017). Sclerostin influences body composition by regulating catabolic and anabolic metabolism in adipocytes. *Proceedings of the National Academy of Sciences of the United States of America*, 114(52), E11238–E11247. <https://doi.org/10.1073/pnas.1707876115>
- Kimura, M., Yamamoto, T., Zhang, J., Itoh, K., Kyo, M., Kamiya, T., Aburatani, H., Katsuoka, F., Kurokawa, H., Tanaka, T., Motohashi, H., & Yamamoto, M. (2007). Molecular basis distinguishing the DNA binding profile of Nrf2-Maf heterodimer from that of Maf homodimer. *Journal of Biological Chemistry*, 282(46), 33681–33690. <https://doi.org/10.1074/jbc.M706863200>
- Klein-Nulend, J., Bonewald, L. F., Bilezikian, J. P., & Raisz, L. G. (2008). Principles of bone biology. *Bilezikian JP, Raisz LG, Martin TJ (Eds.), 1*, 153–174.
- Kobayashi, E. H., Suzuki, T., Funayama, R., Nagashima, T., Hayashi, M., Sekine, H., Tanaka, N., Moriguchi, T., Motohashi, H., Nakayama, K., & Yamamoto, M. (2016). Nrf2 suppresses macrophage inflammatory response by blocking proinflammatory cytokine transcription. *Nature Communications*, 7. <https://doi.org/10.1038/ncomms11624>
- Kogawa, M., Wijenayaka, A. R., Ormsby, R. T., Thomas, G. P., Anderson, P. H., Bonewald, L. F., Findlay, D. M., & Atkins, G. J. (2013). Sclerostin regulates release of bone mineral by osteocytes by induction of carbonic anhydrase 2. *Journal of Bone and Mineral Research*, 28(12), 2436–2448. <https://doi.org/10.1002/jbmr.2003>

- Komarova, S. V., Ataullakhanov, F. I., & Globus, R. K. (2000). Bioenergetics and mitochondrial transmembrane potential during differentiation of cultured osteoblasts. *American Journal of Physiology-Cell Physiology*, 279(4), C1220–C1229. <https://doi.org/10.1152/ajpcell.2000.279.4.C1220>
- Krakauer, J. C., McKenna, M. J., Buderer, N. F., Sudhaker Rao, D., Whitehouse, F. W., & Michael Parfitt, A. (1995). Bone loss and bone turnover in diabetes. *Diabetes*, 44(7), 775–782. <https://doi.org/10.2337/diab.44.7.775>
- Kramer, I., Baertschi, S., Halleux, C., Keller, H., & Kneissel, M. (2012). Mef2c deletion in osteocytes results in increased bone mass. *Journal of Bone and Mineral Research*, 27(2), 360–373. <https://doi.org/10.1002/jbmr.1492>
- Krause, K. H. (2007). Aging: A revisited theory based on free radicals generated by NOX family NADPH oxidases. In *Experimental Gerontology* (Vol. 42, Issue 4, pp. 256–262). <https://doi.org/10.1016/j.exger.2006.10.011>
- Krefting, J., Andrade-Navarro, M. A., & Ibn-Salem, J. (2018). Evolutionary stability of topologically associating domains is associated with conserved gene regulation. *BMC Biology*, 16(1), 87. <https://doi.org/10.1186/s12915-018-0556-x>
- Kronenberg, H. M. (2003). Developmental regulation of the growth plate. In *Nature* (Vol. 423, Issue 6937, pp. 332–336). <https://doi.org/10.1038/nature01657>
- Kugimiya, F., Kawaguchi, H., Ohba, S., Kawamura, N., Hirata, M., Chikuda, H., Azuma, Y., Woodgett, J. R., Nakamura, K., & Chung, U. II. (2007). GSK-3 β controls osteogenesis through regulating Runx2 activity. *PLoS ONE*, 2(9). <https://doi.org/10.1371/journal.pone.0000837>
- Kunkler, K. J., Everett, L. M., Breedlove, D. K., & Kempson, S. A. (1991). Insulin stimulates sodium-dependent phosphate transport by osteoblast-like cells. *The American Journal of Physiology*, 260(5 Pt 1), E751-5. <https://doi.org/10.1152/ajpendo.1991.260.5.E751>
- Kwak, M.-K., Itoh, K., Yamamoto, M., & Kensler, T. W. (2002). Enhanced Expression of the Transcription Factor Nrf2 by Cancer Chemopreventive Agents: Role of Antioxidant Response Element-Like Sequences in the nrf2 Promoter. *Molecular and Cellular Biology*, 22(9), 2883–2892. <https://doi.org/10.1128/mcb.22.9.2883-2892.2002>
- Lai, X., Price, C., Modla, S., Thompson, W. R., Caplan, J., Kirn-Safran, C. B., & Wang, L. (2015). The dependences of osteocyte network on bone compartment, age, and disease. *Bone Research*, 3. <https://doi.org/10.1038/boneres.2015.9>
- Landry, J., Sutton, A., Hesman, T., Min, J., Xu, R.-M., Johnston, M., & Sternglanz, R. (2003). Set2-Catalyzed Methylation of Histone H3 Represses Basal Expression of GAL4 in *Saccharomyces cerevisiae*. *Molecular and Cellular Biology*, 23(17),

5972–5978. <https://doi.org/10.1128/mcb.23.17.5972-5978.2003>

- Laplante, M., & Sabatini, D. M. (2012). mTOR signaling in growth control and disease. In *Cell* (Vol. 149, Issue 2, pp. 274–293). <https://doi.org/10.1016/j.cell.2012.03.017>
- Lau, B. Y. Y., Cohen, D. J. A., Ward, W. E., & Ma, D. W. L. (2013). Investigating the role of polyunsaturated fatty acids in bone development using animal models. In *Molecules* (Vol. 18, Issue 11, pp. 14203–14227). <https://doi.org/10.3390/molecules181114203>
- Lavi-Moshayoff, V., Wasserman, G., Meir, T., Silver, J., & Naveh-Many, T. (2010). PTH increases FGF23 gene expression and mediates the high-FGF23 levels of experimental kidney failure: A bone parathyroid feedback loop. *American Journal of Physiology - Renal Physiology*, 299(4). <https://doi.org/10.1152/ajprenal.00360.2010>
- Lean, J. M., Davies, J. T., Fuller, K., Jagger, C. J., Kirstein, B., Partington, G. A., Urry, Z. L., & Chambers, T. J. (2003). A crucial role for thiol antioxidants in estrogen-deficiency bone loss. *Journal of Clinical Investigation*, 112(6), 915–923. <https://doi.org/10.1172/jci18859>
- Lean, J. M., Jagger, C. J., Kirstein, B., Fuller, K., & Chambers, T. J. (2005). Hydrogen Peroxide Is Essential for Estrogen-Deficiency Bone Loss and Osteoclast Formation. *Endocrinology*, 146(2), 728–735. <https://doi.org/10.1210/en.2004-1021>
- Lecka-Czernik, B. (2017). Diabetes, bone and glucose-lowering agents: basic biology. In *Diabetologia* (Vol. 60, Issue 7, pp. 1163–1169). Springer Verlag. <https://doi.org/10.1007/s00125-017-4269-4>
- Lee, K., Jessop, H., Suswillo, R., Zaman, G., & Lanyon, L. (2003). Bone adaptation requires oestrogen receptor- α . *Nature*, 424(6947), 389. <https://doi.org/10.1038/424389a>
- Lee, N. K., Choi, Y. G., Baik, J. Y., Han, S. Y., Jeong, D. W., Bae, Y. S., Kim, N., & Lee, S. Y. (2005). A crucial role for reactive oxygen species in RANKL-induced osteoclast differentiation. *Blood*, 106(3), 852–859. <https://doi.org/10.1182/blood-2004-09-3662>
- Lee, W. C., Guntur, A. R., Long, F., & Rosen, C. J. (2017). Energy metabolism of the osteoblast: Implications for osteoporosis. In *Endocrine Reviews* (Vol. 38, Issue 3, pp. 255–266). Endocrine Society. <https://doi.org/10.1210/er.2017-00064>
- Lemon, B., Inouye, C., King, D. S., & Tjian, R. (2001). Selectivity of chromatin-remodelling cofactors for ligand-activated transcription. *Nature*, 414(6866),

- 924–928. <https://doi.org/10.1038/414924a>
- Lettgen, B., Hauffa, B., Möhlmann, C., Jeken, C., & Reiners, C. (1995). Bone mineral density in children and adolescents with juvenile diabetes: Selective measurement of bone mineral density of trabecular and cortical bone using peripheral quantitative computed tomography. *Hormone Research in Paediatrics*, *43*(5), 173–175. <https://doi.org/10.1159/000184273>
- Levy, J. R., Murray, E., Manolagas, S., & Olefsky, J. M. (1986). Demonstration of insulin receptors and modulation of alkaline phosphatase activity by insulin in rat osteoblastic cells. *Endocrinology*, *119*(4), 1786–1792. <https://doi.org/10.1210/endo-119-4-1786>
- Li, B., Carey, M., & Workman, J. L. (2007). The Role of Chromatin during Transcription. In *Cell* (Vol. 128, Issue 4, pp. 707–719). Cell Press. <https://doi.org/10.1016/j.cell.2007.01.015>
- Lin, J., Puigserver, P., Donovan, J., Tarr, P., & Spiegelman, B. M. (2002). Peroxisome proliferator-activated receptor γ coactivator 1 β (PGC-1 β), a novel PGC-1-related transcription coactivator associated with host cell factor. *Journal of Biological Chemistry*, *277*(3), 1645–1648. <https://doi.org/10.1074/jbc.C100631200>
- Lin, J., Yang, R., Tarr, P. T., Wu, P. H., Handschin, C., Li, S., Yang, W., Pei, L., Uldry, M., Tontonoz, P., Newgard, C. B., & Spiegelman, B. M. (2005). Hyperlipidemic effects of dietary saturated fats mediated through PGC-1 β coactivation of SREBP. *Cell*, *120*(2), 261–273. <https://doi.org/10.1016/j.cell.2004.11.043>
- Lin, S. C., & Hardie, D. G. (2018). AMPK: Sensing Glucose as well as Cellular Energy Status. In *Cell Metabolism* (Vol. 27, Issue 2, pp. 299–313). Cell Press. <https://doi.org/10.1016/j.cmet.2017.10.009>
- Linares, G. R., Xing, W., Govoni, K. E., Chen, S. T., & Mohan, S. (2009). Glutaredoxin 5 regulates osteoblast apoptosis by protecting against oxidative stress. *Bone*, *44*(5), 795–804. <https://doi.org/10.1016/j.bone.2009.01.003>
- LIU, A., ZHANG, Z., ZHU, B., LIAO, Z., & LIU, Z. (2004). Metallothionein protects bone marrow stromal cells against hydrogen peroxide-induced inhibition of osteoblastic differentiation. *Cell Biology International*, *28*(12), 905–911. <https://doi.org/10.1016/j.cellbi.2004.09.004>
- Liu, G.-S., Chan, E. C., Higuchi, M., Dusting, G. J., & Jiang, F. (2012). Redox mechanisms in regulation of adipocyte differentiation: beyond a general stress response. *Cells*, *1*(4), 976–993. <https://doi.org/10.3390/cells1040976>
- Liu, S., Guo, R., Simpson, L. G., Xiao, Z. S., Burnham, C. E., & Quarles, L. D. (2003). Regulation of fibroblastic growth factor 23 expression but not degradation by

- PHEX. *Journal of Biological Chemistry*, 278(39), 37419–37426. <https://doi.org/10.1074/jbc.M304544200>
- Liu, S., Zhou, J., Tang, W., Jiang, X., Rowe, D. W., & Quarles, L. D. (2006). Pathogenic role of Fgf23 in Hyp mice. *American Journal of Physiology - Endocrinology and Metabolism*, 291(1). <https://doi.org/10.1152/ajpendo.00008.2006>
- Lloyd, A. A., Gludovatz, B., Riedel, C., Luengo, E. A., Saiyed, R., Marty, E., Lorch, D. G., Lane, J. M., Ritchie, R. O., Busse, B., & Donnelly, E. (2017). Atypical fracture with long-term bisphosphonate therapy is associated with altered cortical composition and reduced fracture resistance. *Proceedings of the National Academy of Sciences of the United States of America*, 114(33), 8722–8727. <https://doi.org/10.1073/pnas.1704460114>
- Lo, S. C., & Hannink, M. (2008). PGAM5 tethers a ternary complex containing Keap1 and Nrf2 to mitochondria. *Experimental Cell Research*, 314(8), 1789–1803. <https://doi.org/10.1016/j.yexcr.2008.02.014>
- Loureiro, M. B., Ururahy, M. A. G., Freire-Neto, F. P., Oliveira, G. H. M., Duarte, V. M. G., Luchessi, A. D., Brandão-Neto, J., Hirata, R. D. C., Hirata, M. H., Maciel-Neto, J. J., Arrais, R. F., Almeida, M. G., & Rezende, A. A. (2014). Low bone mineral density is associated to poor glycemic control and increased OPG expression in children and adolescents with type 1 diabetes. *Diabetes Research and Clinical Practice*, 103(3), 452–457. <https://doi.org/10.1016/j.diabres.2013.12.018>
- Lu, H., Kraut, D., Gerstenfeld, L. C., & Graves, D. T. (2003). Diabetes interferes with the bone formation by affecting the expression of transcription factors that regulate osteoblast differentiation. *Endocrinology*, 144(1), 346–352. <https://doi.org/10.1210/en.2002-220072>
- Lu, X. L., Huo, B., Chiang, V., & Guo, X. E. (2012). Osteocytic network is more responsive in calcium signaling than osteoblastic network under fluid flow. *Journal of Bone and Mineral Research*, 27(3), 563–574. <https://doi.org/10.1002/jbmr.1474>
- Luo, X. H., Guo, L. J., Yuan, L. Q., Xie, H., Zhou, H. De, Wu, X. P., & Liao, E. Y. (2005). Adiponectin stimulates human osteoblasts proliferation and differentiation via the MAPK signaling pathway. *Experimental Cell Research*, 309(1), 99–109. <https://doi.org/10.1016/j.yexcr.2005.05.021>
- M., W., T., G., F.L., L., M., H., C., S., M., F., C.L., T., K., S., P., H., A., O., C., P., G.N., D., F., B., Wagegg, M., Gaber, T., Lohanatha, F. L., Hahne, M., Strehl, C., Fangradt, M., ... Buttgerit, F. (2012). Hypoxia Promotes Osteogenesis but Suppresses Adipogenesis of Human Mesenchymal Stromal Cells in a Hypoxia-Inducible Factor-1 Dependent Manner. *PLoS ONE*, 7(9), e46483.

- <https://doi.org/10.1371/journal.pone.0046483> LK
<http://WT3CF4ET2L.search.serialssolutions.com?sid=EMBASE&issn=19326203&id=doi:10.1371%2Fjournal.pone.0046483&atitle=Hypoxia+Promotes+Osteogenesis+but+Suppresses+Adipogenesis+of+Human+Mesenchymal+Stromal+Cells+in+a+Hypoxia-Inducible+Factor-1+Dependent+Manner&stitle=PLoS+ONE&title=PLoS+ONE&volume=7&issue=9&spage=&epage=&aulast=Wagegg&aufirst=Markus&aunit=M.&aufull=Wagegg+M.&coden=&isbn=&pages=-&date=2012&aunit1=M&aunitm=>
- Ma, J., Cai, H., Wu, T., Sobhian, B., Huo, Y., Alcivar, A., Mehta, M., Cheung, K. L., Ganesan, S., Kong, A.-N. T., Zhang, D. D., & Xia, B. (2012). PALB2 Interacts with KEAP1 To Promote NRF2 Nuclear Accumulation and Function. *Molecular and Cellular Biology*, 32(8), 1506–1517. <https://doi.org/10.1128/mcb.06271-11>
- Ma, P., Gu, B., Xiong, W., Tan, B., Geng, W., Li, J., & Liu, H. (2014). Glimepiride promotes osteogenic differentiation in rat osteoblasts via the PI3K/Akt/eNOS pathway in a high glucose microenvironment. *PLoS ONE*, 9(11). <https://doi.org/10.1371/journal.pone.0112243>
- Mabileau, G., Petrova, N. L., Edmonds, M. E., & Sabokbar, A. (2008). Increased osteoclastic activity in acute Charcot’s osteoarthopathy: The role of receptor activator of nuclear factor-kappaB ligand. *Diabetologia*, 51(6), 1035–1040. <https://doi.org/10.1007/s00125-008-0992-1>
- Mainini, G., Rotondi, M., Di Nola, K., Pezzella, M. T., Iervolino, S. A., Seguino, E., D’Eufemia, D., Iannicelli, I., & Torella, M. (2012). Oral supplementation with antioxidant agents containing alpha lipoic acid: Effects on postmenopausal bone mass. *Clinical and Experimental Obstetrics and Gynecology*, 39(4), 489–493.
- Makareeva, E., & Leikin, S. (2013). Collagen Structure, Folding and Function. In *Osteogenesis Imperfecta: A Translational Approach to Brittle Bone Disease* (pp. 71–84). Elsevier Inc. <https://doi.org/10.1016/B978-0-12-397165-4.00007-1>
- Malhotra, D., Portales-Casamar, E., Singh, A., Srivastava, S., Arenillas, D., Happel, C., Shyr, C., Wakabayashi, N., Kensler, T. W., Wasserman, W. W., & Biswal, S. (2010). Global mapping of binding sites for Nrf2 identifies novel targets in cell survival response through ChIP-Seq profiling and network analysis. *Nucleic Acids Research*, 38(17), 5718–5734. <https://doi.org/10.1093/nar/gkq212>
- Malik, S., & Roeder, R. G. (2000). Transcriptional regulation through Mediator-like coactivators in yeast and metazoan cells. *Trends in Biochemical Sciences*, 25(6), 277–283. [https://doi.org/10.1016/S0968-0004\(00\)01596-6](https://doi.org/10.1016/S0968-0004(00)01596-6)
- Manilay, J. O., & Zouali, M. (2014). Tight relationships between B lymphocytes and the skeletal system. In *Trends in Molecular Medicine* (Vol. 20, Issue 7, pp. 405–

- 412). Elsevier Ltd. <https://doi.org/10.1016/j.molmed.2014.03.003>
- Manolagas, S. C., & Almeida, M. (2007). Gone with the Wnts: β -Catenin, T-Cell Factor, Forkhead Box O, and Oxidative Stress in Age-Dependent Diseases of Bone, Lipid, and Glucose Metabolism. *Molecular Endocrinology*, *21*(11), 2605–2614. <https://doi.org/10.1210/me.2007-0259>
- Marenzana, M., & Arnett, T. R. (2013). The Key Role of the Blood Supply to Bone. In *Bone Research* (Vol. 1, Issue 3, pp. 203–215). Sichuan University. <https://doi.org/10.4248/BR201303001>
- Marks, J., Churchill, L. J., Debnam, E. S., & Unwin, R. J. (2008). Matrix extracellular phosphoglycoprotein inhibits phosphate transport. *Journal of the American Society of Nephrology*, *19*(12), 2313–2320. <https://doi.org/10.1681/ASN.2008030315>
- Martin, A., Liu, S., David, V., Li, H., Karydis, A., Feng, J. Q., & Quarles, L. D. (2011). Bone proteins PHEX and DMP1 regulate fibroblastic growth factor Fgf23 expression in osteocytes through a common pathway involving FGF receptor (FGFR) signaling. *FASEB Journal*, *25*(8), 2551–2562. <https://doi.org/10.1096/fj.10-177816>
- Martínez-Redondo, V., Pettersson, A. T., & Ruas, J. L. (2015). The hitchhiker's guide to PGC-1 α isoform structure and biological functions. In *Diabetologia* (Vol. 58, Issue 9, pp. 1969–1977). Springer Verlag. <https://doi.org/10.1007/s00125-015-3671-z>
- Maupin, K. A., Droscha, C. J., & Williams, B. O. (2013). A Comprehensive Overview of Skeletal Phenotypes Associated with Alterations in Wnt/ β -catenin Signaling in Humans and Mice. In *Bone Research* (Vol. 1, pp. 27–71). Sichuan University. <https://doi.org/10.4248/BR201301004>
- McCarthy, I. (2006). The Physiology of Bone Blood Flow: A Review. *The Journal of Bone and Joint Surgery (American)*, *88*(suppl_2), 4. <https://doi.org/10.2106/jbjs.f.00890>
- McMahon, J. M., Boyde, A., & Bromage, T. G. (1995). Pattern of collagen fiber orientation in the ovine calcaneal shaft and its relation to locomotor-induced strain. *The Anatomical Record*, *242*(2), 147–158. <https://doi.org/10.1002/ar.1092420203>
- Meili-Butz, S., Niermann, T., Fasler-Kan, E., Barbosa, V., Butz, N., John, D., Brink, M., Buser, P. T., & Zaugg, C. E. (2008). Dimethyl fumarate, a small molecule drug for psoriasis, inhibits Nuclear Factor- κ B and reduces myocardial infarct size in rats. *European Journal of Pharmacology*, *586*(1–3), 251–258. <https://doi.org/10.1016/j.ejphar.2008.02.038>

- Mercken, E. M., Mitchell, S. J., Martin-Montalvo, A., Minor, R. K., Almeida, M., Gomes, A. P., Scheibye-Knudsen, M., Palacios, H. H., Licata, J. J., Zhang, Y., Becker, K. G., Khraiwesh, H., González-Reyes, J. A., Villalba, J. M., Baur, J. A., Elliott, P., Westphal, C., Vlasuk, G. P., Ellis, J. L., ... de Cabo, R. (2014). SIRT1 extends survival of male mice on a standard diet and preserves bone and muscle mass. *Aging Cell*, *13*(5), 787–796. <https://doi.org/10.1111/accel.12220>
- Miao, W., Hu, L., Scrivens, P. J., & Batist, G. (2005). Transcriptional regulation of NF-E2 p45-related factor (NRF2) expression by the aryl hydrocarbon receptor-xenobiotic response element signaling pathway: Direct cross-talk between phase I and II drug-metabolizing enzymes. *Journal of Biological Chemistry*, *280*(21), 20340–20348. <https://doi.org/10.1074/jbc.M412081200>
- Mihaylova, M. M., & Shaw, R. J. (2011). The AMP-activated protein kinase (AMPK) signaling pathway coordinates cell growth, autophagy, & metabolism. *Nature Cell Biology*, *13*(9), 1016–1023. <https://doi.org/10.1038/ncb2329>
- Miller, S. C., De Saint-Georges, L., Bowman, B. M., & Jee, W. S. S. (1989). Bone lining cells: Structure and function. In *Scanning Microscopy* (Vol. 3, Issue 3, pp. 953–961).
- Mishra, S., & Knothe Tate, M. L. (2003). Effect of lacunocanalicular architecture on hydraulic conductance in bone tissue: Implications for bone health and evolution. *The Anatomical Record*, *273A*(2), 752–762. <https://doi.org/10.1002/ar.a.10079>
- Mitsuishi, Y., Taguchi, K., Kawatani, Y., Shibata, T., Nukiwa, T., Aburatani, H., Yamamoto, M., & Motohashi, H. (2012). Nrf2 Redirects Glucose and Glutamine into Anabolic Pathways in Metabolic Reprogramming. *Cancer Cell*, *22*(1), 66–79. <https://doi.org/10.1016/j.ccr.2012.05.016>
- Miyamoto, K. I., Ito, M., Kuwahata, M., Kato, S., & Segawa, H. (2005). Inhibition of intestinal sodium-dependent inorganic phosphate transport by fibroblast growth factor 23. *Therapeutic Apheresis and Dialysis*, *9*(4), 331–335. <https://doi.org/10.1111/j.1744-9987.2005.00292.x>
- Mödder, U. II, Clowes, J. A., Hoey, K., Peterson, J. M., McCready, L., Oursler, M. J., Riggs, B. L., & Khosla, S. (2011). Regulation of circulating sclerostin levels by sex steroids in women and in men. *Journal of Bone and Mineral Research*, *26*(1), 27–34. <https://doi.org/10.1002/jbmr.128>
- Mödder, U. I., Hoey, K. A., Amin, S., McCready, L. K., Achenbach, S. J., Riggs, B. L., Melton, L. J., & Khosla, S. (2011). Relation of age, gender, and bone mass to circulating sclerostin levels in women and men. *Journal of Bone and Mineral Research*, *26*(2), 373–379. <https://doi.org/10.1002/jbmr.217>

- Mohamed, A. M. F. S. (2008). An overview of bone cells and their regulating factors of differentiation. In *Malaysian Journal of Medical Sciences* (Vol. 15, Issue 1, pp. 4–12).
- Monsalve, M., Wu, Z., Adelmant, G., Puigserver, P., Fan, M., & Spiegelman, B. M. (2000). Direct coupling of transcription and mRNA processing through the thermogenic coactivator PGC-1. *Molecular Cell*, 6(2), 307–316. [https://doi.org/10.1016/S1097-2765\(00\)00031-9](https://doi.org/10.1016/S1097-2765(00)00031-9)
- Morita, K., Miyamoto, T., Fujita, N., Kubota, Y., Ito, K., Takubo, K., Miyamoto, K., Ninomiya, K., Suzuki, T., Iwasaki, R., Yagi, M., Takaishi, H., Toyama, Y., & Suda, T. (2007). Reactive oxygen species induce chondrocyte hypertrophy in endochondral ossification. *Journal of Experimental Medicine*, 204(7), 1613–1623. <https://doi.org/10.1084/jem.20062525>
- Morton, D. J., Barrett-Connor, E. L., & Schneider, D. L. (2001). Vitamin C supplement use and bone mineral density in postmenopausal women. *Journal of Bone and Mineral Research*, 16(1), 135–140. <https://doi.org/10.1359/jbmr.2001.16.1.135>
- Motohashi, H., Katsuoka, F., Shavit, J. A., Engel, J. D., & Yamamoto, M. (2000). Positive or negative MARE-dependent transcriptional regulation is determined by the abundance of small Maf proteins. *Cell*, 103(6), 865–876. [https://doi.org/10.1016/s0092-8674\(00\)00190-2](https://doi.org/10.1016/s0092-8674(00)00190-2)
- Motohashi, H., Kimura, M., Fujita, R., Inoue, A., Pan, X., Takayama, M., Katsuoka, F., Aburatani, H., Bresnick, E. H., & Yamamoto, M. (2010). NF-E2 domination over Nrf2 promotes ROS accumulation and megakaryocytic maturation. *Blood*, 115(3), 677–686. <https://doi.org/10.1182/blood-2009-05-223107>
- Motohashi, H., O'Connor, T., Katsuoka, F., Engel, J. D., & Yamamoto, M. (2002). Integration and diversity of the regulatory network composed of Maf and CNC families of transcription factors. In *Gene* (Vol. 294, Issues 1–2, pp. 1–12). Elsevier. [https://doi.org/10.1016/S0378-1119\(02\)00788-6](https://doi.org/10.1016/S0378-1119(02)00788-6)
- Motyl, K. J., Botolin, S., Irwin, R., Appledorn, D. M., Kadakia, T., Amalfitano, A., Schwartz, R. C., & McCabe, L. R. (2009). Bone inflammation and altered gene expression with type 2 diabetes early onset. *Journal of Cellular Physiology*, 218(3), 575–583. <https://doi.org/10.1002/jcp.21626>
- Mullen, C. A., Haugh, M. G., Schaffler, M. B., Majeska, R. J., & McNamara, L. M. (2013). Osteocyte differentiation is regulated by extracellular matrix stiffness and intercellular separation. *Journal of the Mechanical Behavior of Biomedical Materials*, 28, 183–194. <https://doi.org/10.1016/j.jmbbm.2013.06.013>
- Murad, S., Grove, D., Lindberg, K. A., Reynolds, G., Sivarajah, A., & Pinnell, S. R.

- (1981). Regulation of collagen synthesis by ascorbic acid (prolyl hydroxylation/lysyl hydroxylation/human skin fibroblasts). In *Biochemistry* (Vol. 78, Issue 5).
- Murakami, S., Shimizu, R., Romeo, P.-H., Yamamoto, M., & Motohashi, H. (2014). Keap1-Nrf2 system regulates cell fate determination of hematopoietic stem cells. *Genes to Cells*, 19(3), 239–253. <https://doi.org/10.1111/gtc.12126>
- Murshid, S. A. (2017). The role of osteocytes during experimental orthodontic tooth movement: A review. In *Archives of Oral Biology* (Vol. 73, pp. 25–33). Elsevier Ltd. <https://doi.org/10.1016/j.archoralbio.2016.09.001>
- Nagai, Y., Yonemitsu, S., Erion, D. M., Iwasaki, T., Stark, R., Weismann, D., Dong, J., Zhang, D., Jurczak, M. J., Löffler, M. G., Cresswell, J., Yu, X. X., Murray, S. F., Bhanot, S., Monia, B. P., Bogan, J. S., Samuel, V., & Shulman, G. I. (2009). The Role of Peroxisome Proliferator-Activated Receptor γ Coactivator-1 β in the Pathogenesis of Fructose-Induced Insulin Resistance. *Cell Metabolism*, 9(3), 252–264. <https://doi.org/10.1016/j.cmet.2009.01.011>
- Nagata, T., Kaho, K., Nishikawa, S., Shinohara, H., Wakano, Y., & Ishida, H. (1994). Effect of prostaglandin E2 on mineralization of bone nodules formed by fetal rat calvarial cells. *Calcified Tissue International*, 55(6), 451–457. <https://doi.org/10.1007/bf00298559>
- Nampei, A., Hashimoto, J., Hayashida, K., Tsuboi, H., Shi, K., Tsuji, I., Miyashita, H., Yamada, T., Matsukawa, N., Matsumoto, M., Morimoto, S., Ogihara, T., Ochi, T., & Yoshikawa, H. (2004). Matrix extracellular phosphoglycoprotein (MEPE) is highly expressed in osteocytes in human bone. *Journal of Bone and Mineral Metabolism*, 22(3), 176–184. <https://doi.org/10.1007/s00774-003-0468-9>
- Napoli, N., Chandran, M., Pierroz, D. D., Abrahamsen, B., Schwartz, A. V., & Ferrari, S. L. (2017). Mechanisms of diabetes mellitus-induced bone fragility. In *Nature Reviews Endocrinology* (Vol. 13, Issue 4, pp. 208–219). Nature Publishing Group. <https://doi.org/10.1038/nrendo.2016.153>
- Narapureddy, B., & Dubey, D. (2019). Clinical evaluation of dimethyl fumarate for the treatment of relapsing-remitting multiple sclerosis: Efficacy, safety, patient experience and adherence. *Patient Preference and Adherence*, 13, 1655–1666. <https://doi.org/10.2147/PPA.S187529>
- Narasimhan, M., Patel, D., Vedpathak, D., Rathinam, M., Henderson, G., & Mahimainathan, L. (2012). Identification of Novel microRNAs in Post-Transcriptional Control of Nrf2 Expression and Redox Homeostasis in Neuronal, SH-SY5Y Cells. *PLoS ONE*, 7(12), e51111. <https://doi.org/10.1371/journal.pone.0051111>

- Narimiya, T., Kanzaki, H., Yamaguchi, Y., Wada, S., Katsumata, Y., Tanaka, K., & Tomonari, H. (2019). Nrf2 activation in osteoblasts suppresses osteoclastogenesis via inhibiting IL-6 expression. *Bone Reports*, *11*, 100228. <https://doi.org/10.1016/j.bonr.2019.100228>
- Nguyen, T., Sherratt, P. J., Huang, H. C., Yang, C. S., & Pickett, C. B. (2003). Increased protein stability as a mechanism that enhances Nrf2-mediated transcriptional activation of the antioxidant response element: Degradation of Nrf2 by the 26 S proteasome. *Journal of Biological Chemistry*, *278*(7), 4536–4541. <https://doi.org/10.1074/jbc.M207293200>
- Nicodemus, K. K., & Folsom, A. R. (2001). Type 1 and type 2 diabetes and incident hip fractures in postmenopausal women. *Diabetes Care*, *24*(7), 1192–1197. <https://doi.org/10.2337/diacare.24.7.1192>
- Nijweide, P. J., van der Plas, A., Alblas, M. J., & Klein-Nulend, J. (2003). Osteocyte isolation and culture. *Methods in Molecular Medicine*, *80*, 41–50. <https://doi.org/10.1385/1-59259-366-6:41>
- Noble, B. S. (2008). The osteocyte lineage. In *Archives of Biochemistry and Biophysics* (Vol. 473, Issue 2, pp. 106–111). <https://doi.org/10.1016/j.abb.2008.04.009>
- Norris, D. O., & Carr, J. A. (2013). Regulation of Calcium and Phosphate Homeostasis in Vertebrates. In *Vertebrate Endocrinology* (pp. 501–527). Elsevier. <https://doi.org/10.1016/b978-0-12-394815-1.00014-8>
- Ogata, N., Chikazu, D., Kubota, N., Terauchi, Y., Tobe, K., Azuma, Y., Ohta, T., Kadowaki, T., Nakamura, K., & Kawaguchi, H. (2000). Insulin receptor substrate-1 in osteoblast is indispensable for maintaining bone turnover. *Journal of Clinical Investigation*, *105*(7), 935–943. <https://doi.org/10.1172/JCI9017>
- Ohya, K., & Amagasa, T. (1994). Effects of Insulin on In Vitro Bone Formation in Fetal Rat Parietal Bone. *Endocrine Journal*, *41*(3), 293–300. <https://doi.org/10.1507/endocrj.41.293>
- Okazaki, R., Totsuka, Y., Hamano, K., Ajima, M., Miura, M., Hirota, Y., Hata, K., Fukumoto, S., & Matsumoto, T. (1997). Metabolic improvement of poorly controlled noninsulin-dependent diabetes mellitus decreases bone turnover. *Journal of Clinical Endocrinology and Metabolism*, *82*(9), 2915–2920. <https://doi.org/10.1210/jc.82.9.2915>
- Olagnier, D., Brandtøft, A. M., Gunderstofte, C., Villadsen, N. L., Krapp, C., Thielke, A. L., Laustsen, A., Peri, S., Hansen, A. L., Bonefeld, L., Thyrted, J., Bruun, V., Iversen, M. B., Lin, L., Artegoitia, V. M., Su, C., Yang, L., Lin, R., Balachandran, S., ... Holm, C. K. (2018). Nrf2 negatively regulates STING indicating a link between antiviral sensing and metabolic reprogramming. *Nature Communications*, *9*(1), 309

<https://doi.org/10.1038/s41467-018-05861-7>

- Onal, M., Piemontese, M., Xiong, J., Wang, Y., Han, L., Ye, S., Komatsu, M., Selig, M., Weinstein, R. S., Zhao, H., Jilka, R. L., Almeida, M., Manolagas, S. C., & O'Brien, C. A. (2013). Suppression of autophagy in osteocytes mimics skeletal aging. *Journal of Biological Chemistry*, *288*(24), 17432–17440. <https://doi.org/10.1074/jbc.M112.444190>
- Ornstrup, M. J., Harsløf, T., Kjær, T. N., Langdahl, B. L., & Pedersen, S. B. (2014). Resveratrol increases bone mineral density and bone alkaline phosphatase in obese men: A randomized placebo-controlled trial. *Journal of Clinical Endocrinology and Metabolism*, *99*(12), 4720–4729. <https://doi.org/10.1210/jc.2014-2799>
- Ovcharenko, I., Nobrega, M. A., Loots, G. G., & Stubbs, L. (2004). ECR Browser: a tool for visualizing and accessing data from comparisons of multiple vertebrate genomes. *Nucleic Acids Research*, *32*(Web Server issue), W280–W286. <https://doi.org/10.1093/nar/gkh355>
- Paic, F., Igwe, J. C., Nori, R., Kronenberg, M. S., Franceschetti, T., Harrington, P., Kuo, L., Shin, D. G., Rowe, D. W., Harris, S. E., & Kalajzic, I. (2009). Identification of differentially expressed genes between osteoblasts and osteocytes. *Bone*, *45*(4), 682–692. <https://doi.org/10.1016/j.bone.2009.06.010>
- Pajvani, U. B., Du, X., Combs, T. P., Berg, A. H., Rajala, M. W., Schulthess, T., Engel, J., Brownlee, M., & Scherer, P. E. (2003). Structure-function studies of the adipocyte-secreted hormone Acrp30/adiponectin: Implications for metabolic regulation and bioactivity. *Journal of Biological Chemistry*, *278*(11), 9073–9085. <https://doi.org/10.1074/jbc.M207198200>
- Pajvani, U. B., Hawkins, M., Combs, T. P., Rajala, M. W., Doebber, T., Berger, J. P., Wagner, J. A., Wu, M., Knopps, A., Xiang, A. H., Utzschneider, K. M., Kahn, S. E., Olefsky, J. M., Buchanan, T. A., & Scherer, P. E. (2004). Complex Distribution, Not Absolute Amount of Adiponectin, Correlates with Thiazolidinedione-mediated Improvement in Insulin Sensitivity. *Journal of Biological Chemistry*, *279*(13), 12152–12162. <https://doi.org/10.1074/jbc.M311113200>
- Palumbo, C., Palazzini, S., & Marotti, G. (1990). Morphological study of intercellular junctions during osteocyte differentiation. *Bone*, *11*(6), 401–406. [https://doi.org/10.1016/8756-3282\(90\)90134-K](https://doi.org/10.1016/8756-3282(90)90134-K)
- Papandreou, I., Cairns, R. A., Fontana, L., Lim, A. L., & Denko, N. C. (2006). HIF-1 mediates adaptation to hypoxia by actively downregulating mitochondrial oxygen consumption. *Cell Metabolism*, *3*(3), 187–197. <https://doi.org/10.1016/j.cmet.2006.01.012>

- Park, C. K., Lee, Y., Kim, K. H., Lee, Z. H., Joo, M., & Kim, H. H. (2014a). Nrf2 is a novel regulator of bone acquisition. *Bone*, *63*, 36–46. <https://doi.org/10.1016/j.bone.2014.01.025>
- Park, C. K., Lee, Y., Kim, K. H., Lee, Z. H., Joo, M., & Kim, H. H. (2014b). Nrf2 is a novel regulator of bone acquisition. *Bone*, *63*, 36–46. <https://doi.org/10.1016/j.bone.2014.01.025>
- Paul, R. G., & Bailey, A. J. (1996). Glycation of collagen: The basis of its central role in the late complications of ageing and diabetes. In *International Journal of Biochemistry and Cell Biology* (Vol. 28, Issue 12, pp. 1297–1310). [https://doi.org/10.1016/S1357-2725\(96\)00079-9](https://doi.org/10.1016/S1357-2725(96)00079-9)
- Pavone, V., Testa, G., Giardina, S. M. C., Vescio, A., Restivo, D. A., & Sessa, G. (2017). Pharmacological therapy of osteoporosis: A systematic current review of literature. In *Frontiers in Pharmacology* (Vol. 8, Issue NOV). Frontiers Media S.A. <https://doi.org/10.3389/fphar.2017.00803>
- Peck, W. a, Birge, S. J., & Fedak, S. a. (1964). Bone Cells: Biochemical and Biological Studies after Enzymatic Isolation. *Science*, *146*(3650), 1476–1477. <https://doi.org/10.1126/science.146.3650.1476>
- Pellegrini, G. G., Cregor, M., Mcandrews, K., Morales, C. C., McCabe, L. D., McCabe, G. P., Peacock, M., Burr, D., Weaver, C., & Bellido, T. (2017). NRF2 regulates mass accrual and the antioxidant endogenous response in bone differently depending on the sex and age. *PLoS ONE*, *12*(2). <https://doi.org/10.1371/journal.pone.0171161>
- Perwad, F., Azam, N., Zhang, M. Y. H., Yamashita, T., Tenenhouse, H. S., & Portale, A. A. (2005). Dietary and serum phosphorus regulate fibroblast growth factor 23 expression and 1,25-dihydroxyvitamin D metabolism in mice. *Endocrinology*, *146*(12), 5358–5364. <https://doi.org/10.1210/en.2005-0777>
- Pfander, D., Cramer, T., Schipani, E., & Johnson, R. S. (2003). HIF-1 α controls extracellular matrix synthesis by epiphyseal chondrocytes. *Journal of Cell Science*, *116*(9), 1819–1826. <https://doi.org/10.1242/jcs.00385>
- Pi, J., Leung, L., Xue, P., Wang, W., Hou, Y., Liu, D., Yehuda-Shnaidman, E., Lee, C., Lau, J., Kurtz, T. W., & Chan, J. Y. (2010). Deficiency in the nuclear factor E2-related factor-2 transcription factor results in impaired adipogenesis and protects against diet-induced obesity. *Journal of Biological Chemistry*, *285*(12), 9292–9300. <https://doi.org/10.1074/jbc.M109.093955>
- Poole, K. E. S., Van Bezooijen, R. L., Loveridge, N., Hamersma, H., Papapoulos, S. E., Löwik, C. W., & Reeve, J. (2005). Sclerostin is a delayed secreted product of osteocytes that inhibits bone formation. *FASEB Journal*, *19*(13), 1842–1844.

<https://doi.org/10.1096/fj.05-4221fje>

- Portal-Núñez, S., Lozano, D., Fernández de Castro, L., de Gortázar, A. R., Nogués, X., & Esbrit, P. (2010). Alterations of the Wnt/ β -catenin pathway and its target genes for the N- and C-terminal domains of parathyroid hormone-related protein in bone from diabetic mice. *FEBS Letters*, *584*(14), 3095–3100. <https://doi.org/10.1016/j.febslet.2010.05.047>
- Pouresmaeili, F., Kamalidehghan, B., Kamarehei, M., & Goh, Y. M. (2018). A comprehensive overview on osteoporosis and its risk factors. In *Therapeutics and Clinical Risk Management* (Vol. 14, pp. 2029–2049). Dove Medical Press Ltd. <https://doi.org/10.2147/TCRM.S138000>
- Prabhakar, N. R., & Semenza, G. L. (2012). Adaptive and maladaptive cardiorespiratory responses to continuous and intermittent hypoxia mediated by hypoxia-inducible factors 1 and 2. In *Physiological Reviews* (Vol. 92, Issue 3, pp. 967–1003). <https://doi.org/10.1152/physrev.00030.2011>
- PRITCHARD, J. J. (1952). A cytological and histochemical study of bone and cartilage formation in the rat. *Journal of Anatomy*, *86*(3), 259–277. <http://www.ncbi.nlm.nih.gov/pubmed/12980877>
- Puigserver, P., Adelmant, G., Wu, Z., Fan, M., Xu, J., O'Malley, B., & Spiegelman, B. M. (1999). Activation of PPAR γ coactivator-1 through transcription factor docking. *Science*, *286*(5443), 1368–1371. <https://doi.org/10.1126/science.286.5443.1368>
- Puigserver, P., Rhee, J., Donovan, J., Walkey, C. J., Yoon, J. C., Oriente, F., Kitamura, Y., Altomonte, J., Dong, H., Accili, D., & Spiegelman, B. M. (2003). Insulin-regulated hepatic gluconeogenesis through FOXO1-PGC-1 α interaction. *Nature*, *423*(6939), 550–555. <https://doi.org/10.1038/nature01667>
- Puigserver, P., Wu, Z., Park, C. W., Graves, R., Wright, M., & Spiegelman, B. M. (1998). A cold-inducible coactivator of nuclear receptors linked to adaptive thermogenesis. *Cell*, *92*(6), 829–839. [https://doi.org/10.1016/S0092-8674\(00\)81410-5](https://doi.org/10.1016/S0092-8674(00)81410-5)
- Quinn, J. M. W., Tam, S., Sims, N. A., Saleh, H., McGregor, N. E., Poulton, I. J., Scott, J. W., Gillespie, M. T., Kemp, B. E., & van Denderen, B. J. W. (2010). Germline deletion of AMP-activated protein kinase β subunits reduces bone mass without altering osteoclast differentiation or function. *The FASEB Journal*, *24*(1), 275–285.
- Qutob, S., Dixon, S. J., & Wilson, J. X. (1998). Insulin stimulates vitamin c recycling and ascorbate accumulation in osteoblastic cells. *Endocrinology*, *139*(1), 51–56. <https://doi.org/10.1210/endo.139.1.5659>

- Rached, M. T., Kode, A., Xu, L., Yoshikawa, Y., Paik, J. H., DePinho, R. A., & Kousteni, S. (2010). FoxO1 Is a Positive Regulator of Bone Formation by Favoring Protein Synthesis and Resistance to Oxidative Stress in Osteoblasts. *Cell Metabolism*, *11*(2), 147–160. <https://doi.org/10.1016/j.cmet.2010.01.001>
- Rada, P., Rojo, A. I., Chowdhry, S., McMahon, M., Hayes, J. D., & Cuadrado, A. (2011). SCF/TrCP Promotes Glycogen Synthase Kinase 3-Dependent Degradation of the Nrf2 Transcription Factor in a Keap1-Independent Manner. *Molecular and Cellular Biology*, *31*(6), 1121–1133. <https://doi.org/10.1128/mcb.01204-10>
- Raheja, L. F., Genetos, D. C., & Yellowley, C. E. (2008). Hypoxic osteocytes recruit human MSCs through an OPN/CD44-mediated pathway. *Biochemical and Biophysical Research Communications*, *366*(4), 1061–1066. <https://doi.org/10.1016/j.bbrc.2007.12.076>
- Rana, T., Schultz, M. A., Freeman, M. L., & Biswas, S. (2012). Loss of Nrf2 accelerates ionizing radiation-induced bone loss by upregulating RANKL. *Free Radical Biology and Medicine*, *53*(12), 2298–2307. <https://doi.org/10.1016/j.freeradbiomed.2012.10.536>
- Rasbach, K. A., Gupta, R. K., Ruas, J. L., Wu, J., Naseri, E., Estall, J. L., & Spiegelman, B. M. (2010). PGC-1 α regulates a HIF2 α -dependent switch in skeletal muscle fiber types. *Proceedings of the National Academy of Sciences of the United States of America*, *107*(50), 21866–21871. <https://doi.org/10.1073/pnas.1016089107>
- Ray, P. D., Huang, B.-W., & Tsuji, Y. (2012a). Reactive oxygen species (ROS) homeostasis and redox regulation in cellular signaling. *Cellular Signalling*, *24*(5), 981–990. <https://doi.org/10.1016/j.cellsig.2012.01.008>
- Ray, P. D., Huang, B. W., & Tsuji, Y. (2012b). Reactive oxygen species (ROS) homeostasis and redox regulation in cellular signaling. In *Cellular Signalling* (Vol. 24, Issue 5, pp. 981–990). <https://doi.org/10.1016/j.cellsig.2012.01.008>
- Regan, J. N., Lim, J., Shi, Y., Joeng, K. S., Arbeit, J. M., Shohet, R. V., & Longa, F. (2014). Up-regulation of glycolytic metabolism is required for HIF1 α -driven bone formation. *Proceedings of the National Academy of Sciences of the United States of America*, *111*(23), 8673–8678. <https://doi.org/10.1073/pnas.1324290111>
- Reid, I. R., Evans, M. C., Cooper, G. J., Ames, R. W., & Stapleton, J. (1993). Circulating insulin levels are related to bone density in normal postmenopausal women. *The American Journal of Physiology*, *265*(4 Pt 1), E655–9. <https://doi.org/10.1152/ajpendo.1993.265.4.E655>
- Riddle, R. C., & Clemens, T. L. (2017). Bone cell bioenergetics and skeletal energy

- homeostasis. *Physiological Reviews*, 97(2), 667–698. <https://doi.org/10.1152/physrev.00022.2016>
- Riddle, R. C., Frey, J. L., Tomlinson, R. E., Ferron, M., Li, Y., DiGirolamo, D. J., Faugere, M.-C., Hussain, M. A., Karsenty, G., & Clemens, T. L. (2014). Tsc2 is a molecular checkpoint controlling osteoblast development and glucose homeostasis. *Molecular and Cellular Biology*, 34(10), 1850–1862. <https://doi.org/10.1128/MCB.00075-14>
- Riddle, R. C., Khatri, R., Schipani, E., & Clemens, T. L. (2009). Role of hypoxia-inducible factor-1 α in angiogenic-osteogenic coupling. In *Journal of Molecular Medicine* (Vol. 87, Issue 6, pp. 583–590). <https://doi.org/10.1007/s00109-009-0477-9>
- Rinker, T. E., Hammoudi, T. M., Kemp, M. L., Lu, H., & Temenoff, J. S. (2014). Interactions between mesenchymal stem cells, adipocytes, and osteoblasts in a 3D tri-culture model of hyperglycemic conditions in the bone marrow microenvironment. *Integrative Biology : Quantitative Biosciences from Nano to Macro*, 6(3), 324–337. <https://doi.org/10.1039/c3ib40194d>
- Roadmap Epigenomics Consortium, Kundaje, A., Meuleman, W., Ernst, J., Bilenky, M., Yen, A., Heravi-Moussavi, A., Kheradpour, P., Zhang, Z., Wang, J., Ziller, M. J., Amin, V., Whitaker, J. W., Schultz, M. D., Ward, L. D., Sarkar, A., Quon, G., Sandstrom, R. S., Eaton, M. L., ... Kellis, M. (2015). Integrative analysis of 111 reference human epigenomes. *Nature*, 518(7539), 317–329. <https://doi.org/10.1038/nature14248>
- Robin, M., Almeida, C., Azaïs, T., Haye, B., Illoul, C., Lesieur, J., Giraud-Guille, M. M., Nassif, N., & Hélyary, C. (2016). Involvement of 3D osteoblast migration and bone apatite during in vitro early osteocytogenesis. *Bone*, 88, 146–156. <https://doi.org/10.1016/j.bone.2016.04.031>
- Robling, A. G., Niziolek, P. J., Baldrige, L. A., Condon, K. W., Allen, M. R., Alam, I., Mantila, S. M., Gluhak-Heinrich, J., Bellido, T. M., Harris, S. E., & Turner, C. H. (2008). Mechanical stimulation of bone in vivo reduces osteocyte expression of Sost/sclerostin. *Journal of Biological Chemistry*, 283(9), 5866–5875. <https://doi.org/10.1074/jbc.M705092200>
- Rodríguez-Carballo, Eddie, Gámez, B., & Ventura, F. (2016). p38 MAPK Signaling in Osteoblast Differentiation. *Frontiers in Cell and Developmental Biology*, 4(May), 1–20. <https://doi.org/10.3389/fcell.2016.00040>
- Rodríguez-Carballo, Edgardo, Gámez, B., Méndez-Lucas, A., Sánchez-Freutrie, M., Zorzano, A., Bartrons, R., Alcántara, S., Perales, J. C., & Ventura, F. (2015). p38 α function in osteoblasts influences adipose tissue homeostasis. *FASEB Journal*, 29(4), 1414–1425. <https://doi.org/10.1096/fj.14-261891>

- Romagnoli, C., Marcucci, G., Favilli, F., Zonefrati, R., Mavilia, C., Galli, G., Tanini, A., Iantomasi, T., Brandi, M. L., & Vincenzini, M. T. (2013). Role of GSH/GSSG redox couple in osteogenic activity and osteoclastogenic markers of human osteoblast-like SaOS-2 cells. *FEBS Journal*, *280*(3), 867–879. <https://doi.org/10.1111/febs.12075>
- Romero, R., Sayin, V. I., Davidson, S. M., Bauer, M. R., Singh, S. X., Leboeuf, S. E., Karakousi, T. R., Ellis, D. C., Bhutkar, A., Sánchez-Rivera, F. J., Subbaraj, L., Martinez, B., Bronson, R. T., Prigge, J. R., Schmidt, E. E., Thomas, C. J., Goparaju, C., Davies, A., Dolgalev, I., ... Papagiannakopoulos, T. (2017). Keap1 loss promotes Kras-driven lung cancer and results in dependence on glutaminolysis. *Nature Medicine*, *23*(11), 1362–1368. <https://doi.org/10.1038/nm.4407>
- Rosato, M. T., Schneider, S. H., & Shapses, S. A. (1998). Bone turnover and insulin-like growth factor I levels increase after improved glycemic control in noninsulin-dependent diabetes mellitus. *Calcified Tissue International*, *63*(2), 107–111. <https://doi.org/10.1007/s002239900498>
- Rowe, P. S. N. (2012). Regulation of bone-renal mineral and energy metabolism: The PHEX, FGF23, DMP1, MEPE ASARM pathway. In *Critical Reviews in Eukaryotic Gene Expression* (Vol. 22, Issue 1, pp. 61–86). Begell House Inc. <https://doi.org/10.1615/CritRevEukarGeneExpr.v22.i1.50>
- Rowe, P. S. N., Garrett, I. R., Schwarz, P. M., Carnes, D. L., Lafer, E. M., Mundy, G. R., & Gutierrez, G. E. (2005). Surface plasmon resonance (SPR) confirms that MEPE binds to PHEX via the MEPE-ASARM motif: A model for impaired mineralization in X-linked rickets (HYP). *Bone*, *36*(1), 33–46. <https://doi.org/10.1016/j.bone.2004.09.015>
- Rubin, M. R. (2015). Bone Cells and Bone Turnover in Diabetes Mellitus. In *Current Osteoporosis Reports* (Vol. 13, Issue 3, pp. 186–191). Current Medicine Group LLC 1. <https://doi.org/10.1007/s11914-015-0265-0>
- Rushworth, S. A., Zaitseva, L., Murray, M. Y., Shah, N. M., Bowles, K. M., & MacEwan, D. J. (2012). The high Nrf2 expression in human acute myeloid leukemia is driven by NF-κB and underlies its chemo-resistance. *Blood*, *120*(26), 5188–5198. <https://doi.org/10.1182/blood-2012-04-422121>
- Rutkovskiy, A., Stensløkken, K.-O., & Vaage, I. J. (2016). Osteoblast Differentiation at a Glance. *Medical Science Monitor Basic Research*, *22*, 95–106. <https://doi.org/10.12659/msmbr.901142>
- Ryan, Z. C., Ketha, H., McNulty, M. S., McGee-Lawrence, M., Craig, T. A., Grande, J. P., Westendorf, J. J., Singh, R. J., & Kumar, R. (2013). Sclerostin alters serum vitamin D metabolite and fibroblast growth factor 23 concentrations and the

- urinary excretion of calcium. *Proceedings of the National Academy of Sciences of the United States of America*, 110(15), 6199–6204. <https://doi.org/10.1073/pnas.1221255110>
- Sahni, S., Mangano, K. M., McLean, R. R., Hannan, M. T., & Kiel, D. P. (2015). Dietary Approaches for Bone Health: Lessons from the Framingham Osteoporosis Study. In *Current Osteoporosis Reports* (Vol. 13, Issue 4, pp. 245–255). Current Medicine Group LLC 1. <https://doi.org/10.1007/s11914-015-0272-1>
- Sánchez-De-Diego, C., Antonio Valer, J., Pimenta-Lopes, C., Luis Rosa, J., & Ventura, F. (2019). Interplay between BMPs and reactive oxygen species in cell signaling and pathology. In *Biomolecules* (Vol. 9, Issue 10). MDPI AG. <https://doi.org/10.3390/biom9100534>
- Sánchez-de-Diego, C., Artigas, N., Pimenta-Lopes, C., Valer, J. A., Torrejon, B., Gama-Pérez, P., Villena, J. A., Garcia-Roves, P. M., Rosa, J. L., & Ventura, F. (2019). Glucose restriction promotes osteocyte specification by activating a PGC-1 α -dependent transcriptional program. *iScience*, 0(0). <https://doi.org/10.1016/j.isci.2019.04.015>
- Sanders, K. M., Kotowicz, M. A., & Nicholson, G. C. (2007). Potential role of the antioxidant N-acetylcysteine in slowing bone resorption in early postmenopausal women: a pilot study. In *Translational Research* (Vol. 150, Issue 4, p. 215). Mosby Inc. <https://doi.org/10.1016/j.trsl.2007.03.012>
- Sangokoya, C., Telen, M. J., & Chi, J. T. (2010). microRNA miR-144 modulates oxidative stress tolerance and associates with anemia severity in sickle cell disease. *Blood*, 116(20), 4338–4348. <https://doi.org/10.1182/blood-2009-04-214817>
- Sarmiere, P. D., & Bamburg, J. R. (2004). Regulation of the Neuronal Actin Cytoskeleton by ADF/Cofilin. In *Journal of Neurobiology* (Vol. 58, Issue 1, pp. 103–117). <https://doi.org/10.1002/neu.10267>
- Sato, M., Asada, N., Kawano, Y., Wakahashi, K., Minagawa, K., Kawano, H., Sada, A., Ikeda, K., Matsui, T., & Katayama, Y. (2013). Osteocytes regulate primary lymphoid organs and fat metabolism. *Cell Metabolism*, 18(5), 749–758. <https://doi.org/10.1016/j.cmet.2013.09.014>
- Schaffler, M. B., & Kennedy, O. D. (2012). Osteocyte signaling in bone. *Current Osteoporosis Reports*, 10(2), 118–125. <https://doi.org/10.1007/s11914-012-0105-4>
- Schieber, M., & Chandel, N. S. (2014). ROS function in redox signaling and oxidative stress. *Current Biology : CB*, 24(10), R453–62. <https://doi.org/10.1016/j.cub.2014.03.034>

- Schimrigk, S., Brune, N., Hellwig, K., Lukas, C., Bellenberg, B., Rieks, M., Hoffmann, V., Pöhlau, D., & Przuntek, H. (2006). Oral fumaric acid esters for the treatment of active multiple sclerosis: An open-label, baseline-controlled pilot study. *European Journal of Neurology*, *13*(6), 604–610. <https://doi.org/10.1111/j.1468-1331.2006.01292.x>
- Sebastian, A., & Loots, G. G. (2018). Genetics of Sost/SOST in sclerosteosis and van Buchem disease animal models. *Metabolism: Clinical and Experimental*, *80*, 38–47. <https://doi.org/10.1016/j.metabol.2017.10.005>
- Seibel, M. J., Robins, S. P., & Bilezikian, J. P. (2006). Dynamics of Bone and Cartilage Metabolism. In *Dynamics of Bone and Cartilage Metabolism*. Elsevier Inc. <https://doi.org/10.1016/B978-0-12-088562-6.X5000-6>
- Sendur, O. F., Turan, Y., Tastaban, E., & Serter, M. (2009). Antioxidant status in patients with osteoporosis: A controlled study. *Joint Bone Spine*, *76*(5), 514–518. <https://doi.org/10.1016/j.jbspin.2009.02.005>
- Shah, M., Kola, B., Bataveljic, A., Arnett, T. R., Viollet, B., Saxon, L., Korbonits, M., & Chenu, C. (2010). AMP-activated protein kinase (AMPK) activation regulates in vitro bone formation and bone mass. *Bone*, *47*(2), 309–319. <https://doi.org/10.1016/j.bone.2010.04.596>
- Shaker, J. L., & Deftos, L. (2013). Calcium and Phosphate Homeostasis. In *Endocrine and Reproductive Physiology* (pp. 77-e1). Elsevier. <https://doi.org/10.1016/b978-0-323-08704-9.00004-x>
- Shen, X., Wan, C., Ramaswamy, G., Mavalli, M., Wang, Y., Duvall, C. L., Lian, F. D., Guldberg, R. E., Eberhart, A., Clemens, T. L., & Gilbert, S. R. (2009). Prolyl hydroxylase inhibitors increase neoangiogenesis and callus formation following femur fracture in mice. *Journal of Orthopaedic Research*, *27*(10), 1298–1305. <https://doi.org/10.1002/jor.20886>
- Shimada, T., Kakitani, M., Yamazaki, Y., Hasegawa, H., Takeuchi, Y., Fujita, T., Fukumoto, S., Tomizuka, K., & Yamashita, T. (2004). Targeted ablation of Fgf23 demonstrates an essential physiological role of FGF23 in phosphate and vitamin D metabolism. *Journal of Clinical Investigation*, *113*(4), 561–568. <https://doi.org/10.1172/JCI19081>
- Singh, B., Ronghe, A. M., Chatterjee, A., Bhat, N. K., & Bhat, H. K. (2013). MicroRNA-93 regulates NRF2 expression and is associated with breast carcinogenesis. *Carcinogenesis*, *34*(5), 1165–1172. <https://doi.org/10.1093/carcin/bgt026>
- Singh, S., Grabner, A., Yanucil, C., Schramm, K., Czaya, B., Krick, S., Czaja, M. J., Bartz, R., Abraham, R., Di Marco, G. S., Brand, M., Wolf, M., & Faul, C. (2016). Fibroblast growth factor 23 directly targets hepatocytes to promote

- inflammation in chronic kidney disease. *Kidney International*, 90(5), 985–996. <https://doi.org/10.1016/j.kint.2016.05.019>
- Sinnesael, M., Claessens, F., Laurent, M., Dubois, V., Boonen, S., Deboel, L., & Vanderschueren, D. (2012). Androgen receptor (AR) in osteocytes is important for the maintenance of male skeletal integrity: Evidence from targeted AR disruption in mouse osteocytes. *Journal of Bone and Mineral Research*, 27(12), 2535–2543. <https://doi.org/10.1002/jbmr.1713>
- Sipola, A., Nelo, K., Hautala, T., Ilvesaro, J., & Tuukkanen, J. (2006). Endostatin inhibits VEGF-A induced osteoclastic bone resorption in vitro. *BMC Musculoskeletal Disorders*, 7(1), 56. <https://doi.org/10.1186/1471-2474-7-56>
- Skedros, J. G., Holmes, J. L., Vajda, E. G., & Bloebaum, R. D. (2005). Cement lines of secondary osteons in human bone are not mineral-deficient: New data in a historical perspective. *The Anatomical Record Part A: Discoveries in Molecular, Cellular, and Evolutionary Biology*, 286A(1), 781–803. <https://doi.org/10.1002/ar.a.20214>
- Sodek, J., Ganss, B., & McKee, M. D. (2000). Osteopontin. *Critical Reviews in Oral Biology & Medicine*, 11(3), 279–303. <https://doi.org/10.1177/10454411000110030101>
- Spiegelman, B. M., & Heinrich, R. (2004). Biological control through regulated transcriptional coactivators. In *Cell* (Vol. 119, Issue 2, pp. 157–167). Cell Press. <https://doi.org/10.1016/j.cell.2004.09.037>
- Sprowson, A. P., McCaskie, A. W., & Birch, M. A. (2008). ASARM-truncated MEPE and AC-100 enhance osteogenesis by promoting osteoprogenitor adhesion. *Journal of Orthopaedic Research*, 26(9), 1256–1262. <https://doi.org/10.1002/jor.20606>
- Sroga, G. E., & Vashishth, D. (2012). Effects of bone matrix proteins on fracture and fragility in osteoporosis. *Current Osteoporosis Reports*, 10(2), 141–150. <https://doi.org/10.1007/s11914-012-0103-6>
- Staines, K. A., MacRae, V. E., & Farquharson, C. (2012). The importance of the SIBLING family of proteins on skeletal mineralisation and bone remodelling. In *Journal of Endocrinology* (Vol. 214, Issue 3, pp. 241–255). <https://doi.org/10.1530/JOE-12-0143>
- Stechschulte, L. A., Czernik, P. J., Rotter, Z. C., Tausif, F. N., Corzo, C. A., Marciano, D. P., Asteian, A., Zheng, J., Bruning, J. B., Kamenecka, T. M., Rosen, C. J., Griffin, P. R., & Lecka-Czernik, B. (2016). PPARγ Post-translational Modifications Regulate Bone Formation and Bone Resorption. *EBioMedicine*, 10, 174–184. <https://doi.org/10.1016/j.ebiom.2016.06.040>
- Stegen, S., Van Gastel, N., Eelen, G., Ghesquière, B., D’Anna, F., Thienpont, B.,

- Goveia, J., Torrekens, S., Van Looveren, R., Luyten, F. P., Maxwell, P. H., Wielockx, B., Lambrechts, D., Fendt, S. M., Carmeliet, P., & Carmeliet, G. (2016). HIF-1 α promotes glutamine-mediated redox homeostasis and glycogen-dependent bioenergetics to support postimplantation bone cell survival. *Cell Metabolism*, 23(2), 265–279. <https://doi.org/10.1016/j.cmet.2016.01.002>
- Stern, A. R., Stern, M. M., van Dyke, M. E., Jähn, K., Prideaux, M., & Bonewald, L. F. (2012). Isolation and culture of primary osteocytes from the long bones of skeletally mature and aged mice. *BioTechniques*, 52(6), 361–373. <https://doi.org/10.2144/0000113876>
- Sugawara, Y., Kamioka, H., Honjo, T., Tezuka, K. I., & Takano-Yamamoto, T. (2005). Three-dimensional reconstruction of chick calvarial osteocytes and their cell processes using confocal microscopy. *Bone*, 36(5), 877–883. <https://doi.org/10.1016/j.bone.2004.10.008>
- Role of Nrf2 in bone metabolism, 22 *Journal of Biomedical Science* 101 (2015). <https://doi.org/10.1186/s12929-015-0212-5>
- Sunycz, J. A. (2008). The use of calcium and vitamin D in the management of osteoporosis. In *Therapeutics and Clinical Risk Management* (Vol. 4, Issue 4, pp. 827–836). Dove Press. <https://doi.org/10.2147/tcrm.s3552>
- Tanaka, K. I., Yamaguchi, T., Kanazawa, I., & Sugimoto, T. (2015). Effects of high glucose and advanced glycation end products on the expressions of sclerostin and RANKL as well as apoptosis in osteocyte-like MLO-Y4-A2 cells. *Biochemical and Biophysical Research Communications*, 461(2), 193–199. <https://doi.org/10.1016/j.bbrc.2015.02.091>
- Tatapudy, S., Aloisio, F., Barber, D., & Nystul, T. (2017). Cell fate decisions: emerging roles for metabolic signals and cell morphology. *EMBO Reports*, 18(12), 2105–2118. <https://doi.org/10.15252/embr.201744816>
- Teixeira, M. A., Amorim, M. T. P., & Felgueiras, H. P. (2019). Poly(Vinyl Alcohol)-Based Nanofibrous Electrospun Scaffolds for Tissue Engineering Applications. *Polymers*, 12(1), 7. <https://doi.org/10.3390/polym12010007>
- Theoleyre, S., Wittrant, Y., Tat, S. K., Fortun, Y., Redini, F., & Heymann, D. (2004). The molecular triad OPG/RANK/RANKL: Involvement in the orchestration of pathophysiological bone remodeling. In *Cytokine and Growth Factor Reviews* (Vol. 15, Issue 6, pp. 457–475). <https://doi.org/10.1016/j.cytogfr.2004.06.004>
- Thomas, D. M., Hards, D. K., Rogers, S. D., Ng, K. W., & Best, J. D. (2009). Insulin receptor expression in bone. *Journal of Bone and Mineral Research*, 11(9), 1312–1320. <https://doi.org/10.1002/jbmr.5650110916>

- Thomas, T., Gori, F., Khosla, S., Jensen, M. D., Burguera, B., & Riggs, B. L. (1999). Leptin acts on human marrow stromal cells to enhance differentiation to osteoblasts and to inhibit differentiation to adipocytes. *Endocrinology*, *140*(4), 1630–1638. <https://doi.org/10.1210/endo.140.4.6637>
- Thraillkill, K., Bunn, R. C., Lumpkin, C., Wahl, E., Cockrell, G., Morris, L., Kahn, C. R., Fowlkes, J., & Nyman, J. S. (2014). Loss of insulin receptor in osteoprogenitor cells impairs structural strength of bone. *Journal of Diabetes Research*, *2014*, 703589. <https://doi.org/10.1155/2014/703589>
- Thraillkill, K. M. (2000). Insulin-like growth factor-I in diabetes mellitus: Its physiology, metabolic effects, and potential clinical utility. In *Diabetes Technology and Therapeutics* (Vol. 2, Issue 1, pp. 69–80). <https://doi.org/10.1089/152091599316775>
- Thraillkill, Kathryn M., Clay Bunn, R., Nyman, J. S., Rettiganti, M. R., Cockrell, G. E., Wahl, E. C., Uppuganti, S., Lumpkin, C. K., & Fowlkes, J. L. (2016). SGLT2 inhibitor therapy improves blood glucose but does not prevent diabetic bone disease in diabetic DBA/2J male mice. *Bone*, *82*, 101–107. <https://doi.org/10.1016/j.bone.2015.07.025>
- Tilg, H., Moschen, A. R., Kaser, A., Pines, A., & Dotan, I. (2008). Gut, inflammation and osteoporosis: Basic and clinical concepts. In *Gut* (Vol. 57, Issue 5, pp. 684–694). <https://doi.org/10.1136/gut.2006.117382>
- Tonelli, C., Chio, I. I. C., & Tuveson, D. A. (2018). Transcriptional Regulation by Nrf2. *Antioxidants & Redox Signaling*, *29*(17), 1727–1745. <https://doi.org/10.1089/ars.2017.7342>
- Tong, K. I., Katoh, Y., Kusunoki, H., Itoh, K., Tanaka, T., & Yamamoto, M. (2006). Keap1 Recruits Neh2 through Binding to ETGE and DLG Motifs: Characterization of the Two-Site Molecular Recognition Model. *Molecular and Cellular Biology*, *26*(8), 2887–2900. <https://doi.org/10.1128/mcb.26.8.2887-2900.2006>
- Tresguerres, F. G. F., Torres, J., López-Quiles, J., Hernández, G., Vega, J. A., & Tresguerres, I. F. (2020). The osteocyte: A multifunctional cell within the bone. In *Annals of Anatomy* (Vol. 227). Elsevier GmbH. <https://doi.org/10.1016/j.aanat.2019.151422>
- Tsentidis, C., Gourgiotis, D., Kossiva, L., Doulgeraki, A., Marmarinos, A., Galli-Tsinopoulou, A., & Karavanaki, K. (2016). Higher levels of s-RANKL and osteoprotegerin in children and adolescents with type 1 diabetes mellitus may indicate increased osteoclast signaling and predisposition to lower bone mass: a multivariate cross-sectional analysis. *Osteoporosis International*, *27*(4), 1631–1643. <https://doi.org/10.1007/s00198-015-3422-5>

- Tsourdi, E., Jähn, K., Rauner, M., Busse, B., & Bonewald, L. F. (2018). Physiological and pathological osteocytic osteolysis. In *Journal of Musculoskeletal Neuronal Interactions* (Vol. 18, Issue 3, pp. 292–303). International Society of Musculoskeletal and Neuronal Interactions.
- Urano, T., Shiraki, M., Ouchi, Y., & Inoue, S. (2012). Association of circulating sclerostin levels with fat mass and metabolic disease - Related markers in Japanese postmenopausal women. *Journal of Clinical Endocrinology and Metabolism*, *97*(8). <https://doi.org/10.1210/jc.2012-1218>
- Valko, M., Leibfritz, D., Moncol, J., Cronin, M. T. D., Mazur, M., & Telser, J. (2007). Free radicals and antioxidants in normal physiological functions and human disease. In *International Journal of Biochemistry and Cell Biology* (Vol. 39, Issue 1, pp. 44–84). <https://doi.org/10.1016/j.biocel.2006.07.001>
- Van Der Velde, M., Van Der Eerden, B. C. J., Sun, Y., Almering, J. M. M., Van Der Lely, A. J., Delhanty, P. J. D., Smith, R. G., & Van Leeuwen, J. P. T. M. (2012). An age-dependent interaction with leptin unmasks Ghrelin's bone-protective effects. *Endocrinology*, *153*(8), 3593–3602. <https://doi.org/10.1210/en.2012-1277>
- Varga, P., Pacureanu, A., Langer, M., Suhonen, H., Hesse, B., Grimal, Q., Cloetens, P., Raum, K., & Peyrin, F. (2013). Investigation of the three-dimensional orientation of mineralized collagen fibrils in human lamellar bone using synchrotron X-ray phase nano-tomography. *Acta Biomaterialia*, *9*(9), 8118–8127. <https://doi.org/10.1016/j.actbio.2013.05.015>
- Velling, T., Risteli, J., Wennerberg, K., Mosher, D. F., & Johansson, S. (2002). Polymerization of type I and III collagens is dependent on fibronectin and enhanced by integrins $\alpha 11\beta 1$ and $\alpha 2\beta 1$. *Journal of Biological Chemistry*, *277*(40), 37377–37381. <https://doi.org/10.1074/jbc.M206286200>
- Verborgt, O., Tatton, N. A., Majeska, R. J., & Schaffler, M. B. (2002). Spatial distribution of Bax and Bcl-2 in osteocytes after bone fatigue: Complementary roles in bone remodeling regulation? *Journal of Bone and Mineral Research*, *17*(5), 907–914. <https://doi.org/10.1359/jbmr.2002.17.5.907>
- Veverka, V., Henry, A. J., Slocombe, P. M., Ventom, A., Mulloy, B., Muskett, F. W., Muzylak, M., Greenslade, K., Moore, A., Zhang, L., Gong, J., Qian, X., Paszty, C., Taylor, R. J., Robinson, M. K., & Carr, M. D. (2009). Characterization of the structural features and interactions of sclerostin. Molecular insight into a key regulator of Wnt-mediated bone formation. *Journal of Biological Chemistry*, *284*(16), 10890–10900. <https://doi.org/10.1074/jbc.M807994200>
- Vezeridis, P. S., Semeins, C. M., Chen, Q., & Klein-Nulend, J. (2006). Osteocytes subjected to pulsating fluid flow regulate osteoblast proliferation and

- differentiation. *Biochemical and Biophysical Research Communications*, 348(3), 1082–1088. <https://doi.org/10.1016/j.bbrc.2006.07.146>
- Viégas, M., Costa, C., Lopes, A., Griz, L., Medeiro, M. A., & Bandeira, F. (2011). Prevalence of osteoporosis and vertebral fractures in postmenopausal women with type 2 diabetes mellitus and their relationship with duration of the disease and chronic complications. *Journal of Diabetes and Its Complications*, 25(4), 216–221. <https://doi.org/10.1016/j.jdiacomp.2011.02.004>
- Villarino, M. E., Sánchez, L. M., Bozal, C. B., & Ubios, A. M. (2006). Influence of short-term diabetes on osteocytic lacunae of alveolar bone. A histomorphometric study. *Acta Odontológica Latinoamericana : AOL*, 19(1), 23–28.
- Villena, J. A. (2015). New insights into PGC-1 coactivators: Redefining their role in the regulation of mitochondrial function and beyond. In *FEBS Journal* (Vol. 282, Issue 4, pp. 647–672). <https://doi.org/10.1111/febs.13175>
- Vogt, M. T., Cauley, J. A., Kuller, L. H., & Nevitt, M. C. (1997). Bone mineral density and blood flow to the lower extremities: The study of osteoporotic fractures. *Journal of Bone and Mineral Research*, 12(2), 283–289. <https://doi.org/10.1359/jbmr.1997.12.2.283>
- Wakabayashi, N., Skoko, J. J., Chartoumpekis, D. V., Kimura, S., Slocum, S. L., Noda, K., Palliyaguru, D. L., Fujimuro, M., Boley, P. A., Tanaka, Y., Shigemura, N., Biswal, S., Yamamoto, M., & Kensler, T. W. (2014). Notch-Nrf2 Axis: Regulation of Nrf2 Gene Expression and Cytoprotection by Notch Signaling. *Molecular and Cellular Biology*, 34(4), 653–663. <https://doi.org/10.1128/mcb.01408-13>
- Wakasugi, M., Wakao, R., Tawata, M., Gan, N., Koizumi, K., & Onaya, T. (1993). Bone mineral density measured by dual energy X-ray absorptiometry in patients with non-insulin-dependent diabetes mellitus. *Bone*, 14(1), 29–33. [https://doi.org/10.1016/8756-3282\(93\)90252-6](https://doi.org/10.1016/8756-3282(93)90252-6)
- Wanet, A., Caruso, M., Domelevo Entfellner, J.-B., Najjar, M., Fattaccioli, A., Demazy, C., Evraerts, J., El-Kehdy, H., Pourcher, G., Sokal, E., Arnould, T., Tiffin, N., Najimi, M., & Renard, P. (2017). The Transcription Factor 7-Like 2-Peroxisome Proliferator-Activated Receptor Gamma Coactivator-1 Alpha Axis Connects Mitochondrial Biogenesis and Metabolic Shift with Stem Cell Commitment to Hepatic Differentiation. *STEM CELLS*, 35(10), 2184–2197. <https://doi.org/10.1002/stem.2688>
- Wang, H.-T., Liu, C.-F., Tsai, T.-H., Chen, Y.-L., Chang, H.-W., Tsai, C.-Y., Leu, S., Zhen, Y.-Y., Chai, H.-T., Chung, S.-Y., Chua, S., Yen, C.-H., & Yip, H.-K. (2012). *No Title*. 10(1), 145. <https://doi.org/10.1186/1479-5876-10-145>
- Wang, L. (2018). Solute Transport in the Bone Lacunar-Canalicular System (LCS). In

- Current Osteoporosis Reports* (Vol. 16, Issue 1, pp. 32–41). Current Medicine Group LLC 1. <https://doi.org/10.1007/s11914-018-0414-3>
- Wang, X., Wei, W., Krzeszinski, J. Y., Wang, Y., & Wan, Y. (2015). A Liver-Bone Endocrine Relay by IGFBP1 Promotes Osteoclastogenesis and Mediates FGF21-Induced Bone Resorption. *Cell Metabolism*, 22(5), 811–824. <https://doi.org/10.1016/j.cmet.2015.09.010>
- Wauquier, F., Leotoing, L., Coxam, V., Guicheux, J., & Wittrant, Y. (2009). Oxidative stress in bone remodelling and disease. In *Trends in Molecular Medicine* (Vol. 15, Issue 10, pp. 468–477). Elsevier Ltd. <https://doi.org/10.1016/j.molmed.2009.08.004>
- Wei, J., Shimazu, J., Makinistoglu, M. P., Maurizi, A., Kajimura, D., Zong, H., Takarada, T., Lezaki, T., Pessin, J. E., Hinoi, E., & Karsenty, G. (2015). Glucose Uptake and Runx2 Synergize to Orchestrate Osteoblast Differentiation and Bone Formation. *Cell*, 161(7), 1576–1591. <https://doi.org/10.1016/j.cell.2015.05.029>
- Wei, W., & Wan, Y. (2011). Thiazolidinediones on PPAR γ : the roles in bone remodeling. *PPAR Research*, 2011.
- Wei, W., Wang, X., Yang, M., Smith, L. C., Dechow, P. C., & Wan, Y. (2010). PGC1 β mediates PPAR γ activation of osteoclastogenesis and rosiglitazone-induced bone loss. *Cell Metabolism*, 11(6), 503–516. <https://doi.org/10.1016/j.cmet.2010.04.015>
- Wein, M. N. (2018). Parathyroid Hormone Signaling in Osteocytes. *JBMR Plus*, 2(1), 22–30. <https://doi.org/10.1002/jbm4.10021>
- Weinbaum, S., Cowin, S. C., & Zeng, Y. (1994). A model for the excitation of osteocytes by mechanical loading-induced bone fluid shear stresses. *Journal of Biomechanics*, 27(3), 339–360. [https://doi.org/10.1016/0021-9290\(94\)90010-8](https://doi.org/10.1016/0021-9290(94)90010-8)
- Weinberg, E., Maymon, T., Moses, O., & Weinreb, M. (2014). Streptozotocin-induced diabetes in rats diminishes the size of the osteoprogenitor pool in bone marrow. *Diabetes Research and Clinical Practice*, 103(1), 35–41. <https://doi.org/10.1016/j.diabres.2013.11.015>
- Weinberg, Evgeny, Maymon, T., & Weinreb, M. (2013). AGEs induce caspase-mediated apoptosis of rat BMSCs via TNF α production and oxidative stress. *Journal of Molecular Endocrinology*, 52(1), 67–76. <https://doi.org/10.1530/JME-13-0229>
- WHO | 5. Population nutrient intake goals for preventing diet-related chronic

- diseases. (n.d.). Retrieved March 31, 2020, from https://www.who.int/nutrition/topics/5_population_nutrient/en/index25.html
- Wientroub, S., Eisenberg, D., Tardiman, R., Weissman, S. L., & Salama, R. (1980). Is diabetic osteoporosis due to microangiopathy? *Lancet (London, England)*, 2(8201), 983. [https://doi.org/10.1016/s0140-6736\(80\)92145-5](https://doi.org/10.1016/s0140-6736(80)92145-5)
- Windahl, S. H., Börjesson, A. E., Farman, H. H., Engdahl, C., Movérare-Skrtic, S., Sjögrena, K., Lagerquist, M. K., Kindblom, J. M., Koskela, A., Tuukkanen, J., Pajevic, P. D., Feng, J. Q., Dahlman-Wright, K., Antonson, P., Gustafsson, J. Å., & Ohlsson, C. (2013). Estrogen receptor- α in osteocytes is important for trabecular bone formation in male mice. *Proceedings of the National Academy of Sciences of the United States of America*, 110(6), 2294–2299. <https://doi.org/10.1073/pnas.1220811110>
- Woo, S. M., Rosser, J., Dusevich, V., Kalajzic, I., & Bonewald, L. F. (2011). Cell line IDG-SW3 replicates osteoblast-to-late-osteocyte differentiation in vitro and accelerates bone formation in vivo. *Journal of Bone and Mineral Research : The Official Journal of the American Society for Bone and Mineral Research*, 26(11), 2634–2646. <https://doi.org/10.1002/jbmr.465>
- Wu, S., Levenson, A., Kharitonov, A., & De Luca, F. (2012). Fibroblast growth factor 21 (FGF21) inhibits chondrocyte function and growth hormone action directly at the growth plate. *Journal of Biological Chemistry*, 287(31), 26060–26067. <https://doi.org/10.1074/jbc.M112.343707>
- Wu, T., Zhao, F., Gao, B., Tan, C., Yagishita, N., Nakajima, T., Wong, P. K., Chapman, E., Fang, D., & Zhang, D. D. (2014). Hrd1 suppresses Nrf2-mediated cellular protection during liver cirrhosis. *Genes and Development*, 28(7), 708–722. <https://doi.org/10.1101/gad.238246.114>
- Xi, G., Rosen, C. J., & Clemmons, D. R. (2016). IGF-I and IGFBP-2 stimulate AMPK activation and autophagy, which are required for osteoblast differentiation. *Endocrinology*, 157(1), 268–281. <https://doi.org/10.1210/en.2015-1690>
- Xian, L., Wu, X., Pang, L., Lou, M., Rosen, C. J., Qiu, T., Crane, J., Frassica, F., Zhang, L., Rodriguez, J. P., Jia, X., Yakar, S., Xuan, S., Efstratiadis, A., Wan, M., & Cao, X. (2012). Matrix IGF-1 maintains bone mass by activation of mTOR in mesenchymal stem cells. *Nature Medicine*, 18(7), 1095–1101. <https://doi.org/10.1038/nm.2793>
- Xiong, J., Onal, M., Jilka, R. L., Weinstein, R. S., Manolagas, S. C., & O'Brien, C. A. (2011). Matrix-embedded cells control osteoclast formation. *Nature Medicine*, 17(10), 1235–1241. <https://doi.org/10.1038/nm.2448>

- Xu, D., Rovira, I. I., & Finkel, T. (2002). Oxidants painting the cysteine chapel: Redox regulation of PTPs. In *Developmental Cell* (Vol. 2, Issue 3, pp. 251–252). Cell Press. [https://doi.org/10.1016/S1534-5807\(02\)00132-6](https://doi.org/10.1016/S1534-5807(02)00132-6)
- Xu, Z., Zhang, F., Sun, F., Gu, K., Dong, S., & He, D. (2015). Dimethyl fumarate for multiple sclerosis. In *Cochrane Database of Systematic Reviews* (Vol. 2015, Issue 4). John Wiley and Sons Ltd. <https://doi.org/10.1002/14651858.CD011076.pub2>
- Yamada, C., Yamada, Y., Tsukiyama, K., Yamada, K., Udagawa, N., Takahashi, N., Tanaka, K., Drucker, D. J., Seino, Y., & Inagaki, N. (2008). The murine glucagon-like peptide-1 receptor is essential for control of bone resorption. *Endocrinology*, *149*(2), 574–579. <https://doi.org/10.1210/en.2007-1292>
- Yamaguchi, Y., Kanzaki, H., Katsumata, Y., Itohiya, K., Fukaya, S., Miyamoto, Y., Narimiya, T., Wada, S., & Nakamura, Y. (2018). Dimethyl fumarate inhibits osteoclasts via attenuation of reactive oxygen species signalling by augmented antioxidation. *Journal of Cellular and Molecular Medicine*, *22*(2), 1138–1147. <https://doi.org/10.1111/jcmm.13367>
- Yang, M., Yao, Y., Eades, G., Zhang, Y., & Zhou, Q. (2011). MiR-28 regulates Nrf2 expression through a Keap1-independent mechanism. *Breast Cancer Research and Treatment*, *129*(3), 983–991. <https://doi.org/10.1007/s10549-011-1604-1>
- Yang, W., Lu, Y., Kalajzic, I., Guo, D., Harris, M. A., Gluhak-Heinrich, J., Kotha, S., Bonewald, L. F., Feng, J. Q., Rowe, D. W., Turner, C. H., Robling, A. G., & Harris, S. E. (2005). Dentin matrix protein 1 gene cis-regulation: Use in osteocytes to characterize local responses to mechanical loading in vitro and in vivo. *Journal of Biological Chemistry*, *280*(21), 20680–20690. <https://doi.org/10.1074/jbc.M500104200>
- Yeh, L. C. C., Ford, J. J., Lee, J. C., & Adamo, M. L. (2014). Palmitate attenuates osteoblast differentiation of fetal rat calvarial cells. *Biochemical and Biophysical Research Communications*, *450*(1), 777–781. <https://doi.org/10.1016/j.bbrc.2014.06.063>
- Yin, Y., Corry, K. A., Loughran, J. P., & Li, J. (2020). Moderate Nrf2 Activation by Genetic Disruption of Keap1 Has Sex-Specific Effects on Bone Mass in Mice. *Scientific Reports*, *10*(1), 1–10. <https://doi.org/10.1038/s41598-019-57185-1>
- Yoshikawa, Y., Kode, A., Xu, L., Mosialou, I., Silva, B. C., Ferron, M., Clemens, T. L., Economides, A. N., & Kousteni, S. (2011). Genetic evidence points to an osteocalcin-independent influence of osteoblasts on energy metabolism. *Journal of Bone and Mineral Research*, *26*(9), 2012–2025. <https://doi.org/10.1002/jbmr.417>

- Yoshiko, Y., Wang, H., Minamizaki, T., Ijuin, C., Yamamoto, R., Suemune, S., Kozai, K., Tanne, K., Aubin, J. E., & Maeda, N. (2007). Mineralized tissue cells are a principal source of FGF23. *Bone*, *40*(6), 1565–1573. <https://doi.org/10.1016/j.bone.2007.01.017>
- Yu, T., Robotham, J. L., & Yoon, Y. (2006). Increased production of reactive oxygen species in hyperglycemic conditions requires dynamic change of mitochondrial morphology. *Proceedings of the National Academy of Sciences of the United States of America*, *103*(8), 2653–2658. <https://doi.org/10.1073/pnas.0511154103>
- Zaman, G., Pitsillides, A. A., Rawlinson, S. C. F., Suswillo, R. F. L., Mosley, J. R., Cheng, M. Z., Platts, L. A. M., Hukkanen, M., Polak, J. M., & Lanyon, L. E. (1999). Mechanical strain stimulates nitric oxide production by rapid activation of endothelial nitric oxide synthase in osteocytes. *Journal of Bone and Mineral Research*, *14*(7), 1123–1131. <https://doi.org/10.1359/jbmr.1999.14.7.1123>
- Zhang, C. S., Hawley, S. A., Zong, Y., Li, M., Wang, Z., Gray, A., Ma, T., Cui, J., Feng, J. W., Zhu, M., Wu, Y. Q., Li, T. Y., Ye, Z., Lin, S. Y., Yin, H., Piao, H. L., Hardie, D. G., & Lin, S. C. (2017). Fructose-1,6-bisphosphate and aldolase mediate glucose sensing by AMPK. *Nature*, *548*(7665), 112–116. <https://doi.org/10.1038/nature23275>
- Zhang, J., Wang, X., Vikash, V., Ye, Q., Wu, D., Liu, Y., & Dong, W. (2016). ROS and ROS-Mediated Cellular Signaling. *Oxidative Medicine and Cellular Longevity*, *2016*, 4350965. <https://doi.org/10.1155/2016/4350965>
- Zhang, K., Barragan-Adjemian, C., Ye, L., Kotha, S., Dallas, M., Lu, Y., Zhao, S., Harris, M., Harris, S. E., Feng, J. Q., & Bonewald, L. F. (2006). E11/gp38 Selective Expression in Osteocytes: Regulation by Mechanical Strain and Role in Dendrite Elongation. *Molecular and Cellular Biology*, *26*(12), 4539–4552. <https://doi.org/10.1128/mcb.02120-05>
- Zhang, Keqin, Barragan-Adjemian, C., Ye, L., Kotha, S., Dallas, M., Lu, Y., Zhao, S., Harris, M., Harris, S. E., Feng, J. Q., & Bonewald, L. F. (2006). E11/gp38 selective expression in osteocytes: regulation by mechanical strain and role in dendrite elongation. *Molecular and Cellular Biology*, *26*(12), 4539–4552. <https://doi.org/10.1128/MCB.02120-05>
- Zhang, Y., Rohatgi, N., Veis, D. J., Schilling, J., Teitelbaum, S. L., & Zou, W. (2018). PGC1 β Organizes the Osteoclast Cytoskeleton by Mitochondrial Biogenesis and Activation. *Journal of Bone and Mineral Research*, *33*(6), 1114–1125. <https://doi.org/10.1002/jbmr.3398>
- Zhao, F., Wu, T., Lau, A., Jiang, T., Huang, Z., Wang, X. J., Chen, W., Wong, P. K., & Zhang, D. D. (2009). Nrf2 promotes neuronal cell differentiation. *Free Radical*

Biology and Medicine, 47(6), 867–879.
<https://doi.org/10.1016/j.freeradbiomed.2009.06.029>

Zhong, Q., Ding, K.-H., Mulloy, A. L., Bollag, R. J., & Isales, C. M. (2003). Glucose-dependent insulinotropic peptide stimulates proliferation and TGF-beta release from MG-63 cells. *Peptides*, 24(4), 611–616.
[https://doi.org/10.1016/s0196-9781\(03\)00103-7](https://doi.org/10.1016/s0196-9781(03)00103-7)

Zhou, Y., Li, A., Song, Y., Zhou, H., Li, Y., & Tang, Y. (2013). Role of sclerostin in the bone loss of postmenopausal chinese women with type 2 diabetes. *Chinese Medical Sciences Journal = Chung-Kuo i Hsueh K'o Hsueh Tsa Chih*, 28(3), 135–139. [https://doi.org/10.1016/s1001-9294\(13\)60038-3](https://doi.org/10.1016/s1001-9294(13)60038-3)

Review

Interplay between BMPs and Reactive Oxygen Species in Cell Signaling and Pathology

Cristina Sánchez-de-Diego ¹, José Antonio Valer ¹, Carolina Pimenta-Lopes ¹, José Luis Rosa ^{1,2} and Francesc Ventura ^{1,2,*}

¹ Departament de Ciències Fisiològiques, Universitat de Barcelona, Carrer Feixa Llarga s/n, 08907 L'Hospitalet Llobregat, Spain; csanchezdg@gmail.com (C.S.-d.-D.); j.a.valer@hotmail.com (J.A.V.); carolinapimentacosta@ub.edu (C.P.-L.); joseluisrosa@ub.edu (J.L.R.)

² IDIBELL, Avinguda Granvia de l'Hospitalet 199, 08908 L'Hospitalet de Llobregat, Spain

* Correspondence: fventura@ub.edu; Tel.: +34-934024281; Fax: +34-934024268

Received: 14 August 2019; Accepted: 24 September 2019; Published: 26 September 2019



Abstract: The integration of cell extrinsic and intrinsic signals is required to maintain appropriate cell physiology and homeostasis. Bone morphogenetic proteins (BMPs) are cytokines that belong to the transforming growth factor- β (TGF- β) superfamily, which play a key role in embryogenesis, organogenesis and regulation of whole-body homeostasis. BMPs interact with membrane receptors that transduce information to the nucleus through SMAD-dependent and independent pathways, including PI3K-AKT and MAPKs. Reactive oxygen species (ROS) are intracellular molecules derived from the partial reduction of oxygen. ROS are highly reactive and govern cellular processes by their capacity to regulate signaling pathways (e.g., NF- κ B, MAPKs, KEAP1-NRF2 and PI3K-AKT). Emerging evidence indicates that BMPs and ROS interplay in a number of ways. BMPs stimulate ROS production by inducing NOX expression, while ROS regulate the expression of several BMPs. Moreover, BMPs and ROS influence common signaling pathways, including PI3K/AKT and MAPK. Additionally, dysregulation of BMPs and ROS occurs in several pathologies, including vascular and musculoskeletal diseases, obesity, diabetes and kidney injury. Here, we review the current knowledge on the integration between BMP and ROS signals and its potential applications in the development of new therapeutic strategies.

Keywords: BMP; reactive oxygen species (ROS); NOX; cell signaling; PI3K; MAPK; SMAD; NRF2

1. Introduction

Bone morphogenetic proteins (BMPs) were first described in the 1960s as osteoinductive soluble factors that belong to the transforming growth factor- β (TGF- β) superfamily [1]. BMPs are expressed in multiple cell types and participate in a wide variety of processes, including morphogenesis, cell differentiation and regulation of whole-body homeostasis. Several studies demonstrate that BMPs contribute to gastrulation and mesoderm patterning. In extraembryonic tissues, BMPs are critical for primitive streak formation [2] and to establish left-right patterning [3]. During organogenesis, BMP signaling promotes mesoderm differentiation into heart tissue. In the ectoderm, BMPs induce neural differentiation and are necessary for neural tube formation [4]. In the peripheral nervous system, BMPs induce neuronal lineage commitment and neuronal differentiation whereas in the progenitor cells of the Central Nervous System (CNS), BMPs suppress neuronal or oligodendroglial differentiation and promote astroglial formation [5]. BMPs are also involved in skeletogenesis [6] and bone remodeling after birth [7]. In fact, BMP signaling is required for chondrogenesis [8] and osteogenesis [9]. In kidney organogenesis, BMPs promote the elongation of the ureteric bud and regulate the proliferation and differentiation of the metanephric mesenchyme [10]. BMP signaling is

also critical for the development of vascular system in embryos, and for the regulation of vascular homeostasis in adults and, when altered, being causative for several vascular dysfunctions. For instance, pulmonary arterial hypertension and hereditary hemorrhagic telangiectasia have been directly linked to impaired BMP signaling [11–13]. Finally, BMPs are crucial for a proper reproductive system function. In gonadal differentiation, BMP8 is important for spermatogenesis maintenance [14], while BMP15 is associated with granulosa cell proliferation in the ovary [15]. Due to BMP relevance in organ generation and maintenance, alterations in BMP signaling are associated with several pathologies.

BMPs interact with specific serine-threonine kinase receptors present in the cell membrane. Subsequently, the information is transduced to the nucleus through the SMAD pathway. Besides this signaling mode, several non-canonical, SMAD-independent BMP transducers have been identified, including small GTPases, phosphatidylinositol 3-kinase/AKT (PI3K/AKT) and distinct types of mitogen-activated protein kinases (MAPKs) [16]. In this context, recent evidence suggests that reactive oxygen species (ROS) can also act as second messengers for BMPs.

ROS are highly reactive molecules derived from the reduction of molecular oxygen as a consequence of cellular metabolism or the activity of specific enzymes, such as the NADPH oxidase (NOX) complexes [17]. Since ROS are highly unstable, they react with proteins, nucleic acids, lipids and other cellular components and often disrupt their cellular functions. Therefore, ROS were first considered as harmful molecules. Accordingly, oxidative stress is involved in multiple pathologies such as cardiac and neurodegenerative diseases, vascular disorders, diabetes, infections and cancer [18]. Even though oxidative stress occurs in several pathologies, numerous studies demonstrate that ROS signaling is also important in normal physiology and in the generation of proper redox biological responses [19]. For instance, in skeletal muscle, ROS are required for normal contraction, where they modulate muscle adaptations to exercise [20]. ROS also contribute to immune response activation and regulation [21] and mediate leucocyte adhesion to endothelial cells [22]. Indeed, the physiological role of ROS is based on their capacity to modulate several signaling pathways, including nuclear factor-kappa B (NF- κ B), MAPKs, kelch-like ECH-associated protein 1 (KEAP1)-nuclear factor erythroid 2-related factor 2 (NRF2) and PI3K-AKT [19].

Although little is known about the relationship between BMPs and ROS, both signals share common transducing modules, and their dysregulation occur in several pathologies. In this review, we will describe the putative modes of signaling crosstalk between BMPs and ROS and analyze their implications in physiology and disease.

2. BMP Signals

BMPs structurally belong to the transforming growth factor- β (TGF- β) superfamily [23]. BMPs share seven highly conserved cysteines with other TGF- β family members. Six of them form three intramolecular disulfide bonds, and the seventh one creates a covalent disulfide bond with another monomer to form homo- or heterodimers [24]. BMPs are also sub-classified into several groups, including BMP2/4, BMP5/6/7/8, growth and differentiation factor (GDF)-5/6/7 and BMP9/10 [23]. BMPs diffuse away from the cell of origin or form stable complexes with their cleaved proto-domains.

Outside the cell, BMPs bind to BMP receptors (BMPRs) and initiate an intracellular transduction cascade. BMPRs are serine/threonine kinase receptors with a short extracellular domain, a single transmembrane domain and an intracellular serine/threonine kinase domain. They are classified in two groups: BMPR type I (ACVR1, ACVRL1, BMPR1A and BMPR1B) and BMPR type II (BMPR2, ACVR2 and ACVR2B) [25]. Different BMP subgroups display disparate type I and type II receptor binding specificities [23]. BMP binding induces the formation of a heteromeric complex between type I and type II receptors. Once the complex is established, constitutively active kinase activity present in type II receptors phosphorylates the GS domain (a glycine and serine-rich intracellular region located adjacent to the kinase domain) of type I receptors, an action that leads to its activation. The active complex phosphorylates and activates the SMAD family of transcription factors that transduce the signal to the nucleus [26]. Under basal conditions, receptor-regulated SMADs (R-SMAD) are anchored at the cell

membrane through their interaction with several proteins. In the canonical pathway, type I receptors phosphorylate R-SMADs 1/5/8. R-SMAD phosphorylation releases them from the membrane and disrupts the auto-inhibitory interaction between their N- and C-terminal domains. Then, two active R-SMAD 1/5/8 molecules bind to the common partner SMAD4 and translocate to the nucleus, where they interact with several transcription factors and transcriptional co-activators/repressors [27,28] (Figure 1).

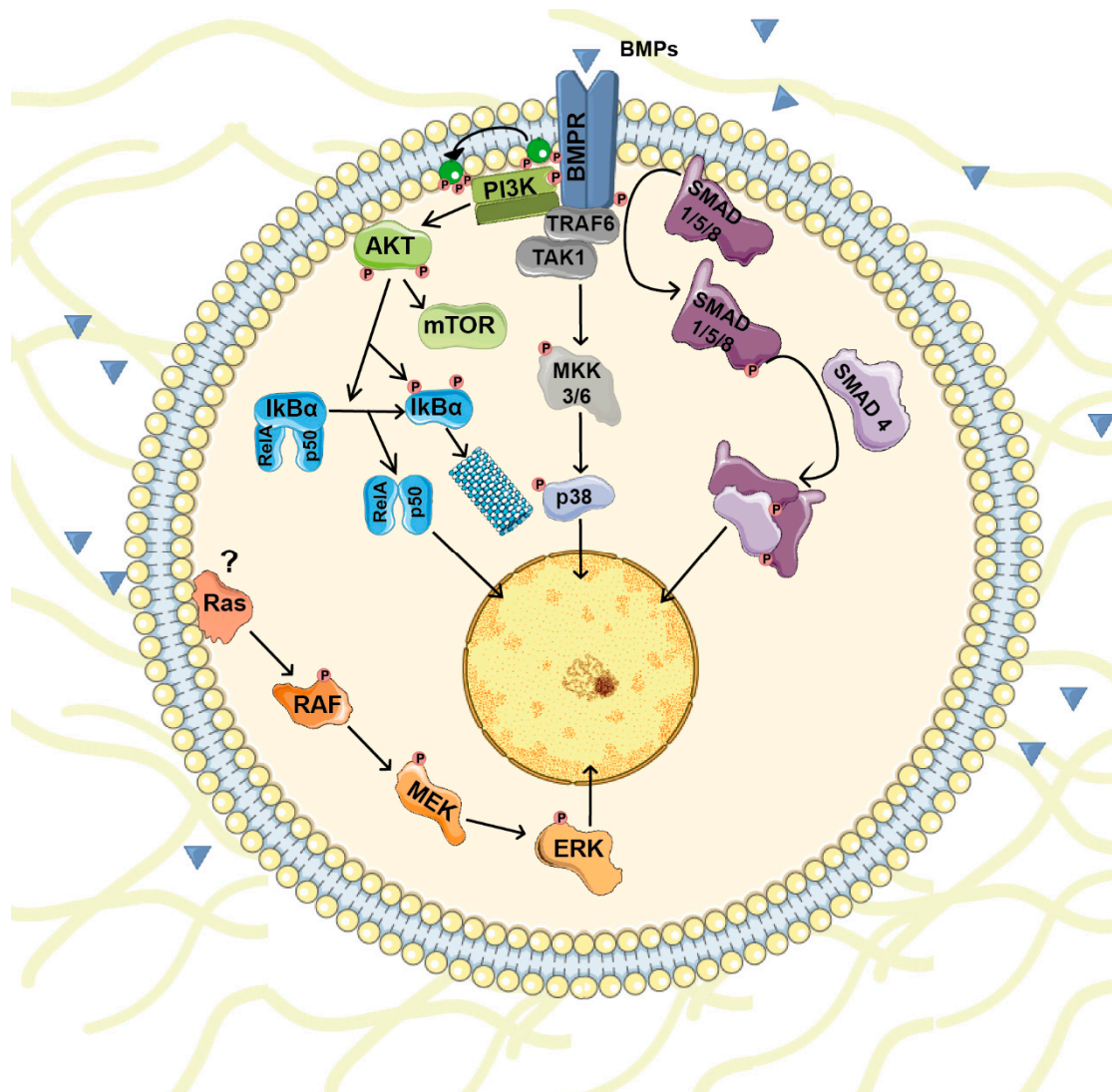


Figure 1. BMP signaling pathways. Once BMP receptors (BMPR) are stimulated they form a complex and initiate an intracellular transduction cascade. In the canonical pathway, BMP receptors phosphorylate and activate the SMAD family of transcription factors that transduce the signal to the nucleus. Besides SMADs, BMPs modulate other intracellular signaling pathways (non-canonical BMP signaling) including PI3K/AKT and various types of MAPKs pathways.

Besides the canonical signaling through SMADs, BMPs modulate other intracellular signaling pathways with important roles in cell physiology. Non-canonical BMP signaling includes small GTPases, PI3K/AKT, lim kinase-1 (LIMK1) and various types of MAPKs [28]. For instance, BMPs regulate p38 activity through TGF- β -associated kinase 1 (TAK1) [29,30]. TAK1 is a member of the MAPK family whose activity is regulated by the E3 ubiquitin ligase TRAF6 in a receptor-kinase-independent manner. Upon BMP/BMPR complex formation, TRAF6 becomes poly-ubiquitinated and recruits and triggers TAK1 activation that induces p38 activity [31] (Figure 1).

BMP signaling is regulated by multiple mechanisms. Intracellularly, several miRNAs regulate the expression of BMPs, BMPRs and downstream effectors. Inhibitory Smads (such as Smad 6 and 7) and methylation of the promoters also regulate BMP signaling. Extracellularly, pseudo-receptors and BMPs antagonists control BMP availability [32,33]. More than 15 antagonists have been discovered which are classified in three subgroups based on the size of the cysteine knot, a common feature of BMPs. First, antagonists with an eight-member ring represented by the DAN family (including DAN, GREM2, Gremlin, Cerberus, Coco and Caronte. second, USAG-1, DANTE and twisted gastrulation (TSG) with a nine-member ring and finally, inhibitors with a ten-member rings including Chordin (CHD), Noggin (NOG), Ventroptin (CHRD1), Follistatin (FST) and FLRG-follistatin-related gene (FSTL3) [32,34]. Finally, the binding of BMPs to several extracellular matrix (ECM) proteins also modulates their bioavailability [34].

3. ROS

ROS are radical and non-radical oxygen species that result from the partial reduction of oxygen [35]. Cellular ROS include the superoxide anion (O_2^-), hydrogen peroxide (H_2O_2), and hydroxyl radical ($OH\cdot$) that arise either as byproducts of aerobic metabolism or as defense mechanisms against xenobiotics or bacterial invasion [36]. Under physiological conditions, ROS act as signaling molecules that are important for adaptation to changes in nutrient supply and the oxidative environment [37]. ROS also contribute to regulate cell proliferation and differentiation. However, increased ROS levels or changes in their compartmentalization can dysregulate oxidation of proteins, lipids and nucleic acids [37]. Therefore, the ROS concentration is in a dynamic equilibrium and is modulated by cellular processes that produce and eliminate ROS.

A primary ROS source is O_2^- , which is generated in the mitochondria by complexes I, and III or in other cellular compartments by the action of several enzymes such as NOXs. Superoxide reacts with molecules to cause molecular damage or turn into H_2O_2 spontaneously or by the action of the enzyme superoxide dismutase (SOD). Other ROS sources are the mitochondrial enzymes monoamine oxidase and cytochrome b5ductase, as well as glycerol-3-phosphate dehydrogenase, aconitase, pyruvate dehydrogenase or α -ketoglutarate dehydrogenase [38].

Since high ROS levels generate cell damage, cells have developed several defense mechanisms to detoxify ROS. H_2O_2 is reduced to generate water by the action of catalase or glutathione peroxidase (GPx). Thioredoxins, peroxiredoxins and GPxs act as antioxidant enzymes by reversing the oxidation of cysteine residues. Finally, cells also have non-enzymatic antioxidants that include low-molecular-weight compounds, such as vitamins C and E, β -carotene, uric acid and glutathione (GSH) [36].

4. ROS-Mediated Cellular Signaling

ROS are highly reactive molecules with the capacity to target several transductor proteins (NF- κ B, MAPKs, KEAP1-NRF2 and PI3K-AKT), ion channels and transporters (Ca^{2+} and mitochondrial permeability transition pore [mPTP]), and thus, impact on cell growth, differentiation, migration and death [37] (Figure 2).

The NF- κ B family of transcription factors are involved in multiple cellular processes such as immune and inflammatory responses, development, cellular growth and apoptosis. NF- κ B dimers are bound to their inhibitors of κ B (I κ Bs) and retained in the cytoplasm. Consequently, NF- κ B activation depends on I κ B degradation, which occurs after its phosphorylation by I κ B kinase (IKK). Activators of the IKK complex include MAPKKKs such as MEKK1, MEKK3 and TAK1, which represent a common hub for several stimuli, including BMPs and ROS. Recent studies demonstrate that ROS can induce I κ B α phosphorylation and degradation [39]. ROS also induce S-glutathionylation and IKK inhibition [40] and other upstream kinases, such as MKK1; these actions hamper NF- κ B activation. Conversely, NF- κ B can alter ROS levels by increasing the expression of antioxidant proteins such as Cu-Zn-SOD, Mn-SOD, GPx and glutathione S-transferase-Pi (GST-Pi) [37].

PI3K-AKT is also susceptible to ROS regulation. PI3K catalyzes phosphatidylinositol 3,4,5-trisphosphate (PIP3) synthesis that recruits it into the plasma membrane and activates proteins that contain the pleckstrin homology domains such as AKT and its upstream activator PDK1. Activation of AKT is induced by its phosphorylation in Thr308 and Ser473 [45]. AKT activity is counteracted by its dephosphorylation by protein phosphatase 2 (PP2A). PP2A is involved in the regulation of WNT, mTOR and MAP kinase pathways, cell cycle progression as well as DNA repair [46]. Inhibition of mTORC1 activates PP2A and subsequent DNA-PK. DNA-PK is required for the repair of DNA double-strand breaks (DSBs). Besides its role in DNA repair, DNA-PK also phosphorylates AKT in Ser473 kinase, under DNA damage conditions [47]. On the other hand, AKT activity can be also reduced through PIP3 dephosphorylation by phosphatase and tensin homolog (PTEN). ROS induce PTEN degradation [48] and may also promote oxidative inactivation of PP2A [49].

ROS also regulate protein kinase pathways through the oxidation of cysteine sulfhydryl groups that are present in several protein kinases, including protein kinase A (PKA) [50], protein kinase C (PKC) [51], protein kinase D (PKD) [52], receptor tyrosine kinases [53] and Ca/calmodulin-dependent protein kinase II (CaMKII) [54]. Recently, a study demonstrated that ROS oxidize Cys17 and 38 of the PKA regulatory subunits, changes that lead to the formation of an inter-subunit disulfide bond that activates PKA independently of cyclic AMP (cAMP) levels [55]. The PKC family contains membrane protein kinases composed of an N-terminal regulatory region and a C-terminal catalytic domain [56]. Both domains contain cysteine-rich motifs targeted by ROS and they play a dual role in PKC regulation. In the regulatory domain, these cysteines form two pairs of zinc fingers that inhibit PKC activity. Low ROS doses destroy the zinc finger conformation, thus activating PKC even in the absence of Ca^{2+} or phospholipids. However, high ROS doses react with cysteine residues in the catalytic domain, and these interactions lead to PKC inactivation [57,58]. Additionally, ROS enhance PKD activation in several ways: they induce the production of DAG, the activation of PKC and the phosphorylation of PKD at Tyr93, which facilitates its binding with PKC [59,60].

The KEAP1-NRF2 pathway is essential for the maintenance of redox balance. Under basal conditions, NRF2 remains in the cytosol associated with KEAP1, which recruits CUL3 that ubiquitinates NRF2, leading to its degradation. Increased ROS levels promote the dissociation of the NRF2-KEAP1 complex by the oxidation of key reactive cysteine residues (Cys151, Cys273 and Cys288) of KEAP1 and/or the activation of kinases such as PKC, PI3K or AMPK that phosphorylate NRF2 [61–64]. Both events reduce NRF2 degradation and facilitate its translocation to the nucleus. Once in the nucleus, NRF2 heterodimerizes with other transcription factors and binds to antioxidant response element (ARE) sequences to promote the expression of target genes [65]. Activation of these different pathways also contributes to ROS scavenging through the induction of NRF2. NF- κ B acts as a transcription factor for NRF2 [66] and, as mentioned above, PKC and PI3K phosphorylate NRF2, an action that stabilizes the protein and promotes its nuclear translocation [62–64]. Simultaneously, ROS activate glycogen synthase kinase 3 β (GSK3 β), which leads to nuclear import of Src kinases that phosphorylate NRF2 at Tyr568 and promote its nuclear export [67].

5. NOXs

NOXs and dual oxidases (DUOXs) are membrane-bound enzymatic complexes that catalyze the transfer of one electron from NADPH to oxygen to generate ROS in response to a stimulus, such as growth factors, cytokines and calcium signals. In the human genome, seven NOX homologues have been identified: NOX1 to NOX5 and DUOX1 and DUOX2. These genes differ in their preferential tissue of expression, the type of ROS released and their regulatory mechanisms. NOXs produce either superoxide (NOX1-3 and NOX5) or H₂O₂ (NOX4 and DUOX1-2) in a NADPH-dependent manner [68]. NOXs are classified in three main groups according to the domains they contain. NOX1, NOX2, NOX3 and NOX4 contain the electron transfer center. NOX5 contains the catalytic domain and an amino-terminal calmodulin-like domain that acts as a regulatory domain. DUOXs contain

the catalytic domain and a calmodulin-like domain connected by an α -helix to an amino-terminal peroxidase-homology domain.

Short-term NOX regulation involves regulatory subunits. NOX1, NOX2 and NOX3 are present as inactive transmembrane monomers, and interaction with other subunits is required for their activity. However, NOX4 is synthesized in a constitutively active form [69]. NOX1 to NOX4 interact with p22phox, which has a scaffold function. NOX5 does not interact with p22phox but requires homo- or multimerization for its stabilization [70] and depends on cytosolic calcium levels for its activation. To activate the NOX catalytic center, three signaling events must occur. First, the regulatory domain (p40phox, p47phox and p67phox), which is in the cytosol, is phosphorylated in the auto-inhibitory region. This process involves protein kinases, including PKC and AKT [71].

Then, phosphorylation of p47phox releases its binding to the SRC-homology 3 (SH3) domain, allowing p47phox to bind to p22phox (in the cell membrane) and to lipids provided by PI3K and phospholipase D [72,73]. Finally, it is required the presence of two guanine nucleotide-binding proteins, RAP1A and RAC2. RAP1A is a membrane protein, while RAC2 localizes in the cytosol in a dimeric complex with its inhibitor guanine nucleotide dissociation inhibitor (Rho-GDI). Upon its activation, RAC2 binds GTP and translocates to the membrane along with p40phox, p47phox and p67phox, that constitute the active complex [74].

NOX enzymes are also regulated at the transcriptional level. This regulation depends on the specific enzyme and cell type. For instance, *NOX1* is strongly induced by the growth factors angiotensin II, platelet-derived growth factor (PDGF) and phorbol esters (in vascular smooth muscle) and keratinocyte growth factor- α (KGF- α) and interferon gamma (IFN- γ) in human colon cells. Comparatively, *NOX4* is regulated by angiotensin II [75].

NOX enzymes participate in several biological processes. In neutrophils, NOXs generate high superoxide concentrations in the phagosome to enhance killing bacteria. In barrier cells, IFN- γ and lipopolysaccharide (LPS) induce *NOX1* expression through Toll-like receptor-4 to help kill invading microorganisms. In addition to host defense, NOX-derived ROS contribute to signal transduction by regulating biological processes such as cell growth, differentiation, angiogenesis and senescence. For instance, *NOX4* overexpression in tumors is associated with apoptosis and cell senescence [75]. *NOX4* is also implicated in angiotensin-II-dependent signaling in vascular smooth-muscle cells [76] and in insulin signaling in adipose tissues [77]. DUOX enzymes are implicated in biosynthetic reactions that involve ECM proteins [75].

6. Interplay between BMPs and ROS Signaling

BMPs stimulate ROS production in several cell types. BMPs stimulate ROS production by activation and/or induction of *NOX1-5* expression. For instance, in adult renal progenitors BMP2 induces *NOX4* and *NOX2* expression and activity [78]. ROS reciprocally regulate the expression of *BMP2* in osteoblasts [79]. Both BMPs and ROS activate several common signaling pathways that should be coordinated (Figure 3). Consequently, unregulated changes in their expression or production or altered signaling could result in severe repercussions.

NOX1, NOX2 and NOX3 require p47phox and p67phox phosphorylation to facilitate translocation of the cytosolic subunits and formation of an active complex. The primary kinase involved in p47 phosphorylation is PKC (α , β , δ , and ζ). Other pathways, including ERK and p38, PKA and AKT, also contribute to NOX activation [80]. Therefore, BMPs can activate NOX enzymes by inducing their expression or through phosphorylation by the non-canonical signaling pathways above mentioned. For instance, in osteoblasts BMP2 enhances ROS production by activating NOX [79], and BMP2, BMP4 and BMP7 upregulate *NOX4*, *NOX1* and *NOX2* expression in osteoblasts, sympathetic neurons and monocytes [79,81,82]. Moreover, in podocytes, BMP2 increases the free cytosolic Ca^{2+} concentration, and the expression of DNA-binding protein inhibitor 1 (ID1). Both events elevate NADPH-dependent ROS production [83].

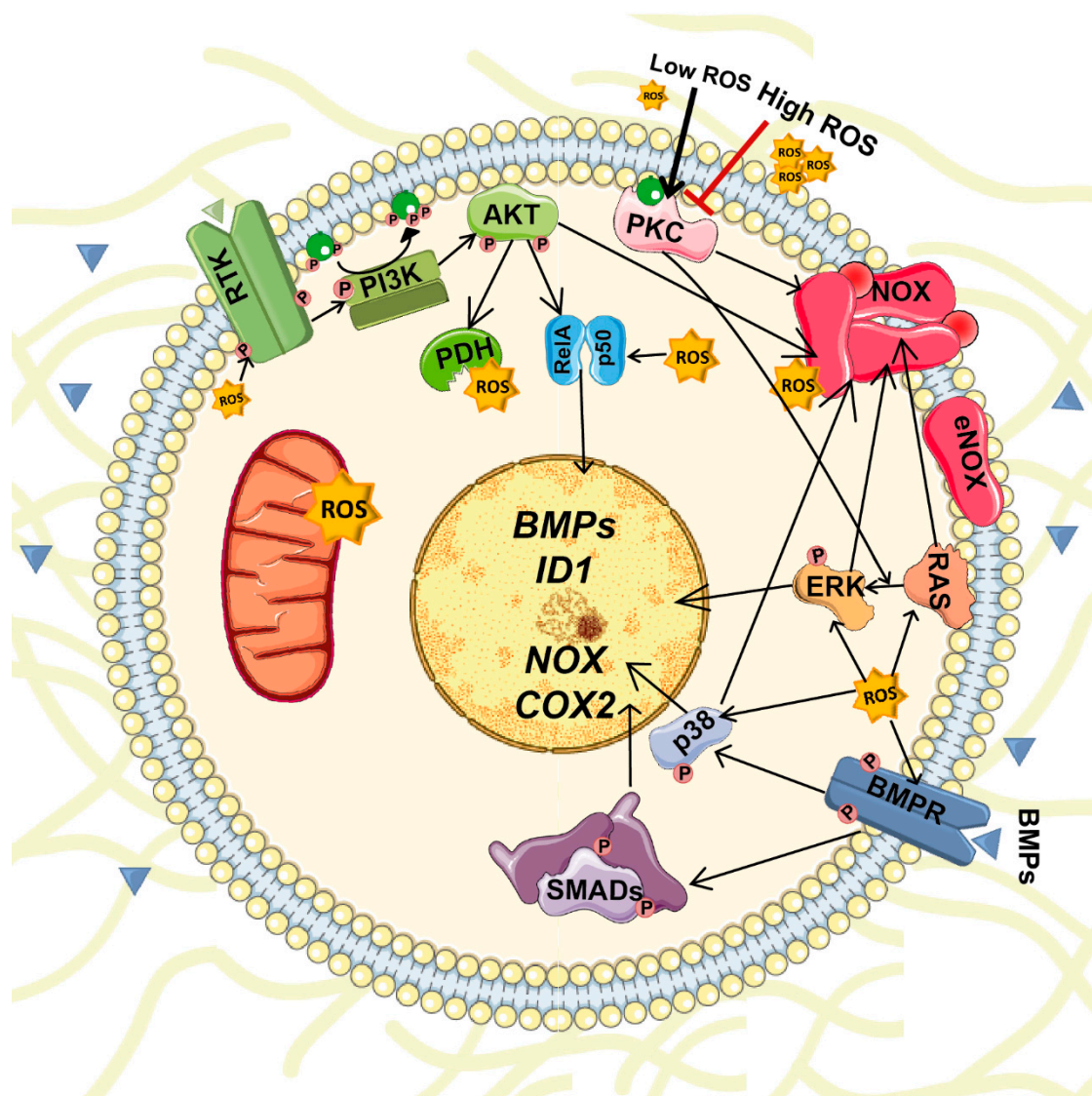


Figure 3. Interplay between BMPs and ROS signaling. Production of BMPs and ROSs are reciprocally regulated. BMPs stimulate ROS production by activation and/or induction of NOX1-5 expression while ROS regulate the expression of several BMPs. Furthermore, both BMPs and ROS activate several common signaling pathways including PI3K-AKT, ERK, JNK and p38 MAPKs.

Activation of non-canonical pathways by BMPs also induces cyclooxygenase 2 (COX2) gene expression [84], which is a source of ROS [85]. Moreover, different prostanoids produced by COX2 modulate NOX activity and regulate ROS production [85]. Finally, PI3K/AKT signaling, which can be activated by BMPs [30], contribute to elevate ROS levels by activating NOX, modulating mitochondrial bioenergetics and enhancing the metabolic rate. In this latter case, AKT phosphorylate GSK3 β , which reduces its activity thus enhancing the activity of pyruvate dehydrogenase and α -ketoglutarate dehydrogenase complexes. Both of these complexes generate superoxide and H₂O₂ [86]. Unlike other NOX isoforms, NOX4 is constitutively active. Thus, its regulation occurs mainly at the transcriptional level. Several cytokines, including BMP2, TGF β and angiotensin II, can upregulate NOX4 expression through PKC and and/or SMAD pathways [78,87].

Reciprocally, ROS contribute to the regulation of BMP expression. In particular, BMP2 and BMP4 are upregulated in conditions associated with oxidative stress [11]. For example, BMP2 autoregulation of its own expression is mediated by SMAD-dependent transcription and can also be modulated by NOX4-derived ROS in osteoblasts [79]. Further, increased H₂O₂ levels, produced by NOX activation or

other conditions such as inflammation, induce NF- κ B activation. Once active, NF- κ B enhances *BMP2* expression [11,88]. Therefore, although the mechanisms are mostly unknown, evidence suggests that there is a positive regulatory loop between ROS and BMP signals. Consequently, alteration of these regulatory loops can lead to oxidative stress and cell dysfunction and contribute to several pathologies.

The crosstalk between BMPs and ROS goes beyond the regulation of their own transcription and activation; it also affects downstream signaling pathways shared by these two molecules. As mentioned above, ROS activate ERK, JNK and p38 MAPKs [42], while BMPs activates TAK1 that acts upstream of JNK and p38 [89]. PI3K-AKT is another intracellular pathway where ROS and BMP signaling converge. BMP2 increases AKT phosphorylation in pancreatic cancer cells [90], while ROS reduces PI3K-AKT downregulation by targeting PTEN and PP2A in embryonic rat heart cells [91].

7. BMPs and ROS in Cell Specification

BMPs were identified as molecules capable of modulating mesenchymal cell specification and inducing bone development. In particular, BMPs regulate osteoblast differentiation through induction of bone-determining transcription factors [92]. ROS generation also influences bone cell differentiation. Undifferentiated mesenchymal stem cells (MSCs) display low levels of ROS and express high levels of antioxidant enzymes. This evidence is linked to MSC self-renewal, as physiological ROS upregulation is required for MSC differentiation. For instance, during MSC osteogenic differentiation, WNT/ β -catenin activation increases ROS [93]. In osteoblast progenitor cells, BMP2 activates *NOX4*, which is highly expressed in pre-osteoblasts, and this activation results in ROS production. Superoxide anions generated by *NOX4* are rapidly converted into H_2O_2 , and ROS produced by *NOX4* induce alkaline phosphatase expression and activate PI3K and SMAD 1/5 signal transduction pathways. MSCs also generate both permanent and transient cartilage. BMP signaling is critical for cartilage formation [94], and ROS generated by *NOX2* and *NOX4* are also essential for the early chondrogenesis stages. ROS also contribute to osteoclast differentiation. Osteoclasts arise from the fusion of multiple monocyte and macrophage precursors in the presence of receptor activator of NF- κ B ligand (RANKL). RANKL stimulates ROS production, which is required for RANKL-induced activation of AKT, NF- κ B and ERK pathways [95]. Moreover, ROS are necessary for the resorptive function of osteoclasts [96].

ROS and BMPs also participate in the cardiovascular system development. In embryonic stem cells, ROS promote differentiation toward both cardiomyogenic and vascular cell lineages through AMP-activated protein kinase (AMPK) pathway activation. ROS and *NOX4* activation are also involved in cardiogenesis and cardiac myofibrillogenesis, since antioxidants and *NOX4* silencing impair the cardiac differentiation of stem cell precursors. In early embryonic mouse heart, *NOX4* is the main *NOX* isoform expressed. *NOX4* generates ROS, an action that leads to p38 phosphorylation and monocyte enhancer factor 2C (MEF2C) nuclear translocation. Both events promote cardiomyocyte specification, transcription of sarcomeric proteins and myofibrillogenesis [97]. ROS also upregulate the expression of other cardiac-specific transcription factors and the expression of *Bmp10* [97]. During embryonic heart formation, BMP10 prevents premature cell cycle withdrawal of mesenchymal cells and regulates the level of expression of several key cardiogenic transcriptional factors [98]. After birth, BMP2 upregulates *NOX4* and enhance ROS-driven p38MAPK activation which promote cardiomyocyte differentiation in stem cells [99]. All these events contribute to the modulation of cardiac growth and function.

BMPs also affect dendritic formation in sympathetic neurons [100], where they promote dendritic growth in hippocampal [101], cortical [102] and retinal ganglion neurons [103]. In sympathetic neurons, BMP7 upregulates *NOX2* expression, which is associated with an increase in oxygen consumption and ROS production. Newly synthesized ROS becomes restricted within certain cell compartments to avoid undesired cellular damage. In these sequestrations, they act as signaling molecules and upregulate the expression of differentiation genes [83]. Antioxidant treatment abolishes the effects of BMP7 on dendrite formation, data that demonstrates the importance of ROS in this phenomenon [81]. Additionally, BMP9 induces and maintains the neuronal cholinergic phenotypes in the central nervous system by inducing gene expression of choline acetyltransferase and vesicular acetylcholine transporter [104]. Interestingly,

BMP9 levels and its bioavailability are reduced by redox-dependent proteolysis [105]. Consequently, increased extracellular ROS levels might be deleterious for neural differentiation. Although these data suggest a functional crosstalk between BMPs and ROS in the coordination of the differentiation of several cell types, further studies regarding the importance of the BMP and ROS interplay in the physiology of other tissues are necessary.

Cancer stem cells (CSC) constitute a small population of cells with the ability to proliferate indefinitely and give rise to the tumors [106]. In addition, differentiated progeny of CSCs create a niche that maintain both CSC and non-CSC components of the tumor hierarchy. BMPs have shown to be important not only for the differentiation of physiological stem cells but also for CSC. BMP2 have shown to induce CSC differentiation in osteosarcoma [107], while BMP4 induce differentiation of colorectal cancer stem cells [108], resulting in a reduction of tumorigenesis in both cases. In gliomas, where BMP2 expression is elevated, CSC secrete BMP antagonists, such as Gremlin1, to maintain their high proliferative capacity [109]. On the other hand, CSC, like normal stem cells have low intracellular levels of ROS, which contribute to their self-renewal capacity and resistance to chemotherapy. Several pathways are involved in controlling ROS levels in CSC. These pathways include PI3K/AKT/mTOR signaling pathway which regulate FOXO, HIF-1 α , ATM, WNT, STAT and NF- κ B pathways [110].

8. BMPs and ROS in Pathology

8.1. ROS and BMPs in Vascular Diseases

Vascular vessels are structures integrated by endothelial, smooth muscle cells (SMCs) and fibroblasts that work in a coordinated manner to adapt to the changes in their environment. Vascular dynamics involve modifications in cell growth, death and migration, and the synthesis or degradation of the ECM. Vascular remodeling responds to physiological and pathological changes in haemodynamic conditions and is driven by the presence of local growth factors, vasoactive substances and hemodynamic stimulus [111].

ROS, as second messengers, induce vessel wall remodeling and influence SMC and endothelial cell growth and survival (Figure 4). Besides mitochondrial respiration, NOXs represent the major ROS source in vascular cells, and their dysregulation is associated with cardiovascular diseases [112]. The superoxide anion (O_2^-) is the major ROS molecule in the vascular wall. It inactivates nitric oxide (NO), a vascular relaxing factor, and thus impairs relaxation [113]. Several pathological conditions, such as inflammation or high blood pressure, activate NOX-derived H_2O_2 production via TNF α . In the endothelium, high pressure increases wall tension, which elevates the calcium concentration, activates PKC and stimulates NOX-dependent. O_2^- and H_2O_2 production [114]. Increased H_2O_2 levels promote I κ B degradation, and the consequent NF- κ B activation induces *BMP2* expression [11,88]. Blood vessel smooth muscle and endothelial cells express *BMP2* and *BMP4* mRNA [88]; expression is higher in endothelial cells. Both *BMP2* and *BMP4* are upregulated in atherosclerotic lesions associated with oxidative stress, inflammation and hyperglycemia [115]. Moreover, plasma *BMP2* levels positively correlate with calcium density of the plaque in hyperglycemia-induced vascular calcification [116].

In SMCs, *BMP2* promotes the expression of the type III sodium-dependent phosphate cotransporter *PIT1* via JNK pathway [117]. This effect is essential in matrix calcification induced by *BMP-2*. *BMP2* also and increases the activity of NOX, which induces oxidative stress. The increase of NOX activity is mediated via activation of the bone morphogenetic protein receptor 2 and SMAD1 [118]. *BMP2*-mediated oxidative stress also induces endoplasmic reticulum (ER) stress that increases the function of GRP78, IRE1 α , and XBP1. XBP1 is a transcription factor that binds to the Runx2 promoter and increases osteogenesis [118]. *BMP2* also increases the levels of the osteogenic marker alkaline phosphatase (ALPL) and decreases the expression of the SMC marker *SM22*, changes that promote SMC transition to the osteochondrogenic phenotype and hence vascular calcification [117].

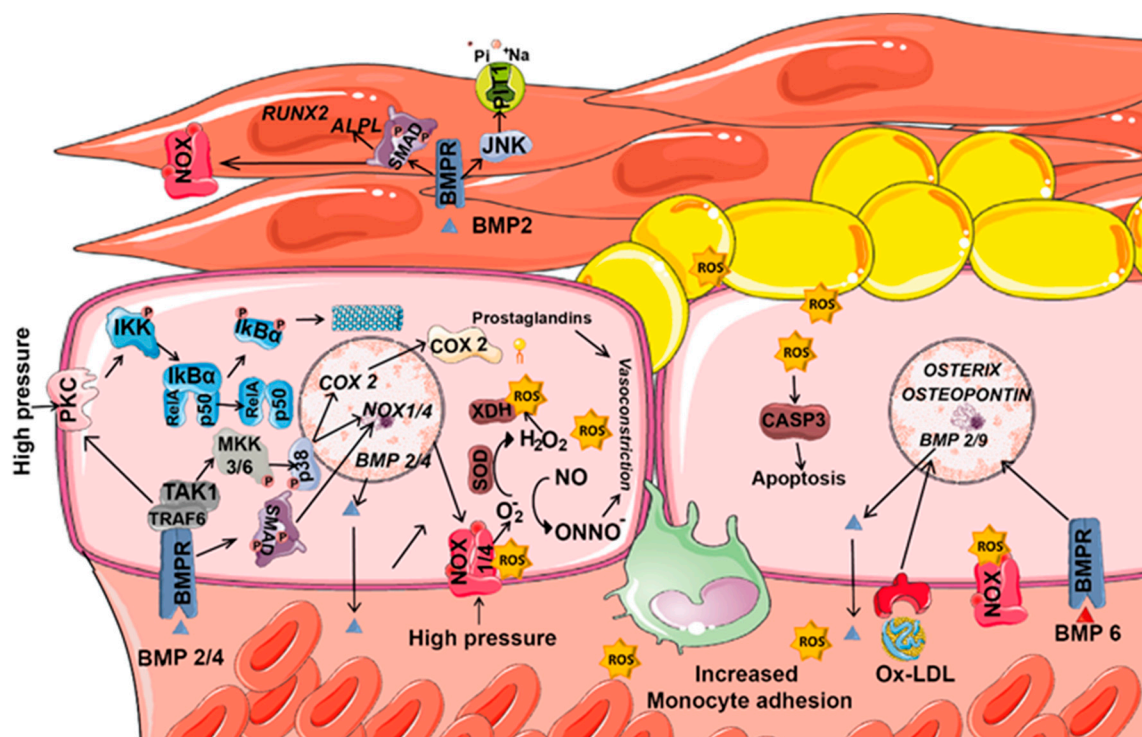


Figure 4. Coordinated contribution of ROS and BMPs to vascular diseases. Vascular vessels are structures integrated by endothelial, smooth muscle cells (SMCs) and fibroblasts. In the endothelium, ROS are mainly produced by NOXs and its levels increase as a response to high pressure. In vascular vessels, ROS induce the expression of several BMPs, inactivates nitric oxide, and stimulate NF- κ B pathway. By its part, BMPs activate MAPK pathways, increase NOX1/4 and COX2 expression and consequently enhance ROS generation. BMP6 and oxidized low-density lipoprotein (oxLDL) increase the expression of the osteoblast markers *Osterix* and *Osteopontin* in a NOX dependent manner. In SMCs, BMPs promotes the expression of the type III sodium-dependent phosphate cotransporter *PIT1*, increases the activity of NOX, and the levels of osteogenic markers (*RUNX2* and *ALPL*).

In endothelial cells, BMP2/4 activate PKC and MAPK pathways, which results in endothelial activation and increases monocyte adhesion. In these cells, MAPK activation is dependent on PKC and subsequent NOX-derived ROS generation [119]. In human coronary artery smooth muscle cells (HCSMC), BMP2 induce NOX via BMPR2 and SMAD1 [118]. In hypertensive patients, BMP2/4 upregulation is associated with impaired endothelial function in systemic blood vessels [120]. Moreover, BMP2/4 administration induces O₂⁻ generation, endothelial dysfunction and hypertension in systemic arteries but does not affect pulmonary blood vessels [121]. In fact, in pulmonary arteries resistant to atherogenesis, BMP4 does not induce ROS production. Consequently, high circulating BMP4 levels selectively induce systemic (but not pulmonary) hypertension. In the endothelium of hypertensive patients, BMP4 upregulates COX2 expression through a BMPR1A/p38 signaling pathway and stimulates NOX1 and NOX4 (but not NOX2), a phenomenon that increases ROS levels [122]. COX2 stimulation increases the release of constrictive prostaglandins, which promotes endothelium-dependent contraction. Induction of NOXs also increases the concentration of superoxide anions that inactivate NO and reduce endothelium dependent relaxations [123]. Besides, superoxide anions produced by NOX4 are converted to H₂O₂ by SOD. Then, H₂O₂ reacts with reduced iron ions, being converted into hydroxyl radicals that cause lipid peroxidation and protein carbonylation. Both modifications contribute to endothelial dysfunction [124]. Moreover, superoxide anions and H₂O₂ activate xanthine oxidase, which further promotes ROS production. All generated ROS initiate an inflammatory cascade and stimulates ICAM-1 expression leading to monocyte adhesion [82,125]. Thus, BMP4 inhibition has a potent anti-inflammatory and anti-atherogenic effect in coronary arteries [82].

In atherosclerosis mice models, BMP6 and oxidized low-density lipoprotein (oxLDL) synergistically regulate the expression of *Osterix (Sp7)* and *Osteopontin*. This process requires NOX activation and ROS production to induce osteogenesis and chondrogenesis in endothelial cells [126]. In the same way, oxLDL requires the activation of the BMP pathway for ROS production, and oxLDL induces the expression of other BMPs such as *BMP2* or *BMP9* [127]. Their combination with oxLDL or H₂O₂ potentiates canonical BMP signaling [126]. Similar effects are obtained in situations where BMP type II receptors are downregulated. Loss of BMPR2 decreases JNK signaling and enhances BMP9-induced mineralization. Both events contribute to the endothelial to mesenchymal transition (EMT) and vascular calcification [128]. Moreover, in models of cardiomyocyte hypertrophy generated by pressure overload or angiotensin II infusion, *Bmp4* expression increases and induces cardiomyocyte hypertrophy, apoptosis, and cardiac fibrosis in a NOX4- and ROS-dependent manner [129]. The pro-apoptotic activation of caspase-3 by BMP2 is triggered by NOX-derived ROS and downstream activation of p38 and JNK [120]. Consequently, BMP4 could be used as a predictor of vascular dysfunction and a pharmacological target to prevent vascular dysfunction [122].

In parallel, drugs that modulate oxidative responses are being investigated as an effective treatment for cardiovascular diseases. For instance, molecules that induce NRF2 transcription inhibit oxLDL production, hence decrease inflammatory cytokine generation and attenuate endothelial injury [130]. Activators of the PI3K/AKT signaling pathway are also useful in the treatment of cardiovascular disease, since they prevent ROS accumulation in the vessels and acts as a vasodilator [131].

8.2. ROS and BMPs in Obesity and Diabetes

Emerging evidence suggests that diabetes leads to depletion of the cellular antioxidant system, increases ROS levels and triggers oxidative stress that is involved in the complications associated with this disease [132]. The ROS sources in diabetes are still controversial. In vitro studies show that hyperglycemia enhances mitochondrial respiration and NOX activity. However, the main in vivo ROS source depends on the tissue and the type of diabetes. In type 1 diabetes mellitus (T1DM), mitochondrial ROS is implicated in cardiac complications, whereas NOX-derived ROS are associated with kidney and vascular injury [133,134]. However, in type 2 diabetes mellitus (T2DM), mitochondrial ROS are associated with kidney [135] and retina injury [136], whereas an increase in NOX activity is implicated in vascular tissue damage [137].

Obesity is associated with chronic inflammation and myocardial dysfunction. In the ventriculus of obese mice, *Nox1* and *Nox2* expression increases [138]. A similar pattern occurs for the expression of fibrotic markers, whereas anti-fibrotic markers BMP2 and active SMAD1/5 are significantly elevated upon reduction of obesity [138]. BMP pathway inhibition in obese mice reduces atherosclerosis and vascular calcification and improves lipid metabolism [127]. For instance, BMP inhibitors reduce apolipoprotein B100 secretion and thus lower the levels of LDL-cholesterol and improve liver steatosis [127]. In the liver, BMP inhibition reduces the levels of hepcidin, an iron regulator. Reduction of hepcidin by BMP inhibition reduces intracellular iron and oxidative stress [139]. In vivo mice models confirm that BMP pathway inhibition limits foam cell formation and atherosclerosis by reducing macrophage intracellular iron and lipid efflux capacity [139]. However, in hypertrophic obesity, upregulation of Gremlin, an antagonist of BMP4/7, impairs BMP4-induced beige/brown adipogenesis, inhibit the capacity of BMP4 to induce commitment and differentiation of preadipocytes and contribute to the dysregulation of the adipose tissue. Silencing *Grem1* and/or adding BMP4 during white adipogenic differentiation reactivated beige/brown markers [140].

In adipose tissue, NOX4-generated H₂O₂ modulates adipogenesis and adipose tissue function. Although ROS, as well as BMP4, mediate preadipocyte differentiation into adipocytes, in mature cells, elevated ROS levels induce adipocyte dysfunction. NOX4-derived ROS from adipocytes in the early stages of obesity initiate the recruitment of immune cells, including macrophages, and this phenomenon worsens insulin resistance and adipose tissue inflammation [141]. All these modifications converge in NOX upregulation and activation of NF- κ B and p38 MAPK pathways that induce

pro-inflammatory gene expression as well as excessive ROS formation in macrophages. Additionally, mitochondria-derived ROS partially maintain insulin resistance and adipose tissue inflammation during the late stages of obesity [141].

One of the main complications in diabetes is endothelial dysfunction. In T1DM, angiotensin II signaling activates NOX1 and induces tetrahydrobiopterin (BH4) deficiency and consequent endothelial nitric oxide synthase (eNOS) uncoupling [142,143]. However, in T2DM animal models, angiotensin II signaling is apparently not the main cause of endothelial dysfunction. Dyslipidemia contributes to elevate BMP4 levels in these animals. BMP4 can also activate NOX1 and induce BH4 deficiency. Further, BMP4 activates COX2 and vascular cell adhesion molecule 1 (VCAM-1) and induces inflammation in T2DM [143]. Diabetes is also associated with medial vascular calcification, also known as Mönckeberg's calcification. This condition correlates with glucose levels in blood and the presence of calcium crystals in the medial layer [144]. Hyperglycemia and diabetes are strong activators of BMP signaling, and BMP2 and BMP4 are associated with atherogenesis in hyperglycemia. Moreover, in diabetic models, BMP4 disturbs blood flow and activates arterial NOXs, phenomena that promote ROS-induced inflammation, endothelial dysfunction and hypertension; BMP2 induces endothelial calcifications via WNT-MSX2 [145–147].

In the kidney, mesangial cells are the major source of glucose-dependent ROS generation. In the glomerular mesangial cells, oxidative stress caused by hyperglycemia activates the PKC ζ isoform, which enhances TGF β expression and increases ECM production. Overproduction of these components promotes morphological changes in the glomeruli. These changes hamper renal function and produce diabetic nephropathy, a serious complication in diabetes [148]. In recent years, recombinant BMP7 emerged as a potential therapy against diabetic nephropathy. BMP7 inhibits the phosphorylation and activation of PKC ζ and JNK and reduces ROS generation and ECM synthesis. BMP7 also rescues podocytes from high-glucose-induced apoptosis by regulating SMAD5 and p38 phosphorylation [149]. Interestingly, high glucose levels induce the expression of *Gremlin*, a BMP antagonist. In mesangial cells, Gremlin induces transdifferentiation of tubular epithelial cells to a fibroblast-like phenotype [150]. In retinal pericytes and in the vascular walls, gremlin antagonizes the antiproliferative effects of BMPs. This action contributes to increased vascular endothelial proliferation and ultimately proliferative retinopathies [151]. Oxidative stress is another key event in the pathogenesis of diabetic retinopathy. In the retina of diabetic patients, the activity of antioxidant enzymes is diminished. The increased concentration of ROS, besides directly affecting cellular structures, activate other metabolic pathways that are detrimental to the development of diabetic retinopathy including PKC [152]. Consequently, modulation of BMP signals and ROS scavenging might serve as targets for high-glucose-associated pathologies.

8.3. ROS and BMPs in Kidney Injury

Sepsis, ischemia and nephrotoxicity are causative of acute kidney injury (AKI), which promotes structural damage and loss of kidney function. When treated quickly, the damage is reversible and kidney function is restored. However, in some cases AKI can lead to chronic kidney disease (CKD), where kidney damage worsens over time and kidney failure could occur [153]. Other conditions such as diabetes, hypertension or heart disease can also cause CKD. A characteristic of renal chronic diseases is the accumulation of excessive ECM and the presence of myofibroblast within the interstitium [154].

In the kidney, BMP2 is expressed by metanephric mesenchymal cells, mesangial cells in the glomerulus and differentiated podocytes. Moreover, in vivo AKI models demonstrate *Bmp2* upregulation in adult renal progenitor cells, where it induces *Sma*, *Col1a1* and *Fibronectin* expression, all of which drive a myofibroblastic transition. Furthermore, in this cell type BMP2 promotes NOX4 expression and activity. NOX4 is also necessary for TGF β -induced kidney myofibroblast activation and to promote the transition of fibroblasts to myofibroblasts [78]. In podocytes, BMP2 increases the Ca²⁺ concentration and stimulates PKC activity, which is involved in the activation of NOX family members. In podocytes, BMP2 also up-regulates ID1, an inductor of NOX activity [83]. Thus, BMP2

stimulates ROS production through NOX enzyme activation in adult renal progenitors and podocytes. Elevated ROS levels induced by BMP promote the EMT, contribute to increased ECM production and hence impair kidney function.

On the other hand, BMP7 negatively regulates TGF β 1 signaling and suppresses inflammation, apoptosis and EMT. Moreover, BMP7 has antifibrotic activity, which prevents ureteral obstruction and diabetic nephropathy [155]. In chronic kidney injury, BMP7 can reverse TGF β 1-induced EMT and repair severe damage to renal tubular epithelial cells, actions that reverse chronic kidney injury [156]. Therefore, BMP7 signaling agonists play a protective role against renal fibrosis in kidney injury models and are postulated as a potential therapy in renal diseases [157,158]. In a similar way, silencing BMP7 antagonists, such as Gremlin, can induce therapeutic effects. For instance, in biopsies from patients with diabetic nephropathy, the levels of Gremlin are upregulated and correlated with elevated serum creatinine levels and tubulointerstitial fibrosis [159]. Inhibition of Gremlin allows the efficient binding of BMP7 to its receptor and improves kidney injury [160]. Furthermore, elevation of the antioxidant system by NRF2 activators appears to be beneficial in renal fibrosis [161,162].

8.4. ROS and BMPs in Musculoskeletal Diseases

Sarcopenia is a syndrome characterized by progressive and generalized loss of skeletal muscle mass and function. Histologically, sarcopenic muscles are characterized by the presence of adipose infiltration, fibrotic tissue and a decline in type II muscle fiber satellite cell content [163]. The cell fate decision between adipocyte and myoblast depends on BMP7 levels. In Myf5+ progenitors, BMP7 represses the expression of the adipogenic inhibitors *Necdin* and preadipocyte factor 1 (*Pref1*) and induces the expression of *Prdm16*, which activates the brown adipogenesis program and blocks the induction of myoblast-specific genes such as *Myf5* and *Myod1* [164]. Consequently, when BMP7 levels are high, Myf5+ progenitors differentiate into brown adipocytes, whereas if BMP7 expression decreases, Myf5+ progenitors can differentiate into the myogenic lineage [165].

In MSCs, chronic oxidative stress leads to S100 calcium-binding protein B (S100B) accumulation, increased NF- κ B transcriptional activity and reduced expression of the promyogenic and anti-adipogenic microRNA-133 (*miR-133*). *miR-133* reduction upregulates *PRDM-16*, which stimulates brown adipogenesis. In parallel, NF- κ B activity also upregulates BMP7 expression that stimulates the myoblast-brown adipocyte transition in an autocrine/paracrine manner [166]. Thus, ROS-mediated BMP7 upregulation might promote sarcopenia, and its inhibition can be beneficial for this disease.

Osteonecrosis arises from the death of bone cells due to decreased blood flow. When osteonecrosis occurs next to the joints, it can lead to osteoarthritis (OA). In bone cells, the hypoxia produced by osteonecrosis increases the production of free oxygen radicals, including O $_2^-$ and H $_2$ O $_2$. Increased BMP2 expression occurs in necrotic lesions [167] and damaged cartilage from OA patients linked to higher ROS production [168]. Moreover, serum BMP2 levels correlate with OA severity, hence it has been suggested that its levels could also be used as a biomarker for this disease [169,170]. Interestingly, after ischemic osteonecrosis, hypoxic chondrocytes within the cartilage transcriptionally activate the BMP2 promoter. BMP2 stimulates proteoglycan synthesis, induces vascularization, promotes endochondral osteogenesis and has anabolic effects on chondrocyte metabolism and function [168,169]. In osteoarthritic cartilage, the increased concentration of BMPs is followed by an up-regulation of BMP antagonists, such as *Gremlin* and *Follistatin*. *Gremlin1* expression is elevated since the early development of OA and its levels correlate with the progression of the disease [171,172]. *Gremlin1* is also highly expressed in synovia and synovial fluids of patients with RA (Rheumatoid Arthritis) and its levels correlate with the concentration of proinflammatory cytokines. Upregulation of *Gremlin1* induce the activation of ERK1/2, AKT, and increased expression of *BCL2* while it reduces the levels of *BAX*. Both facts increase the survival, and capacity of migration of fibroblast-like synoviocytes [173]. Treatment with *Gremlin1* markedly inhibited terminal hypertrophic differentiation with no effects on the chondrogenesis [174] in conclusion, *Gremlin1* could be a good therapeutical target in RA, capable of demoting hyperplastic synovitis [173].

9. Conclusions

Many biochemical, pharmacological and genetic studies confirm the relevance of ROS and BMPs in numerous aspects of cell biology and pathophysiology. Evidence also supports that both signals influence each other: BMP-dependent regulation of ROS production, and vice-versa, increases in the expression of distinct BMPs or modification on the expression of BMP antagonists in response to ROS generated by oxidative stress or NOX activity. However, many questions are still open and much more remains to be learnt regarding the relevance in the interplay between ROS and expression of specific BMPs and their antagonists in the context of normal tissue homeostasis and in pathological conditions. It should be possible to determine the effects of genetic alterations in the BMP signaling on cellular ROS levels or whether the cellular dysfunction associated to oxidative stress also depends on alterations of BMP expression. Additionally, BMPs and ROS share a number of downstream signaling components, suggesting a putative signaling crosstalk between the pathways. For instance, BMP and ROS activation of p38 MAPK or PI3K/AKT are well reported. Such parallel behavior and close signaling connections suggest that BMPs, BMP antagonists and ROS might regulate in coordination cellular physiology. However, despite this compelling rationale, strong evidence that such mechanisms are relevant is still lacking. Elucidation of these molecular mechanisms will not only advance basic biology, it may also provide new strategies for the treatment of a number of pathologies.

Author Contributions: C.S.-d.-D., C.P.-L., J.A.V., J.L.R., and F.V. conceived, analyzed and discussed the manuscript. C.S.-d.-D. and F.V. wrote the manuscript and draw the figures.

Funding: This research was supported by grants from the M.E.C. (BFU2014-56313-P and BFU2017-8 2421-P).

Acknowledgments: Cristina Sánchez de Diego and Carolina Pimenta Costa are the recipient of a F.P.U. fellowship from the Spanish Ministry of Education.

Conflicts of Interest: The authors declare no conflict of interest.

References

1. Urist, M.R.; Rosen, V.; Celeste, A.; Mittleman, L.; Whitters, M.; Kriz, R.; Hewick, R.; Wang, E. *Bone: Formation by Autoinduction*; American Association for the Advancement of Science: Washington, DC, USA, 1965; Volume 150, pp. 893–899.
2. Winnier, G.; Blessing, M.; Labosky, P.A.; Hogan, B.L. Bone morphogenetic protein-4 is required for mesoderm formation and patterning in the mouse. *Genes Dev.* **1995**, *9*, 2105–2116. [[CrossRef](#)] [[PubMed](#)]
3. Fujiwara, T.; Dehart, D.B.; Sulik, K.K.; Hogan, B.L.M. Distinct requirements for extra-embryonic and embryonic bone morphogenetic protein 4 in the formation of the node and primitive streak and coordination of left-right asymmetry in the mouse. *Development* **2002**, *129*, 4685–4696. [[PubMed](#)]
4. Hébert, J.M.; Mishina, Y.; McConnell, S.K. BMP Signaling Is Required Locally to Pattern the Dorsal Telencephalic Midline. *Neuron* **2002**, *35*, 1029–1041. [[CrossRef](#)]
5. Mehler, M.F.; Mabie, P.C.; Zhang, D.; Kessler, J.A. Bone morphogenetic proteins in the nervous system. *Trends Neurosci.* **1997**, *20*, 309–317. [[CrossRef](#)]
6. Storm, E.E.; Huynh, T.V.; Copeland, N.G.; Jenkins, N.A.; Kingsley, D.M.; Lee, S.J. Limb alterations in brachypodism mice due to mutations in a new member of the TGF β -superfamily. *Nature* **1994**, *368*, 639–643. [[CrossRef](#)] [[PubMed](#)]
7. Zhao, M.; Harris, S.E.; Horn, D.; Geng, Z.; Nishimura, R.; Mundy, G.R.; Chen, D. Bone morphogenetic protein receptor signaling is necessary for normal murine postnatal bone formation. *J. Cell Biol.* **2002**, *157*, 1049–1060. [[CrossRef](#)] [[PubMed](#)]
8. Pizette, S.; Niswander, L. BMPs Are Required at Two Steps of Limb Chondrogenesis: Formation of Prechondrogenic Condensations and Their Differentiation into Chondrocytes. *Dev. Biol.* **2000**, *219*, 237–249. [[CrossRef](#)] [[PubMed](#)]
9. Wozney, J.M. The bone morphogenetic protein family and osteogenesis. *Mol. Reprod. Dev.* **1992**, *32*, 160–167. [[CrossRef](#)]
10. Miyazaki, Y.; Oshima, K.; Fogo, A.; Hogan, B.L.; Ichikawa, I. Bone morphogenetic protein 4 regulates the budding site and elongation of the mouse ureter. *J. Clin. Investig.* **2000**, *105*, 863–873. [[CrossRef](#)]

11. Lowery, J.W.; De Caestecker, M.P. BMP signaling in vascular development and disease. *Cytokine Growth Factor Rev.* **2010**, *21*, 287–298. [[CrossRef](#)]
12. De Vinuesa, A.G.; Abdelilah-Seyfried, S.; Knaus, P.; Zwijsen, A.; Bailly, S.; Information, P.E.K.F.C. BMP signaling in vascular biology and dysfunction. *Cytokine Growth Factor Rev.* **2016**, *27*, 65–79. [[CrossRef](#)] [[PubMed](#)]
13. Morrell, N.W.; Bloch, D.B.; Ten Dijke, P.; Goumans, M.J.T.H.; Hata, A.; Smith, J.; Yu, P.B.; Bloch, K.D. Targeting BMP signaling in cardiovascular disease and anaemia. *Nat. Rev. Cardiol.* **2016**, *13*, 106–120. [[CrossRef](#)] [[PubMed](#)]
14. Zhao, G.Q.; Liaw, L.; Hogan, B.L. Bone morphogenetic protein 8A plays a role in the maintenance of spermatogenesis and the integrity of the epididymis. *Development* **1998**, *125*, 1103–1112. [[PubMed](#)]
15. Otsuka, F.; Yao, Z.; Lee, T.; Yamamoto, S.; Erickson, G.F.; Shimasaki, S. Bone morphogenetic protein-15. Identification of target cells and biological functions. *J. Biol. Chem.* **2000**, *275*, 39523–39528. [[CrossRef](#)] [[PubMed](#)]
16. Zhang, Y.E. Non-Smad Signaling Pathways of the TGF- β Family. *Cold Spring Harb. Perspect. Biol.* **2017**, *9*, a022129. [[CrossRef](#)] [[PubMed](#)]
17. Song, P.; Zou, M.H. Roles of Reactive Oxygen Species in Physiology and Pathology. In *Atherosclerosis: Risks, Mechanisms, and Therapies*; Wiley: Hoboken, NJ, USA, 2015; pp. 379–392.
18. Brieger, K.; Schiavone, S.; Miller, F.J.; Krause, K.H. Reactive oxygen species: From health to disease. *Swiss Med. Wkly.* **2012**, *142*, w13659. [[CrossRef](#)] [[PubMed](#)]
19. Roy, J.; Galano, J.M.; Durand, T.; Le Guennec, J.Y.; Lee, J.C.Y. Physiological role of reactive oxygen species as promoters of natural defenses. *FASEB J.* **2017**, *31*, 3729–3745. [[CrossRef](#)]
20. Reid, M.B.; Khawli, F.A.; Moody, M.R. Reactive oxygen in skeletal muscle. III. Contractility of unfatigued muscle. *J. Appl. Physiol.* **1993**, *75*, 1081–1087.
21. Kraaij, M.D.; Savage, N.D.L.; Van Der Kooij, S.W.; Koekkoek, K.; Wang, J.; Berg, J.M.V.D.; Ottenhoff, T.H.M.; Kuijpers, T.W.; Holmdahl, R.; Van Kooten, C.; et al. Induction of regulatory T cells by macrophages is dependent on production of reactive oxygen species. *Proc. Natl. Acad. Sci. USA* **2010**, *107*, 17686–17691. [[CrossRef](#)]
22. Sellak, H.; Franzini, E.; Hakim, J.; Pasquier, C. Reactive oxygen species rapidly increase endothelial ICAM-1 ability to bind neutrophils without detectable upregulation. *Blood* **1994**, *83*, 2669–2677.
23. Kawabata, M. Signal transduction by bone morphogenetic proteins. *Cytokine Growth Factor Rev.* **1998**, *9*, 49–61. [[CrossRef](#)]
24. Nohe, A. Signal transduction of bone morphogenetic protein receptors. *Cell. Signal.* **2004**, *16*, 291–299. [[CrossRef](#)] [[PubMed](#)]
25. Hinck, A.P. Structural studies of the TGF- β s and their receptors—Insights into evolution of the TGF- β superfamily. *FEBS Lett.* **2012**, *586*, 1860–1870. [[CrossRef](#)] [[PubMed](#)]
26. Massagué, J. TGF- β Signal Transduction. *Annu. Rev. Biochem.* **1998**, *67*, 753–791. [[CrossRef](#)] [[PubMed](#)]
27. Shi, Y.; Massagué, J. Mechanisms of TGF-beta signaling from cell membrane to the nucleus. *Cell* **2003**, *113*, 685–700. [[CrossRef](#)]
28. Gámez, B.; Rodríguez-Carballo, E.; Ventura, F. BMP signaling in telencephalic neural cell specification and maturation. *Front. Cell. Neurosci.* **2013**, *7*, 87. [[CrossRef](#)] [[PubMed](#)]
29. Derynck, R.; Zhang, Y.E. Smad-dependent and Smad-independent pathways in TGF- β family signalling. *Nature* **2003**, *425*, 577–584. [[CrossRef](#)]
30. Zhang, Y.E. Non-Smad pathways in TGF-beta signaling. *Cell Res.* **2009**, *19*, 128–139. [[CrossRef](#)]
31. Yamashita, M.; Fatyol, K.; Jin, C.; Wang, X.; Liu, Z.; Zhang, Y.E. TRAF6 mediates Smad-independent activation of JNK and p38 by TGF-beta. *Mol. Cell* **2008**, *31*, 918–924. [[CrossRef](#)]
32. Brazil, D.P.; Church, R.H.; Suraa, S.; Godson, C.; Martin, F. BMP signalling: Agony and antagonism in the family. *Trends Cell Biol.* **2015**, *25*, 249–264. [[CrossRef](#)]
33. Rider, C.C.; Mulloy, B. Bone morphogenetic protein and growth differentiation factor cytokine families and their protein antagonists. *Biochem. J.* **2010**, *429*, 1–12. [[CrossRef](#)] [[PubMed](#)]
34. Bragdon, B.; Moseychuk, O.; Saldanha, S.; King, D.; Julian, J.; Nohe, A. Bone Morphogenetic Proteins: A critical review. *Cell. Signal.* **2011**, *23*, 609–620. [[CrossRef](#)] [[PubMed](#)]
35. Ray, P.D.; Huang, B.W.; Tsuji, Y. Reactive oxygen species (ROS) homeostasis and redox regulation in cellular signaling. *Cell. Signal.* **2012**, *24*, 981–990. [[CrossRef](#)] [[PubMed](#)]

36. Schieber, M.; Chandel, N.S. ROS function in redox signaling and oxidative stress. *Curr. Biol.* **2014**, *24*, R453–R462. [[CrossRef](#)] [[PubMed](#)]
37. Zhang, J.; Wang, X.; Vikash, V.; Ye, Q.; Wu, D.; Liu, Y.; Dong, W. ROS and ROS-Mediated Cellular Signaling. *Oxidative Med. Cell. Longev.* **2016**, *2016*, 4350965. [[CrossRef](#)] [[PubMed](#)]
38. Finkel, T. Signal transduction by reactive oxygen species. *J. Cell Biol.* **2011**, *194*, 7–15. [[CrossRef](#)] [[PubMed](#)]
39. Schoonbroodt, S.; Ferreira, V.; Best-Belpomme, M.; Boelaert, J.R.; Legrand-Poels, S.; Korner, M.; Piette, J. Crucial Role of the Amino-Terminal Tyrosine Residue 42 and the Carboxyl-Terminal PEST Domain of I B in NF- B Activation by an Oxidative Stress. *J. Immunol.* **2000**, *164*, 4292–4300. [[CrossRef](#)] [[PubMed](#)]
40. Reynaert, N.L.; van der Vliet, A.; Guala, A.S.; McGovern, T.; Hristova, M.; Pantano, C.; Heintz, N.H.; Heim, J.; Ho, Y.S.; Matthews, D.E.; et al. Dynamic redox control of NF-kappaB through glutaredoxin-regulated S-glutathionylation of inhibitory kappaB kinase beta. *Proc. Natl. Acad. Sci. USA* **2006**, *103*, 13086–13091. [[CrossRef](#)] [[PubMed](#)]
41. León-Buitimea, A.; Rodríguez-Fragoso, L.; Lauer, F.T.; Bowles, H.; Thompson, T.A.; Burchiel, S.W. Ethanol-induced oxidative stress is associated with EGF receptor phosphorylation in MCF-10A cells overexpressing CYP2E1. *Toxicol. Lett.* **2012**, *209*, 161–165. [[CrossRef](#)]
42. Wentworth, C.C.; Alam, A.; Jones, R.M.; Nusrat, A.; Neish, A.S. Enteric Commensal Bacteria Induce Extracellular Signal-regulated Kinase Pathway Signaling via Formyl Peptide Receptor-dependent Redox Modulation of Dual Specific Phosphatase 3. *J. Biol. Chem.* **2011**, *286*, 38448–38455. [[CrossRef](#)]
43. Banan, A.; Fields, J.Z.; Zhang, Y.; Keshavarzian, A. Phospholipase C-γ inhibition prevents EGF protection of intestinal cytoskeleton and barrier against oxidants. *Am. J. Physiol. Liver Physiol.* **2001**, *281*, G412–G423. [[CrossRef](#)]
44. Matsukawa, J.; Matsuzawa, A.; Takeda, K.; Ichijo, H. The ASK1-MAP Kinase Cascades in Mammalian Stress Response. *J. Biochem.* **2004**, *136*, 261–265. [[CrossRef](#)]
45. Brown, J.S.; Banerji, U. Maximising the potential of AKT inhibitors as anti-cancer treatments. *Pharmacol. Ther.* **2017**, *172*, 101–115. [[CrossRef](#)]
46. Wlodarchak, N.; Xing, Y. PP2A as a master regulator of the cell cycle. *Crit. Rev. Biochem. Mol. Biol.* **2016**, *51*, 162–184. [[CrossRef](#)]
47. Li, Y.; Wang, X.; Yue, P.; Tao, H.; Ramalingam, S.S.; Owonikoko, T.K.; Deng, X.; Wang, Y.; Fu, H.; Khuri, F.R.; et al. Protein Phosphatase 2A and DNA-dependent Protein Kinase Are Involved in Mediating Rapamycin-induced Akt Phosphorylation. *J. Biol. Chem.* **2013**, *288*, 13215–13224. [[CrossRef](#)]
48. Lee, S.R.; Yang, K.S.; Kwon, J.; Jeong, W.; Rhee, S.G.; Lee, C. Reversible Inactivation of the Tumor Suppressor PTEN by H₂O₂. *J. Biol. Chem.* **2002**, *277*, 20336–20342. [[CrossRef](#)]
49. Shimura, T.; Sasatani, M.; Kamiya, K.; Kawai, H.; Inaba, Y.; Kunugita, N. Mitochondrial reactive oxygen species perturb AKT/cyclin D1 cell cycle signaling via oxidative inactivation of PP2A in lowdose irradiated human fibroblasts. *Oncotarget* **2016**, *7*, 3559–3570. [[CrossRef](#)]
50. Srinivasan, S.; Spear, J.; Chandran, K.; Joseph, J.; Kalyanaraman, B.; Avadhani, N.G. Oxidative Stress Induced Mitochondrial Protein Kinase A Mediates Cytochrome C Oxidase Dysfunction. *PLoS ONE* **2013**, *8*, e77129. [[CrossRef](#)]
51. Thompson, J.W.; Narayanan, S.V.; Perez-Pinzon, M.A. Redox Signaling Pathways Involved in Neuronal Ischemic Preconditioning. *Curr. Neuropharmacol.* **2012**, *10*, 354–369. [[CrossRef](#)]
52. Eisenberg-Lerner, A.; Kimchi, A. PKD is a kinase of Vps34 that mediates ROS-induced autophagy downstream of DAPk. *Cell Death Differ.* **2012**, *19*, 788–797. [[CrossRef](#)]
53. Kruk, J.S.; Vasefi, M.S.; Heikkila, J.J.; Beazely, M.A. Reactive Oxygen Species Are Required for 5-HT-Induced Transactivation of Neuronal Platelet-Derived Growth Factor and TrkB Receptors, but Not for ERK1/2 Activation. *PLoS ONE* **2013**, *8*, e77027. [[CrossRef](#)]
54. Luczak, E.D.; Anderson, M.E. CaMKII oxidative activation and the pathogenesis of cardiac disease. *J. Mol. Cell. Cardiol.* **2014**, *73*, 112–116. [[CrossRef](#)]
55. Brennan, J.P.; Bardswell, S.C.; Burgoyne, J.R.; Fuller, W.; Schröder, E.; Wait, R.; Begum, S.; Kentish, J.C.; Eaton, P. Oxidant-induced Activation of Type I Protein Kinase A Is Mediated by RI Subunit Interprotein Disulfide Bond Formation. *J. Biol. Chem.* **2006**, *281*, 21827–21836. [[CrossRef](#)]
56. Newton, A.C. Protein Kinase C: Structure, Function, and Regulation. *J. Biol. Chem.* **1995**, *270*, 28495–28498. [[CrossRef](#)]

57. Gopalakrishna, R.; Jaken, S. Protein kinase C signaling and oxidative stress. *Free. Radic. Biol. Med.* **2000**, *28*, 1349–1361. [[CrossRef](#)]
58. Cosentino-Gomes, D.; Rocco-Machado, N.; Meyer-Fernandes, J.R. Cell Signaling through Protein Kinase C Oxidation and Activation. *Int. J. Mol. Sci.* **2012**, *13*, 10697–10721. [[CrossRef](#)]
59. Cowell, C.F.; Döppler, H.; Yan, I.K.; Hausser, A.; Umezawa, Y.; Storz, P. Mitochondrial diacylglycerol initiates protein-kinase D1-mediated ROS signaling. *J. Cell Sci.* **2009**, *122*, 919–928. [[CrossRef](#)]
60. Wang, Q.J. PKD at the crossroads of DAG and PKC signaling. *Trends Pharmacol. Sci.* **2006**, *27*, 317–323. [[CrossRef](#)]
61. Joo, M.S.; Kim, W.D.; Lee, K.Y.; Kim, J.H.; Koo, J.H.; Kim, S.G. AMPK Facilitates Nuclear Accumulation of Nrf2 by Phosphorylating at Serine 550. *Mol. Cell. Biol.* **2016**, *36*, 1931–1942. [[CrossRef](#)]
62. Silva-Islas, C.A.; Maldonado, P.D. Canonical and non-canonical mechanisms of Nrf2 activation. *Pharmacol. Res.* **2018**, *134*, 92–99. [[CrossRef](#)]
63. Huang, H.C.; Nguyen, T.; Pickett, C.B. Phosphorylation of Nrf2 at Ser-40 by Protein Kinase C Regulates Antioxidant Response Element-mediated Transcription. *J. Biol. Chem.* **2002**, *277*, 42769–42774. [[CrossRef](#)]
64. Nakaso, K.; Yano, H.; Fukuhara, Y.; Takeshima, T.; Wada-Isoe, K.; Nakashima, K. PI3K is a key molecule in the Nrf2-mediated regulation of antioxidative proteins by hemin in human neuroblastoma cells. *FEBS Lett.* **2003**, *546*, 181–184. [[CrossRef](#)]
65. Lee, J.M.; Johnson, J.A. An important role of Nrf2-ARE pathway in the cellular defense mechanism. *J. Biochem. Mol. Biol.* **2004**, *37*, 139–143. [[CrossRef](#)]
66. Rushworth, S.A.; Zaitseva, L.; Murray, M.Y.; Shah, N.M.; Bowles, K.M.; MacEwan, D.J. The high Nrf2 expression in human acute myeloid leukemia is driven by NF- κ B and underlies its chemo-resistance. *Blood* **2012**, *120*, 5188–5198. [[CrossRef](#)]
67. Jain, A.; Jaiswal, A.K. GSK-3 β Acts Upstream of Fyn Kinase in Regulation of Nuclear Export and Degradation of NF-E2 Related Factor 2. *J. Biol. Chem.* **2007**, *282*, 16502–16510. [[CrossRef](#)]
68. Burtenshaw, D.; Hakimjavadi, R.; Redmond, E.M.; Cahill, P.A. Nox, Reactive Oxygen Species and Regulation of Vascular Cell Fate. *Antioxidants* **2017**, *6*, 90. [[CrossRef](#)]
69. Panday, A.; Sahoo, M.K.; Osorio, D.; Batra, S. NADPH oxidases: An overview from structure to innate immunity-associated pathologies. *Cell. Mol. Immunol.* **2015**, *12*, 5–23. [[CrossRef](#)]
70. Brandes, R.P.; Weissmann, N.; Schröder, K. Nox family NADPH oxidases: Molecular mechanisms of activation. *Free. Radic. Biol. Med.* **2014**, *76*, 208–226. [[CrossRef](#)]
71. Hoyal, C.R.; Gutierrez, A.; Young, B.M.; Catz, S.D.; Lin, J.H.; Tschlis, P.N.; Babior, B.M. Modulation of p47PHOX activity by site-specific phosphorylation: Akt-dependent activation of the NADPH oxidase. *Proc. Natl. Acad. Sci. USA* **2003**, *100*, 5130–5135. [[CrossRef](#)]
72. Kanai, F.; Liu, H.; Field, S.J.; Akbary, H.; Matsuo, T.; Brown, G.E.; Cantley, L.C.; Yaffe, M.B. The PX domains of p47phox and p40phox bind to lipid products of PI(3)K. *Nature* **2001**, *3*, 675–678. [[CrossRef](#)]
73. Zhan, Y.; Virbasius, J.V.; Song, X.; Pomerleau, D.P.; Zhou, G.W. The p40phox and p47phox PX domains of NADPH oxidase target cell membranes via direct and indirect recruitment by phosphoinositides. *J. Biol. Chem.* **2002**, *277*, 4512–4518. [[CrossRef](#)]
74. Abo, A.; Pick, E.; Hall, A.; Totty, N.; Teahan, C.G.; Segal, A.W. Activation of the NADPH oxidase involves the small GTP-binding protein p21rac1. *Nature* **1991**, *353*, 668–670. [[CrossRef](#)]
75. Lambeth, J.D. NOX enzymes and the biology of reactive oxygen. *Nat. Rev. Immunol.* **2004**, *4*, 181–189. [[CrossRef](#)]
76. Winkler, K.; Wünsch, S.; Kreutz, R.; Rothermund, L.; Paul, M.; Schmidt, H.H. Upregulation of the vascular NAD(P)H-oxidase isoforms Nox1 and Nox4 by the renin-angiotensin system in vitro and in vivo. *Free Radic. Biol. Med.* **2001**, *31*, 1456–1464. [[CrossRef](#)]
77. Mahadev, K.; Motoshima, H.; Wu, X.; Ruddy, J.M.; Arnold, R.S.; Cheng, G.; Lambeth, J.D.; Goldstein, B.J. The NAD(P)H Oxidase Homolog Nox4 Modulates Insulin-Stimulated Generation of H₂O₂ and Plays an Integral Role in Insulin Signal Transduction. *Mol. Cell. Biol.* **2004**, *24*, 1844–1854. [[CrossRef](#)]
78. Simone, S.; Cosola, C.; Loverre, A.; Cariello, M.; Sallustio, F.; Rascio, F.; Gesualdo, L.; Schena, F.P.; Grandaliano, G.; Pertosa, G. BMP-2 induces a profibrotic phenotype in adult renal progenitor cells through Nox4 activation. *Am. J. Physiol. Physiol.* **2012**, *303*, F23–F34. [[CrossRef](#)]

79. Mandal, C.C.; Ganapathy, S.; Gorin, Y.; Mahadev, K.; Block, K.; Abboud, H.E.; Harris, S.E.; Ghosh-Choudhury, G.; Ghosh-Choudhury, N. Reactive oxygen species derived from Nox4 mediate BMP2 gene transcription and osteoblast differentiation. *Biochem. J.* **2011**, *433*, 393–402. [[CrossRef](#)]
80. Rastogi, R.; Geng, X.; Li, F.; Ding, Y. NOX Activation by Subunit Interaction and Underlying Mechanisms in Disease. *Front. Cell. Neurosci.* **2016**, *10*, 301. [[CrossRef](#)]
81. Chandrasekaran, V.; Lea, C.; Sosa, J.C.; Higgins, D.; Lein, P.J. Reactive oxygen species are involved in BMP-induced dendritic growth in cultured rat sympathetic neurons. *Mol. Cell. Neurosci.* **2015**, *67*, 116–125. [[CrossRef](#)]
82. Sorescu, G.P.; Song, H.; Tressel, S.L.; Hwang, J.; Dikalov, S.; Smith, D.A.; Boyd, N.L.; Platt, M.O.; Lassègue, B.; Griendling, K.K.; et al. Bone Morphogenic Protein 4 Produced in Endothelial Cells by Oscillatory Shear Stress Induces Monocyte Adhesion by Stimulating Reactive Oxygen Species Production From a Nox1-Based NADPH Oxidase. *Circ. Res.* **2004**, *95*, 773–779. [[CrossRef](#)]
83. Pache, G.; Schäfer, C.; Wiesemann, S.; Springer, E.; Liebau, M.; Reinhardt, H.C.; August, C.; Pavenstädt, H.; Bek, M.J. Upregulation of Id-1 via BMP-2 receptors induces reactive oxygen species in podocytes. *Am. J. Physiol. Physiol.* **2006**, *291*, F654–F662. [[CrossRef](#)]
84. Susperregui, A.R.G.; Gamell, C.; Rodríguez-Carballo, E.; Ortuño, M.J.; Bartrons, R.; Rosa, J.L.; Ventura, F. Noncanonical BMP Signaling Regulates Cyclooxygenase-2 Transcription. *Mol. Endocrinol.* **2011**, *25*, 1006–1017. [[CrossRef](#)]
85. Hernanz, R.; Briones, A.M.; Salaces, M.; Alonso, M.J. New roles for old pathways? A circuitous relationship between reactive oxygen species and cyclo-oxygenase in hypertension. *Clin. Sci.* **2014**, *126*, 111–121. [[CrossRef](#)]
86. Koundouros, N.; Poulgiannis, G. Phosphoinositide 3-Kinase/Akt Signaling and Redox Metabolism in Cancer. *Front. Oncol.* **2018**, *8*, 160. [[CrossRef](#)]
87. Sampson, N.; Berger, P.; Zenzmaier, C. Redox Signaling as a Therapeutic Target to Inhibit Myofibroblast Activation in Degenerative Fibrotic Disease. *BioMed Res. Int.* **2014**, *2014*, 1–14. [[CrossRef](#)]
88. Csiszar, A.; Smith, K.E.; Koller, A.; Kaley, G.; Edwards, J.G.; Ungvari, Z. Regulation of Bone Morphogenetic Protein-2 Expression in Endothelial Cells. *Circulation* **2005**, *111*, 2364–2372. [[CrossRef](#)]
89. Moriguchi, T.; Kuroyanagi, N.; Yamaguchi, K.; Gotoh, Y.; Irie, K.; Kano, T.; Shirakabe, K.; Muro, Y.; Shibuya, H.; Matsumoto, K. A Novel Kinase Cascade Mediated by Mitogen-activated Protein Kinase Kinase 6 and MKK3. *J. Biol. Chem.* **1996**, *271*, 13675–13679. [[CrossRef](#)]
90. Chen, X.; Liao, J.; Lu, Y.; Duan, X.; Sun, W. Activation of the PI3K/Akt Pathway Mediates Bone Morphogenetic Protein 2-Induced Invasion of Pancreatic Cancer Cells Panc-1. *Pathol. Oncol. Res.* **2011**, *17*, 257–261. [[CrossRef](#)]
91. Murata, H.; Ihara, Y.; Nakamura, H.; Yodoi, J.; Sumikawa, K.; Kondo, T. Glutaredoxin Exerts an Antiapoptotic Effect by Regulating the Redox State of Akt. *J. Biol. Chem.* **2003**, *278*, 50226–50233. [[CrossRef](#)]
92. Chen, G.; Deng, C.; Li, Y.P. TGF- β and BMP Signaling in Osteoblast Differentiation and Bone Formation. *Int. J. Biol. Sci.* **2012**, *8*, 272–288. [[CrossRef](#)]
93. Hu, C.; Zhao, L.; Peng, C.; Li, L. Regulation of the mitochondrial reactive oxygen species: Strategies to control mesenchymal stem cell fates ex vivo and in vivo. *J. Cell. Mol. Med.* **2018**, *22*, 5196–5207. [[CrossRef](#)] [[PubMed](#)]
94. Li, J.; Dong, S. The Signaling Pathways Involved in Chondrocyte Differentiation and Hypertrophic Differentiation. *Stem Cells Int.* **2016**, *2016*, 1–12. [[CrossRef](#)]
95. Kang, I.S.; Kim, C. NADPH oxidase gp91phox contributes to RANKL-induced osteoclast differentiation by upregulating NFATc1. *Sci. Rep.* **2016**, *6*, 38014. [[CrossRef](#)] [[PubMed](#)]
96. Ha, H.; Kwak, H.B.; Lee, S.W.; Jin, H.M.; Kim, H.M.; Kim, H.H.; Lee, Z.H. Reactive oxygen species mediate RANK signaling in osteoclasts. *Exp. Cell Res.* **2004**, *301*, 119–127. [[CrossRef](#)] [[PubMed](#)]
97. Li, J.; Stouffs, M.; Serrander, L.; Banfi, B.; Bettiol, E.; Charnay, Y.; Steger, K.; Krause, K.H.; Jaconi, M.E. The NADPH Oxidase NOX4 Drives Cardiac Differentiation: Role in Regulating Cardiac Transcription Factors and MAP Kinase Activation. *Mol. Biol. Cell* **2006**, *17*, 3978–3988. [[CrossRef](#)] [[PubMed](#)]
98. Chen, H.; Shi, S.; Acosta, L.; Li, W.; Lu, J.; Bao, S.; Chen, Z.; Yang, Z.; Schneider, M.D.; Chien, K.R.; et al. BMP10 is essential for maintaining cardiac growth during murine cardiogenesis. *Development* **2004**, *131*, 2219–2231. [[CrossRef](#)] [[PubMed](#)]

99. Jiang, C.; Gong, F. BMP-2 and icariin synergistically promote p38MAPK-mediated cardiomyocyte differentiation of mesenchymal stem cells via enhanced NOX4-driven ROS generation. *Med. Chem. Res.* **2017**, *26*, 2547–2556. [[CrossRef](#)]
100. Lein, P.; Johnson, M.; Guo, X.; Rueger, D.; Higgins, D. Osteogenic protein-1 induces dendritic growth in rat sympathetic neurons. *Neuron* **1995**, *15*, 597–605. [[CrossRef](#)]
101. Charette, M.; Banker, G.; Withers, G.S.; Higgins, D. Bone morphogenetic protein-7 enhances dendritic growth and receptivity to innervation in cultured hippocampal neurons. *Eur. J. Neurosci.* **2000**, *12*, 106–116.
102. Le Roux, P.; Behar, S.; Higgins, D.; Charette, M. OP-1 Enhances Dendritic Growth from Cerebral Cortical Neurons in Vitro. *Exp. Neurol.* **1999**, *160*, 151–163. [[CrossRef](#)] [[PubMed](#)]
103. Hocking, J.C.; Hehr, C.L.; Chang, R.Y.; Johnston, J.; McFarlane, S. TGF β ligands promote the initiation of retinal ganglion cell dendrites in vitro and in vivo. *Mol. Cell. Neurosci.* **2008**, *37*, 247–260. [[CrossRef](#)] [[PubMed](#)]
104. Thangnipon, W.; Puangmalai, N.; Suwanna, N.; Soi-Ampornkul, R.; Phonchai, R.; Kotchabhakdi, N.; Mukda, S.; Phermthai, T.; Julavijitphong, S.; Tuchinda, P.; et al. Potential role of N-benzylcinnamide in inducing neuronal differentiation from human amniotic fluid mesenchymal stem cells. *Neurosci. Lett.* **2016**, *610*, 6–12. [[CrossRef](#)] [[PubMed](#)]
105. Wei, Z.; Salmon, R.M.; Upton, P.D.; Morrell, N.W.; Li, W. Regulation of bone morphogenetic protein 9 (BMP9) by redox-dependent proteolysis. *J. Biol. Chem.* **2014**, *289*, 31150–31159. [[CrossRef](#)] [[PubMed](#)]
106. Morrison, S.J.; Weissman, I.L.; Reya, T.; Clarke, M.F. Stem cells, cancer, and cancer stem cells. *Nature* **2001**, *414*, 105–111.
107. Wang, L.; Park, P.; Zhang, H.; La Marca, F.; Claeson, A.; Valdivia, J.; Lin, C.Y. BMP-2 inhibits the tumorigenicity of cancer stem cells in human osteosarcoma OS99-1 cell line. *Cancer Biol. Ther.* **2011**, *11*, 457–463. [[CrossRef](#)] [[PubMed](#)]
108. Lombardo, Y.; Scopelliti, A.; Cammareri, P.; Todaro, M.; Iovino, F.; Ricci-Vitiani, L.; Gulotta, G.; Dieli, F.; De Maria, R.; Stassi, G. Bone Morphogenetic Protein 4 Induces Differentiation of Colorectal Cancer Stem Cells and Increases Their Response to Chemotherapy in Mice. *Gastroenterology* **2011**, *140*, 297–309. [[CrossRef](#)] [[PubMed](#)]
109. Yan, K.; Wu, Q.; Yan, D.H.; Lee, C.H.; Rahim, N.; Tritschler, I.; DeVecchio, J.; Kalady, M.F.; Hjelmeland, A.B.; Rich, J.N. Glioma cancer stem cells secrete Gremlin1 to promote their maintenance within the tumor hierarchy. *Genes Dev.* **2014**, *28*, 1085–1100. [[CrossRef](#)] [[PubMed](#)]
110. Ding, S.; Li, C.; Cheng, N.; Cui, X.; Xu, X.; Zhou, G. Redox Regulation in Cancer Stem Cells. *Oxidative Med. Cell. Longev.* **2015**, *2015*, 1–11. [[CrossRef](#)] [[PubMed](#)]
111. Epstein, F.H.; Gibbons, G.H.; Dzau, V.J. The Emerging Concept of Vascular Remodeling. *N. Engl. J. Med.* **1994**, *330*, 1431–1438. [[CrossRef](#)]
112. Mueller, C.F.H.; Laude, K.; McNally, J.S.; Harrison, D.G. Redox Mechanisms in Blood Vessels. *Arterioscler. Thromb. Vasc. Biol.* **2005**, *25*, 274–278. [[CrossRef](#)]
113. Kojda, G.; Harrison, D. Interactions between NO and reactive oxygen species: Pathophysiological importance in atherosclerosis, hypertension, diabetes and heart failure. *Cardiovasc. Res.* **1999**, *43*, 562–571. [[PubMed](#)]
114. Csiszar, A.; Lehoux, S.; Ungvari, Z. Hemodynamic Forces, Vascular Oxidative Stress, and Regulation of BMP-2/4 Expression. *Antioxid. Redox Signal.* **2009**, *11*, 1683–1697. [[CrossRef](#)] [[PubMed](#)]
115. Hruska, K.A.; Mathew, S.; Saab, G. Bone Morphogenetic Proteins in Vascular Calcification. *Circ. Res.* **2005**, *97*, 105–114. [[CrossRef](#)] [[PubMed](#)]
116. Zhang, M.; Sara, J.D.; Wang, F.L.; Liu, L.P.; Su, L.X.; Zhe, J.; Wu, X.; Liu, J.H. Increased plasma BMP-2 levels are associated with atherosclerosis burden and coronary calcification in type 2 diabetic patients. *Cardiovasc. Diabetol.* **2015**, *14*, 64. [[CrossRef](#)] [[PubMed](#)]
117. Li, X.; Yang, H.Y.; Giachelli, C.M. BMP-2 promotes phosphate uptake, phenotypic modulation, and calcification of human vascular smooth muscle cells. *Atherosclerosis* **2008**, *199*, 271–277. [[CrossRef](#)]
118. Liberman, M.; Johnson, R.C.; Handy, D.E.; Loscalzo, J.; Leopold, J.A. Bone morphogenetic protein-2 activates NADPH oxidase to increase endoplasmic reticulum stress and human coronary artery smooth muscle cell calcification. *Biochem. Biophys. Res. Commun.* **2011**, *413*, 436–441. [[PubMed](#)]
119. Csiszar, A.; Ahmad, M.; Smith, K.E.; Labinskyy, N.; Gao, Q.; Kaley, G.; Edwards, J.G.; Wolin, M.S.; Ungvari, Z. Bone Morphogenetic Protein-2 Induces Proinflammatory Endothelial Phenotype. *Am. J. Pathol.* **2006**, *168*, 629–638. [[CrossRef](#)]

120. Tian, X.Y.; Yung, L.H.; Wong, W.T.; Liu, J.; Leung, F.P.; Liu, L.; Chen, Y.; Kong, S.K.; Kwan, K.M.; Ng, S.M.; et al. Bone morphogenetic protein-4 induces endothelial cell apoptosis through oxidative stress-dependent p38MAPK and JNK pathway. *J. Mol. Cell. Cardiol.* **2012**, *52*, 237–244. [[CrossRef](#)]
121. Csiszar, A.; Labinsky, N.; Jo, H.; Ballabh, P.; Ungvari, Z. Differential proinflammatory and prooxidant effects of bone morphogenetic protein-4 in coronary and pulmonary arterial endothelial cells. *Am. J. Physiol. Circ. Physiol.* **2008**, *295*, H569–H577. [[CrossRef](#)]
122. Wong, W.T.; Tian, X.Y.; Chen, Y.; Leung, F.P.; Liu, L.; Lee, H.K.; Ng, C.F.; Xu, A.; Yao, X.; Vanhoutte, P.M.; et al. Bone Morphogenetic Protein-4 Impairs Endothelial Function Through Oxidative Stress-Dependent Cyclooxygenase-2 Upregulation. *Circ. Res.* **2010**, *107*, 984–991. [[CrossRef](#)]
123. Luo, J.Y.; Zhang, Y.; Wang, L.; Huang, Y. Regulators and effectors of bone morphogenetic protein signalling in the cardiovascular system. *J. Physiol.* **2015**, *593*, 2995–3011. [[CrossRef](#)] [[PubMed](#)]
124. Wong, C.M.; Zhang, Y.; Huang, Y. Bone morphogenetic protein-4-induced oxidant signaling via protein carbonylation for endothelial dysfunction. *Free Radic. Biol. Med.* **2014**, *75*, 178–190. [[CrossRef](#)] [[PubMed](#)]
125. Grgurevic, L.; Christensen, G.L.; Schulz, T.J.; Vukicevic, S.; Information, P.E. Bone morphogenetic proteins in inflammation, glucose homeostasis and adipose tissue energy metabolism. *Cytokine Growth Factor Rev.* **2016**, *27*, 105–118. [[CrossRef](#)]
126. Yung, L.M.; Sánchez-Duffhues, G.; Dijke, P.T.; Yu, P.B. Bone morphogenetic protein 6 and oxidized low-density lipoprotein synergistically recruit osteogenic differentiation in endothelial cells. *Cardiovasc. Res.* **2015**, *108*, 278–287. [[CrossRef](#)] [[PubMed](#)]
127. Derwall, M.; Malhotra, R.; Lai, C.S.; Beppu, Y.; Aikawa, E.; Seehra, J.S.; Zapol, W.M.; Bloch, K.D.; Yu, P.B. Inhibition of bone morphogenetic protein signaling reduces vascular calcification and atherosclerosis. *Arter. Thromb. Vasc. Biol.* **2012**, *32*, 613–622. [[CrossRef](#)] [[PubMed](#)]
128. Sánchez-Duffhues, G.; De Vinuesa, A.G.; Van De Pol, V.; Geerts, M.E.; De Vries, M.R.; Janson, S.G.T.; Van Dam, H.; Lindeman, J.H.; Goumans, M.J.; Dijke, P.T. Inflammation induces endothelial-to-mesenchymal transition and promotes vascular calcification through downregulation of BMPR2. *J. Pathol.* **2019**, *247*, 333–346. [[CrossRef](#)] [[PubMed](#)]
129. Sun, B.; Huo, R.; Sheng, Y.; Li, Y.; Xie, X.; Chen, C.; Liu, H.B.; Li, N.; Li, C.B.; Guo, W.T.; et al. Bone Morphogenetic Protein-4 Mediates Cardiac Hypertrophy, Apoptosis, and Fibrosis in Experimentally Pathological Cardiac Hypertrophy. *Hypertension* **2013**, *61*, 352–360. [[CrossRef](#)] [[PubMed](#)]
130. Mao, H.; Tao, T.; Wang, X.; Liu, M.; Song, D.; Liu, X.; Shi, D. Zedoarondiol Attenuates Endothelial Cells Injury Induced by Oxidized Low-Density Lipoprotein via Nrf2 Activation. *Cell. Physiol. Biochem.* **2018**, *48*, 1468–1479. [[CrossRef](#)] [[PubMed](#)]
131. Lin, X.P.; Cui, H.J.; Yang, A.L.; Luo, J.K.; Tang, T. Astragaloside IV Improves Vasodilatation Function by Regulating the PI3K/Akt/eNOS Signaling Pathway in Rat Aorta Endothelial Cells. *J. Vasc. Res.* **2018**, *55*, 169–176. [[CrossRef](#)] [[PubMed](#)]
132. Rösen, P.; Nawroth, P.P.; King, G.; Möller, W.; Tritschler, H.J.; Packer, L. The role of oxidative stress in the onset and progression of diabetes and its complications: A summary of a Congress Series sponsored by UNESCO-MCBN, the American Diabetes Association and the German Diabetes Society. *Diabetes. Metab. Res. Rev.* **2001**, *17*, 189–212. [[CrossRef](#)] [[PubMed](#)]
133. Asaba, K.; Tojo, A.; Onozato, M.L.; Goto, A.; Quinn, M.T.; Fujita, T.; Wilcox, C.S. Effects of NADPH oxidase inhibitor in diabetic nephropathy. *Kidney Int.* **2005**, *67*, 1890–1898. [[CrossRef](#)] [[PubMed](#)]
134. Martín, A.S.; Du, P.; Dikalova, A.; Lassegue, B.; Aleman, M.; Góngora, M.C.; Brown, K.; Joseph, G.; Harrison, D.G.; Taylor, W.R.; et al. Reactive oxygen species-selective regulation of aortic inflammatory gene expression in Type 2 diabetes. *Am. J. Physiol. Circ. Physiol.* **2007**, *292*, H2073–H2082. [[CrossRef](#)] [[PubMed](#)]
135. Zhen, D.; Chen, Y.; Tang, X. Metformin reverses the deleterious effects of high glucose on osteoblast function. *J. Diabetes Complicat.* **2010**, *24*, 334–344. [[CrossRef](#)] [[PubMed](#)]
136. Kowluru, R.A. Diabetic Retinopathy: Mitochondrial Dysfunction and Retinal Capillary Cell Death. *Antioxid. Redox Signal.* **2005**, *7*, 1581. [[CrossRef](#)]
137. Konior, A.; Schramm, A.; Czesnikiewicz-Guzik, M.; Guzik, T.J. NADPH oxidases in vascular pathology. *Antioxid. Redox Signal.* **2014**, *20*, 2794–2814. [[CrossRef](#)]
138. Wang, H.T.; Liu, C.F.; Tsai, T.H.; Chen, Y.L.; Chang, H.W.; Tsai, C.Y.; Leu, S.; Zhen, Y.Y.; Chai, H.T.; Chung, S.Y.; et al. Effect of obesity reduction on preservation of heart function and attenuation of left ventricular remodeling, oxidative stress and inflammation in obese mice. *J. Transl. Med.* **2012**, *10*, 145. [[CrossRef](#)]

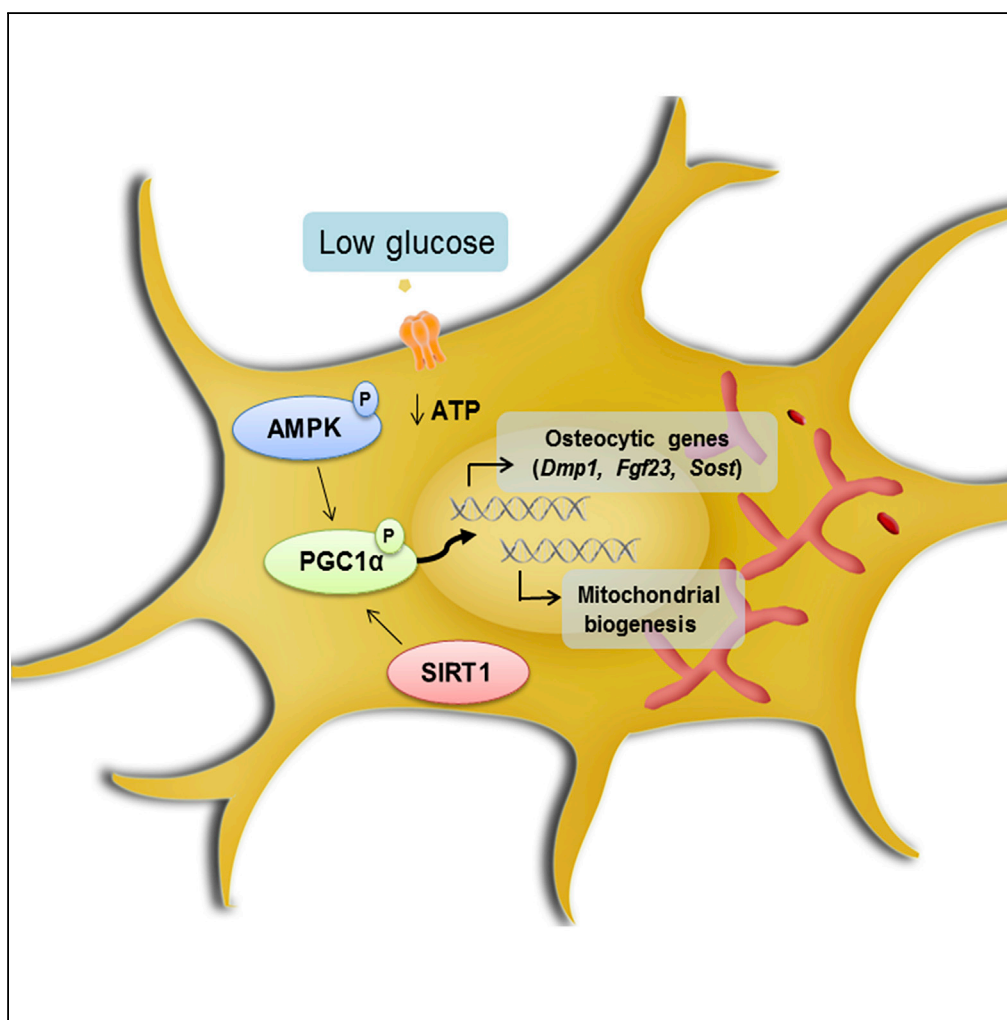
139. Saeed, O.; Otsuka, F.; Polavarapu, R.; Karmali, V.; Weiss, D.; Davis, T.; Rostad, B.; Pachura, K.; Adams, L.; Elliott, J.; et al. Pharmacological suppression of hepcidin increases macrophage cholesterol efflux and reduces foam cell formation and atherosclerosis. *Arterioscler. Thromb. Vasc. Biol.* **2012**, *32*, 299–307. [[CrossRef](#)] [[PubMed](#)]
140. Gustafson, B.; Hammarstedt, A.; Hedjazifar, S.; Hoffmann, J.M.; Svensson, P.A.; Grimsby, J.; Rondinone, C.; Smith, U. BMP4 and BMP Antagonists Regulate Human White and Beige Adipogenesis. *Diabetes* **2015**, *64*, 1670–1681. [[CrossRef](#)]
141. De Villiers, D.; Potgieter, M.; Ambele, M.A.; Adam, L.; Durandt, C.; Pepper, M.S. The Role of Reactive Oxygen Species in Adipogenic Differentiation. In *Genome Editing*; Springer: Cham, Switzerland, 2017; Volume 1083, pp. 125–144.
142. Youn, J.Y.; Gao, L.; Cai, H. The p47phox-and NADPH oxidase organiser 1 (NOXO1)-dependent activation of NADPH oxidase 1 (NOX1) mediates endothelial nitric oxide synthase (eNOS) uncoupling and endothelial dysfunction in a streptozotocin-induced murine model of diabetes. *Diabetology* **2012**, *55*, 2069–2079. [[CrossRef](#)] [[PubMed](#)]
143. Youn, J.Y.; Zhou, J.; Cai, H. Bone Morphogenic Protein 4 Mediates NOX1-Dependent eNOS Uncoupling, Endothelial Dysfunction, and COX₂ Induction in Type 2 Diabetes Mellitus. *Mol. Endocrinol.* **2015**, *29*, 1123–1133. [[CrossRef](#)] [[PubMed](#)]
144. Liu, F.; Zhong, H.; Liang, J.Y.; Fu, P.; Luo, Z.J.; Zhou, L.; Gou, R.; Huang, J. Effect of high glucose levels on the calcification of vascular smooth muscle cells by inducing osteoblastic differentiation and intracellular calcium deposition via BMP-2/Cbfa-1 pathway. *J. Zhejiang Univ. Sci. B* **2010**, *11*, 905–911. [[CrossRef](#)] [[PubMed](#)]
145. Kim, C.W.; Song, H.; Kumar, S.; Nam, D.; Kwon, H.S.; Chang, K.H.; Son, D.J.; Kang, D.W.; Brodie, S.A.; Weiss, D.; et al. Anti-inflammatory and antiatherogenic role of BMP receptor II in endothelial cells. *Arter. Thromb. Vasc. Biol.* **2013**, *33*, 1350–1359. [[CrossRef](#)] [[PubMed](#)]
146. Shao, J.S.; Aly, Z.A.; Lai, C.F.; Cheng, S.L.; Cai, J.; Huang, E.; Behrmann, A.; Towler, D.A. Vascular Bmp Msx2 Wnt Signaling and Oxidative Stress in Arterial Calcification. *Ann. N. Y. Acad. Sci.* **2007**, *1117*, 40–50. [[CrossRef](#)] [[PubMed](#)]
147. Boström, K.I.; Jumabay, M.; Matveyenko, A.; Nicholas, S.B.; Yao, Y. Activation of vascular bone morphogenetic protein signaling in diabetes mellitus. *Circ. Res.* **2011**, *108*, 446–457. [[CrossRef](#)] [[PubMed](#)]
148. Kolset, S.O.; Reinholt, F.P.; Jenssen, T. Diabetic Nephropathy and Extracellular Matrix. *J. Histochem. Cytochem.* **2012**, *60*, 976–986. [[CrossRef](#)] [[PubMed](#)]
149. Yeh, C.H.; Chang, C.K.; Cheng, M.F.; Lin, H.J.; Cheng, J.T. The antioxidative effect of bone morphogenetic protein-7 against high glucose-induced oxidative stress in mesangial cells. *Biochem. Biophys. Res. Commun.* **2009**, *382*, 292–297. [[CrossRef](#)] [[PubMed](#)]
150. Rodrigues-Díez, R.; Lavoz, C.; Carvajal, G.; Rayego-Mateos, S.; Díez, R.R.; Arduan, A.O.; Egido, J.; Mezzano, S.; Ruiz-Ortega, M. Gremlin Is a Downstream Profibrotic Mediator of Transforming Growth Factor-Beta in Cultured Renal Cells. *Nephron Exp. Nephrol.* **2012**, *122*, 62–74. [[CrossRef](#)]
151. Kane, R.; Stevenson, L.; Godson, C.; Stitt, A.W.; O'Brien, C. Gremlin gene expression in bovine retinal pericytes exposed to elevated glucose. *Br. J. Ophthalmol.* **2005**, *89*, 1638–1642. [[CrossRef](#)]
152. Kowluru, R.A.; Chan, P.S. Oxidative Stress and Diabetic Retinopathy. *Exp. Diabetes Res.* **2007**, *2007*, 43603. [[CrossRef](#)]
153. Makris, K.; Spanou, L. Acute Kidney Injury: Definition, Pathophysiology and Clinical Phenotypes. *Clin. Biochem. Rev.* **2016**, *37*, 85–98.
154. Meran, S.; Steadman, R. Fibroblasts and myofibroblasts in renal fibrosis. *Int. J. Exp. Pathol.* **2011**, *92*, 158–167. [[CrossRef](#)] [[PubMed](#)]
155. Wang, S.; Chen, Q.; Simon, T.C.; Strebeck, F.; Chaudhary, L.; Morrissey, J.; Liapis, H.; Klahr, S.; Hruska, K.A. Bone morphogenetic protein-7 (BMP-7), a novel therapy for diabetic nephropathy. Professor Robert Chevalier served as a guest editor for this paper. *Kidney Int.* **2003**, *63*, 2037–2049. [[CrossRef](#)] [[PubMed](#)]
156. Zeisberg, M.; Hanai, J.I.; Sugimoto, H.; Mammoto, T.; Charytan, D.; Strutz, F.; Kalluri, R. BMP-7 counteracts TGF-β1-induced epithelial-to-mesenchymal transition and reverses chronic renal injury. *Nat. Med.* **2003**, *9*, 964–968. [[CrossRef](#)] [[PubMed](#)]
157. Hsing, C.H.; Chou, W.; Wang, J.J.; Chen, H.W.; Yeh, C.H. Propofol increases bone morphogenetic protein-7 and decreases oxidative stress in sepsis-induced acute kidney injury. *Nephrol. Dial. Transplant.* **2011**, *26*, 1162–1172. [[CrossRef](#)] [[PubMed](#)]

158. Lee, H.B.; Ha, H. Mechanisms of Epithelial-Mesenchymal Transition of Peritoneal Mesothelial Cells During Peritoneal Dialysis. *J. Korean Med. Sci.* **2007**, *22*, 943–945. [[CrossRef](#)] [[PubMed](#)]
159. Dolan, V.; Murphy, M.; Sadlier, D.; Lappin, D.; Doran, P.; Godson, C.; Martin, F.; O'Meara, Y.; Schmid, H.; Henger, A.; et al. Expression of gremlin, a bone morphogenetic protein antagonist, in human diabetic nephropathy. *Am. J. Kidney Dis.* **2005**, *45*, 1034–1039. [[CrossRef](#)] [[PubMed](#)]
160. Zhang, Y.; Zhang, Q. Bone morphogenetic protein-7 and Gremlin: New emerging therapeutic targets for diabetic nephropathy. *Biochem. Biophys. Res. Commun.* **2009**, *383*, 1–3. [[CrossRef](#)] [[PubMed](#)]
161. Nezu, M.; Suzuki, N.; Yamamoto, M. Targeting the KEAP1-NRF2 System to Prevent Kidney Disease Progression. *Am. J. Nephrol.* **2017**, *45*, 473–483. [[CrossRef](#)]
162. Choi, B.H.; Kang, K.S.; Kwak, M.K. Effect of Redox Modulating NRF2 Activators on Chronic Kidney Disease. *Molecules* **2014**, *19*, 12727–12759. [[CrossRef](#)]
163. Verdijk, L.B.; Snijders, T.; Drost, M.; Delhaas, T.; Kadi, F.; van Loon, L.J.C. Satellite cells in human skeletal muscle; from birth to old age. *Age (Omaha)* **2014**, *36*, 545–557. [[CrossRef](#)]
164. Frühbeck, G.; Sesma, P.; Burrell, M.A. PRDM16: The interconvertible adipo-myocyte switch. *Trends Cell Biol.* **2009**, *19*, 141–146. [[CrossRef](#)] [[PubMed](#)]
165. Tseng, Y.H.; Kokkotou, E.; Schulz, T.J.; Huang, T.L.; Winnay, J.N.; Taniguchi, C.M.; Tran, T.T.; Suzuki, R.; Espinoza, D.O.; Yamamoto, Y.; et al. New role of bone morphogenetic protein 7 in brown adipogenesis and energy expenditure. *Nature* **2008**, *454*, 1000–1004. [[CrossRef](#)] [[PubMed](#)]
166. Morozzi, G.; Beccafico, S.; Bianchi, R.; Riuizzi, F.; Bellezza, I.; Giambanco, I.; Arcuri, C.; Minelli, A.; Donato, R. Oxidative stress-induced S100B accumulation converts myoblasts into brown adipocytes via an NF- κ B/YY1/miR-133 axis and NF- κ B/YY1/BMP-7 axis. *Cell Death Differ.* **2017**, *24*, 2077–2088. [[CrossRef](#)] [[PubMed](#)]
167. Kim, H.K.; Bian, H.; Aya-Ay, J.; Garces, A.; Morgan, E.F.; Gilbert, S.R. Hypoxia and HIF-1 α expression in the epiphyseal cartilage following ischemic injury to the immature femoral head. *Bone* **2009**, *45*, 280–288. [[CrossRef](#)] [[PubMed](#)]
168. Nakase, T.; Miyaji, T.; Tomita, T.; Kaneko, M.; Kuriyama, K.; Myoui, A.; Sugamoto, K.; Ochi, T.; Yoshikawa, H. Localization of bone morphogenetic protein-2 in human osteoarthritic cartilage and osteophyte. *Osteoarthr. Cartil.* **2003**, *11*, 278–284. [[CrossRef](#)]
169. Kamiya, N.; Shafer, S.; Oxendine, I.; Mortlock, D.P.; Chandler, R.L.; Oxburgh, L.; Kim, H.K. Acute BMP2 upregulation following induction of ischemic osteonecrosis in immature femoral head. *Bone* **2013**, *53*, 239–247. [[CrossRef](#)] [[PubMed](#)]
170. Jiang, M.; Ku, W.Y.; Zhou, Z.; Dellon, E.S.; Falk, G.W.; Nakagawa, H.; Wang, M.L.; Liu, K.; Wang, J.; Katzka, D.A.; et al. BMP-driven NRF2 activation in esophageal basal cell differentiation and eosinophilic esophagitis. *J. Clin. Investig.* **2015**, *125*, 1557–1568. [[CrossRef](#)] [[PubMed](#)]
171. Tardif, G.; Hum, D.; Pelletier, J.P.; Boileau, C.; Ranger, P.; Martel-Pelletier, J. Differential gene expression and regulation of the bone morphogenetic protein antagonists follistatin and gremlin in normal and osteoarthritic human chondrocytes and synovial fibroblasts. *Arthritis Rheum.* **2004**, *50*, 2521–2530. [[CrossRef](#)] [[PubMed](#)]
172. Tardif, G.; Pelletier, J.P.; Boileau, C.; Martel-Pelletier, J. The BMP antagonists follistatin and gremlin in normal and early osteoarthritic cartilage: An immunohistochemical study. *Osteoarthr. Cartil.* **2009**, *17*, 263–270. [[CrossRef](#)]
173. Han, E.J.; Yoo, S.A.; Kim, G.M.; Hwang, D.; Cho, C.S.; You, S.; Kim, W.U. GREM1 Is a Key Regulator of Synovocyte Hyperplasia and Invasiveness. *J. Rheumatol.* **2016**, *43*, 474–485. [[CrossRef](#)]
174. Yi, J.; Jin, Q.; Zhang, B.; Wu, X.; Ge, D. Gremlin-1 Concentrations Are Correlated with the Severity of Knee Osteoarthritis. *Med. Sci. Monit.* **2016**, *22*, 4062–4065. [[CrossRef](#)] [[PubMed](#)]



Article

Glucose Restriction Promotes Osteocyte Specification by Activating a PGC-1 α -Dependent Transcriptional Program



Cristina Sánchez-de-Diego, Natalia Artigas, Carolina Pimenta-Lopes, ..., Pablo M. Garcia-Roves, José Luis Rosa, Francesc Ventura

fventura@ub.edu

HIGHLIGHTS

Glucose restriction promotes osteocytic gene expression and mitochondrial function

Glucose restriction triggers activation of the AMPK/PGC-1 pathway

Effects of glucose restriction on osteocyte gene expression depend on *Ppargc1a/b*

Deletion of *Ppargc1a/b* in osteoblasts and osteocytes leads to osteopenia

Sánchez-de-Diego et al.,
iScience 15, 79–94
May 31, 2019 © 2019 The
Author(s).
[https://doi.org/10.1016/
j.isci.2019.04.015](https://doi.org/10.1016/j.isci.2019.04.015)

Article

Glucose Restriction Promotes Osteocyte Specification by Activating a PGC-1 α -Dependent Transcriptional Program

Cristina Sánchez-de-Diego,¹ Natalia Artigas,¹ Carolina Pimenta-Lopes,¹ José Antonio Valer,¹ Benjamin Torrejon,² Pau Gama-Pérez,¹ Josep A. Villena,³ Pablo M. Garcia-Roves,¹ José Luis Rosa,¹ and Francesc Ventura^{1,4,*}

SUMMARY

Osteocytes, the most abundant of bone cells, differentiate while they remain buried within the bone matrix. This encasement limits their access to nutrients and likely affects their differentiation, a process that remains poorly defined. Here, we show that restriction in glucose supply promotes the osteocyte transcriptional program while also being associated with increased mitochondrial DNA levels. Glucose deprivation triggered the activation of the AMPK/PGC-1 pathway. AMPK and SIRT1 activators or PGC-1 α overexpression are sufficient to enhance osteocyte gene expression in IDG-SW3 cells, murine primary osteoblasts, osteocytes, and organotypic/ex vivo bone cultures. Conversely, osteoblasts and osteocytes deficient in *Ppargc1a* and *b* were refractory to the effects of glucose restriction. Finally, conditional ablation of both genes in osteoblasts and osteocytes generate osteopenia and reduce osteocytic gene expression in mice. Altogether, we uncovered a role for PGC-1 in the regulation of osteocyte gene expression.

INTRODUCTION

Of the major cell types in bone, osteocytes make up over 90% to 95% of total bone cells in the adult skeleton. No longer considered passive placeholders in bone, osteocytes have recently emerged as major orchestrators of bone remodeling, physical mechanosensors, hematopoietic niche cells, and endocrine regulators of whole-body metabolism (Dallas et al., 2013; Sato et al., 2013; Karsenty and Olson, 2016). Lower osteocyte function has been directly linked to mechanical bone fragility, osteopenia associated with aging or diabetes, chronic kidney disease, and atherosclerosis (Dallas et al., 2013; Lai et al., 2015; Napoli et al., 2017).

Osteocytes derive from osteoblasts through an active and dynamic process involving their embedding in mineralized osteoid matrices. During osteocytogenesis dramatic morphological changes occur, including an important restructuring of the cytoskeleton and acquisition of a unique gene expression profile (Bonewald, 2011). As osteocytogenesis progresses, we see the downregulation of some osteoblastic genes and the progressive expression of osteocyte-specific genes such as *Dmp1*, *Fgf23*, and *Sost* (Woo et al., 2011). Yet the genetic and molecular mechanisms that govern the differentiation and maturation of osteocytes are far from clear.

One of the driving forces of osteoblast-osteocyte transition is likely to be their encasement within a mineralized bone matrix. This restricts their access to oxygen and nutrients and can induce modifications in their metabolic profile (Riddle and Clemens, 2017). The lacuno-canalicular system connects osteocytes between these matrices and allows those near the surface to interact with osteoblasts and bone-lining cells (Buenzli and Sims, 2015). However, the mechanisms of diffusion between the bone surface and the osteocytes are challenged to maintain an adequate supply and exchange of nutrients and metabolic products (Piekarski and Munro, 1977; Petrov and Pollack, 2003; Wang, 2018). Therefore we can infer that osteoblasts, as they differentiate into osteocytes, must adapt to a nutrient-restricted environment. For instance, osteocytes are enriched in proteins involved in hypoxic response, and hypoxic conditions promote the expression of osteocytic genes (Hirao et al., 2007; Guo et al., 2010; Dallas et al., 2013).

It has been shown that osteocytes maintain oxidative status utilizing mainly aerobic mitochondrial pathways (Frikha-Benayed et al., 2016). In contrast, osteoprogenitors and osteoblasts represent by far the

¹Departament de Ciències Fisiològiques, Universitat de Barcelona, IDIBELL, L'Hospitalet de Llobregat, 08907 Barcelona, Spain

²Centres Científics i Tecnològics, Universitat de Barcelona, L'Hospitalet de Llobregat, Barcelona 08907, Spain

³Laboratory of Metabolism and Obesity, Vall d'Hebron Institut de Recerca, Universitat Autònoma de Barcelona, Barcelona 08035, Spain

⁴Lead Contact

*Correspondence: fventura@ub.edu

<https://doi.org/10.1016/j.isci.2019.04.015>



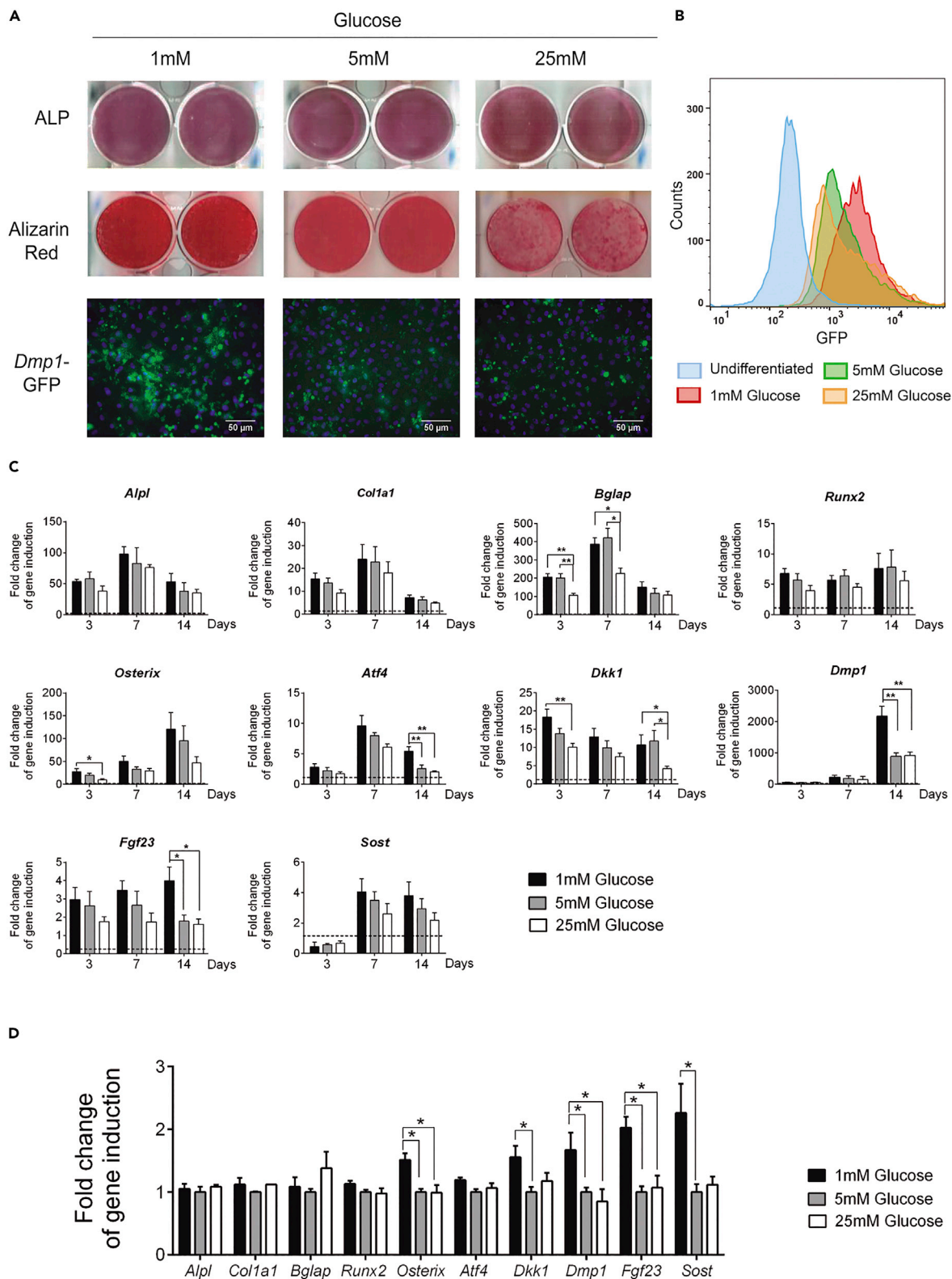


Figure 1. Effect of Glucose Supply in Osteocyte Differentiation

(A) Representative images of alkaline phosphatase staining (ALP), alizarin red staining, and visualization of *Dmp1*-GFP expression in IDG-SW3 differentiated for 14 days in the presence of 1, 5, or 25 mM glucose. Cell nuclei were stained with DAPI (blue).

(B) Flow cytometry analysis of *Dmp1*-GFP expression in IDG-SW3 undifferentiated and differentiated cells for 14 days in the presence of 1, 5, or 25 mM glucose.

(C) mRNA expression profile of osteoblast and osteocyte gene markers during IDG-SW3 differentiation (at 3, 7, and 14 days) in the presence of 1, 5, and 25 mM glucose.

(D) Quantification of mRNA expression levels in primary osteocytes cultured for 4 days in the presence of 1, 5, or 25 mM glucose. mRNA levels were measured by qRT-PCR and normalized to *Tbp* expression.

Results are plotted as expression relative to undifferentiated IDG-SW3 or osteocytes cultured in 5 mM glucose (mean \pm SEM of five to seven independent experiments). * $p < 0.05$ and ** $p < 0.01$ using one-way ANOVA. See also [Figure S1](#).

most glucose-avid cells in bone with relatively sparse uptake in osteocytes (Dirckx et al., 2018). Glucose is not only used by osteoblasts but also its uptake synergizes with Runx2 to determine bone formation and homeostasis throughout life (Wei et al., 2015). Recent studies have further revealed the importance of aerobic glycolysis for the anabolic effects of parathyroid hormone (PTH) and Wnts (Esen et al., 2013, 2015; Regan et al., 2014). These studies pointed out that modulation of AMPK and/or mTORC1/2 is the mechanism involved in the functional link between glucose metabolism and bone formation.

AMPK acts as a cellular energy sensor and has a critical role in adaptive metabolic reprogramming. Several studies demonstrate that AMPK deletion of AMPK α 1, β 1, or β 2 subunits in mice results in reduced trabecular bone without modifying the numbers of osteoclasts and osteoblasts (Quinn et al., 2010). Once active, AMPK activity leads to higher glucose uptake, autophagy, and mitochondrial biogenesis (Hardie, 2018). Some of these functions are mediated by the proliferator-activated receptor γ co-activator-1 (PGC-1). PGC-1s are transcriptional co-activators that respond to a number of environmental cues and coordinate mitochondrial biogenesis and tissue-specific programs of gene regulation (Villena, 2015). Therefore considering that metabolic rewiring is likely to be crucial for bone cell specification, we hypothesize that low glucose concentration can induce metabolic and genetic reprogramming, which promotes osteocytogenesis.

RESULTS**Glucose Restriction Promotes Osteocyte Differentiation**

We investigated the effects of different glucose concentrations, the major source of energy in culture media, on bone cell specification. We differentiated the pre-osteocytic IDG-SW3 cell line and mouse primary osteoblasts in the presence of 1, 5, or 25 mM glucose. Selected glucose concentrations did not affect cell viability or proliferation of IDG-SW3 cells (Figures S1A–S1C). Alkaline phosphatase and alizarin red staining showed the ability of IDG-SW3 cells to differentiate into mature osteoblasts and revealed a decrease in the formation of calcium deposits (alizarin red) when cultured in 25 mM glucose (Figure 1A). Confluent IDG-SW3 cells differentiated into an early stage of osteocyte specification after 14 days in culture at 37°C (Woo et al., 2011). These cells also carry a *Dmp1*-GFP reporter (expression of GFP under the control of the osteocyte-specific *Dmp1* promoter) that facilitates the follow-up of the osteoblast-to-osteocyte transition. Our data showed a negative correlation between osteocytic *Dmp1*-GFP expression and glucose supply. Low glucose supply enhanced the expression of *Dmp1*-GFP, as analyzed by either fluorescence microscopy or fluorescence-activated cell sorting (Figures 1A and 1B). To further characterize the induced phenotype, we quantified mRNAs associated with osteoblasts and osteocytes. Gene expression profiling during the osteoblast-to-osteocyte transition in IDG-SW3 cells indicated that mRNA levels of osteoblastic genes (*Alpl*, *Col1a1*, *Bglap*, or *Atf4*) peaked at the seventh day and decreased thereafter, whereas expression of the osteocytic markers *Dmp1* increased at day 14 (Figure 1C). A high-glucose regime reduced the levels of osteoblast genes, such as *Bglap*, *Osx*, or *Dkk1*. More importantly, glucose restriction (1 mM glucose) significantly increased the expression of the osteocyte markers *Dmp1* and *Fgf23* compared with normoglycemia or hyperglycemia (5 and 25 mM glucose, respectively) (Figure 1C). The effects of distinct glucose concentrations in the osteocytic transcriptional program were independent of changes in the osmotic pressure (Figure S1D). We also investigated the gene expression profile of osteocytes and bone organotypic cultures maintained for 4 and 5 days respectively, with different glucose regimes. As with IDG-SW3 cells, low-glucose media increased the expression of some osteocytic genes (*Dkk1*, *Dmp1*, *Fgf23*, or *Sost*) in osteocytes and bone organotypic cultures (Figures 1D and S1E). Altogether, these data demonstrated that glucose restriction favors osteocytic gene expression.

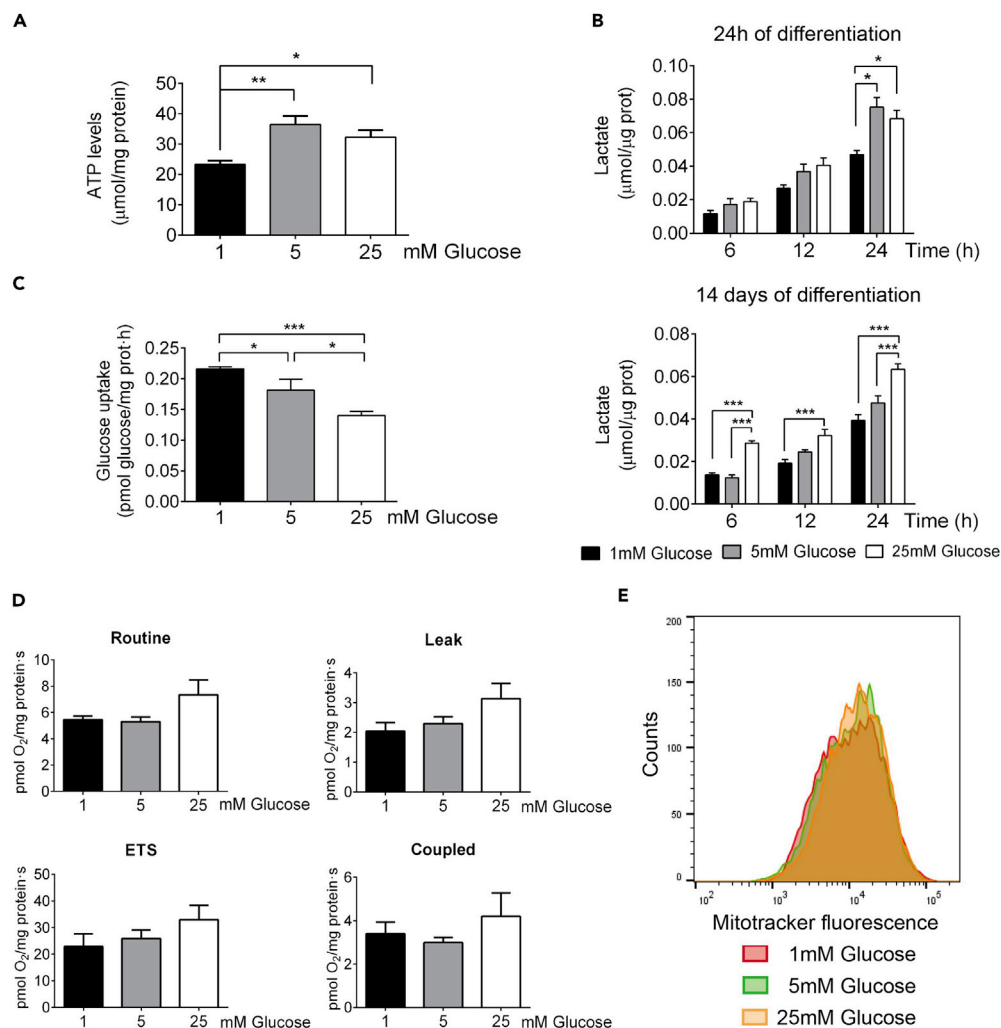


Figure 2. Metabolic Profile Induced by Glucose Supply

(A) ATP levels in IDG-SW3 after 14 days of differentiation in the presence of 1, 5, or 25 mM glucose.

(B) Quantification of lactate release in predifferentiated IDG-SW3 cultured in 1, 5, or 25 mM glucose media for 24 h, and in IDG-SW3 differentiated for 14 days in the presence of 1, 5, or 25 mM glucose.

(C) Determination of the maximal uptake capacity for glucose in IDG-SW3 cells differentiated for 14 days in the presence of 1, 5, or 25 mM glucose.

(D) Determination of routine oxygen consumption, leak respiration (uncoupled), electron transfer capacity (ETS), and coupled respiration of IDG-SW3 differentiated for 14 days in the presence of 1, 5, or 25 mM glucose. A total of 700,000 IDG-SW3 cells were incubated in the respirometry chamber with 1, 5, or 25 mM glucose in α -MEM without FBS during the analysis. All results were expressed relative to protein content. Results are plotted as mean \pm SEM of four to eight independent experiments.

(E) Flow cytometry analysis of IDG-SW3 cells differentiated for 14 days in the presence of 1, 5, or 25 mM glucose and labeled with MitoTracker Deep Red.

* $p < 0.05$, ** $p < 0.01$, and *** $p < 0.001$ using one-way ANOVA. See also [Figure S2](#).

Glucose Supply Modifies Osteoblast and Osteocyte Metabolism

We then aimed to characterize bone cell metabolism by different glucose concentrations. IDG-SW3 cells differentiated in low-glucose conditions had decreased intracellular ATP levels compared with normoglycemia or hyperglycemia, which suggests a compromised energy supply (Figure 2A). We assayed lactate released by IDG-SW3 cells during the initial steps of differentiation (24 h) and after complete differentiation (14 days). As expected, either at 24 h or after differentiation, IDG-SW3 cells cultured in low-glucose medium showed a reduction in lactate production, whereas a high-glucose regime raised lactate production values

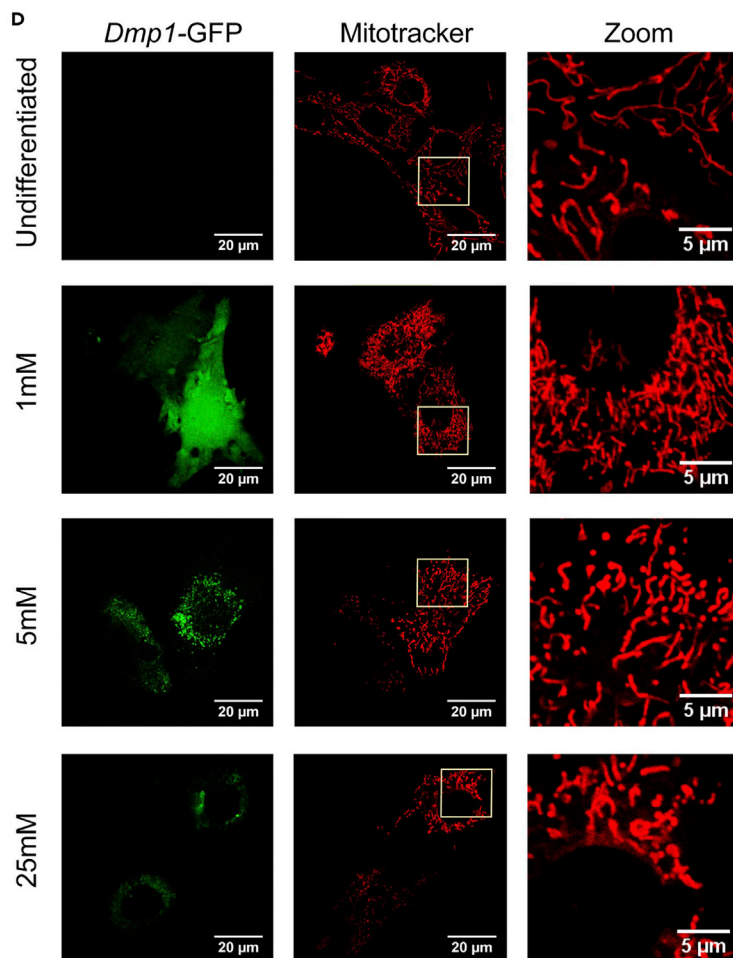
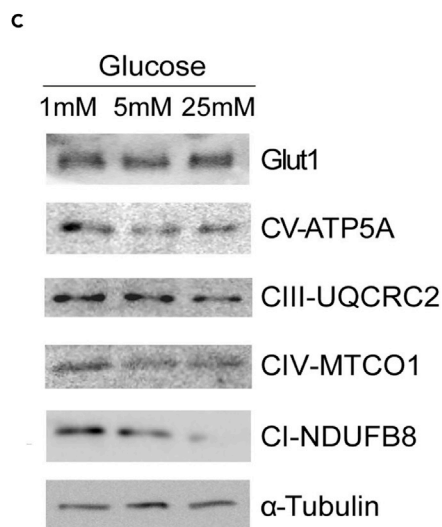
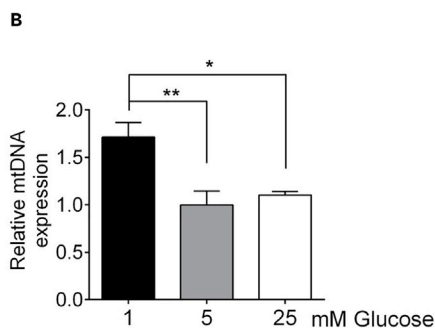
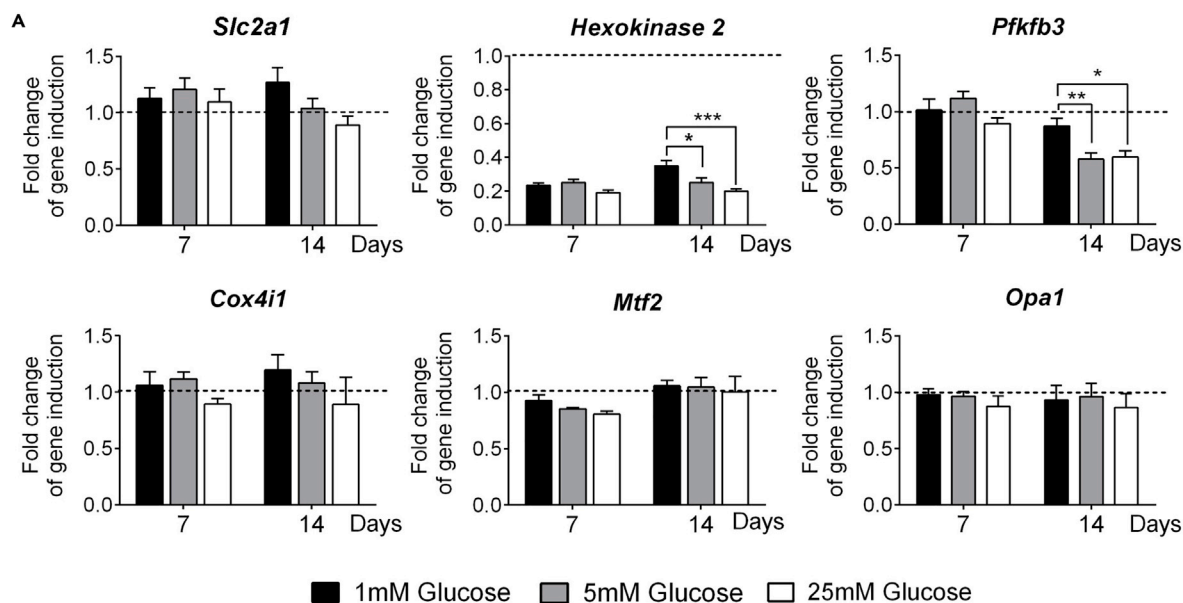


Figure 3. Modification of Glycolytic Gene Expression and Mitochondrial Function Induced by Glucose Supply

(A) mRNA expression levels of glycolytic and mitochondrial genes in IDG-SW3 differentiated for 14 days in the presence of 1, 5, or 25 mM glucose. mRNA expression levels were measured by qRT-PCR and normalized to *Tbp* expression. Results were plotted as expression relative to undifferentiated IDG-SW3 (mean \pm SEM of six independent experiments).

(B) Quantification of mtDNA (*tRNA-Glu*) in IDG-SW3 differentiated for 14 days in the presence of 1, 5, or 25 mM glucose. mtDNA copy number was measured by qPCR and normalized relative to nuclear DNA (*Dmp1* and *Fgf23*). Results are plotted as mean \pm SEM of six independent experiments.

(C) Immunoblot analysis of the expression of Glut1 and mitochondrial complexes in IDG-SW3 differentiated for 14 days in the presence of 1, 5, or 25 mM glucose.

(D) Visualization of mitochondria in IDG-SW3 differentiated for 14 days in the presence of 1, 5, or 25 mM glucose. *Dmp1*-GFP was visualized, and mitochondria were stained with MitoTracker Deep Red.

* $p < 0.05$, ** $p < 0.01$, and *** $p < 0.001$ using one-way ANOVA. See also Figure S3.

(Figure 2B). For a further characterization of metabolic reprogramming, we also analyzed glucose uptake capacity after differentiation for 14 days in 1, 5, and 25 mM glucose. Glucose uptake was tested at 10 μ M glucose for all conditions. Low glucose exposure significantly increased the uptake capacity for glucose, whereas glucose-enriched media decreased it (Figure 2C). We also investigated the bone cell metabolism in primary osteoblasts cultured for 10 days with different glucose concentrations. Mature primary osteoblasts cultured in 1 mM glucose were still able to maintain ATP levels and, as IDG-SW3 cells, osteoblasts increased their glucose uptake capacity in low-glucose conditions (Figures S2A and S2B). Lactate production was also increased when cultured in 25 mM glucose (Figure S2C). Therefore mature osteoblasts in culture can maintain energetic balance and anaerobic glycolysis even at 1 mM glucose. These data suggested a sparing effect in glucose-restricted conditions, maximizing uptake and reducing lactate release, and vice versa under hyperglycemic conditions.

We then measured mitochondrial respiration in intact, differentiated IDG-SW3 cells using the different glucose supplies. These different glucose concentrations were also maintained during the assay as major energy substrate. We determined routine O_2 consumption, leak state (uncoupled respiration after addition of oligomycin into the assay), electron transfer capacity (determination of electron transfer system [ETS] after carbonylcyanide-4- (trifluoromethoxy)-phenyl-hydrazine (FCCP)), and coupled respiration. Differences in respiratory parameters were not significant between groups, and we only observed a slightly increased routine respiration in cells cultured with 25 mM glucose (Figure 2D). Interestingly, IDG-SW3 cells were able to maintain O_2 consumption under glucose restriction conditions. Moreover, total mitochondrial potential was unmodified by the different glucose regimes when analyzed by flow cytometry using a mitochondrial potential-dependent dye (Figure 2E). It is known that routine respiration is controlled by ATP turnover and substrate availability (Brand and Nicholls, 2011). Therefore these data suggested that cells adapt to meet energy demands by increasing glucose uptake and through the diversion of glucose to mitochondrial respiration.

Glucose Restriction Increases the Mitochondrial DNA and Changes Mitochondrial Morphology

To identify further the changes in energy metabolism induced by glucose supply, we quantified the expression of genes involved in glycolysis and mitochondrial function. GLUT1 (*Slc2a1*) is the most expressed glucose transporter in IDG-SW3 cells during osteocyte specification (Figure S3A). In addition, different glucose concentrations did not induce a significant change in expression between GLUT family members (Figures S3B and 3A). IDG-SW3 cells and osteoblasts differentiated under low-glucose conditions had higher expression of the glycolytic genes *Pfkfb3* and *Hk2*, whereas the expression of *Cox4i1* and the genes involved in mitochondrial fusion/fission *Mtf2* and *Opa1* did not show significant differences between distinct glucose regimes (Figures 3A and S3C). As mitochondria are remarkable dynamic organelles that respond to changes in energy demands, we wondered whether glucose concentration would modify mitochondrial content and function. Reduced glucose supply increased the ratio of mitochondrial DNA (mtDNA) to nuclear DNA (Figures 3B and S3D). This increase in mtDNA was consistent with an increase in the protein levels of members of the different oxidative phosphorylation (OXPHOS) complexes (Figures 3C and S3E).

Emerging evidence showed that mitochondria continuously adjust their shape, size, and network organization through fusion or fission events, to regulate their function (Galloway et al., 2012). Confocal images showed dramatic differences in mitochondrial structure and network among the three conditions. IDG-SW3 cells and primary osteoblasts differentiated in 1 mM glucose media arranged their mitochondria in elongated tubules, with higher branching, forming reticular networks (Figures 3D and S3F). In contrast, hyperglycemic conditions increased mitochondrial fragmentation with the formation of ring-like structures in

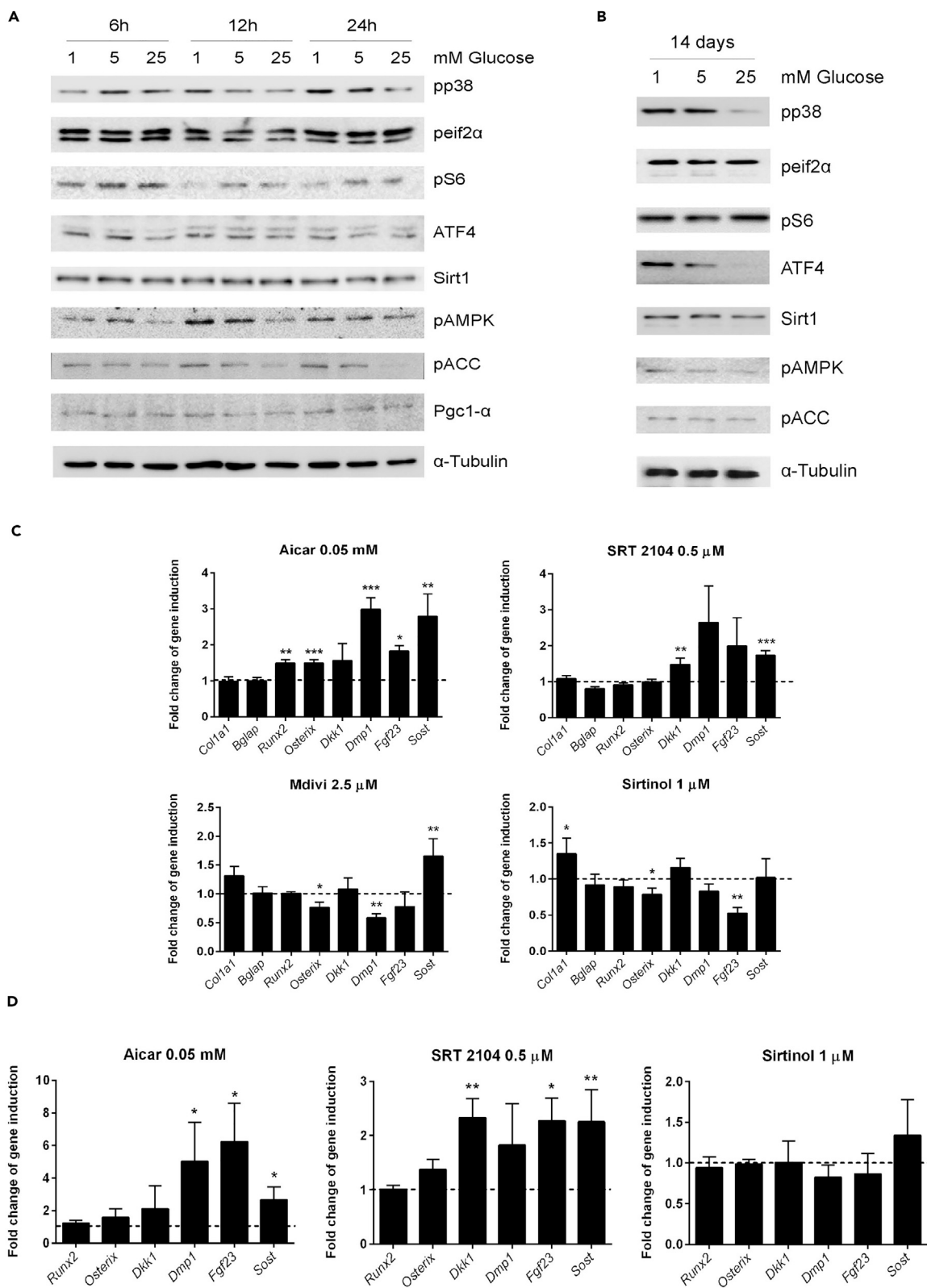


Figure 4. Signaling Pathways Involved in Metabolic and Genetic Reprogramming of Osteocytes

(A and B) Immunoblots from IDG-SW3 cells cultured in 1, 5, and 25 mM glucose media for 6, 12, and 24 h (A) or after 14 days of differentiation in 1, 5, and 25 mM glucose media (B).

(C) mRNA expression of osteoblastic and osteocytic genes in IDG-SW3 differentiated for 14 days in 5 mM glucose and treated with 0.05 mM AICAR (activator of AMPK), 0.5 μ M SRT2104 (activator of SIRT1), 1 μ M sirtinol (inhibitor of SIRT1), and 2.5 μ M Mdivi (inhibitor of mitochondrial fission). mRNA levels were measured by qRT-PCR and normalized to *Tbp* expression. Results were plotted as expression relative to untreated IDG-SW3 (mean \pm SEM of five independent experiments).

(D) mRNA expression of osteoblastic and osteocytic genes in organotypic cultures from mouse femur. Organotypic cultures were maintained in 5 mM glucose media and treated with 0.05 mM AICAR, 0.5 μ M SRT2104, and 1 μ M sirtinol for 5 days. mRNA levels were measured by qRT-PCR and normalized to *Tbp* expression.

Results were expressed as gene expression relative to untreated organotypic cultures (mean \pm SEM of five independent experiments). * $p < 0.05$, ** $p < 0.01$, and *** $p < 0.001$ using Student's *t* test. See also [Figure S4](#).

differentiated IDG-SW3 and osteoblasts ([Figures 3D and S3F](#)). It has been demonstrated that elongated mitochondria are more resistant to mitophagy and more efficient at producing ATP through enhanced cristae density and ATP synthase dimerization ([Gomes et al., 2011](#)). In addition, it is known that ring-like and fragmented mitochondria structures arise from cellular stresses ([Yu et al., 2006](#)). Therefore these data suggest that during osteocyte differentiation, glucose restriction stimulates glycolytic pathways and increases mtDNA and efficiency in an effort to maintain ATP levels.

Glucose Restriction Effects on Osteocyte Gene Expression Depend on AMPK

Nutrient starvation signals through activation of AMPK and mTORC1 energy sensors ([Carroll and Dunlop, 2017](#)). Thus we determined the activation state of signaling pathways likely to be involved in the metabolic and genetic reprogramming of osteocytes. We analyzed early activation of these pathways during the first hours of differentiation and after complete differentiation, in IDG-SW3 and primary osteoblasts. In response to glucose restriction, AMPK and its substrate acetyl-CoA carboxylase (ACC) became phosphorylated ([Figures 4A, 4B, S4A, and S4B](#)). Similarly, the stress kinase p38-MAPK was also activated either at 24 h or after 14 days.

Effects of AMPK on mitochondrial biogenesis rely on PGC-1 (PGC1- α and β) expression and activation ([Hardie, 2018](#)). The PGC-1 family of transcriptional co-activators plays a major role in integrating physiological signals into the expression of nuclear-encoded mitochondrial genes ([Villena, 2015](#)). Posttranslational modifications that activate PGC-1 members include phosphorylation by AMPK and p38 and deacetylation by SIRT1 ([Fan et al., 2004](#); [Gerhart-Hines et al., 2007](#); [Jager et al., 2007](#)). Therefore to further characterize the role of AMPK/SIRT/PGC1 α/β pathways in osteocyte reprogramming and differentiation, we treated IDG-SW3 cells and bone organotypic cultures with different chemical modulators of these pathways. The activation of AMPK by AICAR during differentiation increased the expression of *Runx2* and *Osx* in IDG-SW3 cells and the expression of *Dmp1*, *Fgf23*, and *Sost* osteocyte genes in both IDG-SW3 and bone organotypic cultures ([Figures 4C and 4D](#)). Similarly, the activation of SIRT1 by SRT2104 treatment induced the expression of late osteocyte markers in both experimental models. On the other hand, the inhibition of SIRT1 by sirtinol reduced the levels of *Osx* and *Fgf23* in IDG-SW3 cultures. These results suggested that the activation of AMPK/SIRT1 enhances osteocytic differentiation.

We also evaluated whether induction of mitochondrial fusion and elongation was sufficient for enhancement of osteocytic gene expression. DRP1 is a dynamin-related GTPase that mediates mitochondrial fission ([Galloway et al., 2012](#)). Inhibition of DRP1 by Mdivi-1 increases the number of elongated mitochondria and their reticular network ([Cassidy-Stone et al., 2008](#)). Inhibition of mitochondrial fission by Mdivi-1 during osteocytic differentiation reduced the expression of *Osx* and *Dmp1* but only induced the expression of *Sost* ([Figure 4C](#)). These results suggest that mitochondrial reorganization is not sufficient to enhance osteocytogenesis.

PGC-1 Mediates Enhanced Osteocytic Gene Expression in Response to Reduced Glucose Supply

Next, we determined the expression of *Ppargc1a* and *b* genes during the osteoblast to osteocyte transition in IDG-SW3 cells and primary osteoblasts. Proliferative IDG-SW3 cells expressed higher levels of *Ppargc1a* compared with *Ppargc1b*. Moreover, differentiated cells shifted further toward a major expression of *Ppargc1a* over *Ppargc1b* ([Figure 5A](#)). Similarly, the ratio of expression between *Ppargc1a* and *Ppargc1b*

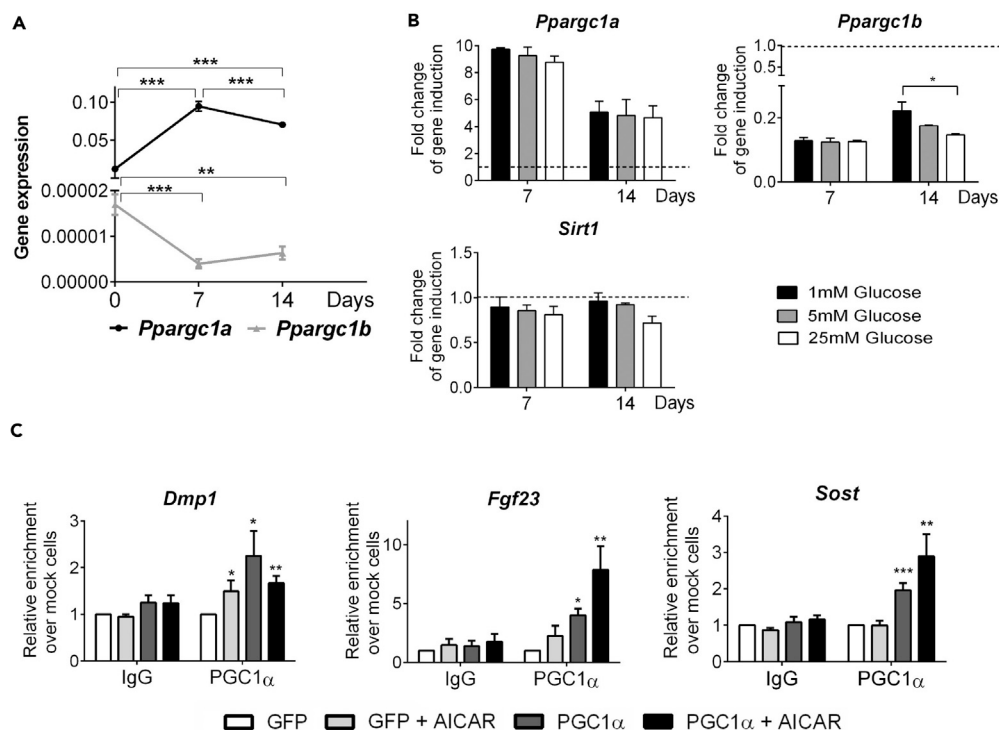


Figure 5. PGC1- α Binds to Osteocytic Promoters

(A) mRNA expression levels of the different isoforms of PGC-1 in IDG-SW3 differentiated for 14 days in 5 mM glucose media. mRNA expression was quantified by qRT-PCR and normalized to *Tbp* expression. Results are plotted as $2^{-\Delta\Delta Ct}$ (mean \pm SEM of six independent experiments).

(B) mRNA expression levels of *Pparg1a*, *Pparg1b*, and *Sirt1* during IDG-SW3 differentiation in 5 mM glucose media. mRNA levels were quantified by qRT-PCR, normalized by *Tbp* and plotted as expression relative to undifferentiated IDG-SW3 (mean \pm SEM of six independent experiments).

(C) Chromatin immunoprecipitation of IDG-SW3 cells infected with control GFP or PGC-1 α expression vectors and differentiated in 5 mM glucose media for 5 days in the presence or absence of 0.5 mM AICAR. Results were normalized to input chromatin and plotted relative to untreated IDG-SW3 cells infected with control GFP vector (mean \pm SEM of four independent experiments). * $p < 0.05$, ** $p < 0.01$, and *** $p < 0.001$ using Student's *t* test. See also Figure S4.

in primary osteoblasts and calvarial mRNA was about 3-fold (data not shown). mRNA levels of PGC-1 α or SIRT1 did not change among the three culture conditions in IDG-SW3 (Figure 5B). On the contrary, in primary osteoblasts, glucose restriction induced *Pparg1a* and *b* mRNA expression (Figure S4C). *Pparg1a* and *b* play redundant roles by regulating gene expression programs through their interaction with a variety of transcription factors such as NRF2, ERR α , PPARs, or MEF2. *In silico* analysis of regulatory motifs present in the promoters of the osteocyte genes *Dmp1*, *Fgf23*, and *Sost* revealed conserved potential binding sites for PGC-1 co-activated factors. We confirmed the recruitment of PGC-1 to these regulatory regions by chromatin immunoprecipitation with an anti-PGC-1 α antibody. Ectopic expression of PGC-1 α and its activation with AICAR increased PGC-1 α occupancy of *Fgf23* and *Sost* promoters in IDG-SW3 cells (Figure 5C). We also determined whether higher PGC-1 α activity could induce expression of these genes. Overexpression of ectopic PGC-1 α in IDG-SW3 and primary osteoblasts led to higher mRNA levels of osteoblastic (*Col1a1*, *Bglap*, *Osx*) and osteocytic (*Dkk1*, *Fgf23*, and *Sost*) genes (Figure 6A). We also analyzed gene expression in primary osteoblasts and osteocytes deficient in PGC-1 α and PGC-1 β . Deletion of *Pparg1a* and *b* did not affect cell proliferation or viability, although it reduced morphological reorganization and hampered the increase in mtDNA induced by glucose restriction (Figure S5). Deletion of *Pparg1a* and *Pparg1b* in primary osteoblasts or osteocytes decreased the levels of *Runx2* and *Osx* irrespective of the glucose regime (Figures 6B and 6C). Furthermore, deletion of *Pparg1a* and *b* genes abolished the induction of the *Dmp1*, *Fgf23*, and *Sost* mRNAs upon glucose restriction. Altogether, these results proved that PGC-1 co-activators act as regulators of osteocyte gene expression.

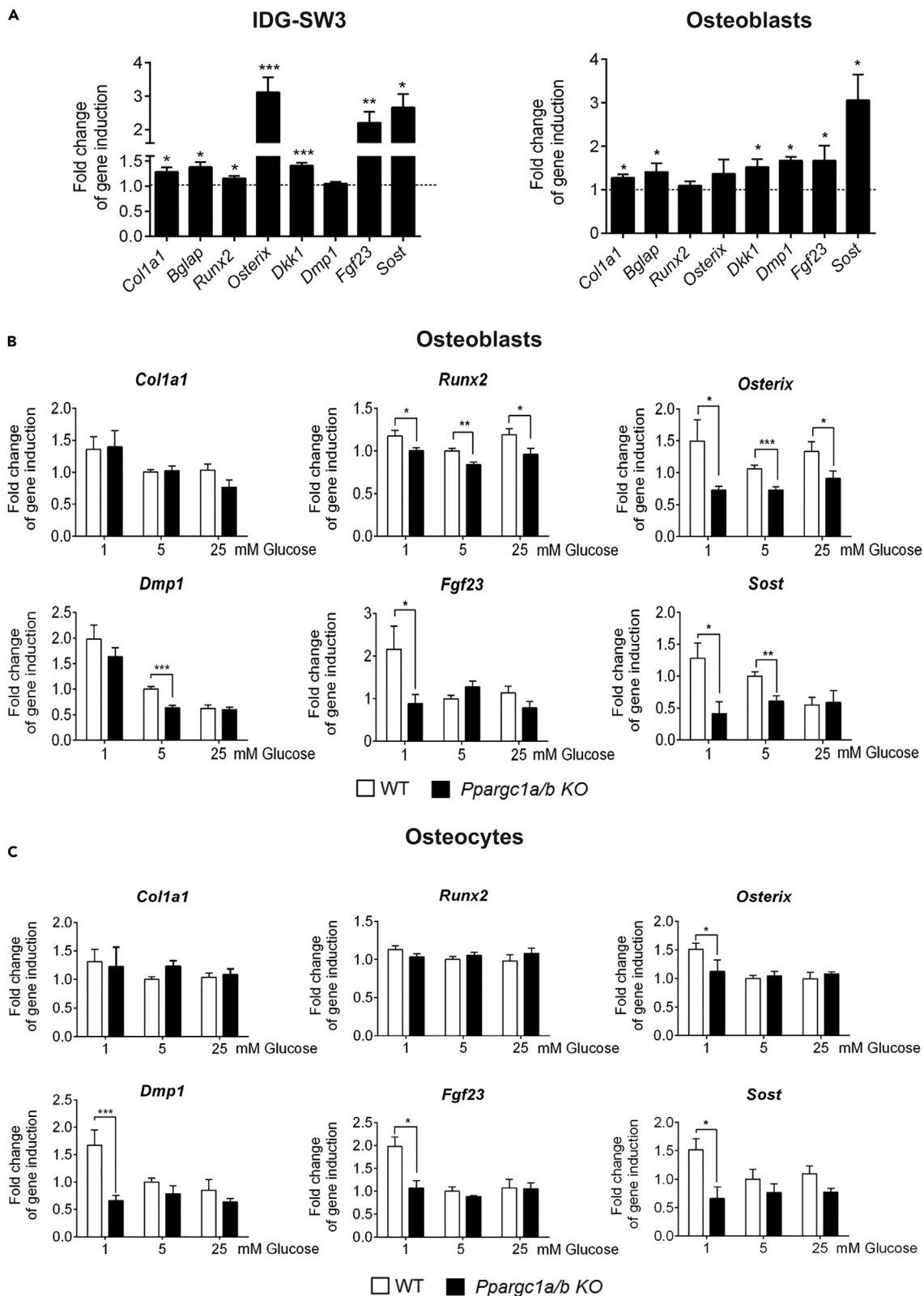


Figure 6. Role of PGC-1 in Osteocyte Differentiation

(A) mRNA expression levels of IDG-SW3 cells (left) and primary osteoblasts (right) infected with GFP or PGC-1 α expression vectors and differentiated in 5 mM glucose media for 5 days. mRNA expression levels were measured by qRT-PCR and normalized to *Tbp* expression. Results were plotted as expression relative to cells infected with GFP vector (mean \pm SEM of six to eight independent experiments).

(B and C) mRNA expression levels of osteocytic and osteoblastic genes in primary osteoblasts (B) and primary osteocytes (C) wild-type and knockout for PGC-1 α/β . Osteoblasts and osteocytes were isolated from calvarias obtained from *Ppargc1a/b*^{fl/fl} mice and infected with pMSCV-Puro or pMSCV-puro-Cre-ERT2 vectors. Infected cells were cultured for five days in 1, 5, or 25 mM glucose media. mRNA expression levels were measured by qRT-PCR and normalized to *Tbp*. Results are plotted as expression relative to control infection (mean \pm SEM of six independent experiments). **p* < 0.05, ***p* < 0.01, and ****p* < 0.001 using Student's *t* test. See also [Figures S5](#) and [S6](#).

Rearrangement of the cytoskeletal organization is a hallmark of osteocytes. In consequence, we examined the arrangement of actin cytoskeleton in IDG-SW3 cells cultured in different glucose concentrations as well as in osteoblasts and osteocytes either wild-type or deficient in *Ppargc1a/b*. We did not find significant differences in any of the conditions ([Figure S6](#)).

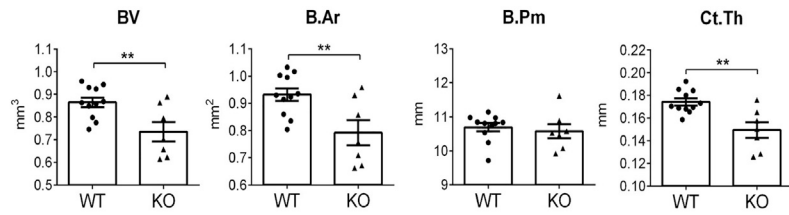
We further explored the role of *Ppargc1a/b* in bone formation and homeostasis in mice. Transgenic mice for Cre under the control of the 2.3-*Col1a1* promoter ([Dacquin et al., 2002](#)) allowed deletion of *Ppargc1a* and *b* in osteoblasts and osteocytes (hereafter *Ppargc1a* *ff/ff*; *Ppargc1b* *ff/ff*; *Col1a1*-Cre; knockout [KO]) ([Figures S7A](#) and [S7B](#)). *Ppargc1a/b* deletion did not affect either body weight or femur length. As expected, *Ppargc1a* and *Ppargc1b* mRNA levels in calvaria from KO mice were significantly reduced in both male and female mice ([Figures S7C](#) and [S7D](#)). We visualized bone formation in male and female mice in distal femurs by micro-computed tomography scanning and histological analysis. In 8 week-old mice, deletion of *Ppargc1a* and *Ppargc1b* led to a decrease in both trabecular and cortical bone architecture. KO male mice presented lower cortical bone volume (BV) associated with reduced cortical thickness, whereas bone perimeter around the midshaft was not affected ([Figure 7A](#)). In addition, distal femurs in males also presented less trabecular bone volume (BV/TV) resulting from a significantly lower trabecular number (Tb.N) and trabecular thickness (Tb.Th) ([Figure 7A](#)). Trabecular analysis of distal femurs in KO females also showed a significant reduction in BV/TV, Tb.N, and Tb.Th. However, reduction in cortical bone parameters were lower in magnitude and did not reach significant differences ([Figure 7B](#)). To clarify the underlying reason for the osteopenic phenotype of the KO mice, we analyzed the expression of osteoblast and osteocyte genes from calvaria. KO male and female mice displayed a reduced expression of osteocyte genes, including *Dmp1*, *Fgf23*, and *Sost*, and increased levels of osteoblastic genes such as *Bglap*, *Runx2*, or *Osx* ([Figure 7C](#)). Reduced osteocyte gene expression occurs without significant changes in either the density of osteocytes per bone area or the number of empty lacunae in cortical bone ([Figures S8](#) and [S9](#)). Mice deficient for *Ppargc1a/\beta* showed reduced *Rankl/Opg* ratio of expression in calvaria ([Figure S10](#)). Similar results were obtained in osteocytes deficient in *Ppargc1a/\beta*. These data suggest that although *Ppargc1a/\beta* affects the expression of *Rankl* and *Opg* in osteocytes, osteopenia in young *Ppargc1a/\beta*-deficient mice does not arise for increased osteoclastogenesis induced directly by an increased *Rankl/Opg* ratio. In conclusion, our data demonstrate the relevant role of PGC-1 in co-activation of the osteoblast and osteocyte transcriptional programs.

DISCUSSION

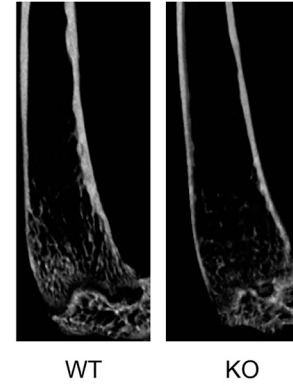
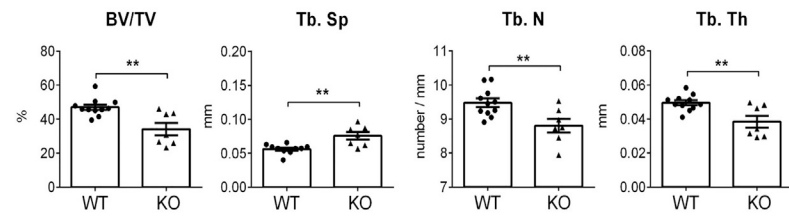
In this study, we identified that a reduced supply of glucose facilitates the expression of osteocytic genes in osteoblast/osteocyte precursors. These effects took place in parallel with an increased mtDNA. Glucose reduction triggers the activation of the AMPK/PGC-1 pathway whereas AMPK and SIRT1 activators were sufficient to increase osteocyte gene expression. Osteoblasts and osteocytes deficient in *Ppargc1a* and *b* were refractory for glucose restriction effects, whereas mice deficient in both genes were osteopenic. Our data strongly support modulation of the metabolic state as a strategy for the differentiation of bone cells.

In recent years, several studies have demonstrated that metabolism of osteoblast lineage cells is programmed to optimize energy production to fulfill functional demands throughout their life cycle ([Riddle and Clemens, 2017](#)). Early stage of osteoblast specification relies on glycolysis to generate ATP, initiate collagen synthesis, and stabilize RUNX2 expression ([Wei et al., 2015](#); [Guntur et al., 2018](#)). Accordingly, molecular signals that determine osteoblast specification, such as Wnt, PTH, or Hypoxia-inducible factor 1 (HIF-1), also promote aerobic glycolysis in osteoblast progenitors ([Esen et al., 2013, 2015](#); [Regan et al., 2014](#); [Dirckx et al., 2018](#)). However, in the adult human skeleton, about 42 billion osteocytes are entrapped in their own mineralized matrix while being connected by cytoplasmic projections with a total length of 175,000 km. These resident osteocytes leave space for just 24 mL extracellular fluid ([Buenzli and Sims,](#)

A Cortical analysis male

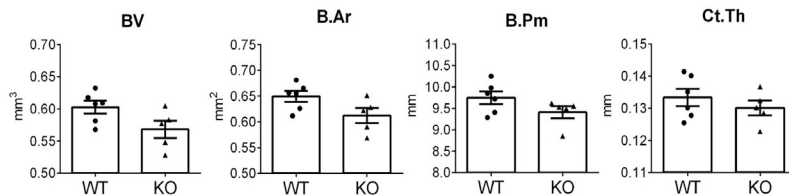


Trabecular analysis male

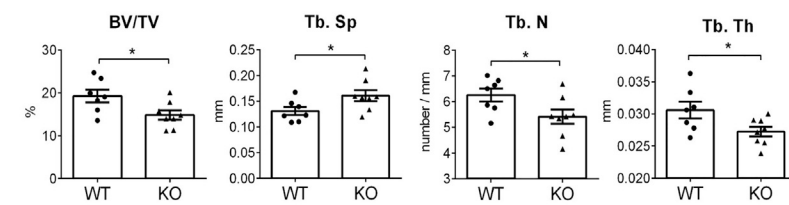


B

Cortical analysis female



Trabecular analysis female



C

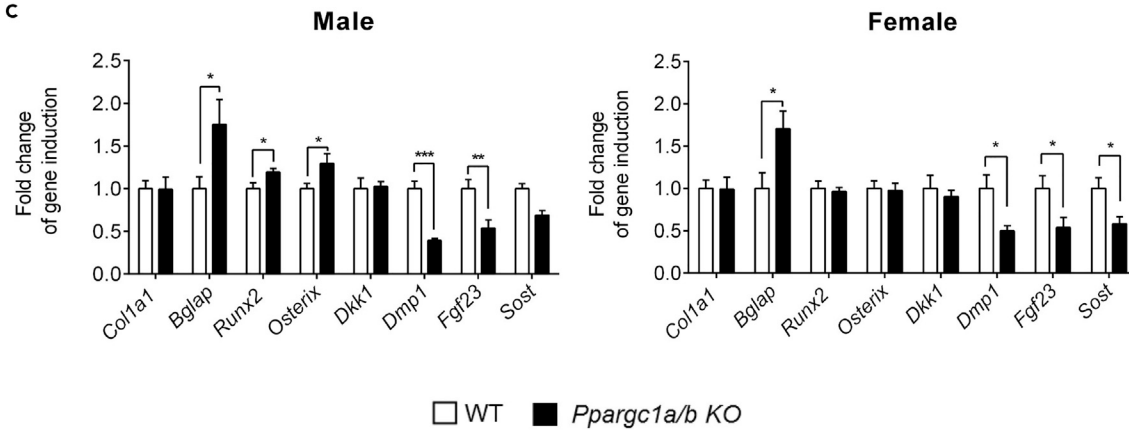


Figure 7. Bone phenotype of *Ppargc1 α / β* Conditional Knockout Mice

(A and B) Micro-computed tomographic analysis and representative images of femurs obtained from male (A) and female (B) *Ppargc1a/b^{fl/fl};Col1a1-Cre* and control (*Ppargc1a/b^{fl/fl}*) mice. Results were plotted as mean \pm SEM of 8–11 independent animals.

(C) mRNA expression levels of osteocytic and osteoblastic genes in calvaria obtained from PGC1 α / β conditional knockout (*Ppargc1a/b^{fl/fl};Col1a1-Cre*) and control mice.

Results are plotted as mean \pm SEM of eight independent animals. mRNA expression levels were measured by qRT-PCR and normalized to *Tbp* expression. * $p < 0.05$, ** $p < 0.01$, and *** $p < 0.001$ using Student's *t* test. B.Ar, bone area; B.Pm, bone perimeter; Ct.Th, cortical thickness; Tb.N, trabecular number; Tb.Sp, trabecular spacing; Tb.Th, trabecular thickness; See also [Figures S7–S10](#).

2015). Therefore osteocyte transition and network formation processes are likely to demand high levels of energy in a nutrient-restricted environment. Our data demonstrate that a shift of the metabolic machinery toward a higher mitochondrial function occurs during the transition of osteoblasts into osteocytes under conditions of glucose restriction. Mitochondria optimize their morphology to cope with reduced caloric supply. Correspondingly, osteocytes *in vivo* have been shown to have numerous mitochondria and to maintain normal oxidative status through mitochondrial pathways (Frikha-Benayed et al., 2016). Osteocytes contribute little to glucose consumption in murine bones compared with osteoprogenitors and osteoblasts (Dirckx et al., 2018). Furthermore, it has been recently shown that bone accumulates a significant fraction of postprandial fatty acids and that suppression of fatty acid oxidation in mature osteoblasts and osteocytes impairs bone accrual (Kim et al., 2017). This link between metabolic reprogramming and cellular specification was already well established for other models of cell specification. For example, higher mitochondrial biogenesis and function is related to the final stage of neurogenesis, astrocytogenesis, hepatic differentiation, and erythropoiesis (Agostini et al., 2016; Xing et al., 2017). On the other hand, we also found that hyperglycemic conditions modify mitochondrial organization and impair osteoblast and osteocyte gene expression. Hyperglycemic microenvironments have been associated with a reduction in osteocyte number and function (Rinker et al., 2014), whereas bone turnover and remodeling have been found to be compromised in patients with diabetes (Kalaitzoglou et al., 2016).

Consistent with its role as regulator of energy homeostasis, we found an inverse correlation between AMPK activity and glucose supply. These results are in agreement with recent evidence showing that AMPK became activated by phosphorylation at Thr172, by sensing not only low cellular energy but also low glucose supply (Lin and Hardie, 2017; Zhang et al., 2017). Activation of AMPK with AMP analogs in normoglycemia was sufficient to induce osteocyte gene expression in IDG-SW3 cells and organotypic bone cultures. Indeed, studies using whole-body and osteoblast-specific genetic abrogation of AMPK activity showed lower cortical and trabecular bone density and enhanced bone turnover (Jeyabalan et al., 2012; Kanazawa et al., 2018). It has been shown that AMPK activation decreases *Rankl* and increases *Sost* expression in osteocytes to delicately coordinate bone turnover (Jeyabalan et al., 2012). Our data also demonstrated that activation of SIRT1 by SRT2104 led to increased osteocyte gene expression program in IDG-SW3 cells and organotypic bone cultures. An increase in bone mineral density was observed in mice fed on a diet supplemented with SRT2104 and shown to be *Sirt1* dependent (Mercken et al., 2014). The beneficial role of SIRT1 in bone formation and remodeling were further confirmed in whole-body and osteoblast-specific *Sirt1*-deficient mice, which displayed low bone mass phenotype (Cohen-Kfir et al., 2011). Moreover, SIRT1 activation gave protection against osteoporosis in both mice and humans (Ornstrup et al., 2014).

We identified a key role of PGC-1, downstream of AMPK, in the coordination of mitochondrial biogenesis and osteocyte specification in cultured cells and murine models. Lessons from other tissues indicate that PGC-1 α and PGC-1 β have a redundant transcriptional role because noticeable phenotypes were only observed when the expression of both co-activators was abolished (Villena, 2015). Our data show that PGC-1 α / β also have a fundamental role in osteoblast and osteocyte function and bone homeostasis. *Ppargc1a* was expressed in osteoblasts and osteocytes in preference to *Ppargc1b*. Moreover, osteoblast-to-osteocyte transition further increased this tendency. Interestingly, PGC-1 β is the main member of the PGC-1 family expressed in osteoclasts and is specifically required for osteoclast function (Wei et al., 2010; Zhang et al., 2018). The functional and therapeutic implications of such cell-type-specific co-activator preferences await further research. For instance, the action of different activators of PGC-1 α in osteoblasts prevents bone loss in type 2 diabetes models without improving diabetes in a PGC-1 α -dependent manner (Khan et al., 2015).

PGC-1 co-activates specific transcription factors, including NRF1, NRF2, PPARs, ER α , ERR α , and MEF2C (Villena, 2015). Co-activation of ER α could account for the milder osteopenic phenotypes that we

obtained in female mice because osteocyte-specific deletion of ER α has been shown to affect bone mineral density only in male mice (Lee et al., 2003; Windahl et al., 2013). Co-activation of diverse transcription factors by PGC-1 has been shown to deeply affect developmental transcriptional programs such as erythropoiesis, chondrogenesis, and differentiation of hepatocytes, cardiomyocytes, and brown adipocytes (Wanet et al., 2017; Cui et al., 2014). Our data show that this would also be the case for osteocytogenesis. For instance, PGC-1 α binds to the *Fgf23* or *Sost* gene promoters, whereas overexpression and loss-of-function experiments produce effects on the expression of *Dmp1*, *Dkk1*, *Fgf23*, *Sost*, or *Osx* genes. We found numerous conserved binding sites for known transcription factors in the promoter and enhancer regions of *Fgf23*, *Sost*, *Dmp1*, or *Osx* genes that could mediate their regulation by PGC-1 α . For instance, it is known that ER α , NRF2, PPARs, ERR α , and MEF2C positively regulate osteocyte gene expression (Kramer et al., 2012; Stechschulte et al., 2016). Therefore PGC-1s are able to co-activate a number of transcription factors with universal and osteocyte-specific functions. Altogether, we have uncovered a central role of PGC-1-mediated transcriptional program required for osteoblast and osteocyte function.

Limitations of Study

Our results demonstrate that glucose restriction promotes osteocytic gene expression through PGC-1-mediated transcriptional co-activation. However, at present, the transcription factors directly involved in this co-activation in specific gene promoters are still unknown and require further investigation. In addition, *Ppargc1a/b* is deleted in both osteoblasts and osteocytes in our mouse model. Therefore we are unable to distinguish the relative contribution in bone homeostasis *in vivo* of PGC-1 expressed in osteoblasts and osteocytes.

METHODS

All methods can be found in the accompanying [Transparent Methods supplemental file](#).

SUPPLEMENTAL INFORMATION

Supplemental Information can be found online at <https://doi.org/10.1016/j.isci.2019.04.015>.

ACKNOWLEDGMENTS

We thank Dr. L. Bonewald for IDG-SW3 cells. We also thank E. Adanero, E. Castaño, B. Barroso, and L. Gómez-Segura for technical assistance. Cristina Sánchez de Diego and Carolina Pimenta Lopes are the recipients of F.P.U. fellowships from the Spanish Ministry of Education. N.A. and Pau Gama are recipients of a fellowship from the University of Barcelona. This research was supported by grants from the M.E.C. (BFU2014-56313-P and BFU2017-8 2421-P) and Fondo Europeo de Desarrollo Regional (FEDER).

AUTHOR CONTRIBUTIONS

Conceived and designed the experiments: C.S.-d.-D., N.A., C.P.-L., B.T., P.M.G.-R., J.L.R., and F.V. Performed the experiments: C.S.-d.-D., N.A., C.P.-L., J.A. Valer, B.T., P.G.-P., P.M.G.-R., J.L.R., and F.V. Analyzed the data: C.S.-d.-D., N.A., C.P.-L., P.M.G.-R., J.L.R., and F.V. Contributed materials J.A. Villena. Wrote the paper: C.S.-d.-D., F.V.

DECLARATION OF INTERESTS

The authors declare no conflicts of interest.

Received: August 22, 2018

Revised: January 16, 2019

Accepted: April 8, 2019

Published: May 31, 2019

REFERENCES

Agostini, M., Romeo, F., Inoue, S., Niklison-Chirou, M.V., Elia, A.J., Dinsdale, D., Morone, N., Knight, R.A., Mak, T.W., Melino, G., et al. (2016).

Metabolic reprogramming during neuronal differentiation. *Cell Death Differ.* 23, 1502–1514.

Bonewald, L.F. (2011). The amazing osteocyte. *J. Bone Miner. Res.* 26, 229–238.

- Brand, M.D., and Nicholls, D.G. (2011). Assessing mitochondrial dysfunction in cells. *Biochem. J.* 437, 575.
- Buenzli, P.R., and Sims, N.A. (2015). Quantifying the osteocyte network in the human skeleton. *Bone* 75, 144–150.
- Carroll, B., and Dunlop, E.A. (2017). The lysosome: a crucial hub for AMPK and mTORC1 signalling. *Biochem. J.* 474, 1453–1466.
- Cassidy-Stone, A., Chipuk, J.E., Ingerman, E., Song, C., Yoo, C., Kuwana, T., Kurth, M.J., Shaw, J.T., Hinshaw, J.E., Green, D.R., et al. (2008). Chemical inhibition of the mitochondrial division dynamin reveals its role in bax/bak-dependent mitochondrial outer membrane permeabilization. *Dev. Cell* 14, 193–204.
- Cohen-Kfir, E., Artsi, H., Levin, A., Abramowitz, E., Bajayo, A., Gurt, I., Zhong, L., D'Urso, A., Toiber, D., Mostoslavsky, R., et al. (2011). Sirt1 is a regulator of bone mass and a repressor of sost encoding for sclerostin, a bone formation inhibitor. *Endocrinology* 152, 4514–4524.
- Cui, S., Tanabe, O., Lim, K.C., Xu, H.E., Zhou, X.E., Lin, J.D., Shi, L., Schmidt, L., Campbell, A., Shimizu, R., et al. (2014). PGC-1 coactivator activity is required for murine erythropoiesis. *Mol. Cell. Biol.* 34, 1956–1965.
- Dacquin, R., Starbuck, M., Schinke, T., and Karsenty, G. (2002). Mouse $\alpha 1(I)$ -collagen promoter is the best known promoter to drive efficient Cre recombinase expression in osteoblast. *Dev. Dyn.* 224, 245–251.
- Dallas, S.L., Prideaux, M., and Bonewald, L.F. (2013). The osteocyte: an endocrine cell... and more. *Endocr. Rev.* 34, 658–690.
- Dirckx, N., Tower, R.J., Mercken, E.M., Vangoitsenhoven, R., Moreau-Triby, C., Breugelmanns, T., Nefyodova, E., Chadoen, R., Mathieu, C., Van der Schueren, B., et al. (2018). Vhl deletion in osteoblasts boosts cellular glycolysis and improves global glucose metabolism. *J. Clin. Invest.* 128, 1087–1105.
- Esen, E., Chen, J., Karner, C.M., Okunade, A.L., Patterson, B.W., and Long, F. (2013). WNT-LRP5 signaling induces warburg effect through mTORC2 activation during osteoblast differentiation. *Cell Metab.* 17, 745–755.
- Esen, E., Lee, S.Y., Wice, B.M., and Long, F. (2015). PTH promotes bone anabolism by stimulating aerobic glycolysis via IGF signaling. *J. Bone Miner. Res.* 30, 1959–1968.
- Fan, M., Rhee, J., St-Pierre, J., Handschin, C., Puigserver, P., Lin, J., Jäeger, S., Erdjument-Bromage, H., Tempst, P., Spiegelman, B.M., et al. (2004). Suppression of mitochondrial respiration through recruitment of p160 myb binding protein to PGC-1 α : modulation by p38 MAPK. *Genes Dev.* 18, 278–289.
- Frikha-Benayed, D., Basta-Pljakic, J., Majeska, R.J., and Schaffler, M.B. (2016). Regional differences in oxidative metabolism and mitochondrial activity among cortical bone osteocytes. *Bone* 90, 15–22.
- Galloway, C.A., Lee, H., and Yoon, Y. (2012). Mitochondrial morphology-emerging role in bioenergetics. *Free Radic. Biol. Med.* 53, 2218–2228.
- Gerhart-Hines, Z., Rodgers, J.T., Bare, O., Lerin, C., Kim, S.H., Mostoslavsky, R., Alt, F.W., Wu, Z., and Puigserver, P. (2007). Metabolic control of muscle mitochondrial function and fatty acid oxidation through SIRT1/PGC-1 α . *EMBO J.* 26, 1913–1923.
- Gomes, L.C., Benedetto, G., and Di Scorrano, L. (2011). During autophagy mitochondria elongate, are spared from degradation and sustain cell viability. *Nat. Cell Biol.* 13, 589–598.
- Guntur, A.R., Gerencser, A.A., Le, P.T., DeMambro, V.E., Bornstein, S.A., Mookerjee, S.A., Maridas, D.E., Clemmons, D.E., Brand, M.D., Rosen, C.J., et al. (2018). Osteoblast like MC3T3-E1 cells prefer glycolysis for ATP production but adipocyte like 3T3-L1 cells prefer oxidative phosphorylation. *J. Bone Miner. Res.* 33, 1052–1065.
- Guo, D., Keightley, A., Guthrie, J., Veno, P.A., Harris, S.E., and Bonewald, L.F. (2010). Identification of osteocyte-selective proteins. *Proteomics* 10, 3688–3698.
- Hardie, D.G. (2018). Keeping the home fires burning: AMP-activated protein kinase. *J. R. Soc. Interface* 15, <https://doi.org/10.1098/rsif.2017.0774>.
- Hirao, M., Hashimoto, J., Yamasaki, N., Ando, W., Tsuboi, H., Myoui, A., and Yoshikawa, H. (2007). Oxygen tension is an important mediator of the transformation of osteoblasts to osteocytes. *J. Bone Miner. Metab.* 25, 266–276.
- Jager, S., Handschin, C., St-Pierre, J., and Spiegelman, B.M. (2007). AMP-activated protein kinase (AMPK) action in skeletal muscle via direct phosphorylation of PGC-1. *Proc. Natl. Acad. Sci. U S A* 104, 12017–12022.
- Jeyabalan, J., Shah, M., Violette, B., and Chenu, C. (2012). AMP-activated protein kinase pathway and bone metabolism. *J. Endocrinol.* 212, 277–290.
- Kalaitzoglou, E., Popescu, I., Bunn, R.C., Fowlkes, J.L., and Thrallkill, K.M. (2016). Effects of type 1 diabetes on osteoblasts, osteocytes, and osteoclasts. *Curr. Osteoporos. Rep.* 14, 310–319.
- Kanazawa, I., Takeno, A., Tanaka, K.I., Notsu, M., and Sugimoto, T. (2018). Osteoblast AMP-activated protein kinase regulates postnatal skeletal development in male mice. *Endocrinology* 159, 597–608.
- Karsenty, G., and Olson, E.N. (2016). Bone and muscle endocrine functions: unexpected paradigms of inter-organ communication. *Cell* 164, 1248–1256.
- Khan, M.P., Singh, A.K., Joharapurkar, A.A., Yadav, M., Shree, S., Kumar, H., Gurjar, A., Mishra, J.S., Tiwari, M.C., Nagar, G.K., et al. (2015). Pathophysiological mechanism of bone loss in type 2 diabetes involves inverse regulation of osteoblast function by pgc-1 α and skeletal muscle atrogens: adipor1 as a potential target for reversing diabetes-induced osteopenia. *Diabetes* 64, 2609–2623.
- Kim, S.P., Li, Z., Zoch, M.L., Frey, J.L., Bowman, C.E., Kushwaha, P., Ryan, K.A., Goh, B.C., Scafidi, S., Pickett, J.E., et al. (2017). Fatty acid oxidation by the osteoblast is required for normal bone acquisition in a sex- and diet-dependent manner. *JCI insight* 2, <https://doi.org/10.1172/jci.insight.92704>.
- Kramer, I., Baertschi, S., Halleux, C., Keller, H., and Kneissel, M. (2012). Mef2c deletion in osteocytes results in increased bone mass. *J. Bone Miner. Res.* 27, 360–373.
- Lai, X., Price, C., Modla, S., Thompson, W.R., Caplan, J., Kirn-Safran, C.B., and Wang, L. (2015). The dependences of osteocyte network on bone compartment, age, and disease. *Bone Res.* 3, <https://doi.org/10.1038/boneres.2015.9>.
- Lee, K., Jessop, H., Suswillo, R., Zaman, G., and Lanyon, L. (2003). Endocrinology: bone adaptation requires oestrogen receptor- α . *Nature* 424, 389.
- Lin, S.C., and Hardie, D.G. (2017). AMPK: sensing glucose as well as cellular energy status. *Cell Metab.* 27, 299–313.
- Mercken, E.M., Mitchell, S.J., Martin-Montalvo, A., Minor, R.K., Almeida, M., Gomes, A.P., Scheibye-Knudsen, M., Palacios, H.H., Licata, J.J., Zhang, Y., et al. (2014). SRT2104 extends survival of male mice on a standard diet and preserves bone and muscle mass. *Aging Cell* 13, 787–796.
- Napoli, N., Chandran, M., Pierroz, D.D., Abrahamsen, B., Schwartz, A.V., and Ferrari, S.L.; IOF Bone and Diabetes Working Group (2017). Mechanisms of diabetes mellitus-induced bone fragility. *Nat. Rev. Endocrinol.* 13, 208–219.
- Ornstrup, M.J., Harsløf, T., Kjær, T.N., Langdahl, B.L., and Pedersen, S.B. (2014). Resveratrol increases bone mineral density and bone alkaline phosphatase in obese men: a randomized placebo-controlled trial. *J. Clin. Endocrinol. Metab.* 99, 4720–4729.
- Petrov, N., and Pollack, S.R. (2003). Comparative analysis of diffusive and stress induced nutrient transport efficiency in the lacunar-canalicular system of osteons. *Biorheology* 40, 347–353.
- Piekarski, K., and Munro, M. (1977). Transport mechanism operating between blood supply and osteocytes in long bones. *Nature* 269, 80–82.
- Quinn, J.M.W., Tam, S., Sims, N.A., Saleh, H., McGregor, N.E., Poulton, I.J., Scott, J.W., Gillespie, M.T., Kemp, B.E., van Denderen, B.J.W., et al. (2010). Germline deletion of AMP-activated protein kinase; ? subunits reduces bone mass without altering osteoclast differentiation or function. *FASEB J.* 24, 275–285.
- Regan, J.N., Lim, J., Shi, Y., Joeng, K.S., Arbeit, J.M., Shohet, R.V., and Long, F. (2014). Up-regulation of glycolytic metabolism is required for HIF1-driven bone formation. *Proc. Natl. Acad. Sci. U S A* 111, 8673–8678.
- Riddle, R.C., and Clemens, T.L. (2017). Bone cell bioenergetics and skeletal energy homeostasis. *Physiol. Rev.* 97, 667–698.
- Rinker, T.E., Hammoudi, T.M., Kemp, M.L., Lu, H., and Temenoff, J.S. (2014). Interactions between mesenchymal stem cells, adipocytes, and osteoblasts in a 3D tri-culture model of hyperglycemic conditions in the bone marrow microenvironment. *Integr. Biol.* 6, 324–337.

Sato, M., Asada, N., Kawano, Y., Wakahashi, K., Minagawa, K., Kawano, H., Sada, A., Ikeda, K., Matsui, T., and Katayama, Y. (2013). Osteocytes regulate primary lymphoid organs and fat metabolism. *Cell Metab.* *18*, 749–758.

Stechschulte, L.A., Czernik, P.J., Rotter, Z.C., Tausif, F.N., Corzo, C.A., Marciano, D.P., Asteian, A., Zheng, J., Bruning, J.B., Kamenecka, T.M., et al. (2016). PPAR γ post-translational modifications regulate bone formation and bone resorption. *EBioMedicine* *10*, 174–184.

Villena, J.A. (2015). New insights into PGC-1 coactivators: redefining their role in the regulation of mitochondrial function and beyond. *FEBS J.* *282*, 647–672.

Wanet, A., Caruso, M., Domelevo Entfellner, J.B., Najjar, M., Fattaccioli, A., Demazy, C., Evraerts, J., El-Kehdy, H., Pourcher, G., Sokal, E., et al. (2017). The transcription factor 7-like 2–peroxisome proliferator-activated receptor gamma coactivator-1 alpha axis connects mitochondrial biogenesis and metabolic shift with stem cell commitment to hepatic differentiation. *Stem Cells* *35*, 2184–2197.

Wang, L. (2018). Solute transport in the bone lacunar-canalicular system (LCS). *Curr. Osteoporos. Rep.* *16*, 32–41.

Wei, J., Shimazu, J., Makinistoglu, M.P., Maurizi, A., Kajimura, D., Zong, H., Takarada, T., Lezaki, T., Pessin, J.E., Hinoi, E., et al. (2015). Glucose Uptake and runx2 synergize to orchestrate osteoblast differentiation and bone formation. *Cell* *161*, 1576–1591.

Wei, W., Wang, X., Yang, M., Smith, L.C., Dechow, P.C., Sonoda, J., Evans, R.M., and Wan, Y. (2010). PGC1beta mediates PPARgamma activation of osteoclastogenesis and rosiglitazone-induced bone loss. *Cell Metab.* *11*, 503–516.

Windahl, S.H., Börjesson, A.E., Farman, H.H., Engdahl, C., Movérare-Skrtic, S., Sjögren, K., Lagerquist, M.K., Kindblom, J.M., Koskela, A., Tuukkanen, J., et al. (2013). Estrogen receptor- in osteocytes is important for trabecular bone formation in male mice. *Proc. Natl. Acad. Sci. U S A* *110*, 2294–2299.

Woo, S.M., Rosser, J., Dusevich, V., Kalajzic, I., and Bonewald, L.F. (2011). Cell line IDG-SW3 replicates osteoblast-to-late-osteocyte differentiation in vitro and accelerates bone

formation in vivo. *J. Bone Miner. Res.* *26*, 2634–2646.

Xing, F., Luan, Y., Cai, J., Wu, S., Mai, J., Gu, J., Zhang, H., Li, K., Lin, Y., Xiao, X., et al. (2017). The anti-warburg effect elicited by the camp-pgc1 α pathway drives differentiation of glioblastoma cells into astrocytes. *Cell Rep.* *18*, 468–481.

Yu, T., Robotham, J.L., and Yoon, Y. (2006). Increased production of reactive oxygen species in hyperglycemic conditions requires dynamic change of mitochondrial morphology. *Proc. Natl. Acad. Sci. U S A* *103*, 2653–2658.

Zhang, C.S., Hawley, S.A., Zong, Y., Li, M., Wang, Z., Gray, A., Ma, T., Cui, J., Feng, J.W., Zhu, M., et al. (2017). Fructose-1,6-bisphosphate and aldolase mediate glucose sensing by AMPK. *Nature* *548*, 112–116.

Zhang, Y., Rohatgi, N., Veis, D.J., Schilling, J., Teitelbaum, S.L., and Zou, W. (2018). PGC1beta organizes the osteoclast cytoskeleton by mitochondrial biogenesis and activation. *J. Bone Miner. Res.* *33*, 1114–1125.

ISCI, Volume 15

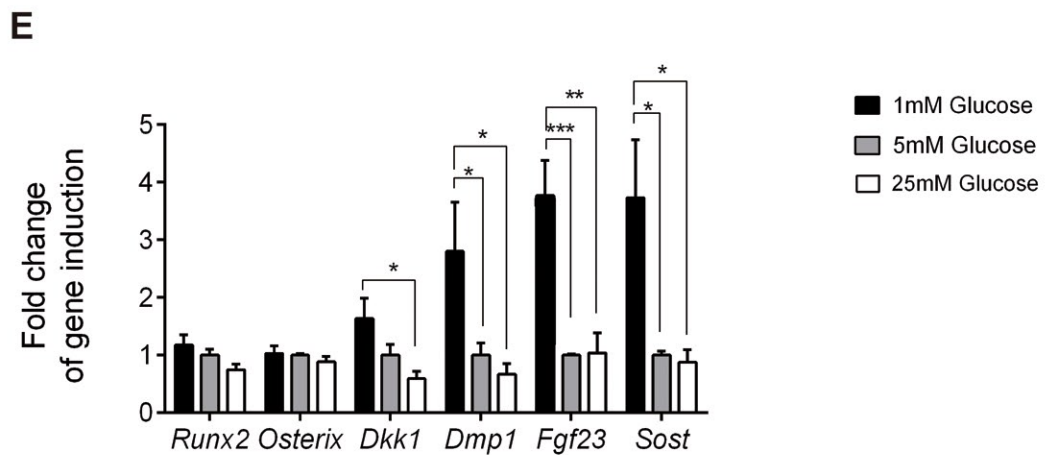
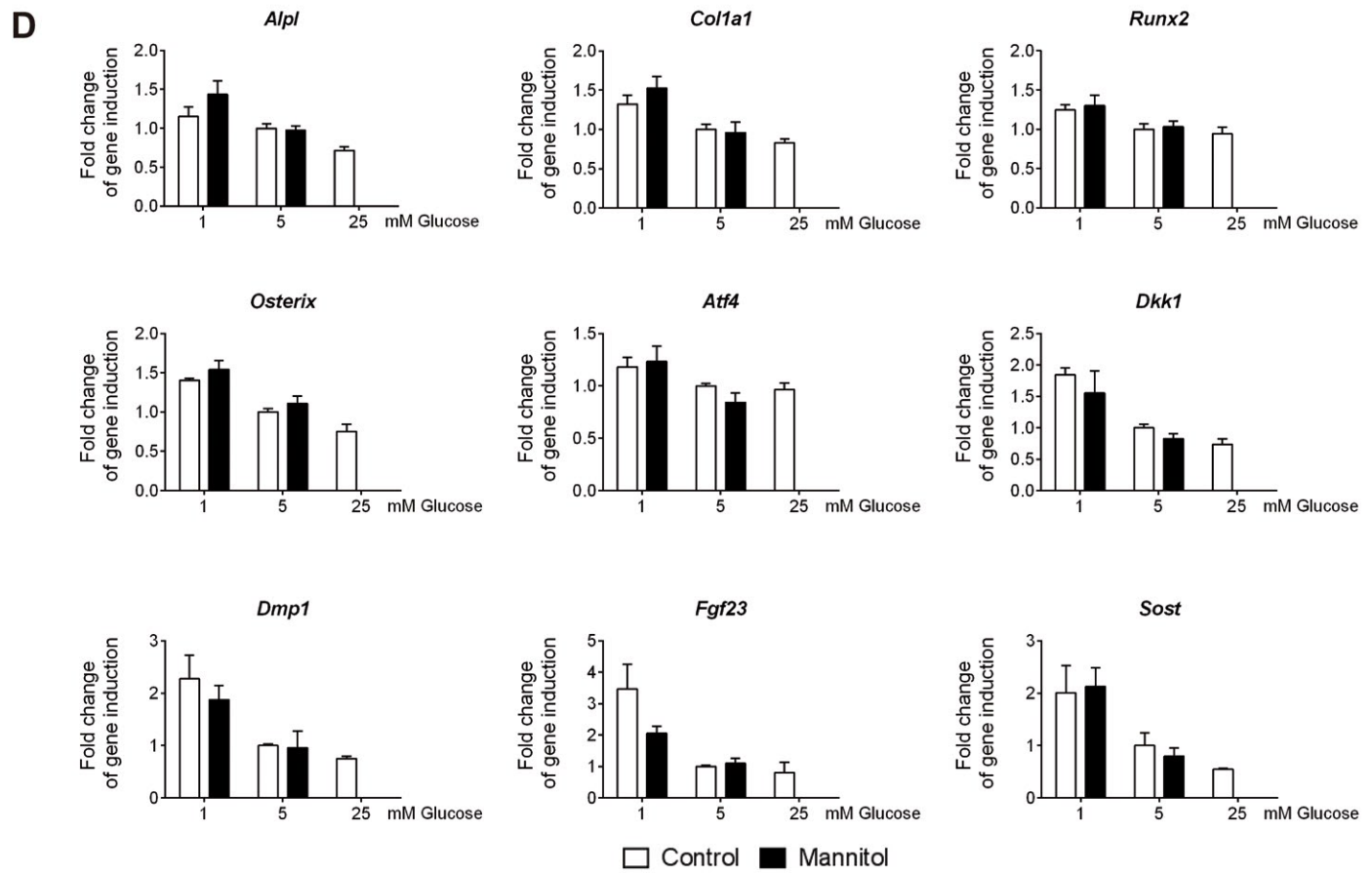
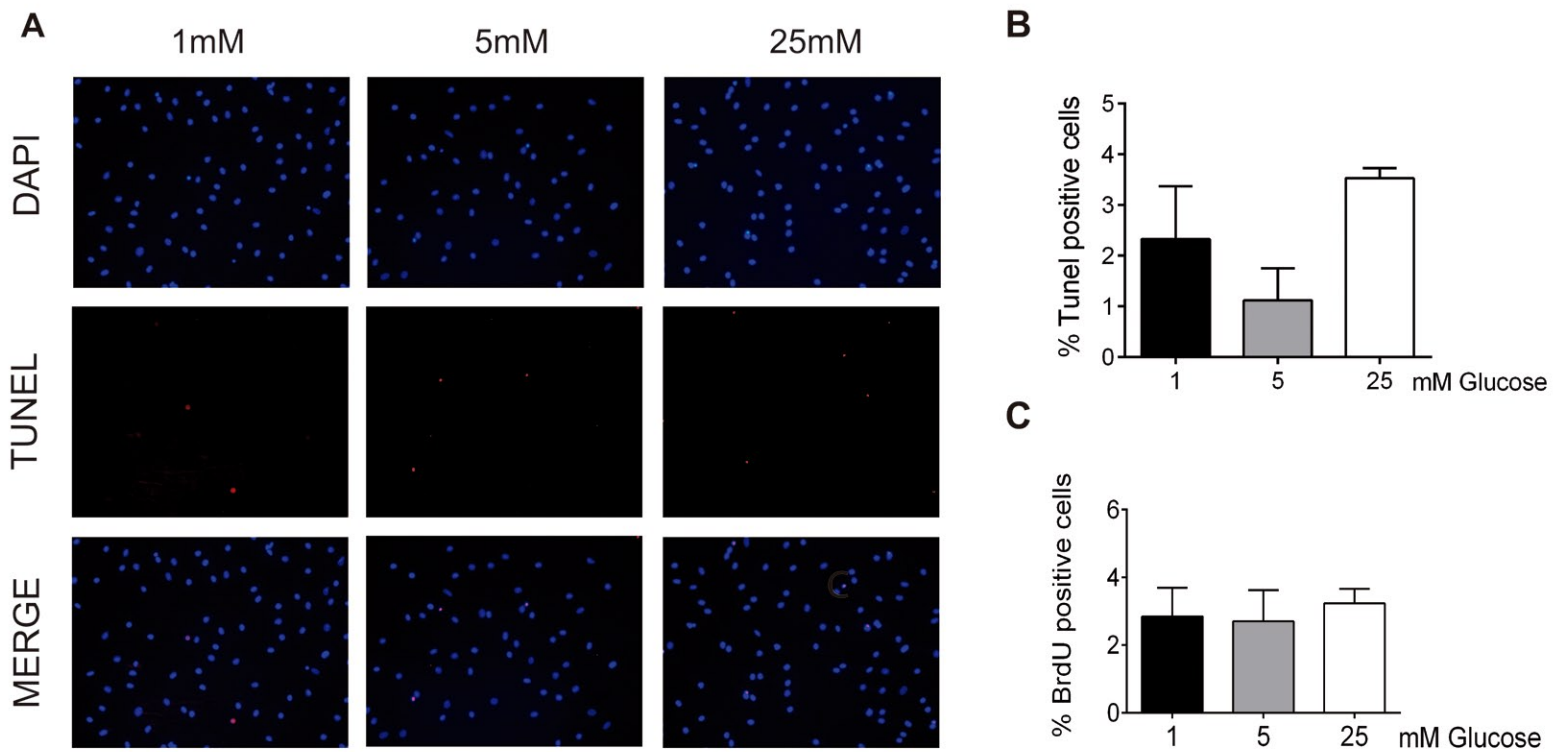
Supplemental Information

Glucose Restriction Promotes Osteocyte

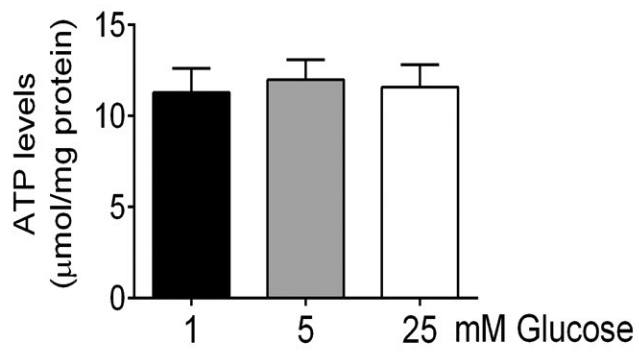
Specification by Activating

a PGC-1 α -Dependent Transcriptional Program

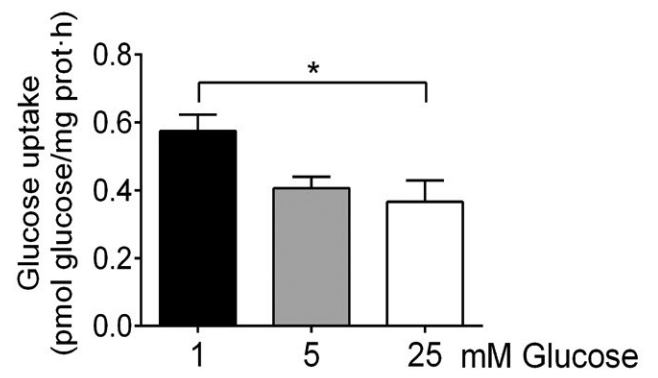
Cristina Sánchez-de-Diego, Natalia Artigas, Carolina Pimenta-Lopes, José Antonio Valer, Benjamin Torrejon, Pau Gama-Pérez, Josep A. Villena, Pablo M. Garcia-Roves, José Luis Rosa, and Francesc Ventura



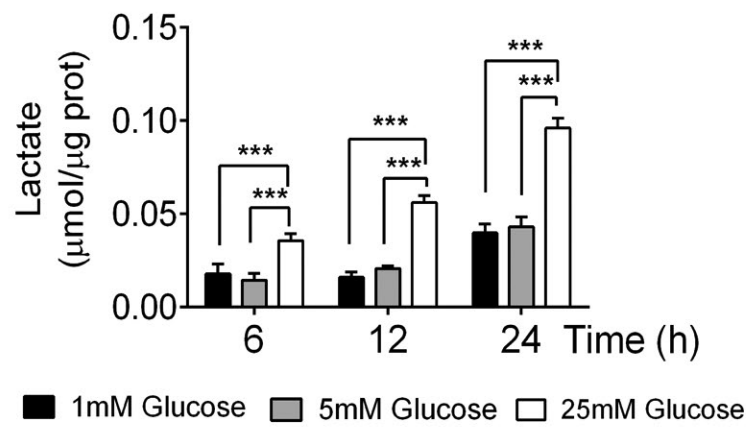
A



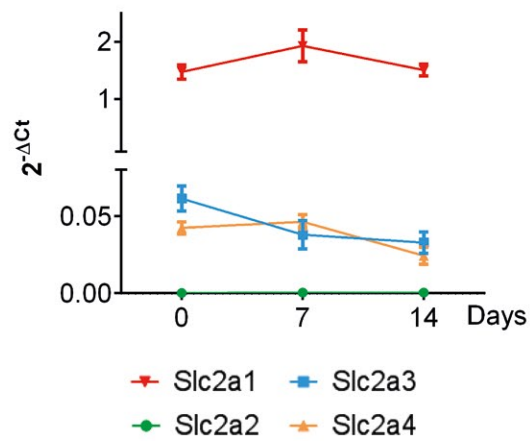
B



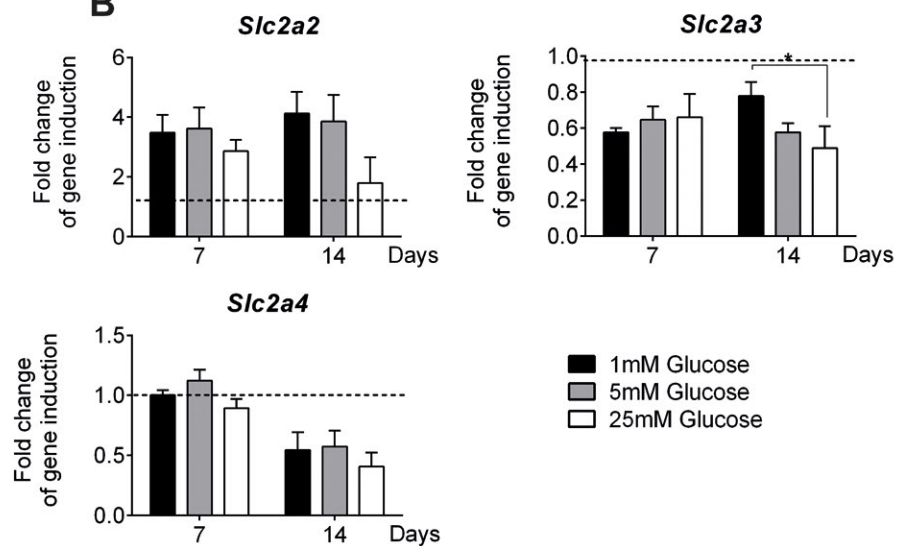
C



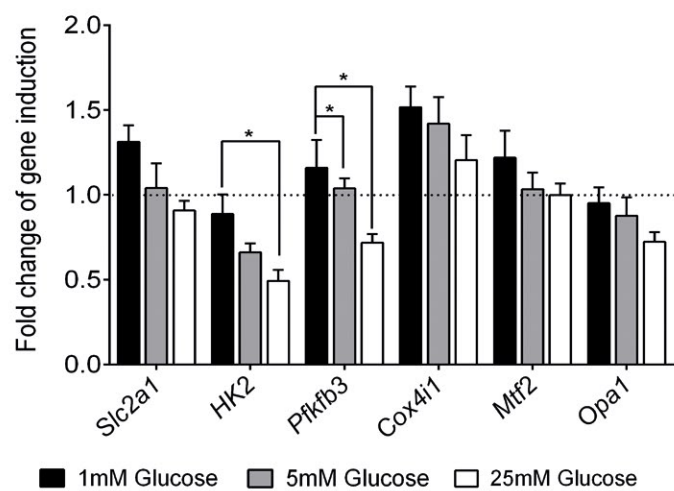
A



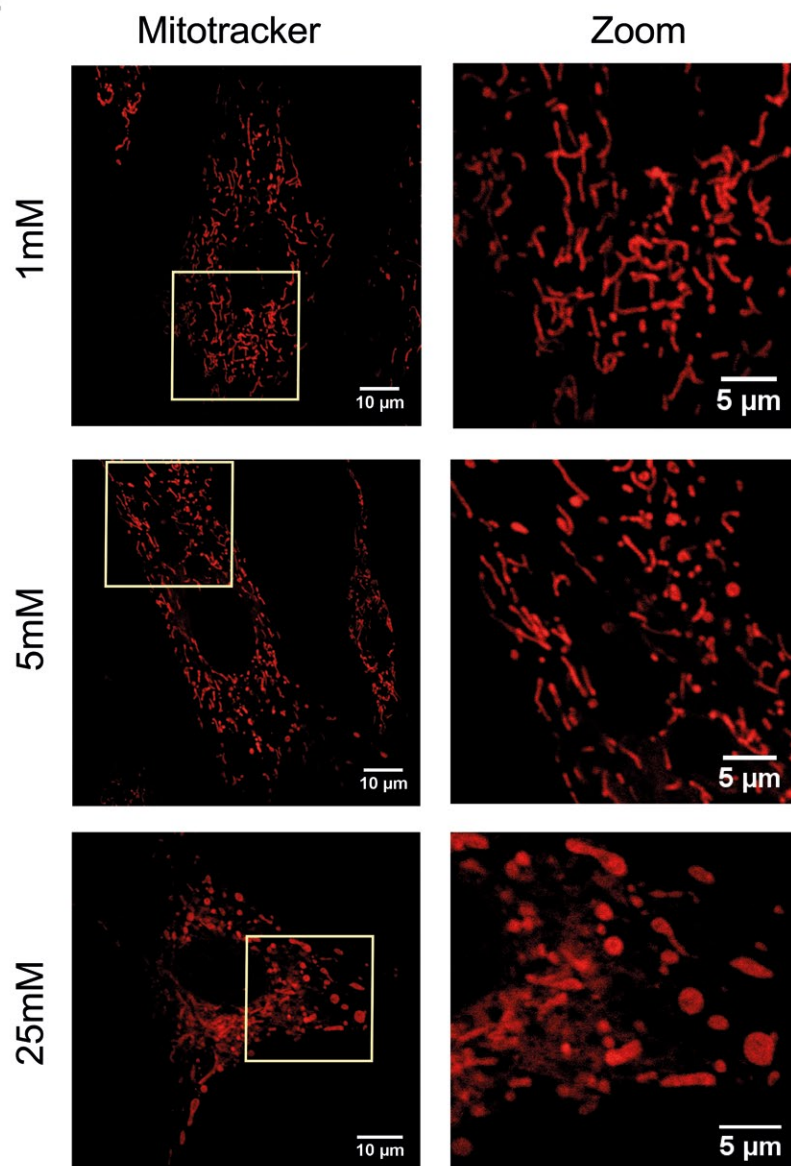
B



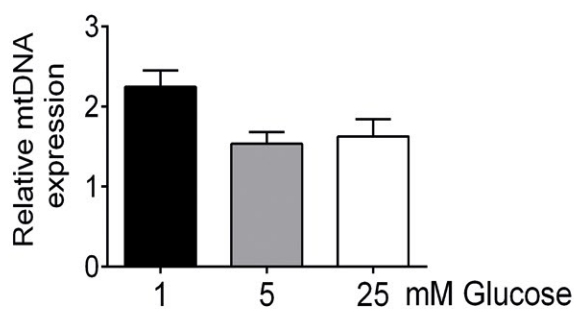
C



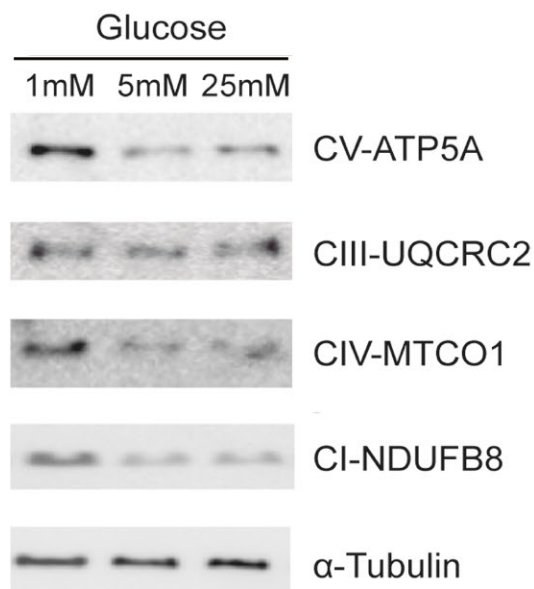
F



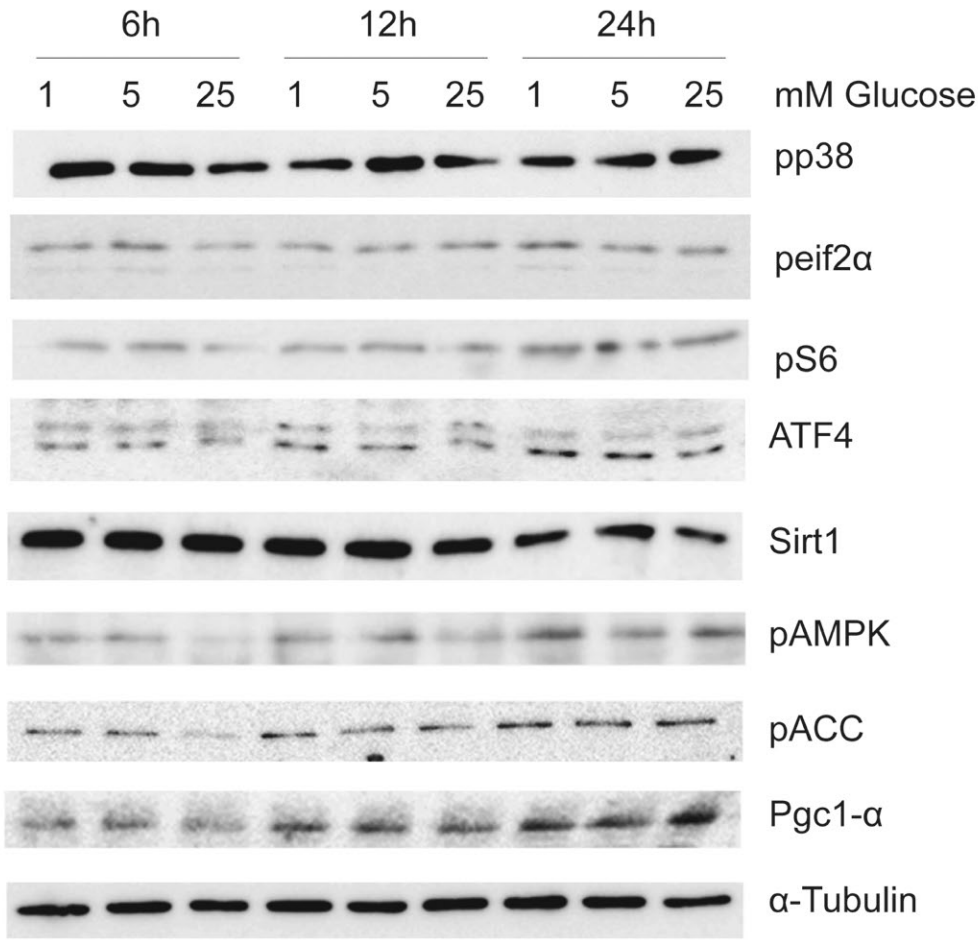
D



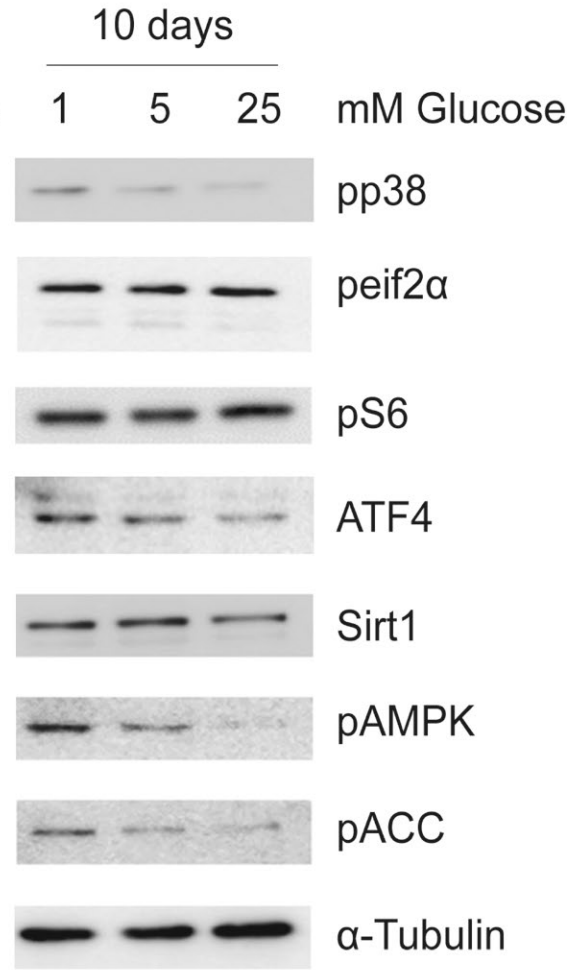
E



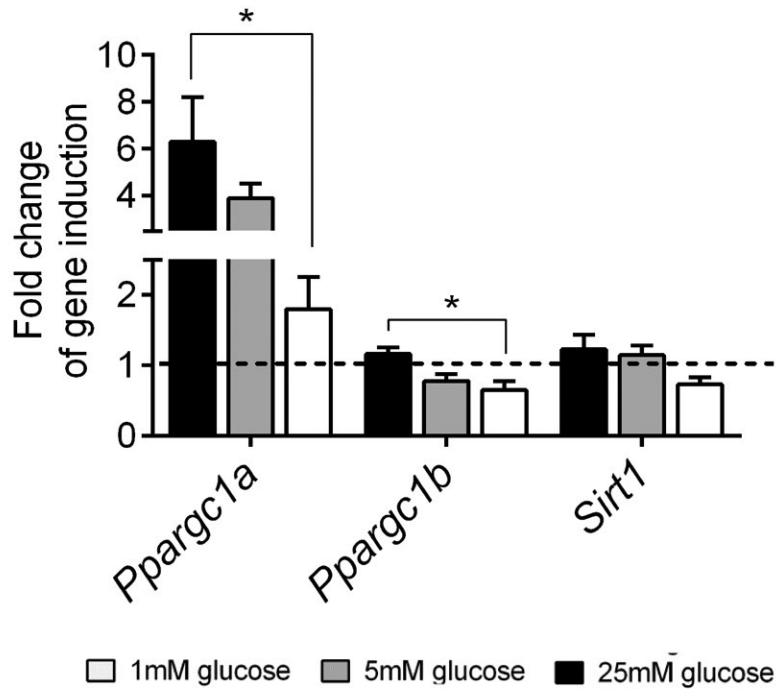
A

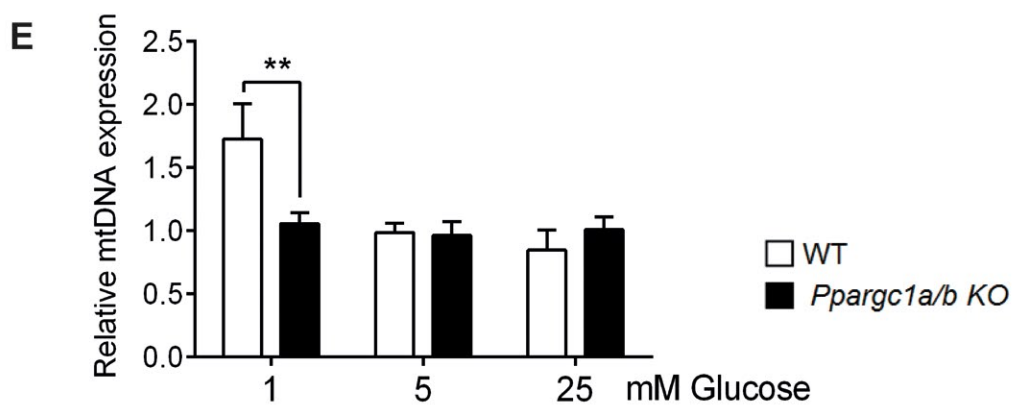
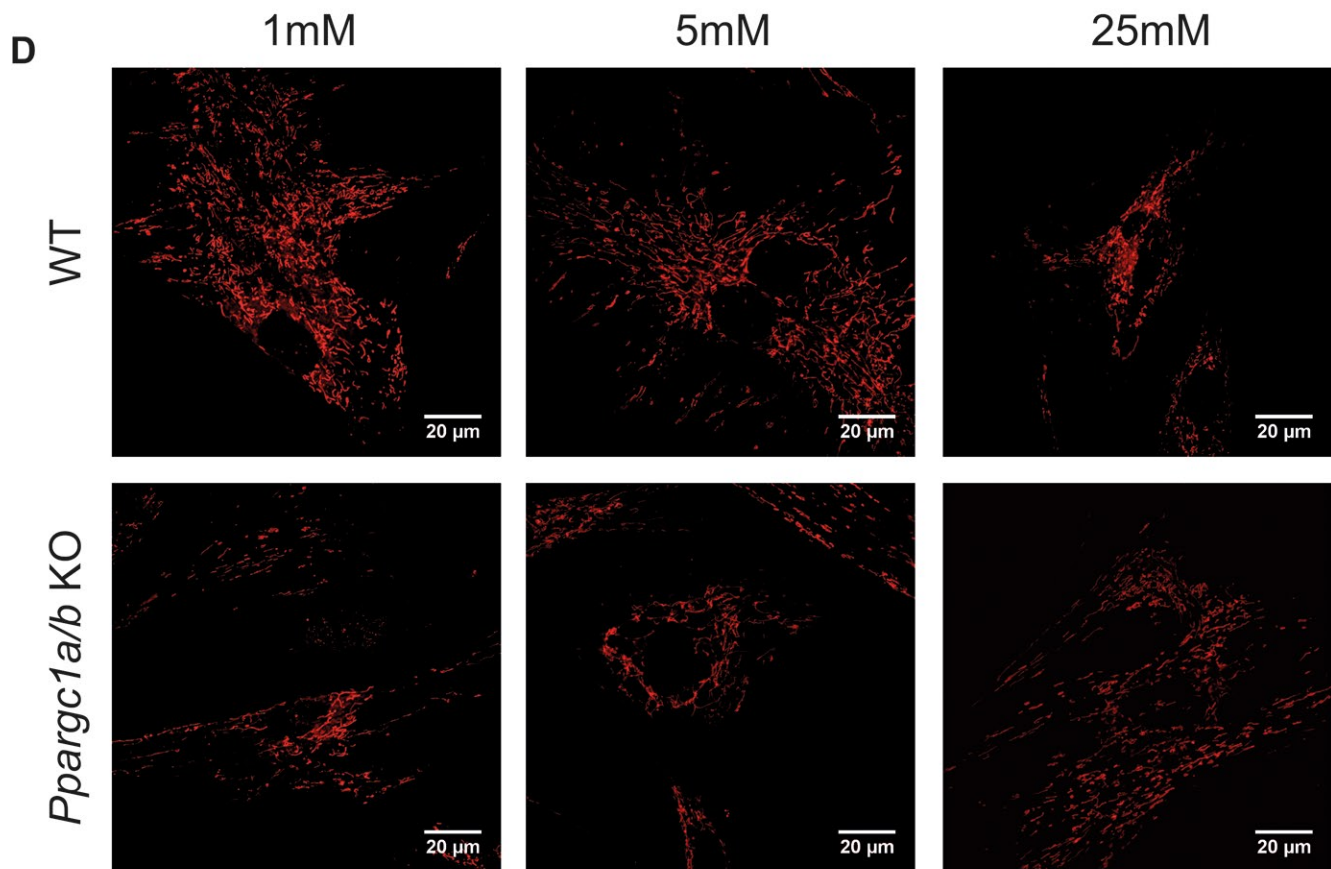
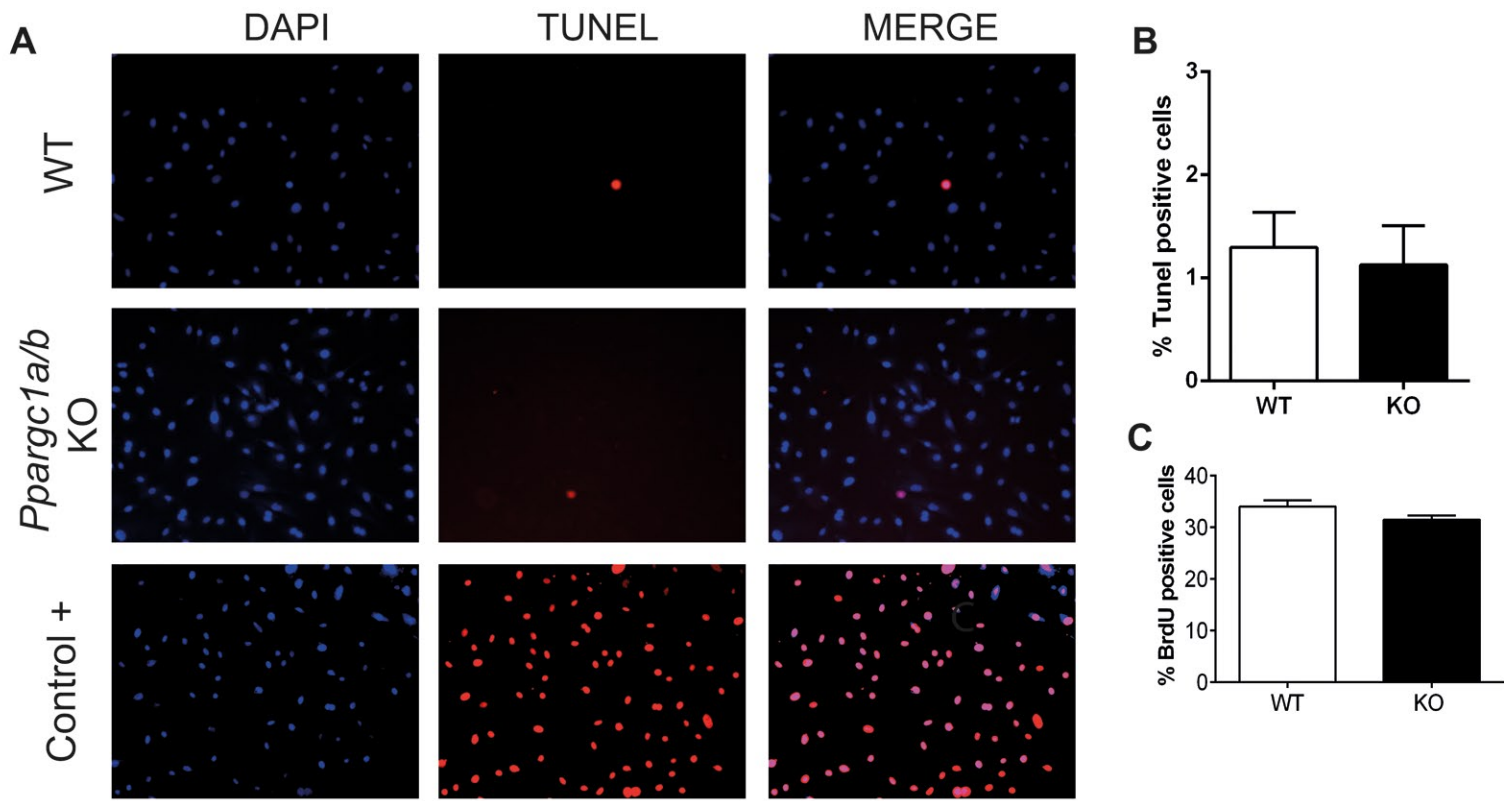


B



C





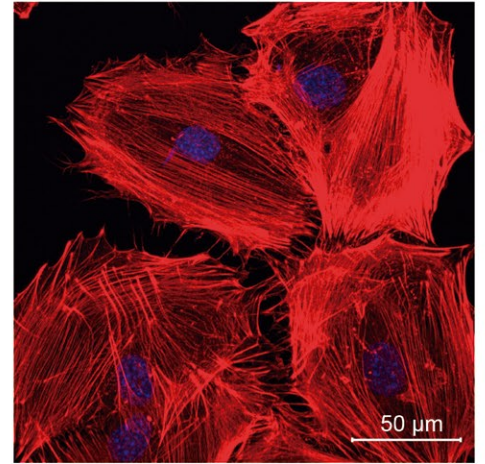
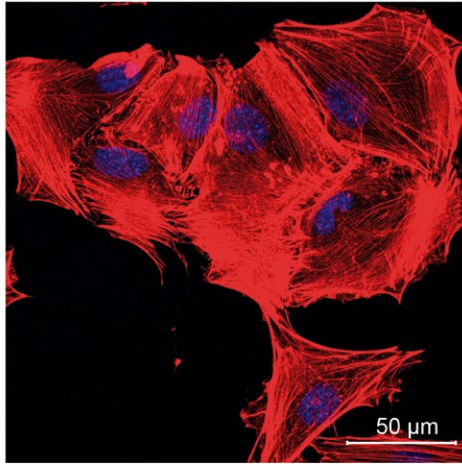
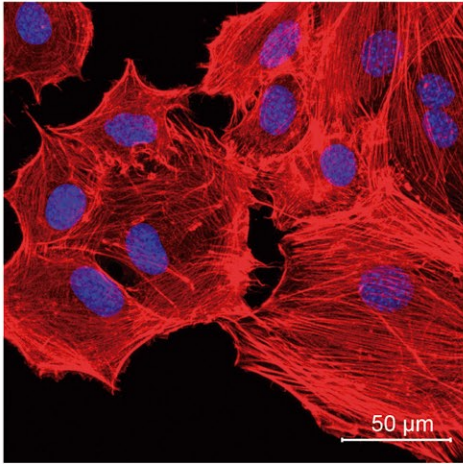
A

IDG-SW3

1mM

5mM

25mM

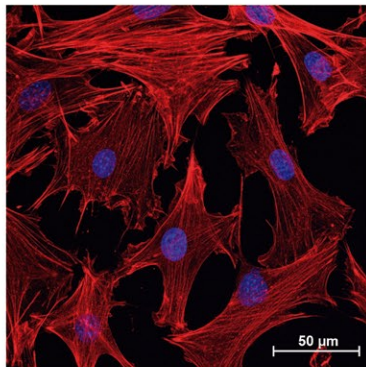
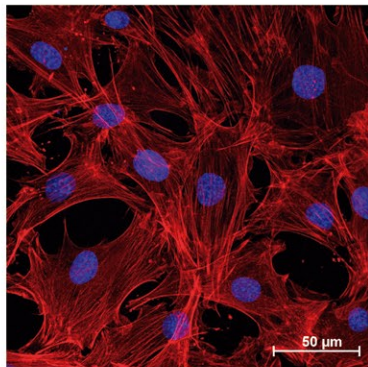
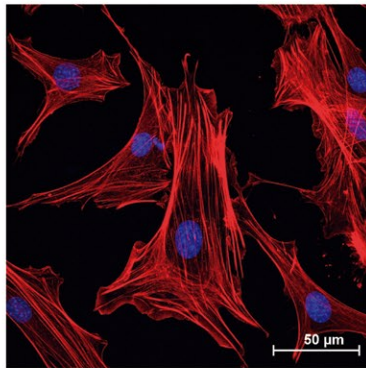
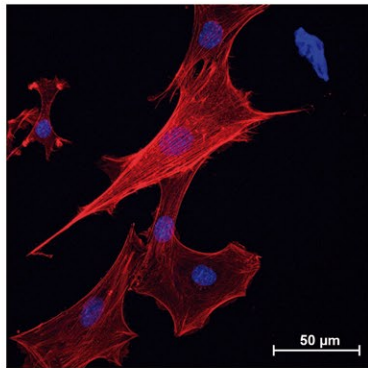


B

Osteoblasts

WT

Ppargc1a/b
KO

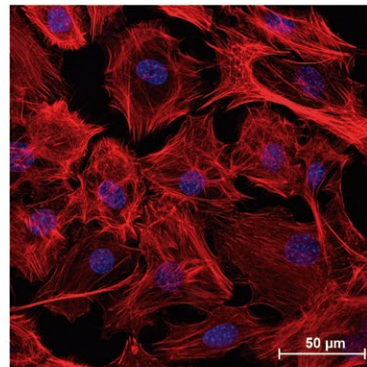
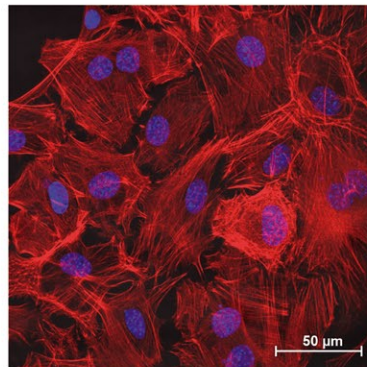
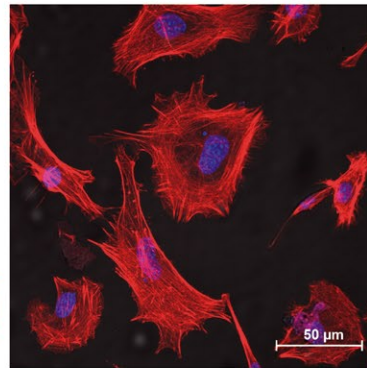
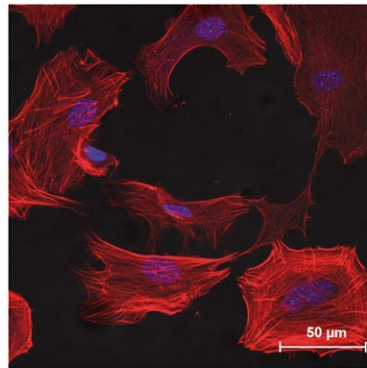


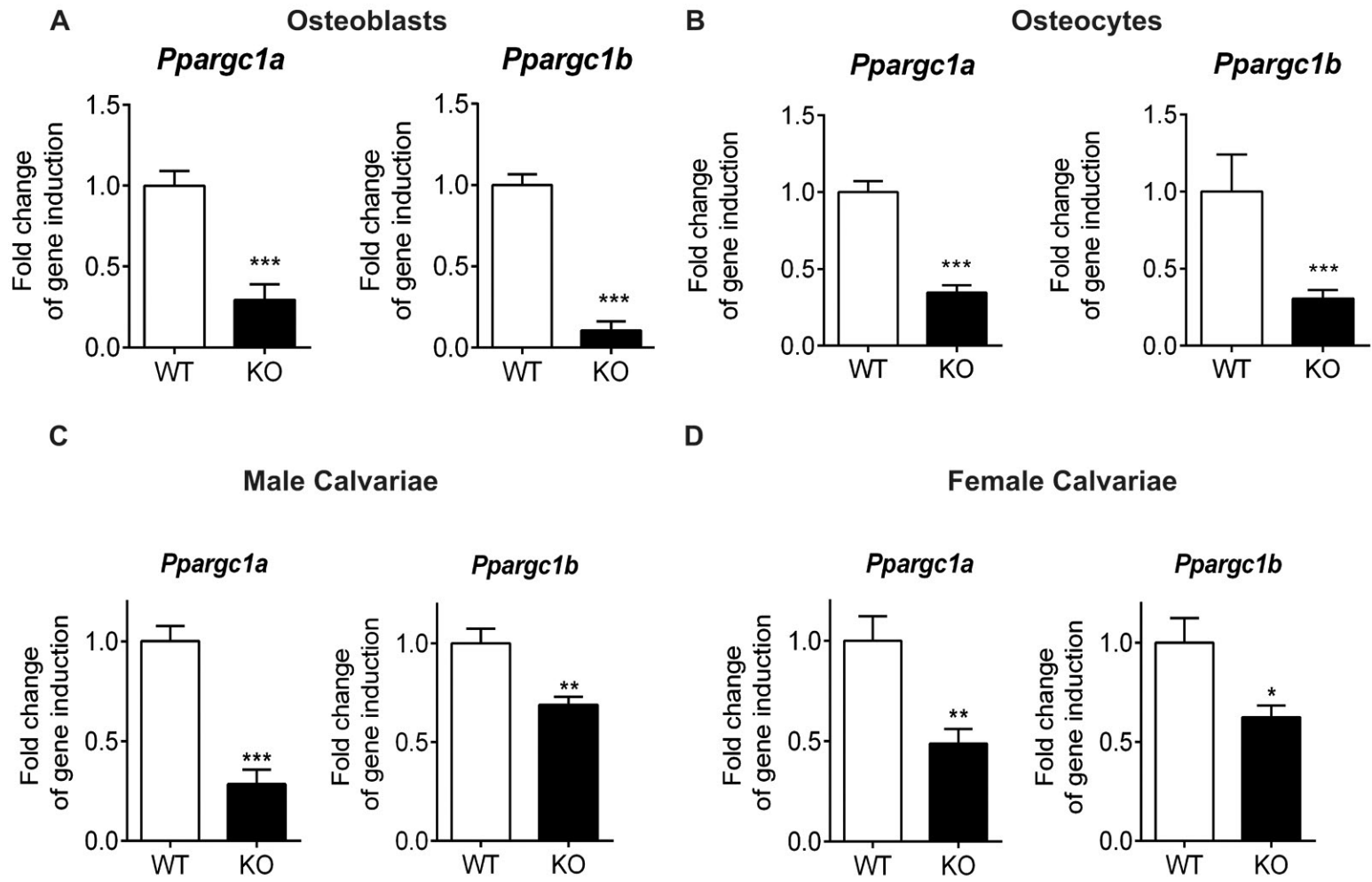
C

Osteocytes

WT

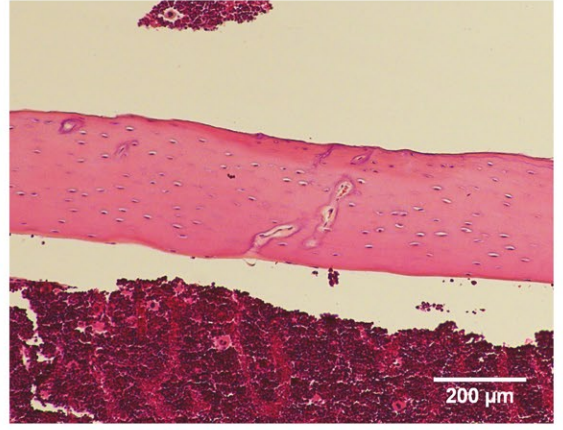
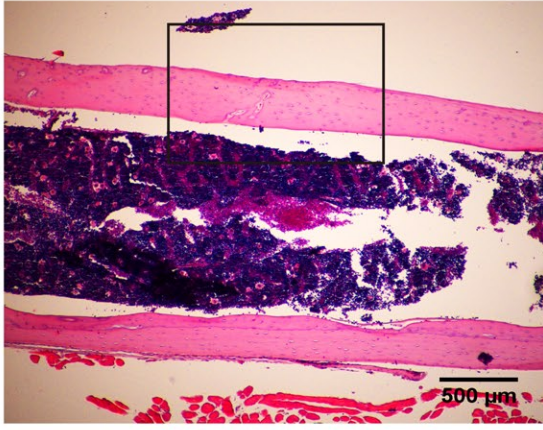
Ppargc1a/b
KO



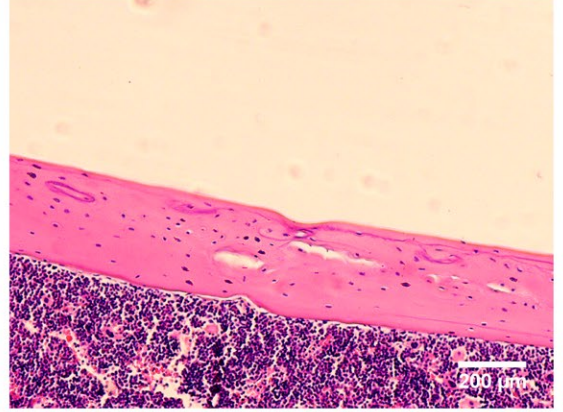
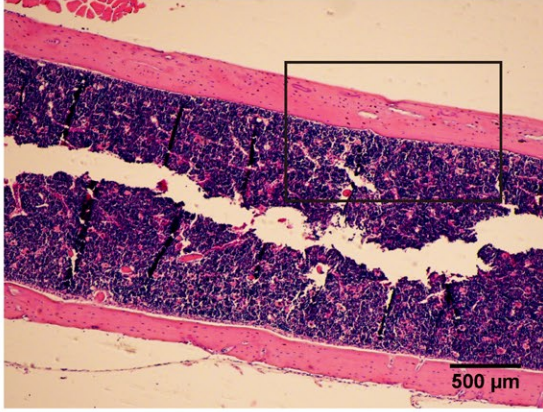


Male

WT

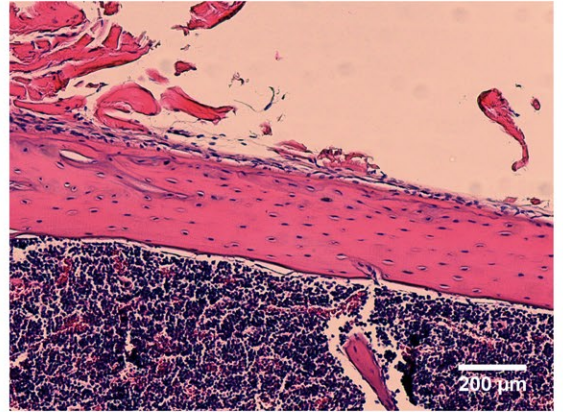
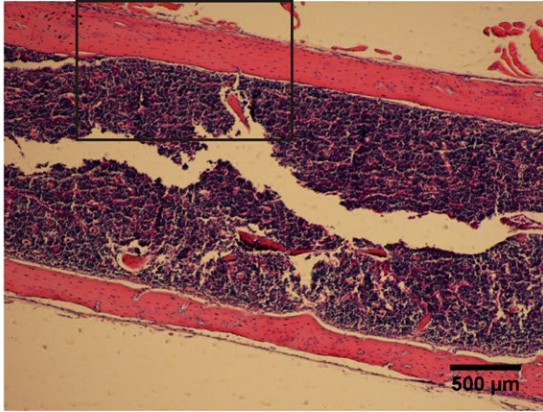


Ppargc1a/b KO

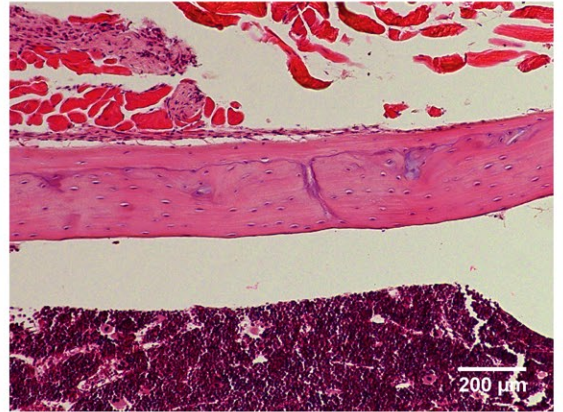
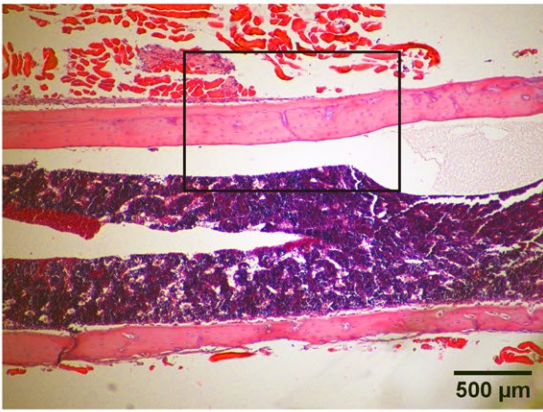


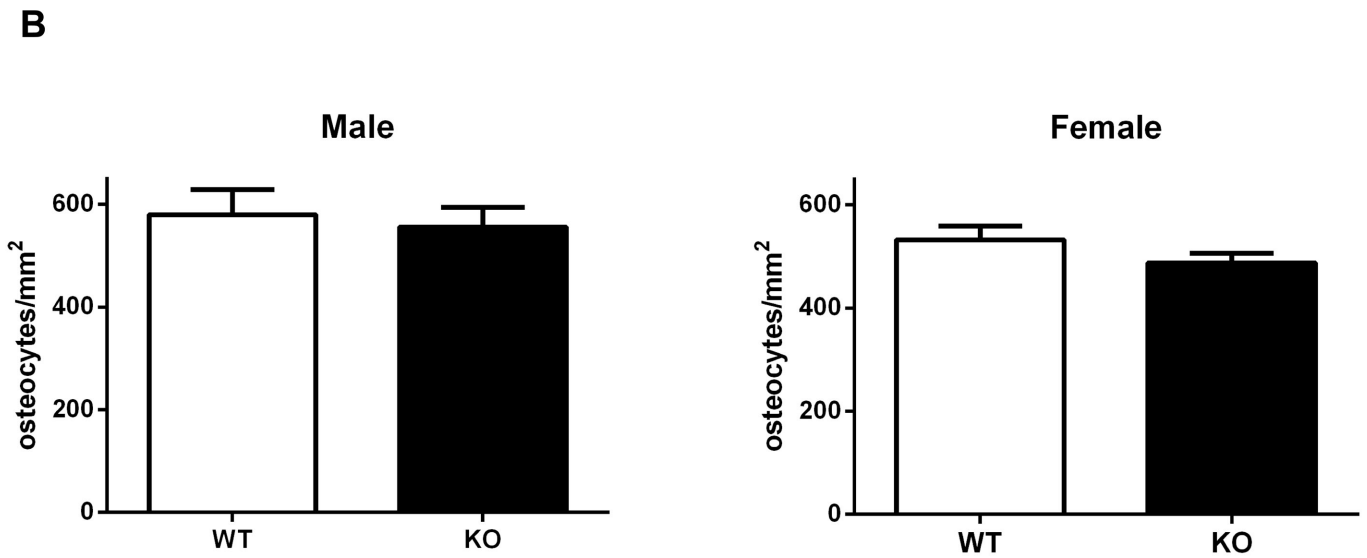
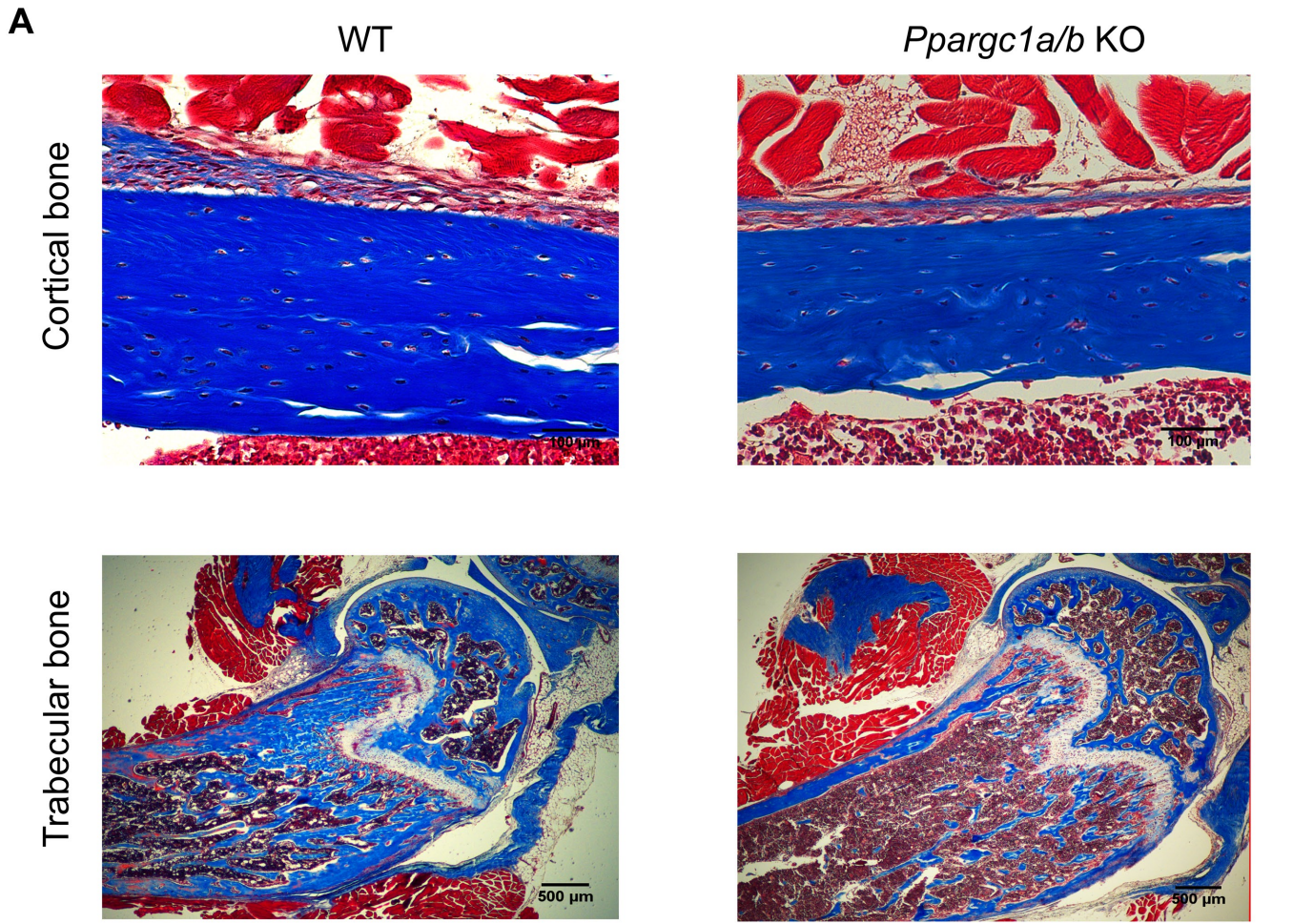
Female

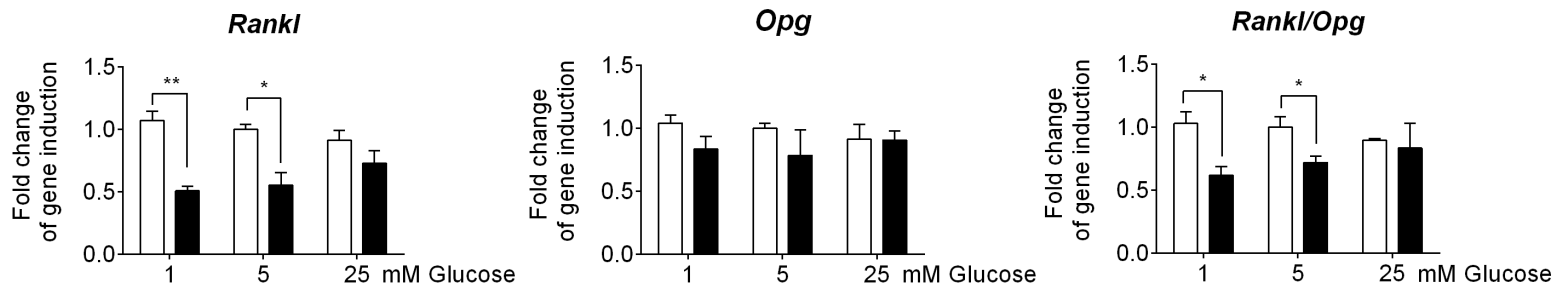
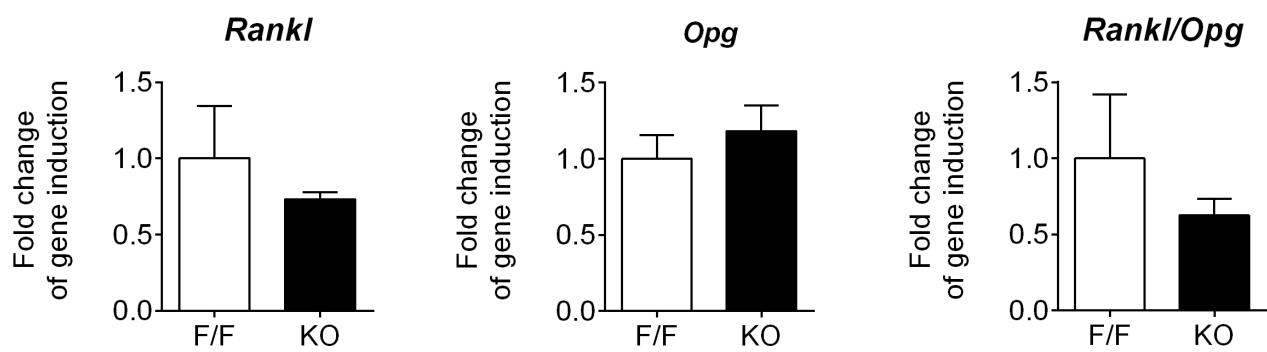
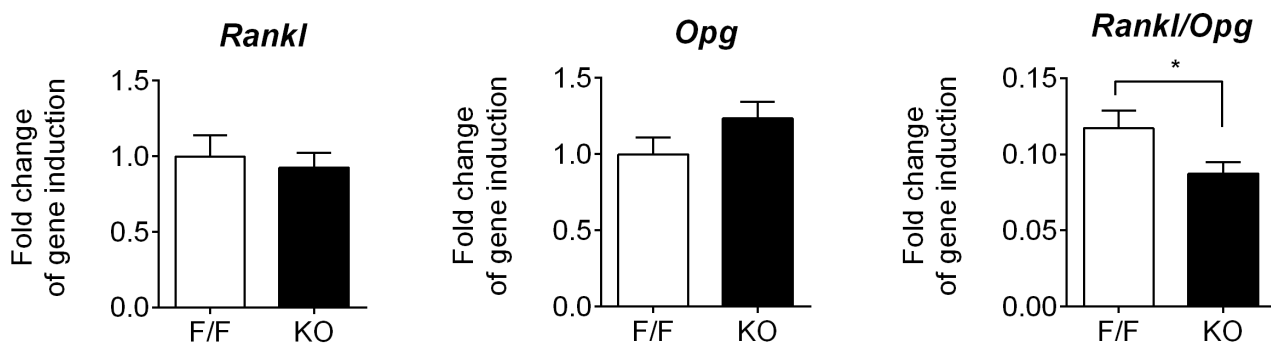
WT



Ppargc1a/b KO





A **Osteocytes****B** **Male Calvaria****C** **Female Calvaria**

SUPPLEMENTARY FIGURE LEGENDS

Figure S1. Glucose supply is responsible for changes in gene expression, related to Figure 1. (A and B) TUNEL staining of IDG-SW3 differentiated for 14 days in the presence of 1, 5 or 25 mM glucose. Representative images (A) and quantitative analysis (B) of TUNEL staining. Results are plotted as mean \pm SEM of three independent experiments. (C) Proliferation rate of IDG-SW3 differentiated for 14 days in presence of 1, 5 or 25 mM glucose. Results are expressed as percentage of BrdU⁺ cells. Data are plotted as mean \pm SEM of three independent experiments. (D) Quantification of mRNA expression levels in IDG-SW3 cells differentiated for 14 days in the presence of 1, 5 or 25 mM glucose or in the presence of 1mM glucose plus 24 mM mannitol and 5 mM glucose plus 20 mM mannitol. Results are plotted as expression relative to IDG-SW3 cells cultured in 5 mM glucose and statistical analysis was performed between conditions with or without mannitol (E) Quantification of mRNA expression levels in organotypic cultures from mouse femur maintained in 1, 5 or 25 mM glucose media. Results are plotted as expression relative to organotypic cultured maintained in 5 mM glucose media. mRNA levels were measured by RT-qPCR and normalized to *Tbp* expression. Results are plotted as mean \pm SEM of six independent experiments. *p<0.05, **p<0.01 and ***p<0.001 using Student's t-test.

Figure S2. Metabolic profile in primary mature osteoblasts under different glucose supplies, Related to Figure 2. (A) ATP levels in osteoblasts after 10 days of differentiation in the presence of 1, 5 or 25 mM glucose. (B) Determination of the maximal uptake capacity for glucose in osteoblast differentiated for 10 days in the presence of 1, 5 or 25 mM glucose. Glucose uptake was tested at 10 μ M glucose for all conditions. (C) Quantification of lactate release in osteoblasts differentiated for 10 days in the presence of 1, 5 or 25 mM glucose.

Figure S3. Changes in glycolytic gene expression and mitochondrial function induced by different glucose concentrations, Related to Figure 3. (A) mRNA expression levels of the different GLUT family members (SLC2a) in IDG-SW3 differentiated for 14 days in 5 mM glucose media. mRNA expression was quantified by RT-qPCR and normalized to *Tbp* expression. Results are plotted as $2^{-\Delta Ct}$ (mean \pm SEM of six independent experiments). (B) mRNA expression levels of *Slc2a2*, *Slc2a3* and *Slc2a4* during IDG-SW3 differentiation in 1, 5 and 25 mM glucose media. mRNA levels were quantified by qRT-PCR, normalized by *Tbp* and plotted as expression relative to undifferentiated IDG-SW3 (mean \pm SEM of six independent experiments). (C) mRNA expression levels of glycolytic and mitochondrial genes in primary osteoblasts differentiated for 10 days in the presence of 1, 5 or 25 mM glucose. Results are plotted as expression relative to undifferentiated primary osteoblasts (mean \pm SEM of six independent experiments). (D) Quantification of mtDNA in primary osteoblasts differentiated for 10 days in the presence of 1, 5 or 25 mM glucose. Results are plotted as expression relative to undifferentiated primary osteoblasts (mean \pm SEM of four independent experiments). (E) Analysis of the levels of mitochondrial complexes in primary osteoblasts differentiated for 10 days in the presence of 1, 5 or 25 mM glucose. (F) Visualization of mitochondria in primary osteoblasts differentiated for 10 days in the presence of 1, 5 or 25 mM glucose. * $p < 0.05$, ** $p < 0.01$ and *** $p < 0.001$ using one-way ANOVA.

Figure S4. Signaling pathways involved in glucose restriction in osteoblasts, Related to Figure 4 and 5. (A and B) Immunoblots from primary osteoblasts during the first 24 hours of differentiation in 1, 5 or 25 mM glucose media (A) or after 10 days of differentiation in 1, 5 and 25 mM glucose media (B). (C) mRNA expression levels of *Pparg1* isoforms and *Sirt1* in primary osteoblasts differentiated for 10 days in 1, 5 or 25

mM glucose media. Results are plotted as $\Delta\Delta\text{Ct}$ relative to undifferentiated osteoblasts at day 0 (mean \pm SEM of five independent experiments).

Figure S5. Loss of PGC-1 α/β does not affect cell viability but abolishes the increase in mitochondrial DNA induced by glucose restriction, Related to Figure 6. (A and B)

TUNEL staining of primary osteoblasts wild-type (WT) and knock-out (KO) for *Ppargc1a/b*. Representative images (A) and quantitative analysis (B) of TUNEL staining.

Results are plotted as mean \pm SEM of three independent experiments. (C) Proliferation

rate of primary osteoblasts wild-type and KO for *Ppargc1a/b*. Results are expressed as percentage of BrdU⁺ cells. Data are plotted as mean \pm SEM of three independent

experiments. (D) Visualization of mitochondria in primary osteoblasts wild-type and KO

for *Ppargc1a/b* differentiated for 10 days in the presence of 1, 5 or 25 mM glucose. (E)

Quantification of mtDNA in primary osteoblasts, wild-type and KO for *Ppargc1a/b*, differentiated for 10 days in the presence of 1, 5 or 25 mM glucose. Results are plotted

relative to the content of wild type osteoblasts cultures at 5 mM glucose as mean \pm SEM

of four independent experiments. * $p < 0.05$, ** $p < 0.01$ and *** $p < 0.001$ using one-way ANOVA.

Figure S6. Different glucose supply or deletion of *Ppgarc1a* and *Ppgarc1b* does not alter actin cytoskeleton organization, Related to Figure 6. (A) Representative images

of Maximum Intensity Projection of IDG-SW3 differentiated in 1, 5, or 25 mM glucose media for 14 days and stained with Alexa 488-phalloidin (red) and DAPI (blue) (B)

Maximum Intensity Projection of primary osteoblasts wild-type and KO for *Ppargc1a/b* stained with Alexa 488-phalloidin (red) and DAPI (blue) (C) Maximum Intensity

Projection of primary osteocytes wild-type and KO for *Ppargc1a/b* stained with Alexa 488-phalloidin (red) and DAPI (blue).

Figure S7. *Ppargc1a* and *Ppargc1b* expression levels in *Ppargc1a/b* deficient (KO) mice, Related to Figure 7. (A). mRNA expression levels of *Ppargc1a* and *Ppargc1b* in primary osteoblast wild-type and KO for *Ppargc1a/b*. Results were plotted as mean \pm SEM of six independent experiments. (B) mRNA expression levels of *Ppargc1a* and *Ppargc1b* in primary osteocytes wild-type and KO for *Ppargc1a/b*. Results were plotted as mean \pm SEM of six independent experiments. (C and D) mRNA expression levels of *Ppargc1a* and *Ppargc1b* in calvaria obtained from *Ppargc1a/b* conditional knockout (*Ppargc1a/b*^{ff};Col1a1-Cre) and control male (C) and female (D) mice. Results were plotted as mean \pm SEM of eight independent animals. mRNA expression levels were measured by RT-qPCR and normalized to *Tbp* expression. *p<0.05, **p<0.01 and ***p<0.001 using Student's t-test.

Figure S8. Histological analysis of femurs of *Ppargc1a* and *Ppargc1b*-deficient mice, Related to Figure 7. Representative images of longitudinal sections of femur from wild type (WT) and *Ppargc1a/b* knock-out (KO) mice stained with hematoxylin and eosin. Images were taken at 4x and 10x magnification.

Figure S9, Related to Figure 7. (A) Representative images of longitudinal sections from middle and distal femur from wild type (WT) and *Ppargc1a/b* knock-out (KO) mice stained with Masson's trichrome stain. Images were taken at 2x and 20x magnification. (B) Osteocyte number normalized by bone area. Results are shown as mean \pm SEM of 12 different fields from 8 different animals.

Figure S10, Related to Figure 7. (A) mRNA expression levels of *Rankl*, *Opg* and *Rankl/Opg* expression ratio in primary osteocytes wild-type and KO for *Ppargc1a/b* cultured in 1, 5, and 25 mM glucose media. Results were plotted as mean \pm SEM of three independent experiments. (B and C) mRNA expression levels of *Rankl*, *Opg* and the

Rankl/*Opg* expression ratio in calvaria obtained from *Ppargc1a/b* conditional knockout (*Ppargc1a/b*^{ff};Col1a1-Cre) and control male (B) and female (C) mice.

TRANSPARENT METHODS

Cell cultures

IDG-SW3 cells (obtained from Dr. L. Bonewald) were cultured as previously described ⁽⁷⁾. Briefly, IDG-SW3 were maintained and expanded in proliferative conditions (33°C in α MEM with 5 mM glucose, 10% FBS, 2 mM glutamine, 1 mM pyruvate, 100 U/ml penicillin, 0.1 mg/ml streptomycin and 50 U/ml IFN- γ) on type I collagen-coated plates. To induce osteogenesis, cells were seeded on type I collagen-coated plates and cultured in osteogenic media (37°C in α MEM with 10% FBS, 1, 5, or 25 mM glucose, 2 mM glutamine, 1 mM pyruvate, 100 U/ml penicillin and 0.1 mg/ml streptomycin with 50 μ g/ml ascorbic acid and 4 mM β -glycerophosphate, in the absence of IFN- γ).

Primary osteoblasts were isolated from calvaria as previously described ⁽²⁴⁾. Briefly, calvaria was dissected from P1-P4 pups, and sutures and soft tissue were discarded. A total of 5 to 10 calvariae were pooled and serially digested in α -MEM, containing trypsin (0.025%)/collagenase II (1 mg/mL). The product of the first 5 minutes of digestion was discarded, while the product of a double 20-minute digestion was centrifuged and seeded on 60-mm culture plates. Cells were used between passages 4 to 6. Osteoblasts were cultured in osteogenic media (as above) and the concentration of glucose adjusted to 1, 5, or 25 mM.

For bone organotypic cultures, bone pieces from mice femurs were digested in DMEM containing collagenase II (1mg/ml) for 2h at 37°C in a shaking water bath. Then, bone pieces were rinsed, plated and incubated overnight in osteogenic media. The next day, bone pieces were washed 4 times with PBS and incubated in osteogenic media for 5 days.

Primary osteocytes were isolated with a protocol derived from Shah et al. (Shah et al. 2016, Bonekey Rep. 5:838). Briefly, mice limbs (tibiae, femur and humeri) and calvariae from 5 mice were pooled, cut and serially digested on a rotating shaker at 37°C. Bone pieces were incubated in collagenase solution (trypsin (0.025%)/collagenase II (1 mg/mL) in α -MEM) for 25 min. The solution was discarded, and the bone pieces were washed in PBS. This was repeated two more times, for a total of three digestions (digestions 1 to 3). Then, bone pieces were incubated with EDTA solution (5 mM EDTA in PBS containing 1% BSA, pH = 7.4) for 25 min. The solution was discarded (digestion 4), and the bone pieces were washed in PBS (digestion 4). Bone pieces were incubated with collagenase solution for 25 min, the solution was discarded, and the bone pieces were washed in PBS (digestion 5). Bone pieces were incubated with EDTA solution for 25 min, the solution was discarded, and the bone pieces were washed in PBS (digestion 6). Bone pieces were incubated with collagenase solution for 25 min, the solution was kept for cell plating, and the bone pieces were washed in PBS (digestion 7). Bone pieces were incubated with EDTA solution for 25 min, the solution was kept for cell plating, and the bone pieces were washed in PBS (digestion 8). Bone pieces were incubated with collagenase solution for 25 min, the solution was kept for cell plating (digestion 9). Digestions 7 to 9 were combined and spun down at 200xg for 5 min. The cell pellet was resuspended in α -MEM culture medium and plated on type-I rat tail collagen coated culture plates. Osteocytes were cultured in α -MEM supplemented with 5% FBS, 5% calf serum, 1mM pyruvate, 100 U/ml penicillin and 0.1 mg/ml of streptomycin. Cells were maintained at 37°C and 5% CO₂ in a humidified incubator up to 7 days.

Animal model

We used eight-week-old C57BL/6 female and male mice. All animal had *ad libitum* access to food (Teklad, 2014: Harlan-Teklad, Indianapolis, IN, USA) and water. Mice

were maintained at 22-24°C on a 12-hour light/12-hour dark cycle. All procedures were approved by the Ethics Committee for Animal Experimentation of the University of Barcelona and the Generalitat de Catalunya. Osteoblast-specific *Ppargc1a/b*-deficient mice (*Ppargc1a/b;Colla1-Cre*) were generated by crossing heterozygous *Colla1-Cre* mice (Tg(*Colla1-cre*)1Kry(21) with mice carrying loxP sites flanking exons 4 and 5 of the *Ppargc1a* ⁽²⁵⁾ and exons 4 and 5 of *Ppargc1b* alleles ⁽²⁶⁾. *Ppargc1a/b f/f;Colla1-Cre* (KO) mice were fertile and born in the Mendelian ratio, and they were crossed with *Ppargc1a/b f/f* to obtain experimental (*Ppargc1a/b f/f;Colla1-Cre*) and control (*Ppargc1a/b f/f*) mice.

Retroviral transduction

Retroviral pMSCV-PGC-1 α (generated from pcDNA4-PGC-1 α from Addgene) and pMSCV-GFP control virus were used for PGC1 α overexpression in primary osteoblasts and IDG-SW3 cells. After infection, cells were cultured for five days in osteogenic media. Retroviral pMSCV-puro-Cre-ERT2, pMSCV-puro and pMSCV-GFP virus were used for *Ppargc1a/b* deletion assays in primary osteoblasts from *Ppargc1a/b f/f* mice. Puromycin (5 μ g/ml) was used for selection of infected cells. 24 hours after selection, tamoxifen was added at 1 μ M for 48 hours. Cells were then cultured for five more days in osteogenic media.

Alkaline phosphatase and Alizarin Red staining

For alkaline phosphatase, staining solution was added to the cells and incubated at room temperature for 30 minutes in the dark. For Alizarin Red staining, fixed cells were incubated with Alizarin Red staining solution at room temperature in the dark for 45 minutes.

Flow cytometry

Differentiated IDG-SW3, osteoblasts and osteocytes were rinsed twice with PBS. Cells were incubated with 0.25% Trypsin and 0.02% EDTA at 37°C for 5-10 min, until cells became rounded and started to detach. Cell suspensions were collected and centrifuged at 150g for 5 min. Cell pellets were rinsed three times with PBS and resuspended in PBS containing 1, 5, or 25 mM glucose, 2 mM glutamine and 1 mM pyruvate. Before flow cytometry analysis, cell suspensions were filtered with a 0.70 µm nylon mesh to remove aggregates. Cell viability was assessed with 7-ADD, ensuring that the analyzed population of cells was alive.

Dmp1-GFP expression

Expression of *Dmp1*-GFP in IDG-SW3 was evaluated after 14 days of differentiation by fluorescence microscopy in a Leica DMIRB fluorescence microscope and flow cytometry in a DB FACS Canto II flow cytometer.

Cell proliferation assay

IDG-SW3, osteoblast and osteocyte proliferation was evaluated using BrdU labeling (BD, CA, USA), following the manufacturer's protocol. Briefly, 2×10^4 cells were seeded and cultured for 14- 10 or 7 days. Then, BrdU (10 µM) was added to the medium for 6 hours. Cells were harvested, fixed and permeabilized. The samples were treated with DNase (300 µg/mL in PBS) for 1 hour at 37°C. BrdU was stained with APC-conjugated anti-BrdU antibody. Cells were analyzed in a DB FACS Canto II flow cytometer.

Cell death detection assay

DNA cleavage was assessed by the TUNEL assay as described by the manufacturer (Roche Molecular Biochemicals). Briefly, IDG-SW3, osteoblast or osteocytes were cultured for 14, 10 or 7 days and then fixed with 4% paraformaldehyde in PBS pH 7.4 at room temperature for 1 h. Cells were permeabilized with 0.1% Triton

X-100 in sodium citrate buffer for 2 min at 4 °C and incubated with TUNEL reaction mixture for 1 h at 37 °C. Total DNA was stained with DAPI (1µg/ml, D9542, Sigma) diluted in PBS for 20 min at room temperature. Coverslip were mounted with ProLong®Gold antifade reagent (P36939, Life Technologies). DNA damage was visualized by fluoresce microscopy in a Nikon E800 microscope. Images were analyzed using ImageJ software.

Fluorescence confocal imaging

IDG-SW3 and primary osteoblasts were cultured in differentiation media for 14 and 10 days, respectively. For Mitochondria visualization, cell cultures were stained with 250nM Mitotracker-Deep-Red (ThermoFisher) for 30 minutes at 37°C. Then, the cells were examined in a Zeiss LSM 880 laser scanning confocal spectral microscope equipped with an incubation control system (37 °C, 5% CO₂). Images corresponding to single confocal sections were taken using a 63x oil immersion objective lens. Images were analyzed using ImageJ software.

For the staining of actin filaments, cells were fixed in 4% paraformaldehyde in PBS for 15 min at room temperature, washed twice in PBS, permeabilized for 15 min in PBS containing 0.1% Triton X-100, and then blocked in PBS containing 1% BSA for 30 min. To visualize F-actin, cells were incubated with 7.5 units of Alexa Fluor 488 phalloidin (Invitrogen) for 1 hour and washed three times with PBS. DNA was stained with DAPI (1µg/ml, D9542, Sigma). Coverslips were air dried and mounted with ProLong Gold antifade reagent (P36939, Life Technologies). Several z-stack images of 0.4 µm were acquired using Zeiss LSM 880 laser scanning confocal spectral microscope and processed using ZEN software 2010 (Zeiss) to obtain a Maximum Intensity Projection for each Z-stack series.

Gene expression

Total RNA was isolated from mouse calvaria, primary osteoblasts or IDG-SW3 cells using TRIsure reagent (Bioline, London, UK). Purified RNA was reverse-transcribed using the High-Capacity cDNA Reverse Transcription Kit (Applied Biosystems, Foster City, CA, USA). Quantitative PCR was carried out using the ABI Prism 7900 HT Fast Real-Time PCR System and a Taqman 5'-nuclease probe method (Applied Biosystems) with SensiFAST Probe Hi-ROX Mix (Bioline). All transcripts were normalized to TATA binding protein (*Tbp*) expression.

Glucose uptake

The uptake of 2-deoxyglucose was studied in IDGs grown for 14 days in 1, 5, and 25 mM glucose in osteogenic media. Cells were washed four times with pre-warmed PBS, incubated with PBS containing 50Ci/mmol of 2-deoxy-D-[G-³H] glucose and 10μM of cold 2-deoxy-D-glucose for 5 min at 37 °C. Monolayers were washed 4 times with cold PBS and lysates were obtained in 0.4M NaOH.

Lactate assay

L-lactate was determined using an enzymatic reaction based on the oxidation of L-lactate to pyruvate by lactate dehydrogenase. Samples were diluted by 1:20 with reaction buffer (0.3M hydrazine sulphate, 0.87M Glycine, 2.5 mM NAD⁺, 0.19M EDTA, pH 9.5). NADH concentration was determined by measuring absorbance at 340 nM using Fluostar Optima BMG Labtech at 0 and 20 minutes after starting reaction.

Intact cell respirometry

Mitochondrial function of intact cells was measured by high-resolution respirometry (Oxygraph-2k, Oroboros Instruments). IDG-SW3 cells were cultured in differentiation media with the indicated glucose concentration for 14days. Cells were trypsinized and resuspended again in differentiation media with 1, 5, or 25 mM glucose without FBS. 700,000 cells were added to the experimental chamber. Endogenous routine

respiration was measured with 1, 5, and 25 mM glucose as substrates. Following stabilization of routine respiration, ATP synthesis was inhibited with 1µg/ml of oligomycin to analyze respiratory uncoupling. Next, carbonylcyanide-4-(trifluoromethoxy)-phenyl-hydrazine 1 µM (FCCP) was titrated to achieve maximum flux through the electron transfer system (ETS). Finally, respiration was inhibited by the sequential addition of rotenone (0.1 µM) and antimycin A (2.5 µM). The remaining O₂ flux after inhibition with antimycin A (O₂ flux independent of the electron transfer system) was subtracted to calculate the different respiratory states. Oxygen flux values were expressed relative to protein content determined by the BCA method.

ATP bioluminescence assay

ATP was detected by luciferin-luciferase-ATP reaction. IDGs were lysed in 500µl of boiling water. Extracts were spin at 12000g and 4°C for 5 minutes and 10 µl of supernatant were used for ATP determination. Luciferin-luciferase assay was performed following the manufacturer's recommendations (rLucHS, Biovision).

Western blot assay

Identification of proteins from cell extracts was performed by immunoblotting against pp38, pEIF2α, pS6, LC3, ATF4, SIRT1, pAMPK, pACC, PGC1α, Oxphos, GLUT1 or α-TUBULIN), diluted at 1:1000. Immuno-reactive bands were detected with horseradish-peroxidase-conjugated secondary antibodies and an EZ-ECL kit (Biological Industries, Cromwell, CT, USA).

Chromatin immunoprecipitation assay

ChIP assay was performed as previously described ⁽²⁷⁾. IDG-SW3 cells were retrovirally-infected with *Ppargc1a* constructs. Cells were cultured for 5 days and fixed in 1% formaldehyde for 10 minutes. ChIP was carried out using 1 µg of anti-PGC-1α

(Abcam) or anti-IgG (Upstate) and purified with 20 μ l Magna CHIP Protein A+G Magnetic Beads (Millipore). Purified DNA fragments were analyzed by qPCR with SYBR Green. The primers used for the analysis for *Dmp1*, *Fgf23* and *Sost* gene promoters are detailed in (Supplementary Table 2).

Determination of mtDNA by qPCR

Two μ g of total DNA were used for mitochondrial DNA determination by qPCR. Primers for a mitochondrial DNA gene (*tRNA-Glu*) and a nuclear DNA gene (*Fgf23*) were used. The cycling conditions used were 43 cycles of 30 seconds at 95°C, 30 seconds at 70°C, and 60 seconds at 72°C.

μ CT analysis

Femurs from mice were dissected, cleaned of soft tissue, and fixed in 4% paraformaldehyde (PFA) for 48 hours. High-resolution images from the femur were acquired using a microCT imaging system (Skyscan 1076, Bruker microCT, Kontich, Belgium) in accordance with the recommendations of the American Society of Bone and Mineral Research (ASBMR). Samples were scanned in air at 50 kV and 200 μ A with an exposure time of 800 ms, using a 1-mm aluminium filter and an isotropic voxel size of 9 μ m. Two-dimensional images were obtained every 1° for 180° rotation and were subsequently reconstructed using NRecon reconstruction software and analyzed with CT-Analyzer (SkyScan). For trabecular measurements, manual VOI was employed, starting at 100 slices from the distal growth plate of the femur and extending to the diaphysis for 150 slices. Cortical measurements were performed by delineating the femur medial cortex for 100 slices around the femoral midshaft. A Gaussian noise filter was applied for the reconstruction, and a global binary threshold was manually established at 20 for trabecular analysis and 100 for cortical analysis.

Histological analysis

For histological preparations, samples were fixed in 4% paraformaldehyde for 48 hours at 4°C, decalcified in 14% EDTA for 4 weeks and paraffin embedded. Samples were cut into 5 µm sections and stained with Hematoxylin/eosin or Masson's trichrome.

Statistical analysis

Statistical analysis was performed using One-way ANOVA or Student's *t* test. Quantitative data are presented as means ± S.E.M. Differences were considered significant at * $p < 0.05$, ** $p < 0.01$ and *** $p < 0.001$.